

# GREAT AUSTRALIAN BIGHT RESEARCH PROGRAM

## RESEARCH REPORT SERIES

### Characterise spatial variability of offshore/slope plankton and micronekton communities

#### Final Report GABRP Project 2.2

Kloser, R.J., van Ruth, P.D., Doubell, M., Downie, R., Flynn, A., Gershwin, L., Patten, N., Revill, A., Richardson, A.E., Ryan, T.E., and Sutton, C.A

GABRP Research Report Series Number 22

October 2017



## DISCLAIMER

The publishers of the Great Australian Bight Research Program advise that the information contained in this publication comprises general statements based on scientific research. The reader is advised that no reliance or actions should be made on the information provided in this report without seeking prior expert professional, scientific and technical advice. To the extent permitted by law, the publishers of the Great Australian Bight Research Program (including its employees and consultants) excludes all liability of any person for any consequences, including but not limited to all losses, damages, costs, expenses and any other compensation, arising directly or indirectly from using this publication (in part or in whole) and any information or material contained in it.

The GABRP Research Report Series is an Administrative Report Series which has not been reviewed outside the Great Australian Bight Research Program and is not considered peer-reviewed literature. Material presented may later be published in formal peer-reviewed scientific literature.

## COPYRIGHT

©2017

## THIS PUBLICATION MAY BE CITED AS:

Kloser, R.J., van Ruth, P.D., Doubell, M., Downie, R., Flynn, A., Gershwin, L., Patten, N., Revill, A., Richardson, A.E., Ryan, T.E. and Sutton, C.A. (2017). Characterise spatial variability of offshore/slope plankton and micronekton communities. Final Report GABRP Project 2.2. Great Australian Bight Research Program, GABRP Research Report Series Number 22, 301pp.

## CONTACT

Dr Rudy Kloser  
CSIRO  
e: [rudy.kloser@csiro.au](mailto:rudy.kloser@csiro.au)

## FOR FURTHER INFORMATION

[www.misa.net.au/GAB](http://www.misa.net.au/GAB)

## GREAT AUSTRALIAN BIGHT RESEARCH PROGRAM

The Great Australian Bight Research Program is a collaboration between BP, CSIRO, the South Australian Research and Development Institute (SARDI), the University of Adelaide, and Flinders University. The Program aims to provide a whole-of-system understanding of the environmental, economic and social values of the region; providing an information source for all to use.

## CONTENTS

Glossary.....	iv
Acknowledgements.....	v
1. Executive summary.....	1
2. Introduction .....	3
2.1 Overview .....	3
2.2 Objectives.....	6
2.3 Methods.....	7
3. Pelagic Habitat .....	12
3.1 Broad scale pelagic habitat .....	12
3.1.1 Introduction .....	12
3.1.2 Methods.....	13
3.1.3 Results and Discussion .....	14
3.1.4 Summary .....	28
3.2 Fine scale pelagic habitat .....	31
3.2.1 Introduction .....	31
3.2.2 Methods.....	31
3.2.3 Results and Discussion .....	32
3.2.4 Summary .....	45
4. Microbes and Plankton .....	49
4.1 Community composition and size structure .....	49
4.1.1 Introduction .....	49
4.1.2 Methods.....	50
4.1.3 Results.....	55
4.1.4 Discussion.....	76
4.1.5 Appendix: Phytoplankton data .....	84
4.2 Physiological process studies, productivity, and food web dynamics .....	88
4.2.1 Introduction .....	88
4.2.2 Methods.....	89
4.2.3 Results.....	93
4.2.4 Discussion.....	106
4.2.5 Summary and conclusions .....	109
5. Zooplankton .....	113
5.1 Large-scale plankton dynamics in the Great Australian Bight .....	115

5.1.1	Introduction .....	115
5.1.2	Methods.....	116
5.1.3	Results.....	120
5.1.4	Discussion.....	132
5.2	Regional comparison of community structure, size and biomass .....	138
5.2.1	Introduction .....	138
5.2.2	Methods.....	139
5.2.3	Results.....	144
5.2.4	Discussion.....	149
5.3	Gelatinous zooplankton .....	155
5.3.1	Introduction .....	155
5.3.2	Methods.....	158
5.3.3	Results.....	158
5.3.4	Discussion.....	159
5.3.5	Sampling challenges and future research focus .....	165
6.	Micronekton.....	176
6.1	Micronekton abundance and diversity regional comparison.....	180
6.1.1	Introduction .....	180
6.1.2	Methods.....	181
6.1.3	Results.....	185
6.1.4	Discussion.....	222
6.1.5	Appendix: Micronekton ancillary data.....	227
6.2	Trophic linkages and food webs based on stable isotopes.....	229
6.2.1	Introduction .....	229
6.2.2	Methods.....	230
6.2.3	Results.....	233
6.2.4	Discussion.....	243
6.3	Bioacoustic spatial and temporal summary.....	248
6.3.1	Introduction .....	248
6.3.2	Methods.....	248
6.3.3	Results.....	254
6.3.4	Discussion.....	265
6.3.5	Conclusions .....	268
6.3.6	Appendix – Additional acoustic figures.....	269



6.4	Fine scale acoustic and optical sampling .....	273
6.4.1	Introduction .....	273
6.4.2	Methods .....	274
6.4.3	Results .....	279
6.4.4	Discussion .....	286
7.	Synthesis and Discussion .....	290
8.	Conclusion .....	295
9.	Appendix: Student Projects .....	297
9.1	Student name .....	297
9.2	Degree type, project title and institution .....	297
9.3	Status of student project .....	297
9.3.1	Aim .....	297
9.3.2	Progress on chapters .....	298
10.	Appendix: project publications .....	299
10.1	Papers .....	299
10.2	Presentations .....	299
10.3	Patents .....	300
10.4	Media Releases .....	300
11.	Appendix: intellectual property .....	301
11.1	Unique discoveries .....	301
11.2	Action plan .....	301

## GLOSSARY

Commonly used and consistent terms and abbreviations used throughout this report are detailed below:

Bathypelagic	A zone of open ocean from 1000 m to 4000 m water depth
Chl-a	Chlorophyll a; a specific form of chlorophyll used in oxygenic photosynthesis
CSIRO	Commonwealth Scientific and Industrial Research Organisation
EAC	Eastern Australian Current
Epipelagic	A zone of open ocean from 0 m to nominally 200 m water depth
EZ net	Easy zooplankton net; a multi net and vertically profiling net used to collect depth stratified zooplankton samples
Folsom plankton splitter	A well known device for subsampling by splitting, developed by Dr Folsom of the Scripps Institution of Oceanography
GAB	Great Australian Bight
IYGPT	International Young Gadid Pelagic Trawl; a type of fishing trawl net
Mesopelagic	A zone of open ocean from nominally 200 m to 1000 m water depth
MIDOC	Mid-water open and closing net; fitted to a trawl net and used to collect depth stratified micronekton samples
MNF	Marine National Facility
NASC	Nautical Area Scattering Coefficient, acoustic measure, see MacLennan et al. 2002 for derivation
Nekton	Marine animals that are able to swim and move independently of currents
Oligotrophic	Low in nutrients and generally not productive in terms of aquatic animal and plant life
PLAOS	Profiling Lagrangian Acoustic Optical System
Pelagic	A zone in the open ocean referring water column as opposed to the ocean floor
Plankton	The taxonomically diverse group of animals that are unable to swim against currents
SARDI	South Australian Research and Development Institute
Seabird9plus	CTD model SBE9+ (serial number 552) with external sensors; Chelsea Fluorometer, Oxygen sensor (SBE43), PAR Biospherical
Shelf	Continental margin seabed depths from 0 m - 200m
Shelf Break	Continental Margin region of the outer shelf where the slope of the seabed increases significantly at 200 m depth
Simrad ITI	a wireless trawl positioning and monitoring system designed to improve control and efficiency in pelagic and bottom trawling
Upper Slope	Continental margin from the shelf break (nominally 200 m) to 750 m depth

## ACKNOWLEDGEMENTS

Physical, chemical, biological, and acoustic data were sourced from the Integrated Marine Observing System (IMOS) – IMOS is a national collaborative research infrastructure, supported by the Australian Government. We thank the voyage participants and CSIRO Marine National facility personnel on IN2015\_C02 for assisting to collect the data, assisting with identifications and recording stations. We thank Terry Visser from PGS for collection of the Ramform Sovereign acoustic data. The CSIRO's Equipment and Technology group for the preparations of the gear used at sea and in particular Matt Sherlock for the Profiling Lagrangian Acoustic Optical Probe. The Continuous Plankton Recorder data collection and analysis was provided by Frank Coman and Wayne Rochester and Gordon Keith for support with the acoustic data and data management at sea. We thank Charles Lemckert from Griffith University for providing the TurboMAP microstructure profiler for use. Finally, we thank the Great Australian Bight Research Program, a collaboration between BP, CSIRO, SARDI, the University of Adelaide and Flinders University, for funding and support.

## 1. EXECUTIVE SUMMARY

The Pelagic Characterisation Theme, Project 2.2 in the Great Australian Bight Research Program (GABRP), has investigated key knowledge gaps in the structure and function of the offshore plankton and micronekton communities of the Great Australian Bight (GAB). This was the first detailed study of the central GAB offshore upper-slope and oceanic pelagic ecosystem that characterised the biota from sizes of microns to meters. Sampling biota from microbes to tuna requires a large diverse team, using a wide range of technologies and methodologies, and is only possible on a large research vessel. Inherent to this study were the multiple spatial and temporal scales that affect the composition, distribution and abundance of species. Given this complexity and the complexities and precision of any one sampling method, a multiple-lines-of-evidence approach was adopted. The potential for bias in interpretation due to fast turn over (days – months) of microbes and plankton, influenced by small-scale local environmental changes, was augmented by characterising slow turn over (years) micronekton species. Similarly, studies of micronekton may be biased by gear selectivity and behaviour, and its temporal and spatial variability. This study provides a comprehensive pelagic ecosystem structure and function of the offshore GAB at a point in time given spatial and temporal context by net primary production derived from satellite ocean colour, physical oceanography modelling and the Continuous Plankton Recorded and bio-acoustics data.

The community structure, dynamics, biodiversity and endemism of microbes (i.e., viruses and bacteria), plankton (i.e., phytoplankton, zooplankton, ichthyoplankton) and micronekton (including squids, small pelagic and mesopelagic fish and gelatinous organisms) were described, highlighting similarities and differences between the eastern and central regions for gradients of distance from the shelf break, day to night, and depth. Most notable was the similarity rather than differences between the eastern and central regions. Key differences were that picoplankton dominated in the central region, with nanoplankton dominant in the east. Notable similarities were that micronekton fish dominated the taxon richness showing that central and eastern GAB regions were similar in diversity and evenness.

This study tested the hypothesis that the “microbial food web” is the dominant planktonic food web over the deep GAB continental margin, particularly in the central GAB where year-round downwelling is thought to be the prevailing cross-margin flow, and that the more efficient “classic food web” only dominates in the eastern GAB during periods of nutrient-rich upwelling. Overall, the study supports this hypothesis, where ecosystem productivity is driven by contrasting food web dynamics between the eastern and central upper slope GAB that are underpinned by variations in dominant nutrient enrichment processes. In the east, enrichment processes are sporadic but intense, and driven primarily by physics (upwelling), with limited influence of biological processes. In the central GAB, there is a stronger influence of biological processes (e.g. nitrification) with only intermittent input of nutrients at the base of the euphotic zone from turbulent fluxes at the shelf edge. Enrichment mechanisms in the central GAB appear to be more constant but constrained.

Despite these differences in food web dynamics, long-term patterns in primary productivity from remote sensed data are relatively similar between the regions, particularly on the upper slope. While primary productivity in the east can be high, it is intermittent and highly variable, with highest rates implicitly linked to upwelling. In the central GAB, primary productivity is more moderate, but linked to a more constant, biologically-mediated supply of nitrogen that ensures that these moderate rates can be maintained over longer periods of time. While remote sensed data, which rely on surface measurements, likely underestimate total primary productivity in the eastern GAB by neglecting

significant sub-surface primary productivity, these results show that the central GAB is an important contributor to overall productivity in the wider GAB region.

Zooplankton and micronekton communities were investigated to compare the eastern and central GAB continental margin in terms of their species composition, size range, biomass and nutrient source/trophic pathways. Nutrient sources and trophic pathways using the compound-specific stable isotope analysis (CSIA) method showed that distinct differences between eastern and central upper slope habitats existed during the study. This was most evident for the crustaceans where source-nitrogen was indicative of an upwelled or higher-latitude water mass in the east, and biologically-fixed nitrogen in the central region. This observation reinforced the differences observed in the dominant production mechanisms. CSIA analysis also showed there were longer trophic pathways in the central GAB for a high number of dominant species. Interestingly, many micronekton fish had a similar or higher trophic level using the CSIA method to the few tuna sampled using the same trophic enrichment factor.

While there were multiple lines of evidence to support dominant differences in nutrient enrichment and trophic pathways between the eastern and central region, the assumed ecological response for zooplankton and micronekton of lower biomass, smaller species and different composition was difficult to assess. Zooplankton and micronekton biomass, size and species composition were similar between the eastern and central regions but differed between species groups and sampling device. The prevailing hypothesis prior to this study was that the central GAB upper slope was an area of constant downwelling, suggesting low nutrients, and hence low production and biomass that explained the sparse (low biomass) benthic fauna when compared to the upwelling eastern and western GAB regions. This study does not support this hypothesis where the yearly production derived from satellite ocean colour and micronekton biomass is similar between the regions and similar to other moderate production regions in Australia. These findings are also supported by the larger spatial and longer temporal Continuous Plankton Recorder (CPR) and bioacoustic sampling.

In conclusion, we hypothesise that the central and eastern regions have similar production, sustained by the biology in the central and eastern GAB and for the eastern upper slope and shelf enrichment driven by the physics (during the summer upwelling season). This is reflected in the base nitrogen and reworked nitrogen trophic transfer to zooplankton and micronekton. We conclude that the central offshore region is an important contributor to the production and biomass of pelagic organisms in the offshore GAB.

To test the generality of this conclusion longer term sampling is required in the following broad areas.

- Longer temporal studies of the biologically-derived nitrogen and nutrient sources.
- A time series of isotopic and trophic measurements through seasons and years is needed to make studies more informative.
- Low-cost monitoring of micronekton with targeted sampling using moorings and ships of opportunity with contribution to the Integrated Marine Observing System (IMOS) Bio-Acoustic Ship Of Opportunity (BASOOP) program.
- Low-cost monitoring of zooplankton with contribution to the IMOS CPR program.

## 2. INTRODUCTION

### 2.1 Overview

The pelagic habitat of the offshore Great Australian Bight (GAB) is nested in a hierarchy of biomes and provinces at global, regional and local scale. At the global scale, the GAB region has been classified within the predominantly southern sub-tropical convergence zone (Longhurst, 2010). Within the Australian pelagic bio-regionalisation, the GAB sits between the Indian Central core water mass and the Northern sub-tropical convergence (Lyne and Hayes, 2005). At a local scale what distinguishes the central GAB within these regional water masses is that the energetics of eddies in the region are low (Figure 2.1-1).

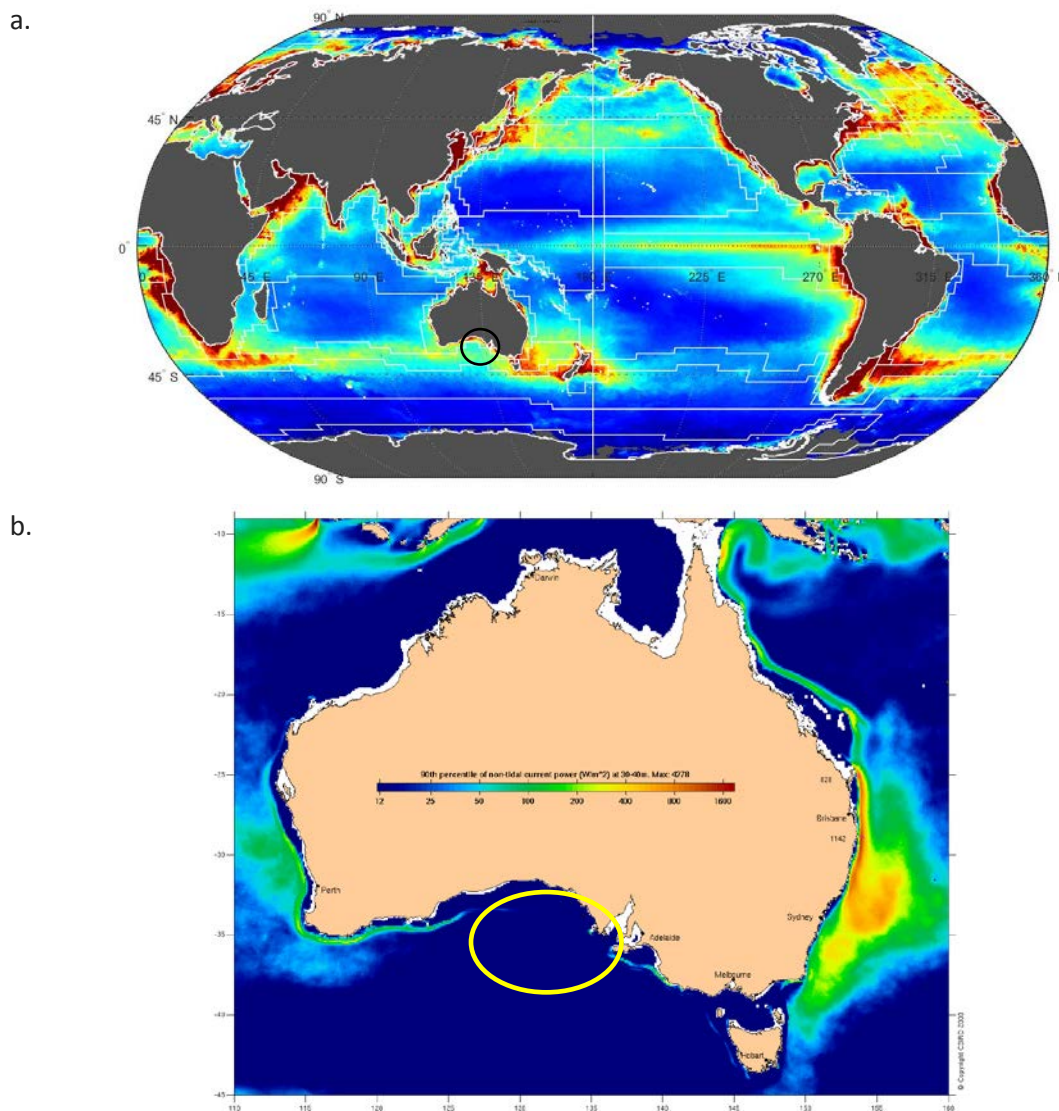


Figure 2.1-1 A. Global bioregionalisation of Longhurst (white lines) with satellite derived annual surface net primary production for 2015 highlighting the GAB (black circle) is classified within the southern sub-tropical convergence zone, and b) the low current power of the central GAB region (yellow circle) compared to the Australian eastern and western boundary currents (Griffin supplied image).

The recent comprehensive scientific review of the GAB (Rogers et al. 2013) hypothesised that contrasting ecological processes predominate in the eastern and central GAB. These are likely driven by spatial and temporal variations in meteorological and oceanographic processes, which govern the supply of nutrients and light that underpin the productivity of these ecosystems. The prevailing

hypothesis is that the central GAB upper slope is an area of constant downwelling, implying low nutrients and hence low production and biomass that explained the sparse (low biomass) benthic fauna when compared to the upwelling eastern and western GAB regions (Middleton et al., 2014). Testing this hypothesis and quantifying differences in pelagic ecology and food web structure will provide conceptual insights into how these systems function, and facilitate the development of tools and protocols for monitoring ecological indicators of the pelagic ecosystem. Monitoring is vital to assess potential impacts of anthropogenic and climate-driven environmental variation on the pelagic ecosystem of the GAB. This will assist in promoting the sustainable management of its marine resources. To underpin sustainable management, two key hypotheses regarding the ecosystem structure, function and dynamics were highlighted in the review to be tested:

- 1) That the “microbial food web” is the dominant planktonic food web over the deep GAB continental margin, particularly in the central GAB where year-round downwelling is thought to be the prevailing cross-margin flow, and that the more efficient “classic food web” only dominates in the eastern GAB during periods of nutrient-rich upwelling (Figure 2.1-2).
- 2) That the zooplankton and micronekton communities of the central GAB continental margin have lower biomass, smaller species, different composition and longer trophic pathways than those on the eastern GAB. This is due to the food source being dominated by the “microbial food web” in the central GAB and the “classical” food web in the eastern GAB during periods of nutrient-rich upwelling (Figure 2.1-2).

To address the above hypotheses Rogers et al. (2013) recommended new studies should focus on collecting data:

1. To provide information on the abundance, community structure, dynamics, biodiversity and endemism of microbes (i.e., viruses and bacteria), plankton (i.e., phytoplankton, zooplankton, ichthyoplankton) and micronekton (including squids, small pelagic and mesopelagic fish and gelatinous organisms).
2. To assess variation in primary and secondary productivity and food web structure in relation to physical drivers, including currents, turbulence, and stratification (upwelling/downwelling), nutrient concentrations, irradiance, and turbidity.
3. To provide information on the microbial, planktonic and micronekton communities that will inform assessments of distributions of key species.

Based on these data and improved knowledge, future developments and potential impacts can be placed in a regional and global context.

Specifically, this project was tasked with improving the following knowledge gaps identified in the literature review:

1. Macro-nutrient concentrations, sources and sinks;
2. Microbial, phytoplankton, zooplankton and ichthyoplankton abundance and community composition;
3. Macrozooplankton and micronekton diversity, distribution, abundance and trophic linkages to iconic and apex predators.

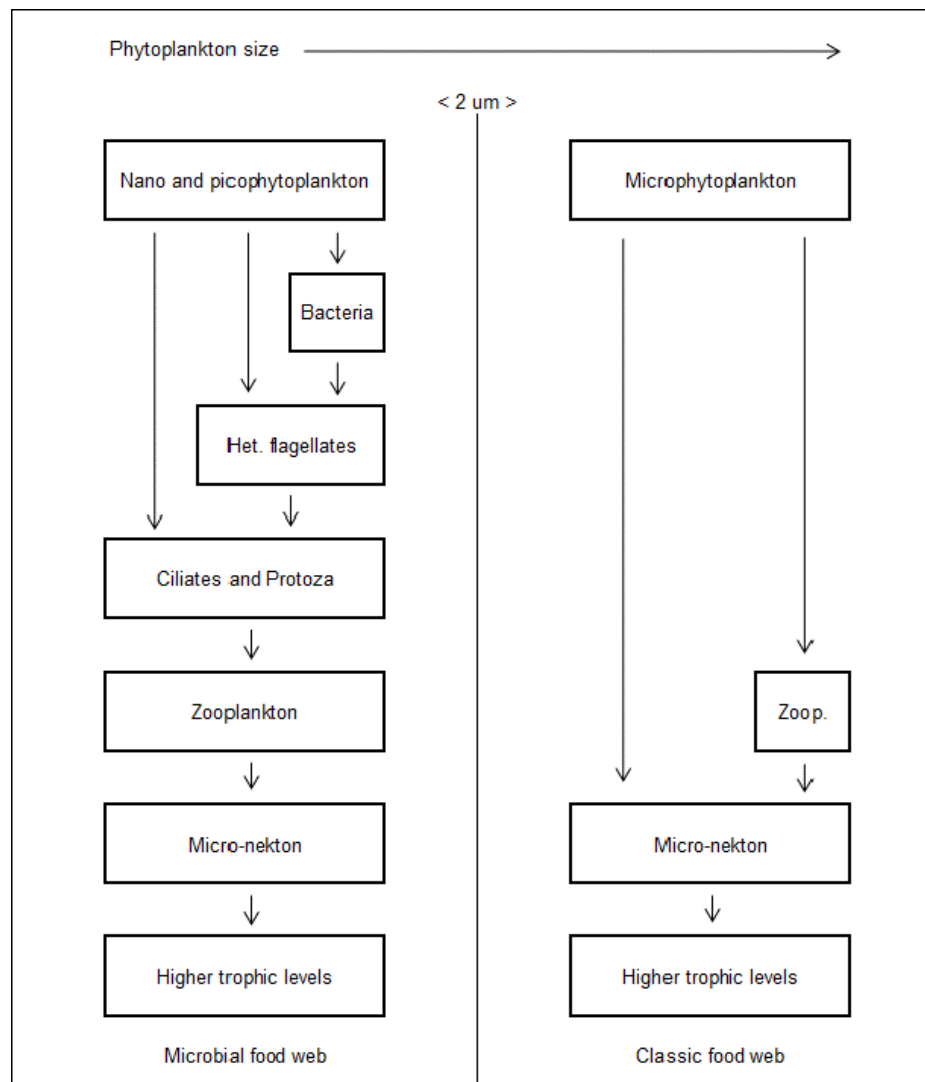


Figure 2.1-2 Example of simplified microbial and classical food webs. The microbial food web is a trophic pathway in the marine food web which is dominated by viruses, bacteria, and nano- and pico-phytoplankton (phytoplankton 2 - 20  $\mu\text{m}$  in diameter). It has two components, one which involves the bacterial recycling of dissolved organic carbon (DOC), and the other which involves carbon fixation at low nutrient concentrations and low irradiances. The microbial food web can be considered a “regenerating” food web and typically operates in the oligotrophic ocean and regions where nutrients are in short supply and  $\text{NH}_4$  is the dominant form of nitrogen. The highly productive classic food web is found in areas subject to some form of nutrient enrichment, such as upwelling. Hence in a more microbial dominated food web the zooplankton and micronekton are expected to have higher nitrogen isotope levels (Miller, 2006).

It was acknowledged that sampling biota from size ranges of bacteria to tuna needs to be placed in context of the very different spatial and temporal scales of their life histories and oceanographic influences (Figure 2.1-3). This study represents a snapshot in time and comparison of biota that have very different life histories and spatial ranging which needs to be considered in interpreting and comparing measurements.



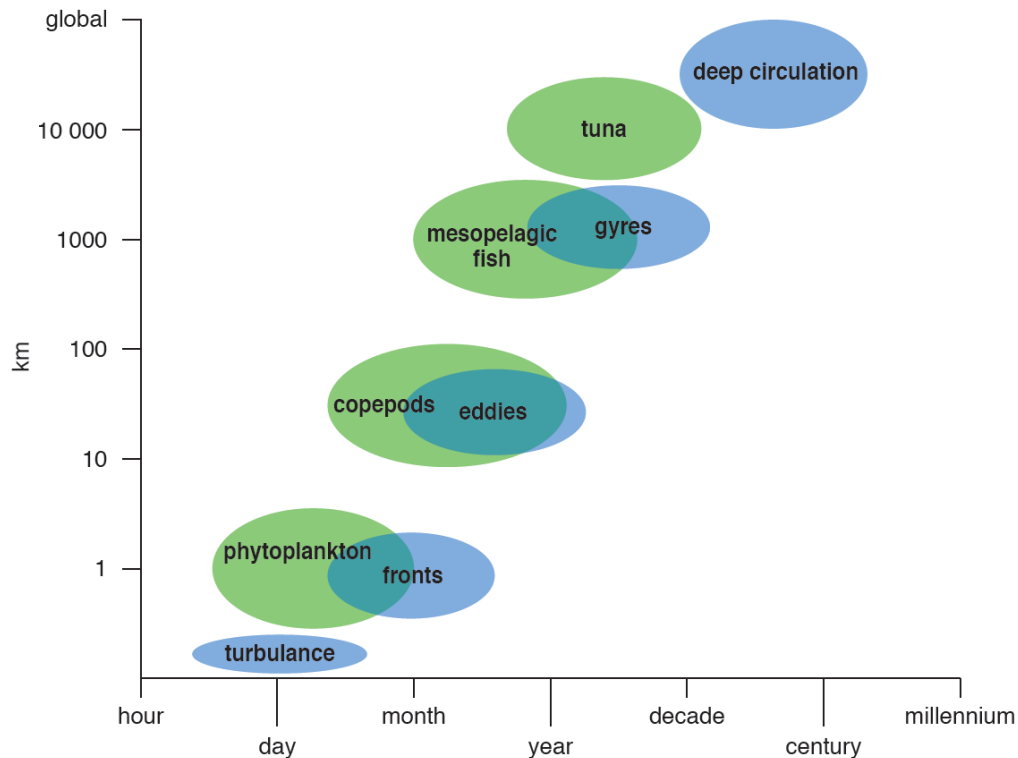


Figure 2.1-3 Logarithmic space- and time- scales showing stylised influence of oceanic circulation and biological size groups in pelagic ecosystems (Steele 1991, Herring 2007).

## 2.2 Objectives

Characterise seasonal and spatial variability of plankton and micronekton communities by:

1. Describing the community structure, dynamics, biodiversity and endemism of microbes (i.e., viruses and bacteria), plankton (i.e., phytoplankton, zooplankton, ichthyoplankton) and micronekton (including squids, small pelagic and mesopelagic fish and gelatinous organisms).
2. Testing the hypothesis that the “microbial food web” is the dominant planktonic food web over the deep GAB continental margin, particularly in the central GAB where year-round downwelling is thought to be the prevailing cross-margin flow, and that the more efficient “classic food web” only dominates in the eastern GAB during periods of nutrient-rich upwelling.
3. Compare the eastern and central GAB continental margin zooplankton and micronekton communities in terms of their species composition, size range, biomass, nutrient source/trophic pathways and habitat. Describe how differences could affect the distribution and abundance of key species.

Changes in the availability of the *RV Investigator* to a single summer voyage reduced the project’s capability to investigate seasonal differences.

## 2.3 Methods

The program objectives had a combination of a dedicated survey and opportunistic sampling as follows:

- Opportunistic trial sampling on the Marine National Facility (MNF) *RV Southern Surveyor* 20 day benthic charter voyage in March 2013 (funded through Benthic Biodiversity Theme).
- Voyage on the MNF *RV Investigator* 22 days (9 days of dedicated pelagic sampling) December 2015.
- Continuous Plankton Recorder (CPR) sampling on a commercial vessel two-monthly from January 2013 to Dec 2015.
- Collection of bio-acoustic data from research, fishing, seismic vessels (with appropriate acoustic equipment) operating within the region.

Details of the sampling for the CPR and bio-acoustic data are provided in the relevant Sections with the core *RV Investigator* December 2015 voyage summarised here. The overall design of the December 2015 survey was based on the combined needs of the GABRP Pelagic and Benthic Themes along six transects T1 to T6 (Figure 2.3-1). The Pelagic sampling design reflected the need for information over three gradients, T2 and T6, along which ecosystem characteristics are expected to vary: east-west (longitude), seabed-water depth and day-night (light). Longitudinal ecosystem differences (between the eastern and central GAB) were expected based on patterns in oceanographic processes, especially upwelling that influences the supply of nutrients and hence production processes. Depth-related ecosystem differences are poorly documented in the GAB, but it was predicted from observations in other deep water ecosystems that there would be marked changes in both benthic and pelagic biological community composition and productivity between the shelf (100 m depth), shelf edge-upper slope (200 – 750 m) and the deep slope/abyss (3000 – 5000 m). Pelagic sampling also needed to capture day night cycles at a given site in production in the epipelagic habitat and diurnal vertical migrations of the zooplankton and micronekton predominantly between the epipelagic and mesopelagic habitat to depths of 1000 m (Figure 2.3-2). Of note is the greater habitat area (factor of 3) of the central regions upper slope compared to the eastern upper slope due to the slope being  $\sim 1.2^\circ$  and  $3.8^\circ$  for the central and eastern regions respectively. The benthic collections were designed to repeat samples obtained in 2013 on the *RV Southern Surveyor* along the five continental slope transects (T1 to T5). Thus, an underlying systematic depth versus longitude stratified design was suited to the four prevalent survey parameters: our hypothesis of ecosystem change over east-west and depth gradients, a general absence of data in the deep GAB region relevant to the project objectives, a large survey area, and limited time available on station.

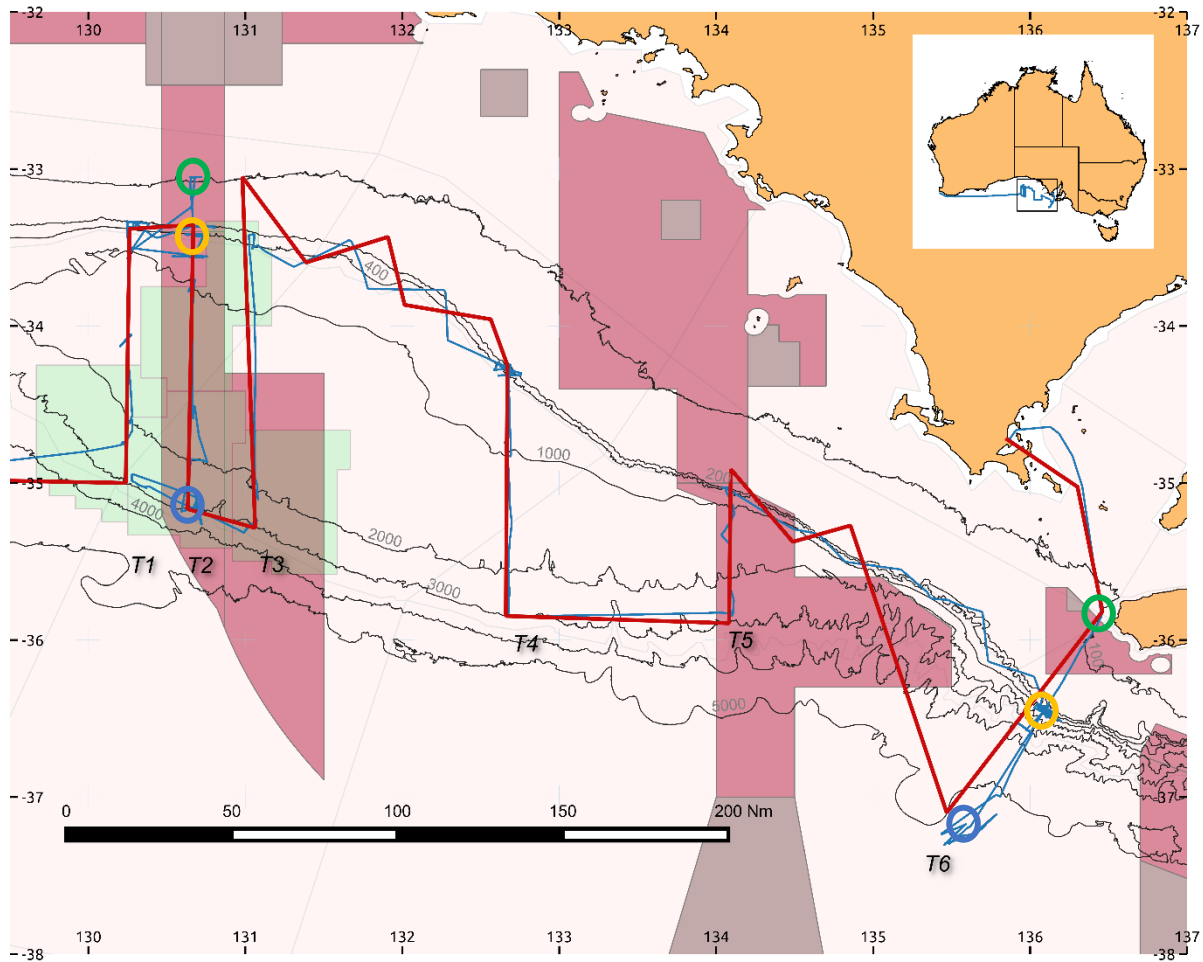


Figure 2.3-1 RV Investigator Dec. 2015 proposed voyage track (red) highlighting the Transects T1 to T6 and the actual track (blue) with the Commonwealth Marine Reserves (Dark Pink) and the BP lease areas (green). The central GAB is located on transect T2 within the Marine reserve and the Eastern transect is T6. The Pelagic regions for biological comparison between the central and eastern region were the outer shelf 100 m (green circles), shelf break/upper slope ~200 – 750 m (orange circles) and the offshore 3000 – 5000 m seabed depth (blue circles) (Kloser et al. 2016).

The 18 days of sampling time were allocated roughly equally to pelagic and benthic sampling, and a mix of pelagic and benthic sampling was undertaken at most individual stations. Sampling involved the use of many gear types, and these were interwoven to maximise the efficiency of the survey, and to meet the time-of-day dependence of much of the pelagic sampling. The voyage started at Transect T6 involving predominately pelagic sampling for the first 4 days. The vessel then moved westward completing the predominately benthic stations of T5 and T4. The rest of the time was then allocated to sampling the Transects, (mainly benthic) T3, (benthic and pelagic) T2 and (mainly benthic) T1 (Figure 2.3-1).

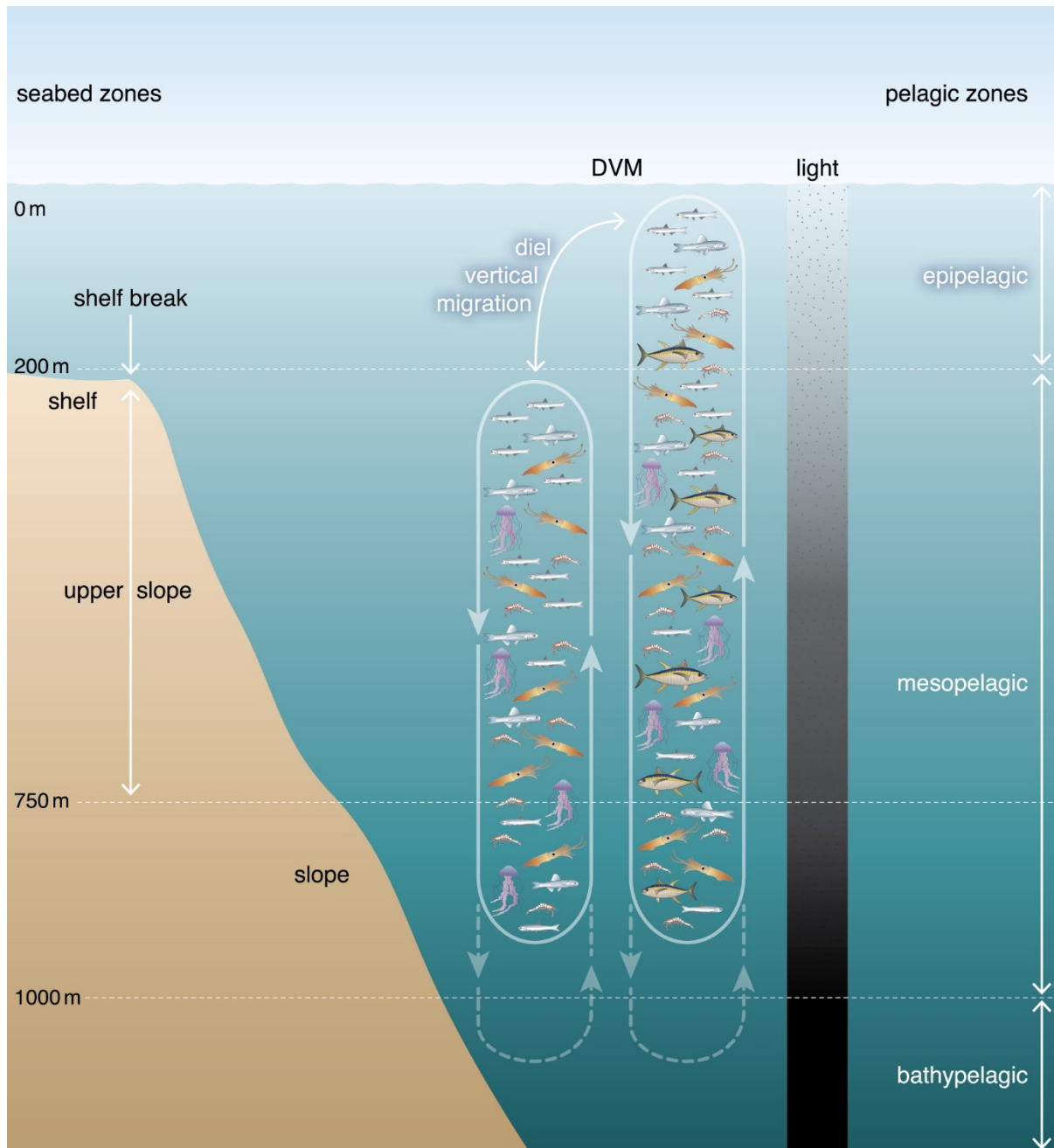


Figure 2.3-2 Cartoon of some descriptive features used in this report highlighting the nominal depths for the shelf, shelf break and upper slope seabed and the epipelagic, mesopelagic and bathypelagic habitat zones. A stylised dynamic of diurnal vertical migration of micronekton that move or remain within the epipelagic, mesopelagic and bathypelagic habitat due to light changes between day and night. A stylised diagram of light levels in the pelagic habitat zone during the day, a dominant driver of vertical movement of larger zooplankton and nekton.

#### *RV Investigator sampling methods*

Details of the sampling and data collection methods from the December 2015 *RV Investigator* voyage can be found in Kloser et al. (2016) summarised briefly below. On this voyage the following samples were collected to address the objectives:

1. Collect and process a full set of water samples to characterise and quantify primary production, microbial communities (virus/bacteria/ picophytoplankton) and determine a variety of water column environmental and chemical parameters.

2. Collect and process phytoplankton, zooplankton and micronekton samples from multiple methods during the day and night using: vertical hauls; surface tows; Easy Zooplankton depth integrated net (EZnet) with attached Laser Optical Particle Counter (LOPC); International Young Gadoid Pelagic Trawl (IYGPT) with attached Midwater Opening and Closing cod-end device (MIDOC); and opportunistically collected nekton (e.g. squids and tuna) for food web studies.
3. Conduct experiments investigating microbial and planktonic physiology and productivity
4. Collect and process profiling lagrangian acoustic, optical (PLAOS) measurements day and night.
5. Collect and process underway pelagic acoustic measurements and target unique layers with TRIAXUS, net and PLAOS samplers.
6. Collect underway acoustic and water chemistry to investigate effects of eddies.

Microbial and planktonic abundance and community composition, primary and secondary productivity, and physical and chemical drivers of these parameters were sampled. CTD and water samples were collected at three depths at stations  $\leq 200$  m depth, with extra water samples for nutrient analysis within and below the euphotic zone. Dissolved nutrients were measured onboard using a Seal AA3HR segmented flow instrument. Samples for chlorophyll a (Chl *a*) and pigments were obtained by filtering 2 L sequentially through 5  $\mu$ m and GF/F filters (nominal pore size  $\sim 0.7$   $\mu$ m) to provide a less than 5  $\mu$ m fraction ( $< 5$   $\mu$ m) and greater than 5  $\mu$ m fraction ( $> 5$   $\mu$ m). Samples for particulate organic matter (POM) were filtered through precombusted GF/F filters. Filters were stored at  $-80$  °C prior to analysis. Picoplankton and virus samples were preserved in glutaraldehyde and stored at  $-80$  °C for further analysis. Samples for molecular studies on bacteria were filtered onto 0.2  $\mu$ m filters and filters stored at  $-80$  °C until analysis. Phytoplankton, zooplankton and ichthyoplankton samples were fixed (with lugol's iodine solution and formalin, respectively) for onshore analysis of abundance and community composition. Primary productivity were examined *in situ* at each station using a Fast Repetition Rate Fluorometer (FRRF). Experimental studies of primary and secondary productivity, and bacterial production were conducted at the upper slope and offshore stations. Assessment of primary productivity were made via  $^{14}\text{C}$  short term incubators (e.g. Parsons et al. 1984; Lohrenz et al. 1993; Mackey et al. 1995). Secondary productivity, micro (and nano-plankton) grazing on phytoplankton were examined via dilution experiments in deck incubators (Landry and Hassett 1982). Pigment concentrations were determined via High Pressure Liquid Chromatography (HPLC) at SARDI Aquatic Sciences. Picoplankton and virus abundance were assessed using flow cytometry. Microbial diversity (16S) and function were assessed. Phytoplankton, zooplankton and ichthyoplankton were enumerated and identified to lowest taxonomic resolution using standard taxonomic methods.

Phytoplankton, zooplankton and micronekton abundance, community composition and trophic linkages were characterised using protocols for plankton above and the following for zooplankton and micronekton. At each station vertical drop nets with three mesh sizes were used to collect mesozooplankton and ichthyoplankton samples. Towed sampling was undertaken for mesozooplankton and ichthyoplankton using a surface net and depth-stratified multiple plankton net system (EZ net). Macro-zooplankton and micronekton were depth-stratified sampled with a multiple cod end system (MIDOC) attached to an International Young Gadoid Pelagic Trawl (IYGPT). Fine scale calibrated multi-frequency acoustic and stereo optical and video sampling (PLAOS) were collected with vertical profiles for target strength and density estimates of dominant zooplankton and micronekton taxa. Biological samples were photographed, identified and weighed to the lowest practical taxonomic unit. Specimens were frozen, or formalin preserved for onshore analysis. Whole

specimen or muscle samples were retained from a range of dominant zooplankton and micronekton species for isotope (carbon, nitrogen) analysis. Underway vessel acoustics were collected at and between stations using calibrated multi-frequency and multi-beam acoustics. Limited time was available to sample, therefore significant uncharacterised water column scattering layers were targeted with the EZ net, PLAOS and MIDOC net to identify unknown zooplankton and micronekton patches. Samples were treated as per the station collections. Larger fauna (zooplankton and pelagic micronekton) were verified to lowest possible taxonomic units or functional group. Taxa were prioritised based on relative and absolute abundance and knowledge of their importance to apex predators. Biological metrics for pelagic fauna were derived to estimate the biomass, trophic linkages, diversity and energetics between regions, sites, depths and day/night differences. For example both bulk and compound specific isotope methods were used on the particulate organic matter (POM), plankton, zooplankton and micronekton samples to elucidate dominate trophic pathways (Post, 2002; Revill et al., 2009). Specific bio-acoustic properties of dominant taxa were derived to enable acoustic modeling (Lavery et al., 2007). Multi-frequency acoustics and optical data were analysed to determine the behaviour and biomass of dominant acoustic groups and the between ground, site and day night differences with reference to broader scale underway acoustic mapping and historic records for the region (e.g. Figure 2.3-3, Kloser et al. 2009).

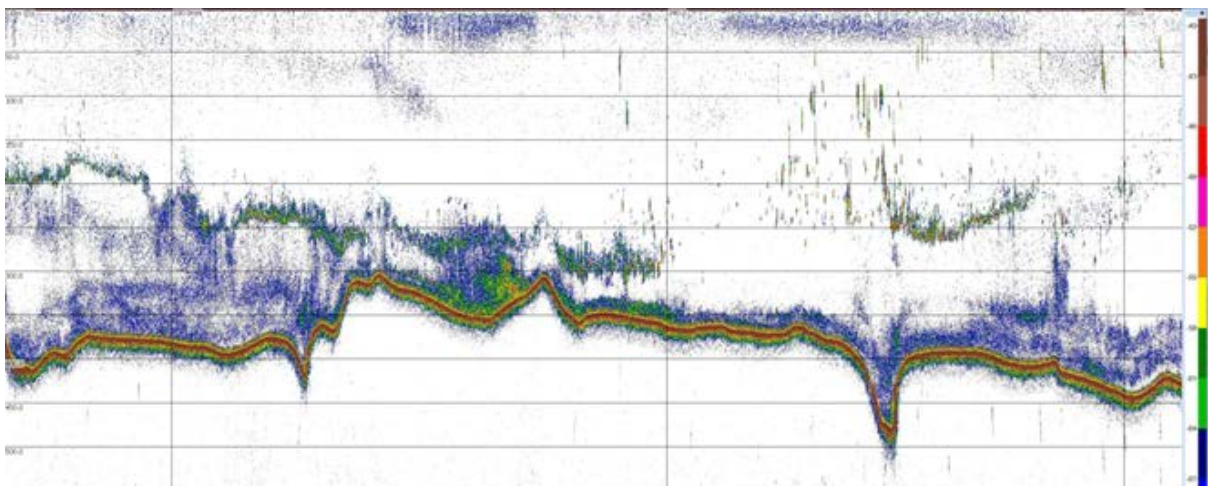


Figure 2.3-3 Example echogram of unverified micronekton schools at 38 kHz (Sv min -76 dB) in the central GAB (131E at 400 m depth) collected on 4 August 2012, 20 nm in length. These data will be reviewed and additional collections gathered for spatial and temporal knowledge.



### 3. PELAGIC HABITAT

Mark Doubell, John Middleton and David Spencer (Griffiths University)

#### 3.1 Broad scale pelagic habitat

##### 3.1.1 Introduction

As a consequence of the summertime circulation pattern in the Great Australian Bight (GAB) it is hypothesised that differences in the physical processes which drive upwelling in the eastern GAB and downwelling in the central GAB may lead to contrasting pelagic ecosystems. So far, the majority of oceanographic studies in the GAB region have focussed on upwelling in the eastern GAB (Lewis, 1981; Kämpf et al., 2004; McClatchie et al., 2006; Kämpf, 2010). However, our understanding of physical processes in the central GAB, and their potential consequences for ecosystem structure and productivity are limited and largely derived from ocean models (Middleton and Cirano, 2002; Middleton and Platov, 2003; Cirano and Middleton, 2004) and remote sensed information (Herzfeld and Tomczak, 1999; Ridgway and Condie, 2004). In this context, comparison of the pelagic oceanographic data collected along transects crossing the continental slope in the central and eastern GAB during early summer provides a novel dataset to test the above hypothesis.

During summer, the GAB region is dominated by large atmospheric high pressure systems which direct winds to the west and lower coastal sea levels (Cirano and Middleton, 2004; Middleton et al., 2017). These conditions, combined with high levels of heating and evaporation, result in a summertime circulation distinct from that experienced in winter. Middleton and Bye, (2007) provide a detailed review of the seasonal circulation patterns characteristic of the GAB. A schematic of the main summertime circulation features and water masses is shown in Figure 3.1-1.

In summary, the formation of an anticyclonic gyre on the shelf drives a weak westward flow near the coast with current velocities of the order  $0.05 \text{ m s}^{-1}$ . Further out on the shelf, the South Australian Current (SAC) flows eastward with current velocities of the order of  $0.20 \text{ m s}^{-1}$  or less (Ridgway and Condie, 2004; Middleton et al., 2017). Along the continental slope, the Flinders Current (FC) flows towards the west (Middleton and Cirano, 2002; Middleton and Platov, 2003) bringing water masses from western Tasmania to the GAB (Richardson, 2015). Numerical simulations indicate the core of the FC to be centred at depths between 300 – 600 m and flow speeds are expected to increase from  $0.05 \text{ m s}^{-1}$  or less in the eastern GAB to approximately  $0.20 \text{ m s}^{-1}$  in the western GAB (Cresswell and Peterson, 1993).

Cross-shelf transport processes are also dominated by the summertime wind-forcing which drive coastal upwelling off the Bonney coast, Kangaroo Island and eastern GAB. In the eastern GAB, upwelling transports cold, nutrient rich water from depths below 200 m onto the shelf (Kämpf et al., 2004; Middleton and Bye, 2007; Kämpf, 2010). The upwelled water resides near the bottom on the shelf to the west of Kangaroo Island and is transported towards the Eyre Peninsula (McClatchie et al., 2006). In the central GAB, convergence of the southward topographic and northward deep ocean Sverdrup transports are predicted to drive downwelling to depths of approximately 250 m at the shelf slope (Middleton et al., 2014; Middleton et al., 2017). Mesoscale eddies and internal waves are further expected to modulate upwelling and downwelling processes in the epipelagic zone over the GAB (Wood and Terray, 2005; Rogers et al., 2013).

The following Section is organised in order to provide the physical context to the 2015 *RV Investigator* voyage. First, a summary of the broad scale metrological and surface oceanographic conditions in the lead up to, and during, the voyage is provided. Observations of the thermohaline collected along transects in the eastern and central GAB are then presented. Water masses are identified and model particle tracking scenarios presented to demonstrate connectivity between the central and eastern GAB, as well as with regions outside of the GAB. Finally, vertical sections of temperature, salinity and macro-nutrients are presented to identify the presence of upwelling and downwelling.

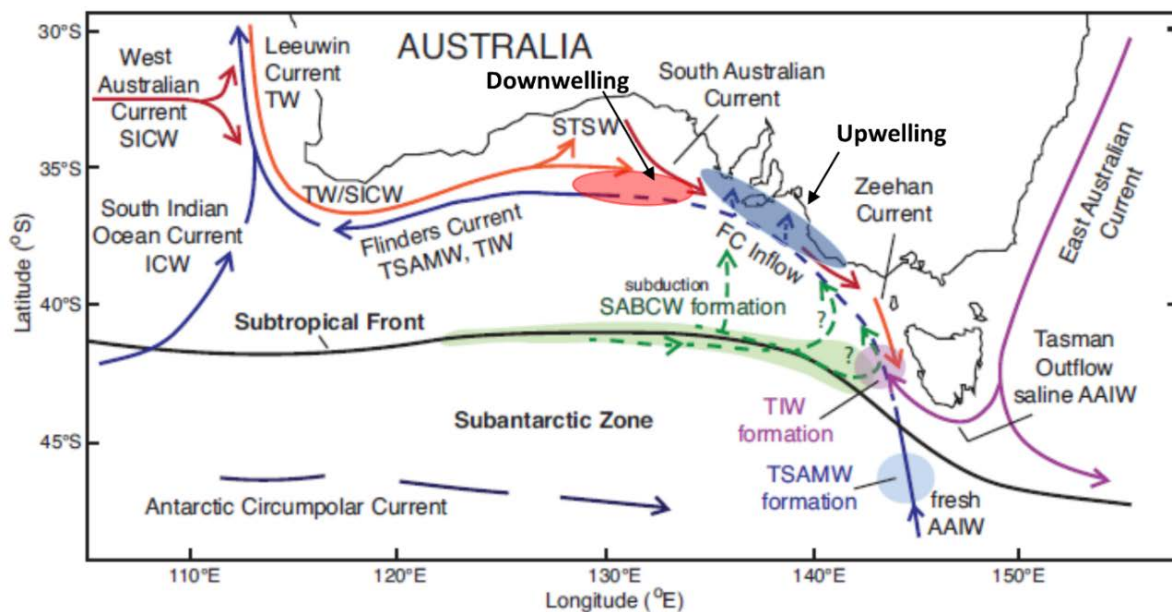


Figure 3.1-1 Schematic of the key summertime circulation features and water masses along the southern Australian shelf modified from Richardson, (2015). Upwelling occurs off the Bonney Coast, Kangaroo Island and the eastern GAB (blue shaded region). Shelf-edge downwelling is expected in the central GAB (red shaded region). Key water masses with connectivity to the Great Australian Bight include: Tasmanian Intermediate Water (TIW), Tasmanian Subantarctic Mode Water (TSAMW), South Australian Basin Central Water (SABCW) and Subtropical Surface Water (STSW).

### 3.1.2 Methods

Images of satellite derived ocean properties were obtained from the IMOS Ocean Current website (<http://oceancurrent.imos.org.au/index.php>). Derived properties included sea surface temperature (SST, °C), sea level height (SLH, m) and geostrophic current velocity ( $\text{ms}^{-1}$ ).

Meteorological information was obtained from the Australian Bureau of Meteorology (BOM; [www.bom.gov.au](http://www.bom.gov.au)). Mean Sea-Level Pressure (MSLP) charts provided a synopsis of the surface wind patterns experienced during the voyage. Hourly wind data were obtained from the BOM Neptune Island automatic weather station. Wind data were standardised to 10 m height and the alongshore component of the wind stress which drives coastal upwelling was determined by rotation of the principal axis relative to the orientation of the coastline consistent with previous analyses for the region (Kämpf et al., 2004). Hourly estimates of the alongshore wind stress (AWS) were vector averaged to provide daily values.

Hydrographic surveys were conducted along transects in the eastern and central GAB during the 2015 *RV Investigator* summer voyage (Figure 3.1-2). Sampling occurred along the eastern GAB transect between November 30<sup>th</sup> and December 4<sup>th</sup> and along the central GAB transect between December 10<sup>th</sup> to December 15<sup>th</sup>. At each station, CTD (conductivity-temperature-depth) profiles were made using a Seabird9+ system fitted with a Chelsea fluorometer for the measurement of chlorophyll *a* fluorescence and a SBE43 dissolved oxygen sensor. CTD profiles were made from the



surface to (near) bottom in waters less than 800 m depth, or a maximum depth of 800 m in waters greater than 800 m depth. At each station, discrete seawater samples were collected at approximately 10, 30, 65, 90, 120, 200, 300, 400 and 800 m depths using Niskin bottles attached to the CTD rosette. Determination of macro-nutrient concentrations including oxides of nitrogen ( $\text{NO}_x$ ; nitrite/nitrate), phosphate ( $\text{PO}_4$ ) and silicate (Si) were made on-board in the *RV Investigator* hydrochemistry laboratory.

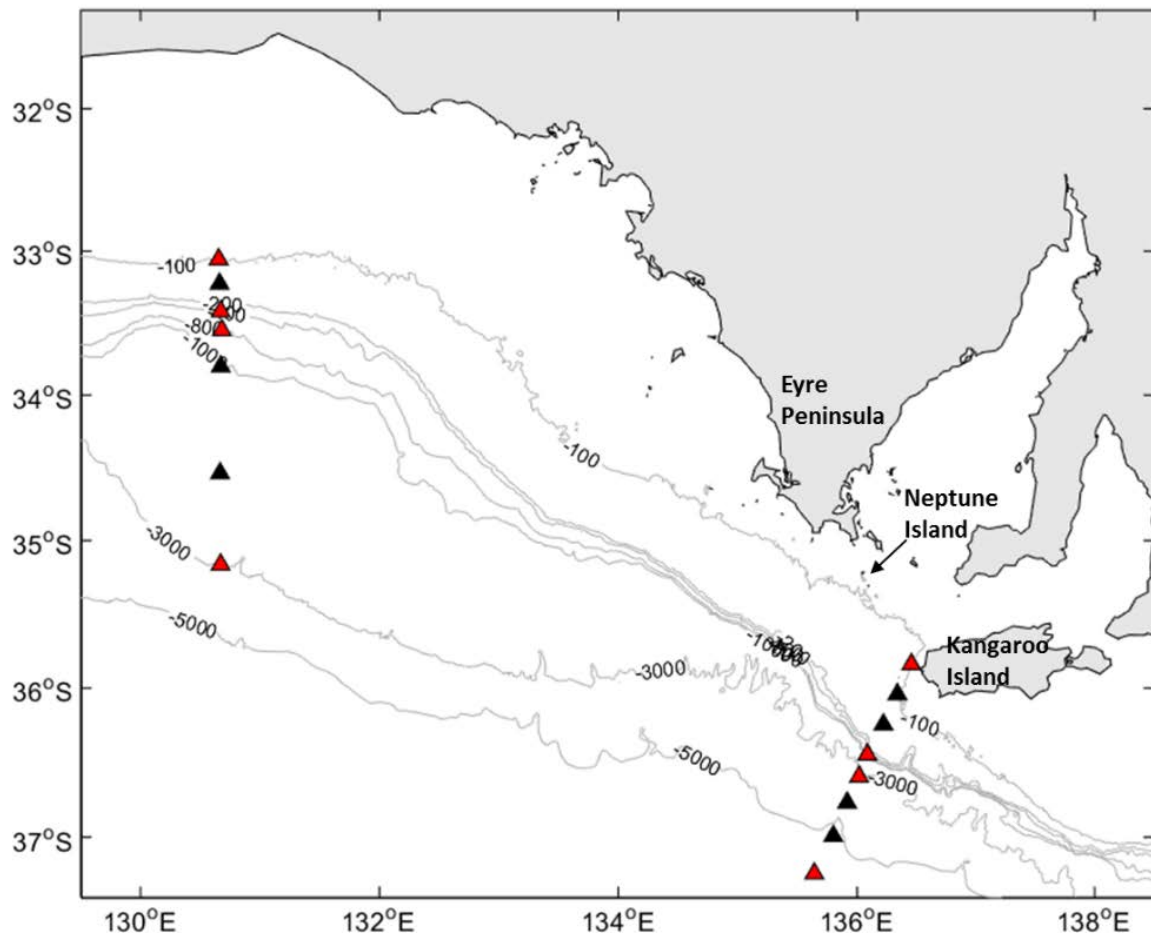


Figure 3.1-2 Location of CTD and microstructure profiling (see 3.2) stations surveyed on the *RV Investigator* voyage in December 2015. The bathymetry of the region is described by the 100, 200, 400, 800, 1000, 3000 and 5000 m isobaths. CTD profiles were made at all stations (triangles) along cross-shelf transects in the central and eastern Great Australian Bight. Microstructure profiles were taken at stations identified by the red filled markers and corresponded with the 'shelf', 'upper slope', 'mid slope' and offshore 'oceanic' stations situated centered on the 100, 400, 800 and greater than 1000 m isobaths, respectively.

### 3.1.3 Results and Discussion

#### Physical context: pre-voyage

Analysis of the alongshore wind stress at Neptune Island shows a general transition from winter downwelling during July and August 2015 to predominantly upwelling favourable conditions throughout the period October to February 2016 (Figure 3.1-3). Variability in the strength and direction of the alongshore wind stress is associated with the passing of atmospheric low and high pressure systems. From early October to mid-November upwelling favourable winds were persistent (Figure 3.1-3). Evidence of active coastal upwelling during this period is indicated by cool SST ( $15^\circ\text{C}$  or less) off the Bonney coast (Figure 3.1-4). Bonney Coast upwelling is generally associated with the simultaneous upwelling off Kangaroo Island and the eastern Eyre Peninsula (Kämpf et al., 2004), but often without a strong surface signature due to the more irregular coastal bathymetry (Middleton

and Bye, 2007). Relaxation of upwelling favourable winds occurred in the fortnight prior to the voyage and between transects (Figure 3.1-3). We note the October-November upwelling will precondition the thermohaline fields to have an upward tilt until downwelling and/or friction and diffusion act to oppose it.

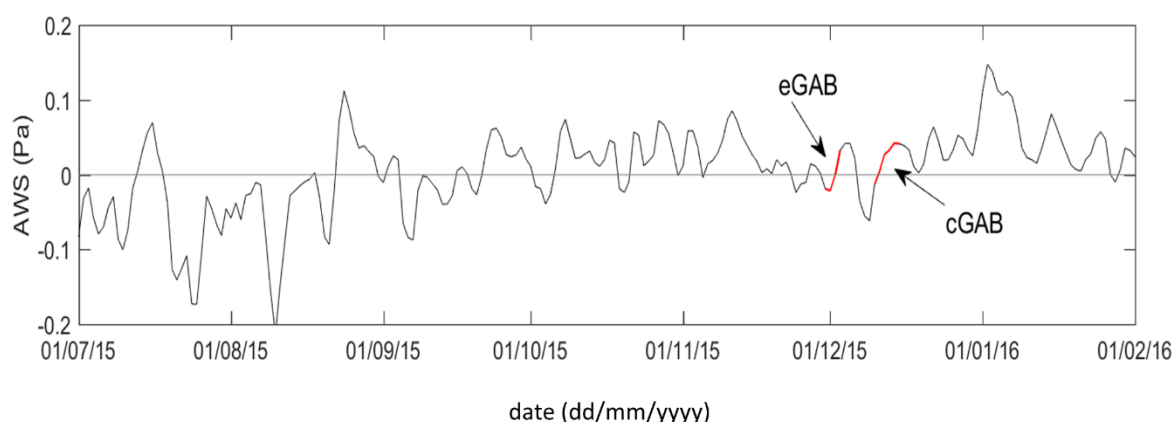


Figure 3.1-3 Daily alongshore wind stress (AWS), low-pass filtered with a 3-day running mean, estimated from the automatic weather station located on Neptune Island situated to the west of Kangaroo Island in the eastern GAB. Positive (negative) values indicate upwelling (downwelling) favourable winds. Red curves correspond to the timing of the RV Investigator hydrographic surveys along transects in the eastern (eGAB) and central (cGAB) GAB.

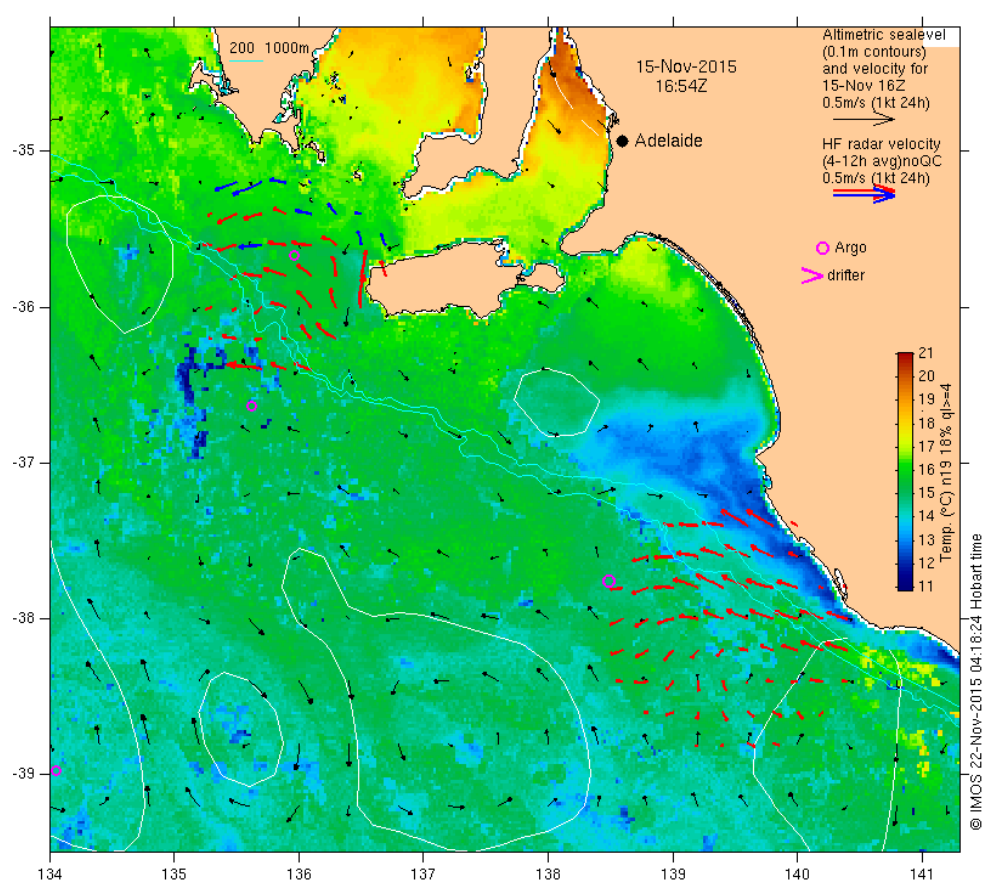


Figure 3.1-4 Sea surface temperature (SST, °C) across south-eastern South Australia showing upwelling along the Bonney Coast on 15-November, 2015 following a month of generally upwelling favourable winds (Figure 3.1-3). Wind direction and speed (red and blue arrows) measured by HF radar off the Bonney Coast and Kangaroo Island show upwelling favourable winds. Sea level height is indicated by the white contours and geostrophic surface velocities (black arrows) are shown with a legend arrow of  $0.5 \text{ m s}^{-1}$ . The cyan line denotes the 200 m isobath and shelf edge (source [oceancurrent.imos.org.au](http://oceancurrent.imos.org.au)).

## Physical context from satellite data: during Voyage

Consistent with the summertime meteorology of southern Australia, high pressure systems were a predominant feature in the GAB during the voyage (Figure 3.1-5). High pressure systems are responsible for driving (geostrophic) winds in an anti-clockwise direction that can lead to coastal upwelling when the winds are directed alongshore from the south-east. During the eastern GAB transect, winds are anticyclonic (Figure 3.1-5) but were not directed alongshore in the central or eastern GAB. Note, the wind data from Neptune Island (Figure 3.1-3) indicated there was an alongshore component to the wind during this period as shown by the weak positive upwelling wind stress of up to 0.05 Pa present for 2 to 3 days in early December. The corresponding SST image (December 2<sup>nd</sup>) is shown in Figure 3.1-6A. It showed slightly cooler temperatures in the eastern GAB (15–17 °C) relative to the central GAB (17 – 20 °C) and evidence of coastal upwelling off Kangaroo Island, the Eyre Peninsula and Streaky Bay in the west. This is possibly due to the short 2 – 3 day burst of upwelling or remnants of the upwelling that occurred earlier in November (Figure 3.1-4).

The SST image in Figure 3.1-6A also shows weak to non-existent currents over the shelf that are consistent with the atmospheric forcing for December 2<sup>nd</sup> (Figure 3.1-5A). At this time, the high is positioned such that the gradients of atmospheric pressure (and winds) are smallest over the eastern GAB. Farther offshore, the SSH (white contours) and associated black vectors indicate the presence of weak high (anti-cyclonic) and low (cyclonic) pressure mesoscale eddies in the deep ocean of the central GAB with surface speeds of 0.10 to 0.20 m s<sup>-1</sup> (or about 10 – 20 km d<sup>-1</sup>). As they grow and deepen, low pressure eddies also act as sites of internal upwelling (Suthers et al., 2011). In addition, it should be noted that eddies for the GAB are typically much weaker than those found in the major boundary current systems of the world where average and maximum speeds can exceed 0.5 and 1 m s<sup>-1</sup> (Andrews, 1977; Mata et al., 2006).

For the central GAB, the atmospheric high shown in Figure 3.1-5A has migrated east to the Tasman Sea and has been replaced by a much weaker high (Figure 3.1-5B) that drives weak surface currents (0.10 m s<sup>-1</sup>) near the shelf edge (Figure 3.1-6B) and weak to non-existent surface currents on the shelf and further offshore in oceanic waters. Evidence of weak coastal upwelling off Kangaroo Island, the Eyre Peninsula and Streaky Bay in the west is again weak and possibly due to the short 2 to 3 day burst of upwelling and/or remnants of the previous upwelling events (Figure 3.1-4). A mesoscale high pressure ocean eddy lies to the south of the central GAB transect and a very weak low pressure eddy to the west of the transect.

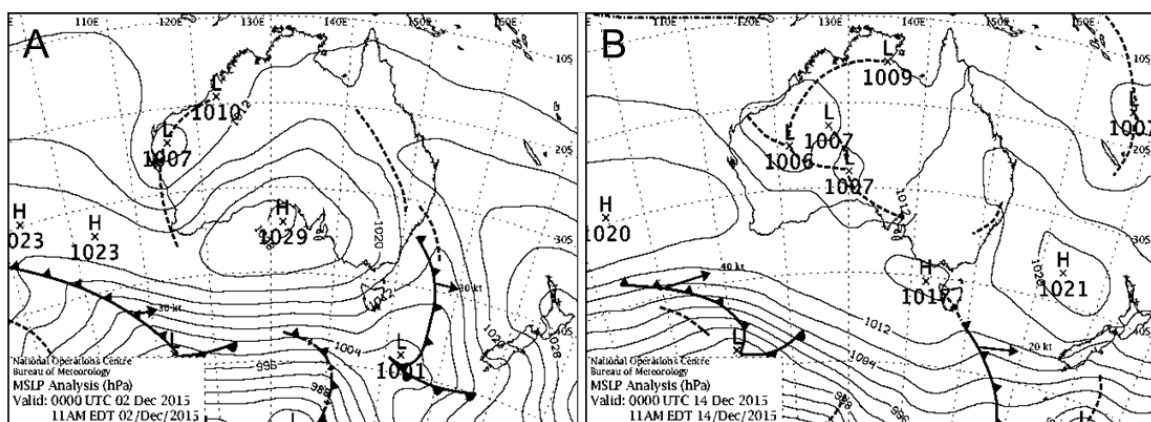


Figure 3.1-5 Snapshots of the mean sea level pressure (MSLP; hPa) for Australia on (A) 2<sup>nd</sup> December 2015 during sampling of the eastern GAB transect and (B) 14<sup>th</sup> December 2015 during sampling of the central GAB transect. High pressure systems dominate the GAB region and are characteristic of the summertime meteorology of South Australia (source: [www.bom.gov.au](http://www.bom.gov.au)).



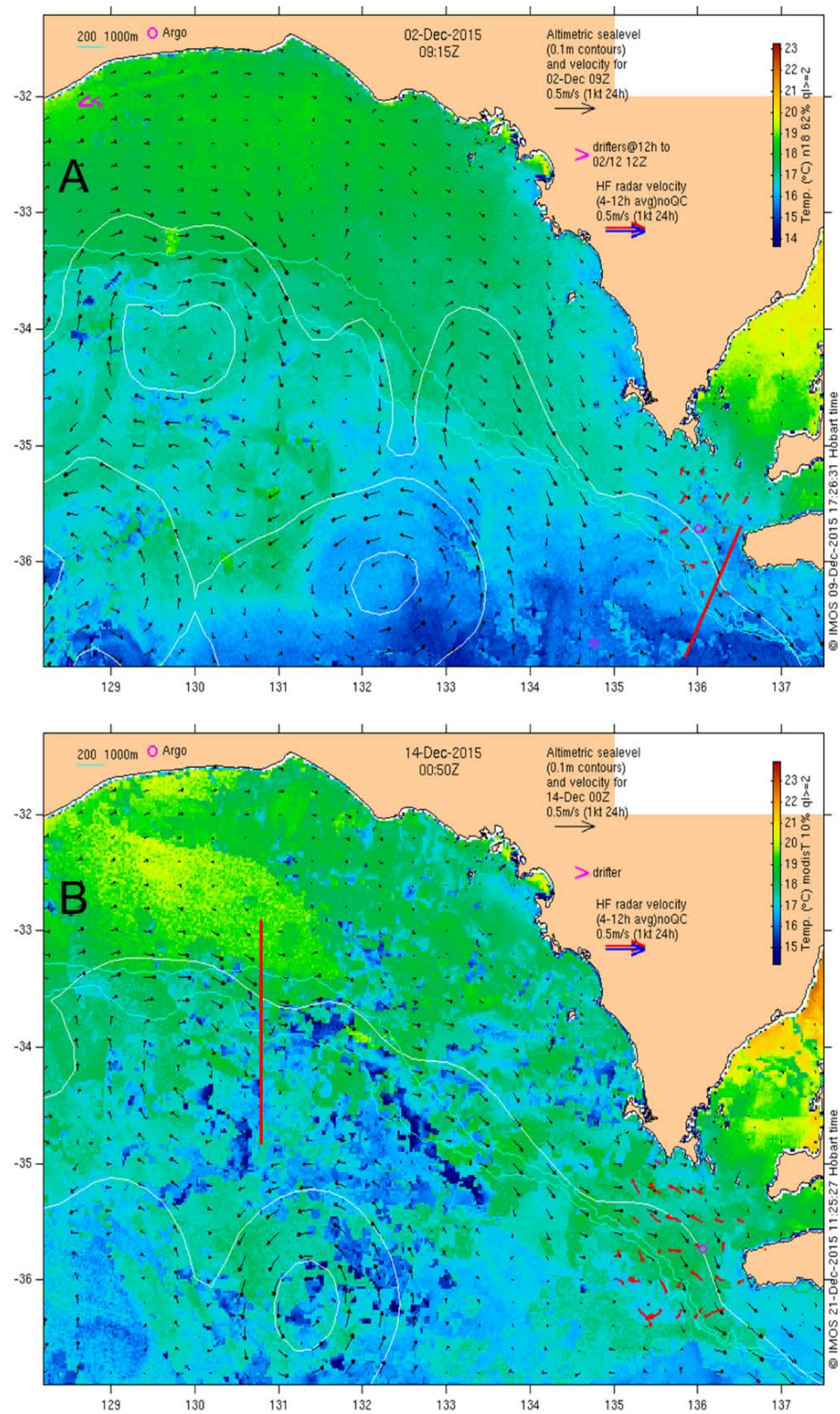


Figure 3.1-6 Remote sensed images of sea surface temperature (SST) taken on (A) 2<sup>nd</sup> December during sampling of the eastern GAB transect and (B): 14<sup>th</sup> December during sampling of the central GAB transect. Surface currents (red arrows) measured by HF radar off Kangaroo Island are indicated. Sea level height is indicated by the white contours and geostrophic surface velocities (black arrows) are shown with a legend arrow of 0.5 m s<sup>-1</sup>. The cyan line denotes the 200m (shelf edge) and 100 m isobaths. The red solid line shows the location of transects sampled in central (B) and eastern (A) Great Australian Bight (source [oceancurrent.imos.org.au](http://oceancurrent.imos.org.au)).

## Physical context from in situ data: during Voyage

To examine the distribution of water masses in the GAB, a scatter plot of temperature versus salinity is presented using the CTD data collected from the central and eastern transects (Figure 3.1-7). As defined by Richardson, (2015) well defined water masses below 200 m depth include; Tasmanian Intermediate Water (TIW), Tasmanian Subantarctic Mode Water (TSAMW) and South Australian Basin Central Water (SABCW). All three of these water mass are formed off the west coast of Tasmania (Figure 3.1-1) and are transported to the GAB by the Flinders Current (depths 400 to 1200 m; Richardson, 2015). SABCW is also likely formed at the subtropical front and subducted towards the shelves (Figure 3.1-1). These deep water masses are readily identified in the collected data (Figure 3.1-7) and closely follow those presented by Richardson, (2015) using all available data from Tasmania to Albany and are independent of season and surface eddies.

Above 200 m depth, several other water masses may be defined. Slope Water (SW) is found on the upper shelf during summer and is associated with the upwelling of SABCW onto the shelf and mixing with Subtropical Surface Water (STSW); a dominant water mass that is associated with GAB shelf water (Richardson, 2015). The large scatter in temperature and salinity observed at depths shallower than 200 m is associated with regional variations in heating and evaporation resulting in the formation and mixing of local water masses on the shelf (Richardson, 2015). Subtropical Surface Water (STSW) is modified by localised heating and evaporation to form Evaporated Water (EW). Vertical mixing with deeper, cooler SW generates the formation of Cooled Evaporated Water (CEW). Similarly, Mixed Slope Water (MSW) is generated when SW mixes with STSW during upwelling events.

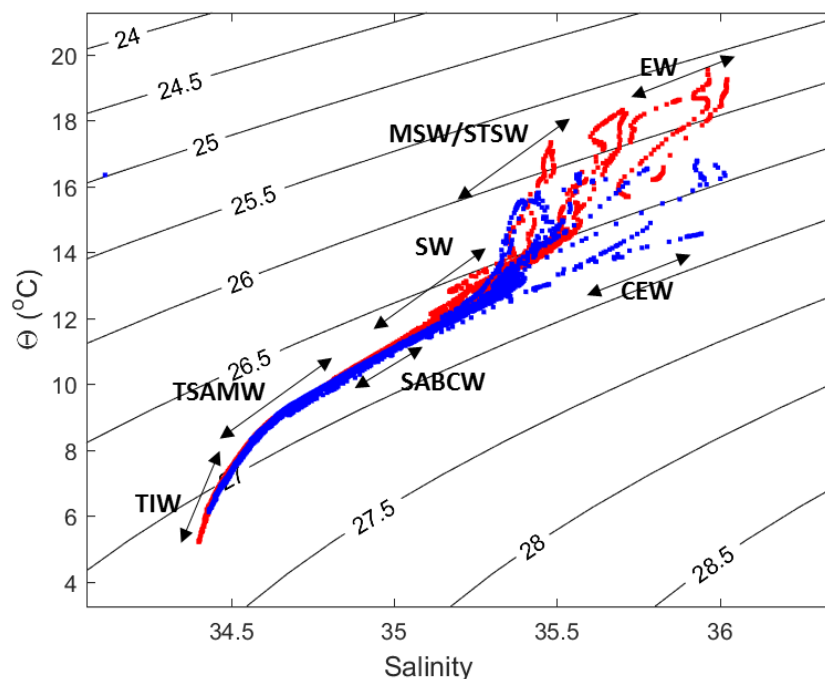


Figure 3.1-7 Temperature-salinity plot from CTD profiling to 800m depth taken during the 2015 RV Investigator Voyage. Red dots are for the central Great Australian Bight (GAB) and blue dots for the eastern GAB. Potential temperature  $\theta$  (°C) is plotted on the y-axis and contour lines of potential density  $\sigma_\theta$  ( $\text{kg m}^{-3}$ ) are shown. Identified water masses, as defined by Richardson (2015), are labelled. Key water masses with connectivity to the Great Australian Bight include: Tasmanian Intermediate Water (TIW), Tasmanian Subantarctic Mode Water (TSAMW), and South Australian Basin Central Water (SABCW). Locally formed water masses include Slope Water (SW), Subtropical Surface Water (STSW), Mixed Slope Water (MSW), Cooled Evaporated Water (CEW) and Evaporated Water (EW).

To further investigate the summertime connectivity between the central and eastern GAB results from particle tracking studies using the validated GABROMS model (Middleton et al., 2017) are presented in Figure 3.1-8. Particles were released at three depths (surface, mid, deep) along transects situated in the central (130.5 E) and eastern (138 E) GAB.

For the central GAB transect at 130.5 E (Figure 3.1-8A), the red particles nearest the coast (50 m initial water depth) move to the west as expected for the wind driven flow and also, at the bottom, towards the coast consistent with bottom Ekman upwelling. Farther offshore, both the purple and green particles (initial water depths 100 m and 200 m) move to the east again consistent with the flow of the South Australian Current (Figure 3.1-1). The mid-depth (100 m) green particles are found as far as the Bonney Coast over the 70 days of trajectory calculation. The mid-depth deep (700 m) blue particles indicate a weak cyclonic eddy which is non-existent at the bottom. Bottom displacements from 130.5 E are relatively small and to the east.

For the far eastern transect at 136 E (Figure 3.1-8B), the surface deployed particles present a chaotic display with red and purple particles moving into the Spencer Gulf and offshore, respectively. At the mid-depth (25 m and 50 m) the red and purple particles display a north-westward flow as expected for upwelling winds. At a depth of 100 m, the mid-depth green particles move to the south-east consistent with the flow of the South Australian Current and opposite to that expected for summer winds. At the bottom depths, the green particles cluster around the southern waters south of Kangaroo Island, while the red and purple trajectories at the bottom are similar to those at mid-depth. In summary, only the very near-shore trajectories for initial water depth of less than 50 m generally move to the north-west in accordance with the expected upwelling favourable winds. Farther offshore, currents are in the opposite direction and generally to the south-east; consistent with a strong and extensive South Australian Current (Figure 3.1-1).

The above results for 2013 are similar to those obtained for 2012, but differ from those for 2011 and 2014 where the coastal trajectories (red and purple; initial water depths of 50 and 100m ) are directed more to the north-east and along the west coast of the Eyre Peninsula. This suggests inter-annual variability in the regional connectivity is likely to occur due to changes associated with the relative strength of the dominant current systems (e.g. Leeuwin current, SAC). Whilst these differences are unresolved for the December 2015 voyage, the results of the particle tracking studies do not show any direct connection of possibly nutrient rich waters of the eastern GAB, Kangaroo Island and Bonney Coast regions with the central GAB within the 70 day simulation periods. These findings suggest the regional connectivity of the eastern GAB to the central GAB through the deep (300 m or greater) westward movement of the Flinders Current indicated by water mass analysis (Figure 3.1-7) is weak and occurs over timescales longer than those simulated in the particle tracking studies.

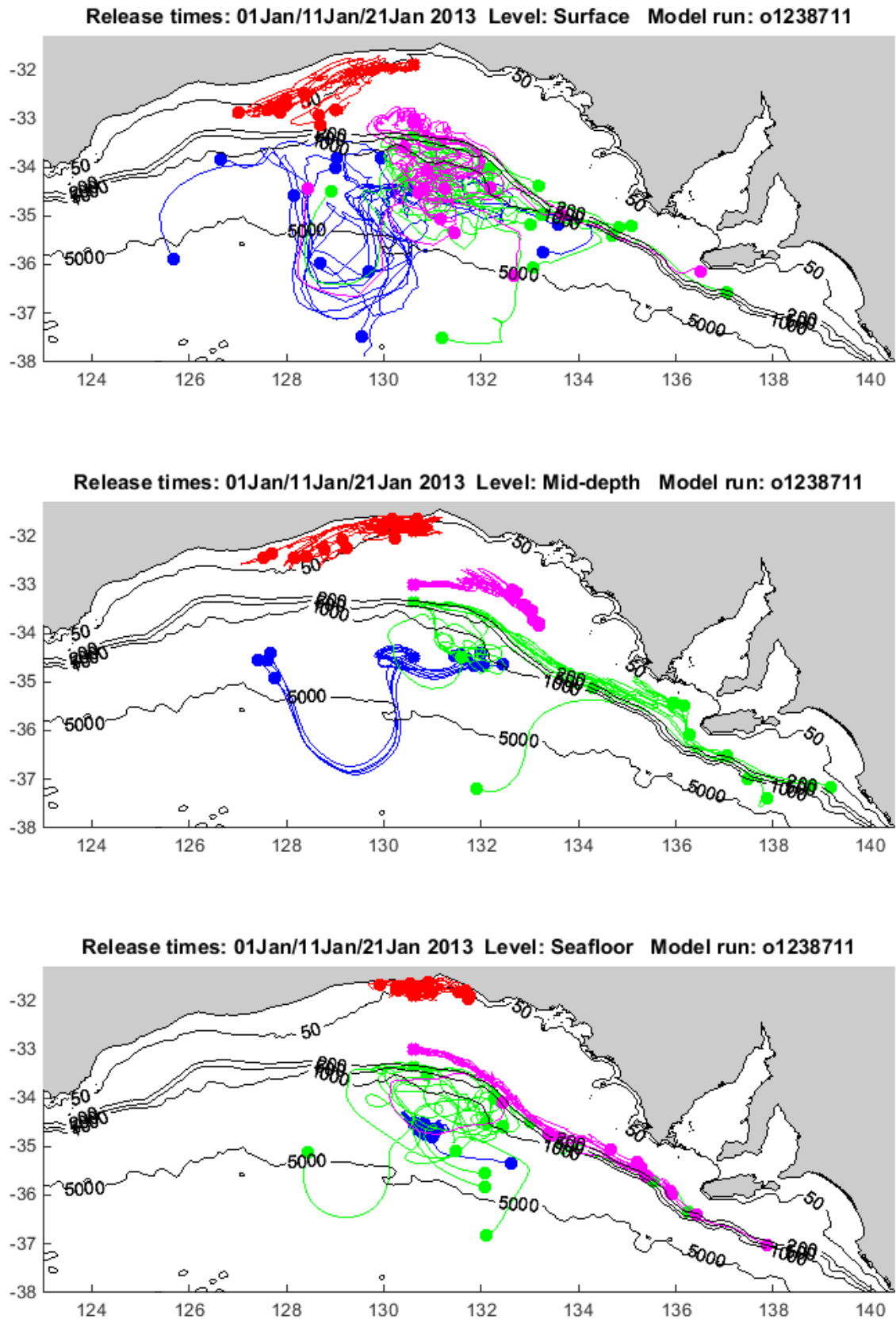


Figure 3.1-8 (A) Plan view of float tracks for floats released at four sites along the mid-GAB transect at 130.5 °E, at the surface (top panel), mid-depth (middle panel), and bottom (bottom panel), during summer 2013. The 4 sites are over the 50 m isobath in red, 100 m isobath in purple, 200 m isobath in green and 1400 m isobath in blue. Filled circles represent positions 70 days after release.



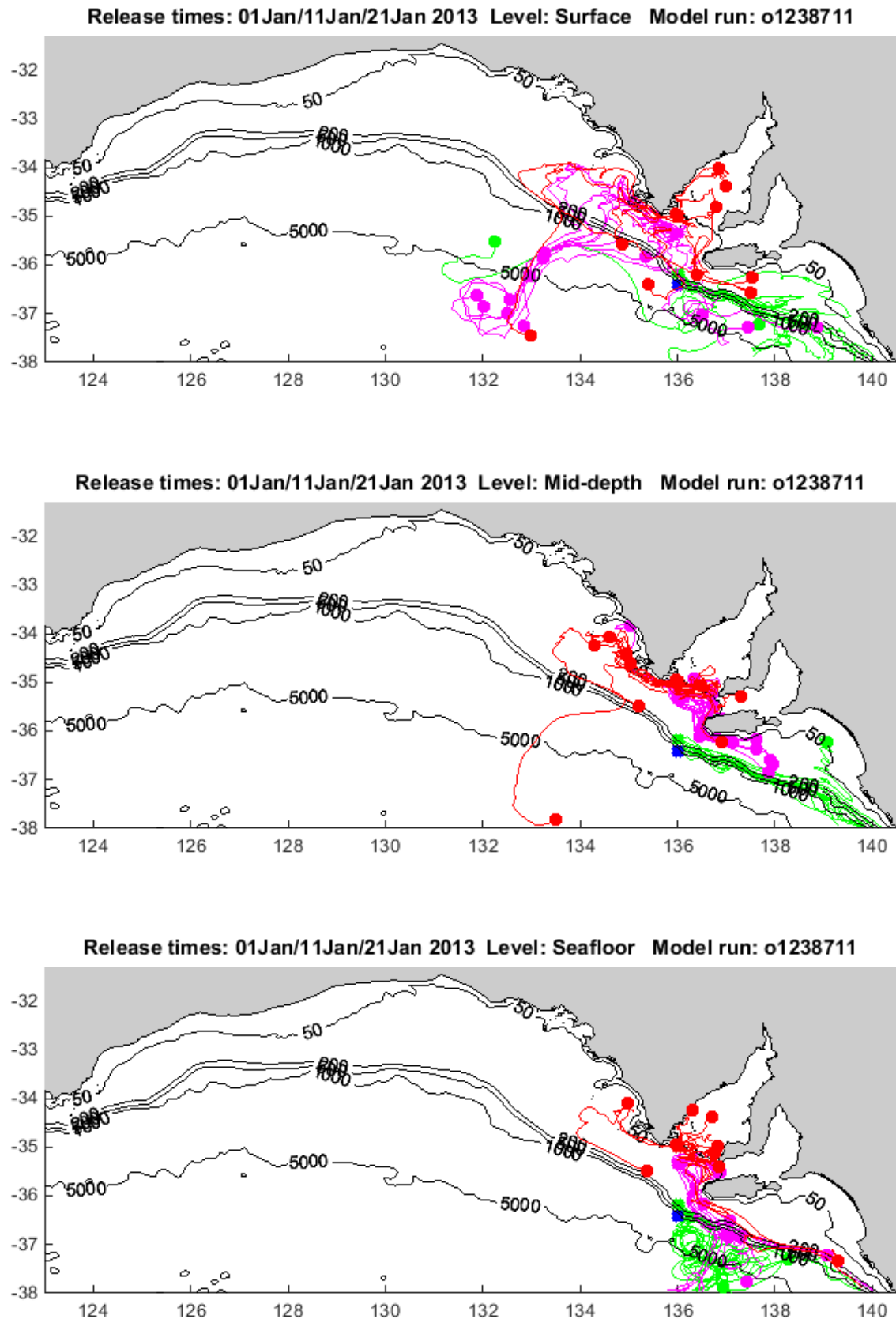


Figure 3.1- 8 (B). Plan view of float tracks for floats released at four sites along the eastern transect at 136.0 °E, at the surface (top panel), mid-depth (middle panel), and bottom (bottom panel), during summer 2013. The 4 sites are over the 50 m isobath in red, 100 m isobath in purple, 200 m isobath in green and 1400 m isobath in blue. Filled circles represent positions 70 days after release.



Finally, vertical sections of potential temperature, salinity and potential density to a depth of 800 m are presented for the central and eastern GAB transects in Figure 3.1-9 and Figure 3.1-10. Equivalent sections focusing on the upper 250 m of the water column are presented in section 3.2 (Figure 3.1-1 and Figure 3.2-2). Temperature and salinity sections here demonstrate the strong vertical thermohaline contrasts in the upper ocean down to 200 m depth. Across both transects, a surface mixed layer of relatively uniform low density, warm-saline water overlies relatively cool-fresh waters of higher density. Surface mixed layers were generally deeper in the central GAB (50 – 75m) relative to those in the eastern GAB (25 – 50 m), with the major differences in mixed layer depths between the central and east occurring in shelf waters inshore from the upper slope region.

Below the surface mixed layer strong stratification, indicated by the small separation of isopycnals between  $\sigma_\theta = 26.2\text{--}26.5 \text{ kg m}^{-3}$ , was driven by sharp decreases in temperature (Figure 3.1-9) and salinity (Figure 3.1-10). Strong vertical changes in salinity were particularly evident on the shelf compared to offshore waters. In the central GAB, sloping isopycnals below the surface mixed layer show downwelling at the shelf slope to a depth of approximately 250 m. Such a result is consistent with previous studies (Middleton et al., 2014; Middleton et al., 2017) and supports the conclusion that downwelling occurs in the central GAB all year round. At greater depths (500 – 800 m), upwelling at the continental shelf edge is indicated by the upward sloping isopycnals and is the expected signature of the Flinders Current (Middleton and Bye, 2007).

In the eastern GAB, sloping isopycnals between  $\sigma_\theta = 26.4\text{--}26.7 \text{ kg m}^{-3}$  show evidence for the coastal upwelling of cool-fresh water onto the shelf. The presence of a weak “high” pressure eddy centred in deep water and between 36.8 and 37.4 °S is a possible interpretation of the downwelled temperature, salinity signals and resultant density contours observed offshore from the slope ( $\sigma_\theta = 26.6\text{--}26.7 \text{ kg m}^{-3}$ ) (Figure 3.1-9B and Figure 3.1-10B). In the euphotic zone (upper 100 m), the maximum downwelling is of order 30 to 40 m and small. Notably, the presence of the high pressure eddy is not seen in the altimeter data shown in Figure 3.1-6. A possible reason for this is that the colder waters are found farther offshore which act to sit lower in the water column and mask the “high” sea level expected of the eddy.

Vertical sections of the average macro-nutrient concentrations for  $\text{NO}_x$ , phosphate and silicate are presented in Figure 3.1-11 to Figure 3.1-13. Nutrient concentrations within the surface mixed layer were very low and decrease to near zero at the surface. The relative influence of downwelling and upwelling processes on the distribution of nutrients, associated with  $\sigma_\theta = 26.3$  to  $26.6 \text{ kg m}^{-3}$ , is evident in the shelf waters of central and eastern GAB, respectively. In the central GAB, nutrients at the shelf slope are downwelled to depths of 100 – 250 m and remain low in waters on the shelf. In the eastern GAB, nutrients are upwelled onto the shelf to depths of 40 – 50 m (also see Figure 3.2-3 for a high resolution transect of  $\text{NO}_x$  focusing on the upper 250 m of the water column).

Below the mixed layer and offshore from the slope, nutrient concentrations generally increased with increasing depth; with similar concentrations observed along lines of constant density in the central and eastern GAB regions. High concentrations of all three macro-nutrients are found at depths greater than 300 to 400 m. Differences in the distributions of each nutrient species (e.g.  $\text{NO}_x$  versus  $\text{PO}_4$ ) were observed within each transect. A possible reason for this may be due to the limited number of discrete water samples taken and the variability observed within replicate samples taken at each depth. Nonetheless, the observed vertical distribution of nutrient concentrations are generally consistent with long-term CSIRO Atlas of Regional Seas (CARS) climatological average distributions found along Australia’s southern margin (Richardson, 2015) and show nutrient rich waters at depths greater than 300 m are present along the slope .

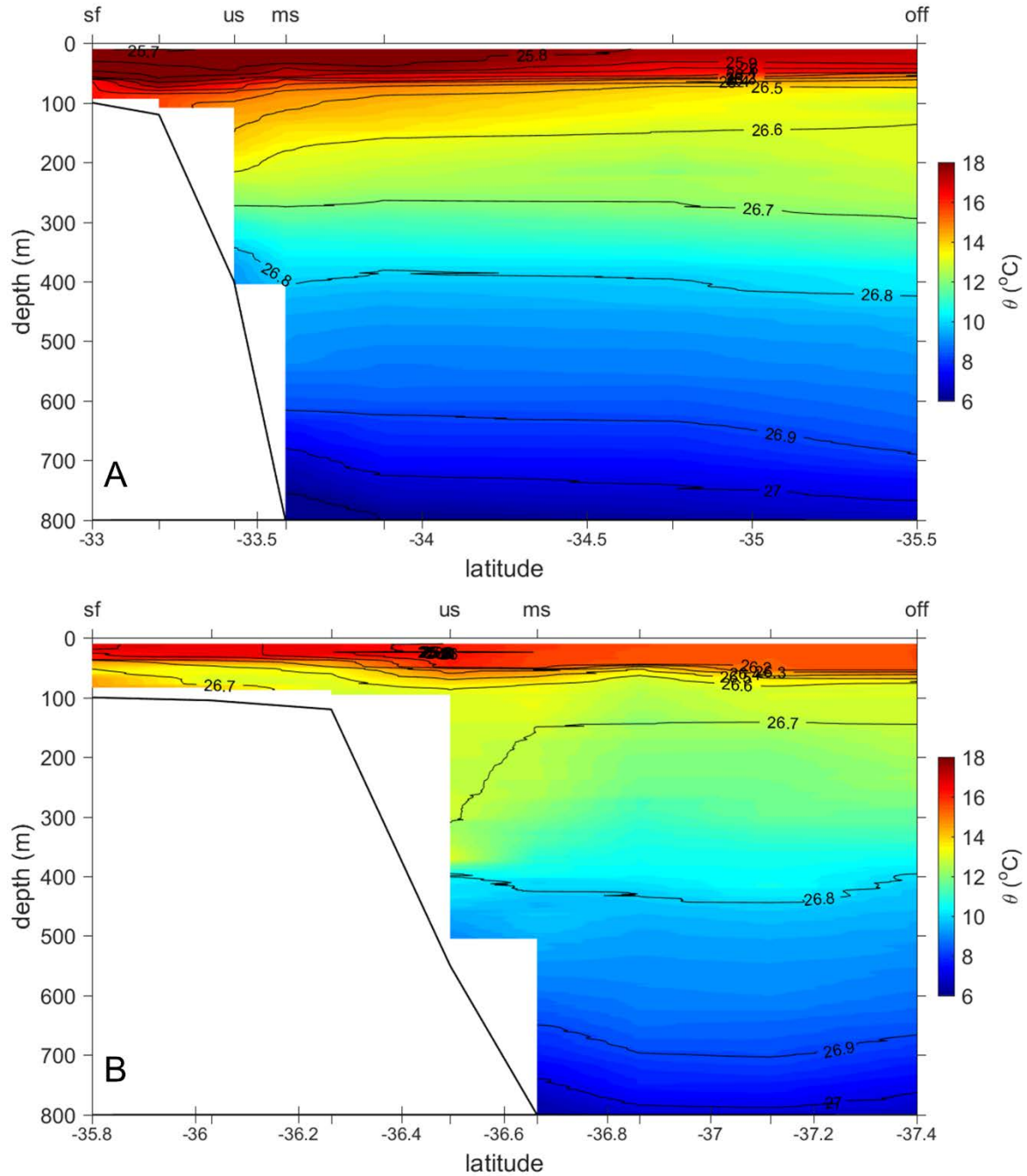


Figure 3.1-9 Results from the observational transects constructed from CTD profiles showing the vertical distribution of potential temperature ( $\theta$ , °C) for (A) the central GAB, and (B) the eastern GAB. Contours show lines of potential density ( $\sigma_\theta$ ,  $\text{kgm}^{-3}$ ). The locations of stations shown in Figure 3.1-2 are marked as small ticks along the top and bottom abscissa. The corresponding position of stations sampled in approximately 100, 400, 800 and 1000 m water depth or greater are indicated by the top abscissa labels 'sf' for shelf, 'us' for the upper slope, 'ms' for the mid slope and 'off' for offshore stations, respectively.

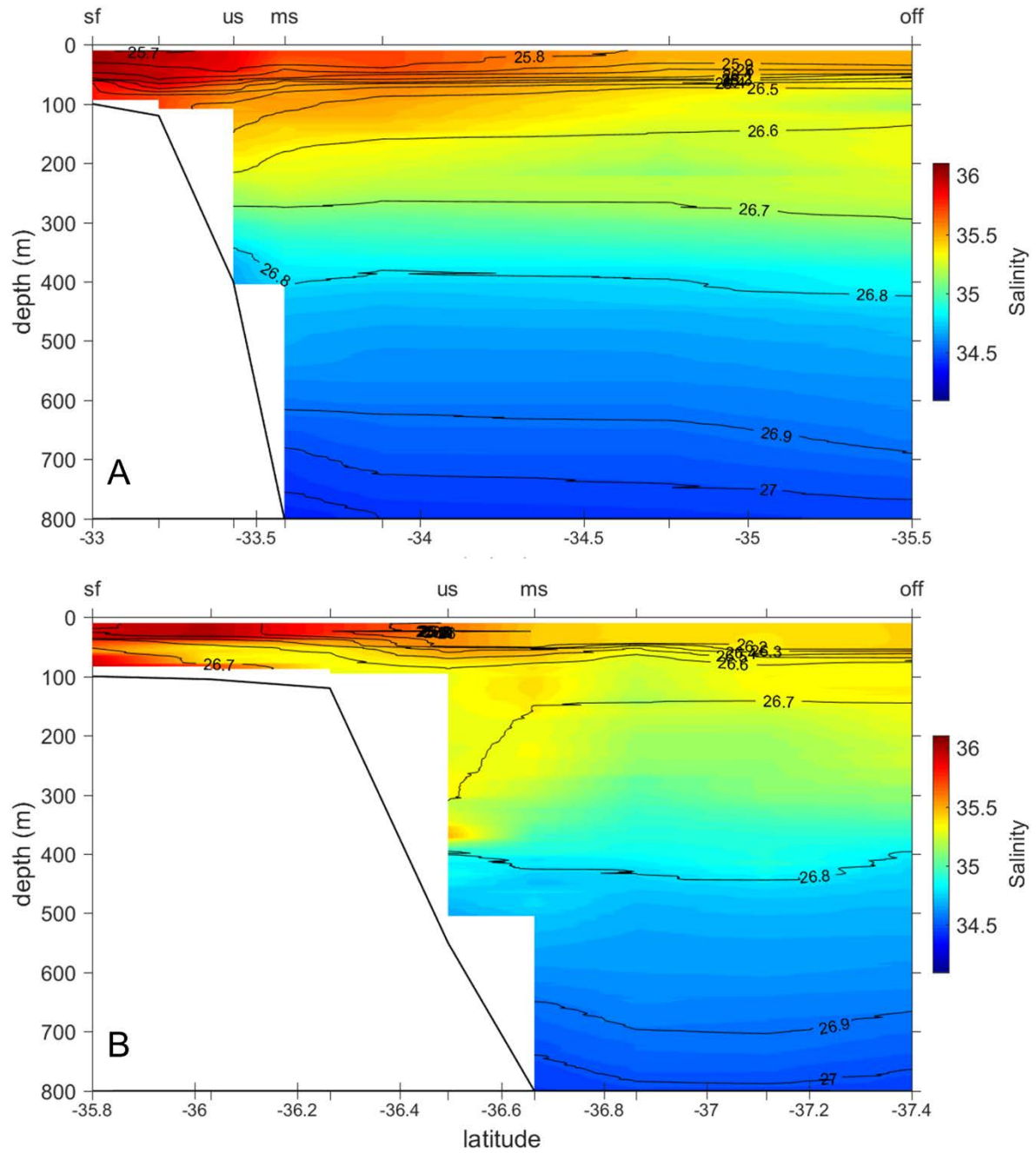


Figure 3.1-10 Results from the observational transects constructed from CTD profiling showing the vertical distribution of salinity for (A) the central GAB, and (B) the eastern GAB. Contours show lines of potential density ( $\sigma_\theta$ ,  $\text{kg m}^{-3}$ ). The locations of stations shown in Figure 3.1-2 are marked as small ticks along the top and bottom abscissa. The corresponding position of stations sampled in approximately 100, 400, 800 and 1000 m water depth or greater are indicated by the top abscissa labels 'sf' for shelf, 'us' for the upper slope, 'ms' for the mid slope and 'off' for offshore stations, respectively.

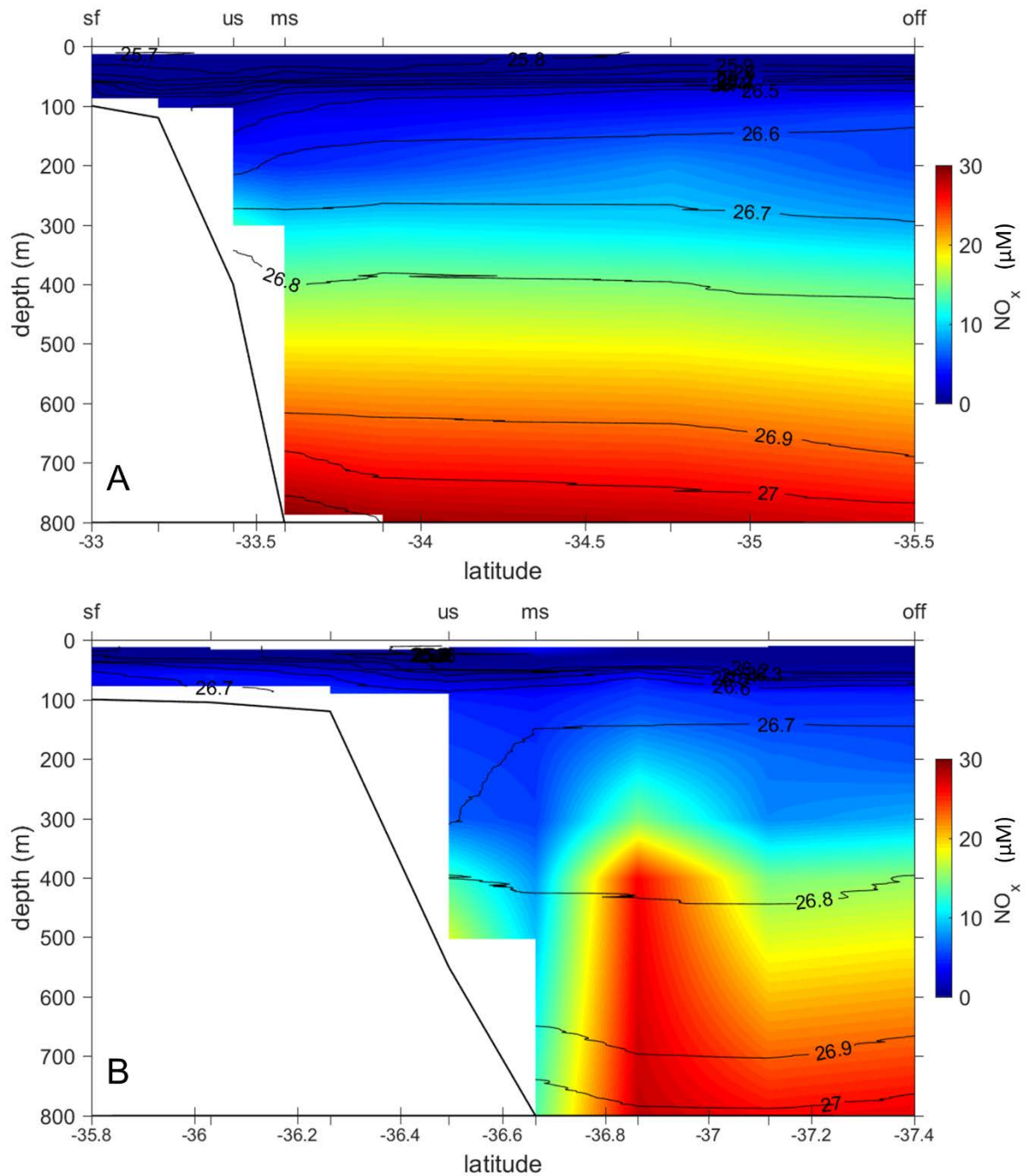


Figure 3.1-11 Results from the observational transects constructed from CTD profiles showing the vertical distribution of  $\text{NO}_x$  ( $\mu\text{M}$ ) for (A) the central GAB, and (B) the eastern GAB. Contours show lines of potential density ( $\sigma_\theta$ ,  $\text{kg m}^{-3}$ ). The locations of stations shown in Figure 3.1-2 are marked as small ticks along the top and bottom abscissa. The corresponding position of stations sampled in approximately 100, 400, 800 and 1000 m water depth or greater are indicated by the top abscissa labels 'sf' for shelf, 'us' for the upper slope, 'ms' for the mid slope and 'off' for offshore stations, respectively.

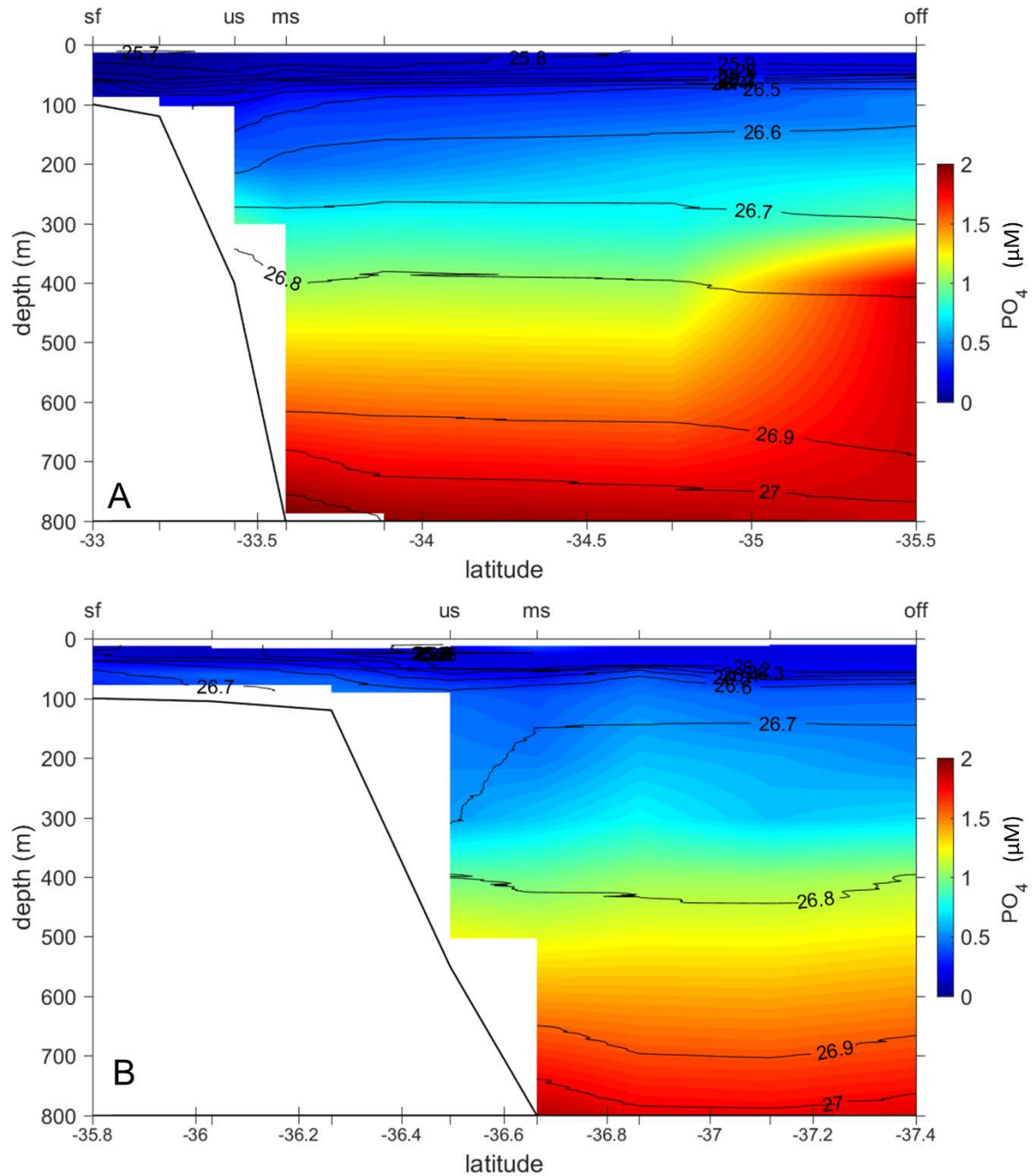


Figure 3.1-12 Results from the observational transects constructed from CTD profiles showing the vertical distribution of phosphate ( $\text{PO}_4$ ,  $\mu\text{M}$ ) for (A) the central GAB, and (B) the eastern GAB. Contours show lines show the potential density ( $\sigma_\theta$ ,  $\text{kg m}^{-3}$ ). The locations of stations shown in Figure 3.1-2 are marked as small ticks along the top and bottom abscissa. The corresponding position of stations sampled in approximately 100, 400, 800 and 1000 m water depth or greater are indicated by the top abscissa labels 'sf' for shelf, 'us' for the upper slope, 'ms' for the mid slope and 'off' for offshore stations, respectively



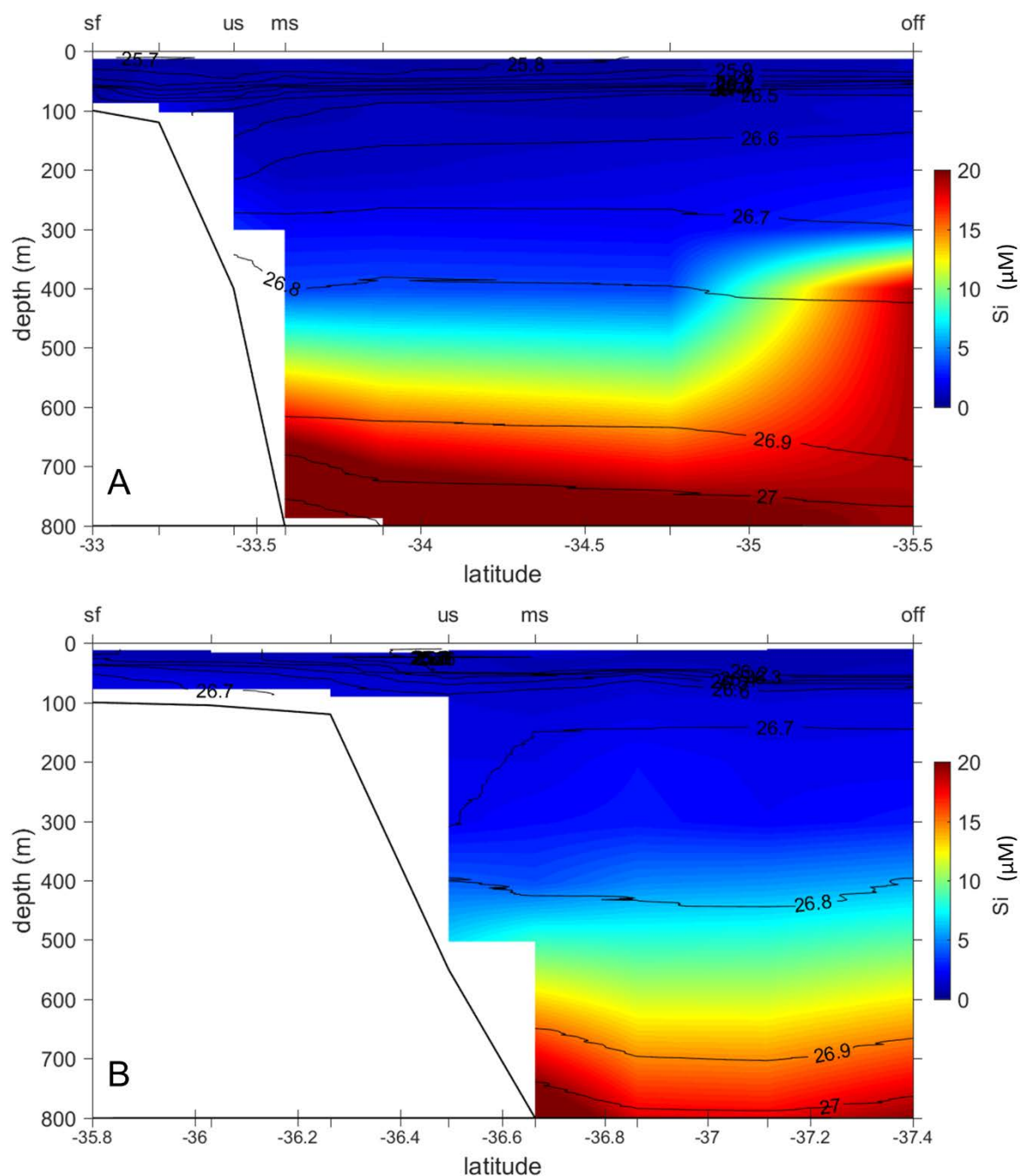


Figure 3.1-13 Results from the observational transects constructed from CTD profiles showing the vertical distribution of silicate ( $\text{Si}$ ,  $\mu\text{M}$ ) for (A) the central GAB, and (B) the eastern GAB. Contours show lines show the potential density ( $\sigma_\theta$ ,  $\text{kg m}^{-3}$ ). The locations of stations shown in Figure 3.1-2 are marked as small ticks along the top and bottom abscissa. The corresponding position of stations sampled in approximately 100, 400, 800 and 1000 m water depth or greater are indicated by the top abscissa labels 'sf' for shelf, 'us' for the upper slope, 'ms' for the mid slope and 'off' for offshore stations, respectively.

### 3.1.4 Summary

Observations of the meteorological (Figure 3.1-3 and Figure 3.1-5) and oceanographic conditions (Figure 3.1-4) prior to the *RV Investigator* voyage indicate the summer upwelling season had been active for a period of at least one month. Consistent with previous analyses of the summertime wind forcing (Kämpf et al., 2004; Middleton and Bye, 2007) several distinct upwelling favourable events spanning periods of 3 – 7 days were observed prior to the cruise (Figure 3.1-3). These events resulted in cool sea surface temperatures off the Bonney coast (Figure 3.1-6) and are indicative of active upwelling. Upwelling occurs simultaneously along the Bonney coast and eastern GAB regions (Kämpf et al., 2004; Middleton et al., 2017) and shows a moderate level of connectivity through the prevailing shelf currents (Middleton et al., 2017). However, it is likely that the timescales of connectivity between the Bonney coast and eastern GAB greatly exceed those related to phytoplankton nutrient uptake, such that nutrient supply to each of these regions is driven by the localised upwelling.

During the voyage, the continued presence of atmospheric high pressure systems in the GAB (Figure 3.1-3) meant winds were weakly upwelling favourable during transect periods (Figure 3.1-5). The surface signature of upwelling was not strong for the sampling in the eastern GAB and even weaker during sampling in the central GAB (Figure 3.1-6). Shelf currents in both cases were weak (Figure 3.1-6), although a  $0.10 \text{ m s}^{-1}$  shelf edge current is observed during sampling in the central GAB. Model particle tracking studies (Figure 3.1-8) supported the presence of an eastward flowing South Australian Current over the GAB region.

Mesoscale oceanic eddies, with diameters of 100 – 200 km, were present during the voyage although not near transects (Figure 3.1-6) where they might otherwise lead to upwelling or downwelling. As mentioned above, observed geostrophic current velocities were substantially lower than the mean velocities ( $0.5 \text{ m s}^{-1}$ ) associated with mesoscale eddies in the West (Andrews, 1977) and East Australian Current (Mata et al., 2006) systems. Considering a current velocity of  $0.1 \text{ m s}^{-1}$  is equivalent to a horizontal displacement of approximately  $8.5 \text{ km day}^{-1}$ , the horizontal transport of water masses due to eddies experienced during the voyage is relatively small compared to the spatial (20 – 200 km) and temporal (1 – 5 days) distribution of sampling effort along transects.

The identification of Tasmanian Intermediate Water (TIW), Tasmanian Subantarctic Mode Water (TSAMW) and South Australian Basin Central Water (SABCW) in the central and eastern GAB (Figure 3.1-7) support the expected regional connectivity of the GAB to deep water masses formed outside of the GAB region (Figure 3.1-1) and a general westward flow from the Bonney Coast to the central GAB via the Flinders Current (Middleton and Bye, 2007; Richardson, 2015). These deep water masses are not affected by mesoscale eddies or local mixing processes. Observations of deep upwelling along the continental slope in the central and eastern GAB at depths of 350 to 400 m provides further evidence for the presence of the Flinders current and is consistent with its expected summertime depth distribution and dynamics (Middleton and Platov, 2003; Cirano and Middleton, 2004). Additionally, summertime particle tracking modelling studies (Figure 3.1-8) indicate the deep westward movement of the Flinders Current identified by water mass analysis (Figure 3.1-7) is weak and occurs over timescales much longer than the 70 day model simulation periods.

Locally formed water masses, defined by Richardson (2015) using water mass and isotope analysis, were identified in the upper 200 m of the water column in the shelf and upper slope regions of the GAB (Figure 3.1-7). The formation of these water masses has implications for the mixing of nutrient-rich upwelled waters with nutrient-deplete surface waters (Figure 3.1-11 to Figure 3.1-13) and hence regional pelagic ecosystem structure and productivity (McClatchie et al., 2006). Section 3.2 provides a detailed inspection of the observed fine-scale epipelagic habitat structure and quantifies the role of mixing process on the vertical transport of nutrients to the euphotic zone.

Finally, along transect vertical sections of temperature, salinity and density (Figure 3.1-9 and Figure 3.1-10) demonstrated surface mixed layers were generally deeper in the central GAB (50-75m) relative to the eastern GAB (25 – 50 m). Shelf-edge downwelling to depths of 250 m was observed in the central GAB, whilst upwelling of relatively cool-fresh and nutrient rich water onto the shelf (Figure 3.1-11 to Figure 3.1-13) was observed in the eastern GAB. Collectively, the abovementioned observations are consistent with the known characteristics, and our conceptual understanding, of the met-ocean processes operating during summer in the GAB (Middleton and Bye, 2007; Rogers et al., 2013).

## References

- Andrews, J. C. 1977. Eddy structure and the West Australian current. *Deep Sea Research*, 24: 1133-1148.
- Cirano, M., and Middleton, J. F. 2004. Aspects of the mean wintertime circulation along Australia's southern shelves: Numerical studies. *Journal of Physical Oceanography*, 34: 668-684.
- Cresswell, G., and Peterson, J. 1993. The Leeuwin Current south of Western Australia. *Marine and Freshwater Research*, 44: 285-303.
- Herzfeld, M., and Tomczak, M. 1999. Bottom-driven upwelling generated by eastern intensification in closed and semi-closed basins with a sloping bottom. *Marine and Freshwater Research*, 50: 613-627.
- Kämpf, J. 2010. On preconditioning of coastal upwelling in the eastern Great Australian Bight. *Journal of Geophysical Research: Oceans*, 115: doi:10.1029/2010JC006294.
- Kämpf, J., Doubell, M., Griffin, D., Matthews, R., L., and Ward, T. M. 2004. Evidence of a large seasonal coastal upwelling system along the southern shelf of Australia. *Geophysical Research Letters*, 31: doi:1029/2003GL019221.
- Lewis, R. 1981. Seasonal upwelling along the south-eastern coastline of South Australia. *Marine and Freshwater Research*, 32: 843-854.
- Mata, M. M., Wijffels, S. E., Church, J. A., and Tomczak, M. 2006. Eddy shedding and energy conversions in the East Australian Current. *Journal of Geophysical Research: Oceans*, 111: doi:1029/2006JC003592.
- McClatchie, S., Middleton, J. F., and Ward, T. M. 2006. Water mass analysis and alongshore variation in upwelling intensity in the eastern Great Australian Bight. *Journal of Geophysical Research: Oceans*, 111: doi:10.1029/2004JC002699.
- Middleton, J. F., and Bye, J. A. 2007. A review of the shelf-slope circulation along Australia's southern shelves: Cape Leeuwin to Portland. *Progress in Oceanography*, 75: 1-41.
- Middleton, J. F., and Cirano, M. 2002. A northern boundary current along Australia's southern shelves: The Flinders Current. *Journal of Geophysical Research: Oceans*, 107: doi:10.1029/2000JC000701,2002.
- Middleton, J. F., Griffin, D., Luick, J., Herzfeld, M., James, C., and Oke, P. 2017. Physical oceanography of the Great Australian bight: the science that underpins. Final Report GABRP Project 1.1. Great Australian Bight Research Program, GABRP Research Report Number 20, 109pp.
- Middleton, J. F., James, N. P., James, C., and Bone, Y. 2014. Cross-shelf seawater exchange controls the distribution of temperature, salinity, and neritic carbonate sediments in the Great Australian Bight. *Journal of Geophysical Research: Oceans*, 119: 2539-2549.
- Middleton, J. F., and Platov, G. 2003. The mean summertime circulation along Australia's southern



- shelves: a numerical study. *Journal of Physical Oceanography*, 33: 2270-2287.
- Richardson, L. E. 2015. Water Mass connectivity and mixing along the southern margin of Australia: hydrographic and stable isotope analyses. The Australian National University, ACT, Australia.
- Ridgway, K., and Condie, S. 2004. The 5500-km-long boundary flow off western and southern Australia. *Journal of Geophysical Research: Oceans*, 109, C04017: doi:10.1029/2003JC001921.
- Rogers, P. J., Ward, T. M., van Ruth, P. D., Williams, A., Bruce, B. D., Connell, S. D., Currie, D. R., et al. 2013. Physical processes, biodiversity and ecology of the Great Australian Bight region: a literature review. CSIRO, Australia.
- Suthers, I. M., Young, J. W., Baird, M. E., Roughan, M., Everett, J. D., Brassington, G. B., Byrne, M., et al. 2011. The strengthening East Australian Current, its eddies and biological effects — an introduction and overview. *Deep Sea Research Part II: Topical Studies in Oceanography*, 58: 538-546.
- Wood, J., and Terray, E. 2005. Ocean current, temperature, and wave observations at the Amrit-1 location offshore of southern Victoria, Australia. Final Report April–October 2004, Ocean Data Technologies Inc.

## 3.2 Fine scale pelagic habitat

### 3.2.1 Introduction

The summertime climatology experienced in the Great Australian Bight (GAB) during the *RV Investigator* voyage gave rise to upwelling in the eastern GAB and downwelling in the central GAB (see Section 3.1.1). Under upwelling conditions in the relatively narrow-shelf eastern GAB, the strength of the stratification below the surface mixed layer is amplified as a result of strong temperature gradients as cool-fresh, nutrient rich waters are drawn up onto the shelf (Figure 3.1-9 and Figure 3.1-10; McClatchie et al., 2006). Shelf waters of the much wider central GAB are also subjected to intense heating and evaporation during summer. This, again, results in the formation of a warm-saline ocean surface layer overlying waters with a lower temperature and salinity. Hence across the GAB, the hydrographic structure of the water column is characterised by complex vertical profiles of temperature and salinity due to different shelf widths and oceanographic mechanisms of cross-shelf transport (i.e. downwelling and upwelling).

The formation of new water masses on the shelf and slope regions (Figure 3.1-7) requires microscale mixing processes which are associated with cross-isopycnal tracer fluxes (e.g. temperature, salt and nutrients). The two major mixing processes driving cross-isopycnal fluxes are mechanical turbulent mixing and double-diffusive convective mixing (Thorpe, 2007). Mechanical turbulent mixing is typically driven by instabilities arising from either the differential motion of water (e.g. wind and internal wave generated shear). Double-diffusive convective mixing arises from instabilities arising from the different molecular diffusion coefficients of heat and salt and is recognised as a potentially important process influencing upper ocean nutrient supply and primary productivity (St. Laurent and Schmitt, 1999; Glessmer et al., 2008). Numerical simulations indicate that double-diffusive driven nutrient supply to the euphotic zone may, at times, be as important as fluxes associated with mechanical turbulence and mesoscale eddies (Oschlies et al., 2003).

The following section provides a finescale assessment of the thermohaline structure observed across the upper water column to 250 m depth, and its relation to the distribution of nitrate and phytoplankton biomass, during the *RV Investigator* voyage. In order to understand and quantify mixing processes across the GAB, direct measurements of turbulence microstructure were conducted. Estimates of the vertical diffusivity are calculated and discussed in relation to vertical nutrient fluxes. To our knowledge, this study presents the first survey of small-scale mixing processes in the GAB.

### 3.2.2 Methods

Hydrographic CTD (conductivity-temperature-depth) and microstructure observations were conducted along cross-shelf transects in the eastern and central GAB during the 2015 *RV Investigator* summer voyage (Figure 3.1-2). Sampling occurred along the eastern GAB transect between November 30<sup>th</sup> and December 4<sup>th</sup> and along the central GAB transect between December 10<sup>th</sup> to December 15<sup>th</sup>. CTD profiles of hydrographic properties were made using a Seabird9plus with external sensors for the measurement of chlorophyll *a* fluorescence and dissolved oxygen concentrations. The fluorometer attached to the CTD provides an uncalibrated, relative measure of the chlorophyll *a* concentration, a proxy for phytoplankton biomass. CTD profiles were made from the surface to (near) bottom in waters less than 800 m depth, or a maximum depth of 800 m in waters greater than 800 m depth. At each station, discrete seawater samples were collected at approximately 10, 30, 65, 90, 120, 200, 300, 400 and 800 m depths using Niskin bottles attached to the CTD rosette. Determination of macro-nutrient concentrations; oxides of nitrogen (NO<sub>x</sub>; nitrite/nitrate), phosphate (PO<sub>4</sub>) and silicate (Si) were made on-board in the *RV Investigator* hydrochemistry laboratory. Here, we report on the distribution of NO<sub>x</sub> which is representative of the

nitrogen source supporting new production (Dugdale and Goering, 1967).

Microstructure measurements were taken at 4 stations on each transect (Figure 3.1-2). At microstructure stations, two consecutive microstructure profiles were made following CTD profiling. Microstructure measurements were made using a TurboMAP profiler (Wolk et al., 2002; Doubell et al., 2009). TurboMAP is a free-fall instrument which is equipped with sensors for the microscale measurement of turbulent shear ( $\partial u' / \partial z$ ,  $\partial v' / \partial z$ ; where  $u'$  and  $v'$  are the horizontal shear fluctuations and  $z$  is depth) and temperature gradient ( $\partial T' / \partial z$  where  $T'$  is the microscale temperature fluctuation) and standard hydrographic parameters (CTD). Shear and temperature gradient data are sampled at a rate of 512 Hz and CTD sensors are sampled at 64 Hz. Typical profiling speeds were  $0.5 \text{ m s}^{-1}$  and profiling was limited to maximum depth of approximately 180 m.

### 3.2.3 Results and Discussion

#### Hydrographic structure

Vertical sections obtained from CTD profiling, focusing on the upper 250 m of the water column along transects in the central and eastern GAB, are presented in Figure 3.2-1 to Figure 3.2-5. Common to both transects is the existence of a warm–saline surface layer that extends from north to south above a layer of relatively cool–fresh water. However, temperature (Figure 3.2-1) and salinity (Figure 3.2-2) Sections clearly demonstrate a strong contrast between the vertical thermohaline structure resulting from downwelling in the central GAB and upwelling in the eastern GAB.

In the central GAB (Figure 3.2-1 A; Figure 3.2-2 A), downwelling at the shelf-break is evident to depths of approximately 250 m and the waters are warmer than those found in the eastern GAB. The reason for this is illustrated by the schematic of the expected summer circulation shown in Figure 3.1-1. Within the wide shelf of the central GAB, the relatively shallow depths (particularly near the coast) lead to greater heating and evaporation. This water “collides” with the equatorward deep ocean Sverdrup transport at the shelf slope and leads to downwelling (Middleton and Platov, 2003; Middleton et al., 2014).

For the eastern GAB (Figure 3.2-1 B and Figure 3.2-2 B), sloping isopycnals between  $\sigma_\theta = 26.2$ – $26.5 \text{ kg m}^{-3}$  show cold–fresh water has been upwelled onto the shelf below the surface mixed layer and to depths of approximately 35 m. This result is consistent with the SST data presented in Figure 3.1-6. In open-ocean waters offshore from the continental slope, upwelled water is associated with the top of the sub-surface mesoscale eddy identified above (Figure 3.1-11) and centred between  $36.8$  and  $37.4^\circ \text{ S}$ . It is likely this eddy anticyclonic in the upper half and cyclonic in the lower half since the net depth integrated density difference with surrounding water is small as indicated by the lack of a visible eddy in the surface SSH data from the altimeter data (Figure 3.1-6).

The influence of upwelling and downwelling on the distribution of  $\text{NO}_x$  is shown in Figure 3.2-3. For the central GAB, similar  $\text{NO}_x$  concentrations associated with  $\sigma_\theta = 26.5 \text{ kg m}^{-3}$  are found below depths of approximately 75 m in open-ocean waters and are downwelled to depths of 140 – 150 m at the shelf slope. A noteworthy feature is the large  $\text{NO}_x$  concentration (greater than  $10 \mu\text{M}$ ) found at depths below approximately 200 m across the region (also see Figure 3.1-11 for  $\text{NO}_x$  distribution to 800 m depth). Notably, as the result of upwelling in the eastern GAB, elevated concentrations of  $\text{NO}_x$  relative to those observed in the central GAB are observed across the upper 150 m of the water column, with  $\text{NO}_x$  concentrations of up to  $5 \mu\text{M}$  associated with the  $\sigma_\theta = 26.5 \text{ kg m}^{-3}$  observed on the shelf below the surface mixed layer and to depths of approximately 30 m. In surface waters of the eastern and central GAB  $\text{NO}_x$  concentrations are drawn to very low values approaching zero.

Figure 3.2-4 and Figure 3.2-5 show the corresponding distributions of chlorophyll *a* fluorescence and dissolved oxygen. For both transects, maximum concentrations of fluorescence are observed in bands below the surface mixed layer and are concentrated between approximately  $\sigma_\theta = 26.3$  –

$26.6 \text{ kg m}^{-3}$ . This band of high fluorescence is narrower, more concentrated, and sits higher in the water column in the east (approximately 40 to 75 m depth) relative to the central GAB (approximately 60 to 110 m depth). Surface mixed layer fluorescence levels on the shelf are comparable between the central and eastern GAB. However, offshore from the shelf slope, surface fluorescence concentrations in the central GAB are much lower than those observed offshore in the eastern GAB. Fluorescence concentrations correspond closely with elevated dissolved oxygen levels and the location of the nutricline reflecting active uptake by phytoplankton.

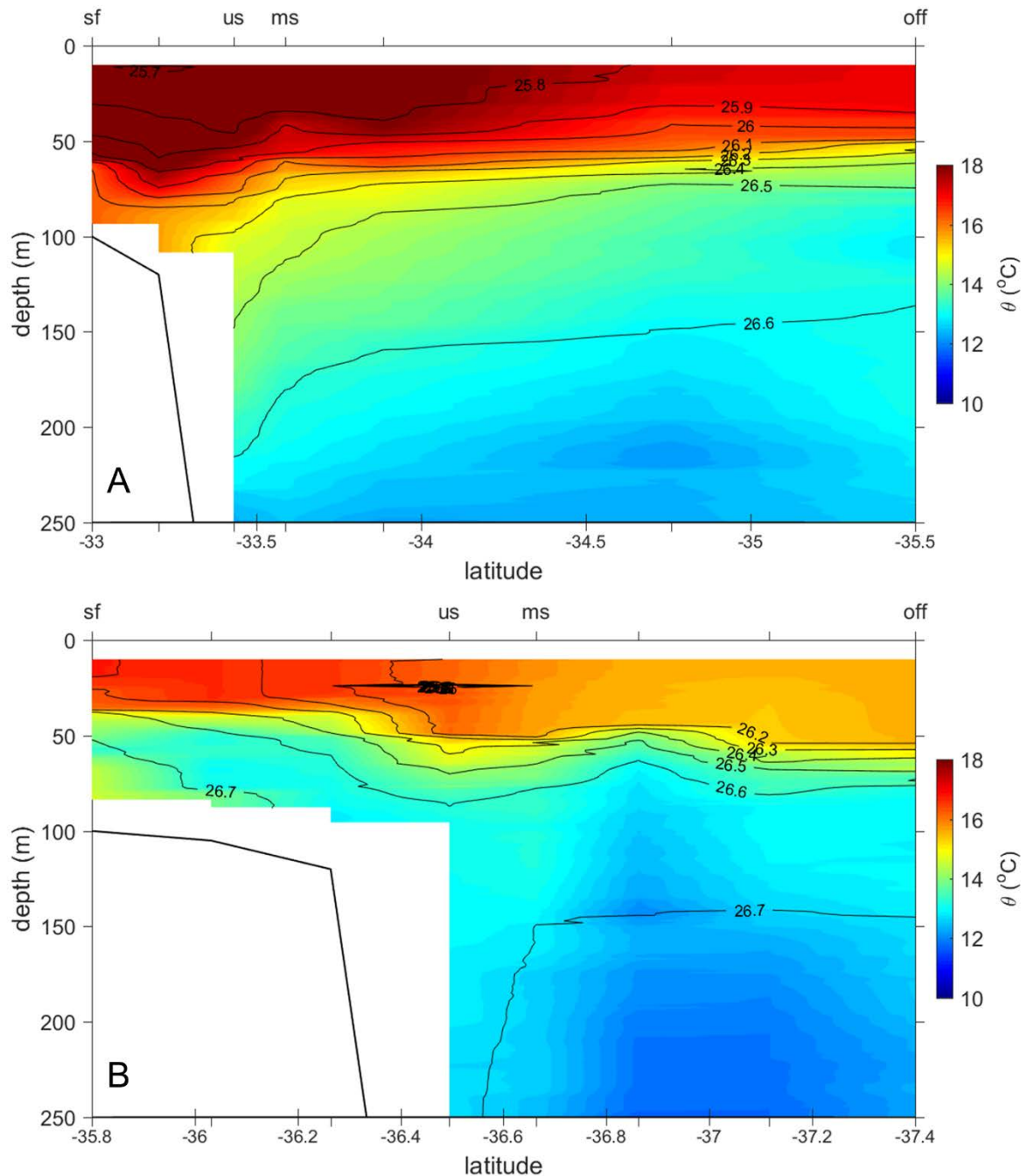


Figure 3.2-1 Results from the observational transects constructed from CTD profiles showing the vertical distribution of potential temperature ( $\theta$ ,  $^{\circ}\text{C}$ ) to depths of 250 m for (A) the central GAB, and (B) the eastern GAB. Contours show lines show the potential density ( $\sigma_{\theta}$ ,  $\text{kg m}^{-3}$ ). The locations of stations shown in Figure 3.1-2 are marked as small ticks along the top and bottom abscissa. The corresponding position of microstructure stations sampled in approximately 100, 400, 800 and 1000 m water depth or greater are indicated by the top abscissa labels 'sf' for shelf, 'us' for the upper slope, 'ms' for the mid slope and 'off' for offshore stations, respectively.

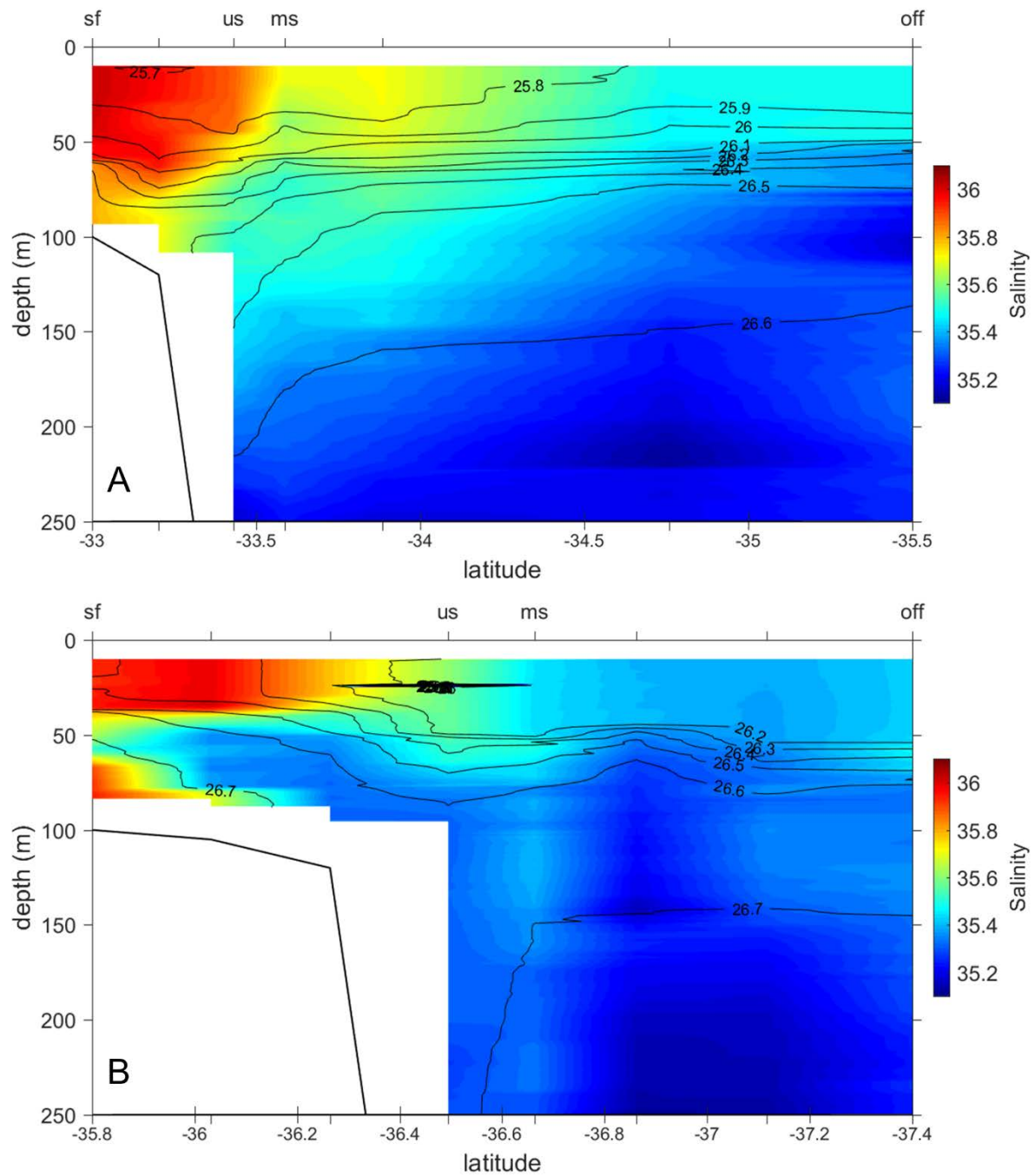


Figure 3.2-2 Results from the observational transects constructed from CTD profiles showing the vertical distribution of salinity ( $S$ ) to depths of 250 m for (A) the central GAB, and (B) the eastern GAB. Contours show lines of potential density ( $\sigma_\theta$ ,  $\text{kg m}^{-3}$ ). The locations of stations shown in Figure 3.1-2 are marked as small ticks along the top and bottom abscissa. The corresponding position of microstructure stations sampled in approximately 100, 400, 800 and 1000 m water depth or greater are indicated by the top abscissa labels 'sf' for shelf, 'us' for the upper slope, 'ms' for the mid slope and 'off' for offshore stations, respectively.



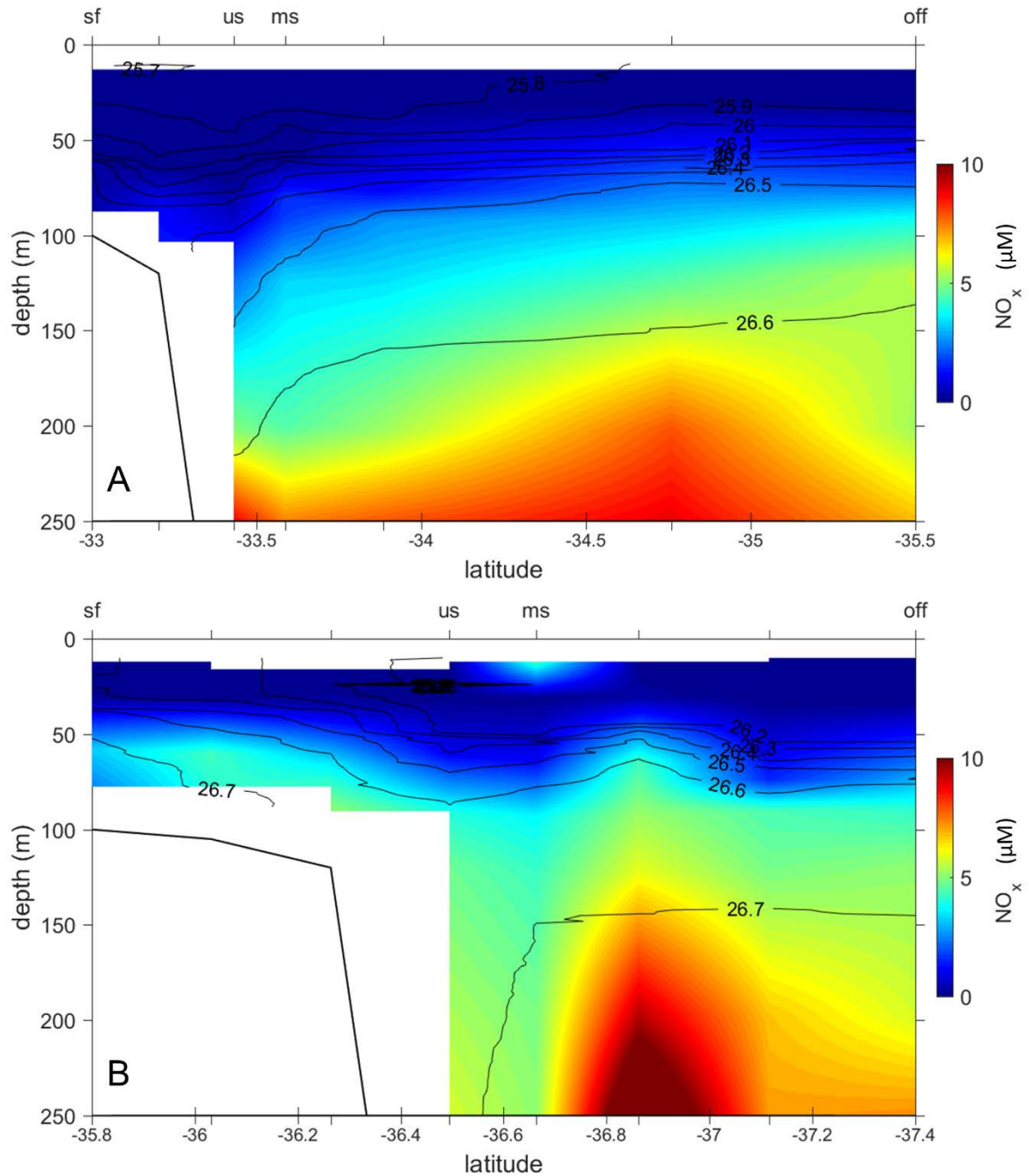


Figure 3.2-3 Results from the observational transects constructed from CTD profiles showing the vertical distribution of  $\text{NO}_x$  ( $\mu\text{M}$ ) to depths of 250 m for (A) the central GAB, and (B) the eastern GAB. Contours show lines of potential density ( $\sigma_\theta$ ,  $\text{kg m}^{-3}$ ). The locations of stations shown in Figure 3.1-2 are marked as small ticks along the top and bottom abscissa. The corresponding position of stations sampled in approximately 100, 400, 800 and 1000 m water depth or greater are indicated by the top abscissa labels 'sf' for shelf, 'us' for the upper slope, 'ms' for the mid slope and 'off' for offshore stations, respectively.



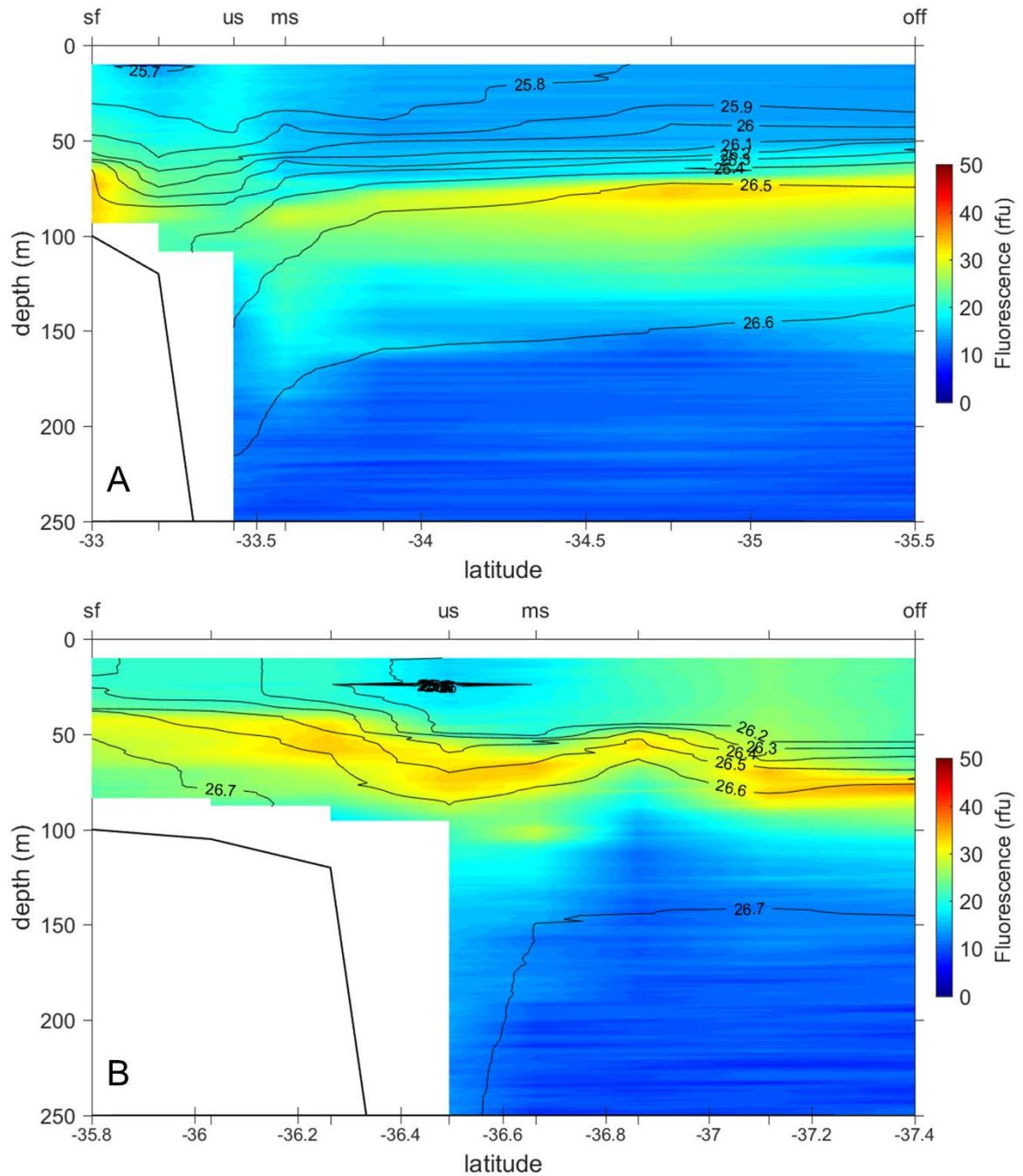


Figure 3.2-4 Results from the observational transects constructed from CTD profiles showing the vertical distribution of chlorophyll a fluorescence (relative fluorescence units) to depths of 250 m for (A) the central GAB, and (B) the eastern GAB. Contours show lines of potential density ( $\sigma_\theta$ ,  $\text{kg m}^{-3}$ ). The locations of stations shown in Figure 3.1-2 are marked as small ticks along the top and bottom abscissa. The corresponding position of stations sampled in approximately 100, 400, 800 and 1000 m water depth or greater are indicated by the top abscissa labels 'sf' for shelf, 'us' for the upper slope, 'ms' for the mid slope and 'off' for offshore stations, respectively.

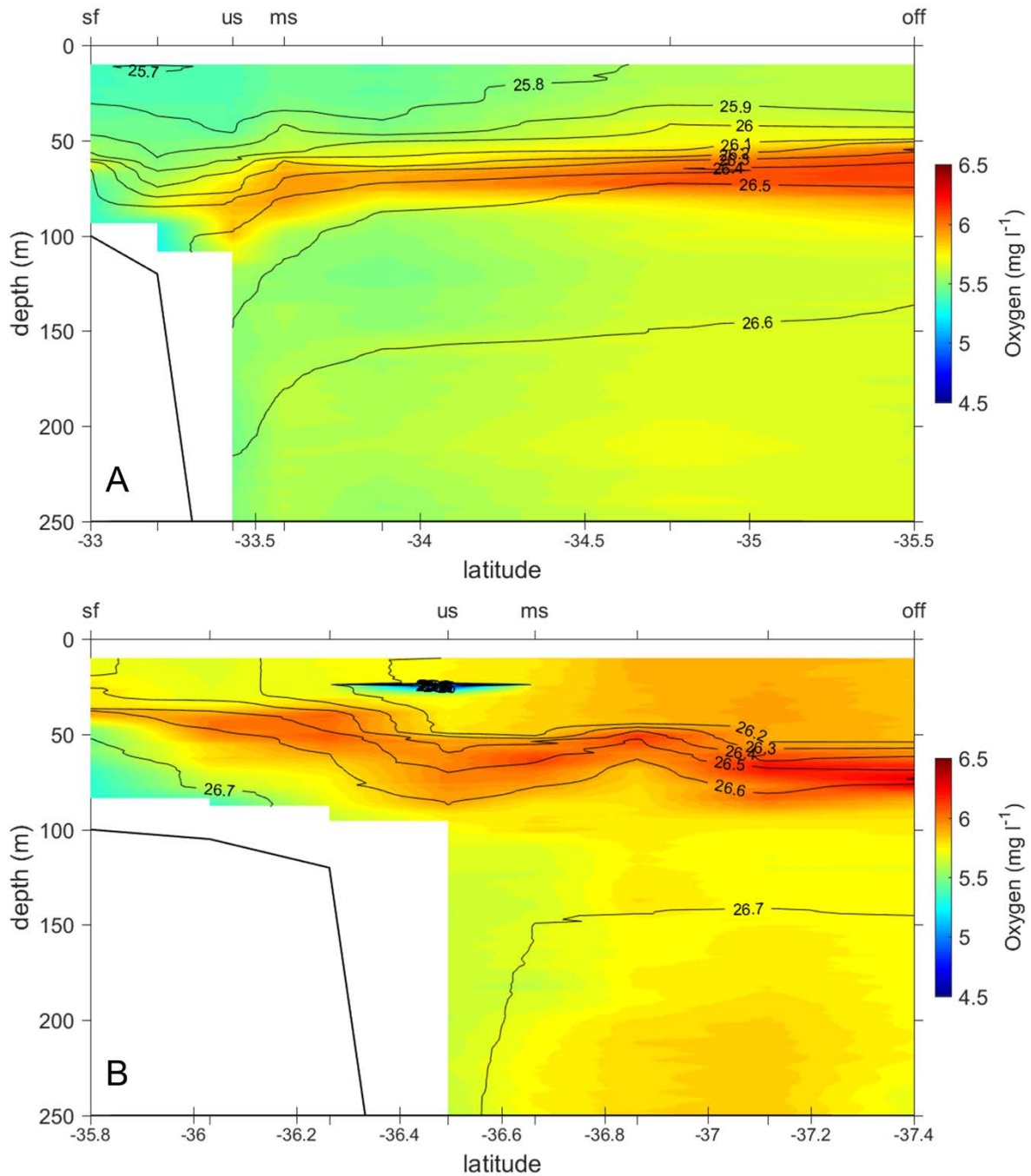


Figure 3.2-5 Results from the observational transects constructed from CTD profiles showing the vertical distribution of dissolved oxygen (mg l<sup>-1</sup>) to depths of 250 m for (A) the central GAB, and (B) the eastern GAB. Contours show lines of potential density ( $\sigma_t$ , kg m<sup>-3</sup>). The locations of stations shown in Figure 3.1-2 are marked as small ticks along the top and bottom abscissa. The corresponding position of stations sampled in approximately 100, 400, 800 and 1000 m water depth or greater are indicated by the top abscissa labels 'sf' for shelf, 'us' for the upper slope, 'ms' for the mid slope and 'off' for offshore stations, respectively.

### Mixing processes

To clarify the role of mixing processes, including the potential for double-diffusive convection, the strength of the competing temperature and salinity gradients, expressed by the Turner angle was calculated by Ruddick, (1983)

$$Tu = \arctan\left[\left(\beta \frac{\partial S}{\partial z} + \alpha \frac{\partial \theta}{\partial z}\right) / \left(\beta \frac{\partial S}{\partial z} - \alpha \frac{\partial \theta}{\partial z}\right)\right] \quad (1)$$

where  $\alpha$  is the thermal expansion coefficient,  $\beta$  is the haline contraction coefficient,  $\partial\theta/\partial z$  is the mean vertical gradient of potential temperature and  $\partial S/\partial z$  is that for salinity.

When  $45^\circ < Tu < 90^\circ$  the thermohaline stratification is favourable for salt-fingering and when  $-45^\circ < Tu < -90^\circ$  for double-diffusive convection. Salt-fingering is a form of double-diffusive instability that arises when an unstable vertical salinity gradient is stabilised by temperature given the molecular diffusion of heat is approximately 100 times greater than salt (Stern and Turner, 1969).

Cross-shelf variations in the 4-m average Turner angle indicate the high potential for salt-fingering in both the central and eastern GAB (Figure 3.2-6). Salt-fingering favourable  $Tu$  accounted for 75 % of the water column to 800 m depth in the central GAB and was strongly salt-fingering favourable ( $75^\circ < Tu < 90^\circ$ ) at depths between 250 and 500 m in waters extending offshore from the continental slope. In the eastern GAB, salt-fingering favourable  $Tu$  accounted for 45 % of the water column to 800 m depth, with regions most favourable observed at depths below 250 m offshore from the continental slope. Here, intermittent patches favourable for double-diffusion were observed at depth on the shelf and upper slope region in response to a reversal in the thermohaline gradients beneath the upwelled water mass (Figure 3.2-1 and Figure 3.2-2).

Considering the high potential for salt-fingering indicated by  $Tu$ , and in order to evaluate mixing processes, microstructure measurements of turbulent shear and temperature gradient were used to compute turbulent kinetic energy dissipation rates ( $\varepsilon$ ) and the microscale temperature dissipation rate ( $\chi$ ). A detailed description of the methods followed to process the shear and temperature microstructure data and the associated derivation of mixing parameters is presented in Ishizu et al., (2013).

In brief, assuming isotropic conditions (St. Laurent and Schmitt, 1999),  $\varepsilon$  was estimated from the shear spectrum as,

$$\varepsilon = 7.5\nu\langle u'^2_z \rangle \quad (2)$$

where the operator  $\langle \cdot \rangle$  is the ensemble average,  $\langle u'^2_z \rangle$  is the shear variance of the horizontal small-scale velocity and  $\nu$  is the kinematic viscosity (Tennekes and Lumley, 1972).

The shear variance over 4-m Sections was calculated by integrating the power spectra of the velocity shear between 1 cycle per minute (cpm) and half the Kolmogorov wavenumber. A correction was made to recover the unresolved variance in the high wavenumber region using the Nasmyth empirical spectrum (Oakey, 1982). Resulting  $\varepsilon$  values for each shear probe were quality screened and, where appropriate, averaged. The noise level for  $\varepsilon$  was approximately  $1.0 \times 10^{-10} \text{ W kg}^{-1}$  (Wolk et al., 2002).

Similarly, assuming local isotropy,  $\chi$  was estimated as (Osborn and Cox, 1972),

$$\chi = 6\kappa_T\langle T'^2_z \rangle \quad (3)$$

where  $\kappa_T$  is the molecular thermal diffusivity equal to  $1.4 \times 10^{-7} \text{ m}^2 \text{ s}^{-1}$  and  $\langle T'^2_z \rangle$  is the variance of the vertical small-scale temperature gradient. The variance of the temperature gradient data was initially calculated by integrating the power spectra between 1 cpm and the Batchelor wavenumber for each corresponding 4-m Section. An improved estimate of  $\chi$  was then determined by re-selecting an upper wavenumber limit below the region where electronic noise influences the integration. A

correction was made to recover the unresolved variance in the high wavenumber region using the Batchelor empirical spectrum (Dillon and Caldwell, 1980). The noise level for  $\chi$  was approximately  $1.0 \times 10^{-12} \text{ C}^2 \text{ s}^{-1}$  (Wolk et al., 2002).

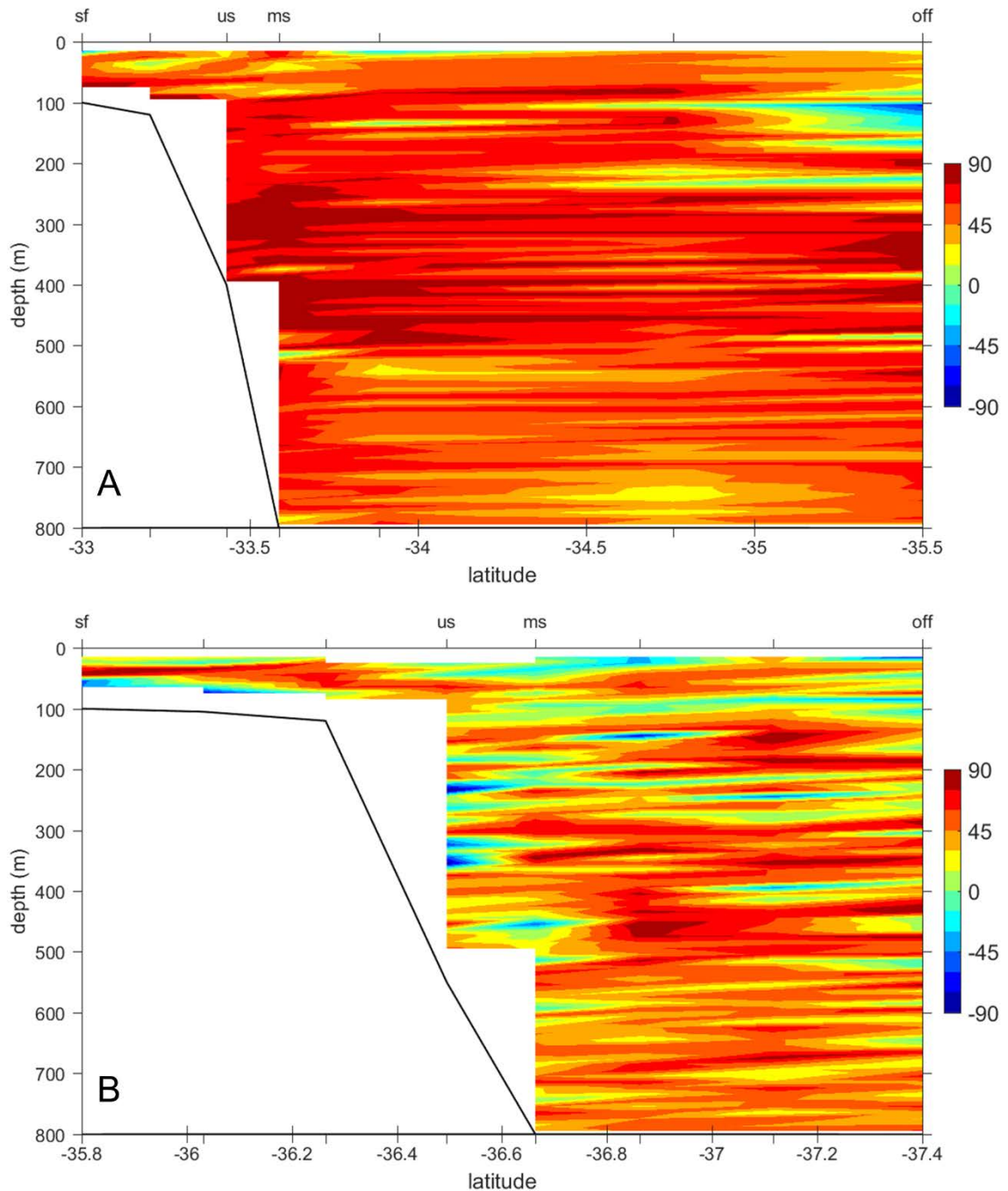


Figure 3.2-6 Results from the observational transects constructed from CTD profiles showing the vertical distribution of the Turner angle (degrees) to depths of 250 m for (A) the central GAB, and (B) the eastern GAB. Contours show lines of potential density ( $\sigma_\theta$ ,  $\text{kg m}^{-3}$ ). The locations of stations shown in Figure 3.1-2 are marked as small ticks along the top and bottom abscissa. The corresponding position of stations sampled in approximately 100, 400, 800 and 1000 m water depth or greater are indicated by the top abscissa labels 'sf' for shelf, 'us' for the upper slope, 'ms' for the mid slope and 'off' for offshore stations, respectively.

Figure 3.2-7 shows an example of the high-resolution hydrographic, shear and temperature microstructure data collected at the mid-shelf station in the eastern GAB. Corresponding estimates



of  $\varepsilon$  and  $\chi$ , derived from the microstructure shear and temperature gradient data, are shown. Microstructure shear data are weaker below the surface mixed layer resulting with  $\varepsilon$  values of the order  $10^{-9} \text{ W kg}^{-1}$ . Elevated one-sided temperature gradient microstructure was observed below the mixed layer in association with sharp vertical microscale temperature gradients and resulted in elevated  $\chi$  values of the order  $10^{-7} \text{ }^\circ\text{C}^2 \text{ s}^{-1}$ .

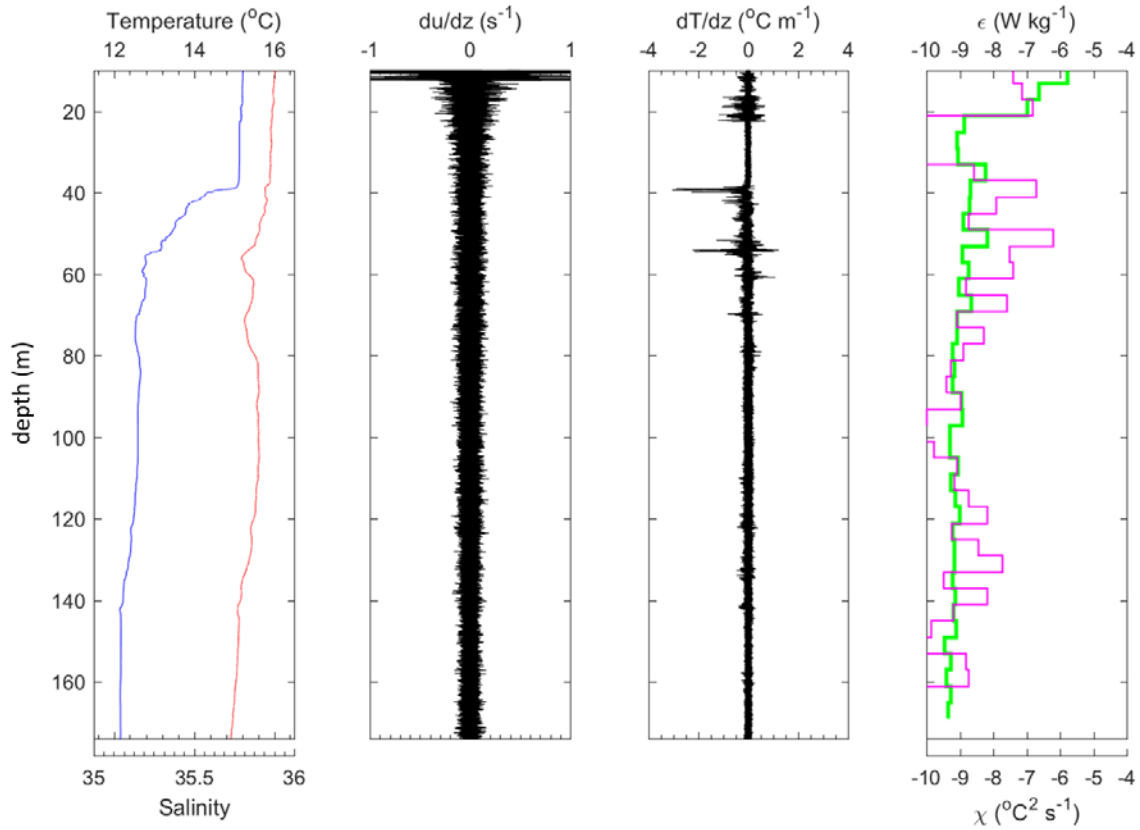


Figure 3.2-7 Representative microstructure profile taken mid-slope in the eastern GAB in approximately 800 m water depth. Profiles are shown of (from left to right): (1) high-resolution temperature ( $^\circ\text{C}$ ) and salinity, (2) shear ( $du'/dz$ ,  $\text{s}^{-1}$ ), (3) temperature gradient ( $dT'/dz$ ,  $^\circ\text{C m}^{-1}$ ) and (4) the kinetic energy dissipation rate,  $\varepsilon$  ( $\text{W kg}^{-1}$ ) (green line) and thermal dissipation rate,  $\chi$  ( $^\circ\text{C}^2 \text{ s}^{-1}$ ) (grey line) in logarithm scale.

Cross shelf distributions (Figure 3.2-8) showed that the largest values of  $\varepsilon$  at  $\sim 10^{-7}$  to  $10^{-5} \text{ W kg}^{-1}$  were commonly found within the surface mixed layer (50 m depth or less) in both the central and eastern GAB. Due to strong stratification at the base of the surface mixed layer (Figure 3.2-1 and Figure 3.2-2), reduced  $\varepsilon$  values typically ranging between approximately  $10^{-9}$  to  $10^{-8} \text{ W kg}^{-1}$  were observed below the surface mixed layer on the slope and in open-ocean waters and were of similar magnitude in the east and central GAB. On the shelf, values of  $\varepsilon$  at  $\sim 10^{-7} \text{ W kg}^{-1}$  in the eastern GAB generally exceeded those observed in the central GAB by over an order of magnitude.

Values of  $\chi$  were generally largest at  $\sim 10^{-7} - 10^{-6} \text{ }^\circ\text{C}^2 \text{ s}^{-1}$  at depths of 40 – 60 m in both the central and eastern GAB and were associated with the strong temperature gradients present at the base of the surface mixed layer (thermocline) across both transects (Figure 3.2-1 and Figure 3.2-7). Increased variability in  $\chi$  was observed relative to  $\varepsilon$  at the slope and offshore in open-ocean waters for both transects. At slope and offshore stations in the central GAB,  $\chi$  was regularly observed to be larger than corresponding  $\varepsilon$  estimates, particularly at depths below 50 m (Figure 3.2-6). These increased measures of  $\chi$  were associated with strong vertical gradients in temperature and are indicative of potential salt-fingering.

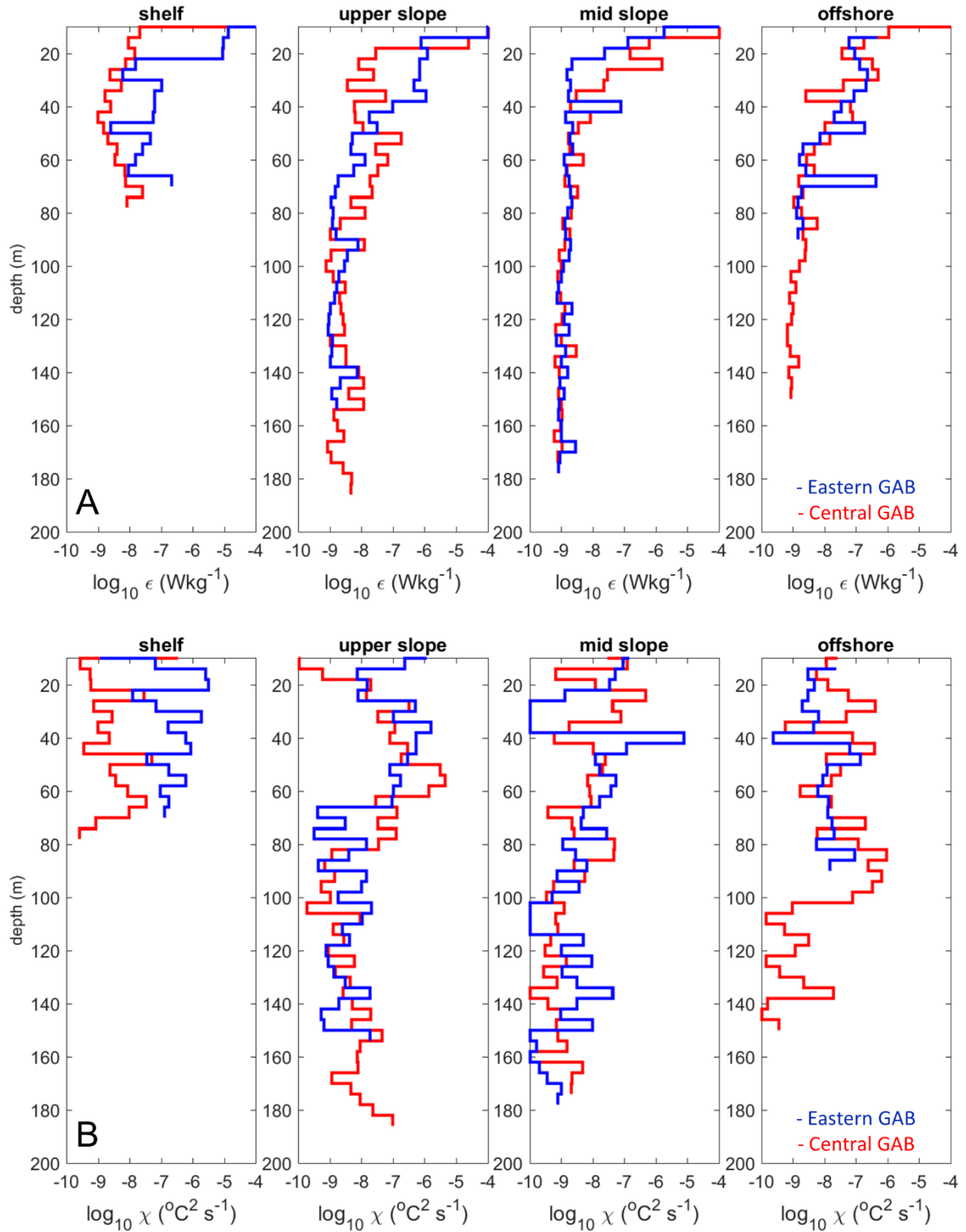


Figure 3.2-8 Representative profiles of (A) the kinetic energy dissipation rate,  $\epsilon \text{ (W kg}^{-1}\text{)}$  and (B) thermal dissipation rate  $\chi \text{ (}^{\circ}\text{C}^2 \text{ s}^{-1}\text{)}$  in logarithm scale. Red lines are for the central Great Australian Bight (GAB) and blue lines for the eastern GAB. The position of stations where microstructure profiles were taken in approximately 100, 400, 800 and 1000 m water depth or greater are indicated by the labels 'shelf', 'upper slope', 'mid slope' and 'offshore', respectively.



Large thermal dissipation rates and low turbulence suggest the onset of double diffusion (Inoue et al., 2007). To examine whether mechanical turbulence or double-diffusion was active we examined the dissipation ratio which provides a more direct measure of the dominant mixing process. The dissipation ratio is given by,

$$\Gamma = (\chi N^2) / (2\varepsilon(\partial\bar{\theta}/\partial z)^2) \quad (4)$$

where  $N^2 = g\alpha(\partial\bar{\theta}/\partial z)$  is the square of the buoyancy frequency and  $g$  is the acceleration due to gravity. Values of  $\Gamma$  greater than 1 indicate the dominance of double-diffusion and, conversely, values of  $\Gamma$  less than 1 indicate mechanical turbulent mixing is the dominant mixing process (Oakey, 1988). A comparison of estimated  $\Gamma$  and  $Tu$  values (Figure 3.2-9) shows that double diffusion is only likely to be active in a very small fraction (approximately 1 %) of the regions where  $Tu$  suggests salt-fingering favourable conditions. Hence, despite the thermohaline structure being favourable for double-diffusion, mechanical turbulence is likely to be the dominant mixing process influencing vertical diapycnal fluxes.

When mechanical turbulent mixing dominates, as indicated in Figure 3.2-8, the vertical eddy diffusivities for the different scalar variables (i.e. density  $K_\rho$ , heat  $K_\theta$ , and salt  $K_S$ ) are assumed to be the same. The vertical eddy diffusivity for density,  $K_\rho$ , can be estimated from (Osborn, 1980; Oakey, 1982; Oakey, 1985) as,

$$K_\rho = \Gamma \varepsilon / N^2 \quad (5)$$

where  $\Gamma$  is the observed dissipation ratio and  $N^2$  is the previously defined square of the buoyancy frequency.

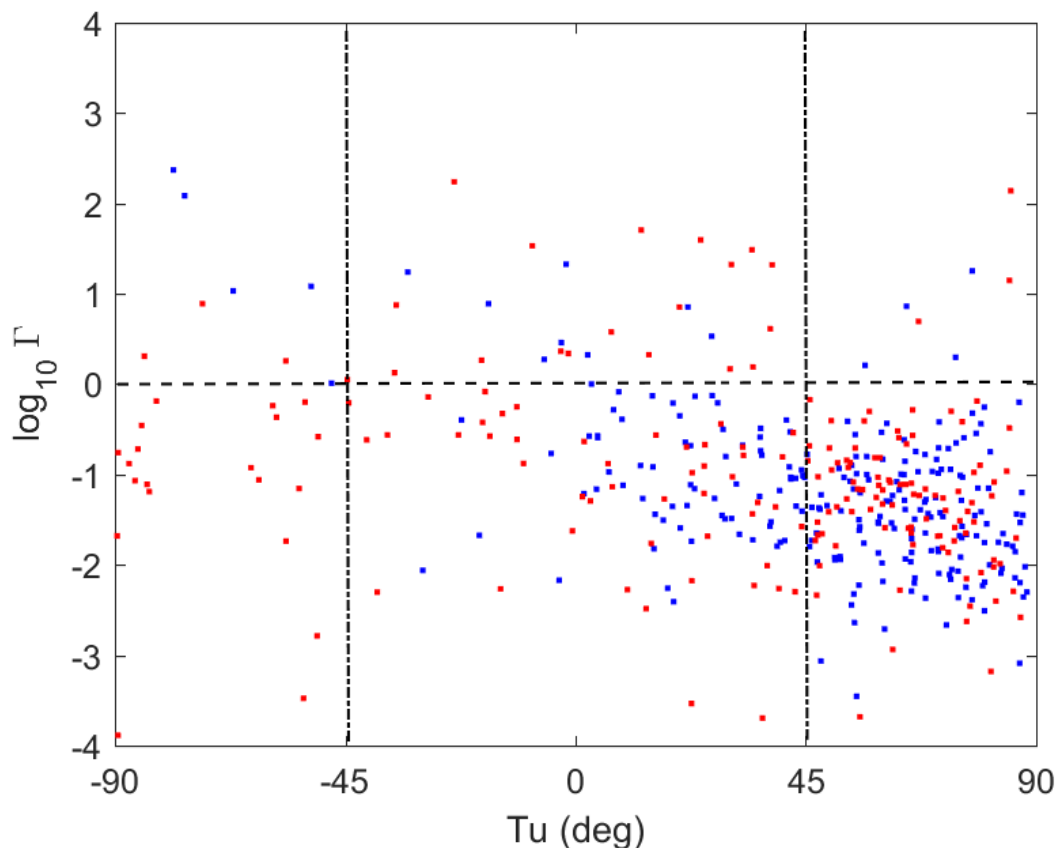


Figure 3.2-9 Scatter plot of the dissipation ratio ( $\Gamma$ ) versus the turner angle ( $Tu$ , degrees). Red dots are for the central Great Australian Bight (GAB) and blue dots for the eastern GAB.

Figure 3.2-10 plots the vertical distribution of  $K_\rho$  for representative profiles made at each station along transects in the central and eastern GAB. Due to intermittent nature of  $\varepsilon$ , the vertical distribution of  $K_\rho$  was also variable. The vertical eddy diffusivity of density showed large spatial variability, spanning six orders of magnitude ( $10^{-8}$  to  $10^{-2} \text{ m}^2 \text{ s}^{-1}$ ) in both the central and eastern GAB. Average  $K_\rho$  values of the order  $10^{-5} \text{ m}^2 \text{ s}^{-1}$  were observed in the pycnocline between  $\sigma_\theta = 26.2$ - $26.5 \text{ kg m}^{-3}$ . Below the base of the surface mixed layer (pycnocline) and approximately 180 m depth, average values of  $K_\rho$  of the order  $10^{-4} \text{ m}^2 \text{ s}^{-1}$  in the central GAB were approximately an order of magnitude smaller than those ( $10^{-3} \text{ m}^2 \text{ s}^{-1}$ ) measured in the eastern GAB.

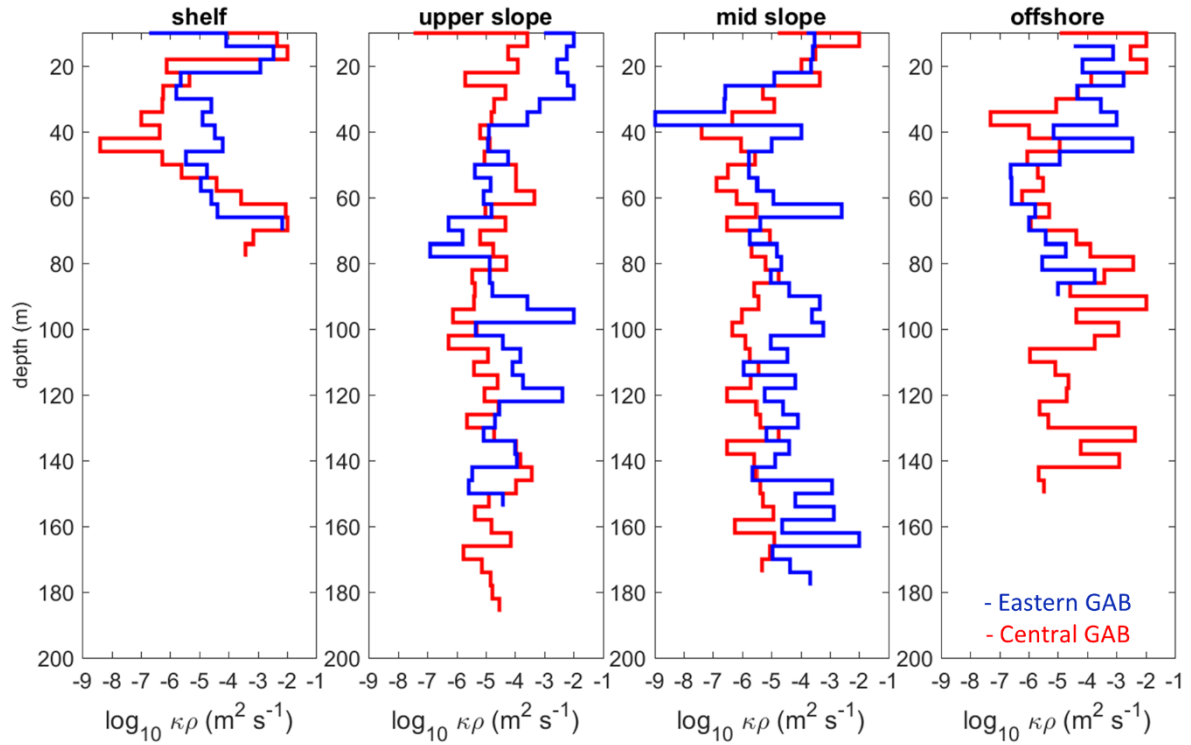


Figure 3.2-10 Representative profiles of the vertical eddy diffusivity of density,  $\kappa_\rho (\text{m}^2 \text{ s}^{-1})$  in logarithm scale. Red lines are for the central Great Australian Bight (GAB) and blue lines for the eastern GAB. The position of stations where microstructure profiles were taken in approximately 100, 400, 800 and 1000 m water depth or greater are indicated by the labels 'shelf', 'upper slope', 'mid slope' and 'offshore', respectively.

With knowledge of  $K_\rho$ , the mean vertical flux of  $\text{NO}_x$  can then be determined as,

$$\bar{F}_{\text{NO}_x} = -\kappa_\rho \partial \bar{C} / \partial z \quad (6)$$

where  $\bar{C}$  is the mean  $\text{NO}_x$  concentration and  $-\partial \bar{C} / \partial z$  is the mean vertical gradient of  $\text{NO}_x$  (upward is positive).

Surface water  $\text{NO}_x$  concentrations from water samples were very low ( $0.05 \mu\text{M}$  or less) down to 30 m depth along both transects, before increasing significantly across the pycnocline to approximately 1.9 and  $4.1 \mu\text{M}$  at 90 m depth in the central and eastern GAB, respectively (Figure 3.2-3).  $\text{NO}_x$  concentrations of approximately  $6 \mu\text{M}$  were observed at about 200 m depth in both the eastern and central GAB. Applying the above mentioned average vertical eddy diffusivities for the eastern and central GAB to the nutrient gradients observed between the base the mixed layer (approximately 50 m) and 100 m depth (approximate base of the euphotic zone) in each regions gives upward  $\text{NO}_x$

flux due to mechanical turbulent mixing of 0.32 and 2.70  $\mu\text{M m}^{-2} \text{d}^{-1}$  for the central and eastern GAB, respectively. As expected, variability in  $K_p$  and nutrient gradients, yielded equally variable flux estimates, with maximum  $\text{NO}_x$  fluxes of 1.04 and 15.38  $\mu\text{M m}^{-2} \text{d}^{-1}$  estimated for the central and eastern GAB, respectively.

In the context of regional upwelling (and downwelling) process which control the bulk advective transport of nutrients along isopycnal surfaces, turbulent mixing importantly transports nutrients across isopycnal surfaces. The abovementioned results, obtained at several locations crossing the slope, show a continuous, yet intermittent, upward flux of nutrients across euphotic zone to the base of the surface mixed layer (pycnocline) where they are readily used by phytoplankton.

To demonstrate the significance of the cross-isopycnal transport of nutrients, we compare the vertical displacements expected under advective upwelling and downwelling processes to those expected for turbulent diffusion. Another evaluation of the observed diffusivities on vertical displacement can be given by examining the spread of a point source of a passive scalar (e.g. nutrients). The root mean square vertical spread of a point source is given by,

$$\sigma = \sqrt{(2\kappa_p t)} \quad (7)$$

where  $t$  is time. For  $\kappa_p = 10^{-4}$  and  $10^{-3} \text{ m}^2 \text{s}^{-1}$ , and  $t = 30$  days a vertical spread of approximately 20 and 50 m is expected in the central and eastern GAB, respectively.

In the eastern GAB, advective transport due to upwelling is estimated to be approximately of 50 m per month (Petrusevics et al., 2011). For the central GAB, numerical experiments using the GAB ROMS model (Middleton et al., 2007) under summertime downwelling conditions show the vertical displacement of  $\text{NO}_x$  to be up to 100 m. This is demonstrated in Figure 3.2-11, where the CARS (annual average) vertical distribution of  $\text{NO}_x$  was incorporated into the ocean model for the entire domain as a passive scalar that is mixed and advected by the fully forced, “simulated” currents and diffusion for each January 15-25<sup>th</sup> period for the years 2011 to 2014. The results show that the initial nutrient distributions (the flat dashed curves) are either neutral or upwelled in places and for some years (e.g., 2014; 2011 at 150 m depth), but otherwise downwelled (e.g., 2011) in deep water (400 m depth) and by up to 100 m. These model results are generally consistent with the observed downwelling in the central GAB (Figure 3.1-11 and Figure 3.2-3). Here,  $\text{NO}_x$  concentrations observed offshore in open-ocean waters at 60 m depth are downwelled to approximately 100 m depth at the upper slope.

Hence, for the eastern GAB upward diffusive transports of 50 m over a month are comparable to advective transport due to upwelling. For the shelf slope and open-ocean regions of the central GAB, whilst downwelling is generally expected turbulent diffusion should at times and at some depths, appear to be a possible mechanism for nutrient supply.

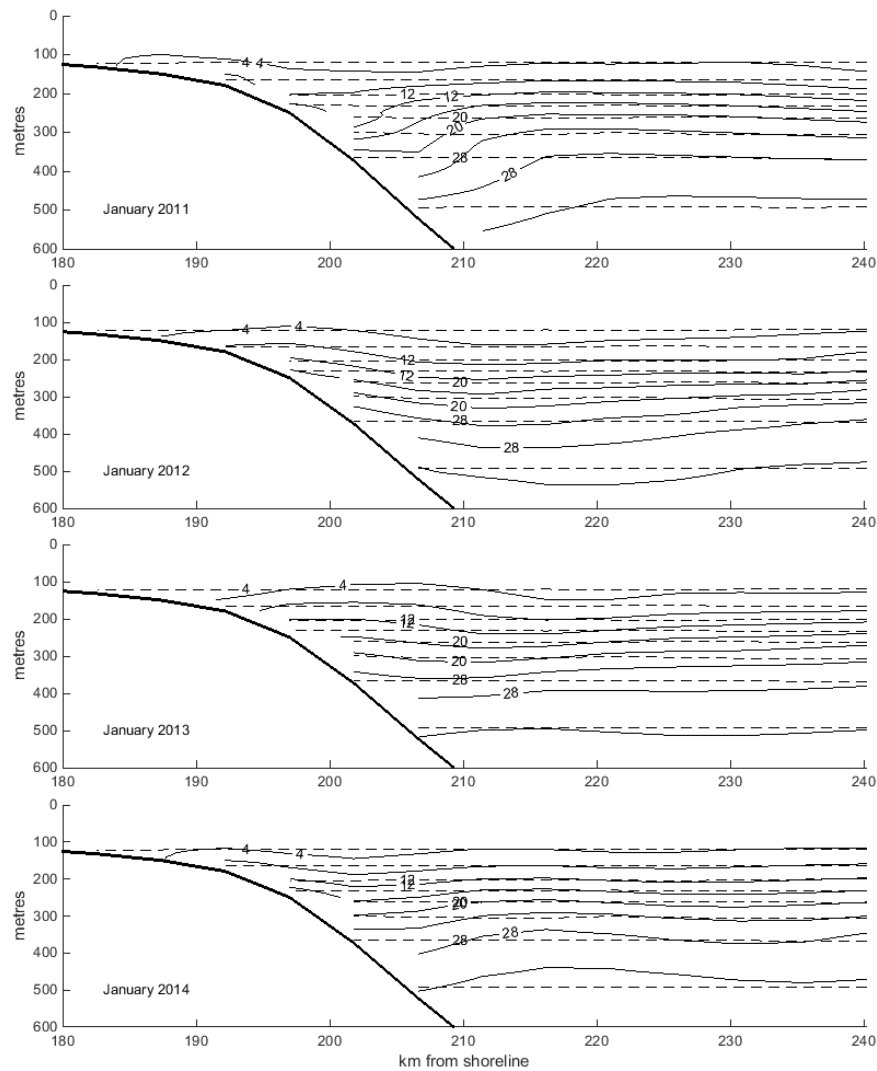


Figure 3.2-11 Simulated January cross-Sections of  $\text{NO}_x$  ( $\mu\text{M}$ ) at  $130.7^\circ\text{E}$ , at two times separated by ten days. Dashed: day 0. Solid: day 10.

### 3.2.4 Summary

Hydrographic and microstructure observations were made along two cross shelf transects under conditions in the eastern and central GAB. For the eastern GAB, nutrient rich water was upwelled from the shelf break on to the shelf. For the central GAB, downwelling was observed to depths of 250 m at the shelf slope. In response to upwelling and downwelling processes, the distribution of chlorophyll fluorescence was characterised by a subsurface maximum band located at depths between approximately 45 and 75 m in the eastern GAB, consistent with previous observations of a subsurface chlorophyll maxima in the area (Kämpf et al., 2004; McClatchie et al., 2006). Slightly lower peak fluorescence concentrations were observed in the central GAB and the depth of fluorescence maximum band was located at depths between 60 and 110 m. For both regions, the concurrent positioning of the fluorescence and oxygen maximums (Figure 3.2-4 and Figure 3.2-5) in relation to the strong vertical gradient in nutrients (Figure 3.2-3) suggests that nitrogen is removed from the water by photosynthesis occurring at the subsurface fluorescence maximum.

Hydrographic measurements showed the existence of a shallow warm, salty surface layer overlying a cool, fresher water across the GAB. As a consequence of the competing temperature and salinity gradients, unstable conditions indicated by the distribution of the Turner angle (Figure 3.2-6), demonstrated a high potential for double-diffusive mixing. To evaluate whether turbulent mixing or

double-diffusive convection dominated the mixing of water masses and vertical tracer fluxes, direct measurements of microscale shear and temperature gradient were made (Figure 3.2-8). Although measures of the turbulent kinetic dissipation rate ( $\epsilon$ ) and thermal dissipation rate ( $\chi$ ) did not always show corresponding magnitudes, calculation of the dissipation ratio showed that mechanical turbulent mixing was the dominant mixing process at the time of the study (Figure 3.2-9).

Considering the present study was conducted during the early onset of the summer season, our findings suggest double-diffusive mixing processes, particularly in the central GAB, may become an increasingly important process later in summer when the strength of competing temperature and salinity gradients increase.

Estimates of the vertical turbulent eddy diffusivity were found to be highly variable in space (Figure 3.2-10), spanning six orders of magnitude, with average values of the order  $10^{-4} \text{ m}^2 \text{ s}^{-1}$  and  $10^{-3} \text{ m}^2 \text{ s}^{-1}$  below the base of the pycnocline to approximately 180 m depth in the central and eastern GAB, respectively. The observed values are consistent with values of turbulent diffusion typically measured in and below the ocean pycnocline (Thorpe, 2007) and in upwelling regions (Hales et al., 2005). Importantly, while the upwelling and downwelling circulation experienced across the region is responsible for the advection of nutrients on- and offshore, turbulent diffusion provides a persistent, predominantly upward cross-diapycnal flux to the euphotic zone with average estimates of 1.04 and 15.38  $\mu\text{M NO}_x \text{ m}^{-2} \text{ d}^{-1}$  estimated for the central and eastern GAB, respectively.

In conclusion, our results suggest that the increased phytoplankton levels (Figure 3.2-4) observed below the surface mixed layer in the GAB during summer are largely controlled by vertical nutrient fluxes. In the eastern GAB, elevated nutrient fluxes resulting from both enhanced turbulent diffusion and wind-driven upwelling are likely to play an important role in influencing and enhancing the local primary productivity (van Ruth et al., 2010). Our results also suggest turbulence may potentially play an important role in the central GAB by supporting the vertical transport of nutrients from deep waters on the shelf slope and offshore to the euphotic zone where downwelling dominates.

This study presents the first study of the interaction between upwelling/downwelling and turbulence in the GAB. As the findings presented here are limited to two transects being representative of a wide area taken over a short sampling period, future studies may be improved by examining the variability of vertical nutrient fluxes and its relationship to phytoplankton dynamics over broader temporal and spatial scales.

## References

- Dillon, T. M., and Caldwell, D. R. 1980. The Batchelor spectrum and dissipation in the upper ocean. *Journal of Geophysical Research: Oceans*, 85: 1910-1916.
- Doubell, M. J., Yamazaki, H., Li, H., and Kokubu, Y. 2009. An advanced laser-based fluorescence microstructure profiler (TurboMAP-L) for measuring bio-physical coupling in aquatic systems. *Journal of plankton research*, 31: 1441-1452.
- Dugdale, R., and Goering, J. 1967. Uptake of new and regenerated forms of nitrogen in primary productivity. *Limnology and oceanography*, 12: 196-206.
- Glessmer, M. S., Oschlies, A., and Yool, A. 2008. Simulated impact of double-diffusive mixing on physical and biogeochemical upper ocean properties. *Journal of Geophysical Research: Oceans*, 113: C08029: doi:10.1029/2007JC004455.
- Hales, B., Moum, J. N., Covert, P., and Perlin, A. 2005. Irreversible nitrate fluxes due to turbulent mixing in a coastal upwelling system. *Journal of Geophysical Research: Oceans*, 110: C10S11: doi:10.1029/2004JC002685.
- Inoue, R., Yamazaki, H., Wolk, F., Kono, T., and Yoshida, J. 2007. An estimation of buoyancy flux for a

- mixture of turbulence and double diffusion. *Journal of Physical Oceanography*, 37: 611-624.
- Ishizu, M., Kitade, Y., and Michida, Y. 2013. Mixing process on the northeast coast of Hokkaido in summer. *Journal of oceanography*, 69: 1-13.
- Kämpf, J., Doubell, M., Griffin, D., Matthews, R., L., and Ward, T. M. 2004. Evidence of a large seasonal coastal upwelling system along the southern shelf of Australia. *Geophysical Research Letters*, 31: doi:10.29/2003GL019221.
- McClatchie, S., Middleton, J. F., and Ward, T. M. 2006. Water mass analysis and alongshore variation in upwelling intensity in the eastern Great Australian Bight. *Journal of Geophysical Research: Oceans*, 111: doi:10.1029/2004JC002699.
- Middleton, J. F., Arthur, C., Van Ruth, P., Ward, T. M., McClean, J. L., Maltrud, M. E., Gill, P., et al. 2007. El Nino effects and upwelling off South Australia. *Journal of Physical Oceanography*, 37: 2458-2477.
- Middleton, J. F., James, N. P., James, C., and Bone, Y. 2014. Cross-shelf seawater exchange controls the distribution of temperature, salinity, and neritic carbonate sediments in the Great Australian Bight. *Journal of Geophysical Research: Oceans*, 119: 2539-2549.
- Middleton, J. F., and Platov, G. 2003. The mean summertime circulation along Australia's southern shelves: a numerical study. *Journal of Physical Oceanography*, 33: 2270-2287.
- Oakey, N. 1982. Determination of the rate of dissipation of turbulent energy from simultaneous temperature and velocity shear microstructure measurements. *Journal of Physical Oceanography*, 12: 256-271.
- Oakey, N. 1985. Statistics of mixing parameters in the upper ocean during JASIN Phase 2. *Journal of Physical Oceanography*, 15: 1662-1675.
- Oakey, N. S. 1988. Estimates of mixing inferred from temperature and velocity microstructure. *Elsevier oceanography series*, 46: 239-247.
- Osborn, T. 1980. Estimates of the local rate of vertical diffusion from dissipation measurements. *Journal of Physical Oceanography*, 10: 83-89.
- Osborn, T. R., and Cox, C. S. 1972. Oceanic fine structure. *Geophysical & Astrophysical Fluid Dynamics*, 3: 321-345.
- Oschlies, A., Dietze, H., and Kähler, P. 2003. Salt-finger driven enhancement of upper ocean nutrient supply. *Geophysical Research Letters*, 30: 2204: doi:2210.1029/2003GL018552.
- Petrusevics, P., Bye, J., Luick, J., and Teixeira, C. E. 2011. Summer sea surface temperature fronts and elevated chlorophyll-a in the entrance to Spencer Gulf, South Australia. *Continental Shelf Research*, 31: 849-856.
- Ruddick, B. 1983. A practical indicator of the stability of the water column to double-diffusive activity. *Deep Sea Research Part A. Oceanographic Research Papers*, 30: 1105-1107.
- St. Laurent, L., and Schmitt, R. W. 1999. The contribution of salt fingers to vertical mixing in the North Atlantic Tracer Release Experiment. *Journal of Physical Oceanography*, 29: 1404-1424.
- Stern, M. E., and Stewart Turner, J. 1969. Salt fingers and convecting layers. *Deep Sea Research and Oceanographic Abstracts*, 16: 497-511.
- Tennekes, H., and Lumley, J. L. 1972. *A first course in turbulence*, MIT press.
- Thorpe, S. A. 2007. *An introduction to ocean turbulence*, Cambridge University Press.



- van Ruth, P. D., Ganf, G. G., and Ward, T. M. 2010. Hot-spots of primary productivity: an alternative interpretation to conventional upwelling models. *Estuarine, Coastal and Shelf Science*, 90: 142-158.
- Wolk, F., Yamazaki, H., Seuront, L., and Lueck, R. G. 2002. A new free-fall profiler for measuring biophysical microstructure. *Journal of Atmospheric and Oceanic Technology*, 19: 780-793.

## 4. MICROBES AND PLANKTON

### 4.1 Community composition and size structure

Nicole Patten and Paul van Ruth

#### 4.1.1 Introduction

The size structure and composition of plankton communities have important implications for the flow of carbon through marine systems and ultimately, ecosystem function (Marañón, 2009). The relative abundance of small and large phytoplankton influence the amount of material either recycled within the euphotic zone, transferred to higher trophic levels or loss via sedimentation (Legendre and Rassoulzadegan, 1996). For example, small phytoplankton dominate in oligotrophic waters due to their high surface area to volume ratios. At these times, tight coupling occurs between picophytoplankton, bacteria and their protist grazers leading to complex interactions and the recycling of nutrients within the microbial food web (Azam, 1983). The high rates of respiration and the multiple steps through relatively small planktonic organisms sees the microbial food web as the most inefficient route for carbon transfer toward higher trophic levels (Legendre and Rassoulzadegan, 1995). Viral lysis of bacteria (and picophytoplankton) and subsequent release of bacterial derived dissolved organic matter further add to tight coupling and nutrient recycling within the microbial food web (Fuhrman, 1999; Suttle, 2007). In contrast, large phytoplankton dominate in waters subject to nutrient enrichment (e.g. via upwelling) due to their capacity for nutrient storage and ability to outcompete the often saturated growth rates of smaller phytoplankton (Barber and Hiscock, 2006; Finkel, 2001). Under these conditions, simpler trophic pathways from diatoms to zooplankton to fish (i.e. the classical food web (Ryther, 1969)) permit more efficient transfer of carbon to higher trophic levels.

The Great Australian Bight (GAB) is a region supporting a large and valuable proportion of Australia's total fishery production (Ward et al., 2006) and has global conservation significance for resident and migratory apex predators (Rogers et al., 2013). However, there is limited information on the planktonic communities supporting this production (reviewed in Rogers et al. 2013). In the eastern GAB, coastal upwelling processes occurring during the austral summer are known to promote elevated phytoplankton biomass and primary production (Kämpf et al., 2004; McClatchie et al., 2006; van Ruth et al., 2010a; van Ruth et al., 2010b) resulting in enhanced biomass of zooplankton and small pelagic fish (Ward et al., 2006; van Ruth and Ward, 2009). It is predicted that under these conditions, a large fraction of the biomass is attributed to large phytoplankton and trophic pathways most closely reflect a classical food web. The central GAB region is not influenced by the localised upwelling processes occurring to the east; instead, downwelling processes are thought to occur year round (Middleton and Bye, 2007). Under these oligotrophic conditions, it is predicted that small phytoplankton and bacteria (and viruses) dominate. Similarly, under periods of downwelling in the eastern GAB, a microbial food web is predicted to be the dominant trophic pathway.

The first detailed set of studies on the lower trophic food web in eastern GAB shelf waters showed a shift from a system dominated by small ( $< 1 \mu\text{m}$ ) autotrophic prokaryotes (*Prochlorococcus* and *Synechococcus*) during periods of downwelling, towards one with increased abundances of unicellular picoeukaryotes ( $\sim 1 - 2 \mu\text{m}$ ) in waters influenced by upwelling (van Dongen-Vogels et al., 2011; van Dongen-Vogels et al., 2012). A decrease in *Synechococcus* and picoeukaryotes abundances occurred with distance from the shelf during an upwelling event in the eastern GAB, concomitant with highest nutrient concentrations and phytoplankton biomass at the chlorophyll fluorescence

maximum on the shelf (Paterson et al., 2013b). *Prochlorococcus*, bacteria and viruses however exhibited variable distributions from the shelf to offshore waters (Paterson et al., 2013b). A 2 year study with ~ seasonal sampling on the shelf in the eastern GAB showed using pigment data, that cryptophytes, chlororophytes, prymnesiophytes and diatoms were dominant groups contributing to autotrophic biomass (Thompson et al., 2011). These results indicated the importance of (2 – 20  $\mu\text{m}$ ) and microphytoplankton (20 – 200  $\mu\text{m}$ ) in eastern GAB shelf waters. Large scale satellite derived estimates of picoplankton (< 2  $\mu\text{m}$ ), nanoplankton and microplankton confirm this, with nanoplankton estimated to represent a significant (~ 50%) fraction of the averaged total phytoplankton biomass in the GAB (Rogers et al., 2013).

Much less is known of the central GAB autotrophic community structure. The only study known focusing on the microbial food web (picophytoplankton, bacteria and viruses) in the central GAB, showed enhanced picophytoplankton biomass (due to picoeukaryotes) in slope waters; and decreasing picophytoplankton biomass and cell abundances with distance from the shelf to offshore waters (SARDI unpublished data). Contributions of each of pico-, nano- and micro-phytoplankton fractions, and further details of the phytoplankton community composition are not known in the central GAB beyond large scale satellite derived estimates (Rogers et al., 2013). Information on the consumers of the different size fractions of phytoplankton is further limited in the central GAB, but the occurrence of high abundances of micronekton and crustaceans at the shelf break (Young et al., 1999) does not match entirely with the prediction of the dominance of small cells, where carbon transfer to higher trophic levels would be limited.

This work aims to address current gaps in our knowledge of planktonic communities in the GAB, by determining the abundance and biomass of planktonic organisms from viruses through the mesozooplankton, in shelf, slope and offshore waters of the central and eastern GAB. The overarching hypothesis is that a microbial food web dominates in waters off the continental shelf in the GAB, particularly in the central GAB where downwelling conditions occur year-round, and that the classical food web operates only under nutrient enrichment (via upwelling) in the eastern GAB. Given the forcing of nutrient resources and/or physical drivers on phytoplankton size and community structure for coastal through to ocean waters worldwide (Marañón et al., 2012; 2015) environmental drivers of planktonic communities in the GAB are further investigated.

### 4.1.2 Methods

#### Study area, CTD transects and water sampling

Sampling was conducted at the start of the austral summer (late November through to mid-December) in 2015 across two shelf to offshore transects (Figure 4.1-1), one in the central GAB (Transect 2; T2) and one in the eastern GAB (Transect 6; T6) on board the *RV Investigator*. Four stations were sampled along each transect representing the shelf (bottom depth ~ 90 – 100 m), upper slope (bottom depth ~ 400 m), mid slope (bottom depth ~ 800 m) and offshore waters (bottom depth ~ 3000 - 5000 m) (Table 4.1-1). Day and night sampling occurred at the upper slope and offshore stations (Table 4.1-1).

Vertical profiles of temperature, salinity, fluorescence and dissolved oxygen were obtained at each station (down to ~ 10 - 20 m above the bottom; except for deeper (> 800 m) water stations where profiles were taken to ~ 800 m) using a Seabird SBE 9+ Conductivity-temperature-depth (CTD) instrument, which was fitted with an oxygen (SBE43) and fluorescence sensor (Chelsea).

Seawater was sampled at three depths for a range of biological parameters (see below); 10 m 'surface', at the chlorophyll fluorescence maximum (cmax) (as determined from *in situ* fluorescence profiles), and at 120 m (deep), using 12 L Niskin bottles mounted on a rosette. Deep samples at shelf stations were collected at ~90 m. Additional depths, spanning within and below the photic zone were also sampled for dissolved nutrients.

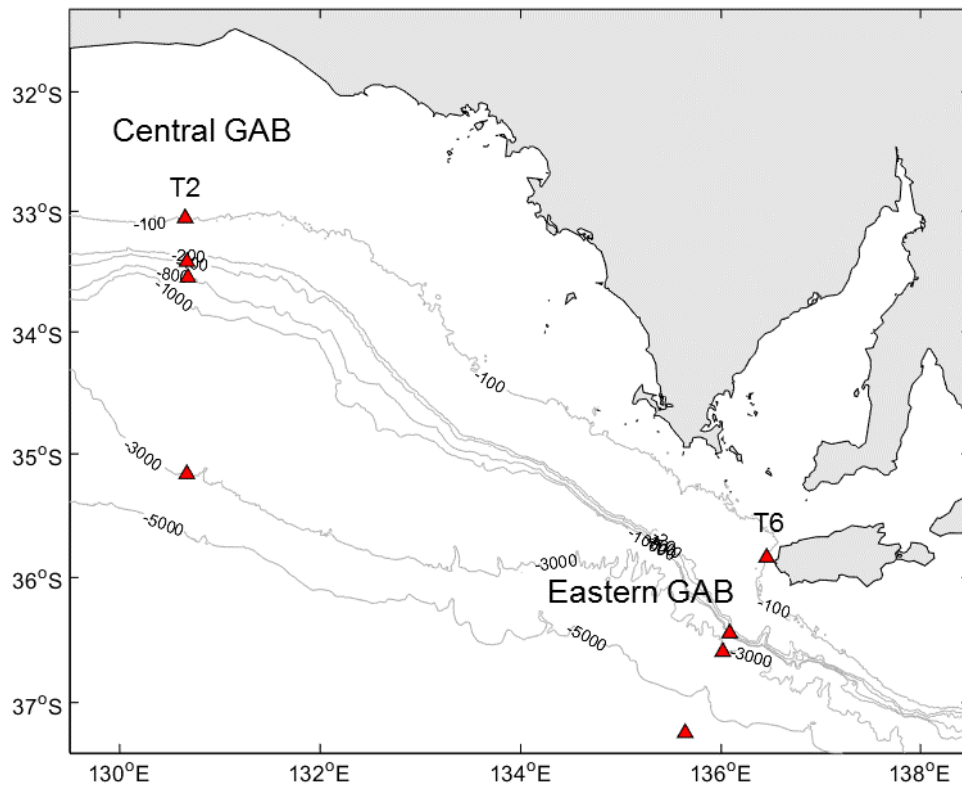


Figure 4.1-1 Location of the study area in the Great Australian Bight (GAB). Transect 2 (T2) is located in the central GAB and Transect 6 (T6) is located in the eastern GAB. Red triangles represent stations on each transect on the shelf, upper slope, mid slope and offshore.

## Microbes and plankton

Table 4.1-1 Bio-chemical sampling overview for the central (Transect 2) and eastern (Transect 6) Great Australian Bight (GAB).

Parameter	Depth	Transect 2 - Central GAB							Transect 6 - Eastern GAB						
		C-Sf-D	C-Us-N	C-Us-D	C-Ms-N	C-Ms-D	C-Off-N	C-Off-D	E-Sf-N	E-Us-N	E-Us-D	E-Ms-N	E-Ms-D	E-Off-N	E-Off-D
Dissolved nutrients *	D1	×	×	×	×	×	×	×	×	×	×	×	×	×	×
	D2	×	×	×	×	×	×	×	×	×	×	×	×	×	×
	D3	×	×	×	×	×	×	×	×	×	×	×	×	×	×
Picophytoplankton	D1	×	×	×	×	×	×	×	×	×	×		×	×	×
	D2	×	×	×	×	×	×	×	×	×	×		×	×	×
	D3	×	×	×	×	×	×	×	×	×	×		×	×	×
Pigments < 5µm	D1	×	×	×		×	×	×	×	×	×		×	×	×
	D2	×	×	×		×	×	×	×	×	×		×	×	×
	D3	×	×	×		×	×	×	×	×	×		×	×	×
Pigments > 5µm	D1	×	×	×		×	×	×	×	×	×		×	×	×
	D2	×	×	×		×	×	×	×	×	×		×	×	×
	D3	×	×	×		×	×	×	×	×	×		×	×	×
Phytoplankton (> 5 µm)	D1	×		×		×		×	×		×		×		×
	D2	×		×		×		×	×		×		×		×
	D3	×		×		×		×	×		×		×		×
Bacteria/Virus	D1	×	×	×	×	×	×	×	×	×	×		×	×	×
	D2	×	×	×	×	×	×	×	×	×	×		×	×	×
	D3	×	×	×	×	×	×	×	×	×	×		×	×	×
Zooplankton (64 µm net) abundance and biomass	D1	×	×	×	×	×	×	×	×	×	×		×	×	×
	D2	×	×	×	×	×	×	×	×	×	×		×	×	×
	D3	×	×	×	×	×	×	×	×	×	×		×	×	×
Zooplankton (150 µm net) abundance and biomass	D1	×	×	×	×	×	×	×	×	×	×		×	×	×
	D2	×	×	×	×	×	×	×	×	×	×		×	×	×
	D3	×	×	×	×	×	×	×	×	×	×		×	×	×

\* Additional nutrient samples were also taken within and below the euphotic zone. Prefix 'C' refers to Central GAB and prefix 'E' refers to Eastern GAB. Sf = shelf; Us = upper slope; Ms = mid slope; Off = offshore. Suffix 'N' and 'D' refer to night and day sampling respectively.

### Nutrient analysis

Dissolved nutrients were analysed onboard using a Seal AA3HR segmented flow instrument. Detection limits were 0.02 µM for Nitrate + Nitrite, nitrite, ammonia and phosphate and 0.2 µM for silicate. Nitrate was determined by subtracting nitrite from nitrate + nitrite.

### Chlorophyll *a* and accessory pigments

Samples for chlorophyll *a* (chl *a*) and pigments were obtained by filtering 2 L sequentially through 5 µm and GF/F filters (nominal pore size ~ 0.7 µm) to provide a less than 5 µm fraction (< 5 µm), and a greater than 5 µm fraction (> 5 µm). Filters were stored at -80 °C prior to analysis. Pigments were analysed via the gradient elution procedure of Van Heukelem and Thomas (2001) on an Agilent 1200 series High Pressure Liquid Chromatography (HPLC) system in the environmental chemistry laboratory at the Aquatic Sciences division of the South Australian Research and Development Institute (SARDI).

Biomarker pigments were used to infer the distribution of dominant algal classes and functional groups. For the fractionated samples, total chl *a* (Tchl *a*) was calculated as the sum of chl *a*, divinyl chl *a* (DVchl *a*), chl *a* allomer and chl *a* epimer in the less than 5 µm fraction plus the greater than 5 µm fraction. Bio-marker pigments were then used to infer dominant algal classes and functional groups following Jeffrey (1997) (Table 4.1-2). Size fractionated pigment data provided additional information on the autotrophic community, particularly on the small nanophytoplankton, which are difficult to enumerate with flow cytometry and which are missed with traditional phytoplankton identification via microscopy given their small size.

Table 4.1-2 Characteristic pigments, pigment abbreviations and their representative algal taxa

Pigment	Abbreviation	Taxa
Chlorophyll <i>a</i>	chl <i>a</i>	all photosynthetic algae
Divinyl Chl <i>a</i>	DVchl <i>a</i>	prochlorophytes ( <i>Prochlorococcus</i> spp.)
Chlorophyll <i>b</i>	chl <i>b</i>	dominant in green algae (e.g. chlorophytes, euglenophytes, prasinophytes)
Zeaxanthin	zea	cyanobacteria (e.g. <i>Synechococcus</i> ); also prochlorophytes ( <i>Prochlorococcus</i> )
19'hexanoyloxyfucoxanthin	19Hex	prymnesiophytes; some dinoflagellates with endosymbionts)
19'butanoloxyfucoxanthin	19But	chrysophytes; some prymnesiophytes and some dinoflagellates with endosymbionts
Alloxanthin	allo	cryptophytes; also some dinoflagellates with endosymbionts
Peridinin	peri	photosynthetic dinoflagellates, except those containing endosymbionts of other algal classes
Fucoxanthin	fuco	diatoms; also Prymesioophytes, Chrysophytes and some dinoflagellates with endosymbionts
Prasinolanthin	pras	prasinophytes

Phytoplankton community size structure was further investigated according to the approach of Vidussi et al., (2001) and Uitz et al.,(2008). However, instead of identifying three size classes; pico (< 2 µm); nano (2 – 20 µm) and micro (> 20 µm), we modified the approach to further divide the nanoplankton into a 2 – 5 µm fraction and 5 – 20 µm fraction. To do this, pico and nano groups were first calculated from the < 5 µm fraction, according to the following equations:

$$pico = 0.86 \times Zea + 1.01 \times (chl\ b)$$

$$nano = 0.60 \times allo + 0.35 \times 19but + 1.27 \times 19hex$$



The micro fraction was assumed to equal zero. Next, the nano and micro fractions were calculated from the greater than 5 µm fraction using the equations:

$$\text{nano} = 0.60 \times \text{allo} + 0.35 \times \text{19but} + 1.27 \times \text{19hex}$$

$$\text{micro} = 1.41 \times \text{fuco} + 1.41 \times \text{Peri}$$

The weighted sum of the concentration of pigments for the two size fractions (wDP < 5 µm and wDP > 5 µm) were then calculated separately where:

$$\text{wDP} < 5 \mu\text{m} = 0.60 \times \text{allo} + 0.35 \times \text{19but} + 1.27 \times \text{19hex} + 0.86 \times \text{zea} + 1.01 \times (\text{Chl } b)$$

$$\text{wDP} > 5 \mu\text{m} = 1.41 \times \text{fuco} + 1.41 \times \text{peri} + 0.60 \times \text{allo} + 0.35 \times \text{19but} + 1.27 \times \text{19Hex}$$

The proportion of each of the four size groups were then calculated by dividing by their respective wDP.

### Picophytoplankton, bacteria and viruses

Triplicate samples for picophytoplankton were fixed in glutaraldehyde (0.25 % final concentration), and triplicate samples for bacteria and viruses were fixed in glutaraldehyde (0.5 % final concentration), in the dark for 15 minutes, quick frozen in liquid nitrogen and stored at - 80 °C until analysis. Picophytoplankton samples were thawed at 37 °C, 1 µm beads (Polysciences) added as an internal reference and samples analysed on a FACSVerse (Becton Dickinson) flow cytometer within 2 months of collection. Acquisition was run for 3 minutes on medium flow rate. Picophytoplankton groups were discriminated on the basis of red and orange auto fluorescence of chlorophyll and the accessory pigment phycoerythrin and light scatter properties of side-angle light scatter (SSC) and forward-angle light scatter (FSC), using the flow cytometry analysis software FlowJo®.

Bacteria and viruses were thawed as above, diluted 10 fold in Tris EDTA (pH = 8.0, Sigma-Aldrich), stained with SYBR I green ( $0.5 \times 10^{-4}$  final concentration, Molecular Probes) in the dark at 80°C for 10 minutes and then 1 µm fluorescent beads added an internal reference (Brussaard, 2004). Bacteria and viruses were analysed using the same flow cytometer as above with acquisition run for 2 minutes on a low flow rate. Bacteria and viruses were discriminated on the basis of green fluorescence, SSC and FSC using FlowJo® flow cytometry analysis software. Bacteria and viruses were separated on plots of side scatter (SSC) and green (SYBR) fluorescence and SSC and red (chl *a*) fluorescence. In deep samples, *Prochlorococcus* could clearly be discriminated from bacteria in SSC and red fluorescence plots (and SSC and green fluorescence), however in surface and SFM, *Prochlorococcus* often coincided within the bacteria group. To correct for this in the stained samples, *Prochlorococcus* were included within the bacterial group for all three depths in the analysis. Bacteria counts were then corrected for by subtracting total counts of *Prochlorococcus* (obtained from non-stained samples) from the bacteria group.

### Phytoplankton

Water samples (1 L) were preserved using Lugol's solution for phytoplankton taxonomy. Phytoplankton (> 5 µm) were identified by Microalgal services (<http://microalgal.com.au>) to lowest taxonomic resolution using standard taxonomic methods.

## Zooplankton

Zooplankton were collected via vertical tows spanning the upper 200 m of the water column (or upper ~ 100 m on the shelf). A bongo net (64  $\mu\text{m}$  and 150  $\mu\text{m}$  mesh nets) with a net mouth diameters of 30 cm was retrieved vertically at approximately 1  $\text{m s}^{-1}$ . General Oceanics flow meters were mounted in the net mouths. Upon retrieval, the contents of each net was split into two portions; one for biomass and one for identification. The biomass sample was filtered through pre-weighed 64  $\mu\text{m}$  47 mm diameter filters and frozen at -20 °C until analysis. The sample for identification was fixed in 5 % formalin. Filters for zooplankton biomass were oven dried at 60 °C for 24 hours, placed in a desiccator for 2 hours and filters were then re-weighed. Zooplankton biomass was then recorded as biomass ( $\text{mg m}^{-3}$ ) in the water column using the volume swept by the net, calculated as the distance travelled by the net multiplied by the area of the net mouth. In the laboratory, samples for identification were rinsed through a 35  $\mu\text{m}$  mesh sieve. Enumeration and identification of zooplankton was performed to lowest taxonomic level possible. Organism numbers were recorded as individuals  $\text{m}^{-3}$  in the water column using the volume swept by the net, as above.

## Data analysis.

All values reported in the text are means  $\pm$  standard error unless otherwise indicated. Multivariate analyses were performed in PRIMER Version 6 (PRIMER-E, Plymouth, UK). Abundances of viruses, bacteria and picophytoplankton subgroups were  $\log_{10}(x + 1)$  transformed and treated using the Gower metric similarity coefficient, which provides equal weighting when abundances vary by several orders of magnitude (Thomson et al. 2006). Pigment concentrations, phytoplankton and zooplankton abundances were fourth root transformed and Bray-Curtis distance measures applied.

Multidimensional scaling ordination (MDS) plots were used to visualise the autotrophic plankton community compositions (picophytoplankton, phytoplankton and pigments) between regions, locations and depths. PERMANOVA (Region x Depth) was used to statistically test differences in picophytoplankton, phytoplankton and pigment composition. A location test within and between the eastern and central GAB was not conducted given one location (shelf, upper slope, lower slope and offshore) was sampled within each region.

The BEST correlation-based procedure (PRIMER-E, Plymouth, UK) was applied to define the environmental variables (nitrate, nitrite, phosphate, silicate, ammonium, temperature, salinity, oxygen and chl *a* (where chl *a* was only used for non-autotrophic groups; i.e. bacteria/virus and zooplankton) best explaining patterns in biotic (bacteria/viruses, phytoplankton, pigments and zooplankton) matrices (Clarke and Warwick, 2001). The test was conducted by maximizing a Spearman rank correlation ( $\rho$ ) between the resemblance matrices of environmental variables (Euclidean distance) and the biological community structure (Gower or Bray-Curtis - outlined above). The significance of these results was tested using permutation tests, with  $P < 0.05$  considered to be statistically significant.

Pearson correlation coefficients,  $r$ , were also computed between individual virus, bacterial and picophytoplankton groups for each region (all data  $\log_{10}(x + 1)$  transformed).

### 4.1.3 Results

## Nutrients

The depth of the nutricline was approximately 25 m deeper in the central GAB than in the eastern GAB (Figure 4.1-2), sitting just below the  $c_{\text{max}}$  (i.e.  $c_{\text{max}}$ ; 40 – 75 m in the eastern GAB and 70 –

100 m in the central GAB – see Section 4.1-2). Nitrate + nitrite concentrations were close to or below detection ( $\sim 0.02 \mu\text{M}$ ) in surface waters in both the central and eastern GAB (Figure 4.1-2A – B). In the cmax, nitrate + nitrite were  $1.14 \pm 0.26 \mu\text{M}$  and  $2.58 \pm 0.57 \mu\text{M}$  in the central and eastern GAB respectively, while in deep water (120 m) concentrations were  $3.45 \pm 0.63 \mu\text{M}$  and  $4.48 \pm 0.42 \mu\text{M}$  respectively. Phosphate and silicate followed the same trend as nitrate + nitrite with higher concentrations occurring in the eastern GAB compared to the central GAB in the cmax (1.4-fold and 2.3-fold higher for phosphate and silicate respectively) and deep water (1.2-fold and 1.6-fold higher for phosphate and silicate respectively), but also in surface waters (1.7-fold and 1.3-fold higher for phosphate and silicate respectively) (Figure 4.1-2C – F). Relatively high concentrations of nitrate + nitrite, phosphate and silicate occurred in the cmax on the shelf in the eastern GAB compared to the central GAB (for e.g.  $3.23 \mu\text{M}$  versus  $0.252 \mu\text{M}$  for nitrate + nitrate respectively).

The difference between the central and eastern GAB was less apparent offshore with highest concentrations of nitrate + nitrite observed in deep water (at 120 m) in the central GAB (up to  $7.2 \mu\text{M}$ ) compared to the eastern GAB ( up to  $4.9 \mu\text{M}$ ) (Figure 4.1-2A – B). Between the shelf and upper slope locations (at approximately 150 m bottom depth), additional nutrient profiles (collected together with CTD profiles) showed a peak in silicate reaching  $0.7 \mu\text{M}$  at 30 m depth and  $2.0 \mu\text{M}$  at  $\sim 85$  m and below (Figure 4.1-2E) which was not reflected in high nitrate + nitrite or phosphate concentrations (Figure 4.1-2A – D) suggesting a source of silicate in shelf waters, distinct from enrichment via upwelling. Ammonium concentrations were patchy in their distribution, ranging from below detection to  $0.36 \mu\text{M}$  in the eastern GAB and  $0.10 \mu\text{M}$  in the central GAB in the upper 120 m of the water column, but with elevated concentrations occurring in near surface shelf waters of the eastern and central GAB.

Examination of stoichiometric ratios indicated potential N limitation (N:P ratios below Redfield ratio of 16:1) for waters down to 120 m over the whole region (Figure 4.1.3A). Potential silicate limitation (Si:N Redfield ratios  $< 1$ ) was evident at times for upper surface waters in the GAB (Figure 4.1-3B).

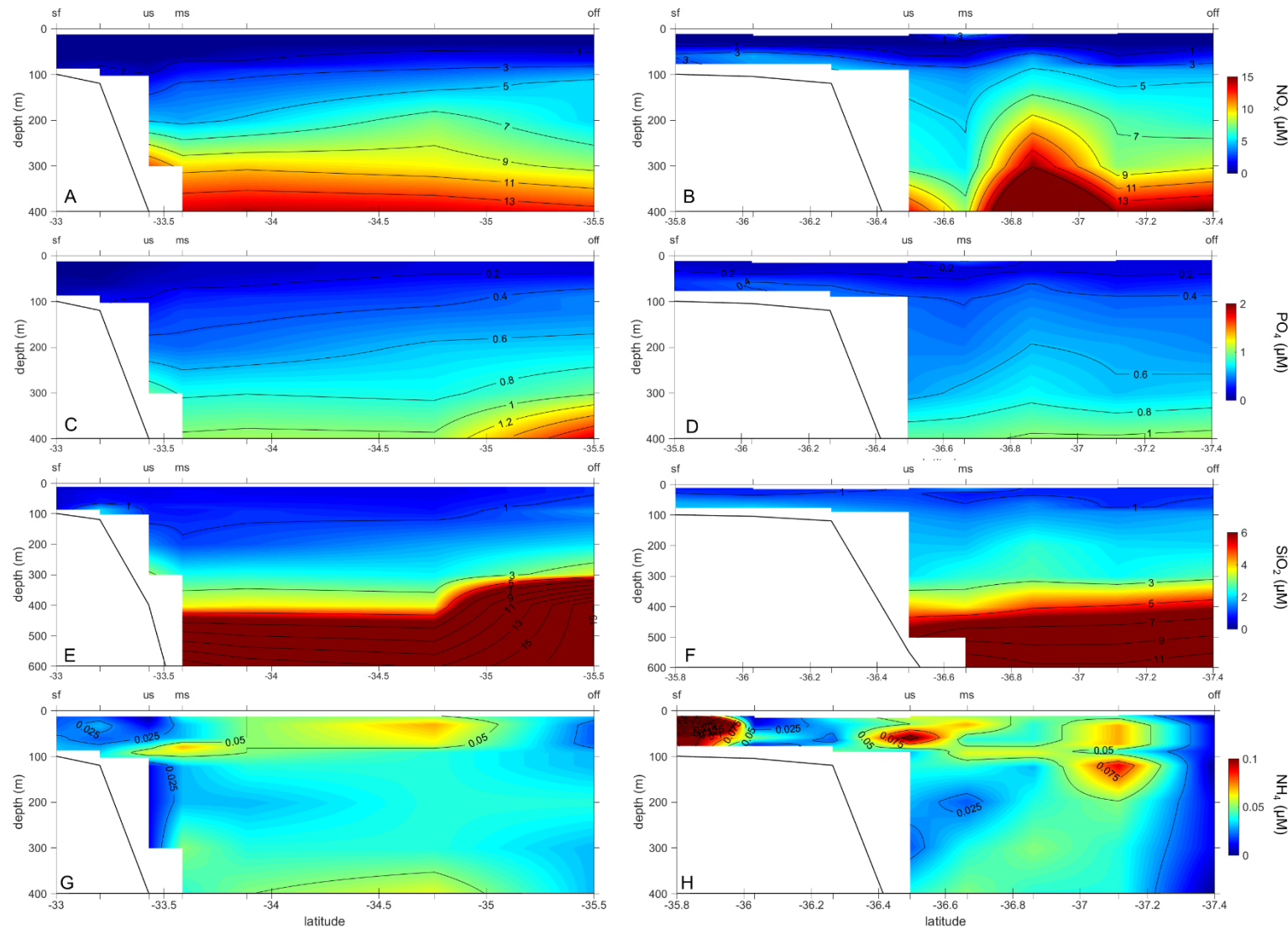


Figure 4.1-2 Dissolved nutrient plots of Nitrate + Nitrite ( $\text{NO}_x$ ) (A – B), Phosphate ( $\text{PO}_4$ ) (C – D), Silicate ( $\text{SiO}_2$ ) (E – F) and Ammonium ( $\text{NH}_4$ ) (G – H) in the central (A, C, E, G) and the eastern (B, D, F, H) Great Australian Bight (GAB).

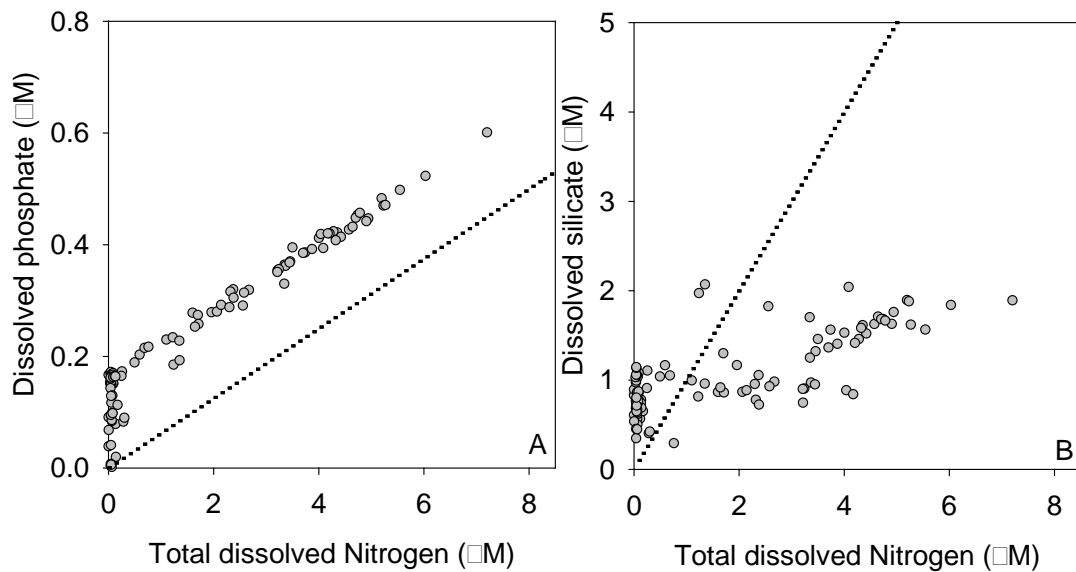


Figure 4.1-3 Plots of Total Inorganic Nitrogen to Phosphate (A) and Total Inorganic Nitrogen to Silicate (B). The straight line for each plot represent the Redfield ratio of 16:1 (N:P) (A) and 1:1 (N:Si) (B).

### Chlorophyll *a*

Chl *a* in the cmax always exceeded chl *a* in surface and deep water, with cmax chl *a* concentrations ranging from 0.16 – 1.24  $\mu\text{g L}^{-1}$  and 0.24 – 0.67  $\mu\text{g L}^{-1}$  in the central and eastern GAB respectively (Figure 4.1-4). Surface and deep water Tchl *a* concentrations were overall low ( $< 0.20 \mu\text{g L}^{-1}$ ), with the exception of the central GAB shelf waters, where the highest Tchl *a* recorded for the region at the time for the study (1.24  $\mu\text{g L}^{-1}$ ) persisted from the cmax to deep water and with ~ 61 % of the Tchl *a* attributed to phytoplankton greater than 5  $\mu\text{m}$  in size. This contrasted with eastern GAB shelf waters, where Tchl *a* was overall low (reaching maximum concentrations of 0.24  $\mu\text{g L}^{-1}$  in the cmax) and where phytoplankton less than 5  $\mu\text{m}$  dominated the biomass (78 – 100 % of Tchl *a*). Upper slope waters in both the central and eastern GAB were dominated by phytoplankton less than 5  $\mu\text{m}$  in size ( $> 94$  % of Tchl *a*) but Tchl *a* in the eastern GAB upper slope waters exceeded Tchl *a* in the central GAB by up to 3.4-fold. Excluding shelf stations however, Tchl *a* was 1.7-fold higher in the eastern GAB than the central GAB. Mid slope and offshore waters of the central GAB showed slightly lower Tchl *a* concentrations compared to the eastern GAB, but for both regions there was an increased contribution of phytoplankton greater than 5  $\mu\text{m}$  in size (up to 24 % in mid slope waters of the central GAB, and up to 26 % in the offshore waters of the eastern GAB).

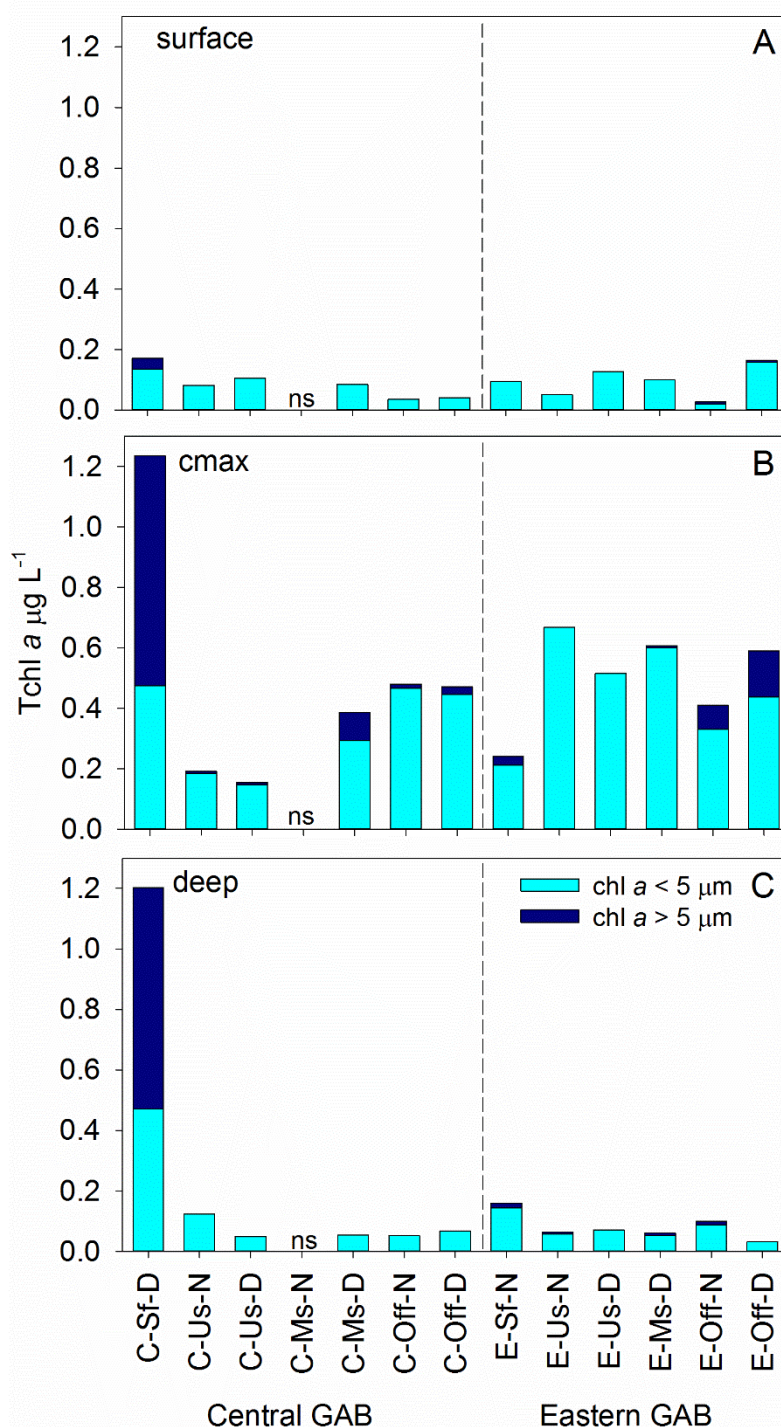


Figure 4.1-4 Size fractionated chlorophyll *a* (< 5  $\mu\text{m}$ , > 5  $\mu\text{m}$ ) making up total chlorophyll *a* (Tchl *a*) in surface (A), cmix (B) and deep water (C) in the Great Australian Bight (GAB). Prefix 'C' refers to Central GAB (to left of dashed line) and prefix 'E' refers to Eastern GAB (to the right of dashed line). Sf = shelf; Us = upper slope; Ms = mid slope; Off = offshore. Suffix 'N' and 'D' refer to night and day sampling respectively.

#### Picophytoplankton

Three groups of picophytoplankton could be discriminated with flow cytometry, *Prochlorococcus*, *Synechococcus*, and picoeukaryotes. In the central GAB, with the exception of the offshore station, highest picophytoplankton abundances occurred in surface waters (Figure 4.1-5). The opposite



occurred for the eastern GAB for the upper slope and mid slope, with highest abundances occurring in the cmax. Unusually low total picophytoplankton abundances ( $10.0 \times 10^6$  cells ml<sup>-1</sup> in the cmax) occurred in eastern GAB shelf waters throughout the water column, with *Prochlorococcus* low to absent. While picophytoplankton abundances were similarly scaled in offshore surface waters in the central and eastern GAB, picophytoplankton abundances at the cmax in the central GAB were on average up to 2.9-fold higher than in the eastern GAB. Picophytoplankton abundances were overall low in deep water, with some picophytoplankton groups sometimes absent at this depth. While *Prochlorococcus* dominated cell counts in both regions, *Synechococcus* and picoeukaryotes abundances were higher and made up a greater proportion of the total picophytoplankton counts in the eastern GAB. All groups of picophytoplankton were significantly positively correlated to each other in both the central and eastern GAB (Table 4.1-3).

Table 4.1-3 Linear correlation coefficients (*r*) between subgroups of viruses (V1, V2, V3 and V4), bacteria (low DNA (LDNA) and high DNA (HDNA)) and picophytoplankton (*Pro* = *Prochlorococcus*, *Syn* = *Synechococcus*, *Peuk* = picoeukaryotes) for the central GAB and eastern GAB. Coefficients *r* in bold are significant (*P* < 0.05).

Region	Group	V1	V2	V3	V4	LDNA	HDNA	<i>Pro</i>	<i>Syn</i>
Central	V1								
	V2	<b>0.64</b>							
	V3	<b>0.48</b>	<b>0.82</b>						
	V4	<b>0.65</b>	<b>0.52</b>	<b>0.52</b>					
	LDNA	<b>0.60</b>	<b>0.80</b>	<b>0.59</b>	<b>0.66</b>				
	HDNA	<b>0.48</b>	0.42	0.15	0.20	<b>0.55</b>			
	<i>Pro</i>	0.37	<b>0.75</b>	<b>0.84</b>	<b>0.58</b>	<b>0.70</b>	-0.01		
	<i>Syn</i>	<b>0.51</b>	<b>0.82</b>	<b>0.83</b>	<b>0.65</b>	<b>0.85</b>	0.22	<b>0.88</b>	
	<i>Peuk</i>	<b>0.66</b>	<b>0.74</b>	<b>0.64</b>	<b>0.68</b>	<b>0.88</b>	0.41	<b>0.74</b>	
East	V1								
	V2	<b>0.51</b>							
	V3	<b>0.51</b>	<b>0.89</b>						
	V4	<b>0.72</b>	<b>0.62</b>	<b>0.70</b>					
	LDNA	<b>0.55</b>	<b>0.66</b>	<b>0.71</b>	<b>0.86</b>				
	HDNA	0.46	<b>0.50</b>	<b>0.51</b>	0.42	0.40			
	<i>Pro</i>	0.49	<b>0.75</b>	<b>0.90</b>	<b>0.80</b>	<b>0.73</b>	0.28		
	<i>Syn</i>	<b>0.54</b>	<b>0.89</b>	<b>0.92</b>	<b>0.80</b>	<b>0.80</b>	0.41	<b>0.93</b>	
	<i>Peuk</i>	<b>0.51</b>	<b>0.87</b>	<b>0.82</b>	<b>0.80</b>	<b>0.83</b>	<b>0.50</b>	<b>0.82</b>	

In MDS plots, picophytoplankton communities in deep water clearly separated from those in the surface and the cmax (Fig. 4.1-6A). Clear differences in the picophytoplankton communities between the central and eastern GAB were more difficult to visualise in two dimensional space in the MDS plot. PERMANOVA (Region × Depth) however revealed significant differences between the central and eastern GAB picophytoplankton communities with significant interaction (*P* < 0.05), so that surface and deep water picophytoplankton communities in the central GAB differed to those in the eastern GAB at the same depth. Within each region, picophytoplankton communities in the surface and cmax were similar (*P* > 0.05) and differed to picophytoplankton communities in deep water.

The BEST analysis was applied to investigate which environmental parameters best explained the picophytoplankton community structure. The combination of nitrate and silicate showed the highest correlation ( $\rho = 0.50$ ) with picophytoplankton community structure (Table 4.1-4).

Table 4.1-4 Results from BEST analysis of picophytoplankton, bacteria/virus, phytoplankton ( $> 5 \mu\text{m}$ ). Pigments ( $< 5 \mu\text{m}$ ), zooplankton ( $64 \mu\text{m}$  net and  $150 \mu\text{m}$ ) community composition (based on abundances) and environmental parameters. Spearman coefficient ( $\rho$ ) is given for the best combination of parameters explaining community composition, marked by  $\times$ . The single best predictor is highlighted in bold  $\times$ .  $\rho$  values are all significant ( $P < 0.01$ ).

Group	$\rho$	Temp	Sal	O <sub>2</sub>	NO <sub>3</sub>	NO <sub>2</sub>	NH <sub>4</sub>	PO <sub>4</sub>	SiO <sub>2</sub>	chl <i>a</i> $> 5 \mu\text{m}$
picophytoplankton	0.50				$\times$				$\times$	
bacteria/virus	0.43				$\times$			$\times$	$\times$	
phytoplankton	0.39	$\times$				$\times$		$\times$		
pigments ( $< 5 \mu\text{m}$ )	0.26					$\times$				
zooplankton ( $64 \mu\text{m}$ net)	0.72			$\times$		$\times$	$\times$			
zooplankton ( $150 \mu\text{m}$ net)	0.72					$\times$	$\times$			$\times$

Note no single predictor was best for the zooplankton in the  $150 \mu\text{m}$  net. Also note, chl *a* (of any fraction) was not used in the analysis for any of the autotrophs (picophytoplankton, phytoplankton or pigments  $< 5 \mu\text{m}$ ), given it is a proxy itself for autotrophic biomass.

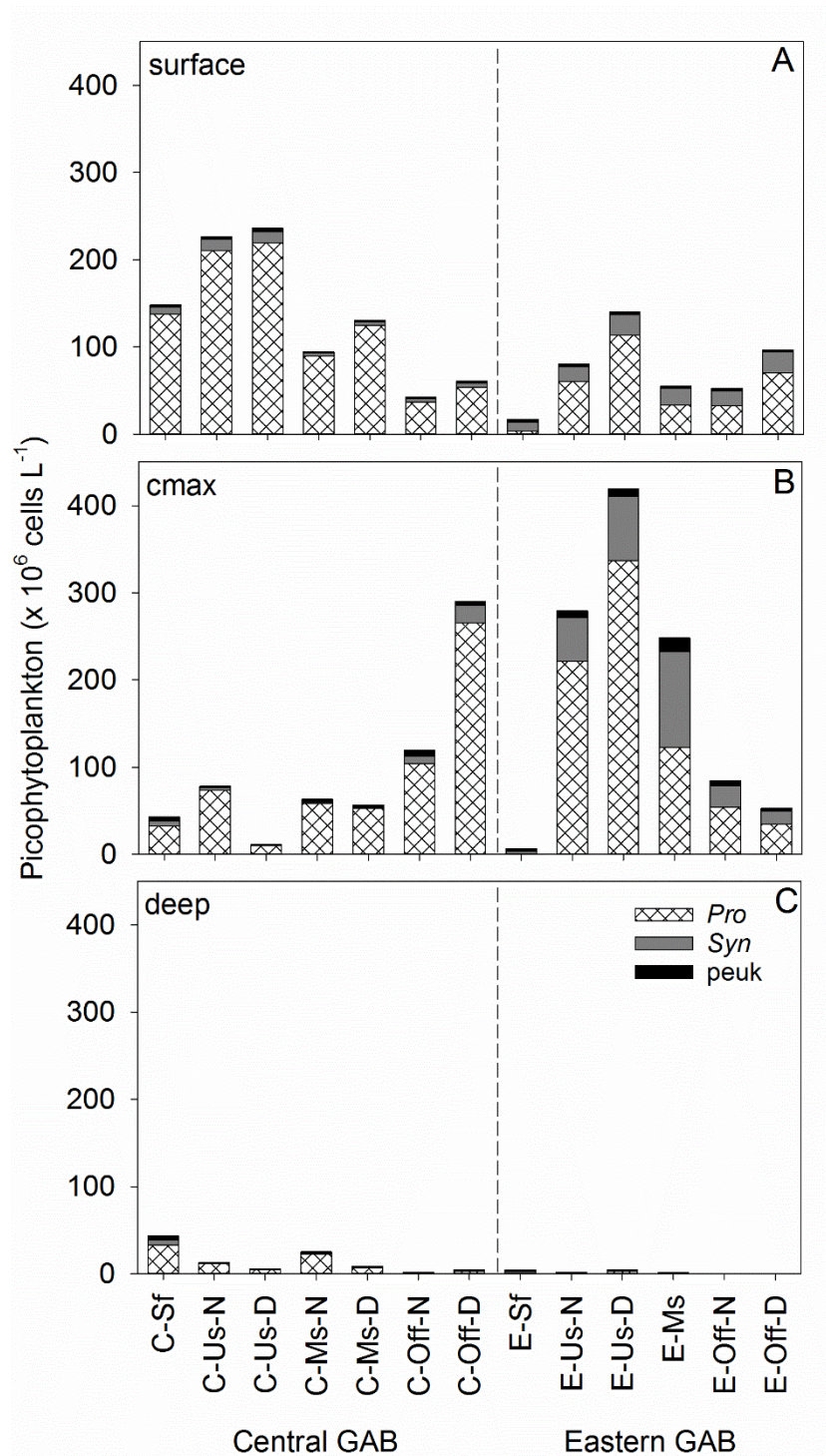


Figure 4.1-5 Picophytoplankton abundances ( $\times 10^6$  cells  $L^{-1}$ ) in surface (A), cmax (B) and deep water (C) in the Great Australian Bight (GAB). Prefix 'C' refers to Central GAB (to left of dashed line) and prefix 'E' refers to Eastern GAB (to the right of dashed line). Sf = shelf; Us = upper slope; Ms = mid slope; Off = offshore. Suffix 'N' and 'D' refer to night and day sampling respectively. Pro = *Prochlorococcus*, Syn = *Synechococcus* and peuk = picoeukaryotes.

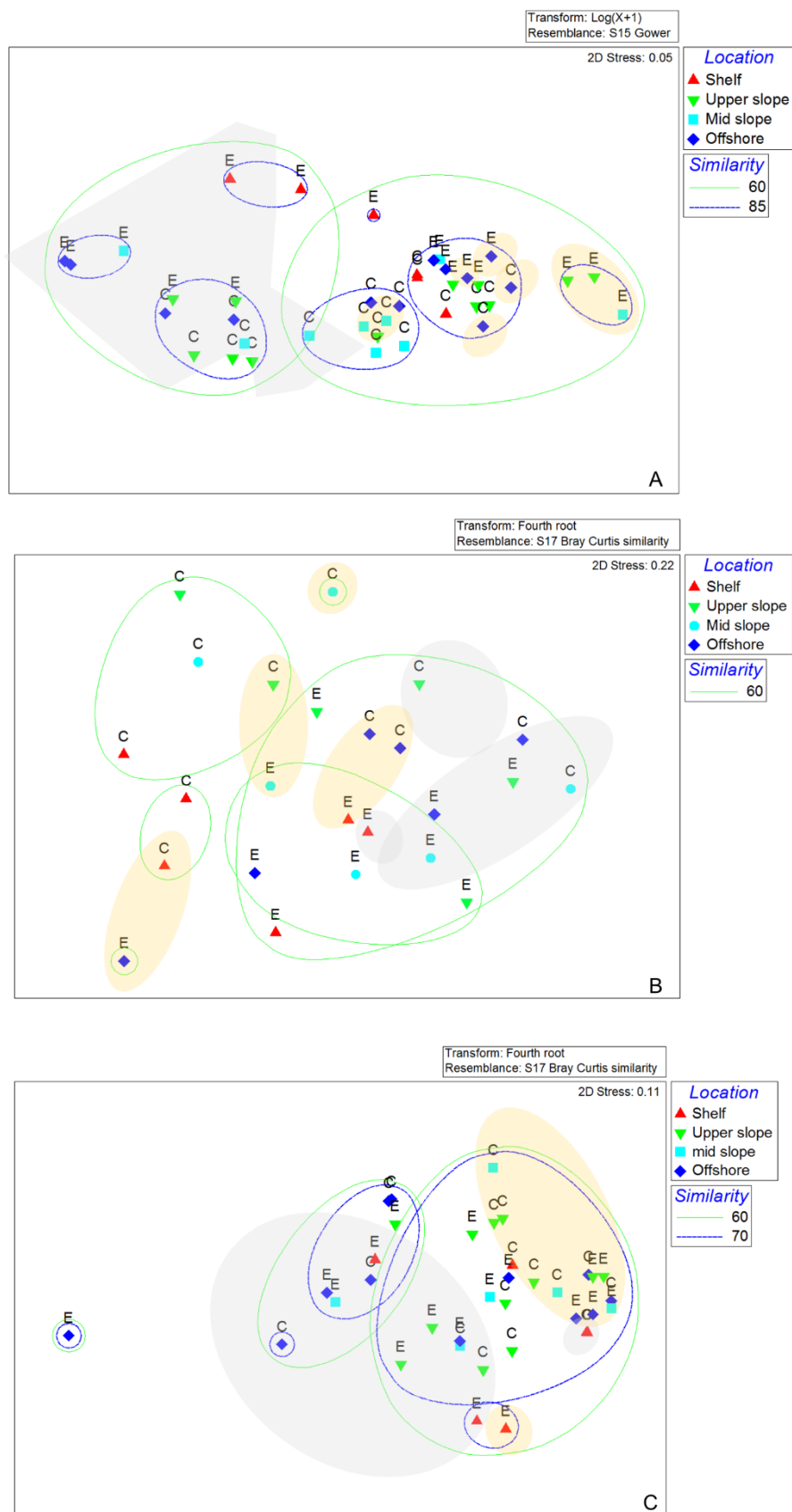


Figure 4.1-6 MDS ordinations of picophytoplankton (A), phytoplankton (B) and pigments (< 5  $\mu$ m) coupled to a cluster analysis. Prefix 'C' refers to Central GAB and prefix 'E' refers to Eastern GAB. No shading indicates surface; orange shading indicates the cmx and grey shading indicates deep water.

### Phytoplankton (> 5 µm)

Highest phytoplankton abundances ( $20.9 \times 10^3$  cells L<sup>-1</sup>), concomitant with highest Tchl *a* concentrations (Figure 4.1-7), occurred on the shelf in the central GAB in deep water (~ 90 m) but relatively high abundances also occurred at the cmax at this location (Figure 4.1-7). However, shifts in the community composition were evident. Central GAB surface waters were dominated by dinoflagellates (Gymnodinioid group, *Gyrodinium* spp. and *Heterocapsa* spp. and *Gonyaulax* spp.), while the cmax was dominated by diatoms (*Nitzschia* spp., *Chaetoceros* spp. and *Rhizosolenia* spp.). In deep water, dinoflagellates dominated (Gymnodinioid group, *Gyrodinium* spp., and *Heterocapsa* spp.), but there were still relatively high numbers of diatoms (*Nitzschia* spp., *Chaetoceros* spp., and *Guinardia striata*) (see Appendix Table 4.1-54). In the central GAB, phytoplankton abundances showed a decreasing trend moving from the shelf to offshore, with a shift towards dinoflagellate dominated communities.

In the east, the trend was different in that highest phytoplankton abundances occurred in offshore waters in the cmax (Figure 4.1-7), with diatoms dominating total phytoplankton abundances and with similar dominant taxa (to genus level) for diatoms to those in the cmax and deep shelf waters of the central GAB (*Nitzschia* spp. and *Chaetoceros* spp.), but also with high abundances of *Guinardia striata* (Appendix Table 4.1-6). The most abundant dinoflagellates in surface waters in the offshore eastern GAB were a Gymnodinioid group, *Gyrodinium* spp. and *Heterocapsa* spp., with these three groups present at relatively high abundances right across the GAB in the surface and cmax. Other dominant phytoplankton taxa made up at most 17.3 % of the total phytoplankton abundance, with cryptophytes (*Hemiselmis* sp., *Leucocryptos* spp. and *Plagioselmis prolunga*) generally the next most abundant taxa after diatoms and dinoflagellates in the eastern GAB, and prasinophytes (*Nephroselmis* spp., *Pyraminonas* spp.) generally, the next most abundant taxa (after dinoflagellates and diatoms) in the central GAB (Appendix Table 4.1-5).

MDS plots showed the central shelf and offshore eastern GAB phytoplankton communities to sit closely in two dimensional space and for the deep water communities (except on the shelf in the central GAB) to be more closely grouped and separated from the surface and cmax phytoplankton communities (Fig. 4.1-6B). PERMANOVA (Region x Depth) however revealed statistical differences between the central and eastern GAB ( $P < 0.05$ ) with no significant interaction ( $P > 0.05$ ). As for picophytoplankton, similar phytoplankton communities occurred between the surface and cmax and with these communities differing to those in deep water ( $P < 0.05$ ). The BEST analysis showed that temperature and phosphate were the best predictors of phytoplankton community structure ( $p = 0.39$ ) (Table 4.1-4).

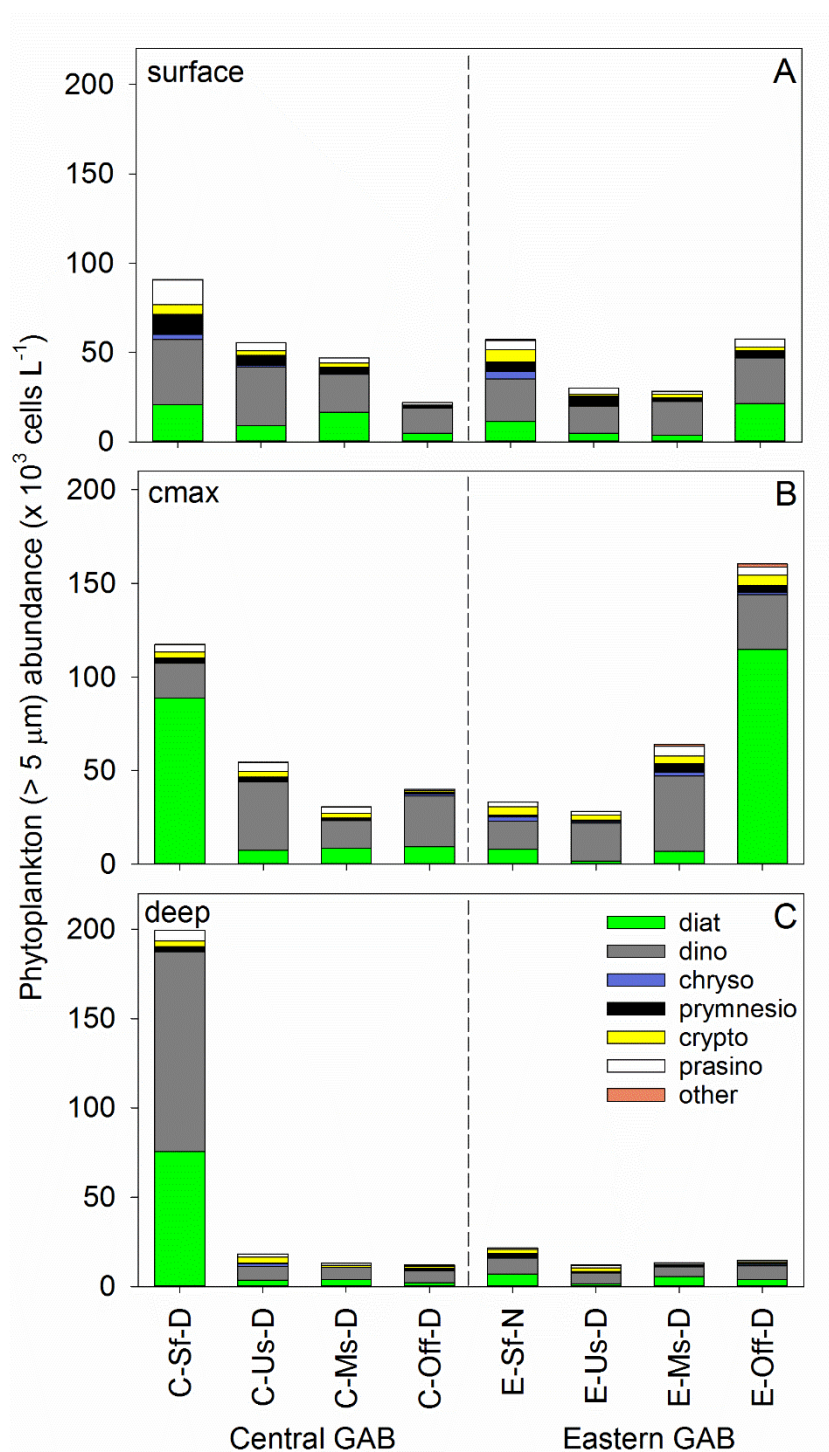


Figure 4.1-7 Phytoplankton ( $> 5 \mu\text{m}$ ) abundances ( $\times 10^3 \text{ cells L}^{-1}$ ) in surface (A), cmax (B) and deep water (C) in the Great Australian Bight (GAB). Prefix 'C' refers to Central GAB (to left of dashed line) and prefix 'E' refers to Eastern GAB (to the right of dashed line). Sf = shelf; Us = upper slope; Ms = mid slope; Off = offshore. Suffix 'N' and 'D' refer to night and day sampling respectively. diat = diatoms; dino = dinoflagellates; chryso = chrysophytes; prymnesio = prymnesiophytes, crypto = cryptophytes; prasino = prasinophytes and other = other flagellates not included in previous groups.



## Pigments

Size fractionation of pigments allowed further differentiation of the phytoplankton community. DVchl *a* (*Prochlorococcus*) and zeaxanthin (*Synechococcus*) made up the largest proportion of the combined biomarker pigment concentrations in the central GAB surface waters (Figure 4.1-8). This was also true of the eastern GAB, however in addition to DVchl *a* and zeaxanthin, 19hex (*prymnesiophytes*) also comprised a large fraction of biomass that was on average, 2.0-fold higher than in the central GAB. Relatively high concentrations of 19hex persisted down to the cmax in the east, and were ~ 1.7-fold higher compared to the central GAB, with chl *b* (chlorophytes), zeaxanthin and DVchl *a* further contributing similarly to the total biomarker concentration. The exception to this was on the shelf in the east, where zeaxanthin and DVchl *a* were absent, and where 19but (*chrysophytes*, some *prymnesiophytes*) occurred at similar concentrations to 19hex. While 19but was present in the cmax at all times over the central and eastern GAB, the overall concentration of this pigment was 1.9-fold higher in the east. Relatively high concentrations of fucoxanthin ( $0.12 \mu\text{g L}^{-1}$ ) occurred in the less than 5  $\mu\text{m}$  fraction in shelf waters of the central GAB persisting down to deep water. Fucoxanthin was also present at all stations in the cmax in the less than 5  $\mu\text{m}$  fraction, indicating this pigment was more likely a biomarker of other nanoplankton (i.e. *prymnesiophytes* or *chrysophytes*) given that most diatoms are larger than 5  $\mu\text{m}$ .

In the greater than 5  $\mu\text{m}$  fraction, the only biomarkers present were, fucoxanthin, 19but, 19hex and (on one occasion) chl *b*. Highest concentrations of fucoxanthin observed for this study ( $0.40 \mu\text{g L}^{-1}$ ) occurred in shelf waters of the central GAB, matching the high concentrations of diatoms observed via microscopy (Figure 4.1-7). Fucoxanthin concentrations of  $0.08 \mu\text{g L}^{-1}$  also occurred offshore in the east. The biomarker peridinin (representative of autotrophic dinoflagellates) was absent at all times, as was the biomarker alloxanthin (representative of cryptophytes).

Pigment compositions in the central and eastern GAB exhibited some separation in two dimensional space in MDS plots but with clearer separation between surface, cmax and deep water (Fig. 4.1-6C). PERMANOVA (Region x Depth) confirmed differences in pigment composition between regions ( $P < 0.05$ ) with no interaction occurring with depth ( $P > 0.05$ ). However within each region, the pigment composition at the cmax differed to pigment composition in surface and deep waters (all  $P < 0.05$ ). The BEST analysis showed a relatively low correlation ( $\rho = 0.26$ ) for the best predictor (nitrite) of the less than 5  $\mu\text{m}$  community (Table 4.1-4).

Estimates of the contribution of each of the picoplankton, nanoplankton 2 – 5  $\mu\text{m}$ , nanoplankton 5 – 20  $\mu\text{m}$  and microphytoplankton to total phytoplankton biomass showed that overall, picoplankton dominated Tchl *a* biomass in the central GAB in surface and cmax waters ( $49.6 \pm 2.6 \%$ ,  $52.2 \pm 7.7 \%$  respectively), but not in deep water where nanoplankton 2 – 5  $\mu\text{m}$  dominated (Figure 4.1-9). In the eastern GAB, nanoplankton (2 – 5  $\mu\text{m}$ ) dominated biomass in the surface, cmax and in deep water ( $74.3 \pm 8.3 \%$ ,  $48.5 \pm 4.4 \%$  and  $79.2 \pm 6.7 \%$  respectively) at the time of the study. The relatively high concentrations of Tchl *a* greater than 5  $\mu\text{m}$  which occurred in shelf waters of the central GAB was due to the dominance of microphytoplankton. The contribution of nanoplankton 5 – 20  $\mu\text{m}$  was low across the GAB, commonly contributing 0 % and with a maximum of 12.0 % (mid slope in the central GAB).

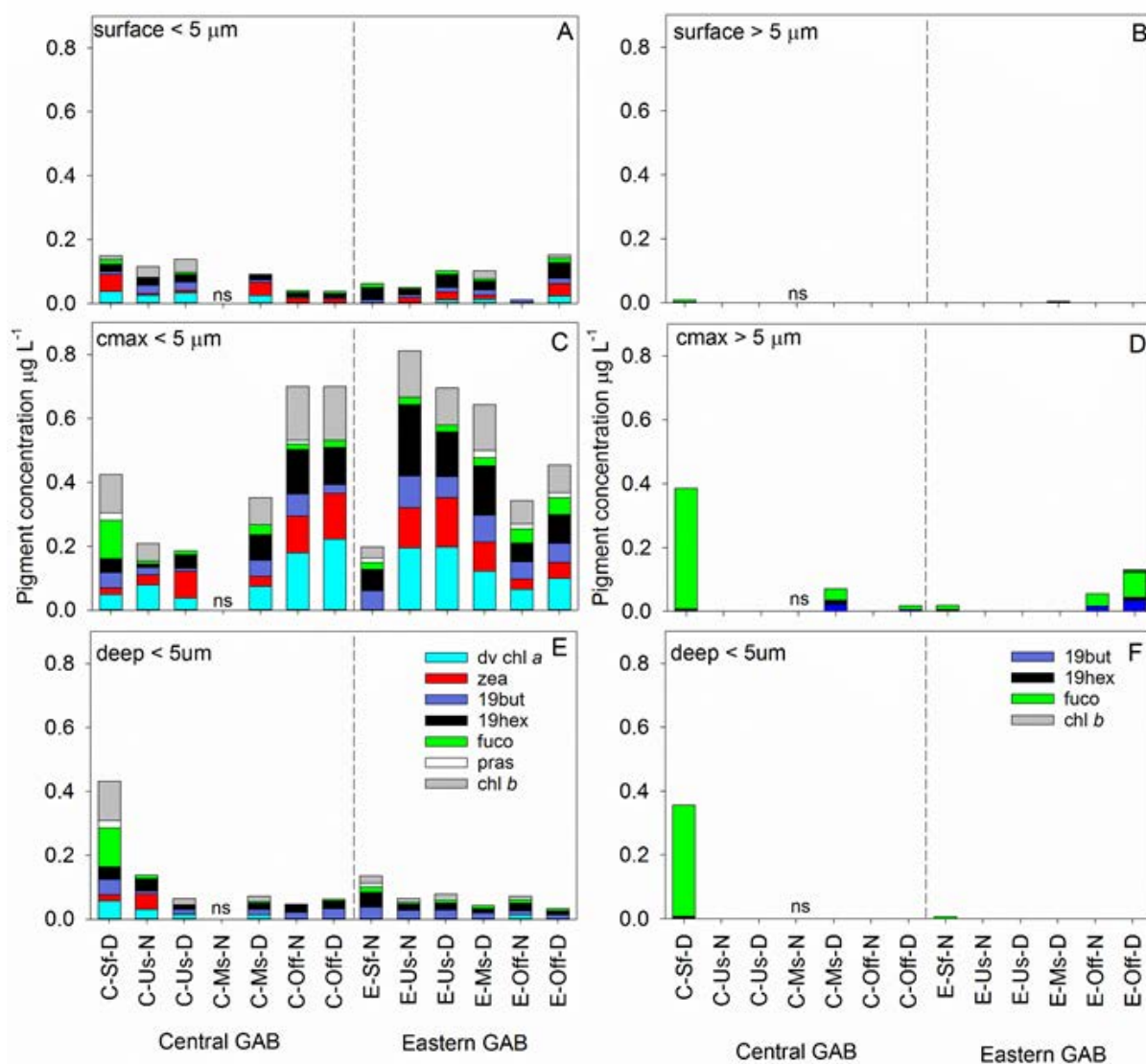


Figure 4.1-8 Distribution of accessory pigments (< 5  $\mu\text{m}$ ) (A, C, E) and (> 5  $\mu\text{m}$ ) (B, D, F) in surface (A – B), cmx (C – D) and deep water (E – F) in the Great Australian Bight (GAB). Prefix 'C' refers to Central GAB (to left of dashed line) and prefix 'E' refers to Eastern GAB (to the right of dashed line). Sf = shelf; Us = upper slope; Ms = mid slope; Off = offshore. Suffix 'N' and 'D' refer to night and day sampling respectively. See Table 4.1-2 for full names of pigments. ns = not sampled.

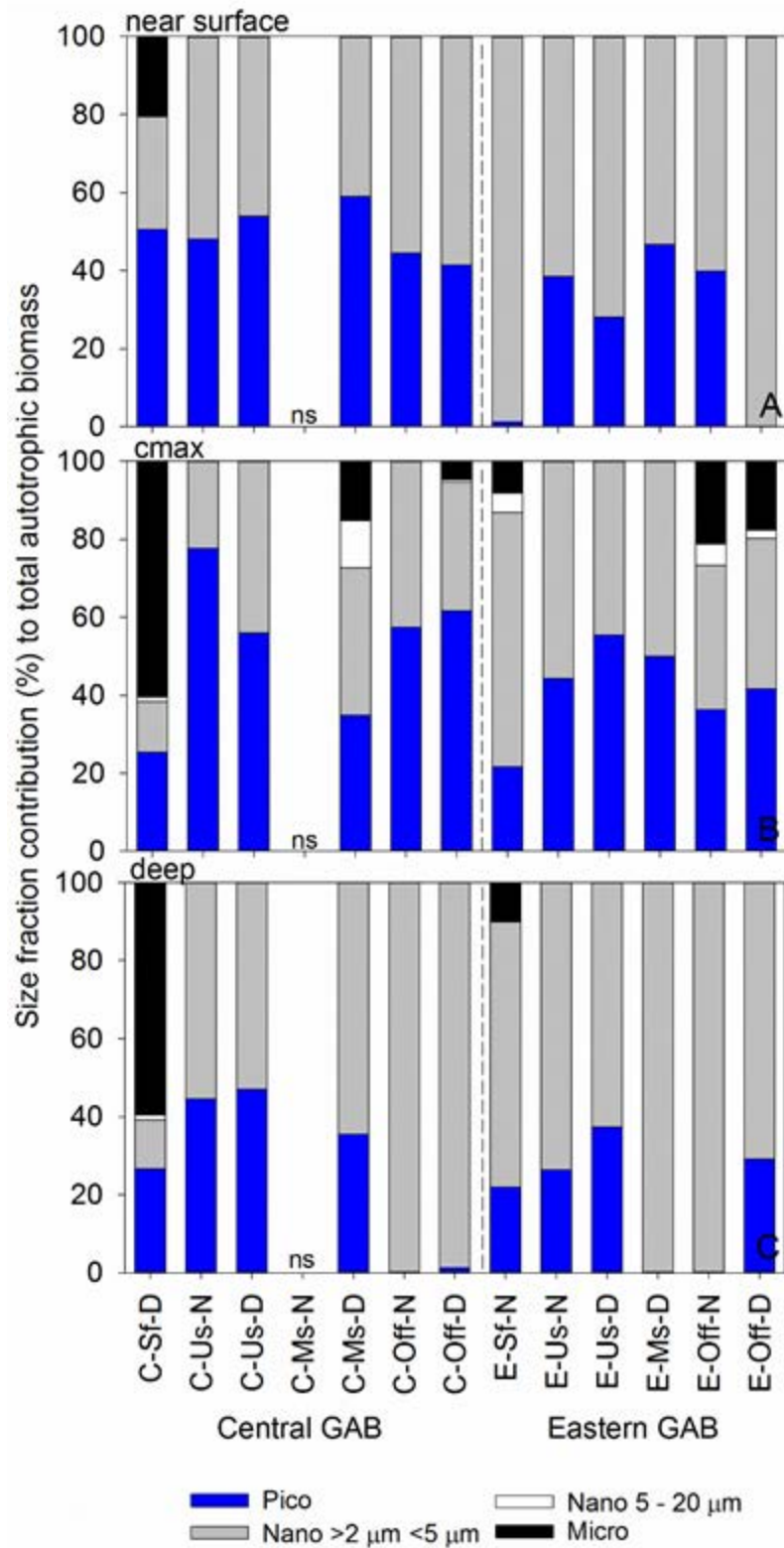


Figure 4.1-9 Percent (%) contribution of picophytoplankton (Pico), Nanophytoplankton > 2 μm < 5 μm (Nano > 2 μm < 5 μm), nanophytoplankton 5 – 20 μm (Nano 5 – 20 μm) and microphytoplankton (20 – 200 μm) to total autotrophic biomass in surface (A), cmx (B) and deep water (C) in the Great Australian Bight (GAB). Prefix 'C' refers to Central GAB (to left of dashed line) and prefix 'E' refers to Eastern GAB (to the right of dashed line). Sf = shelf; Us = upper slope; Ms = mid slope; Off = offshore. Suffix 'N' and 'D' refer to night and day sampling respectively. ns = not sampled.

### Bacteria and viruses

There was no clear regional trend or shelf to offshore trend for the abundances of bacteria (Figure 4.1-10). Highest bacterial abundances, reaching  $3.95 \times 10^8$  cells  $L^{-1}$  occurred on the shelf in the central GAB persisting down to deep water ( $\sim 90$  m). Similarly scaled bacterial abundances also occurred in the cmax on the mid slope in the eastern GAB. Lowest bacterial abundances occurred in the upper slope at the cmax in the central GAB ( $0.70 \times 10^8$  cells  $L^{-1}$ ) with these abundances similarly scaled to those in deep water. Flow cytometric analysis allowed further differentiation of the bacterial community into high DNA (HDNA) and low DNA (LDNA) groups (based on SYBR green fluorescence and side scatter). In the central GAB, the percent of HDNA bacteria (% HDNA) was always higher in the cmax and/or deep water compared with surface water except for the offshore station, where % HDNA cells was low in the cmax ( $\sim 24$  %) compared to surface and deep water (59 – 64 %). In the east, on the shelf and offshore, a similar % HDNA (57 – 60 %) occurred for surface, cmax and deep water, while the highest % HDNA (74 %) occurred in surface waters on the mid slope in the eastern GAB.

Four groups of viruses could be discriminated with flow cytometry, V1 made up the largest portion of total virus abundances, followed by V2, V3 and then V4 (Figure 4.1-11). Viruses abundance showed overall low variation between the central and eastern GAB and between the shelf through to offshore for each transect/region, ranging between  $26.1 \times 10^8$  cell  $L^{-1}$  and  $79.3 \times 10^8$  cell  $L^{-1}$  and varying at most by 3.0 fold in the east (Figure 4.1-11).

In the Central GAB, all virus groups were positively correlated with LDNA but not to HDNA, with the exception of V1 with HDNA. Similarly in the Eastern GAB, V1 was better correlated with LDNA than HDNA (Table 4.1-3). V2 showed significant positive correlations with all bacterial and picophytoplankton subgroups in the eastern and central GAB with the exception for HDNA in the central GAB (Table 4.1-3). While V3 and V4 exhibited significant positive correlations with all bacterial and picophytoplankton subgroups in both the central and eastern GAB, overall higher correlation coefficients occurred for the picophytoplankton subgroups (Table 4.1-3).

The BEST analysis showed phosphate, nitrate and silicate to have the highest correlation ( $\rho = 0.43$ ) with the bacterial and viral communities (Table 4.1-43).

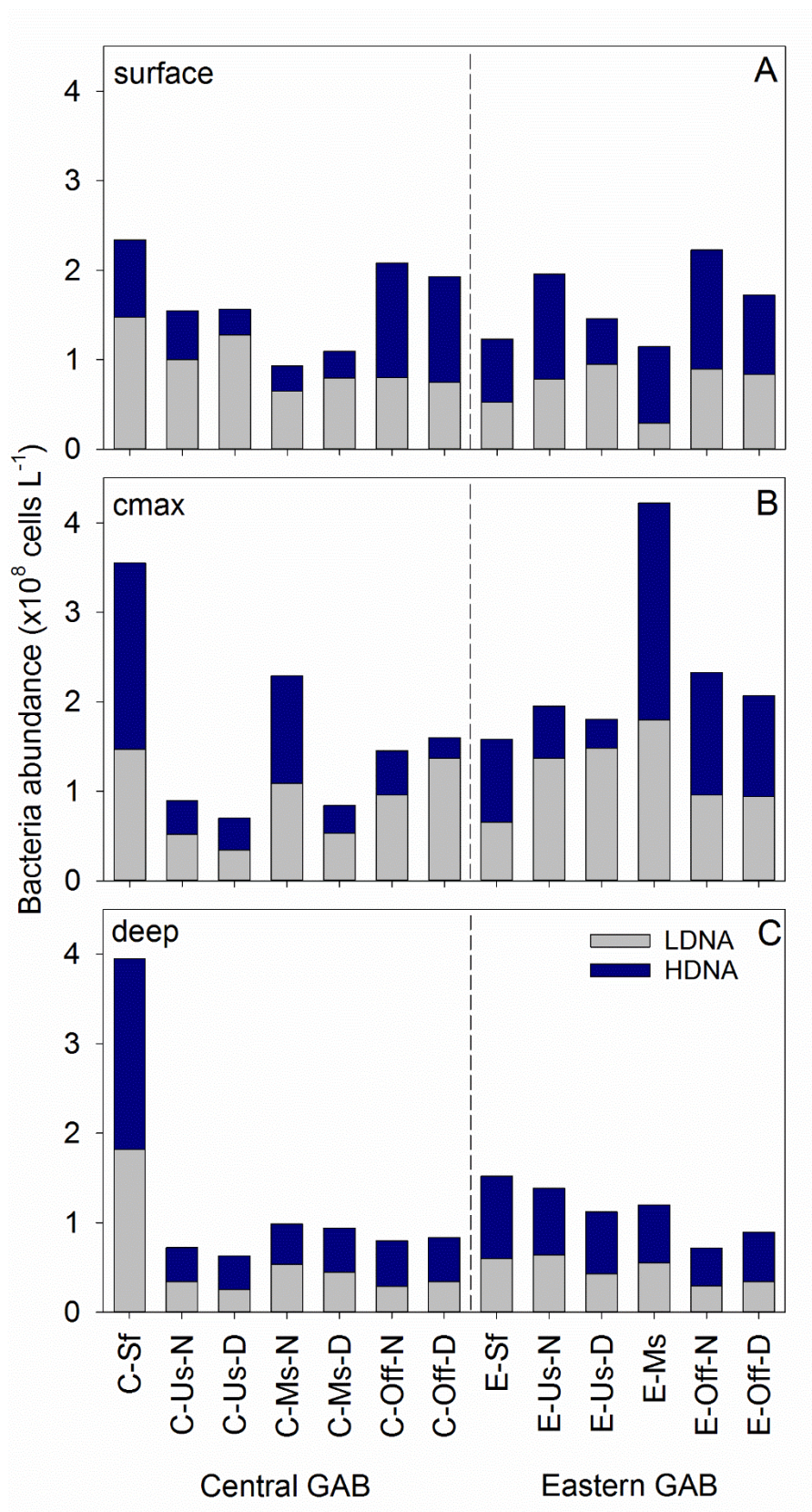


Figure 4.1-10 Bacterial abundances ( $\times 10^8$  cells  $L^{-1}$ ) in surface (A), cmax (B) and deep water (C) in the Great Australian Bight (GAB). Prefix 'C' refers to Central GAB (to left of dashed line) and prefix 'E' refers to Eastern GAB (to the right of dashed line). Sf = shelf; Us = upper slope; Ms = mid slope; Off = offshore. Suffix 'N' and 'D' refer to night and day sampling respectively. LDNA = low DNA bacteria and HDNA = high DNA bacteria.



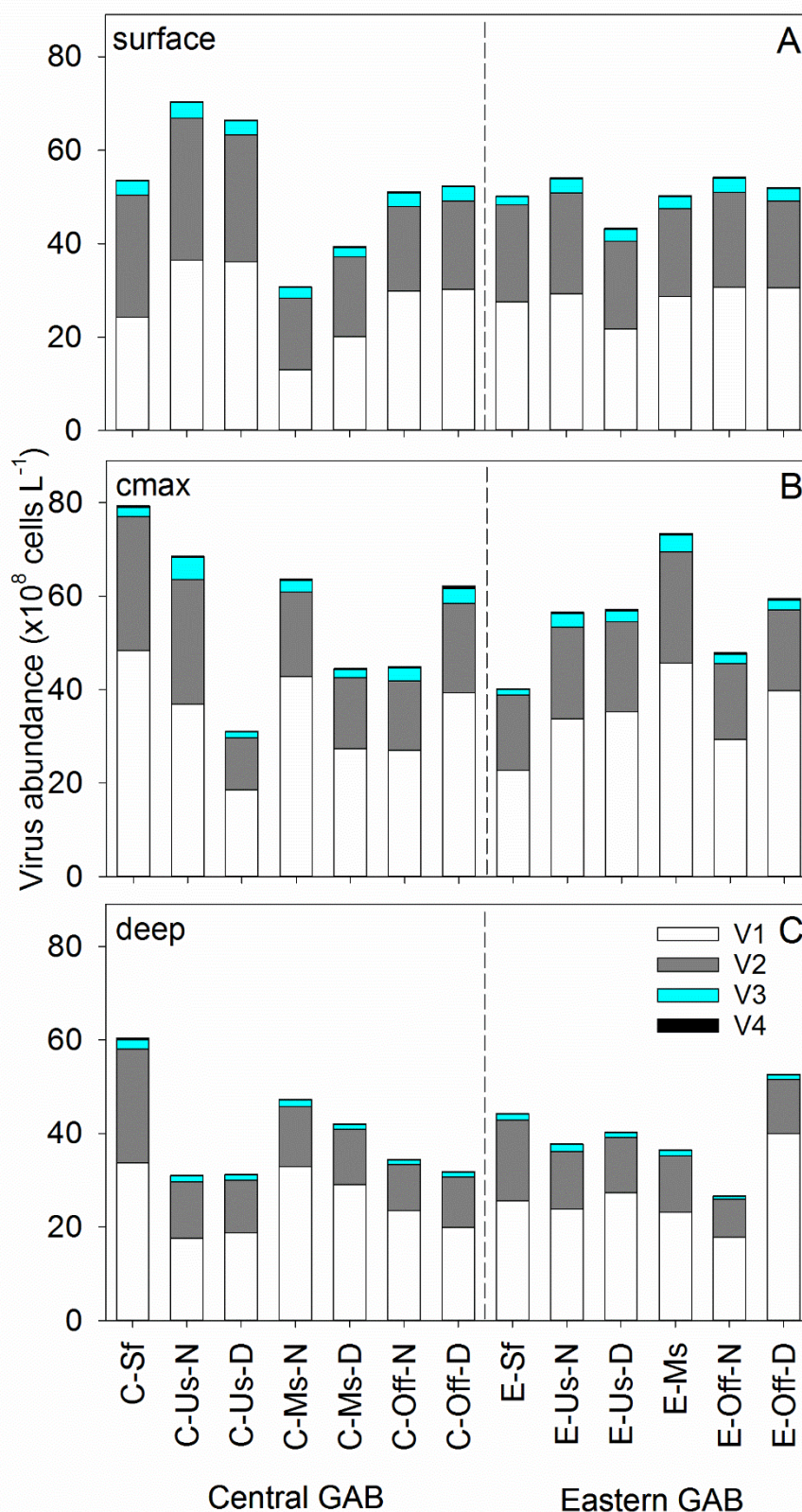


Figure 4.1-11 Viral abundances (x 10<sup>8</sup> cells L<sup>-1</sup>) in surface (A), cmax (B) and deep water (C) in the Great Australian Bight (GAB). Prefix 'C' refers to Central GAB (to left of dashed line) and prefix 'E' refers to Eastern GAB (to the right of dashed line). Sf = shelf; Us = upper slope; Ms = mid slope; Off = offshore. Suffix 'N' and 'D' refer to night and day sampling respectively. V1 = Virus group 1, V2 = Virus group 2, V3 = Virus group 3 and V4 = Virus group 4.



#### Zooplankton (64 $\mu\text{m}$ and 150 $\mu\text{m}$ nets)

Overall, zooplankton biomass was ~2-fold higher and with number of individuals ~5-fold higher in the eastern GAB compared to the central GAB (Figure 4.1-112). Highest zooplankton biomass and concentration of individuals occurred on the shelf. However, on the shelf in the eastern GAB, zooplankton biomass (58.9  $\text{mg m}^{-3}$  and 77.0  $\text{mg m}^{-3}$  for the 64  $\mu\text{m}$  and 150  $\mu\text{m}$  net respectively) was up to 7.8-fold higher, with abundances ( $200.0 \times 10^3$  and  $9.8 \times 10^3$  individuals  $\text{m}^{-3}$  for the 64  $\mu\text{m}$  and 150  $\mu\text{m}$  net respectively) up to 20.4-fold higher than on the shelf in the central GAB. Excluding the shelf stations, biomass was similar between the central GAB and eastern GAB; however, the eastern GAB had 2-fold higher abundances of zooplankton in the 150  $\mu\text{m}$  net, but lower abundances of zooplankton in the 64  $\mu\text{m}$  net.

Further shifts occurred between locations within the central and eastern GAB (Figure 4.1-12). For example, in the eastern GAB, total zooplankton biomass and abundance in the 64  $\mu\text{m}$  net was similar between the upper shelf (7.22  $\text{mg m}^{-3}$  and  $2.25 \times 10^3$  individuals  $\text{m}^{-3}$ ) and offshore waters (5.48  $\text{mg m}^{-3}$  and  $2.10 \times 10^3$  individuals  $\text{m}^{-3}$ ). However, higher biomass occurred in the 150  $\mu\text{m}$  net concomitant with lower (~3-fold) number of individuals in the upper slope compared to offshore waters, indicating relatively larger organisms were contributing to the biomass in upper slope waters. In the central GAB in the 64  $\mu\text{m}$  net, higher biomass and numbers of individuals occurred at the upper slope compared to offshore, however for the 150  $\mu\text{m}$  net, total abundances and zooplankton biomass were similar.

Trends in copepod abundances reflected the overall trends in total zooplankton abundances (Figure 4.1-13). The exception to this was the high number of copepods occurring offshore in the east in the 150  $\mu\text{m}$  net (and with low relative abundances in the 64  $\mu\text{m}$  net), dominated by harpacticoids and with high numbers of copepod nauplii. Apart from the elevated abundances occurring in shelf waters in the east, shelf waters also differed to those elsewhere in the eastern GAB and the central GAB, in that here, nauplii were not the dominant group; instead, calanoids and cyclopoid copepods made up similar contributions (~36 % each) to total copepod abundances.

A similar overall trend to total zooplankton abundance and biomass was followed by other identified major zooplankton taxonomic groups, with highest abundances recorded in shelf waters in the eastern GAB (Figure 4.1-14). In the eastern GAB on the shelf, appendicularians, cladocerans, echinoderms and the predatory dinoflagellate *Noctiluca* were dominant taxa and with amphipods also present in higher abundances than for any other location. In the central GAB on the shelf, echinoderms, thaliaceans and cladocerans were dominant taxa with appendicularians also present in relatively high abundances in the 64  $\mu\text{m}$  net. Elsewhere in the central GAB, appendicularians and thaliaceans were also dominant taxa, except with increased numbers of ostracods, gastropods and amphipods in offshore waters. In the eastern GAB, relatively low abundances of zooplankton taxa occurred on the upper shelf and mid shelf, but with offshore waters showing higher proportions and absolute numbers of appendicularians, chaetognaths and ostracods.

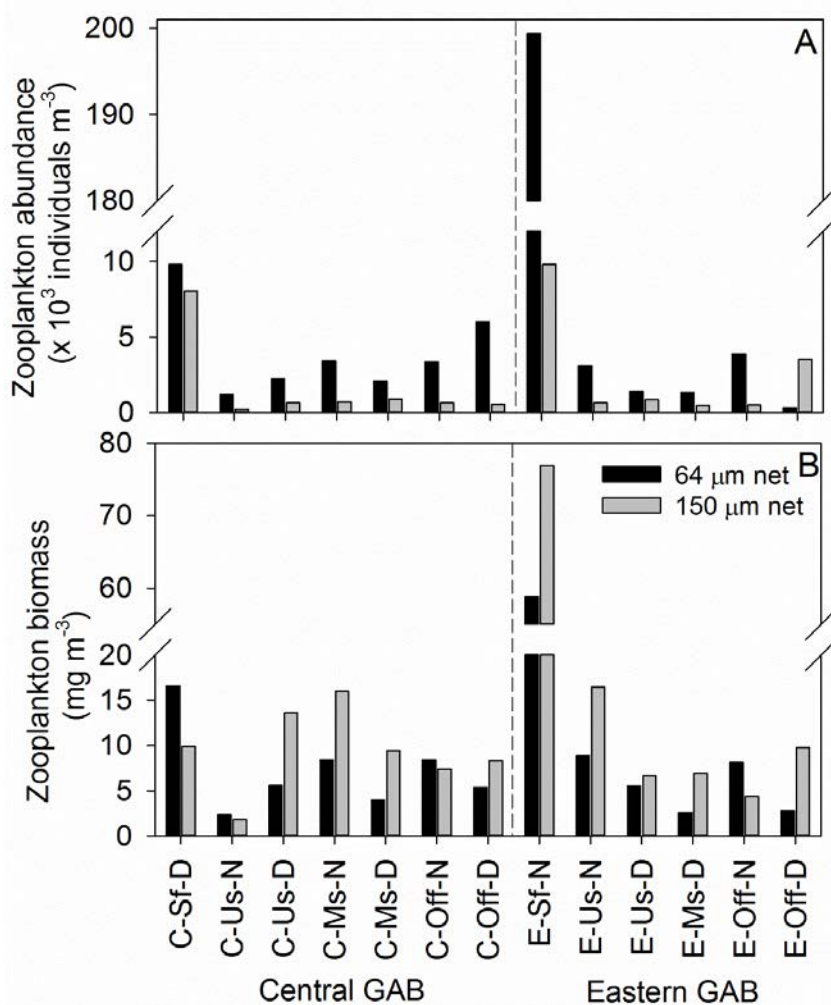


Figure 4.1-12 Zooplankton abundance ( $\times 10^3$  individuals  $m^{-3}$ ) and biomass ( $mg\ m^{-3}$ ) in the 64  $\mu m$  and 150  $\mu m$  net in the Great Australian Bight (GAB). Prefix 'C' refers to Central GAB (to left of dashed line) and prefix 'E' refers to Eastern GAB (to the right of dashed line). Sf = shelf; Us = upper slope; Ms = mid slope; Off = offshore. Suffix 'N' and 'D' refer to night and day sampling respectively.

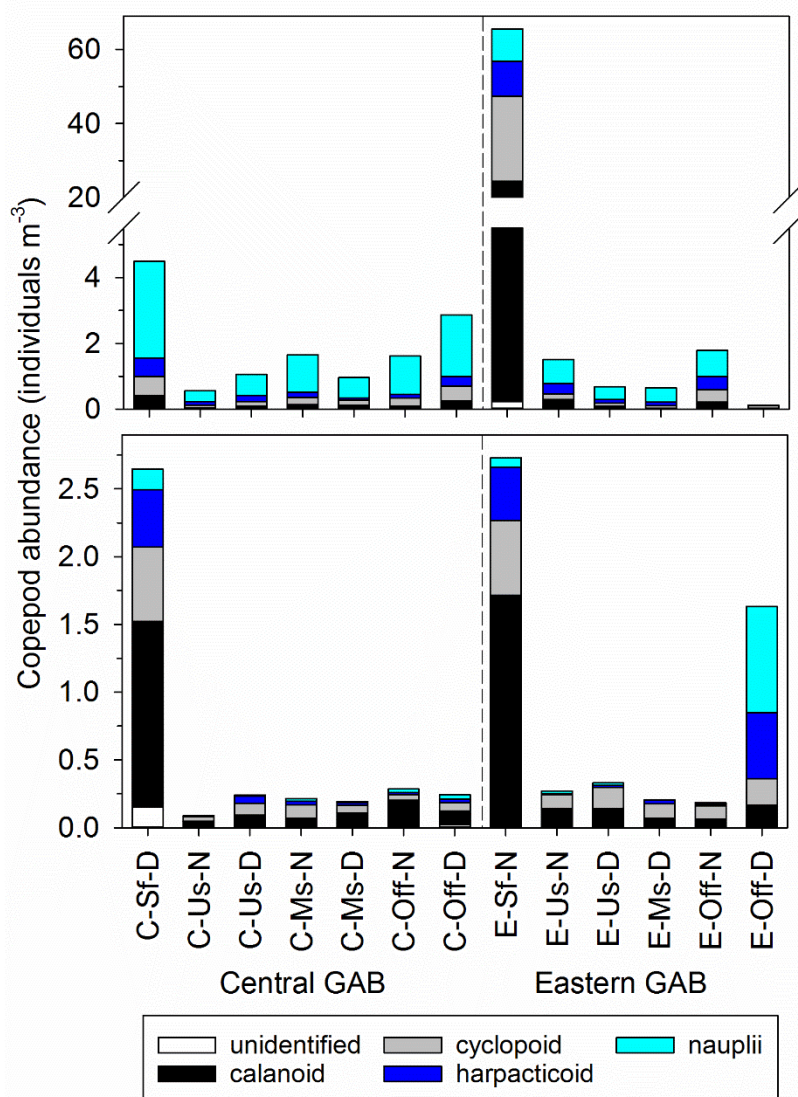


Figure 4.1-13 Copepod abundance ( $\times 10^3$  individuals  $m^{-3}$ ) in the 64  $\mu m$  (A) and 150  $\mu m$  (B) net in the Great Australian Bight (GAB). Prefix 'C' refers to Central GAB (to left of dashed line) and prefix 'E' refers to Eastern GAB (to the right of dashed line). Sf = shelf; Us = upper slope; Ms = mid slope; Off = offshore. Suffix 'N' and 'D' refer to night and day sampling respectively.

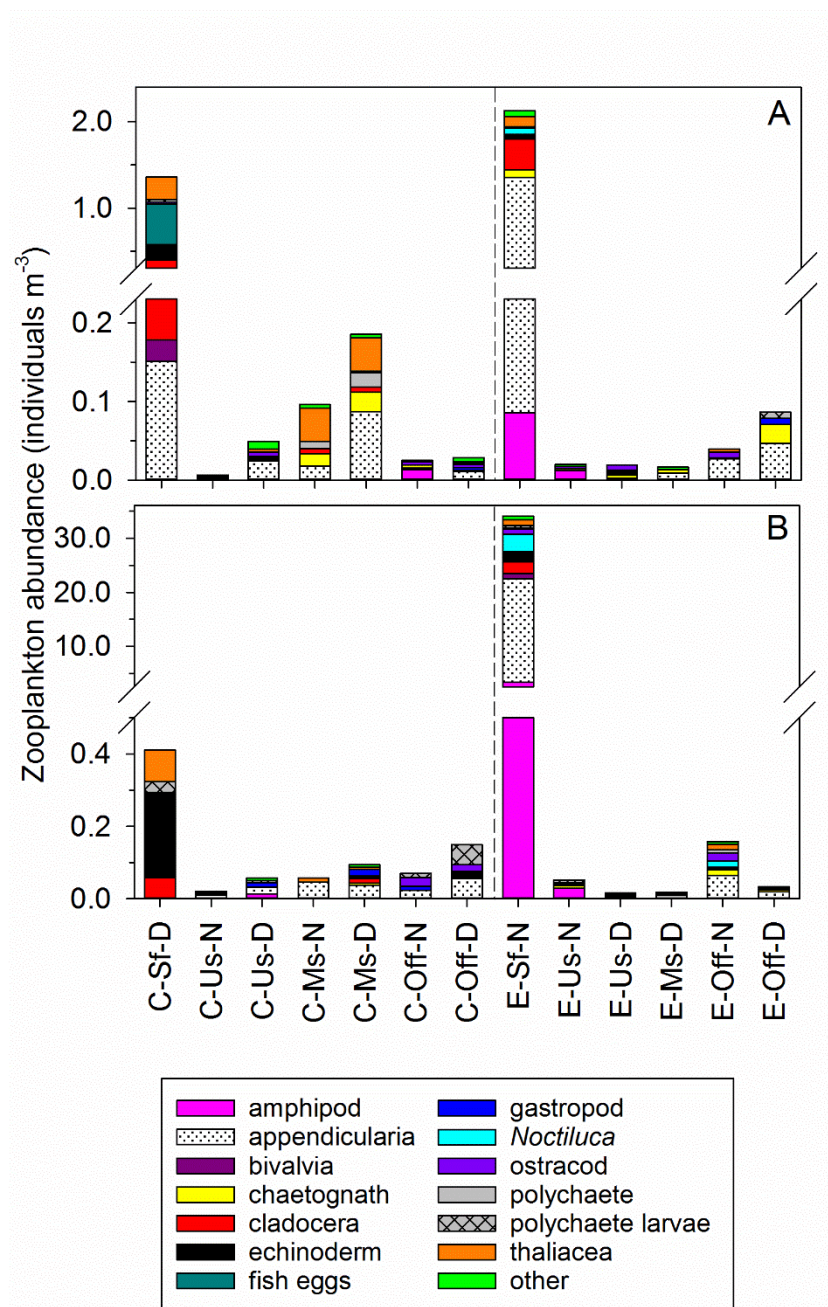


Figure 4.1-14 Major zooplankton taxa (excluding copepods) ( $\times 10^3$  individuals  $m^{-3}$ ) in the 64  $\mu m$  (A) and 150  $\mu m$  (B) net in the Great Australian Bight (GAB). Prefix 'C' refers to Central GAB (to left of dashed line) and prefix 'E' refers to Eastern GAB (to the right of dashed line). Sf = shelf; Us = upper slope; Ms = mid slope; Off = offshore. Suffix 'N' and 'D' refer to night and day sampling respectively.

#### 4.1.4 Discussion

Surface waters of the central and eastern GAB were oligotrophic overall, with nitrate + nitrite concentrations commonly close to or below detection limit. These results are consistent with studies in the eastern GAB shelf showing a nutrient-deplete surface layer, concomitant with stratification occurring during the austral summer (van Ruth et al., 2010a; van Ruth et al., 2010b; van Dongen-Vogels et al., 2011; van Dongen-Vogels et al., 2012; Paterson et al., 2013b) and in shelf waters to the west of the central GAB (Motoda et al., 1978). However, below the surface mixed layer, the nutrient regime of the central GAB differed to that of the east at the time of the study, with the nutricline (and pycnocline – see Section 3.2) ~ 25 m deeper in the central GAB, and with the nutrient pool in the cmax and deep water (120 m) 2.3-fold and 1.3-fold higher respectively in the east. The upper 60 – 80 m of the water column, however, appeared to be nitrogen limited at the time of the study.

In line with these regional differences in the nutrient regime, and differences in the oceanographic and mixing processes at the time of the study (see Section 3.2), autotrophic communities differed between regions. Excluding shelf stations (discussed separately below), Tchl *a* was 1.7-fold higher in the eastern GAB than the central GAB. Highest autotrophic biomass (as Tchl *a*) always occurred below the surface, at depths of ~ 60 m in the eastern GAB, and ~ 70 – 90 m in the central GAB, likely reflecting the nutricline (and pycnocline) position in each region. Previous studies in the eastern GAB (Kämpf et al., 2004; van Ruth et al., 2010a; van Ruth et al., 2010b; van Dongen-Vogels et al., 2011; van Dongen-Vogels et al., 2012; Paterson et al., 2013b) have confirmed the presence of a sub-surface chlorophyll fluorescence maxima occurring commonly ~ 40 m or below in late October to March/April. Indeed, chl *a* concentrations up to ~ 1.3 µg L<sup>-1</sup> have been reported in the cmax on the eastern GAB shelf (van Ruth et al., 2010a; van Dongen-Vogels et al., 2011; van Dongen-Vogels et al., 2012). The occurrence of a sub-surface chlorophyll maxima is a consistent feature in many ocean realms (e.g. North Sea (Weston et al., 2005), Antarctic waters (Holm-Hansen and Hewes, 2004), Atlantic Ocean and Gulf of Mexico (Hobson and Lorenzen, 1972), Pacific Ocean (Furuya and Marumo, 1983) including the east and west coasts of Australia (Hanson et al., 2005; 2007; Thompson et al., 2011)). These sub-surface layers commonly represent enhanced autotrophic biomass (as in this study) and production compared to surface waters (Hanson et al., 2007; van Ruth et al., 2010a). As highlighted for the west coast of Australia (Hanson et al., 2007) and the eastern GAB (van Ruth et al., 2010a) the presence of these sub-surface peaks in phytoplankton biomass have important implications for the use of satellite derived surface estimates of phytoplankton biomass and productivity and their input into biogeochemical models, given surface signatures will likely underestimate productivity of the region.

The exception to the overall higher Tchl *a* in the slope and offshore waters of the eastern GAB, was on the shelf in the central GAB. Here, highest Tchl *a* was recorded for the region at the time of the study (1.24 µg L<sup>-1</sup>) and with > 60% of the biomass attributed to large (> 5 µm) phytoplankton, with the diatoms *Nitzschia* spp., *Chaetoceros* spp. and *Rhizosolenia* spp. dominating (in the cmax) and dinoflagellates dominating close to the benthos but with relatively high numbers of diatoms still present. *Nitzschia* spp. are commonly of benthic origin (Hallegraeff et al., 2010) and high abundances (up to 7.7 × 10<sup>3</sup> cells L<sup>-1</sup>; the highest abundance of any other diatom taxa at the time of the study) may indicate these diatoms are resuspended from the benthos. While in low abundances, *Pleurosigma* spp., considered a benthic diatom (Hallegraeff et al., 2010) was only present in shelf and upper slope waters of the central GAB.

Given downwelling conditions in the central GAB (Section 4.2.1), and oligotrophic surface waters, the relatively high phytoplankton biomass in the central GAB was unexpected. Elevated silicate, which did not coincide with elevated nitrate + nitrite (or phosphate) occurred over the shelf,



suggesting an independent source of silicate exists on the shelf, possibly resuspension following remineralization in the sediments, or entering shelf waters via groundwater inflow. The extent of high autotrophic biomass in central GAB shelf waters is unclear given the paucity of data for the region and the one shelf sample taken during this study. While Motoda et al., (1978) showed overall lower chl *a* (reaching  $\sim 0.4 \mu\text{g L}^{-1}$ ) in their study on the western side of the central GAB, they also showed relatively high chl *a* in the mid water column and persisting down to near the benthos on the shelf. Our finding of relatively high phytoplankton biomass in central GAB shelf waters may link in with the high biomass of higher trophic organisms known to occur off the shelf in the central GAB (Young et al., 1999) (see Section 6). Possible sources and/or origins of silicate and the extent of high autotrophic biomass should be a focus of future research in the central GAB.

Excluding the central GAB shelf, phytoplankton less than  $5 \mu\text{m}$  dominated both regions. Differences in the size structure of autotrophic plankton communities was further evident in this less than  $5 \mu\text{m}$  fraction. For example, higher picophytoplankton abundances occurred in surface waters in the central GAB, with higher picophytoplankton abundances found in the cmax in the eastern GAB. While *Prochlorococcus* dominated cell counts in both regions, there was a shift towards increased cell abundances of all picophytoplankton groups in the east, and with a higher fraction of the community comprising *Synechococcus* and picoeukaryotes. Relatively high *Prochlorococcus* abundances fell within ranges previously reported in the eastern GAB (van Dongen-Vogels et al., 2011; van Dongen-Vogels et al., 2012; Paterson et al., 2013b), central GAB (SARDI unpublished data) and other tropical regions (e.g. Ningaloo, north-western Australia (Patten et al., 2011)), and which were an order of magnitude higher than *Prochlorococcus* abundances occurring in south western Australia waters (Paterson et al., 2013a). *Synechococcus* abundances reported here similarly fell within ranges previously reported in the eastern GAB, Ningaloo (Patten et al., 2011) and in the Kimberley (Jones et al., 2014), however Paterson et al., (2013b) reported *Synechococcus* abundances as high as  $\sim 65 \times 10^8 \text{ L}^{-1}$  to occur during periods of strong upwelling in the eastern GAB. Picoeukaryote abundances were on the lower end of the high numbers reported during upwelling events in the eastern GAB (van Dongen-Vogels et al., 2011; van Dongen-Vogels et al., 2012; Paterson et al., 2013b) but aligned with those previously reported in the central GAB (SARDI unpublished data).

Further shifts in the phytoplankton community less than  $5 \mu\text{m}$  in size was observed in the distributions and concentrations of biomarker pigments. For example, pigments indicative of *Prochlorococcus* (DVchl *a*) and *Synechococcus* (zea) made up the largest proportion of the combined biomarker pigment concentrations in the central GAB surface waters, with zea in the central and eastern GAB closely matching those relatively high concentrations (i.e.  $> 0.1 \mu\text{g L}^{-1}$ ) occurring in tropical waters off the eastern Australian coast (Thompson et al., 2011).

In addition to DVchl *a* and zea, 19hex ( $\sim$  Prymesiophytes), Chl *b* ( $\sim$  Chlorophytes) and 19but ( $\sim$  CXhrysophytes) made up a larger proportion of total biomass in the eastern GAB, indicative of a nanoplankton community. Similar concentrations of 19hex and 19but as shown here in the eastern GAB, were estimated by Thompson et al. (2011) for the same region. The presence of fuco in the less than  $5 \mu\text{m}$  fraction was most likely attributed to phytoplankton other than diatoms (i.e. prymnesiophytes or chrysophytes). In the greater than  $5 \mu\text{m}$  fraction, however, fuco concentrations up to  $0.40 \mu\text{g L}^{-1}$  and occurring at the high end of those reported for the east coast of Australia (Thompson et al., 2011) followed overall trends in diatom abundance determined via microscopy in both the central and eastern GAB.

Dinoflagellates made up a significant proportion of phytoplankton abundance via microscopy counts yet the biomarker pigment of autotrophic dinoflagellates, peri, was absent at all times in this study.



While this contrasts with (Thompson et al., 2015) who showed that at times, autotrophic dinoflagellates accounted for ~ 10 % of the community, our results suggest that the dinoflagellate community contained endosymbionts of other algal taxa, and/or that the community was primarily mixotrophic or heterotrophic. Mixotrophy is widely common in dinoflagellates (Stoecker, 1999)(Stoecker, 1999), which are known to feed on diverse taxa from bacteria, picoeukaryotes, to nanophytoplankton and other dinoflagellates (reviewed in Jeong et al., (2010)). Thompson et al., (2015) previously reported the presence of relatively large dinoflagellates (e.g. *Noctiluca*, *Ceratium*, *Gyrodinium* and *Protoperdinium*) and highlighted the abundant dinoflagellate community in eastern GAB shelf waters compared to other IMOS National Reference Stations around Australia. In this study, the most abundant dinoflagellates (Gymnodinioid group, *Gyrodinium* spp., and *Heterocapsa* spp.) prevailed in relatively high abundances through the central and eastern GAB. In other regions, dinoflagellates of the genus *Gyrodinium* and *Heterocapsa* have been shown to feed on bacteria, cyanobacteria, haptophytes, cryptophytes, Rhaphidophytes and small diatoms, while *Gyrodinium* is known to feed on cryptophytes (Jeong et al., 2010). Grazing by dinoflagellates on bacteria through to phytoplankton may represent a significant trophic pathway in GAB waters.

Estimates of the contribution of each of the picoplankton, nanoplankton 2 – 5 µm, nanoplankton 5 – 20 µm and microplankton, showed that overall, picophytoplankton dominated autotrophic biomass in the central GAB, and nanoplankton (2 – 5 µm) dominated in the eastern GAB. The significance of a high proportion of nanoplankton in the 2 – 5 µm fraction, particularly in the eastern GAB, is in line with growing evidence highlighting the importance of these relatively small and often missed autotrophs to biogeochemical cycling (Not et al., 2008; Worden et al., 2015). Concomitant with the relatively high proportion of nanoplankton 2 – 5 µm in size the eastern GAB, the microphytoplankton biomass was relatively high, together with highest diatom counts reported for the study ( $115 \times 10^3$  cells l<sup>-1</sup>). Here, the diatoms *Chaetoceros* spp. and *Guinardia striata* dominated but with *Nitzschia* spp. also present at relatively high concentrations. This peak in phytoplankton abundance in offshore waters may be due to nutrient enrichment of the photic zone via the presence of a cyclonic eddy at the time of sampling (see Section 3.2 and discussion below).

In contrast to the overall Tchl *a*, highest zooplankton abundance and biomass occurred on the shelf in the eastern GAB. Zooplankton biomass was an order of magnitude higher than previously reported for the eastern GAB and exceeded all zooplankton biomass measures for all IMOS National Reference Stations in 2010 and 2011 (Thompson et al., 2015). Copepods were dominated by cyclopoids and calanoids with nauplii making up the smallest fraction of total copepod abundance for any other station. Other dominant zooplankton taxa in shelf waters of the eastern GAB were cladocerans, appendicularians, thaliaceans, echinoderms and the predatory dinoflagellate *Noctiluca*. The significantly elevated zooplankton abundance on the eastern GAB shelf likely indicates an upwelling event in the prior ~ 2 weeks. The contradiction between high zooplankton biomass and low phytoplankton biomass is most likely due to the different time responses of plankton at different trophic positions. For example, small pico- and nano- phytoplankton will be the first groups to respond (~ days) to nutrient enrichment, larger microphytoplankton following after given sufficient nutrient uptake and growth (days to ~ a week) and predators of the phytoplankton (~ days – weeks). Approximately 2 weeks prior to sampling at the same station, relatively high nitrate + nitrite occurred within the photic zone (3.5 µM at 50 m depth) concomitant with cool (< 15°C) seawater temperatures indicative of upwelled water (McClatchie et al., 2006; van Ruth et al., 2010a; van Ruth et al., 2010b; van Dongen-Vogels et al., 2011; van Dongen-Vogels et al., 2012) at this same depth (unpublished IMOS data). Low phytoplankton here likely reflects high grazing rates on the phytoplankton, which translated into the elevated zooplankton biomass observed in this study.

Excluding the shelf stations, zooplankton biomass was similar between the central and eastern GAB. Differences in community structure were evident, however, with higher numbers of relatively smaller zooplankton occurring in the central GAB. These results support isotope results (Section 6.2) indicating a shorter food web (i.e. more efficient biomass transfer to high trophic levels) in the eastern GAB compared to the central GAB. Highest numbers of copepod nauplii occurring in offshore waters of the eastern GAB, concomitant with modest phytoplankton biomass, but with increased biomass of microphytoplankton also suggest a more recent enrichment event (~ days to 1 week) compared to that of the upwelling event described above. The mechanism or exact timing of this hypothesised enrichment is not clear, however the presence of a cyclonic eddy in offshore waters of the eastern GAB at the time of sampling, may be the source of nutrients, given uplift of the nutricline was shown to occur within the eddy (Figure 4.1.2 and see Section 3.2).

Bacteria and viruses showed the lowest variability between regions, depth and location within regions. Bacteria abundances fell within ranges previously found in the eastern and central GAB (Paterson et al., 2012; Paterson et al., 2013b; SARDI unpublished data) however virus abundances were overall lower than previously found from the same stations in the central and eastern GAB sampled in April 2013 (SARDI unpublished data). Relatively uniform bacterial abundances are well known to occur over large distances and oceanographic regimes (del Giorgio and Scarborough, 1995). However, the slight increase in the % HDNA bacteria in the eastern GAB may indicate these cells are larger and more metabolically active than the LDNA bacteria, which could represent smaller cells with low activity, and include dead and dormant cells (Troussellier et al., 1999; Gasol and Del Giorgio, 2000). Viruses were positively correlated with bacteria in both the central and eastern GAB suggesting bacteria to be major hosts of viruses. Significant positive relationships of the viral subgroups V2, V3 and V4 with all picophytoplankton groups also suggest viral infection of picophytoplankton in GAB waters. These results overall suggest a functioning microbial food web occurring over the central and eastern GAB region despite differences in nutrient sources and plankton community structure.

Variations in picophytoplankton, bacteria and virus communities were shown to be driven by changes in nitrate concentrations; or a co-varying and significantly related parameter (i.e. temperature, phosphate or silicate). Moving from smaller to larger planktonic organisms, this influence became weaker (as seen with lower correlation coefficients, Table 4.1-3). For zooplankton, recycled and intermediate nitrogen forms were better predictors of the community structure (Table 4.1-3). These differences are likely due to the time lag response of zooplankton following enrichment of the water column in the ~2 weeks prior.

Using multiple lines of evidence, our results indicate significant differences in the phytoplankton communities between the central and eastern GAB. Overall, in the central GAB, there was a dominance of picophytoplankton, particularly in surface waters, with the smallest picophytoplankton group, *Prochlorococcus*, numerically dominating cell counts (shown via flow cytometry) and with its accessory pigment, DV chl *a*, comprising a larger fraction of chl *a* biomass than in the east. While high abundances of *Prochlorococcus* also occurred in the eastern GAB in the cmax, the larger of the picophytoplankton, *Synechococcus* and picoeukaryotes, occurred in higher numbers and comprised a larger amount of chl *a* biomass than in the central GAB. In the eastern GAB, small nanophytoplankton (2 – 5 µm) comprised the largest fraction of chl *a* biomass (shown via pigment analysis), with Chlorophytes, Prymnesiophytes and Chrysophytes the dominant groups within this size fraction. A different trend was observed on the shelf in the central GAB and in the offshore station of the eastern GAB, where microphytoplankton dominated biomass (shown via pigments; with high biomass of Fuco) or showed relatively high abundances (via microscopy). At

these stations, picophytoplankton, bacteria and viruses also showed relatively high abundances. Therefore, our results do not suggest a displacement of a microbial food web with that of a classical food web (Ryther, 1969), but support a growing body of evidence showing growth of all autotrophic groups; albeit with different groups having different nutrient affinities and growth kinetics, with nutrient enrichment of the photic zone (Barber and Hiscock, 2006). However, biomass accumulation of small in comparison to larger phytoplankton is often modest due to high grazing rates on the former (Barber and Hiscock, 2006). High growth rates of diatoms under enrichment, which likely exceed those growth rates of pico- and nanophytoplankton, would then result in microphytoplankton biomass build up. The elevated diatom abundances in some locations in the central and eastern GAB may then indicate shorter and more efficient food chains at these times. The high numbers of dinoflagellates in addition to smaller flagellates, also point to high levels of grazing, and tight coupling between production and biomass accumulation in the GAB.

## References

- Azam, F. 1983. The ecological role of water-column microbes in the sea. *Marine Ecology Progress Series*, 10: 257-263.
- Barber, R., and Hiscock, M. 2006. A rising tide lifts all phytoplankton: Growth response of other phytoplankton taxa in diatom-dominated blooms. *Global Biogeochemical Cycles*, 20: GB4S03, doi:10.1029/2006GB002726.
- Brussaard, C. P. D. 2004. Optimization of procedures for counting viruses by flow cytometry. *Applied and Environmental Microbiology*, 70: 1506-1513.
- del Giorgio, P. A., and Scarborough, G. 1995. Increase in the proportion of metabolically active bacteria along gradients of enrichment in freshwater and marine plankton: implications for estimates of bacterial growth and production rates. *Journal of Plankton Research*, 17: 1905-1924.
- Finkel, Z. V. 2001. Light absorption and size scaling of light-limited metabolism in marine diatoms. *Limnology and Oceanography*, 46: 86-94.
- Fuhrman, J. A. 1999. Marine viruses and their biogeochemical effects. *Nature*, 399: 541-548.
- Furuya, K., and Marumo, R. 1983. The structure of the phytoplankton community in the subsurface chlorophyll maxima in the western North Pacific Ocean. *Journal of Plankton Research*, 5: 393-406.
- Gasol, J., M., and Del Giorgio, P., A. 2000. Using flow cytometry for counting natural planktonic bacteria and understanding the structure of planktonic bacterial communities. *Scientia Marina*, 64: 197-224.
- Hallegraeff, G. M., Bolch, C. J. S., Hill, D. R. A., Jameson, I., LeRoi, J.-M., McMinn, A., Murray, S., et al. 2010. *Algae of Australia: Phytoplankton of temperate coastal waters*, CSIRO Publishing, Melbourne.
- Hanson, C. E., Pattiaratchi, C. B., and Waite, A. M. 2005. Sporadic upwelling on a downwelling coast: Phytoplankton responses to spatially variable nutrient dynamics off the Gascoyne region of Western Australia. *Continental Shelf Research*, 25: 1561-1582.
- Hanson, C. E., Pesant, S., Waite, A. M., and Pattiaratchi, C. B. 2007. Assessing the magnitude and significance of deep chlorophyll maxima of the coastal eastern Indian Ocean. *Deep Sea Research Part II: Topical Studies in Oceanography*, 54: 884-901.

- Hobson, L. A., and Lorenzen, C. J. 1972. Relationships of chlorophyll maxima to density structure in the Atlantic Ocean and gulf of Mexico. *Deep Sea Research and Oceanographic Abstracts*, 19: 297-306.
- Holm-Hansen, O., and Hewes, C. D. 2004. Deep chlorophyll-a maxima (DCMs) in Antarctic waters. *Polar Biology*, 27: 699-710.
- Jeffrey, S. W. 1997. Application of pigment methods to oceanography. *In* *Phytoplankton pigments in oceanography: guidelines to modern methods*, pp. 127-166. Ed. by S. W. Jeffrey, R. F. C. Mantoura, and S. W. Wright. UNESCO, Paris.
- Jeong, H. J., Yoo, Y. D., Kim, J. S., Seong, K. A., Kang, N. S., and Kim, T. H. 2010. Growth, feeding and ecological roles of the mixotrophic and heterotrophic dinoflagellates in marine planktonic food webs. *Ocean Science Journal*, 45: 65-91.
- Jones, N. L., Patten, N. L., Krikke, D. L., Lowe, R. J., Waite, A. M., and Ivey, G. N. 2014. Biophysical characteristics of a morphologically-complex macrotidal tropical coastal system during a dry season. *Estuarine, Coastal and Shelf Science*, 149: 96-108.
- Kämpf, J., Doubell, M., Griffin, D., Matthews, R., L., and Ward, T. M. 2004. Evidence of a large seasonal coastal upwelling system along the southern shelf of Australia. *Geophysical Research Letters*, 31: doi:10.29/2003GL019221.
- Legendre, L., and Rassoulzadegan, F. 1995. Plankton and nutrient dynamics in marine waters. *Ophelia*, 41: 153-172.
- Legendre, L., and Rassoulzadegan, F. 1996. Food-web mediated export of biogenic carbon in oceans: Hydrodynamic control. *Marine Ecology Progress Series*, 145: 179-193.
- Marañón, E. 2009. Phytoplankton size structure. *In* *Encyclopedia of Ocean Science*, pp. 4252-4256. Ed. by J. H. Steele, K. K. Turekian, and S. A. Thorpe. Academic Press, Italy.
- Marañón, E., Cermeño, P., Latasa, M., and Tadonlécé, R. D. 2012. Temperature, resources, and phytoplankton size structure in the ocean. *Limnology and Oceanography*, 57: 1266-1278.
- Marañón, E., Cermeño, P., Latasa, M., and Tadonlécé, R. D. 2015. Resource supply alone explains the variability of marine phytoplankton size structure. *Limnology and Oceanography*, 60: 1848-1854.
- McClatchie, S., Middleton, J. F., and Ward, T. M. 2006. Water mass analysis and alongshore variation in upwelling intensity in the eastern Great Australian Bight. *Journal of Geophysical Research: Oceans*, 111: doi:10.1029/2004JC002699.
- Middleton, J. F., and Bye, J. A. T. 2007. A review of the shelf-slope circulation along Australia's southern shelves: Cape Leeuwin to Portland. *Progress in Oceanography*, 75: 1-41.
- Motoda, S., Kawamura, T., and Taniguchi, A. 1978. Differences in productivities between the Great Australian Bight and the Gulf of Carpentaria, Australia, in summer. *Marine Biology*, 46: 93-99.
- Not, F., Latasa, M., Scharek, R., Viprey, M., Karleskind, P., Balagué, V., Ontoria-Oviedo, I., et al. 2008. Protistan assemblages across the Indian Ocean, with a specific emphasis on the picoeukaryotes. *Deep Sea Research Part I: Oceanographic Research Papers*, 55: 1456-1473.
- Paterson, H., Heel, K., and Waite, A. 2013a. A warm-core eddy linking shelf, Leeuwin Current and oceanic waters demonstrated by near-shelf distribution patterns of *Synechococcus* spp. and *Prochlorococcus* spp. in the eastern Indian Ocean. *Marine and Freshwater Research*, 64: 1011-1021.

- Paterson, J. S., Nayar, S., Mitchell, J. G., and Seuront, L. 2012. A local upwelling controls viral and microbial community structure in South Australian continental shelf waters. *Estuarine, Coastal and Shelf Science*, 96: 197-208.
- Paterson, J. S., Nayar, S., Mitchell, J. G., and Seuront, L. 2013b. Population-specific shifts in viral and microbial abundance within a cryptic upwelling. *Journal of Marine Systems*, 113–114: 52-61.
- Patten, N. L., Wyatt, A. S. J., Lowe, R. J., and Waite, A. M. 2011. Uptake of picophytoplankton, bacterioplankton and viroplankton by a fringing coral reef community (Ningaloo Reef, Australia). *Coral Reefs*, 30: 555-567.
- Rogers, P. J., Ward, T. M., van Ruth, P. D., Williams, A., Bruce, B. D., Connell, S. D., Currie, D. R., et al. 2013. Physical processes, biodiversity and ecology of the Great Australian Bight region: a literature review. CSIRO, Australia.
- Ryther, J. H. 1969. Photosynthesis and fish production in the sea. *Science*, 166: 72-76.
- Stoecker, D. K. 1999. Mixotrophy among Dinoflagellates. *Journal of Eukaryotic Microbiology*, 46: 397-401.
- Suttle, C. A. 2007. Marine viruses - major players in the global ecosystem. *Nature Reviews Microbiology*, 5: 801-811.
- Thomson, P. G., Davidson, A. T., and Maher, L. 2016. Increasing CO<sub>2</sub> changes community composition of pico- and nano-sized protists and prokaryotes at a coastal Antarctic site. *Marine Ecology Progress Series*, 554: 51-69.
- Thompson, P., Bonham, P., Waite, A., Clementson, L., Cherukuru, N., Hassler, C., and Doblin, M. 2011. Contrasting oceanographic conditions and phytoplankton communities on the east and west coasts of Australia. *Deep Sea Research Part II: Topical Studies in Oceanography*, 58: 645-663.
- Thompson, P. A., Bonham, P., Thomson, P., Rochester, W., Doblin, M. A., Waite, A. M., Richardson, A., et al. 2015. Climate variability drives plankton community composition changes: the 2010–2011 El Niño to La Niña transition around Australia. *Journal of Plankton Research*, 37: 966-984.
- Troussellier, M., Courties, C., Lebaron, P., and Servais, P. 1999. Flow cytometric discrimination of bacterial populations in seawater based on SYTO 13 staining of nucleic acids. *FEMS Microbiology Ecology*, 29: 319-330.
- Uitz, J., Huot, Y., Bruyant, F., Babin, M., and Claustre, H. 2008. Relating phytoplankton photophysiological properties to community structure on large scales. *Limnology and Oceanography*, 53: 614-630.
- van Dongen-Vogels, V., Seymour, J. R., Middleton, J. F., Mitchell, J. G., and Seuront, L. 2011. Influence of local physical events on picophytoplankton spatial and temporal dynamics in South Australian continental shelf waters. *Journal of Plankton Research*, 33: 1825-1841.
- van Dongen-Vogels, V., Seymour, J. R., Middleton, J. F., Mitchell, J. G., and Seuront, L. 2012. Shifts in picophytoplankton community structure influenced by changing upwelling conditions. *Estuarine, Coastal and Shelf Science*, 109: 81-90.
- Van Heukelem, L., and Thomas, C., S. 2001. Computer-assisted high-performance liquid chromatography method development with applications to the isolation and analysis of phytoplankton pigments. *Journal of Chromatography A*, 910: 31-49.
- van Ruth, P. D., Ganf, G. G., and Ward, T. M. 2010a. Hot-spots of primary productivity: An alternative interpretation to conventional upwelling models. *Estuarine, Coastal and Shelf Science*, 90: 142-158.

- van Ruth, P. D., Ganf, G. G., and Ward, T. M. 2010b. The influence of mixing on primary productivity: A unique application of classical critical depth theory. *Progress in Oceanography*, 85: 224-235.
- van Ruth, P. D., and Ward, T. M. 2009. Meso-zooplankton abundance, distribution and community composition in the eastern Great Australian Bight. *Transactions of the Royal Society of South Australia*, 133: 274-283.
- Vidussi, F., Claustre, H., Manca, B. B., Luchetta, A., and Marty, J.-C. 2001. Phytoplankton pigment distribution in relation to upper thermocline circulation in the eastern Mediterranean Sea during winter. *Journal of Geophysical Research: Oceans*, 106: 19939-19956.
- Ward, T. M., McLeay, L. J., Dimmlich, W. F., Rogers, P. J., McClatchie, S. A. M., Matthews, R., Kämpf, J., et al. 2006. Pelagic ecology of a northern boundary current system: effects of upwelling on the production and distribution of sardine (*Sardinops sagax*), anchovy (*Engraulis australis*) and southern bluefin tuna (*Thunnus maccoyii*) in the Great Australian Bight. *Fisheries Oceanography*, 15: 191-207.
- Weston, K., Fernand, L., Mills, D. K., Delahunty, R., and Brown, J. 2005. Primary production in the deep chlorophyll maximum of the central North Sea. *Journal of Plankton Research*, 27: 909-922.
- Worden, A. Z., Follows, M. J., Giovannoni, S. J., Wilken, S., Zimmerman, A. E., and Keeling, P. J. 2015. Rethinking the marine carbon cycle: Factoring in the multifarious lifestyles of microbes. *Science*, 347.
- Young, J., Nishida, T., and Stanley, C. 1999. A Preliminary survey of the summer hydrography and plankton biomass of the eastern Great Australian Bight, Australia. Southern Bluefin Tuna Recruitment Monitoring and Tagging Program. CSIRO, Hobart, 15 pp.



## Microbes and plankton

### 4.1.5 Appendix: Phytoplankton data

Table 4.1-5 Phytoplankton abundances (cells L<sup>-1</sup>) per sampled depth at the shelf, upper slope, mid slope and offshore stations in the central and eastern Great Australian Bight (GAB).

Group	Species/Genus	C-Sf-D			C-Us-D			C-Ms-D			C-Off-D			E-Sf-N			E-Us-D			E-Ms-D			E-Off-D		
		Surface	cmax	Deep	Surface	cmax	Deep	Surface	cmax	Deep	Surface	cmax	Deep	Surface	cmax	Deep	Surface	cmax	Deep	Surface	cmax	Deep	Surface	cmax	Deep
Diatom	<i>Amphora</i> sp.	0	0	200	0	0	0	0	0	0	100	0	0	0	0	0	0	0	0	0	0	0	0	250	0
Diatom	<i>Asterionellopsis glacialis</i>	0	0	0	0	0	0	0	0	0	0	0	0	0	0	0	0	0	0	0	0	0	400	0	0
Diatom	<i>Attheya</i> sp.	250	0	0	0	0	0	0	0	0	0	0	0	0	0	0	0	0	0	25	0	0	0	0	0
Diatom	<i>Bacteriastrium elegans</i>	750	0	0	75	0	25	0	0	0	0	0	0	0	130	0	0	0	0	400	0	0	0	500	0
Diatom	<i>Cerataulina pelagica</i>	0	0	0	0	0	0	0	0	0	0	0	0	1000	2800	600	0	0	0	0	0	0	0	4000	0
Diatom	<i>Ceratoneis/Cylindrotheca closterium</i>	750	400	1000	0	200	25	0	400	400	0	50	0	1000	400	400	25	0	0	25	0	100	800	7000	300
Diatom	<i>Chaetoceros</i> spp.	4000	1600	3000	2200	3800	150	7300	3000	900	1200	600	200	250	1000	900	0	0	200	1000	2800	0	11000	39000	600
Diatom	<i>Climacodium frauenfeldianum</i>	350	0	600	25	0	0	0	0	0	0	0	0	0	0	0	0	0	0	0	0	0	0	0	0
Diatom	<i>Cocconeis</i> spp.	500	0	400	0	200	0	0	0	100	0	200	300	500	200	300	25	200	100	200	0	800	0	0	100
Diatom	<i>Corethron criophilum</i>	0	0	0	0	200	75	0	50	25	0	25	0	0	0	0	0	0	0	0	0	0	0	250	0
Diatom	<i>Coscinodiscus</i> spp.	0	0	0	0	0	0	25	75	0	0	75	0	0	0	0	0	0	25	0	0	50	0	250	0
Diatom	<i>Cyclotella</i> spp.	2800	1000	1200	2400	1000	1500	2800	800	1900	1700	600	1300	3500	400	900	2600	600	1000	1000	1300	2400	4400	4000	1000
Diatom	<i>Dactyliosolen fragilissimus</i>	500	600	0	0	0	25	3300	150	0	0	0	0	500	0	50	0	0	0	0	0	0	0	0	0
Diatom	<i>Diploneis</i> sp.	0	75	50	0	0	0	0	0	0	0	0	0	0	0	0	0	0	0	0	0	0	0	0	0
Diatom	<i>Entomoneis</i> sp.	0	400	0	0	0	0	0	0	0	0	0	0	0	25	0	0	0	0	0	0	0	0	0	0
Diatom	<i>Ephmera</i> sp.	0	0	0	0	0	0	0	50	0	0	50	0	0	0	0	0	0	0	0	0	0	0	0	0
Diatom	<i>Eucampia zodiacus</i>	0	0	0	0	0	75	0	130	0	0	0	0	0	0	0	0	0	0	0	0	0	0	4000	0
Diatom	<i>Fragilaria</i> sp.	0	1000	0	25	0	0	0	200	100	0	25	0	0	0	0	0	0	0	0	0	0	0	0	0
Diatom	<i>Grammotophora marina</i>	0	0	0	0	0	50	0	0	0	0	0	0	0	0	0	0	0	0	0	0	0	0	0	0
Diatom	<i>Guinardia flaccida</i>	0	25	0	0	0	0	0	0	0	0	0	0	0	50	0	0	0	0	0	0	0	0	0	25
Diatom	<i>Guinardia striata</i>	100	800	2000	0	0	25	500	25	0	0	0	0	75	0	150	0	0	0	0	0	130	0	17000	75
Diatom	<i>Hemiaulus membranaceus</i>	1800	0	0	100	50	0	250	0	0	0	0	0	0	0	0	0	0	0	0	0	0	0	2000	0
Diatom	<i>Hemidiscus</i> sp.	0	25	0	0	0	0	0	0	0	0	0	0	0	0	0	0	0	0	0	0	0	0	0	0
Diatom	<i>Lauderia annulata</i>	0	0	0	0	0	0	0	0	0	0	0	0	0	800	300	0	0	0	0	0	0	0	0	0
Diatom	<i>Leptocylindrus danicus</i>	2300	0	800	1600	150	500	0	200	0	0	0	0	130	330	400	0	0	0	200	0	0	0	0	25
Diatom	<i>Licmophora</i> sp.	250	0	0	0	0	0	0	0	0	0	0	0	0	0	0	0	0	0	0	0	0	0	0	0
Diatom	<i>Lioloma pacificum</i>	0	400	100	0	0	250	0	0	0	0	200	0	0	0	0	0	0	0	0	0	0	600	250	0
Diatom	<i>Minidiscus trioculatus</i>	0	0	0	0	0	0	0	0	0	0	0	0	500	0	0	0	200	0	0	0	0	0	0	0
Diatom	<i>Naviculoid</i> spp.	500	1400	1200	0	200	25	0	25	0	200	400	0	1500	400	400	200	0	100	0	0	200	200	2000	0
Diatom	<i>Nitzschia</i> spp.	2500	77000	62000	800	800	700	1000	2800	400	1200	6600	500	2000	800	2200	1400	600	200	600	1800	900	800	14000	1100

## 4.1-5 continued

Group	Species/Genus	C-Sf-D			C-Us-D			C-Ms-D			C-Off-D			E-Sf-N			E-Us-D			E-Ms-D			E-Off-D		
		Surface	cmax	Deep	Surface	cmax	Deep	Surface	cmax	Deep	Surface	cmax	Deep	Surface	cmax	Deep	Surface	cmax	Deep	Surface	cmax	Deep	Surface	cmax	Deep
Diatom	<i>Paralia sulcata</i>	0	100	0	0	0	0	0	0	0	0	0	0	0	0	0	0	0	0	0	0	0	0	0	0
Diatom	<i>Planktoniella</i> sp.	0	0	50	0	0	0	0	25	0	0	0	0	0	0	0	0	0	0	0	0	25	0	250	0
Diatom	<i>Pleurosigma</i> sp.	500	400	600	0	200	25	25	400	0	50	50	0	25	0	0	0	25	0	0	0	0	25	0	0
Diatom	<i>Proboscia alata</i>	1300	1200	350	0	400	0	250	0	0	0	0	0	0	0	0	0	0	0	100	0	75	1200	5000	0
Diatom	<i>Pseudo-nitzschia delicatissima</i> group	0	0	0	0	0	0	0	0	0	0	0	0	0	0	0	0	0	0	0	500	0	0	4000	0
Diatom	<i>Pseudosolenia calcar-avis</i>	0	200	180	0	0	0	0	0	0	0	0	0	0	0	0	0	0	0	0	0	0	0	0	0
Diatom	<i>Rhizosolenia setigera</i>	0	0	400	1000	130	50	500	0	0	0	0	0	0	0	0	0	0	0	0	0	0	0	0	0
Diatom	<i>Rhizosolenia</i> spp.	1300	1600	400	0	0	100	0	75	75	300	280	0	500	25	25	0	0	25	75	0	100	1400	4000	500
Diatom	<i>Skeletonema costatum/pseudocostatum</i>	0	0	0	0	0	0	0	0	0	0	0	0	0	0	0	400	0	0	0	0	0	0	0	0
Diatom	<i>Thalassionema</i> sp.	500	200	800	600	25	0	0	0	0	0	130	0	0	0	0	0	0	25	0	0	0	0	0	0
Diatom	<i>Thalassiosira</i> sp.	0	400	130	200	0	0	0	0	0	0	0	0	600	400	0	0	0	0	75	100	600	7000	300	0
Diatom	<i>Thalassiosira</i> cf. <i>mala</i>	0	0	0	0	0	0	0	0	0	0	0	0	0	0	0	0	0	0	500	600	0	0	0	0
Dinoflagellate	<i>Amphidinium</i> sp.	0	0	0	0	0	100	0	0	0	0	0	0	0	0	0	0	0	0	0	0	0	0	0	100
Dinoflagellate	<i>Amphisolenia globifera</i>	0	0	0	0	0	0	0	25	0	0	0	0	0	0	0	0	0	0	0	0	0	0	0	0
Dinoflagellate	<i>Blepharocysta splendor-maris</i>	25	0	0	0	0	0	0	0	0	0	0	0	0	0	0	0	0	0	0	0	0	0	0	0
Dinoflagellate	<i>Ceratium furca</i>	0	0	0	0	0	0	0	25	0	0	0	0	0	0	0	25	0	0	0	0	0	0	0	0
Dinoflagellate	<i>Ceratium fusus</i>	100	50	200	50	0	0	0	0	0	0	25	0	0	0	0	0	0	0	0	0	0	25	0	0
Dinoflagellate	<i>Ceratium lineatum</i>	0	0	0	0	0	0	0	25	0	0	0	0	0	0	0	0	25	0	0	0	0	0	500	0
Dinoflagellate	<i>Ceratium tenue</i>	25	0	0	0	0	0	25	0	0	0	0	0	25	0	0	0	0	0	25	0	0	0	0	0
Dinoflagellate	<i>Ceratium teres</i>	25	0	0	0	0	0	250	0	0	25	0	0	0	0	0	0	0	0	0	0	0	25	0	0
Dinoflagellate	<i>Ceratocorys horridum</i>	25	0	0	25	0	0	0	0	0	0	0	0	0	0	0	0	0	0	0	0	0	0	0	0
Dinoflagellate	<i>Cochlodinium</i> spp.	250	200	0	0	130	50	0	200	0	0	0	0	0	75	300	0	800	0	0	1500	50	50	1000	75
Dinoflagellate	<i>Corythodinium constrictum</i>	0	0	0	0	0	25	0	0	0	0	0	0	0	0	0	0	0	0	0	0	0	0	0	0
Dinoflagellate	<i>Goniodoma polyedricum</i>	100	0	0	0	0	0	0	0	0	0	0	0	0	0	0	0	0	0	0	0	0	25	0	0
Dinoflagellate	<i>Gonyaulax</i> spp.	2800	0	0	100	0	0	25	25	0	0	0	0	0	0	25	25	0	0	0	25	25	50	1000	25
Dinoflagellate	Gymnodinioid group	17000	11000	17000	12000	18000	3200	8800	7800	3600	6600	14000	3800	8000	7200	5000	7000	10000	3000	10000	17000	2700	14000	12000	4100
Dinoflagellate	<i>Gyrodinium</i> spp.	6800	4600	90000	7000	10000	2900	4300	2200	2000	2100	7200	2000	4000	1800	2100	4200	5400	1600	3200	13000	1500	4600	6000	1800
Dinoflagellate	<i>Heterocapsa</i> spp.	5000	1400	1200	6600	3200	500	5800	1200	0	2900	4000	300	7500	3800	400	800	2000	0	3000	3500	300	2800	4000	400
Dinoflagellate	<i>Karenia mikimotoi</i>	0	0	0	0	25	0	0	0	0	0	0	0	0	0	0	0	0	0	50	0	0	0	0	0
Dinoflagellate	<i>Karenia</i> sp.	0	0	0	0	0	0	0	0	0	50	0	0	0	0	0	0	0	0	0	0	25	0	0	50
Dinoflagellate	<i>Karlodinium</i> sp.	0	50	0	0	0	0	0	0	0	250	150	0	150	100	130	100	75	500	0	100	50	130	0	0

## Microbes and plankton

### 4.1-5 continued

		C-Sf-D			C-Us-D			C-Ms-D			C-Off-D			E-Sf-N			E-Us-D			E-Ms-D			E-Off-D		
Group	Species/Genus	Surface	cmax	Deep	Surface	cmax	Deep	Surface	cmax	Deep	Surface	cmax	Deep	Surface	cmax	Deep	Surface	cmax	Deep	Surface	cmax	Deep	Surface	cmax	Deep
Dinoflagellate	<i>Katodinium glaucum</i>	25	0	0	0	600	0	0	200	0	75	0	0	500	75	25	800	400	0	0	25	100	200	500	25
Dinoflagellate	<i>Kryptoperidium</i> sp.	0	0	0	0	0	0	0	0	0	0	0	0	25	0	0	0	0	0	0	0	0	0	0	0
Dinoflagellate	<i>Lepidodinium chlorophorum</i>	0	0	0	0	0	0	0	0	0	0	0	0	0	0	0	0	0	0	0	0	0	250	0	0
Dinoflagellate	<i>Mesoporus perforatus</i>	100	0	0	0	0	0	0	0	0	0	0	0	0	0	0	0	0	0	0	0	0	0	0	0
Dinoflagellate	<i>Noctiluca scintillans</i>	0	0	0	0	0	0	0	0	0	0	0	0	0	0	0	0	0	0	25	0	0	0	0	0
Dinoflagellate	<i>Oxytoxum subulatum</i>	0	0	0	0	0	25	0	0	0	0	0	0	0	0	0	0	0	0	0	0	0	25	0	0
Dinoflagellate	<i>Oxytoxum</i> spp.	3300	600	2400	6800	3800	130	2000	2800	700	1200	1200	130	2500	1600	700	1800	800	400	1800	4000	700	2800	600	300
Dinoflagellate	<i>Peridinium</i> sp.	750	400	200	0	400	200	0	0	200	700	200	0	25	25	25	400	0	100	200	0	25	25	500	0
Dinoflagellate	<i>Phalacroma mitra</i>	0	0	0	0	0	0	0	0	0	0	0	0	0	0	0	0	0	0	25	0	0	0	0	0
Dinoflagellate	<i>Phalacroma rotundatum</i>	0	0	0	0	0	0	0	0	0	0	0	0	0	0	0	0	25	0	0	0	25	0	0	25
Dinoflagellate	<i>Podolampas bipes</i>	0	0	0	0	0	0	0	0	0	0	0	0	0	0	0	0	0	25	0	0	0	0	0	0
Dinoflagellate	<i>Podolampas palmipes</i>	0	0	0	0	0	0	0	0	0	0	0	0	0	0	0	0	0	0	0	0	0	0	0	25
Dinoflagellate	<i>Podolampas spinifera</i>	0	0	0	0	0	0	0	0	0	0	0	0	0	0	0	0	0	25	0	0	0	0	0	0
Dinoflagellate	<i>Pronoctiluca spinifera</i>	0	0	0	0	0	75	0	0	0	75	25	25	25	25	0	0	0	0	25	0	25	0	0	25
Dinoflagellate	<i>Prorocentrum concavum</i>	25	0	0	0	0	0	0	0	0	0	0	0	25	0	0	0	0	0	0	0	0	0	0	0
Dinoflagellate	<i>Prorocentrum cordatum</i>	0	0	0	0	0	100	0	75	0	25	25	0	150	25	0	25	0	0	250	0	0	250	50	0
Dinoflagellate	<i>Prorocentrum dentatum</i>	0	0	0	0	0	0	0	0	0	0	50	0	250	0	0	0	400	0	0	25	0	25	250	0
Dinoflagellate	<i>Prorocentrum rhathymum</i>	0	200	0	0	0	0	0	0	0	0	0	0	0	0	0	0	0	0	0	0	0	25	0	0
Dinoflagellate	<i>Prorocentrum</i> sp.(cf. balticum)	0	0	0	0	0	0	0	0	0	0	0	0	0	0	0	0	0	0	0	0	0	25	250	0
Dinoflagellate	<i>Protoperidinium</i> spp.	0	25	0	0	400	0	0	0	0	0	0	0	25	50	25	0	0	0	200	25	75	25	250	25
Dinoflagellate	<i>Pselodinium</i> sp.	0	0	0	0	0	0	0	0	0	0	0	0	0	0	0	0	0	0	0	0	0	50	0	0
Dinoflagellate	<i>Scrippsiella</i> spp.	50	25	400	0	0	0	100	0	0	50	50	0	100	0	25	25	0	0	50	130	25	25	750	25
Dinoflagellate	<i>Takayama</i> spp.	0	0	0	0	0	0	0	0	0	50	0	0	250	75	0	50	0	0	0	25	0	200	750	0
Dinoflagellate	<i>Torodinium</i> sp.	0	25	400	0	0	200	0	200	200	25	25	75	25	130	130	0	400	300	400	200	50	400	500	500
Dinoflagellate	<i>Warnowia</i> spp.	50	0	25	25	130	200	0	0	0	0	200	0	0	0	0	0	0	50	0	130	0	75	0	50
Cryophytes	<i>Dinobryon</i> sp.	1500	0	0	400	200	200	0	0	25	0	200	0	0	25	0	200	0	25	0	750	0	0	0	0
Cryophytes	<i>Ochromonas</i> spp.	1300	0	600	600	400	1200	500	0	0	500	800	400	4500	2200	400	400	800	200	0	1300	300	200	1000	700
Prymnesiophytes	<i>Chrysochromulina</i> spp.	11000	2600	2200	5800	2000	500	2800	1200	100	900	1000	1100	3000	1200	1900	4400	600	300	1800	4000	200	3200	3000	500
Prymnesiophytes	<i>Emiliana huxleyi</i>	0	0	200	0	0	0	750	200	0	0	0	0	2000	0	200	800	0	200	200	750	0	600	1000	100
Prymnesiophytes	<i>Prymnesium patellifera</i>	0	0	0	0	0	0	0	0	0	0	0	0	0	0	0	0	200	0	0	0	0	0	0	0

## 4.1-5 continued

Group	Species/Genus	C-Sf-D			C-Us-D			C-Ms-D			C-Off-D			E-Sf-N			E-Us-D			E-Ms-D			E-Off-D		
		Surface	cmax	Deep	Surface	cmax	Deep	Surface	cmax	Deep	Surface	cmax	Deep	Surface	cmax	Deep	Surface	cmax	Deep	Surface	cmax	Deep	Surface	cmax	Deep
Cryptophytes	<i>Hemiselmis</i> sp.	4300	1000	2200	2400	1800	2100	1300	800	400	0	200	800	3000	1400	1500	600	600	1000	600	750	100	200	3000	300
Cryptophytes	<i>Leucocryptos</i> spp.	750	400	400	0	1200	400	750	800	200	200	200	300	0	1400	500	200	800	200	400	1000	100	400	250	400
Cryptophytes	<i>Plagioselmis prolunga</i>	500	2000	400	0	0	800	250	0	600	200	400	100	4000	1600	300	0	1000	700	1000	2000	200	1200	2000	200
Cryptophytes	<i>Rhodomonas salina</i>	0	0	0	0	0	0	0	800	0	0	0	0	0	0	0	0	0	0	0	25	0	0	0	0
Cryptophytes	<i>Teleaulax acuta</i>	0	0	0	0	0	0	0	0	0	0	0	100	0	0	100	0	400	100	0	250	0	200	0	200
Prasinophytes	<i>Cymbomonas tetramitiformis</i>	1000	0	800	0	0	0	0	0	300	300	0	0	500	0	100	0	0	0	400	0	0	0	0	0
Prasinophytes	<i>Halosphaera viride</i>	1800	1000	600	0	0	75	0	0	0	0	0	0	500	25	100	800	600	100	200	750	100	1400	500	0
Prasinophytes	<i>Nephroselmis</i> spp.	4000	800	1200	1600	2200	1200	1300	1400	0	200	400	500	0	400	100	1000	200	600	0	1000	200	0	1000	100
Prasinophytes	<i>Pterosperma</i> sp.	1300	0	200	600	800	0	250	0	0	200	0	0	25	0	0	600	0	0	600	250	500	1000	0	0
Prasinophytes	<i>Pyramimonas</i> spp.	5800	2000	3000	2400	1600	500	1300	2000	500	600	400	100	4000	1800	200	1200	800	700	400	2000	200	1400	3000	500
Prasinophytes	<i>Tetraselmis</i> spp.	0	0	200	0	0	0	0	0	200	0	0	0	0	0	100	0	200	100	0	1300	100	600	0	0
Euglenophyta	<i>Eutreptiella</i> spp.	0	0	0	0	25	100	0	0	25	0	0	200	0	0	130	0	0	200	200	250	100	200	1000	0
Other flagellates	<i>Apedinella spinifera</i>	0	0	0	0	0	0	0	200	0	0	0	0	0	0	0	0	0	0	0	500	0	0	0	0
Other flagellates	<i>Dictyocha fibula</i>	0	200	0	25	25	0	0	0	100	0	75	25	0	0	0	0	50	25	0	0	75	0	500	100
Other flagellates	<i>Heterosigma akashiwo</i>	0	0	0	0	0	0	50	0	0	0	0	0	500	0	0	0	25	0	0	0	0	0	0	0
Other flagellates	<i>Paulinella</i> sp.	250	0	0	0	0	0	0	0	0	0	0	0	0	0	0	0	0	0	0	0	0	0	0	0
Other flagellates	<i>Telonema subtilis</i>	0	0	0	0	200	0	0	0	0	0	0	0	0	0	0	0	0	0	0	0	0	0	0	0
Other flagellates	<i>Mesodinium rubrum</i>	0	0	0	0	0	0	0	0	0	0	0	0	0	0	0	0	0	0	0	250	0	0	0	0

## 4.2 Physiological process studies, productivity, and food web dynamics

van Ruth, P.D., Patten, N.L., Redondo, A., Laverock, B., Seymour, J.

### 4.2.1 Introduction

Understanding variations in ecosystem productivity requires close examination of changes in the biomass and size distribution of the different trophic levels of the food web. Using this information alone, however, often results in incorrect conclusions. For example, it is often suggested that low chlorophyll *a* (chl *a*) concentrations equate to low productivity, but this is not necessarily always the case. It is possible for primary productivity to be high when chl *a* is low (e.g. van Ruth et al. 2009). Such conditions would occur at the onset of bloom development, or could indicate significant grazing of phytoplankton biomass. To fully comprehend the drivers of variation in ecosystem productivity, it is necessary to not only assess biomass, but consider the rates of the physiological processes that facilitate the accumulation and transfer of this biomass. In the case of the lower trophic ecosystem, the main processes affecting productivity include primary production (new carbon production), and grazing (transfer of carbon up the food web to higher trophic levels). Rates of these processes, and ultimately overall ecosystem productivity, will be determined by food web dynamics (i.e. the biomass and size distribution of plankton communities and the physical and optical properties of the water column in which they reside). Differences in food web dynamics between regions will have associated implications for ecosystem productivity.

Estimates of primary productivity are typically modelled as a function of a given depth in the water column (e.g. mixed layer depth, euphotic depth), the surface irradiance, the surface concentration of phytoplankton biomass (chl *a*), and the rate of photosynthesis, calculated as a function of sea surface temperature (e.g. Platt et al. 1991, Behrenfeld and Falkowski 1997). A deeper understanding of influence of variations in phytoplankton size structure on primary productivity can be gained by using size fractionated chl *a* data (if available). Thus, changes in food web dynamics between regions will have a significant effect on primary productivity, and the amount and size of food available for the primary consumers. This will, in turn, dictate the size and community composition of the primary consumers (e.g. heterotrophic bacteria, heterotrophic phytoplankton, micro- or mesozooplankton), and the efficiency of energy transfer up the food web to higher trophic levels. Thus, understanding the drivers of shifts in food web dynamics will provide new insights into the factors controlling overall ecosystem productivity in the GAB.

Van Ruth et al. (2010a) have previously characterised primary productivity in shelf regions of the eastern and central GAB according to three levels of classification:

- Offshore areas of the eastern and central GAB have low daily integral productivities ( $< 800 \text{ mg C m}^{-2} \text{ d}^{-1}$ ) that are comparable to values reported for the oligotrophic waters of the Leeuwin current off south west Western Australia ( $110 - 520 \text{ mg C m}^{-2} \text{ d}^{-1}$ , Hanson et al. 2005), the Australia – Indonesia Coastal (AuSW) and South Sub-tropical Convergence (SSTC) provinces of Longhurst et al. (1995) and the north and south Atlantic sub-tropical gyres ( $18 - 362 \text{ mg C m}^{-2} \text{ d}^{-1}$ , Maranon et al. 2003).
- Mid-shelf and coastal waters have intermediate productivities ( $800 - 1600 \text{ mg C m}^{-2} \text{ d}^{-1}$ ) that are comparable to those reported for localised upwellings off south west Western Australia ( $840 - 1310 \text{ mg C m}^{-2} \text{ d}^{-1}$ , Hanson et al. 2005), and for the waters of Bass Strait and the east coast of Tasmania ( $336 - 2880 \text{ mg C m}^{-2} \text{ d}^{-1}$ , highest rates associated with the spring bloom, Harris et al. 1987).

- Higher productivities also occur, but are restricted to distinct hotspots in the region. Productivity levels in coastal waters off south western Eyre Peninsula and south western Kangaroo Island in the east, and Cape Adieu in the central GAB ( $1600\text{--}3900\text{ mg C m}^{-2}\text{ d}^{-1}$ ) were within the range of productivities measured in the highly productive upwelling systems of the Benguela current off southern Africa ( $1000\text{--}3500\text{ mg C m}^{-2}\text{ d}^{-1}$ , Brown et al. 1991), and the Humboldt current off the coast of Chile ( $800\text{--}5100\text{ mg C m}^{-2}\text{ d}^{-1}$ , Daneri et al. 2000).

Slope and offshore waters of the eastern and central GAB fall within the SSTC province of Longhurst et al. (1995) and can hence be considered low in primary productivity. This study represents the first opportunity to assess the accuracy of this information with estimates of daily integral primary productivity calculated using *in situ* data.

Other microbial and planktonic processes may also provide information to assist our understanding of food web dynamics and productivity in the GAB. For example, ammonia oxidation is the first key step in the nitrification process, which involves the transformation of ammonium ( $\text{NH}_4^+$ ) to nitrite ( $\text{NO}_2^-$ ), and subsequently to nitrate ( $\text{NO}_3^-$ ). This is important within marine environments, because all three forms of inorganic nitrogen support primary production, with  $\text{NH}_4^+$  uptake typically being favoured by smaller phytoplankton, whereas  $\text{NO}_2^-$  and  $\text{NO}_3^-$  (collectively,  $\text{NO}_x$ ) are typically assimilated by larger taxa (Beman et al., 2011).  $\text{NH}_4^+$  concentrations are traditionally viewed as representing the supply of “regenerated” nitrogen, as opposed to “new”  $\text{NO}_x$  from upwelling for example. However, nitrification acts as a supply chain for regenerated  $\text{NO}_x$ , and can therefore impact the distribution and productivity of phytoplankton.

Dimethylsulfoniopropionate (DMSP) is an algal metabolite, produced by a variety of phytoplankton taxa and some bacteria. DMSP supports phytoplankton, primarily by scavenging reactive oxygen species associated with physiological stress (Sunda et al., 2002). DMSP is released from the phytoplankton cell in its dissolved form (DMSPd), which can provide up to 60% of bacterial carbon (C) demand, and 90% of bacterial sulphur (S) demand (Kiene and Lynn, 2000). DMSP is most prominently produced by dinoflagellates, prymnesiophytes and chrysophytes (Yoch 2002), all members of the  $>5\text{ }\mu\text{m}$  size fraction of phytoplankton communities. Variations in rates of DMSP production can thus provide insights into differences in phytoplankton community composition and size distribution between regions, and related changes in food web dynamics and productivity.

This chapter links physical, chemical and biological (biomass and abundance) data from Sections 3.1, 3.2 and 4.1 with information on microbial and planktonic physiological processes to provide new insights into the food webs of the eastern and central GAB. Data were analysed with the objective of testing one of the key hypotheses of the pelagic theme:

*That the “microbial food web” is the dominant planktonic food web over the deep GAB continental margin, particularly in the central GAB where year-round downwelling is thought to be the prevailing cross-margin flow, and that the more efficient “classic food web” only dominates in the eastern GAB during periods of nutrient-rich upwelling.*

#### 4.2.2 Methods

Physiological studies were conducted using samples or data collected from sampling locations outlined in Section 4.1 (see Figure 4.1-1). Sampling and analytical methods for characterising microbial and plankton biomass are also reported in Section 4.1. Techniques that make use of this information to examine microbial and planktonic physiological processes that may assist in explaining variation in food web dynamics between the central and eastern GAB are detailed below.



### Physical, optical and biological layer characterisation

To assist in the estimation of variation in primary productivity in the GAB, important physical, optical and biological layers were defined. The mixed layer depth (MLD) was calculated from CTD temperature profiles using a threshold method, with the criteria of de Boyer Montegut et al. (2004) (i.e. a temperature difference of 0.2°C). The measurement closest to 10 dbar is used as the reference value. The threshold MLDs were interpolated to exactly match the threshold criteria.

Euphotic depths ( $Z_{eu}$ ) were defined using CTD profiles of photosynthetically active radiation (PAR). The attenuation coefficient for downwelled irradiance ( $K_d$ ) was calculated as the slope of the regression line of the log-transformed PAR with respect to depth, which yields  $Z_{eu}$  when substituted into the Beer-Lambert equation:

$$Z_{eu} = \frac{1}{K_d} * \ln\left(\frac{100}{1}\right)$$

Irradiance profiles can be influenced by the shadow of the vessel, hence we calculated  $Z_{eu}$  using only PAR values from depths greater than 5 m. The depth of the chlorophyll maximum (DCM) was estimated from CTD fluorescence profiles. The layer below the DCM was calculated as the depth from the DCM to the base of  $Z_{eu}$ .

### Primary productivity

To provide context for our single-voyage data, primary productivity was first examined using data extracted from MODIS Aqua database using the Australian Ocean Data Network (AODN) portal. Chlorophyll *a* (chl *a*) from the OC3M algorithm was used, together with remote sensed sea surface temperature (SST), to estimate primary productivity using the Vertically Generalized Production Model (VGPM) of Behrenfeld and Falkowski (1997), modified following Eppley (1972), as implemented by Antoine and Morel (1996). One Km resolution data, centered around shelf, slope and offshore stations on Transect 2 (central GAB) and transect 6 (eastern GAB), were used to examine variations in monthly, climatological (seasonal) and long-term mean primary productivity in the euphotic zone in these regions, from 2002 to present day, according to the equation:

$$PP_{eu} = C_{sat} * P_{opt}^b * D_{irr} * \left[ 0.66125 * \frac{E_o}{(E_o + 4.1)} \right] * Z_{eu}$$

The  $C_{sat}$  is the remote-sensed surface chlorophyll concentration,  $P_{opt}^b$  is the optimal specific photosynthetic rate,  $D_{irr}$  is daylength in decimal hours,  $E_o$  is the monthly mean surface irradiance, and  $Z_{eu}$  is the euphotic depth.  $P_{opt}^b$  is estimated from SST according to the exponential relationship described by Morel (1991):

$$P_{opt}^b = 1.54 * 10^{[(0.0275 * sst) - 0.07]}$$

Euphotic depth ( $Z_{eu}$ ) can be estimated from  $C_{sat}$  following:

$$Z_{eu} = \begin{cases} 568.2(C_{tot})^{-0.746} \rightarrow \text{if } C_{tot} < 102 \\ 200.0(C_{tot})^{-0.293} \rightarrow \text{if } C_{tot} > 102 \end{cases}$$

Where

$$C_{tot} = \begin{cases} 38.0(C_{sat})^{0.425} \rightarrow \text{if } C_{sat} < 1.0 \\ 40.2(C_{sat})^{0.507} \rightarrow \text{if } C_{sat} \geq 1.0 \end{cases}$$

*In situ* voyage data was used in the Eppley-VGPM to provide a more accurate estimation of daily integral primary productivity in the two regions at the time of the voyage. Surface extracted chl *a* concentrations ( $C_{surf}$ ), measured via High Pressure Liquid Chromatography (HPLC, as detailed in 4.1.2) were substituted into the equations above in place of  $C_{sat}$ .  $P_{bopt}$  was estimated using CTD measured SST. The daily mean surface irradiance, provided by the Bureau of Meteorology (<http://www.bom.gov.au/climate/>) from Nullarbor (central GAB) and Neptune Islands (eastern GAB) weather stations, was used in place of  $E_o$ . Daylength was calculated using sunrise/sunset times for Nullarbor and Neptune Islands, extracted from the Geoscience Australia Website (<http://www.ga.gov.au/geodesy/astro/sunrise.jsp>). The above parameters were used to estimate levels of daily integral productivity across important vertical layers within the water column; within the euphotic zone, the surface mixed layer (SML), and the layer from the surface down to the chlorophyll maximum (DCM). Productivity was also estimated for the layer below the chlorophyll maximum (sub-DCM), with the extracted chl *a* concentration at the chlorophyll maximum used in place of  $C_{surf}$ . Daily mean surface irradiance was adjusted to the level corresponding to that at the chlorophyll maximum, corrected as a proportion of the surface level following an examination of the vertical irradiance profile measured by the CTD.  $P_{opt}^b$  was estimated using CTD-measured temperature at the chlorophyll maximum. Daylength was calculated as above. Finally, daily integral productivity calculated for the layer from the surface down to the chlorophyll maximum was added to daily integral productivity calculated for the layer below the chlorophyll maximum to provide corrected value for daily integral primary productivity in the euphotic zone that takes into account the increased productivity at the chlorophyll maximum.

In order to examine spatial variation in the contribution of the large and small size fractions of phytoplankton biomass to total primary productivity, the above calculations were repeated using values reported in 4.1.3 for the < 5  $\mu\text{m}$  and > 5  $\mu\text{m}$  size fractions, and total chl *a* (sum of chl *a* from the < 5  $\mu\text{m}$  and > 5  $\mu\text{m}$  fractions)

#### *Micro-zooplankton grazing*

Microzooplankton grazing experiments were conducted from water collected at the chlorophyll maximum at stations 2\_1, 2\_3, 2\_4, 2\_7, 6\_4 and 6\_8 (note the experiments did not work at 6\_8 and were not conducted at 6\_1 due to time constraints on this station). Whole seawater (WSW) was collected using niskin bottles mounted on the rosette and gently filtered through 200  $\mu\text{m}$  mesh to remove mesozooplankton predators. A portion of the seawater was gravity-filtered through a 0.8/0.2  $\mu\text{m}$  filter (PALL Acropak) to yield filtered seawater (FSW). WSW was diluted with FSW to 20 % WSW. For each dilution (100 % and 20 %), duplicate 2 L polycarbonate bottles were filled gently to the top using silicon tubing, bottles were screened to *in situ* light levels and incubated at ambient seawater temperature for 24 hours in a flow-through seawater chamber. Additional duplicate bottles were filled for samples taken at the commencement of the incubation. For a set of experiments at each station, an additional set of bottles were set up and amended with  $\text{KH}_2\text{PO}_4$  (0.03  $\mu\text{M}$ ),  $\text{NH}_4\text{Cl}$  (0.5  $\mu\text{M}$ ),  $\text{FeSO}_4$  (1.0 nM) and  $\text{MnSO}_4$  (0.1 nM) (Landry et al. 1995) to determine whether nutrient limitation occurred. From each bottle, samples for picophytoplankton, bacteria, and Chl *a* were taken at the start ( $t_0$ ) and end ( $t_{24}$ ) of the experiment. Bottles, silicon tubing and filters were acid-washed (give HLC grade) prior to each experiment to eliminate toxicity effects (Fitzwater, Knauer et al. 1982).

For picophytoplankton duplicate samples were fixed in glutaraldehyde (0.25 % final concentration) in the dark for 15 minutes, quick frozen in liquid nitrogen and stored at  $-80^\circ\text{C}$  until analysis. Picophytoplankton samples were thawed at  $37^\circ\text{C}$ , 1  $\mu\text{m}$  beads (Polysciences) added as an internal

reference and samples analysed on a FACSVerse (Becton Dickenson) flow cytometer within 2 months of collection. Acquisition was on medium flow-rate for 3 minutes. Picophytoplankton groups were discriminated on the basis of red and orange auto-fluorescence of chlorophyll and the accessory pigment phycoerythrin and light scatter properties of side-angle light scatter (SSC) and forward-angle light scatter (FSC) (Marie, Partensky et al. 1999), using the flow cytometry analysis software FlowJo®.

For bacteria duplicate 1 ml seawater samples were fixed in glutaraldehyde (0.5 % final concentration) in the dark for 15 minutes, quick frozen in liquid nitrogen and stored at -80°C until analysis. Bacteria samples were thawed as above, diluted 10-fold in Tris EDTA (pH = 8.0, Sigma-Aldrich), stained with SYBR I green (0.5 x 10<sup>-4</sup> final concentration, Molecular Probes) in the dark at 80°C for 10 minutes and then 1.0 µm fluorescent beads (Polysciences) were added as an internal standard (Marie, Partensky et al. 1999). Bacteria were analysed using the same flow cytometers as above with acquisition run for 2 minutes on a low flow rate. Bacteria were discriminated on the basis of green fluorescence, side-angle light scatter (SSC) and forward-angle light scatter (FSC) using FlowJo® flow cytometry analysis software.

Samples for Chl *a* were obtained by filtering 2 L sequentially through GF/F filters (nominal pore size ~ 0.7 µm). Filters were stored at -20 °C prior to analysis. Chlorophyll *a* concentrations were fluorometrically determined on 90 % acetone extracts (Parsons et al. 1984). Samples were acidified with 10% HCl to correct for phaeopigments.

Net picoplankton growth rates and grazer-induced mortality rates were measured using the 2-point modification (Landry, R. et al. 1995, Worden and Binder 2003, Landry, Brown et al. 2008, Strom and Fredrickson 2008) of the dilution method (Landry and Hassett 1982). The grazing rate estimates based on this 2-point modification method provides a minimum estimate of grazing pressure. Net rates of growth (*k*) were calculated for the undiluted and diluted treatments (*k* and *k<sub>d</sub>* respectively) according to (Landry, Haas et al. 1984):

$$k = 1/t \times \ln(P_t/P_0) \text{ and } k_d = 1/t \times \ln(P_t/P_0)$$

where *P<sub>t</sub>* and *P<sub>0</sub>* are the final and initial concentrations of a given parameter for that given treatment.

From the measured differences in the two treatments, grazing rate (*m*) and net picoplankton growth rate (*μ*) were calculated following Landry et al. (2008), where

$$m = (k_d - k)/1 - x$$

where *x* = is the dilution factor (0.2), and

$$\mu = k + m$$

#### *Meso-zooplankton grazing*

Meso-zooplankton grazing pressure was estimated using temperature-dependent biomass relationships. Potential growth of the mesozooplankton was estimated via the empirical relationship of Huntley and Boyd (1984):

$$G'_{\max} = 0.0542e^{(0.110T)}$$

Where *T* is surface temperature measured by CTD, and *G'\_{\max}* is the maximum mass-specific food-saturated growth rate, which can be used to estimate the assimilative capacity (AC) of the mesozooplankton community:

$$AC = 0.7G'_{\max}$$

Where 0.7 is the estimate of 70 % assimilative efficiency proposed by Conover (1978). The assimilative capacity was multiplied by biomass to give an estimate of the potential grazing rate of the mesozooplankton community. Meso-zooplankton dry mass (DM, mg m<sup>-3</sup> see Section 4.2.1) was converted to carbon mass (CM, mg C m<sup>-3</sup>) as described by Wiebe (1988):

$$\log_{10}(CM) = (\log_{10}(DM) + 0.499)/0.991$$

### Nitrification

At each sampling station, water from three depths (10 m, the chlorophyll maximum as determined from CTD fluorescence, and 120 m) was used to examine ammonia oxidation rates via colourimetric determination of NO<sub>2</sub><sup>-</sup> concentrations (Grasshof, 1976), as described by Kitidis et al. (2011). Briefly, allylthiourea (ATU; 100 mM) and sodium chlorate (NaClO<sub>3</sub>; 100 mM) were used to inhibit the first and second stages of the nitrification process, respectively, and the ammonia oxidation rate was calculated as the difference in NO<sub>2</sub><sup>-</sup> concentration over 48 hours: ([NO<sub>2</sub><sup>-</sup>]<sub>NaClO<sub>3</sub></sub> – [NO<sub>2</sub><sup>-</sup>]<sub>ATU</sub>)/t. As ammonia oxidation is the rate-limiting step of the nitrification process, rate measurements are therefore used as an indication of nitrification rates.

### Dimethylsulfoniopropionate (DMSP) production

DMSP concentrations were measured at each sampling station, in water collected from three depths (10 m, the chlorophyll maximum as determined from CTD fluorescence, and 120 m), using sulphur-specific gas chromatography with flame photometric detector (GC-FPD). DMSP is degraded by bacteria via one of two pathways: the demethylation pathway, in which sulphur is incorporated into cellular protein, and the cleavage pathway, which produces the climatically important volatile, dimethyl sulphide (DMS). Bacterial taxa responsible for DMSP degradation were quantified using qPCR (Levine et al., 2012). Six groups of demethylating bacteria were enumerated using subclade-specific primers targeting the *dmdA* gene, and the dominant DMSP cleaving groups were quantified using primers for the *dddP* gene.

## 4.2.3 Results

### Physical, optical and biological layer characterisation

MLD were variable across the waters of the GAB (Table 4.2-1). In the east, MLD increased with distance from shore, from 18 m depth on the shelf to 51 m depth at the offshore station. In the central GAB, MLD ranged from 19.5 m to 40.5 m, with the shallowest occurring at the mid-slope station, and the deepest at the upper-slope station. Euphotic depth (*Z<sub>eu</sub>*) was also variable across the GAB, though there was no variation in the east (Table 4.2-1). In the central GAB, *Z<sub>eu</sub>* ranged between 76.2 m and 95 m, with shallower values at the shelf and offshore stations, and deeper values on the slope. In the central GAB, the surface mixed layer made up ~ 30% of the euphotic zone on the shelf, ~ 40% on the upper-slope, ~20% on the mid-slope, and ~ 40% in offshore waters (Figure 4.2-1a). In the east, proportions were ~ 20% for the shelf and upper slope, and ~40% for mid-slope and offshore waters. In general, the chlorophyll maximum occurred in shallower waters in the eastern GAB than the central region. In the east, the depth of the chlorophyll maximum followed the pattern of MLD, increasing with distance from shore from 39.0 m on the shelf to 73.0 m at the offshore station. The depth of the chlorophyll maximum was generally much deeper in the central GAB,

ranging from 69.0 m on the shelf to 91 m at the upper slope station. This pattern led to wide variation in the magnitude of the layer below the chlorophyll maximum yet within the euphotic zone, the sub-DCM layer (Table 4.2-1). This layer was generally much larger in the east, decreasing with distance from shore from 43.2 m on the shelf to 9.2 m at the offshore station. In the central GAB, the sub-DCM layer was largest at the mid-slope station and smallest at the upper-slope, ranging from 10.0 to 4.0 m. Accordingly, the proportion of the euphotic zone made up by the sub-DCM layer was much greater in the eastern GAB than the central GAB (Figure 4.2-1a).

*Table 4.2-1 Physical, optical and biological depth characterisation parameters defined using CTD data collected on the RV Investigator during the IN2015\_C02 voyage in the Great Australian Bight in December 2015. MLD = Mixed layer depth (m),  $K_d$  = the attenuation coefficient for downwelled irradiance ( $m^{-1}$ ),  $Z_{eu}$  = the euphotic depth (m),  $Z_{DCM}$  = depth of chlorophyll maximum (m), sub-DCM = the depth of the layer below the chlorophyll maximum to the base of  $Z_{eu}$  (m). Stations with the prefix C are located in the central GAB, with the prefix E in the east. Sf is the shelf station in each location, Us the upper slope, Ms the mid slope, and Off the offshore station.*

	MLD	$K_d$	$Z_{eu}$	$Z_{DCM}$	Sub-DCM
C-Sf	24.5	0.060	76.2	69.0	7.2
C-Us	40.5	0.048	95.0	91.0	4.0
C-Ms	19.5	0.054	85.0	75.0	10.0
C-Off	31.5	0.060	76.2	70.0	6.2
E-Sf	18.0	0.056	82.2	39.0	43.2
E-Us	25.0	0.056	82.2	51.0	31.2
E-Ms	45.0	0.056	82.2	62.0	20.2
E-Off	51.0	0.056	82.2	73.0	9.2

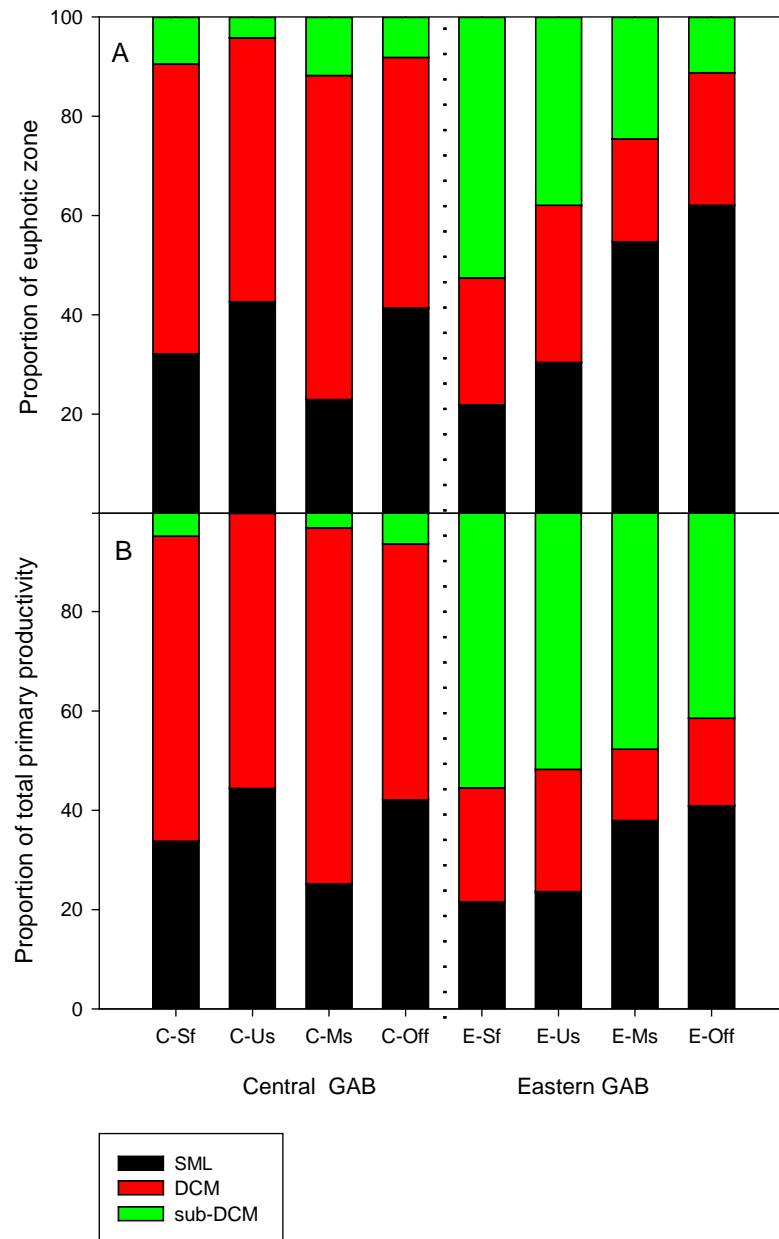


Figure 4.2-1 (a) Proportion of euphotic zone made up by the surface mixed layer (SML), the layer down to depth of the chlorophyll maximum (DCM), and the layer below DCM yet still within the euphotic zone (sub-DCM). B) Proportion of total primary productivity in the euphotic zone made up by productivity in the layer down to the DCM, and productivity in the layer sub-DCM. Note: DCM includes SML (i.e. DCM = red + black). Stations with the prefix C are located in the central GAB, with the prefix E in the east. Sf is the shelf station in each location, Us the upper slope, Ms the mid slope, and Off the offshore station.

### Primary productivity

Long-term patterns in primary productivity from remote-sensed data indicate that productivity across the GAB is generally highest through the austral summer and lowest through the austral winter (Figure 4.2-2). Monthly and climatological means, however, indicate that while primary productivity in the east may at times be much higher than that in the central GAB, it is sporadic and more variable, and primary productivity in the central GAB, while more moderate, is also more constant. There were several instances of peaks in monthly mean primary productivity in the east



that were  $> 600 \text{ mg C m}^{-2} \text{ d}^{-1}$ , particularly in shelf waters. In contrast, monthly mean primary productivity in the central GAB only exceeded  $600 \text{ mg C m}^{-2} \text{ d}^{-1}$  on one occasion (on the shelf in 2005). Coefficients of variation associated with the monthly means were always higher for eastern GAB regions. Despite these differences, long-term mean primary productivity was similar between analogous regions. Indeed, t-tests indicated that there was no significant difference between the long-term mean productivity levels in the slope regions of the eastern and central GAB ( $p = 0.38$ ).

Estimates of  $PP_{eu}$  calculated using *in situ* data indicate that the highest primary productivity was occurring on the shelf in the central GAB (Figure 4.2-3). Levels in the central GAB decrease with distance from shore, from  $443.1 \text{ mg C m}^{-2} \text{ d}^{-1}$  on the shelf to  $91.6 \text{ mg C m}^{-2} \text{ d}^{-1}$  in offshore waters. In the east, primary productivity was  $\sim 50\%$  lower on the shelf at  $210.6 \text{ mg C m}^{-2} \text{ d}^{-1}$ , increasing to  $298.4 \text{ mg C m}^{-2} \text{ d}^{-1}$  over the upper slope, decreasing again to  $57.8 \text{ mg C m}^{-2} \text{ d}^{-1}$  in offshore waters. Primary productivity in the surface mixed layer ( $PP_{SML}$ ) contributes a relatively small amount to total primary productivity in the euphotic zone across the GAB (Figure 4.2-B; Figure 4.2-3). There is a clear contrast, however, in the proportion of  $PP_{eu}$  made up by productivity levels in the layer down to depth of the chlorophyll maximum ( $PP_{DCM}$ ), and productivity levels in the layer below the chlorophyll maximum but still within the euphotic zone ( $PP_{sub-DCM}$ ), with the  $PP_{sub-DCM}$  contributing significantly more  $PP_{eu}$  in the eastern GAB than in the central GAB (Figure 4.2-1 b; Figure 4.2-3). This was reflected in the corrected  $PP_{eu}$  ( $Corr PP_{eu}$ ), which was higher than  $PP_{eu}$  in the east, but lower the  $PP_{eu}$  in the central GAB (Figure 4.2-3). Analysis of primary productivity by size fraction indicates that the vast majority of productivity is occurring in the  $< 5 \mu\text{m}$  autotrophic fraction across the GAB, with the only significant contribution from the  $> 5 \mu\text{m}$  autotrophic fraction occurring on the shelf in the central GAB (Figure 4.2-4).

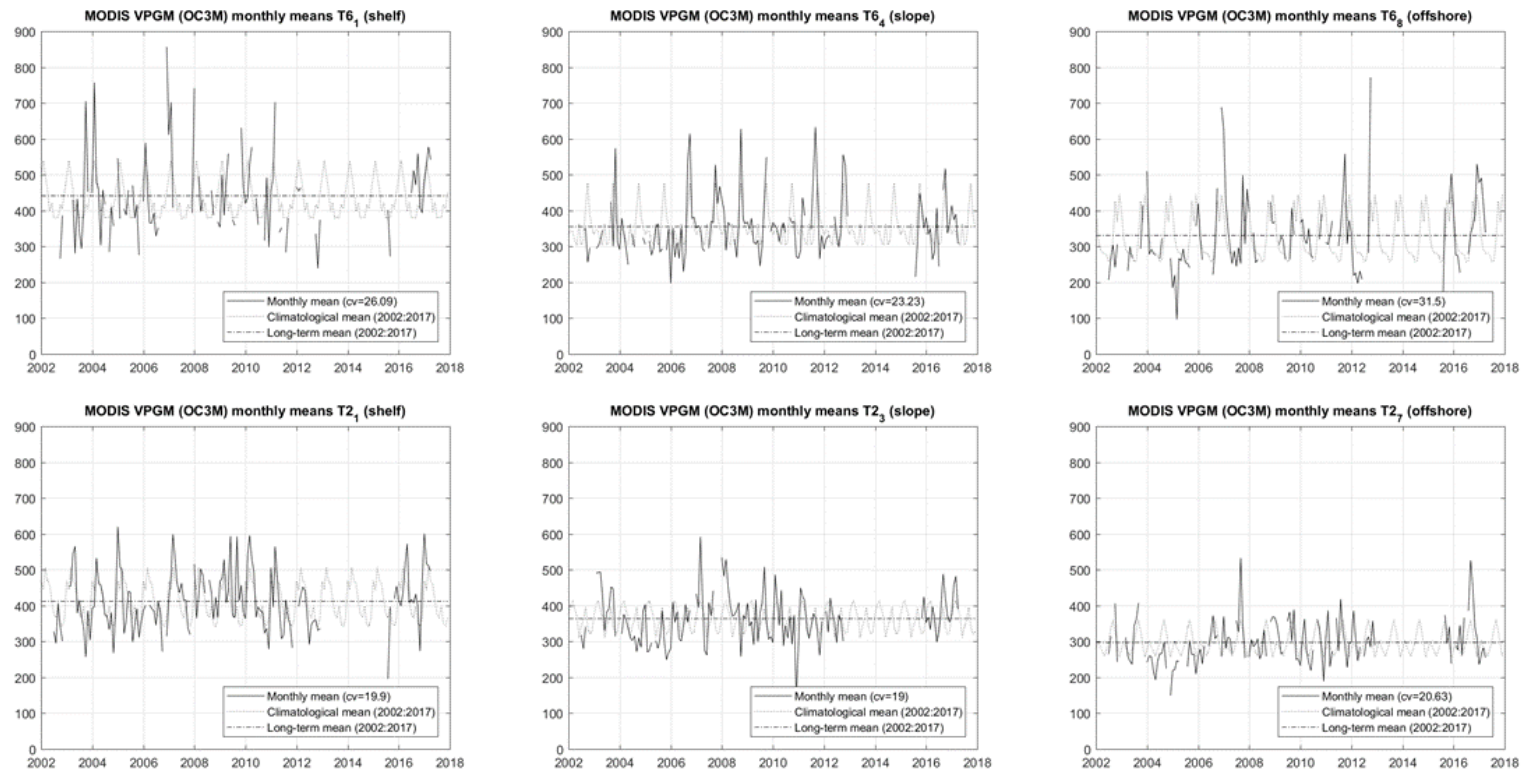


Figure 4.2-2 Primary productivity (mg C m<sup>-2</sup> d<sup>-1</sup>) extracted from MODIS Aqua, calculated using the vertically generalized production model (VGPM) and chl *a* from the OC3M algorithm. 1 Km resolution centered around shelf, slope and offshore stations on transect 2 (central GAB) and transect 6 (eastern GAB) from 2002 - 2017. Each plot includes monthly mean (with coefficient of variation), climatological mean, and long-term mean for the data.

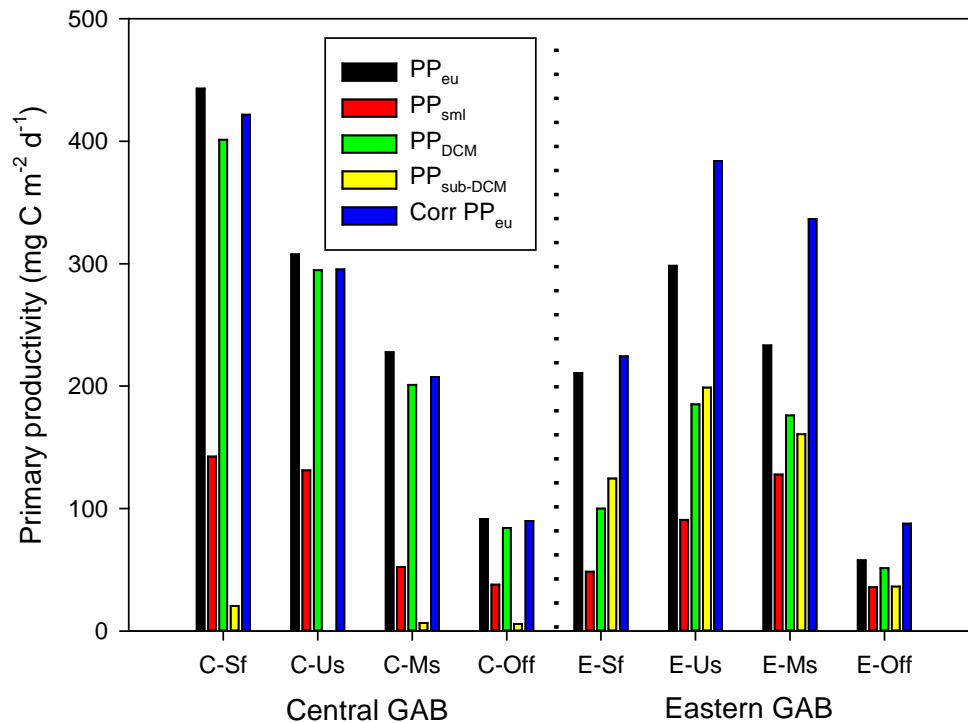


Figure 4.2-3 Daily integral primary productivity levels in the Great Australian Bight in the euphotic zone ( $PP_{eu}$ ), in the surface mixed layer ( $PP_{sml}$ ), in the layer down to the depth of the chlorophyll maximum ( $PP_{DCM}$ ), in the layer below the depth of the chlorophyll maximum but within the euphotic zone ( $PP_{sub-DCM}$ ), and in the euphotic zone, corrected for productivity occurring in the layer sub-DCM ( $Corr PP_{eu}$ ). Stations with the prefix C are located in the central GAB, with the prefix E in the east. Sf is the shelf station in each location, Us the upper slope, Ms the mid slope, and Off the offshore station.

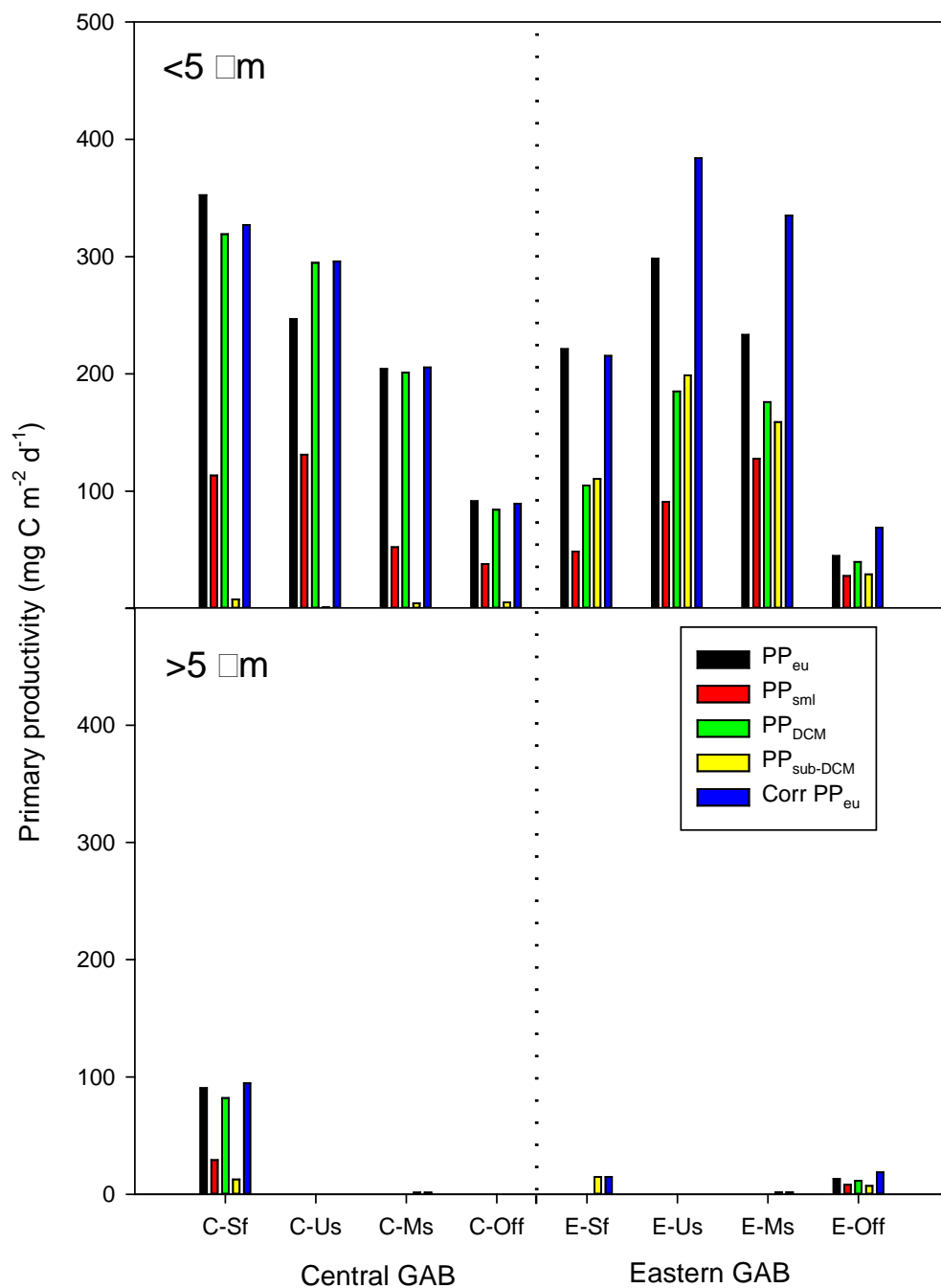


Figure 4.2-4 Size fractionated daily integral primary productivity levels in the Great Australian Bight in the euphotic zone ( $PP_{eu}$ ), in the surface mixed layer ( $PP_{sml}$ ), in the layer down to the depth of the chlorophyll maximum ( $PP_{DCM}$ ), in the layer below the depth of the chlorophyll maximum but within the euphotic zone ( $PP_{sub-DCM}$ ), and in the euphotic zone, corrected for productivity occurring in the layer sub-DCM ( $Corr PP_{eu}$ ). Stations with the prefix C are located in the central GAB, with the prefix E in the east. Sf is the shelf station in each location, Us the upper slope, Ms the mid slope, and Off the offshore station.

#### Micro-zooplankton grazing

Net growth rates ( $\mu$ ) and grazing rates ( $m$ ) for chl *a* (a proxy of total phytoplankton biomass) yielded negative values of  $m$  and  $\mu$  for all experiments/stations (data not shown). Reasons for these negative

values are unclear but might be the result of low chlorophyll concentrations to start with (often as low as  $0.2 \mu\text{g l}^{-1}$ ) and low analytical resolution of the fluorometer at these low concentrations.

Net growth rates ( $\mu$ ) and mortality rates ( $m$ ) of bacteria and *Synechococcus* were the only reliable data from the different picoplankton groups, with *Prochlorococcus* and picoeukaryotes (except for upper slope in the central GAB for picoeukaryotes – see below) both showing negative values for  $\mu$  and  $m$  (like for Chl *a*) (Table 4.2-2).

Over all dilution experiments, mortality rates of bacteria ranged from  $0.25 \text{ d}^{-1}$  to  $1.36 \text{ d}^{-1}$ , with bacterial growth rates ranging from  $0.24 \text{ d}^{-1}$  to  $1.60 \text{ d}^{-1}$  (Table 4.2-2). Similar bacterial mortality rates ( $0.47 \text{ d}^{-1}$  –  $0.76 \text{ d}^{-1}$ ) and growth rates ( $0.50 \text{ d}^{-1}$  –  $0.70 \text{ d}^{-1}$ ) occurred on the shelf and upper slope in the central GAB, with no difference occurring in nutrient-amended experiments, indicating nutrients were not limiting in these waters (for bacteria) and that overall, grazing rates were near equal to growth rates. On the lower slope and offshore, mortality rates of bacteria in nutrient-amended experiments were 1.8-fold and 4.2-fold higher, respectively, compared with dilutions having no added nutrients. Net bacterial growth rates were similarly higher (3.2-fold) in nutrient-amended dilutions for both slope and offshore waters, but with growth rates slightly exceeding grazing rates in these waters. While in the east, only one experiment (upper slope) produced positive  $m$  and  $u$  rates, the opposite trend occurred with highest growth rates  $1.33 \text{ d}^{-1}$  occurring in dilutions with no added nutrients. In contrast, grazing rates were slightly higher in nutrient amended experiments ( $0.49 \text{ d}^{-1}$  vs  $0.33 \text{ d}^{-1}$ ).

*Synechococcus* mortality and net growth rates ranged from  $-0.07$  to  $2.01 \text{ d}^{-1}$  and growth rates of  $0.18$  to  $1.09 \text{ d}^{-1}$ , with highest grazing and growth rates ( $2.01 \text{ d}^{-1}$  and  $1.09 \text{ d}^{-1}$ , respectively) occurring on the central upper slope (with no nutrients added) (Table 4.2-2). A similar trend to that of bacteria occurred in shelf and upper slope waters for *Synechococcus* with grazing and growth rates in non-amended dilutions exceeding those in nutrient amended dilutions (indicating no nutrient limitation in these waters for *Synechococcus*). Grazing equalled or exceeded *Synechococcus* growth in shelf and upper slope waters in the central GAB. In lower slope and offshore waters, grazing and growth rates were lower than on the shelf in the central GAB with no clear difference between dilutions with and without nutrients added, and with growth rates (slightly overall) exceeding grazing rates. In the east, grazing and growth rates of *Synechococcus* in the upper and lower shelf were similar ( $0.17 \text{ d}^{-1}$  –  $0.26 \text{ d}^{-1}$ ) and ( $0.20 \text{ d}^{-1}$  to  $0.55 \text{ d}^{-1}$ ) with no clear difference between dilutions with and without nutrients. These rates in the east were more comparable to those occurring in lower shelf and offshore waters of the central GAB.

For the one experiment that provided positive values of  $m$  and  $\mu$  for *Prochlorococcus* (offshore in eastern GAB, no nutrients added), low grazing rates ( $0.24 \text{ d}^{-1}$ ) were only slightly lower than growth rates ( $0.35 \text{ d}^{-1}$ ). Only one experiment provided positive values of  $m$  and  $\mu$  for picoeukaryotes (in upper slope waters of the central GAB, for non-amended dilutions only). Here, high picoeukaryote growth ( $2.43 \text{ d}^{-1}$ ) was coupled with high rates of mortality ( $4.15 \text{ d}^{-1}$ ).

Table 4.2-2 Grazing mortality rate ( $m$ ) and net picoplankton growth rate ( $\mu$ ) of bacteria (Bac), *Prochlorococcus* (Pro), *Synechococcus* (Syn) and picoeukaryotes (Peuk) determined from the 2-point modification of the dilution method. Blanks in the table indicate negative values were obtained. '-'; no nutrient amendment, '+'; nutrient amendment.

Station	Nut.	Bac		Pro		Syn		Peuk	
		$m$	$\mu$	$m$	$\mu$	$m$	$\mu$	$m$	$\mu$
C-Sf	-	0.49	0.54			0.58	0.58		
	+	0.48	0.5			0.08	0.26		
C-Us	-	0.76	0.69			2.01	1.09	4.15	2.43
	+	0.47	0.7			0.61	0.09		
C-Ms	-	0.43	0.93			-0.06	0.31		
	+	1.36	1.63			0.17	0.39		
C-Off	-	0.25	0.24			-0.07	0.36		
	+	0.8	1			0.11	0.18		
E-Us	-	0.33	1.33			0.18	0.2		
	+	0.49	0.54			0.17	0.55		
E-Ms	-			0.06	0.17	0.21	0.34		
	+					0.26	0.31		

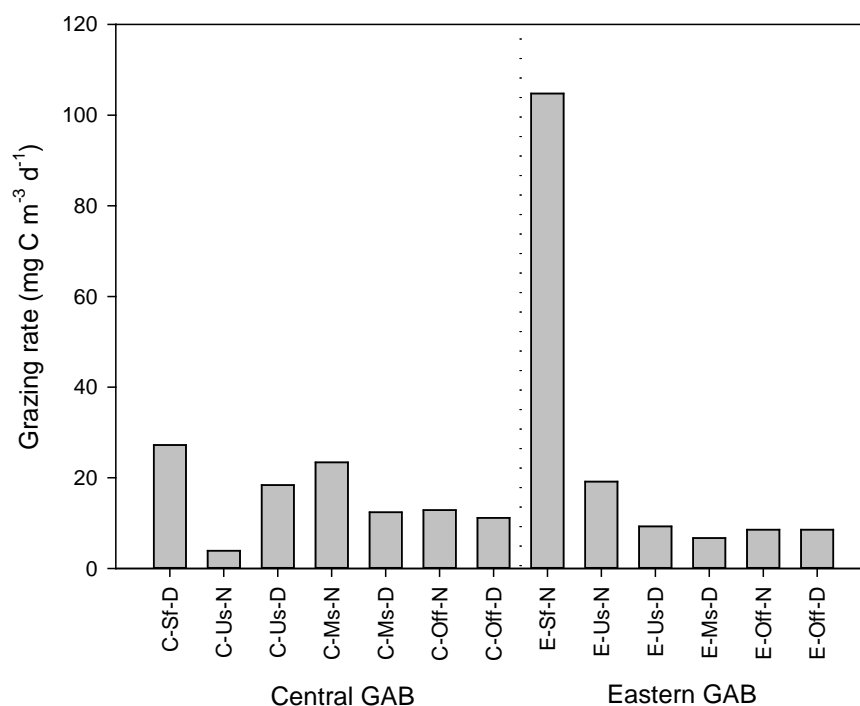


Figure 4.2-5 Total mesozooplankton grazing rates calculated using biomass (dry mass) collected in the 64  $\mu\text{m}$  and 150  $\mu\text{m}$  mesh nets during December 2015 in the Great Australian Bight (GAB). Prefix 'C' refers to Central GAB (to left of dashed line) and prefix 'E' refers to eastern GAB (to the right of dashed line). Sf = shelf; Us = upper slope; Ms = mid slope; Off = offshore. Suffix 'N' and 'D' refer to night and day sampling respectively.

#### Meso-zooplankton grazing

Generally, mesozooplankton grazing rates were higher on the shelf, decreasing offshore, though this pattern was clearer in the eastern GAB (Figure 4.2-5, Table 4.2-3). There were no clear differences



evident in grazing rates between day and night measurements. Highest total mesozooplankton grazing rate occurred on the shelf in the eastern GAB, and was nearly four times as high as the rate on the shelf in the central GAB (104.8 vs 27.2 mg C m<sup>-2</sup> d<sup>-1</sup>). However, grazing rates on the upper and mid slope and in offshore waters in the central GAB were generally double the rates in the eastern GAB. On the shelf in the east, highest grazing rates came from larger mesozooplankton (caught in the 150 µm mesh net), with the opposite trend on the shelf in the central GAB (Table 4.2-3). This pattern continued over slope and offshore waters in the east, but reversed in these waters in the central GAB (Table 4.2-3).

Table 4.2-3 Variation in zooplankton dry mass (mg m<sup>-3</sup>) carbon mass (mg C m<sup>-3</sup>) and grazing rate (mg C m<sup>-3</sup> d<sup>-1</sup>) for samples collected in nets of different mesh sizes (64 µm mesh and 150 µm mesh). Temperature = surface temperature from CTD (°C),  $G'_{max}$  = potential growth rate (d<sup>-1</sup>). For station names, prefix 'C' refers to Central GAB and prefix 'E' refers to Eastern GAB. Sf = shelf; Us = upper slope; Ms = mid slope; Off = offshore. Suffix 'N' and 'D' refer to night and day sampling respectively.

Station/sample time	Mesh size	Dry mass	Carbon mass	Temperature	G'max	Grazing rate
C-Sf-D	150	9.9	32.2	19.2	0.45	10.1
C-Us-N	150	1.8	5.9	18.6	0.42	1.7
C-Us-D	150	13.6	44.4	18.6	0.42	13.1
C-Ms-N	150	16.0	52.3	18.6	0.42	15.3
C-Ms-D	150	9.4	30.7	18.3	0.40	8.7
C-Off-N	150	7.4	24.1	17.1	0.36	6.0
C-Off-D	150	8.3	27.1	17.2	0.36	6.8
E-Sf-N	150	77.0	255.2	16.5	0.33	59.4
E-Us-N	150	16.5	53.8	16.4	0.33	12.5
E-Us-D	150	6.7	21.6	16.5	0.33	5.1
E-Ms-D	150	6.9	22.5	15.8	0.31	4.9
E-Off-N	150	4.4	14.3	15.6	0.30	3.0
E-Off-D	150	9.8	31.8	15.5	0.30	6.7
C-Sf-D	64	16.6	54.2	19.2	0.45	17.1
C-Us-N	64	2.3	7.5	18.6	0.42	2.2
C-Us-D	64	5.6	18.0	18.6	0.42	5.3
C-Ms-N	64	8.4	27.4	18.6	0.42	8.0
C-Ms-D	64	4.0	13.0	18.3	0.40	3.7
C-Off-N	64	8.4	27.4	17.1	0.36	6.8
C-Off-D	64	5.4	17.4	17.2	0.36	4.4
E-Sf-N	64	58.8	194.7	16.5	0.33	45.3
E-Us-N	64	8.9	28.8	16.4	0.33	6.7
E-Us-D	64	5.6	18.0	16.5	0.33	4.2
E-Ms-D	64	2.6	8.4	15.8	0.31	1.8
E-Off-N	64	8.1	26.4	15.6	0.30	5.6
E-Off-D	64	2.8	9.1	15.5	0.30	1.9

### Nitrification

In the eastern GAB, nitrification rates were greatest at the DCM and sub-chlorophyll maximum waters of the offshore station (average nitrification rate 93 nM NH<sub>4</sub><sup>+</sup> day<sup>-1</sup>, Figure 4.2-6A). The average nitrification rate for in the eastern GAB was 42 nM NH<sub>4</sub><sup>+</sup> day<sup>-1</sup>. In the central GAB, nitrification rates were greatest in sub-DCM waters of slope stations (average nitrification rate 99 nM NH<sub>4</sub><sup>+</sup> day<sup>-1</sup>, Figure 4.2-6B). The average nitrification rate in the central GAB was 52 nM NH<sub>4</sub><sup>+</sup> day<sup>-1</sup>.

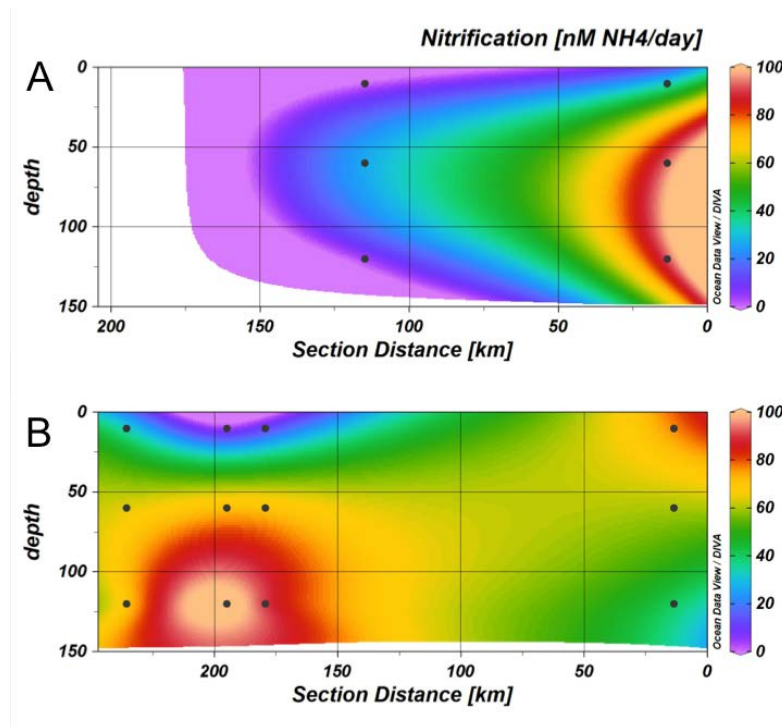


Figure 4.2-6 Ammonia oxidation rates ( $\text{nM NH}_4 \text{ day}^{-1}$ ) in (A) the eastern GAB, and (B) the central GAB. Sampling locations are indicated by black dots. Transects are shown from shelf waters on the left to offshore (ocean) waters on the right (broadly, from north to south). Data were plotted in Ocean Data View (ODV) using DIVA gridding.

Ammonia oxidising archaea (AOA) and bacteria (AOB) were quantified for the euphotic zone (upper 60 m) of each site using qPCR, (Abell et al., 2013). AOA were strongly driven by water depth ( $F 135$ ,  $p < 0.001$ ; Figure 4.2.7 A), with gene copies being at least 1000-fold more abundant at the chlorophyll maximum than in surface waters. Average AOA abundances were greater in the central GAB than the eastern GAB ( $1.74 \times 10^6$  gene copies  $\text{l}^{-1}$  and  $1.56 \times 10^6$  gene copies  $\text{l}^{-1}$ , respectively); however, this was not significant.

AOB gene abundances were significantly greater in the central GAB than the eastern GAB (average  $2.23 \times 10^6$  gene copies  $\text{l}^{-1}$  and  $1.23$  gene copies  $\text{l}^{-1}$ , respectively;  $F 35.14$ ,  $p < 0.001$ ) (Figure 4.2.7 B), and AOB were also more abundant at the chlorophyll maximum than in surface waters ( $F 10.75$ ,  $p < 0.01$ ). When AOB abundances were normalised to abundances of the universal bacterial 16S rRNA gene, the relative abundance (RA) in the central GAB was 2.32 %, compared to 1.35 % in the eastern GAB. In particular, the average RA at the chlorophyll maximum of station 2\_3 was 4.67 %, representing a 2- to 3-fold increase, compared to other sites in the euphotic zone. This was due to a decrease in the abundance of bacterial 16S rRNA genes, rather than an increase in AOB (Figure 4.2-7B).

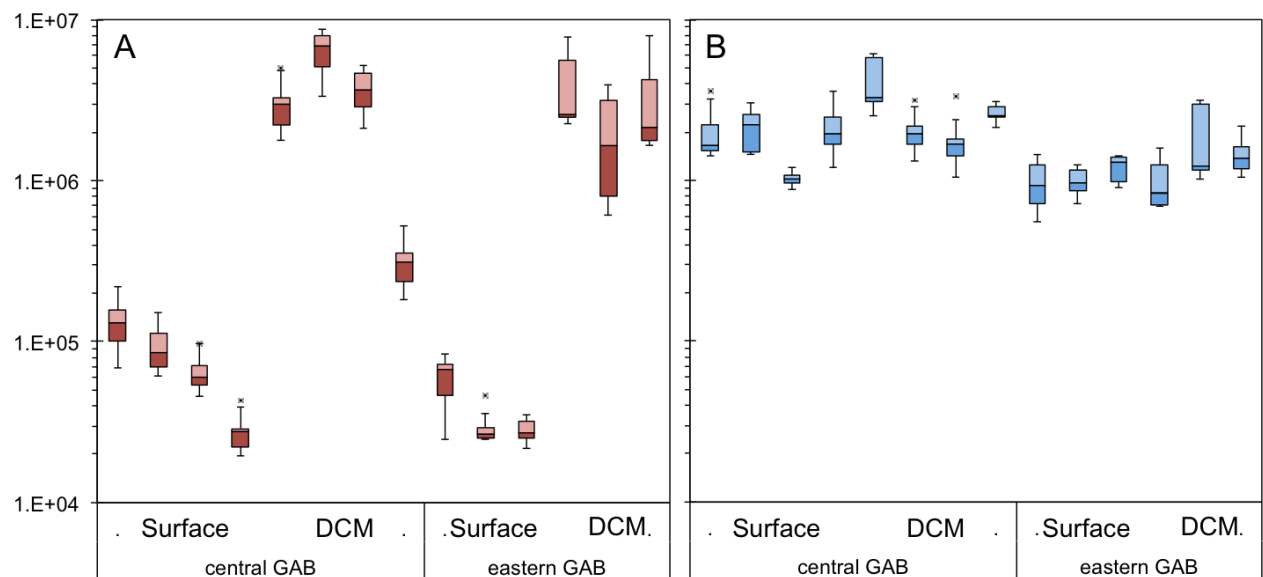


Figure 4.2-7 Abundances (gene copies l-1) of (A) ammonia oxidising archaea, AOA, and (B) ammonia oxidising bacteria, AOB. Samples are ordered, left to right, from shelf water to offshore (oceanic) waters for each depth horizon: surface (10 m depth) and the depth of the chlorophyll maximum (DCM, 60 m depth). Boxes indicate the interquartile range (IQR), calculated from 9 replicate qPCR reactions for each sample, and bisected by the median. Error bar limits are 1.5\*IQR, and outliers are shown as asterisks.

#### DMSP production

DMSP concentrations were 7-fold greater in the eastern GAB than in the central GAB (average across all depths 2.59 nM and 16.92 nM, respectively;  $F=11.95$ ,  $p<0.01$ , Figure 4.2.8). Overall, the relative abundance (RA) of demethylating bacteria in the euphotic zone was greater in the central GAB (average 25.23% and 27.17% for surface and DCM samples, respectively) than in the eastern GAB (24.76% and 23.71%, respectively) ( $F=11.95$ ,  $P < 0.01$ ; Figure 4.2-9). In contrast, the cleavage gene *dddP* was of greater abundance in the eastern GAB (average 2.60% and 2.29% for surface and DCM samples, respectively) than in the central GAB (1.52% and 1.71%, respectively) ( $F=6.71$ ,  $p < 0.05$ ; Figure 4.2-9).

The dominant demethylators (Figure 4.2-9, subclades D1, D3 and C2) belong to the SAR11 clade of bacteria: the most abundant and ubiquitous organisms in the ocean. This group is highly abundant in shelf and slope waters of the central GAB (Figure 4.2-9); particularly at the chlorophyll maximum of the upper slope station, where demethylating SAR11 comprise almost 40% of the total bacterial community (Figure 4.2-9B).

In order to explore this dynamic further, we examined SAR11 gene expression using qPCR with cDNA synthesised from RNA. We found that, conversely to the gene abundance data, SAR11 *dmdA* expression levels were greater in the eastern GAB ( $F=28.03$ ,  $p<0.01$ ; Figure 4.2.10).

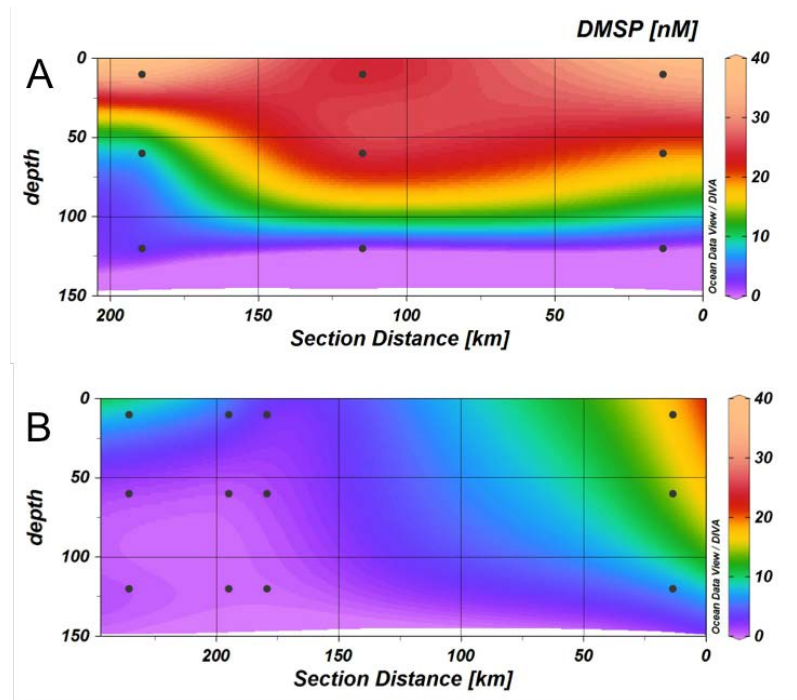


Figure 4.2-8 DMSP concentrations (nM) in (A) the eastern GAB, and (B) the central GAB. Sampling locations are indicated by black dots. Transects are shown from shelf waters on the left to offshore (ocean) waters on the right (broadly, from north to south). Data were plotted in Ocean Data View (ODV) using DIVA gridding.

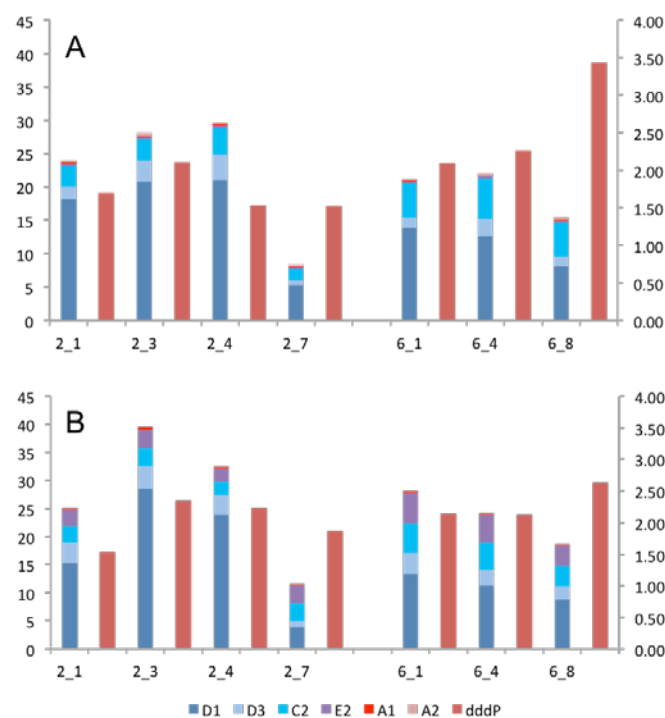


Figure 4.2-9 Relative abundances (%) of demethylating (D1, D3, C2, E2, A1, A2; left-hand axis) and DMSP cleavage (dddP; right-hand axis) genes in (A) surface, and (B) DCM samples. Sites within the central GAB are shown on the left, and sites within the eastern GAB are shown on the right. Relative abundances were calculated from gene copy numbers normalised to abundances of the 16S rRNA gene.

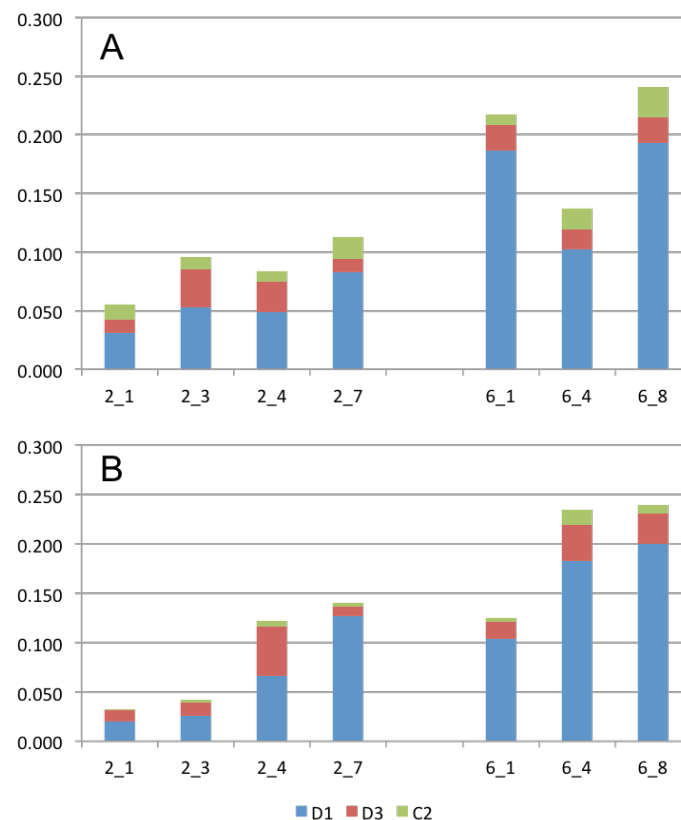


Figure 4.2-10 Expression (%) of demethylating SAR11 genes (D1, D3, C2) in (A) surface, and (B) DCM samples. Sites within the central GAB are shown on the left, and sites within the eastern GAB are shown on the right. Expression levels were calculated from gene transcript numbers normalised to the relevant gene copy number for each gene.

#### 4.2.4 Discussion

Contrasts in microbial and plankton physiology can provide insights into differences in food web dynamics between the eastern and central GAB, but must be considered together with information about changes in physical and chemical oceanographic parameters (Sections 3.1 and 3.2), and microbial and planktonic biomass and abundance (Section 4.1). Accurate insights into variations in the lower trophic ecosystem, and their influence on overall ecosystem productivity, can only be gained through assessment of a full suite of these parameters, particularly when dealing with single voyage, spot measurements such as those from this study. The following discussion will build upon key outcomes from Sections 3.1, 3.2, and 4.1.

Variations in food web dynamics between the eastern and central GAB at the time of the voyage (i.e. during the upwelling season) were driven by differences in the enrichment processes that underpin autotrophic production and alter the influence of different physical, optical and biological layers on  $PP_{eu}$ . In the east, the chlorophyll maximum and nutricline occurred at ~ 40 – 60 m. Enrichment processes, which are sporadic but intense in nature, were driven primarily by physics (upwelling, Section 3.2), with limited influence of biological processes (i.e. low nitrification). The relatively shallow surface mixed layer on the shelf and upper slope (which makes up only 20 – 30% of the euphotic zone) means there was a large volume of upwelled water present within the euphotic zone in these areas where irradiances were still relatively high (~ 6 – 8% of surface values), in which high productivity can occur. The sub-DCM layer made up > 50% of the euphotic zone on the shelf, and >

40% on the upper slope, and was responsible for > 50% of total primary productivity in these regions. It also contributed a significant proportion of total primary productivity in mid-shelf and offshore waters in the eastern GAB. In contrast, in the central GAB, the chlorophyll maximum and nutricline were approximately 20 – 30 m deeper than in the east. There was a stronger influence of biological processes (i.e. high nitrification) on enrichment in the central GAB, with intermittent input from turbulent fluxes at the shelf edge (Section 3.2). Enrichment mechanisms in the central GAB appear to be more constant but constrained. Surface mixed layers were also relatively shallow in this region, but the DCM occurred close to the nutricline at the base of the euphotic zone. The volume of water available for higher productivity was thus very small in the central GAB (~5–10% of the euphotic depth), and irradiances at the DCM were very low (~1–2% of surface values). The sub-DCM layer thus contributed little to total primary productivity in the euphotic zone in the central GAB. These results have implications for estimates of primary productivity generated using surface values of chl *a*, which don't account for increased productivity in the bottom layer of the euphotic depth. Using surface chl *a* alone leads to significant underestimation of  $PP_{eu}$  in the eastern GAB in the austral summer. This further highlights the importance of ground-truthing modelled estimates and remote sensed information with *in situ* data that have been collected according to well researched, regionally appropriate sampling plans that are designed to unravel the complex dynamics that underpin ecosystem productivity.

Daily integral primary productivity calculated using *in situ* data were comparable to climatological and long-term means in shelf and slope waters in the central GAB and in slope waters in the eastern GAB. However, on the shelf in the east and in offshore waters in the eastern and central GAB, rates of daily integral primary productivity were half to a third that of the climatological and long-term means. These represent the first estimates of daily integral primary productivity calculated using *in situ* data in slope and offshore waters of the GAB, and thus the first chance to ground-truth remote sensed information in these regions. Previous studies have characterised shelf-edge regions in the GAB as having low daily integral productivities (< 800 mg C m<sup>-2</sup> d<sup>-1</sup>, van Ruth et al. 2010a), comparable to those reported for the oligotrophic waters of the Leeuwin current off south west Western Australia (< 550mg C m<sup>-2</sup> d<sup>-1</sup>, Hanson et al. 2005), the AuSW and SSTC provinces of Longhurst et al (1995), and the north and south Atlantic sub-tropical gyres (<400 mg C m<sup>-2</sup> d<sup>-1</sup>, Maranon et al. 2003). Slope and offshore waters can now be characterised in the same way.

The relatively low phytoplankton biomass (Section 4.1) and low daily integral primary productivity in shelf waters in the east was somewhat surprising but not inexplicable. Given the influence of upwelling in eastern GAB shelf and slope waters, one would expect to observe high phytoplankton biomass, particularly in the larger size fraction, and high daily integral primary productivity, in line with the first key hypothesis of this study. Primary productivity in this region has previously been reported to be intermediate (800 –1600 mg C m<sup>-2</sup> d<sup>-1</sup>, van Ruth et al. 2010a), comparable to rates in localised upwellings off southwest Western Australia (Hanson et al. 2005) and spring bloom conditions off Tasmania (Harris et al. 1987), or even high (1600 – 3900mg C m<sup>-2</sup> d<sup>-1</sup>) and within the range of productivities measured in the highly productive Benguela and Humboldt current upwelling systems (Brown et al. 1991, Daneri et al. 2000). Highest rates of primary productivity in the eastern GAB have previously been associated with the upwelled water mass during periods of active upwelling (van Ruth et al. 2010a, b), but upwelling in the region has been shown to be highly variable, both within and between seasons (van Ruth et al. 2010a, b; Sections 3.1 and 3.2). However, productivity estimates calculated from spot measurements such as those used in this study will depend on the oceanographic conditions that prevailed in the lead up to sampling. In this case, it is clear from wind stress data and temperature profiles that an upwelling event had occurred ~2 weeks prior to our voyage (Section 3.1).



We therefore observed; in shelf waters of the eastern GAB during our sampling; the ecosystem dynamics two weeks after an enrichment event. The initial response (within days of the event) would have been increased phytoplankton biomass, followed by the micro and mesozooplankton response (weeks) to the increase in available food resulting in decreased phytoplankton biomass as nutrient levels waned in the wake of the upwelling event. Indeed, upon our sampling, ~ 2 weeks post enrichment, we observed low chl *a* concentrations and high mesozooplankton biomass on the shelf in the eastern GAB (Section 4.2). Meso-zooplankton grazing rates were also significantly higher on the shelf in the eastern GAB than any other region sampled. This high grazing pressure, driven by high mesozooplankton biomass, caused the low phytoplankton biomass that was present at the time of sampling for this study, which, when used in the VGPM to model daily integral primary productivity, resulted in lower than expected rates of primary productivity on the shelf in the eastern GAB. If we “correct” our modelled estimates of primary productivity for grazing, we will get a more accurate indication of the true magnitude of daily integral primary productivity in the eastern and central GAB. Assuming a C:chl ratio of 75:1, we can convert grazing rates from mg C m<sup>-3</sup> to mg chl m<sup>-3</sup>; this is the amount of chlorophyll that has been “lost” through grazing. When we add this to our measured values for chl *a* and re-calculate daily integral primary productivity through the VGPM, we get “grazing corrected” productivities of 1175.4 mg C m<sup>-2</sup> d<sup>-1</sup> on the shelf in the east, and 542.0 mg C m<sup>-2</sup> d<sup>-1</sup> on the shelf in the central GAB. This new figure would classify eastern GAB as intermediate, as is in better agreement with previous studies in the region (van Ruth et al. 2010a, b).

The low biomass and daily integral primary productivity levels of phytoplankton in the > 5 µm size fraction in the eastern GAB contradicts the first key hypothesis of this study. The expectation was that upwelling events in the eastern GAB would promote a food web underpinned by larger phytoplankton, but our biomass results do not support this contention. However, it is highly likely that mesozooplankton were preferentially grazing on larger phytoplankton on the shelf in the east, hence the lack of biomass and productivity in the >5 µm size fraction. Elsewhere in the GAB, the lack of biomass and productivity are more likely to reflect unfavourable conditions for growth of larger phytoplankton, related to either nutrient availability, differences in enrichment processes and/or levels of irradiance.

Growth rates of, and grazing pressure on, picophytoplankton was also highly variable across the GAB. Higher grazing rates of *Synechococcus* and bacteria occurred in shelf and upper slope waters of the central GAB. Growth rates of *Synechococcus*, bacteria and (perhaps even picoeukaryotes), were not nutrient limited in these waters. This contrasts with *Synechococcus* communities in lower shelf and offshore waters, where nutrient limitation was observed. Growth rates of *Synechococcus* were overall similar to those reported for other oceanic systems (i.e. Californian Current, Sargasso Sea (Worden and Binder 2003)), however, in the central GAB on the shelf and upper slope specifically, grazing rates on *Synechococcus* were more than double the rate reported in those previous studies at the same locations. Grazing rates in the eastern GAB were more comparable to those in the Californian Current and Sargasso Sea (Worden and Binder 2003). Overall, bacterial growth and mortality rates reflected those occurring in the southern limit of Californian Current System, even when for that system, Chl *a* values were an order of magnitude higher (Linacre et al. 2010).

In the central GAB, in shelf and upper slope waters, grazing on *Synechococcus* exceeded *Synechococcus* growth, and with bacterial growth only slightly higher than bacterial mortality associated with grazing. Low grazing (averaging 0.04 d<sup>-1</sup>) on *Synechococcus* in lower central GAB slope and offshore waters, together with reasonably high rates of grazing on bacteria relative to bacterial growth rates, indicates potential shifts in the (nanoplanktonic) communities grazing on the different picoplankton groups with distance from the shelf/slope. Despite lower mortality rates of

*Synechococcus* in the eastern GAB, nano-microzooplankton grazing still accounted for the removal of > 50% of *Synechococcus* cell abundance. Together, these results indicate a substantial removal of bacterial biomass through microbial web dominated processes across different oceanographically influenced areas/regions of the GAB, and increased grazing pressure on *Synechococcus* in shelf/upper slope waters of the central GAB. With only one reliable estimate of  $m$  and  $\mu$  for picoeukaryotes, it is difficult to make overall conclusions. However, the high grazing rates recorded for picoeukaryotes, which exceeded high picoeukaryote growth rates, are indicative of the potentially important role picoeukaryotes have as a food source for higher trophic levels in upper slope waters of the central GAB.

While nitrification rates were highest in the central GAB, there was still significant nitrification occurring in the east, indicating that the process is important for nitrogen cycling and enrichment across the GAB. However, in the absence of physical enrichment mechanisms, biologically mediated enrichment via nitrification provides a critically important yet previously undocumented source of nitrogen for primary producers in the central GAB. As previously documented for other oceanic environments (e.g. Beman et al., 2008; Church et al., 2010; Santoro et al., 2013), nitrification rates correlated strongly with AOA abundances in the euphotic zone, and less strongly with AOB abundances. In the California current upwelling system, AOA abundance has been related to competition for  $\text{NH}_4^+$  with phytoplankton, and to light inhibition of different AOA ecotypes (Smith et al., 2014 a,b). Our observations support these previous studies, and suggest that ammonia oxidation at the DCM and below is predominantly carried out by archaea. It appears that archaea in the central GAB are outcompeting phytoplankton for ammonium and converting it to nitrate. Thus, while our original hypothesis of a dominant microbial food web in the central GAB appears to hold true, primary productivity is underpinned by regenerated nitrate, not regenerated ammonium as first thought.

Variations in DMSP concentrations across the GAB reflect broad differences in phytoplankton community structure between the central and eastern GAB, with a dominance of non- or low-DMSP producing phytoplankton taxa (e.g. diatoms, picoeukaryotes, cyanobacteria) in the central GAB, compared to high-DMSP producers (e.g. prymnesiophytes, dinoflagellates) in the eastern GAB, in agreement with phytoplankton abundance data presented in Section 4.1. The greatest abundances of the *dddP* gene, which primarily belongs to the *Roseobacter* lineage, corresponded with high DMSP concentrations in the eastern GAB. *Roseobacter* are motile, and are strongly attracted to the DMSP exuded by phytoplankton, which they use as a carbon source (Seymour et al., 2010). Together, these data provide further evidence that the central GAB supports a functionally different microbial and planktonic community to that in the east.

#### 4.2.5 Summary and conclusions

Overall, ecosystem productivity in the GAB is driven by contrasting food web dynamics between the eastern and central GAB that are underpinned by variations in dominant nutrient enrichment processes. In the east, enrichment processes are sporadic but intense, and driven primarily by physics (upwelling), with limited influence of biological processes. The chlorophyll maximum and nutricline occur around the middle of the euphotic zone, with low rates of nitrification rates and high rates of DMSP production. Nano-phytoplankton dominate the autotrophic community, with higher rates of primary productivity driven by a large volume of nutrient rich water above the euphotic depth, which contributes a significant proportion of total primary productivity in the euphotic zone.

Meso-zooplankton are abundant in the region, and associated grazing rates are high. Together these results indicate a shorter food web in the east, driven predominantly by upwelled nitrogen.

In the central GAB, there is a stronger influence of biological processes (e.g. nitrification) with only intermittent input of nutrients at the base of the euphotic zone from turbulent fluxes at the shelf edge. Enrichment mechanisms in the central GAB appear to be more constant but constrained. The chlorophyll maximum and nutricline occur toward the base of the euphotic zone, with high rates of nitrification, but lower rates of DMSP production. The phytoplankton community is dominated by smaller pico-phytoplankton, with highest rates of primary productivity at the base of the euphotic zone. Grazing by mesozooplankton is less intense in the central GAB, but rates of micro-zooplankton grazing on small picoplankton are much higher than in the east. Together these results suggest a longer food web in the central GAB, driven by regenerated nitrogen.

Despite these differences in food web dynamics, long-term patterns in primary productivity are relatively similar between the regions, particularly on the slope. While primary productivity in the east can be high, it is intermittent and highly variable, with highest rates implicitly linked to upwelling. In the central GAB, primary productivity is more moderate, but linked to a more constant, biologically mediated supply of nitrogen that ensures that these moderate rates can be maintained over longer periods of time. These results show that the central GAB is an important contributor to overall productivity in the wider GAB region.

## References

- Abell G.C.J., Ross D.J., Keane J.P., Oakes J.M., Eyre B.D., Robert S.S., and Volkman J.K. 2013. Nitrifying and denitrifying microbial communities and their relationship to nutrient fluxes and sediment geochemistry in the Derwent Estuary, Tasmania. *Aquat. Microb. Ecol.*, 70: 63-75.
- Antoine, D. and Morel, A. 1996. Oceanic primary production: 1. Adaptation of a spectral light-photosynthesis model in view of application to satellite chlorophyll observations. *Global Biogeochemical Cycles*, 10(1): 43-55.
- Behrenfeld, M. J. and Falkowski P. G., 1997. Photosynthetic rates derived from satellite-based chlorophyll concentration. *Limnology and Oceanography*, 42(1): 1-20.
- Beman J.M., Popp B.N., and Francis C.A. 2008. Molecular and biogeochemical evidence for ammonia oxidation by marine Crenarchaeota in the Gulf of California. *ISME J.*, 2:429-441.
- Beman J.M., Chow C.E., King A.L., Feng Y., Fuhrman J.A., Andersson A., Bates N.R., Popp B.N., and Hutchins D.A. 2011. Global declines in oceanic nitrification rates as a consequence of ocean acidification. *Proc. Natl. Acad. Sci.*, 108: 208-213.
- Brown, P. C., Painting, S. J., Cochraine, K. L., 1991. Estimates of phytoplankton and bacterial biomass and production in the northern and southern Benguela ecosystems. *South African Journal of Marine Science*, 11: 537-564.
- Church M.J., Wai B., Karl D.M., DeLong E.F. 2010. Abundances of crenarchaeal amoA genes and transcripts in the Pacific Ocean. *Environ. Microbiol.*, 12: 679-668.
- Conover, R. J. 1978. Transformation of organic matter. *In: Marine Ecology IV*. O. Kinne (ed), pp 221-500, Wiley, New York.
- Daneri, G., Dellarossa, V., Quinones, R., Jacob, B., Montero, P., and Ulloa, O., 2000. Primary production and community respiration in the Humboldt Current System off Chile and associated oceanic areas. *Marine Ecology Progress Series*, 197: 41-49.
- de Boyer Montégut, C., G. Madec, A. S. Fischer, A. Lazar, and Iudicone, D. 2004. Mixed layer depth over the global ocean: an examination of profile data and a profile-based climatology. *J. Geophys. Res.*, 109, C12003. doi:10.1029/2004JC002378, pdf
- Eppley, R. W. 1972. Temperature and phytoplankton growth in the sea. *Fish. Bull.*, 70(4): 1063-1085.

- Fitzwater, S. E., G. A. Knauer and Martin, J. H. 1982. Metal contamination and its effect on primary production measurements. *Limnology and Oceanography*, 27(3): 544-551.
- Grasshoff K. 1976. *Methods of seawater analysis*. Verlag Chemie, Weinheim.
- Hanson, C. E., Pattiaratchi, C. B., and Waite, A. M., 2005. Sporadic upwelling on a downwelling coast: Phytoplankton responses to spatially variable nutrient dynamics off the Gascoyne region of Western Australia. *Continental Shelf Research*, 25: 1561-1582.
- Harris, G., Nilsson, C., Clementson, L., and Thomas, D., 1987. The water masses of the east coast of Tasmania: seasonal and interannual variability and the influence on phytoplankton biomass and productivity. *Australian Journal of Marine and Freshwater Research*, 38: 569-590.
- Huntley, M. and C. M. Boyd 1984. Food limited growth of marine zooplankton. *The American Naturalist*, 124: 455-478.
- Kiene R.P., and Linn L.J. 2000. The fate of dissolved dimethylsulfoniopropionate (DMSP) in seawater: tracer studies using  $^{35}\text{S}$ -DMSP. *Geochim. Cosmochim. Acta.*, 64: 2797-2810.
- Kitidis V., Laverock B., McNeil C.L., Beesley A., Cummings D., Tait K., Osborn M., Widdicombe S. 2011. Impact of ocean acidification on benthic and water column ammonia oxidation. *Geophys. Res. Lett.*, 38: L21603.
- Landry, M. R., Kirshtein, J., and Constantinou J. 1995. A refined dilution technique for measuring the community grazing impact of microzooplankton, with experimental tests in the central equatorial Pacific. *Marine Ecology Progress Series*, 120: 53-63.
- Landry, M., Haas L. and Fagerness, V. 1984. Dynamics of microbial plankton communities: experiments in Kaneohe Bay, Hawaii. *Marine Ecology Progress Series*, 16: 127-133.
- Landry, M. R., Brown, S. L., Rii, Y. M., Selph, K. E., Bidigare, R. R., Yang, E. J., and Simmons, M. P. 2008) Depth-stratified phytoplankton dynamics in Cyclone Opal, a subtropical mesoscale eddy. *Deep Sea Research Part II: Topical Studies in Oceanography* 55(10–13): 1348-1359.
- Landry, M. R. and Hassett, R. P. 1982. Estimating the grazing impact of marine micro-zooplankton. *Marine Biology*, 67(3): 283-288.
- Levine, N.M., Varaljay, V.A., Toole, D.A., Dacey, J.W.H., Doney, S.C., Moran. M.A.. 2012. Environmental, biochemical and genetic drivers of DMSP degradation and DMS production in the Sargasso Sea. *Environ. Microbiol.*, 14: 1210-1223.
- Linacre, L. P., Landry, M. R., Lara-Lara, J. R., Hernández-Ayón, J. M., and Bazán-Guzmán, C. 2010. Picoplankton dynamics during contrasting seasonal oceanographic conditions at a coastal upwelling station off Northern Baja California, México. *Journal of Plankton Research*, 32(4): 539-557.
- Longhurst, A., Sathyendranath, S., Platt, T., Caverhill, C., 1995. An estimate of global primary production in the ocean from satellite radiometer data. *Journal of Plankton Research*, 17: 1245-1271.
- Maranon, E., Behrenfeld, M. J., Gonzalez, N., Mourino, B., Zubkov, M. V., 2003. High variability of primary production in oligotrophic waters of the Atlantic Ocean: uncoupling from phytoplankton biomass and size structure. *Marine Ecology Progress Series*, 257: 1-11.
- Marie, D., Partensky, F., Vaulot, D. and Brussard, C. 1999. Enumeration of phytoplankton, bacteria, and viruses in marine samples. *In* Current protocols in cytometry. J. P. Robinson (ed), pp. 11.11.11-11.11.15. John Wiley & Sons, New York.
- Morel, A. 1991. Light and marine photosynthesis: a spectral model with geochemical and climatological implications. *Progress in oceanography*, 26(3): 263-306.
- Parsons, T. R., Maita, Y. and Lalli, C. M. 1984. *A Manual of Chemical and Biological Methods for Seawater Analysis*, Pergamon Press, New York.

- Platt, T., Bird, D. F., Sathyendranath, S., 1991. Critical depth and marine primary production. *Proceedings of the Royal Society of London B*, 246: 205-217.
- Santoro, A.E., Sakamoto, C.M., Smith, J.M., Plant, J.N., Gehman, A.L., Worden, A.Z. et al. 2013. Measurements of nitrite production and nitrite-producing organisms in and around the primary nitrite maximum in the central California Current. *Biogeosci Discuss.*, 10:5803-5840.
- Seymour, J.R., Simo, R., Ahmed, T., Stocker, R. 2010. Chemoattraction to dimethylsulfoniopropionate throughout the marine microbial food web. *Science*, 329: 342-345.
- Smith, J.M., Chavez, F.P., Francis, C.A. 2014. Ammonium uptake by phytoplankton regulates nitrification in the sunlit ocean. *PLOS One* 9:e108173.
- Smith, J.M., Casciotti, K.L., Chavez, F.P., Francis, C.A. 2014. Differential contributions of archaeal ammonia oxidiser ecotypes to nitrification in coastal surface waters. *ISME J.*, 8: 1704-1714.
- Sunda, W., Kieber, D.J., Kiene, R.P., Hunstman, S. 2001. An antioxidant role for DMSP and DMS in marine algae. *Nature*, 418: 317-320.
- Strom, S. L. and K. A. Fredrickson 2008. Intense stratification leads to phytoplankton nutrient limitation and reduced microzooplankton grazing in the southeastern Bering Sea. *Deep Sea Research Part II*, 55(16–17): 1761-1774.
- van Ruth, P., Thompson, P., Bonham, P., and Jones, E. 2009. Primary productivity and zooplankton ecology in the Port Lincoln Tuna Farming Zone. Technical report, Aquafin CRC Project 4.6, FRDC Project 2005/059. Aquafin CRC, Fisheries Research & Development Corporation and South Australian Research & Development Institute (Aquatic Sciences), Adelaide. SARDI Publication No F2008/000789-1, SARDI Research Report Series No 343, 58 pp.
- van Ruth, P. D., Ganf, G. G., and Ward, T. M. 2010a. Hot-spots of primary productivity: An alternative interpretation to conventional upwelling models. *Estuarine, Coastal and Shelf Science*, 90: 142-158.
- van Ruth, P. D., Ganf, G. G., and Ward, T. M. 2010b. The influence of mixing on primary productivity: A unique application of classical critical depth theory. *Progress in Oceanography*, 85: 224-235.
- Wiebe, P. H. 1988. Functional regression equations for zooplankton displacement volume, wet weight, dry weight, and carbon: a correction. *Fish. Bull.*, 86: 833-835.
- Worden, A. Z. and Binder, B. J. 2003. Application of dilution experiments for measuring growth and mortality rates among *Prochlorococcus* and *Synechococcus* populations in oligotrophic environments. *Aquatic Microbial Ecology*, 30(2): 159-174.
- Yoch, D.C. 2002. Dimethylsulfoniopropionate: Its Sources, Role in the Marine Food Web, and Biological Degradation to Dimethylsulfide. *Applied and Environmental Microbiology*, 68(12): 5804-5815.

## 5. ZOOPLANKTON

Marine zooplankton comprise three intermediate trophic groups in pelagic foodwebs, all are heterotrophic and responsible for the transfer of organic carbon/energy to higher trophic levels (Figure 5-1). Zooplankton are taxonomically diverse and are classified into three, functional groups which are size based; micro, meso and macro zooplankton whose main constituents are ciliates, copepods and krill respectively. Zooplankton forage on bacteria, phytoplankton, zooplankton, detritus and the ratio of herbivorous to omnivorous-carnivorous zooplankton varies on rates of regional primary productivity. In regions of the world's oceans where primary productivity is limited, small cells dominate phytoplankton communities and a lower proportion of herbivorous to omnivorous-carnivorous zooplankton is observed (Zhou et al., 2009; Marañón et al., 2015). While in nutrient rich waters large phytoplankton cells dominate phytoplankton communities, and a greater abundance of large herbivorous and carnivorous zooplankton are observed (Legendre and Rassoulzadegan, 1995). Thus the relative abundance of different size classes of zooplankton communities provide an insight into ecosystem structure and function (Zhou et al., 2009).

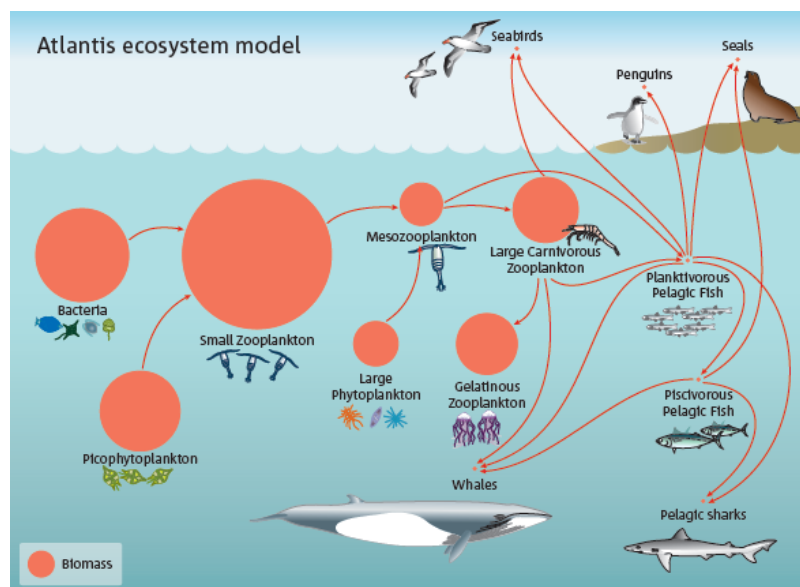


Figure 5-1 Diagram of a shelf marine foodweb in Southern Australia, with size of the spheres representing biomass of each trophic group.

A literature review of GAB ecosystem processes identified that zooplankton communities on the continental shelf in the eastern GAB have been well-described, but substantial knowledge gaps exist in offshore waters (>200 m) in the central and eastern GAB (Rogers, 2013). Prior studies in continental shelf waters of the eastern GAB, report that copepods numerically dominate zooplankton communities year-round. However during periods of nutrient enrichment and elevated primary productivity there is a ~ 25% net increase in zooplankton biomass. This increase can in part be attributed to the relative increase in abundance of species with fast growth rates and short development phases such as salps, cladocera and planktonic larvae (Van Ruth and Ward, 2009).

The objective of this chapter is to characterise relationships between environmental variables and the vertical, horizontal, regional, seasonal and inter-annual trends of zooplankton communities in the pelagic waters of the GAB. In this chapter the following datasets are used to describe patterns in zooplankton communities:

- 1) The temporally and spatially extensive CPR (continuous plankton recorder) dataset.



- 2) Surface and vertically resolved samples from net and laser optical plankton counter in the eastern and central GAB using data collected on IN2015\_C02.
- 3) A description and discussion of the gelatinous zooplankton collected and observed on IN2015\_C02.

### References

- Legendre, L., Rassoulzadegan, F., 1995. Plankton and nutrient dynamics in marine waters. *Ophelia* 41, 153-172.
- Marañón, E., Cermeño, P., Latasa, M., Tadonlécé, R.D., 2015. Resource supply alone explains the variability of marine phytoplankton size structure. *Limnology and Oceanography* 60, 1848-1854.
- Rogers, P.J., 2013. Physical processes, biodiversity and ecology of the Great Australian Bight region : a literature review / Paul Rogers, Tim Ward, Paul van Ruth, Alan Williams ; contributing authors, Barry Bruce, Sean Connell, David Currie, Campbell Davies, Karen Evans, Bronwyn Gillanders, Simon Goldsworthy, David Griffin, Nick Hardman-Mountford, Alex Ivey, Rudy Kloser, John Middleton, Anthony Richardson, Andrew Ross, Jason Tanner and Jock Young. CSIRO, [Hobart, Tasmania].
- Van Ruth, P.D., Ward, T.M., 2009. Meso-Zooplankton Abundance, Distribution and Community Composition in the Eastern Great Australian Bight. *Transactions of the Royal Society of South Australia* 133, 274-283.
- Zhou, M., Tande, K.S., Zhu, Y., Basedow, S., 2009. Productivity, trophic levels and size spectra of zooplankton in northern Norwegian shelf regions. *Deep Sea Research Part II: Topical Studies in Oceanography* 56, 1934-1944.

## 5.1 Large-scale plankton dynamics in the Great Australian Bight

Anthony Richardson, Wayne Rochester and Frank Colman

### 5.1.1 Introduction

Shelf waters of the Great Australian Bight (GAB) are economically and ecologically important, especially in the east. They support a diverse pelagic ecosystem that includes important predators such as Australian sea lions (*Neophoca cinerea*), New Zealand fur seals (*Arctocephalus forsteri*) and southern blue fin tuna (*Thunnus maccoyii*) (Page et al. 2006; Ward et al. 2006; Fowler et al. 2007; Goldsworthy and Page 2007). They support rock lobster, scale-fish and sardine fisheries, and a steadily growing aquaculture industry. The eastern GAB also supports a significant recreational fishery and fishing-based tourism generates significant revenue for the region. The higher trophic levels are ultimately supported by phytoplankton and zooplankton at the base of the foodweb. Careful and sustainable management of these higher trophic levels thus requires an understanding of the structure, function and variability of the plankton community that supports them.

Uncertainty remains about how the plankton of the GAB supports such productive and diverse higher trophic levels (Rogers et al. 2013). We hypothesize that the “classic food web” – with large phytoplankton such as diatoms and large zooplankton such as big copepods – dominates in the eastern GAB during periods of nutrient-rich upwelling. van Ruth and Ward (2009) found that copepods and cladocerans dominate mesozooplankton abundance in all seasons and that seasonal upwelling events generate elevated productivity and increased the abundance and biomass of mesozooplankton. This higher biomass of phytoplankton and zooplankton should lead to more efficient food web transfer to higher trophic levels. By contrast, the “microbial loop” is thought to dominate in the central and western GAB where year-round downwelling is thought to prevail, and in waters off the continental shelf. These conditions lead to smaller phytoplankton (often dominated by flagellates) and smaller copepods and lower biomass. However, observations of phytoplankton and zooplankton in the GAB are limited in central and offshore waters >200 m water depth (Rogers et al. 2013), limiting the ability to test these hypotheses, especially outside the eastern GAB and covering different seasons.

We sampled the phytoplankton and zooplankton community in the GAB using a Continuous Plankton Recorder (CPR) towed behind Ships of Opportunity (SOOP). CPRs have been towed regularly in the North Atlantic since 1948 and Australian waters since 2009 as part of the Integrated Marine Observing System (IMOS) Australian Continuous Plankton Recorder (AusCPR) survey. The CPR is ideal for supplementing snapshots from one-off process-oriented cruises because it provides a longer-time perspective suited to analysis of interannual, seasonal and regional differences. Because the device is towed behind SOOP whilst underway, data can be collected all year round, even during winter storms.

Here we analyse CPR data to characterise the longer-term and larger-scale variability in phytoplankton and zooplankton of the GAB. We describe the interannual, seasonal and regional variation in plankton communities in terms of their environmental drivers. We interpret our findings in terms of the potential efficiency of the foodweb to support higher trophic levels, with particular reference to the hypothesised more-traditional foodweb on the eastern shelf of the GAB and a more-microbial foodweb in central and offshore waters.

### 5.1.2 Methods

#### *Plankton data*

As part of the GABRP (Theme 2) and in conjunction with IMOS, plankton data have been collected across the GAB using a CPR.

#### *The CPR device and sample collection*

The CPR samples continuously at a depth of ~7 m. Water enters the CPR through a square aperture of (1.61 cm<sup>2</sup>), about the size of a thumbnail, and flows down an expanding tunnel, which effectively reduces the water pressure to minimise damage to the captured plankton, and exits through the rear of the device (Figure 5.1-1). The movement of the water past the CPR turns an external propeller at the rear of the device that operates a drive shaft and gear system, which advances a silk filtering mesh. Plankton in the water are filtered onto this constantly moving band of silk. The filtering silk meets a second band of covering silk, effectively sandwiching the plankton, and is then wound onto a spool in a storage tank containing formalin. The CPR not only give an adequate representation of mesozooplankton, but also gives an indication of blooms of large phytoplankton.

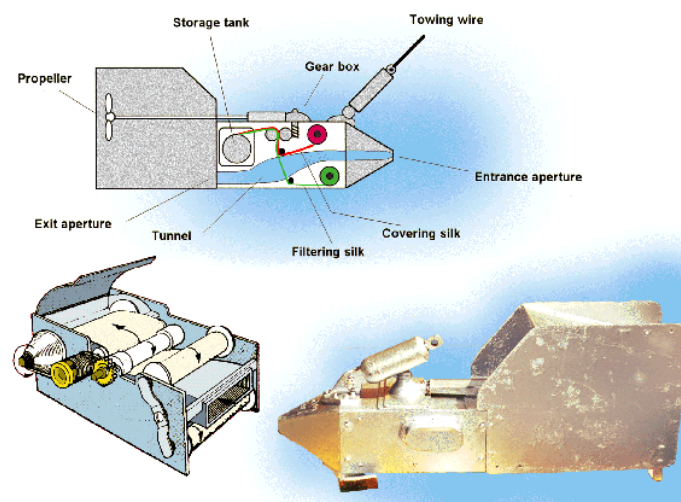


*Figure 5.1-1 The Continuous Plankton Recorder.*

When the CPR is returned to the laboratory after towing, the filtering silk, a continuous record of the plankton on that tow, is removed from the internal mechanism and unwound (typically a 500 nm tow will use about 5 m of silk). For ease of plankton counting, the silk is then divided into samples representing 5 nautical miles of tow. Position (latitude and longitude) and local time for each sample are calculated based on log sheets filled in on the vessel. The volume of water filtered for each 5 nautical mile sample is 1.5 m<sup>3</sup> and is used to standardise abundance estimates. On every 4<sup>th</sup> sample, phytoplankton and zooplankton are counted to the lowest taxonomic level. The copepods are abundant and robust, and can be identified to species, whereas most other zooplankton can only be identified to family. Many of the phytoplankton can only be identified to genus using light microscopy. More than 500 different phytoplankton and zooplankton taxa have been recorded.

### Sampling in the GAB

We have collected and analysed 294 CPR samples from Adelaide across the GAB. There is considerable variation in the number of samples collected each year. Additional CPR data in the area collected on an ad hoc basis in 2010 and 2011 aboard the *RV Southern Surveyor* were included in the analysis (Figure 5.1-2 and Table 5.1-1). Although there were more CPR samples available to use from the area, we restricted the analysis to routes that traversed the same region through time. This CPR transect from Adelaide across the GAB is still in operation.

Because CPR routes follow shipping lanes, this has the advantage of making the routes consistent through time, allowing better comparison, but has the disadvantage of not necessarily sampling a region comprehensively. We split the CPR data in the GAB into four regions: GAB East Shelf (from 132.5°E to Adelaide and <200 m isobath); GAB East offshore (Off) (east of 132.5°E and offshore of the 200 m isobath); GAB Central offshore (Off) (from 129°E to 132.5°E and offshore of the 200 m isobath); and GAB West Offshore (west of Albany at 118°E to 129°E and offshore of the 200 m isobath). Other samples in the region are shown in grey but were not included in analyses.

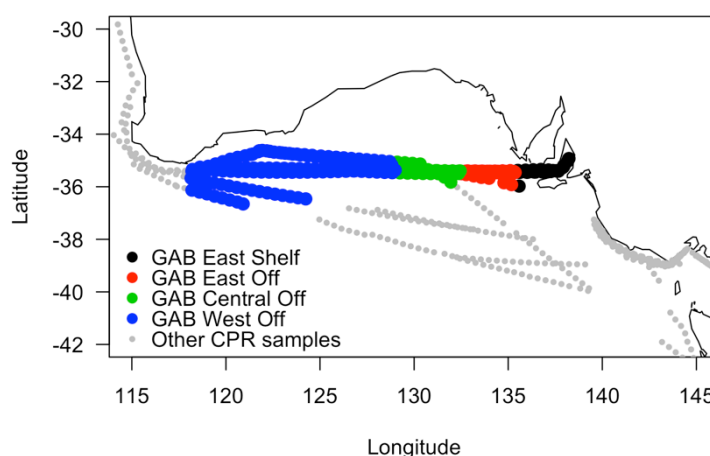


Figure 5.1-2. Map of all CPR samples in Southern Australia, including the focal regions on the GAB.

Table 5.1-1. The number of CPR samples counted from each region each year. Note that due to shipping routes there are no CPR samples from the GAB Central shelf.

Year	Region	Number of samples
2016	GAB West Off	16
<b>2015</b>	<b>GAB East Off</b>	<b>8</b>
<b>2015</b>	<b>GAB Central Off</b>	<b>8</b>
2015	GAB West Off	31
<b>2014</b>	<b>GAB East Shelf</b>	<b>33</b>
<b>2014</b>	<b>GAB East Off</b>	<b>34</b>
<b>2014</b>	<b>GAB Central Off</b>	<b>33</b>
2014	GAB West Off	47
<b>2011</b>	<b>GAB East Shelf</b>	<b>1</b>
<b>2011</b>	<b>GAB East Off</b>	<b>6</b>
<b>2011</b>	<b>GAB Central Off</b>	<b>8</b>
2011	GAB West Off	38
<b>2010</b>	<b>GAB Central Off</b>	<b>7</b>
2010	GAB West Off	24
	TOTAL	294

### *Caveats associated with using Continuous Plankton Recorder (CPR) data*

There are several caveats to consider when using CPR data. Firstly, the device provides a semi-quantitative estimate of phytoplankton and zooplankton abundances, particularly the smaller phytoplankton species (Batten et al. 2003; Richardson et al. 2004, 2006). CPR data are sensitive enough to describe subtle changes in seasonal cycles with climate change (Edwards and Richardson 2004), large-scale movement of plankton communities (Chivers et al. 2017), connectivity between trophic levels (Richardson and Schoeman 2004), and rapid regime shifts (Beaugrand et al. 2009). Secondly, the CPR is deployed at ~7 m depth, so it collects near-surface plankton. However, the sample is probably indicative of the mixed layer, as the device is towed behind large commercial vessels with a substantial draft and turbulence behind the ship. As it is towed during the day and night, it also captures species at night that are moving from deeper waters to feed near the surface. Lastly, the location of routes is determined by shipping routes and these cannot be altered as they can in research cruises.

In summary, although there are limitations with using the data especially for quantitative estimates, the standardised method and taxonomy are robust for analyses over regional to basin spatial scales and from seasonal to interannual time scales.

### *Statistical analysis*

To investigate potential drivers of zooplankton abundance/community composition and environmental variables, we obtained satellite remote sensing products for SST and Chl *a* from IMOS. Based on the sample time and location, we extracted sea surface temperature (SST) and Chl *a* data from weekly SeaWiFS composites. Chl *a* is a proxy phytoplankton biomass, the primary food source for zooplankton. SST data were obtained from satellite NOAA AVHRR (Advanced Very High Resolution Radiometer) data. Temperature is correlated with nutrient concentrations (e.g. cooler water generally has more nitrate) and determines physiological rate processes, and is a primary driver of plankton composition. Considering the lifespan of phytoplankton is less than a month, we feel that the weekly composites provide an adequate tradeoff between daily SST and Chl *a* data with lots of missing data due to clouds, and a monthly time scale with virtually no missing environmental data but that might miss important processes.

### *Univariate analysis of abundance and community metrics*

To investigate the potential environmental drivers of plankton abundance and community metrics, we used a model-building approach. In the early analysis phase, we identified that relationships between our key biological and environmental variables were generally linear, so we used linear models. Further, linear models help better estimate the contributions of different predictors, which is useful considering the unbalanced designs here.

We developed separate models for the abundance of key phytoplankton functional groups (total phytoplankton, diatoms and dinoflagellates) and key zooplankton functional groups (copepods, non-copepod zooplankton, and then key groups within these including cladocera, chaetognaths, euphausiids, and copepod juveniles). It should be noted that euphausiids captured by the CPR are larval/juvenile stages and not adults. After inspection of the residual plots, all linear models for abundance were log<sub>10</sub>-transformed to improve the assumptions of homogeneity of variance and normality. We developed linear models for several univariate community metrics: the mean size of copepods in a sample (weighted by abundance of each species), copepod richness (number of species), the ratio of predominantly herbivorous copepods to total copepods (Herbivore : Total Copepods), and the “conversion efficiency” between zooplankton and phytoplankton (Zooplankton :

Phytoplankton). We used information from Boltovskoy (1999) on the preferred diet of copepod species and genera to partition species as herbivores or carnivores/omnivores. Zooplankton : Phytoplankton is the simple ratio of total zooplankton abundance to total phytoplankton abundance – we assume that higher values suggest more zooplankton is supported relative to phytoplankton abundance and thus there is more efficient transfer to zooplankton (potentially through carnivorous/recycled matter pathways). On visual inspection of residuals, the response copepod size and the Herbivore: Total copepod ratio was untransformed. The Zooplankton : Phytoplankton was log10-transformed to improve the residuals. Copepod richness (a count variable), was modelled as a generalized linear model with a Poisson error structure and a log link function. Plots show the mean effect and 95 % confidence errors or bands.

We included a suite of predictors that represent various potential drivers of plankton abundance and community structure: time variables (Year, Season), space variables (Depth of the water column and Region (GAB East Shelf, GAB East Off, GAB Central Off, GAB West Off)) and environmental variables (SST, Chl *a*). During the early analysis phase, we included Time of Day as a non-linear variable (cubic spline) to assess whether there was a diel vertical migration signal. Time of Day was never significant and we thus dropped it from all subsequent analyses to reduce the number of parameters in the model.

We used a backward stepwise modelling approach, where we removed each term one at a time and used an F-test to determine whether the model without the variable had significantly worse explanatory power. We included one two-way interaction, Region\*Season, as we were particularly interested in whether there were different seasonal cycles in different regions. We did not include other two-way or higher interactions because of the potential for over-parameterizing the model. All linear and generalized linear models were conducted in R3.2 Statistical Software Package.

#### Multivariate community analysis

To examine how the zooplankton community responds to environmental variables, we performed non-metric Multidimensional Scaling (nMDS) analysis (Clarke et al., 2014). nMDS is an ordination technique that seeks to preserve the rank dissimilarities between objects (here samples) based on a suite of variables (here species). In the 2-D ordinations, the closer the two samples the more similar are their species. We used the Bray-Curtis dissimilarity measure because it is robust to joint absences (when samples look more similar because they have no species in common) and is thus used extensively in ecology (Clarke et al., 2014).

Copepods are an ideal species for this type of analysis because they are the most abundant multicellular animals, dominate pelagic zooplankton communities, are an important food source for higher trophic levels, and are readily identifiable to species. We removed species that were present in < 5 % of samples, leaving 26 species. To ensure abundant species did not dominate the ordination, the Hellinger transformation was applied to the raw species abundances (Legendre and Gallagher, 2001). This transformation divides the abundance of a species by the total abundance of all species in each sample, and then takes the square root. We performed 1000 iterations using the metaMDS function in the statistical package Vegan (Oksanen 2017). To aid interpretation, we included vector plots of environmental variables using, plotted species scores, and included the 99% confidence limit of the centroid for the factor. To assess significant differences among groups and for continuous predictors, we performed a Permutational Multivariate Analysis of Variance (ADONIS) (Anderson, 2001). This gives the significance and the proportion of variance in the multivariate data (here copepod communities) explained by each of the environmental predictors.

To identify copepod species that were driving the different communities in the four regions in the GAB, we used the Dufrene-Legendre Indicator Species Analysis (Dufrene and Legendre, 1997) in the package *labdsv*. We then investigated in more detail the species highlighted by the Indicator Species Analysis that generated differences among regions.

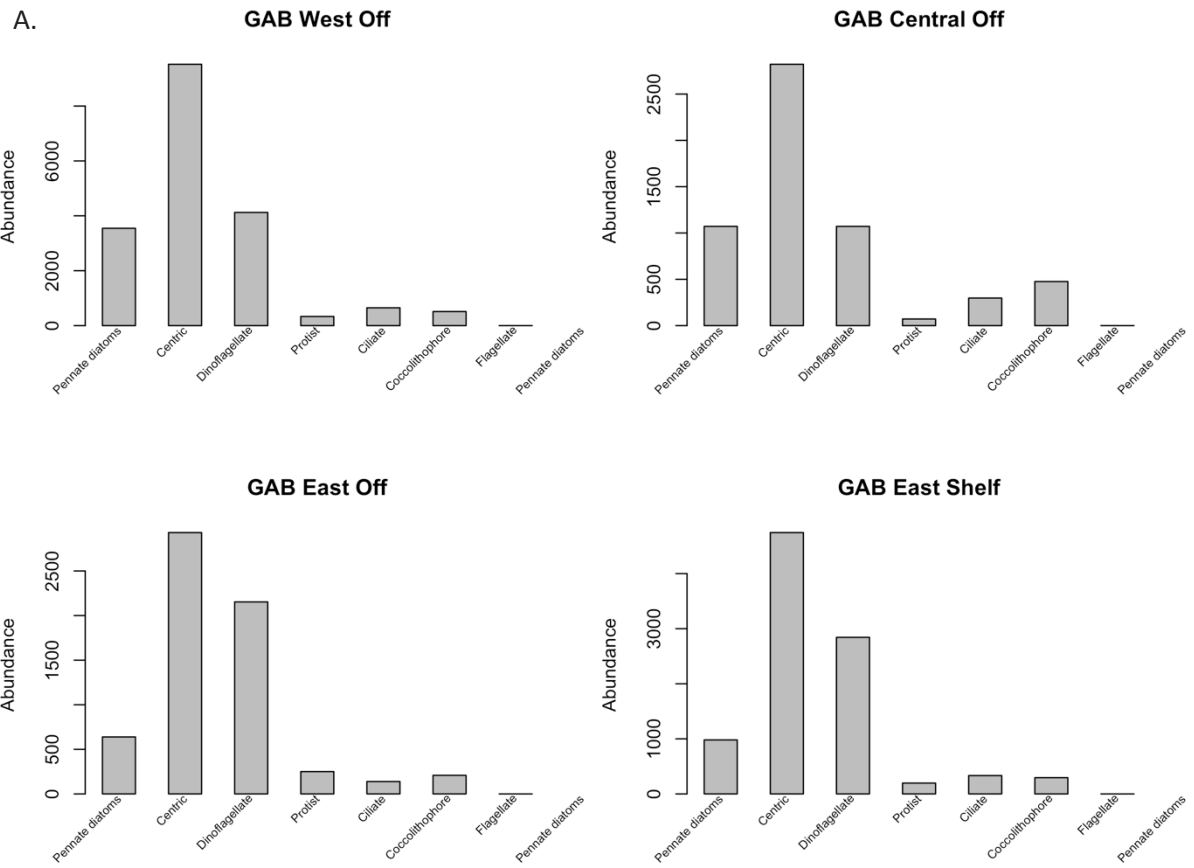
### 5.1.3 Results

#### *Overall plankton composition*

For phytoplankton, there is relatively little difference in the relative contribution of the main functional groups (Figure 5.1-3a). Pennate diatoms dominate the phytoplankton community, constituting between 46.3% and 50.9% of the community. The next most important group is the dinoflagellates, which constitute ~32% of the phytoplankton community on the eastern GAB and this drops to ~20% on the Central and Western offshore regions. In terms of pennate diatoms, they are 10% of the community on the eastern GAB and increase to 19% on the GAB Central Off and GAB West Off.

Overall, copepods were the most important zooplankton group in the GAB, constituting 50% of the community (Figure 5.1-3b). Copepods make up less of the zooplankton in the eastern GAB, with a total of 35.5% on the GAB East Shelf and 37.7% on the GAB East Off; this increases to 54.7% on the GAB Central Off and 72.5% on the GAB West Off. Shelf waters of GAB East were often dominated by cladocerans, which made up 49.5% of the community by abundance. While cladocerans were virtually absent from the offshore waters, making up <2.5% of the community. Larvaceans were important in GAB East Off waters, constituting 34.3% of the zooplankton, but contributed <14% to all other regions. Chaetognaths (arrow worms) were important in the GAB Central Off (22.2%) and in the GAB East Off (14.6%) but were rare in GAB East Shelf (1.7%) and GAB West Off (5.9%). Tintinnids (3-6%) and euphausiids (1-2%) were found in offshore waters, and were absent on the GAB East Shelf. All other zooplankton functional groups were rare.





## Zooplankton

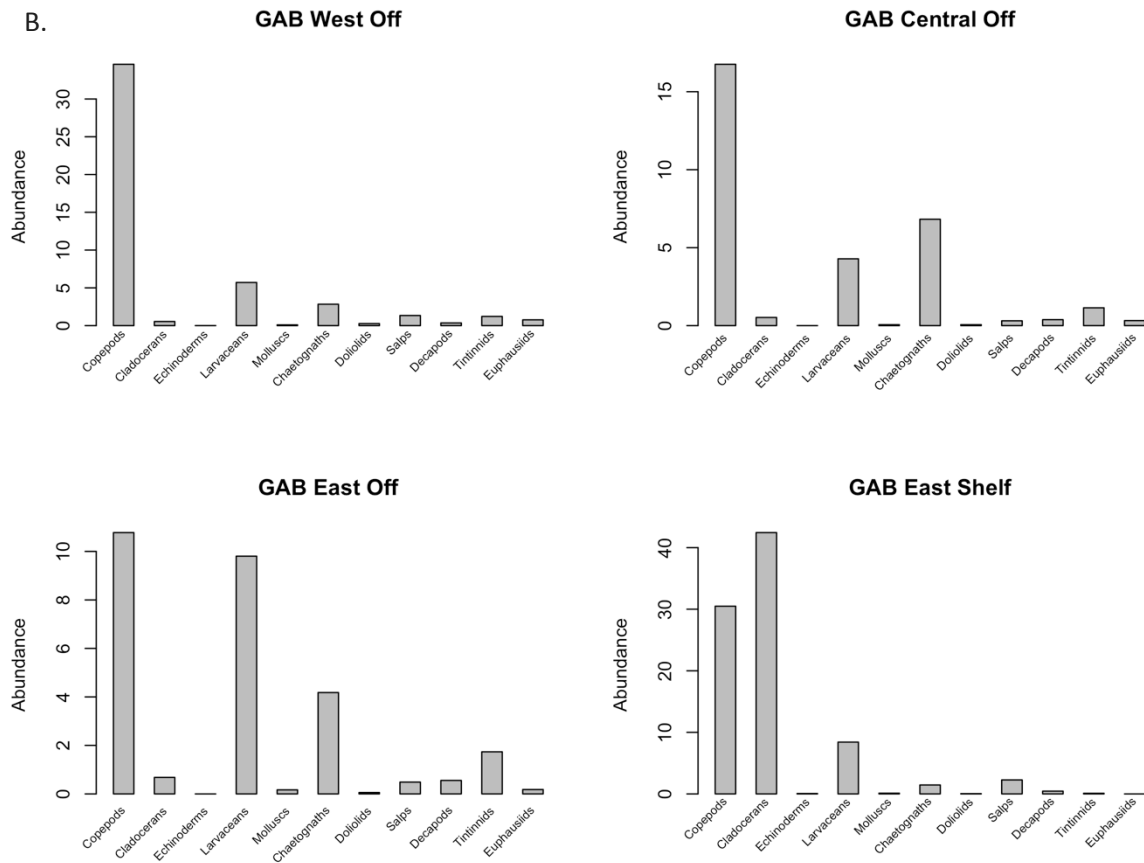


Figure 5.1-3. Relative abundance of functional groups. (A) Phytoplankton. (B) Zooplankton.

### Phytoplankton functional groups

Total diatom abundance was significantly related to Year, Depth, and Region\*Season ( $r^2=21.3\%$ ), but not to SST or Chl *a* (Figure 5.1-4). There are more diatoms in shallower waters. On the GAB East Shelf there are more diatoms in autumn than other seasons. Further offshore on the Central and Western GAB, there are more diatoms in spring and summer.

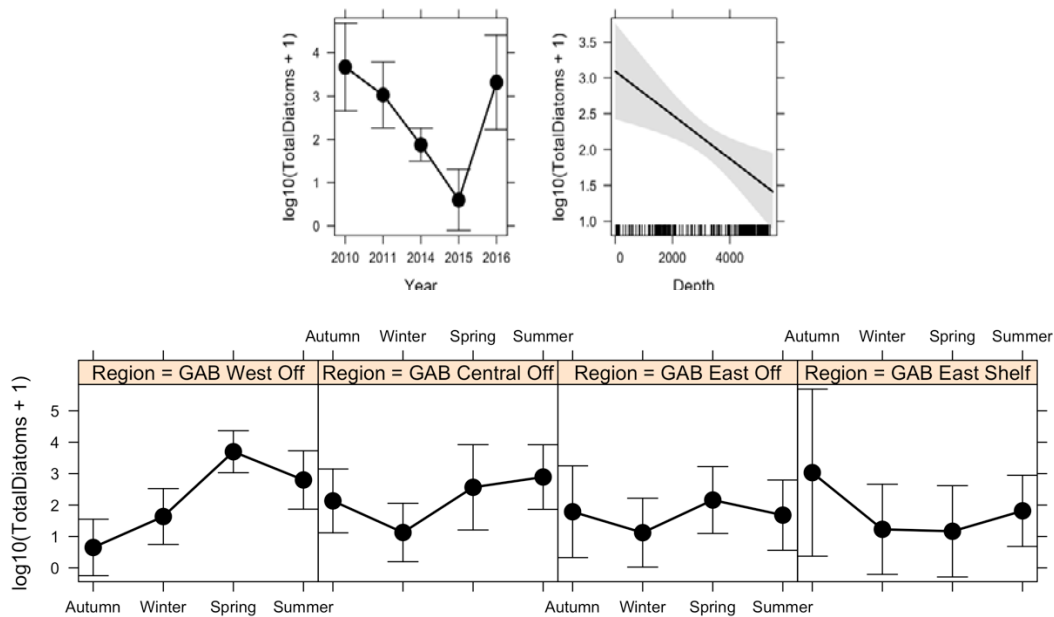


Figure 5.1-4 Effects plot of final linear model of total diatoms (log10-transformed) against predictors showing means  $\pm$  95% confidence limits.

Dinoflagellate abundance was significantly related to Year and Season ( $r^2=18.7\%$ ), but not to SST, Chl  $a$ , Depth or Region (Figure 5.1-11). As with many other response variables, there is a large increase over time in the abundance of dinoflagellates. There are also more dinoflagellates in autumn and summer, and fewer in spring.

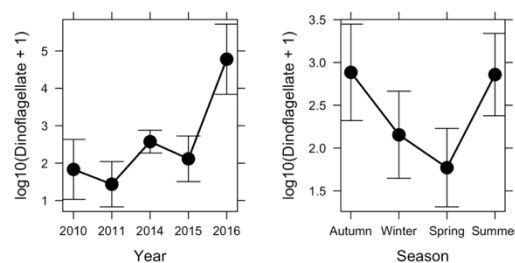


Figure 5.1-5. Effects plot of final linear model of total dinoflagellates (log10 transformed) against predictors showing means  $\pm$  95% confidence limits.

### Zooplankton functional groups

Total copepod abundance was significantly related to Year, Chl  $a$  and Region\*Season ( $r^2=57.4\%$ ), but not SST or Depth (Figure 5.1-6). Total copepod abundance varied by more than an order of magnitude interannually. There were substantially more copepods in warmer waters of the GAB and in waters with higher Chl  $a$ . The Region : Season interaction was significant, implying that different regions in the GAB had different seasonal cycles. For example, copepod abundance on the GAB East Shelf declined by an order of magnitude from autumn to spring, whereas the offshore regions had a more muted seasonal cycle, especially the GAB West Offshore. Despite these differences there were some strikingly similar seasonal patterns across the regions, with generally high copepod abundance in autumn and winter and lower in spring and summer.

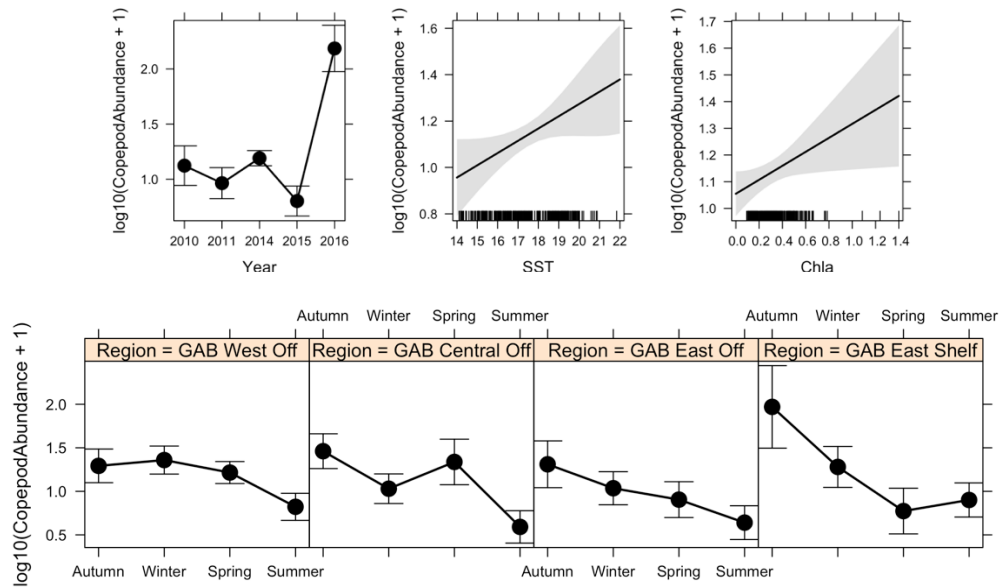


Figure 5.1-6. Effects plot of final linear model of total copepod abundance (log10-transformed) against predictors showing means  $\pm$  95% confidence limits.

Non-copepod zooplankton abundance was significantly related to Year, SST, and Region\*Season ( $r^2=43.8\%$ ), but not Chl *a* or Depth (Figure 5.1-7). Similar to copepods, non-copepod zooplankton abundance varied by an order of magnitude interannually and increased in warmer waters. Non-copepod zooplankton was highest in winter on the GAB East Shelf. Similarly to copepods, the GAB East Shelf had greater seasonality than the offshore regions.

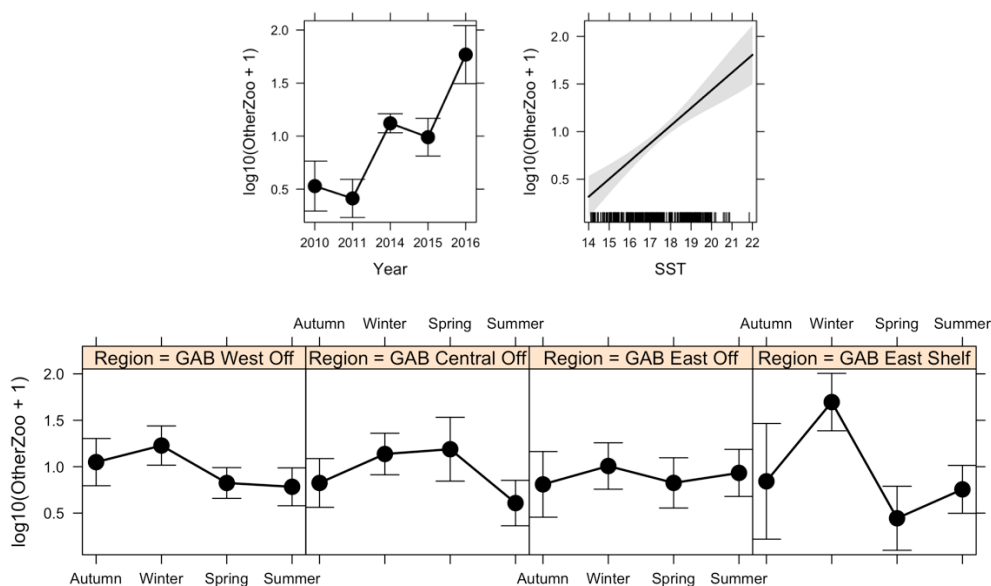


Figure 5.1-7. Effects plot of final linear model of non-copepod zooplankton abundance (log10-transformed) against predictors showing means  $\pm$  95% confidence limits.

Cladoceran abundance was significantly related to Chl *a* and Region\*Season ( $r^2=49.8\%$ ), but did not vary by Year, SST or Depth (Figure 5.1-8). Cladoceran abundance increased in higher Chl *a* water. There were contrasting seasonal cycles between the GAB East Shelf, with highest densities in winter,

and offshore regions that had low abundances all year round, except for GAB East Off where there were elevated Cladoceran densities in autumn.

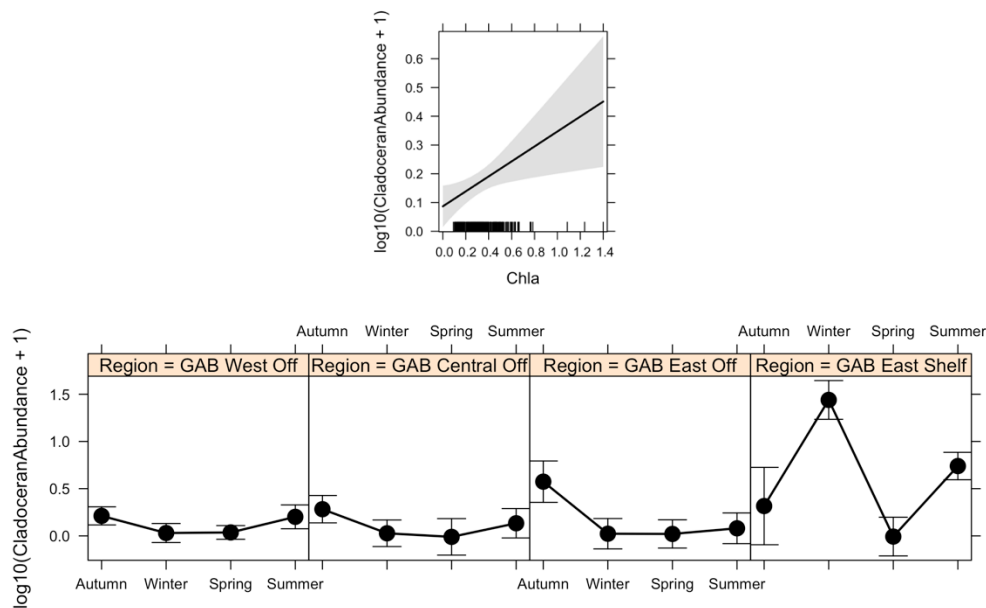


Figure 5.1-8. Effects plot of final linear model of total cladoceran abundance ( $\log_{10}$ -transformed) against predictors showing means  $\pm$  95% confidence limits.

Larvaceans were significantly related to Year, SST, and Region\*Season ( $r^2=21.0\%$ ), but not to Chl *a* or Depth (Figure 5.1-11). The interannual trend was variable. There was an increase in larvaceans in warmer water. The seasonal cycles in the different regions were very different. Larvaceans were most abundant in spring in offshore regions.

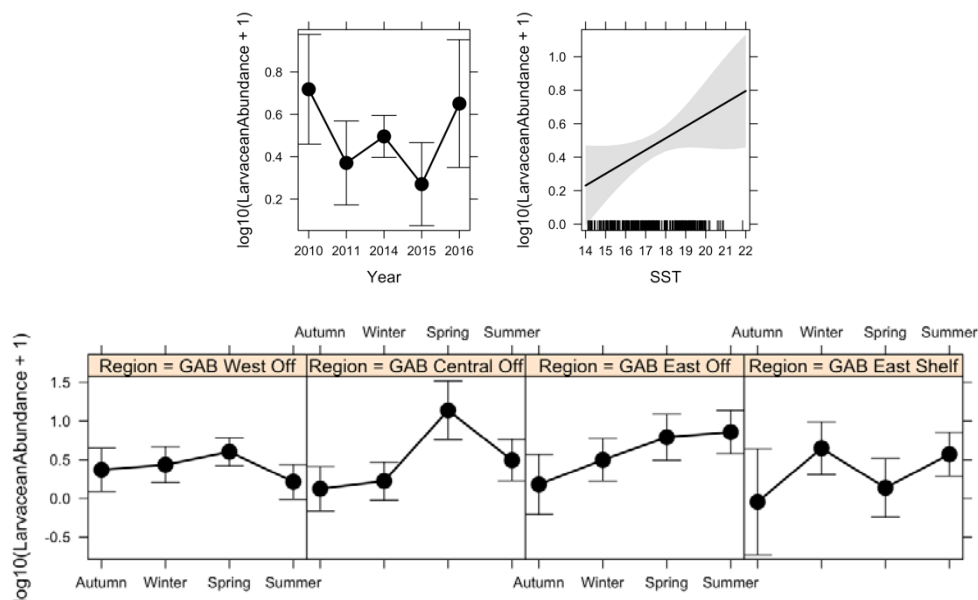


Figure 5.1-9. Effects plot of final linear model of total larvacean abundance ( $\log_{10}$ -transformed) against predictors showing means  $\pm$  95% confidence limits.

Chaetognaths were significantly related to Year, and Region\*Season ( $r^2=55.0\%$ ), but not to SST and Depth (Figure 5.1-10). There was a general increase in chaetognath abundance over time. They were strongly related to SST, with an order of magnitude more chaetognaths in 21°C than 14°C water.

## Zooplankton

There were many more chaetognaths in offshore waters, particularly the GAB Central Offshore and GAB West Offshore. Across the regions, chaetognaths increased from autumn to a peak in winter and then declined in spring and summer.

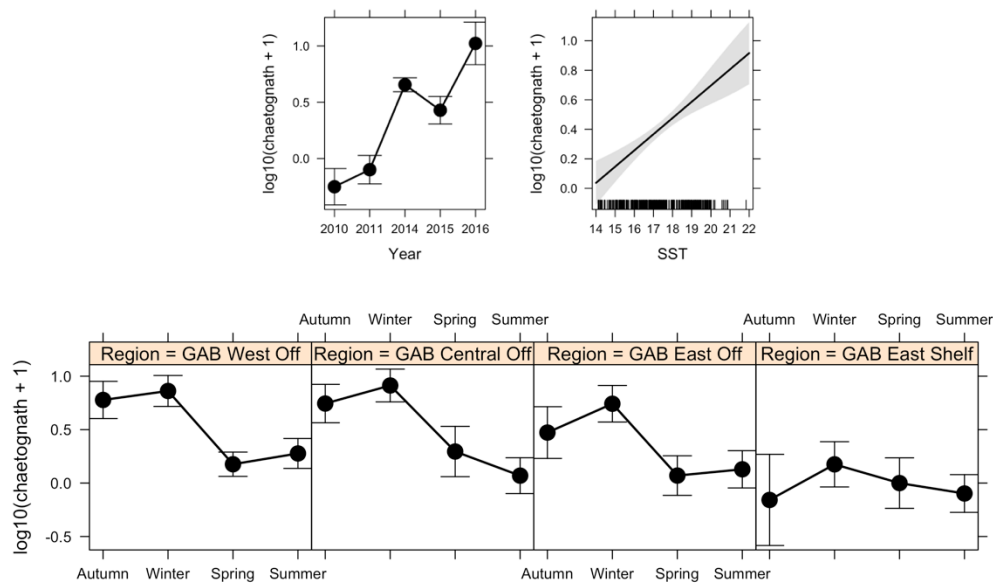


Figure 5.1-10. Effects plot of final linear model of total chaetognath abundance (log10-transformed) against predictors showing means  $\pm$  95% confidence limits.

Euphausiids were significantly related to Year, Chl *a*, Region and Season ( $r^2=35.6\%$ ), but not to SST or Depth (Figure 5.1-11). As with many other response variables, there was a general increase over the last few years in the abundance of euphausiids. They were strongly related to Chl *a*, with more euphausiids in waters with more phytoplankton. There were more Euphausiids offshore on the GAB than on the shelf, especially on GAB Central Offshore and GAB West Offshore. Across the regions, euphausiids peaked in autumn and then were less abundant in other seasons.

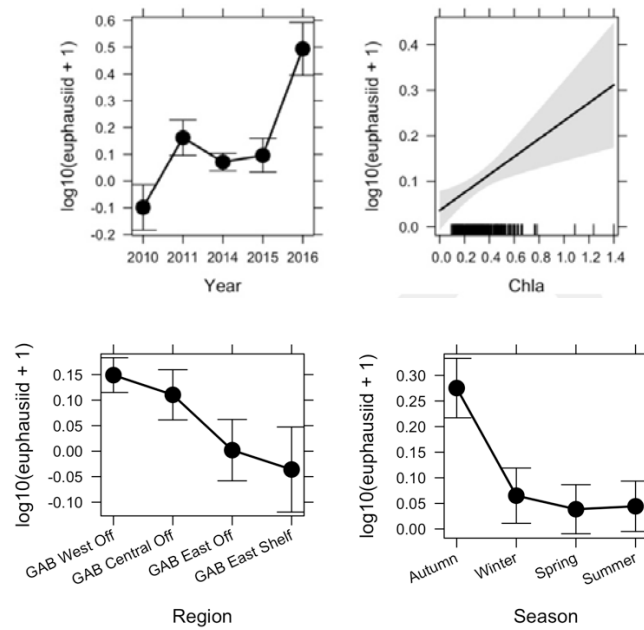


Figure 5.1-11. Effects plot of final linear model of total euphausiid abundance (log10-transformed) against predictors showing means  $\pm$  95% confidence limits.

#### Community metrics

Copepod richness was significantly related to Year, SST, Depth, Region and Season ( $r^2=54.8\%$ ), but not to Chl *a* (Figure 5.1-12). Similar to many of the response variables, there has been an increase in richness over the last few years. Copepod richness was strongly related to temperature, with nearly three times as many species in 21°C than 14°C waters. Copepod size was positively but more weakly related to Chl *a*. The Region\*Season interaction is significant, but the general seasonal trend is still clear among regions: the copepod community was most diverse in autumn and then it decreased through winter, spring and summer.



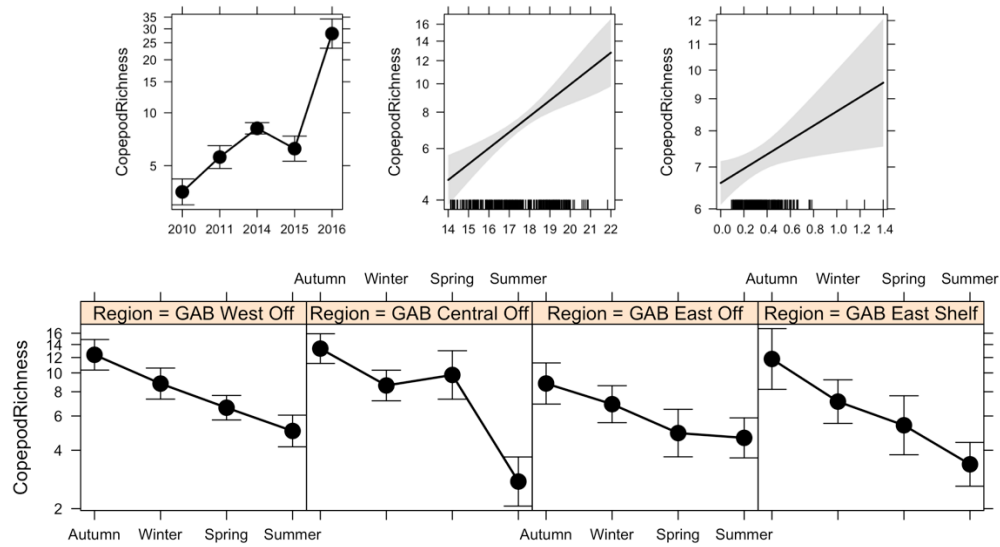


Figure 5.1-12. Effects plot of final generalized linear model of copepod richness against predictors showing means  $\pm$  95 % confidence limits.

Copepod size was significantly related to Year, SST, Depth, Region and Season ( $r^2=21.1\%$ ), but not to Chl *a* (Figure 5.1-13). Copepod size was greater in 2016 than other years. Copepods were larger in warmer water and offshore. The interaction Region\*Season was not significant, implying a similar seasonal cycle in the different regions, which shows largest copepods in winter and spring. Copepods were largest in the GAB Central Offshore region.

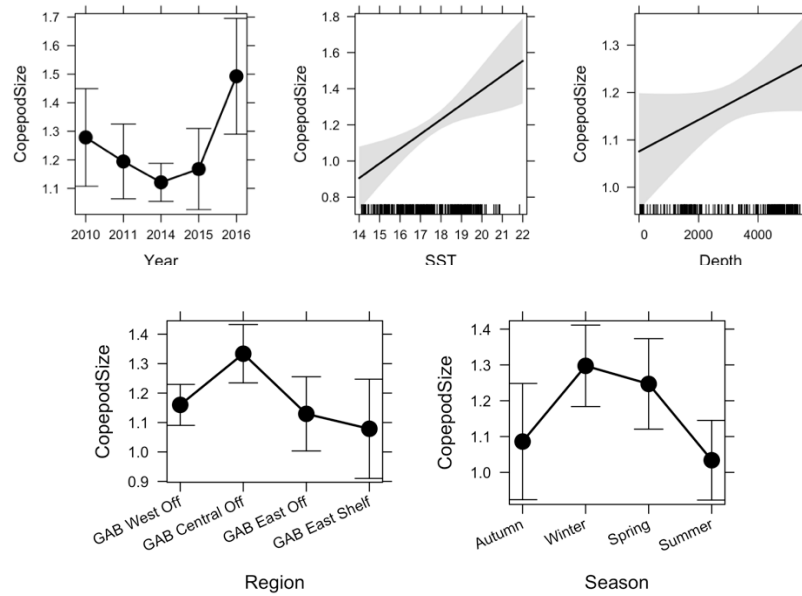


Figure 5.1-13. Effects plot of final linear model of copepod size against predictors showing means  $\pm$  95 % confidence limits.

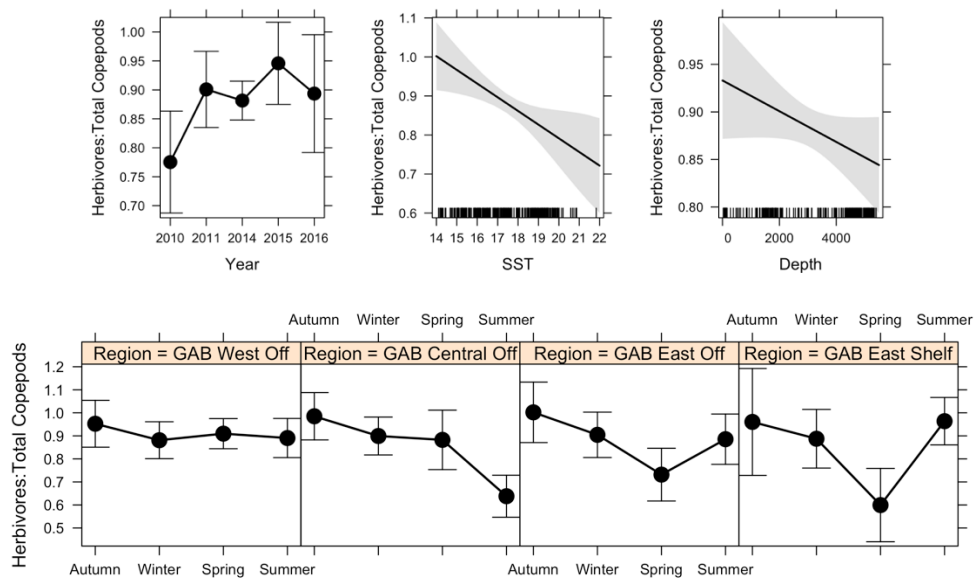


Figure 5.1-14. Effects plot of final linear model of herbivore:total copepod ratio against predictors showing means  $\pm$  95 % confidence limits.

Copepod herbivore:total copepod was significantly related to Year, SST, Depth, and Region\*Season ( $r^2=28.5\%$ ), but not to Chl *a* (Figure 5.1-14). Copepods that are primarily herbivorous dominate the copepod community, constituting 88.8%. Over the past few years, 90-95% of the copepod community have been primarily herbivorous. There were substantially fewer herbivores in colder and deeper waters. In all regions, there were relatively more herbivorous copepods in autumn than other seasons.

## Zooplankton

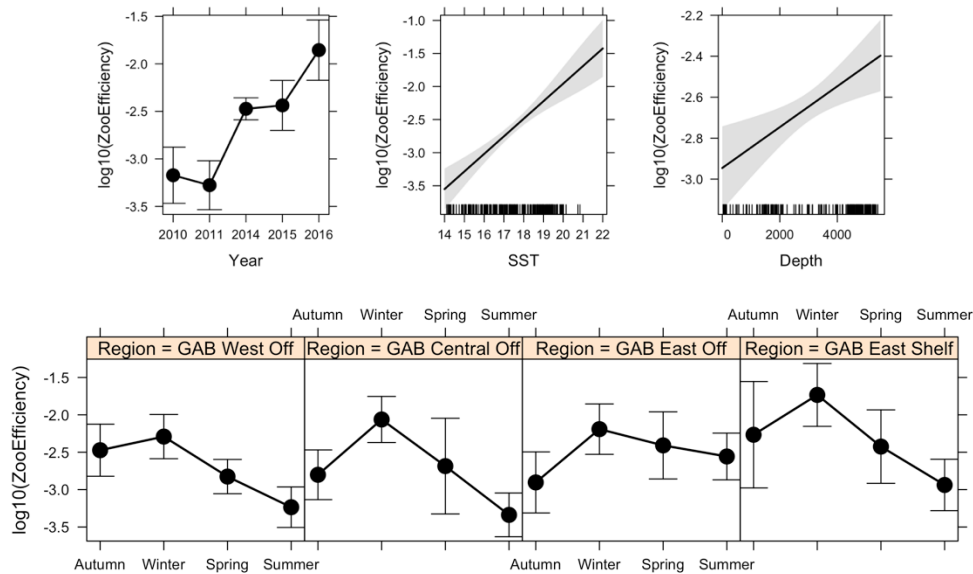


Figure 5.1-15. Effects plot of final linear model of zooplankton:phytoplankton ratio ( $\log_{10}$ -transformed) against predictors showing means  $\pm$  95% confidence limits.

The zooplankton:phytoplankton ratio was significantly related to Year, SST, Depth and Region\*Season ( $r^2=44.5\%$ ), but not to Chl  $a$  (Figure 5.1-11). There has been relatively more zooplankton relative to phytoplankton through time. There was more zooplankton relative to phytoplankton in warmer waters and also in deeper water. The shape of the seasonal cycle was similar among regions, with the highest zooplankton:phytoplankton ratio in winter and lowest in autumn and summer.

### Multivariate community analysis

The nMDS of the copepod assemblage had a stress of 0.138, indicating a good ordination. Each of these figures shows the same nMDS, but with the different factors of Region, Season and Year superimposed. The ADONIS permutation test for all environmental variables simultaneously explained 28.1% of the variation in copepod communities and confirms that Region ( $r^2=6.9\%$ ,  $p<0.001$ ), Year ( $r^2=11.7\%$ ,  $p<0.001$ ), Season ( $r^2=6.5\%$ ,  $p<0.001$ ), Depth (1.2%,  $p<0.001$ ), and SST ( $r^2=1.7\%$ ,  $p<0.001$ ) were all significant and explain variation in copepod communities; Chl  $a$  was not significant.

The nMDS ordination shows distinctly different copepod communities across regions (Figure 5.1-16A). The 99% confidence limits of the means show that the copepod community on the GAB East Shelf is different from other regions. It is most similar to GAB East Off, and this region is different from both GAB Central Off and GAB West Off, which have similar copepod communities (overlapping confidence limits). In terms of relationship to environmental variables, all vectors were significant except Chl  $a$ , which is short and not significant ( $p>0.05$ ). Offshore regions were positively related to the Depth vector. Samples in the bottom left corner are generally from warmer conditions.

The nMDS ordination also clearly shows different copepod communities seasonally (Figure 5.1-16B). The 99% confidence limits of the means show that the copepod communities in winter and autumn overlap, but are distinct from those in spring and summer. Autumn and spring communities are found in warmer waters, and those in spring appear to experience the coolest conditions.

The nMDS ordination also show that copepod communities vary interannually (Figure 5.1-16C). The 99% confidence limits of the means show that the copepod community in 2010 and 2011 were similar, and in 2015 and 2016 were similar, and both pairs of years were different from each other and from 2014. Communities in 2010 and 2011 experienced warmer waters, while those in 2015 and 2016 experienced cooler conditions.

By plotting the species scores in ordination space (Figure 5.1-16D), species appearing close to each other imply that they are distributed similarly and are thus part of the same community. For example, *Farranula rostrata* and *Clausocalanus ingens* are species found off the shelf, and *Centropages australiensis*, *Acartia tranteri*, *Acartia fossae*, and *Centropages furcatus* are found in shallow water. *Lucicutia flavicornis*, *Candacea bipinnata*, and *Temora turbinata* are all warm-water species, and *Paracalanus indicus*, *Acartia negligens*, and *Oithona plumifera* are cold-water species.

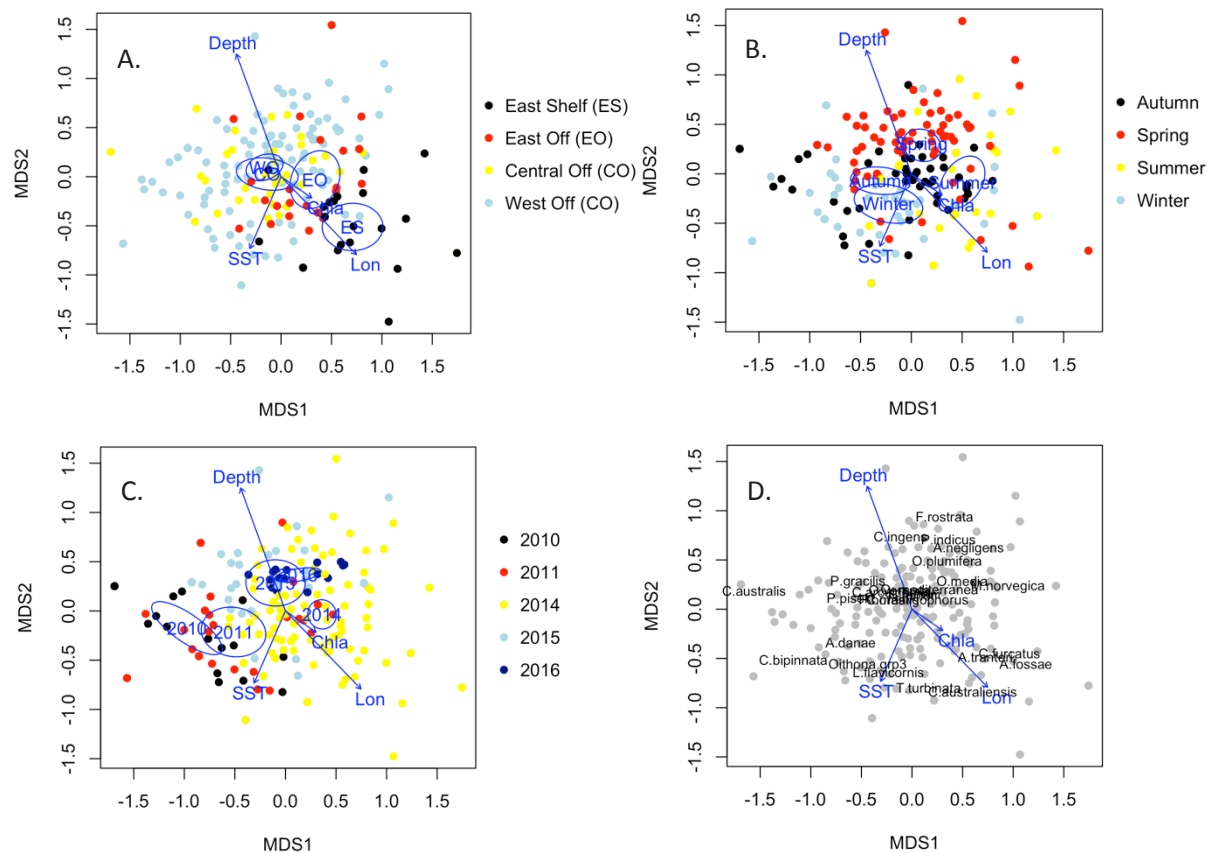


Figure 5.1-16. nMDS of the most common 26 copepod species. with Season superimposed and with environmental vectors.

The indicator value analysis highlighted species indicative of particular regions. For example, *Clausocalanus furcatus* (IV=0.3164,  $p<0.001$ , A), *Centropages australiensis* (IV=0.2130,  $p<0.001$ , B), *Temora turbinata* (IV=0.2062,  $p<0.009$ , C), and *Acartia tranteri* (IV=0.1292,  $p<0.011$ , E) were indicative of GAB East Shelf waters. *Lucicutia flavicornis* (IV=0.1287,  $p<0.035$ , D) was indicative of GAB East Offshore waters. *Nannocalanus minor* (IV=0.3000,  $p<0.001$ , F), *Clausocalanus arcuicornis* (IV=0.2561,  $p<0.003$ , G), *Pleuromamma piseki* (IV=0.1809,  $p<0.011$ , H), *Clausocalanus mastigophorus* (IV=0.1738,  $p<0.002$ , K), and *Pleuromamma gracilis* (IV=0.1537,  $p<0.015$ , I) was indicative of GAB Central Offshore. *Paracalanus indicus* (IV=0.1909,  $p<0.016$ , J) is an excellent indicator of GAB West Offshore waters.

A.

B.

C.

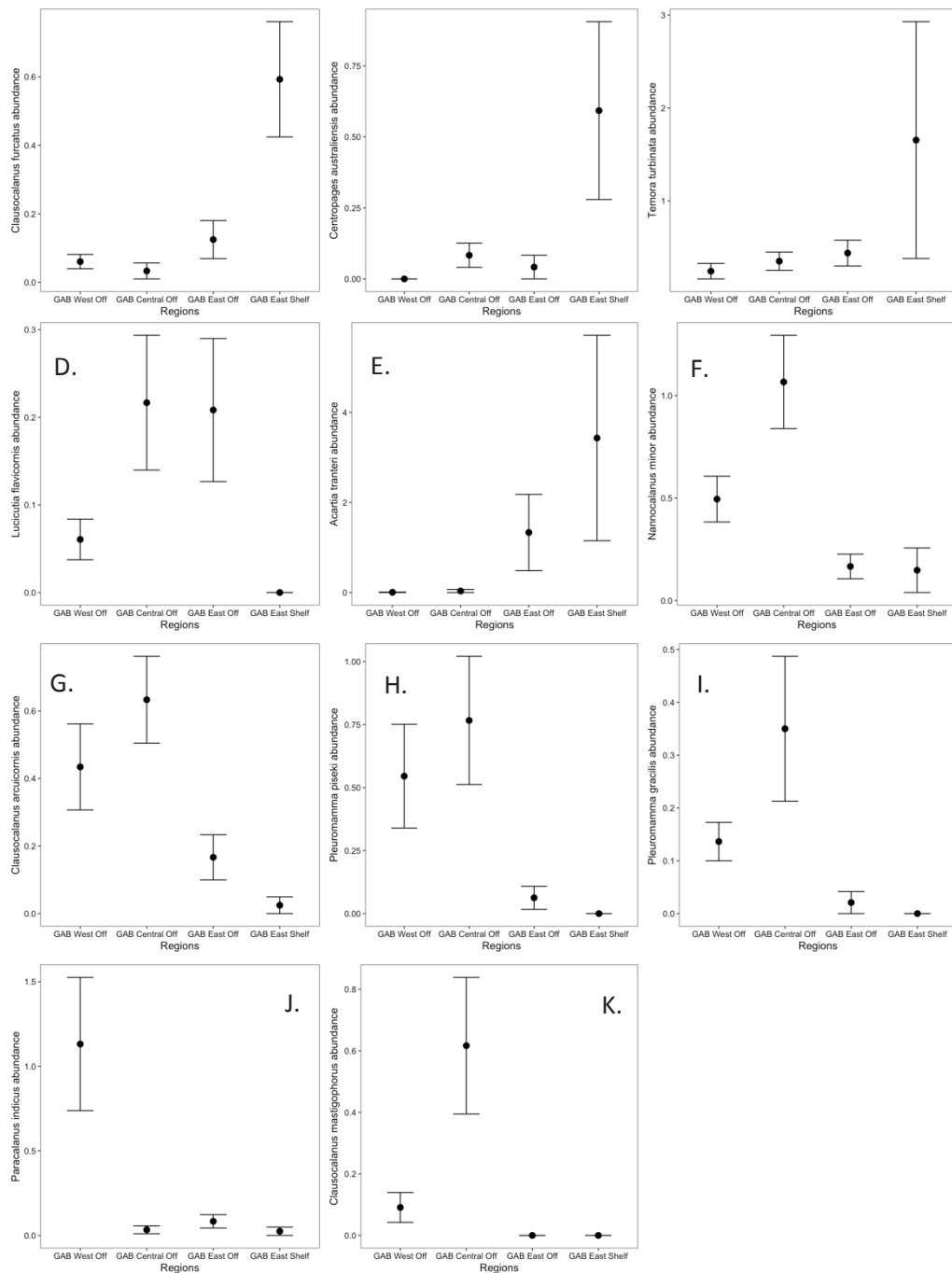


Figure 5.1-17. Mean ( $\pm$  standard error) abundance of the key species that separate regions based on an Indicator Species Analysis.

### 5.1.4 Discussion

The current study has provided a number of new insights into plankton dynamics in the GAB. First, we have established that there are distinct functional groups of phytoplankton and zooplankton and characteristic copepod species in different seasons and regions of the GAB. Second, we have found that there is marked seasonality in plankton dynamics in all regions, with peaks in abundance generally in Winter and Autumn, rather than Spring and Summer on the eastern GAB shelf as found by van Ruth and Ward (2009) in their more coastal sampling. Last, we showed that there was considerable interannual variation in many plankton functional groups, often greater than the regional and seasonal variation.

These findings provide new perspectives on our original hypothesis that the eastern GAB shelf has an efficient classical foodweb with high plankton abundance and large size, and that offshore regions and the central and western bank have a microbial foodweb with low plankton abundance and small size. Consistent with our original hypothesis, we found that compared with offshore regions the eastern GAB shelf generally had higher zooplankton abundance, a higher zooplankton : phytoplankton ratio, and a higher herbivore : total copepod ratio. However, contrary to our original hypothesis, we found that the size of copepods was smaller in the eastern GAB.

#### *Shelf waters of the eastern GAB: A productive classical foodweb*

The abundance of cladocerans, copepods, and non-copepod zooplankton was highest on the eastern GAB shelf, consistent with a classical foodweb, similar to findings of van Ruth and Ward (2009). Cladocerans can outnumber copepods in coastal and shelf waters (Jagger et al., 1988). Their populations can expand extremely rapidly in response to phytoplankton blooms via asexual reproduction (Kim *et al.* 1989) and thus they do well in productive coastal waters. Cladocerans are herbivorous and eat large diatoms (Jagger et al., 1988) and can be considered part of a classical food web, albeit a coastal one.

The highest abundance of copepods was on the eastern GAB shelf. We also found that the highest herbivore:total copepod ratio was in the eastern GAB, indicating that herbivores dominate the community in this region. Herbivorous and omnivorous copepod primarily graze on microplankton (20-200  $\mu\text{m}$ ) and their feeding efficiency decreases below 10  $\mu\text{m}$  (Berggreen et al. 1988), so they prefer large phytoplankton cells that are more common on the shelf in the eastern GAB (van Ruth and Ward 2009). Because herbivorous copepods have a relatively high predator:prey mass ratio (Wirtz, 2012), they transfer energy efficiently from phytoplankton to zooplankton and to fish (Heneghan et al., 2016). This is consistent with the idea that the eastern shelf is more productive and supports larger biomasses of zooplankton and higher trophic levels than offshore waters.

We also found that the zooplankton:phytoplankton ratio was a maximum on the shelf of the eastern GAB and lower in offshore regions. The zooplankton:phytoplankton ratio is commonly used in lakes as a measure of trophic efficiency, and is highest in temperate lakes with a classical foodweb and lowest in subtropical lakes dependent on a more microbial foodweb (Havens and Beaver 2013). Thus the higher zooplankton:phytoplankton ratio in the eastern GAB in our study suggests more efficient energy transfer to zooplankton than in offshore waters. This ratio, as well as the abundance of zooplankton and copepods, peaks in Winter, suggesting that Winter could be more important for conversion of secondary production to higher trophic levels than previously thought.

We hypothesised that the size of copepods would be larger on the shelf in the eastern GAB and smaller in offshore regions. However, we found the opposite. The common copepods on the eastern GAB shelf were small to medium in size (e.g., *Acartia fassae*, *Acartia tranteri*, *Centropages australiensis*, see Figure Figure 5.1-16D), whereas copepods in offshore waters had a range of sizes from small (e.g., *Clausocalanus ingens*) to large (e.g., *Pleuromamma piseki*, *Pleuromamma gracilis*). These larger species off the shelf undergo extensive diel vertical migrations and thus are better adapted to deep chlorophyll maxima (Hays et al., 1994). The eastern GAB shelf also had a high abundance of juvenile copepods suggesting rapidly growing populations, especially during the Winter, which makes the mean size of the copepod community smaller.

### *Offshore waters of the GAB: A 'productive' microbial foodweb*

The abundance of larvaceans was highest in offshore regions. Larvaceans were by far the most important group after copepods in the central and western GAB, and rivalled copepods in abundance on the eastern GAB, consistent with previous work in the region (van Ruth and Ward, 2009). Larvaceans are the second most abundant zooplankton group in the world when appropriately sampled (Hopcroft and Roff, 1998) and are the most competitive zooplankton in low food concentrations (Gorsky and Fenaux, 1998). Larvaceans are generally more abundant in warm water (Jaspers et al. 2009), and we found more larvaceans in warmer waters in our study. The relatively high abundance of larvaceans, especially offshore of the eastern GAB, is likely to lead to relatively efficient transfer of energy to higher trophic levels. This is because larvaceans grow quickly even in oligotrophic regions and their production can exceed that of copepods (Jaspers et al. 2009). Larvaceans are adapted to living in low nutrient waters, with feeding mechanisms that efficiently filter smaller picoplankton and nanoplankton (Wirtz 2012) that generally dominate these low nutrient regions, including offshore waters of the GAB (van Ruth and Ward 2009). Due to their specialised feeding mode, larvaceans are able to use directly the picoplankton dominated primary production in oligotrophic ecosystems, where 80% of the algae are  $<3\ \mu\text{m}$  (Goerick, 1998), while copepods are dependent on protozoans as intermediates to access the primary producers in oligotrophic areas. This ability to feed on small particles means that larvaceans have a high predator to prey mass ratio (Wirtz, 2012), so they can efficiently help transfer energy to higher trophic levels (Heneghan et al., 2016). This has been termed the “larvacean shunt” (Deibel and Lee, 1992) and is likely to support larger zooplankton and higher trophic levels in offshore GAB waters.

The abundance of chaetognaths was highest in offshore waters, especially on the central and western GAB. Chaetognaths (arrow worms) constitute 10-30% of the biomass of copepods in the global oceans (Bone, 1991). Their main food has been considered copepods (Bone, 1991) as they have large feeding hooks on their heads, and copepods can be identified in their guts.

Recent work suggests, however, that chaetognaths can gulp seawater, taking in dissolved and thin particulate organic matter produced by viruses and bacteria (Casanova et al. 2012). This diet could explain the high abundance of chaetognaths in oligotrophic waters such as the offshore GAB. Their relatively large size (up to 2.5 cm) means they make good food for higher trophic levels.

The abundance of euphausiids was highest in offshore waters. Euphausiids often have their highest abundances in shelf-edge and adjacent oceanic waters (Gibbons, 1995). Higher euphausiid abundance in offshore waters of the GAB is also not surprising given the region is likely to be heavily influenced by cold waters of the Southern Ocean. Euphausiids are omnivorous, increasing their degree of carnivory in oligotrophic waters (Henschke et al. 2015). Euphausiids are common along the shelf break because of passive accumulation and the likelihood of shelf-edge upwelling (Gibbons 1995). Euphausiids are generally long-lived species (a few years) and thus can survive the intermittent food availability along the shelf-edge and oceanic waters. Being large (up to 6 cm), nutritious (as are all crustaceans), and having a higher predator:prey mass ratio (i.e., the relative size of predator and prey) than other zooplankton except salps and crustaceans, euphausiids are an excellent food source for higher trophic levels.

Tintinnids also increased in offshore waters. These single-celled ciliates (up to  $200\ \mu\text{m}$  in size) graze pico- and nanophytoplankton and are important in the diet of copepods and euphausiids (Montagnes 2013), and thus sustain other zooplankton populations.

It thus appears that offshore regions of the GAB with their less seasonally variable zooplankton abundance, the high predator:prey mass ratios of larvaceans and euphausiids, the ability of



larvaceans and tintinnids to feed directly on nanophytoplankton, the typical high abundances of euphausiids at the shelf edge, and the potential ability for chaetognaths to extract nutrition directly from dissolved organic matter and bacteria, could support higher levels of larger zooplankton (e.g., siphonophores) and higher trophic levels such as micronekton than previously thought.

## References

- Anderson, M.J. 2001. A new method for non-parametric multivariate analysis of variance. *Austral Ecology*, 26: 32-46.
- Batten, S. D., Clark, R. A., Flinkman, J., Hays, G. C., John, E. H., John, A. W. G., et al. 2003. CPR sampling – the technical background, materials and methods, consistency and comparability. *Progress in Oceanography*, 58: 193–215.
- Beaugrand G, Luczak, C., and Edwards, M. 2009. Rapid biogeographical plankton shifts in the North Atlantic Ocean. *Global Change Biology*, 15: 179-1803.
- Berggreen U., Hansen B., and Kiørboe T. 1988. Food Size Spectra, Ingestion and Growth of the Copepod *Acartia tonsa* during development—implications for determination of copepod production. *Marine Biology*, 99: 341–352.
- Boltovskoy D. (Ed.) 1999. South Atlantic Zooplankton. Backhuys Publishers, Leiden.
- Bone, Q.H., Kapp, H., and Pierrot-Bults, A.C. 1991. The biology of the chaetognaths. Oxford University Press, New York, 173 pp.
- Casanova, J.-P., Barthélémy, R.-M., Duvert, M., and Faure, E. 2012. Chaetognaths feed primarily on dissolved and fine particulate organic matter, not on prey: implications for marine food webs. *Hypotheses in the Life Sciences*, 2(1): 20-29.
- Chivers, W. J., Walne, A. W. and G. C. Hays 2017. Mismatch between marine plankton range movements and the velocity of climate change. *Nature Communications* 8.
- Clarke, K.R., Gorley, R.N., Somerfield, P.J., and Warwick, R.M. 2014. Change in marine communities: an approach to statistical analysis and interpretation, 3rd edition. PRIMER-E, Plymouth, 260 pp.
- Edwards M., and Richardson A.J. 2004. Impact of climate change on marine pelagic phenology and trophic mismatch. *Nature*, 430: 881-884.
- Deibel D., and Lee S. H. 1992. Retention efficiency of submicrometer particles by the pharyngeal filter of the pelagic tunicate *Oikopleura vanhoeffeni*. *Marine Ecology Progress Series*, 81: 25–30.
- Dufrene, M. and Legendre, P. 1997. Species assemblages and indicator species: the need for a flexible asymmetrical approach. *Ecol. Monogr.*, 67(3): 345-366.
- Fowler, S. L., Costa, D. P., and Gales, N., 2007. Ontogeny of movements and foraging ranges in the Australian sea lion. *Marine Mammal Science*, 23: 598-614.
- Gibbons, M.J. 1995. Observation of euphausiid assemblages of the south coast of South Africa. *South African Journal of Marine Science*, 16: 141-148.
- Goericke R. 1998. Response of phytoplankton community structure and taxon-specific growth rates to seasonally varying physical forcing in the Sargasso Sea off Bermuda. *Limnology Oceanography*, 43: 921–935.
- Goldsworthy, S. D., and Page, B. C., 2007. A risk assessment approach to evaluating the significance of seal bycatch in two Australian fisheries. *Biological Conservation*, 139: 269-285.
- Gorsky G., and Fenaux R. 1998. The role of appendicularians in marine food webs. In: Bone Q., editor. *The Biology of Pelagic Tunicates*. Oxford University Press, New York, pp. 161–170.

- Havens, K.E. and Beaver, J.R. 2013. Zooplankton to phytoplankton biomass ratios in shallow Florida lakes: an evaluation of seasonality and hypotheses about factors controlling variability. *Hydrobiologia*, 703: 177-187.
- Hays, G.C., Proctor, C.A., John, A.W.G., and Warner, A.J. 1994. Interspecific differences in the diel vertical migration of marine copepods: The implications of size, color, and morphology. *Limnology and Oceanography*, 39: 1621-1629.
- Heneghan, R.F., Everett, J.D., Blanchard, J.L., and Richardson, A.J. 2016. Zooplankton are not fish: improving zooplankton realism in size-based models mediates energy transfer in food webs. *Frontiers in Marine Science*, 3: 1-15.
- Henschke, N., Everett, J.D., Suthers, I.M., Smith, J.A., Hunt, B.P.V., Doblin, M.A., and Taylor, M.D. 2015. Zooplankton trophic niches respond to different water types of the western Tasman Sea: A stable isotope analysis. *Deep-Sea Research*, 104: 1-8.
- Hopcroft R. R., and Roff J. C. 1998. Production of tropical larvaceans in Kingston Harbour, Jamaica: are we ignoring an important secondary producer? *Journal of Plankton Research*, 20: 557–569.
- Jaspers, C., Nielsen, T.G., Carstensen, J., Hopcroft, R.R., Møller, E.F. 2009. Metazooplankton distribution across the Southern Indian Ocean with emphasis on the role of Larvaceans. *Journal of Plankton Research*, 31: 525-540.
- Jagger, R.A., Kimmerer, W.J., Jenkins, G.P. 1988. Food of the cladoceran *Podon intermedius* in a marine embayment. *Marine Ecology Progress Series*, 43, 245-250.
- Kim, S. W., Onbe, T. and Yoon, Y. H. 1989. Feeding habits of marine cladocerans in the inland sea of Japan. *Marine Biology*, 100: 313-318.
- Legendre, P., Gallagher, E.D. 2001. Ecologically meaningful transformations for ordination of species data. *Oecologia*, 129: 271-280.
- Montagnes, D.J.S. 2013. Ecophysiology and behavior of tintinnids. In: Dolan JR, Montagnes DJS, Agatha S, Coats WD, Stoecker DK, editors. *The biology and ecology of tintinnid ciliates: models for marine plankton*. West Sussex: Wiley-Blackwell. p. 85-121.
- Oksanen, J. (2017). Package ‘vegan’. 292 pp.
- Page, B. C., McKenzie, J., Sumner, M. D., Coyne, M., and Goldsworthy, S. D., 2006. Spatial separation of foraging habits among New Zealand fur seals. *Marine Ecology Progress Series*, 323: 263-279.
- Richardson, A.J., John, E., Irigoien, X., Harris, R.P., Hays, G.C. (2004) How well does the Continuous Plankton Recorder (CPR) sample zooplankton? A comparison with the Longhurst Hardy Plankton Recorder (LHPR) in the northeast Atlantic. *Deep-Sea Research*, 51: 1283-1294.
- Richardson, A.J., Schoeman, D.S. 2004. Climate impact on plankton ecosystems in the Northeast Atlantic. *Science*, 305: 1609-1612.
- Richardson, A.J., Walne, A.W., John, A.W.G., Jonas, T.D., Lindley, J.A., Sims, D.W., and Witt, M. 2006. Using Continuous Plankton Recorder Data. *Progress in Oceanography*, 68: 27-74.
- Rogers, P.J., 2013. Physical processes, biodiversity and ecology of the Great Australian Bight region : a literature review / Paul Rogers, Tim Ward, Paul van Ruth, Alan Williams ; contributing authors, Barry Bruce, Sean Connell, David Currie, Campbell Davies, Karen Evans, Bronwyn Gillanders, Simon Goldsworthy, David Griffin, Nick Hardman-Mountford, Alex Ivey, Rudy Kloser, John Middleton, Anthony Richardson, Andrew Ross, Jason Tanner and Jock Young. CSIRO, [Hobart, Tasmania].
- van Ruth, P.D., and Ward, T.M., 2009. Meso-Zooplankton Abundance, Distribution and Community Composition in the Eastern Great Australian Bight. *Transactions of the Royal Society of South Australia*, 133: 274-283.

- Ward, T. M., McLeay, L. J., Dimmlich, W. F., Rogers, P. J., McClatchie, S. A. M., Matthews, R., Kampf, J., and Van Ruth, P. D. 2006. Pelagic ecology of a northern boundary current system: effects of upwelling on the production and distribution of sardine (*Sardinops sagax*), anchovy (*Engraulis australis*) and southern bluefin tuna (*Thunnus maccoyii*) in the Great Australian Bight. *Fisheries Oceanography*, 15(3): 191-207.
- Wirtz, K. W. 2012. Who is eating whom? Morphology and feeding type determine the size relation between planktonic predators and their ideal prey. *Mar. Ecol. Prog. Ser.*, 445: 1–12.

## 5.2 Regional comparison of community structure, size and biomass

Ryan Downie, Anthony Richardson and Rudy Kloser

### 5.2.1 Introduction

Pelagic ecosystems of the Great Australian Bight (GAB) serve as important nursery grounds for highly migratory pelagic finfish, sharks, pinnipeds and cetaceans that are of conservation concern (Rogers, 2013). These ecosystems also support two of Australia's largest fisheries, sardine and southern bluefin tuna, which contribute approximately \$50 million annually to the South Australian economy, and the South Australian seafood industry supports approximately 3000 jobs state-wide (PIRSA, 2015; ABRES 2016). Despite the conservation and commercial importance of pelagic ecosystems to the region, the biophysical processes that support this higher trophic level productivity remain uncertain (Rogers, 2013).

Previous empirical studies have identified that pelagic ecosystems on the continental shelf (0 – 200 m) in the eastern GAB experience episodic upwelling events in summer/autumn, that draw nutrient rich waters into the photic zone creating 'hotspots' of elevated primary and secondary productivity, but little work has been done in waters of the continental slope (400 - 1000 m water column depth) and further offshore (> 1000 m water column depth) in the eastern or central GAB (Kämpf et al., 2004; Ward et al., 2006; van Ruth et al., 2010; Rogers, 2013). We presume that large scale biophysical processes support ecosystem function in slope and offshore waters of the GAB. In particular, in summer/autumn productivity is nitrate-limited due to low wind stress and shallow mixed layer depths and ecosystem productivity is supported by microbial nitrification processes (Longhurst, 1995; Moore et al., 2013). However in autumn and spring, strengthening westerly winds deepen the mixed layer, which replenishes nutrients in the photic zone stimulates productivity, but ecosystems remain oligotrophic ( $<300 \text{ mg C m}^{-2} \text{ d}^{-1}$ ) (Longhurst, 1995; Uitz et al., 2010). Uncertainty and knowledge gaps exist around how accurate these estimates are and how energy is transferred to higher trophic levels, given the abundance of marine life that these ecosystems support. Here we aim to characterise the size structure and biovolume (a proxy for biomass) of meso-zooplankton in eastern upper-slope (E-Us), central upper-slope (C-Us), eastern offshore (E-Off) and central offshore waters (C-Off) in the GAB, early in the summer upwelling season.

Continental slope and offshore waters of the GAB display low annual variation in production and are termed oligotrophic ( $<300 \text{ mg C m}^{-3} \text{ d}^{-1}$ ) (Jitts, 1969; Motoda et al., 1978; Hanson et al., 2007; Uitz et al., 2010). Two mechanisms drive ecosystem productivity in sub-tropical/temperate oligotrophic waters: i) shoaling of the thermocline/nutricline within the photic zone and/or ii) the microbial regeneration of nutrients (Cullen, 1982; Treusch et al., 2009; Mignot et al., 2014). The relative contribution of these two processes vary temporally and spatially, and may result in the formation of deep chlorophyll maximum layers (Cullen, 1982; Cullen, 2015). Deep chlorophyll maximum layers persist year round in subtropical/temperate gyres and play an important role in regional production of these vast ocean provinces and have been found to contribute 30-70% to regional primary productivity in offshore waters of Western Australia (Hanson et al., 2007; Kemp and Villareal, 2013; Mignot et al., 2014; Signorini et al., 2015). It was anticipated that deep chlorophyll layers are a feature of slope and offshore waters of the GAB, and the aim of this project was to characterise relationships between primary and secondary production in slope and offshore waters of the GAB, given the importance of these habitats to higher trophic level foraging.

Waters of the continental shelf in the GAB experience seasonal variation in their properties. Observed variation is explain by seasonal climatic and oceanographic conditions which generate year round downwelling in the central GAB, and microbial regeneration of nutrients is thought to underpin areal production of pelagic ecosystems (Rogers, 2013). While in the summer/autumn episodic south-easterly wind events draw nutrient rich subsurface waters into the photic zone of shelf waters in the eastern GAB elevating ecosystem production (Middleton and Platov, 2003; Cirano and Middleton, 2004; Kämpf, 2010; van Ruth et al., 2010). Nutrient enrichment events in the eastern

GAB, have been demonstrated to stimulate elevated primary and secondary production in shelf and downstream coastal waters of the GAB, which triggers a shift in the community composition of phytoplankton and meso-zooplankton (Van Ruth and Ward, 2009; van Ruth et al., 2010). Copepods numerically dominate zooplankton communities year-round in the GAB, but during periods of elevated production species with fast growth rates and short development phases including salps, cladocera and meroplankton experience increases in relative abundances which results in a ~25% net increase in zooplankton biomass (Van Ruth and Ward, 2009). The extent which E-Us and E-Off stations are influenced by upwelling and the influence they have on ecosystem productivity is explored in this study. It was anticipated that deep chlorophyll maximum layers are a common feature of continental slope and offshore ecosystems in the eastern and central GAB, and should upwellings be observed, we would expect to observe higher biovolume of meso-zooplankton size classes in nutrient rich waters.

Since Sheldon's foundational work describing the size spectra of particles in the ocean (Sheldon et al., 1972), size based metrics have been used to characterise ecosystem structure and efficiency under different productivity regimes (Zhou et al., 2009; Blanchard et al., 2017). Rates of primary productivity have been demonstrated to influence the size structure and biovolume of zooplankton communities: in regions of high production the proportion of small herbivorous zooplankton increases, while in periods of low production an increase in the relative abundance of larger omnivorous- carnivorous zooplankton occurs (Zhou et al., 2009). One common metric used to summarise relationships between size spectra and abundance of organisms within ecosystems is the linear regression coefficient, slope. Slope metrics capture seasonal shifts in zooplankton communities, where more negative slopes are observed during periods of elevated production explained by the increased abundance of small herbivorous zooplankton, compared to when production is low slopes are flatter due to the relative increase abundance of omnivorous – carnivorous zooplankton (Zhou et al., 2009; Dai et al., 2016). Steeper slopes are associated with more efficient ecosystems where the transfer of carbon/energy to higher trophics happens through less trophic steps compared to ecosystems that display flatter slopes. Here we will use size spectra metrics to characterise zooplankton communities in pelagic ecosystems of the Great Australian Bight, comparing results to interpret regional differences in ecosystem efficiency.

### 5.2.2 Methods

The GAB accounts for approximately 1300 km of Australia's southern continental margin: it is crescent shaped and extends from Israelite Bay, WA to Kangaroo Island, SA. The continental shelf extends on average 100 km offshore and is at its greatest extent in the central GAB (230 km). The continental slope displays notable variation in its gradient, in the east it is approximately 70 km from the coast and drops from the shelf break (200 m) to 3000 m depth over 14 km (strait line distance), whereas in the central GAB the shelf break is approximately 200 km from the coast and drops to 3000 m over 200 km (straight line distance) (Figure 5.2-1).

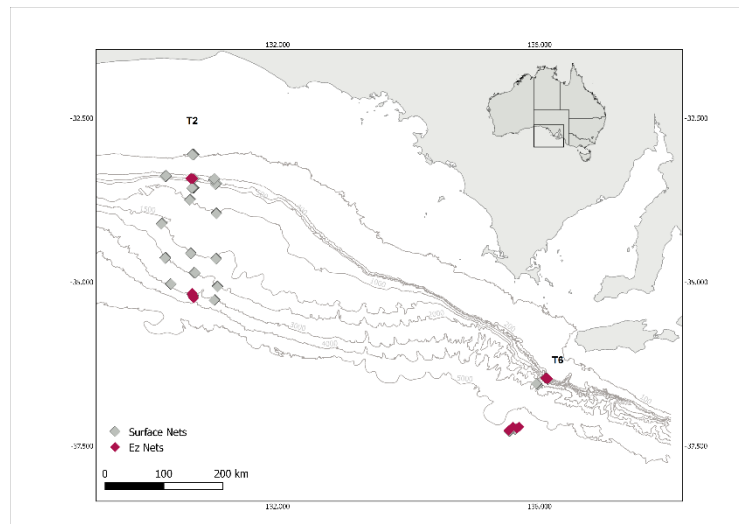


Figure 5.2-1. Location of Surface Net and Depth stratified (EZ net) samples, from the IN2015-C02 cruise

This body of work aims to characterise meso-zooplankton communities of the upper slope and offshore waters of the eastern and central GAB. The driving hypothesis of the program was that the microbial food-web is dominant year round, and episodic wind-stress events generate regional upwelling in shelf waters of the eastern GAB in summer/autumn, waters which support elevated primary and secondary productivity, important foraging grounds for marine mammals, pelagic sharks and large pelagic fisheries. The survey was designed to characterise the physical and biological components of regional ecosystems, describing each trophic level in terms of their taxonomic classification, size range, biomass and trophic relationships. Zooplankton communities were sampled using 1.2 m diameter surface net, multiple opening-closing deep deployed net system and a Laser Optical Plankton Counter (LOPC™). A subtle systematic bias is present in methods used to quantify zooplankton size spectra, which are based on an organism's equivalent spherical diameter (ESD). High resolution flat-bed scanning methods (ZooScan) measure non-living particles in a constant volume of water, where particles orientate according to their centre of gravity, compared to the LOPC where organisms are free-swimming and randomly orientated during measurement. ZooScan methods are more likely to measure maximum ESD, while LOPC methods are more likely to measure the mean orientation of an organism in its natural environment.

## Sampling stations and frequency

The deep-water GAB pelagic and benthic ecosystem survey ran from 30 November to 22 December 2015, a total of 23 days. Sampling time was dedicated to characterising the physical and ecological processes associated with the eastern and central GAB, with a focus on the upper slope (400-1000 m water depth) and offshore waters (> 1000 m water depth). Characterisation of pelagic ecosystems was focused on T2 and T6 (Figure 5.2-1). Opportunistic zooplankton sampling was additionally conducted along two transects (T1 and T3). Sampling stations were located at approximately 400 m, 1000 m and >3000 m water depths. At each pelagic sampling station, day and night samples were obtained to characterise diurnal movements of biota, while on some transects (T1 and T3) surface net samples were obtained opportunistically and time of day accounted for by recording the time the net was deployed.

Bottom depth at station determined the site's pelagic habitat classification. Sites with a bottom depth between 400-1000 m were classified as "slope" communities; herein referred to as East Upper Slope (E-Us) and Central Upper Slope (C-Us). While sites >1000 m bottom depth were classified as

“offshore” herein referred to as C-Off and E-Off for central and eastern offshore stations respectively. Transects T1-T3 are considered the central GAB; transect T6 represents the eastern GAB.

#### *Environmental data*

Vertical profiles of temperature, fluorescence and dissolved oxygen were obtained at each pelagic sampling station (down to ~ 20 m above the seafloor; except at deeper (> 800 m) water stations where profiles were taken to ~ 800 m). A Seabird SBE 9+ Conductivity-temperature-depth (CTD), dissolved oxygen sensor (Sea-Bird Scientific, SBE43) and a fluorometer (Chelsea Technologies Group Ltd, Aqua Tracker III) were fitted to a water sampling rosette frame.

Nutrients were analysed from water samples at 16 locations during 21 sampling events, samples were collected at 10m ‘surface’, the deep chlorophyll (fluorescence) maximum (cmax) and at 120m ‘deep’, using 12L Niskin bottles mounted on 36 bottle rosette. Water samples were collected to measure dissolved nutrient concentrations, the following nutrients were measured: ammonia, nitrite, nitrate, phosphate, silica, dissolved oxygen and salinity. Samples were analysed on-board using a Seal AA3HR segmented flow instrument, run by trained Marine National Facility hydrochemistry staff. Detection limits were 0.02µm for Nitrate + Nitrite, nitrite, ammonia and phosphate and 0.2 µM for silicate.

#### *Surface net sampling*

Surface samples were obtained by towing a 1.2 m diameter ring net, fitted with 335 µm mesh net for 10 minutes at 1m depth. Three replicate tows were obtained at each pelagic and benthic station. Samples were generally collected opportunistically during other deep-water operations to maximise sampling efficiency, vessel speed through water averaged 3 knots during sampling. A total of 117 surface tows were collected, 70 samples were processed for analysis due to time constraints. Samples at pelagic sampling stations on T2 and T6 were split into three size classes (0.3 - 1 mm, 1 - 4 mm and > 4 mm) using a series of three stacked sieves. Each size fraction was then split in half using a Folsom plankton splitter and frozen separately for size based and stable isotope analysis. Samples obtained from T1 and T3 were only split into three size classes. All samples were frozen at -20°C and defrosted for analysis. Thawed samples appeared structurally intact and no morphological damage was detected. Due to unreliable readings from flow meters, the filtered volume for each tow was calculated by multiplying the area of the net mouth, by the sampling time of each net, by the average speed of the vessel during sampling.

#### *Community and size spectra analysis - ZooScan*

The size structure and functional taxonomy of zooplankton samples were quantified using ZooScan (Grosjean et al., 2004). ZooScan is an image processing technique that obtains estimates of particle size from a high resolution flatbed scanner, which is suited to the analysis of biotic material with an equivalent spherical diameter (ESD) >300 µm. Scans are analysed using ZooProcess, which extracts individual particles “vignettes” and derives a range of parameters relating to its size and colour (Gorsky et al., 2010). Vignettes are then analysed using Plankton ID, which uses a neural network algorithm and assigns vignettes to a broad taxonomic groups, based on characteristics of groups in a reference library (Gorsky et al., 2010; Vandromme et al., 2012). Results were cross validated by a trained observer to remove incorrect classifications, inorganic material and scanning artefacts. In excess of 210,000 measurements of individual organisms were generated to quantify patterns in the size structure of zooplankton communities in the GAB. Output from multiple scans from different size fractions (derived from sieving) were merged using automated methods developed in R



statistical software (R, 2013). Size-based metrics were then calculated to compare the size structure of zooplankton communities. The Normalised Biovolume Size Spectra (NBSS) of each sample was calculated using methods described in Vandromme et al. (2012). A linear model was fitted to the NBSS data and the derived slope coefficient was used as a metric to summarise relationships between abundance and body size. Standardised mean size and total biovolume metrics were calculated to summarise general patterns in communities.

### *Surface net statistical analysis*

#### *Significance testing*

Summary metrics from size spectra data were generated to compare communities of interest; slope (linear regression coefficient), total biovolume (a proxy for biomass) and mean size. Metrics were analysed to test for differences between Regions (2 levels; fixed; east/central), Habitats (2 levels; fixed; slope/offshore) and time of day (2 levels; fixed; day/night) using a three-way ANOVA in R (R, 2013). Metrics were log 10-transformed to improve the assumptions of homogeneity of variance and normality if necessary. The most parsimonious model was determined by using a backward-fitting approach, where all terms and possible interactions were included in the first run of the model and sequentially removed if not found to account for significant variation. Where a statistically significant interaction or effect was detected, pair-wise comparisons were used to interpret the interaction and identify which levels and the direction of differences between levels. Time of Day was never significant and we thus dropped it from all subsequent analyses to reduce the number of parameters in the model.

#### *Size spectra and constrained ordination analysis*

A Redundancy analysis (RDA: constrained ordination) was used to explore the relationship between linear normalised biovolume size spectra data and 6 environmental variables to find which environmental variables explained significant variation. The benefit of a constrained RDA is that the ordination outputs the variation that is explained by environmental variables. Bi-plots were generated to depict the relationships between size spectra and explanatory variables. Rarely-observed size classes were removed from data to simplify the dataset as rare observations unduly influence constrained ordination, as recommended by Cao et al. (2001). To ensure abundant functional groups did not dominate the ordination, a Hellinger transformation was applied to linear normalised biovolume data (Legendre and Gallagher, 2001). Size classes were deemed to be rare if not found to occur within 14% of samples or 9 of the 67 samples. Given that variation increases with size spectra, data were scaled/standardized within the analysis so that analysis was not dominated by species with highest variation. Environmental variables were screened for collinearity using correlation analysis; bivariate relationships that displayed R-squared values  $\geq 0.75$  were removed, to avoid over-fitting and simplify the model for interpretation purposes. Redundant variables were removed based on informed opinion to ensure remaining variables retained the greatest portion of variation. RDA axes were tested for significance using a permutation ANOVA, to evaluate if the variation explained by retained variables was higher than would be explained by randomly generated variables (Legendre et al., 2011). The most parsimonious RDA model was selected using the R-squared goodness-of-fit approach.

*Depth integrated sampling**Depth stratified net sampling*

Depth-stratified sampling was achieved by towing a multiple opening-closing net (MOCNESS referred to herein as EZ net with a 1m x 1m sampling area). The EZ net was fitted with 5 x 335  $\mu\text{m}$  mesh nets, and was deployed at each pelagic sampling station on T2 and T6. Nets were sampled at 100 m depth intervals obliquely, and each 100 m interval was sampled for 10 minutes. At offshore stations, a sample was collected from 600 - 400 m, over 20 minutes. Nets were triggered through an optic fibre connection and verified to have fired through a live video feed. The EZ net was fitted with a Seabird SBE 9+ Conductivity-temperature-depth (CTD) sensor and a Laser optical plankton counter (LOPC). Samples were processed using the same methodology as described above for the Surface Net samples; samples were sieved into three size classes and then each size fraction spit in half and frozen separately for size-based and isotope analyses.

*LOPC – vertical characterisation of zooplankton communities*

Laser Optical Plankton Counter profiles provide highly resolved vertical profiles of particulate matter representative of meso-zooplankton communities (Herman et al., 2004). A LOPC and a Seabird electronics CTD were fitted to the main frame of the EZ net system to characterise vertical structure of meso-zooplankton size spectra at high resolution. The system was lowered to 400 m and retrieved at a rate of 10 meters per minute. The vessel towed the system at 3 knots. Volume filtered was estimated by multiplying the sampling area of the LOPC ( $0.006 \text{ m}^2$ ) by sampling time per depth interval (sec), by speed of the vessel ( $\text{m sec}^{-1}$ ). Observations from surface waters ( $<10\text{m}$ ) were excluded from this analysis to avoid the potential confounding effects of turbulent bubbles from the ship.

Data recorded from LOPC is reported in two formats, Single Element Plankton (SEP) and Multi-Element plankton (Herman et al., 2004). SEP is reported as count data in 15  $\mu\text{m}$  bins of particles Equivalent Spherical Diameter (ESD). Multi-element Plankton ESD was calculated following methods described in Herman et al. (2004) and the LOPC system integration guide. LOPCs are effective at observing particles between 0.2 - 10 mm to densities around  $10^6 \text{ m}^{-3}$ , see Herman et al. (2004) for further details. Normalised Biovolume of each defined size bin was calculated for each 5 m depth interval using methods described in Vandromme et al. (2012) and summarised here; a particles spherical biovolume was calculated ( $\text{mm}^3$ ), particles were then assigned a logarithmic scaled size bin based on its spherical biovolume. The biovolume of all particles within a respective size bin were summed and standardised for volume filtered ( $\text{m}^3$ ), and normalised by dividing by the range of the size bin ( $\text{mm}^3$ ). Biovolume of SEP data was based on the median size of particles within log-spaced size classes. The mean of derived normalised biovolume estimates are derived for 5 m depth intervals and plotted against depth to characterise the vertical structure of zooplankton communities down to 200 m.

*EZ net - vertical characterisation of zooplankton communities*

EZ net samples were analysed using ZooScan methods, and derived total biovolume and mean size metrics were calculated. Metrics were analysed using a boxplot-style analysis. These are reported in relation to the region, habitat and depth in which the samples were collected. Inconsistencies between net and LOPC observations are expected due to the practical limitations of sampling devices, where the mesh size of the EZ net was 300  $\mu\text{m}$  and LOPC are capable of sampling particles with ESD  $> 200 \mu\text{m}$ .

### 5.2.3 Results

#### *Meso-zooplankton communities in surface waters*

Derived NBSS plots indicate that meso-zooplankton communities observed at E-Us stations had a greater abundance of smaller size classes, when compared to stations further offshore and in the central GAB (Figure 5.2-2). The greater abundance of smaller size classes at E-Us generated significantly steeper slopes than C-Us, C-Off and E-Off stations ( $F = 30.0$ ,  $p < 0.001$ ) (Figure 5.2-3 a). The E-Us had variable but statistically higher total biovolume of meso-zooplankton than C-Us, C-Off and E-Off stations ( $F = 7.85$ ,  $p < 0.01$ ) (Figure 5.2-3 b). The mean size of meso-zooplankton in E-Us was statistically smaller than C-Us, C-Off and E-Off communities ( $F = 7.69$ ,  $p < 0.01$ ) (Figure 5.2-3 c).

A redundancy analysis explored the relationship between the size structure of communities and environmental variables (Figure 5.2-4). A correlation analysis between environmental variables, detected collinearity between multiple explanatory variables (salinity, oxygen, NO<sub>x</sub>, Phosphate and silicate), which were removed to avoid over-fitting and simplify the model for interpretation purposes. Variables retained were fluorescence, ammonia and temperature, which collectively explained a significant portion of total variation of meso-zooplankton size structure. Bi-plots depicted that size structure of E-Us communities group and are best explained by elevated fluorescence values. Fluorescence explained 71% of observed variation.

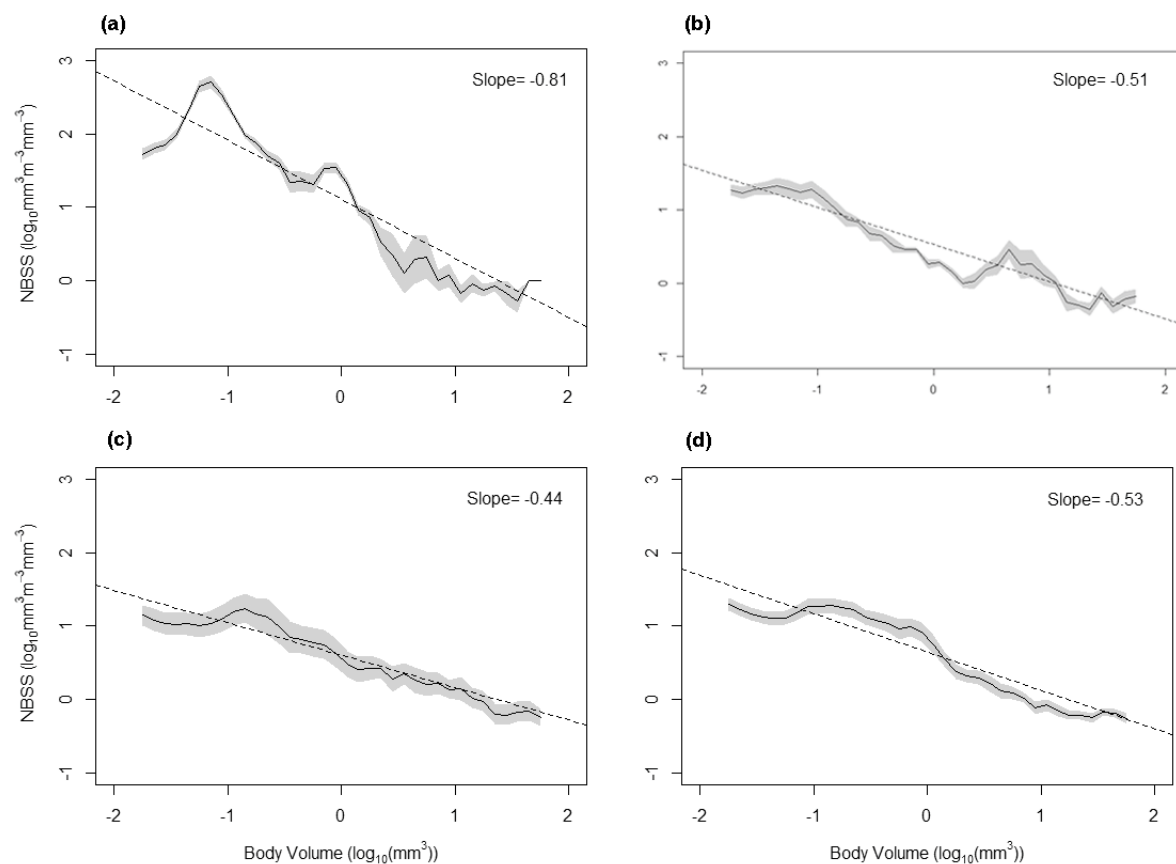


Figure 5.2-2. Normalised Biovolume size spectrum plots from (a) E-US, (b) E-Off, (c) C-Us and (d) C-Off. Text inset report linear regression coefficient slope.

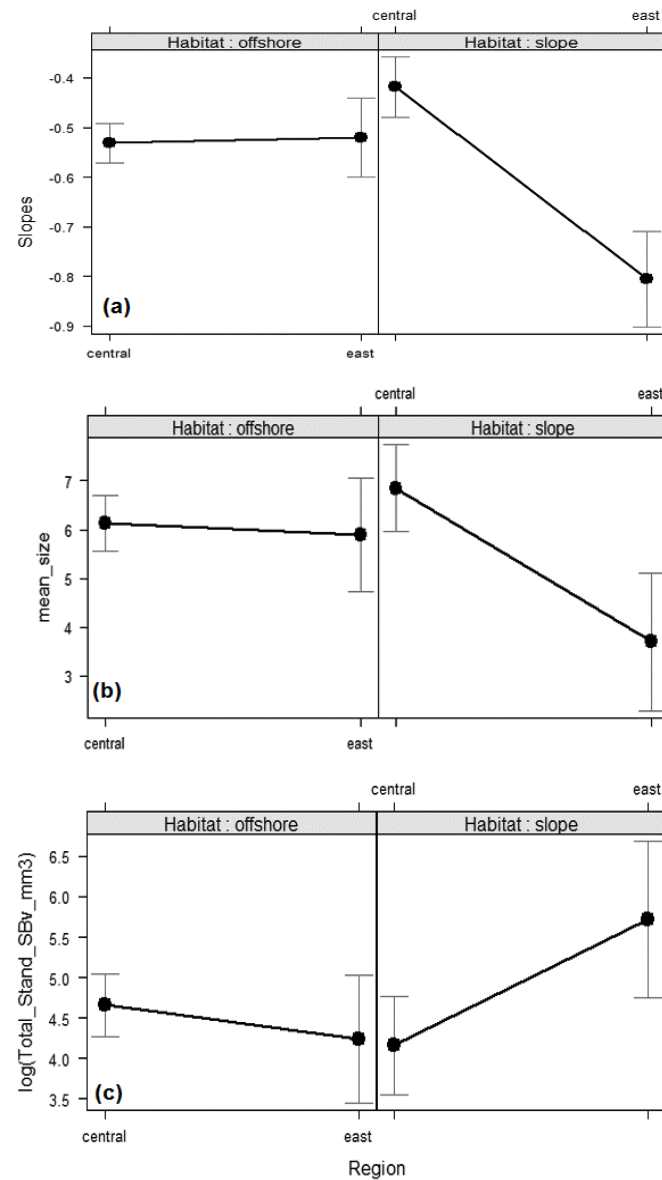


Figure 5.2-3. Metrics from surface net Normalised Biovolume Size Spectra ANOVA interaction plots that summarise a) Slope by region and habitat, b) the mean size of meso-zooplankton by region and habitat (c) Total Biovolume of meso-zooplankton by region and habitat.

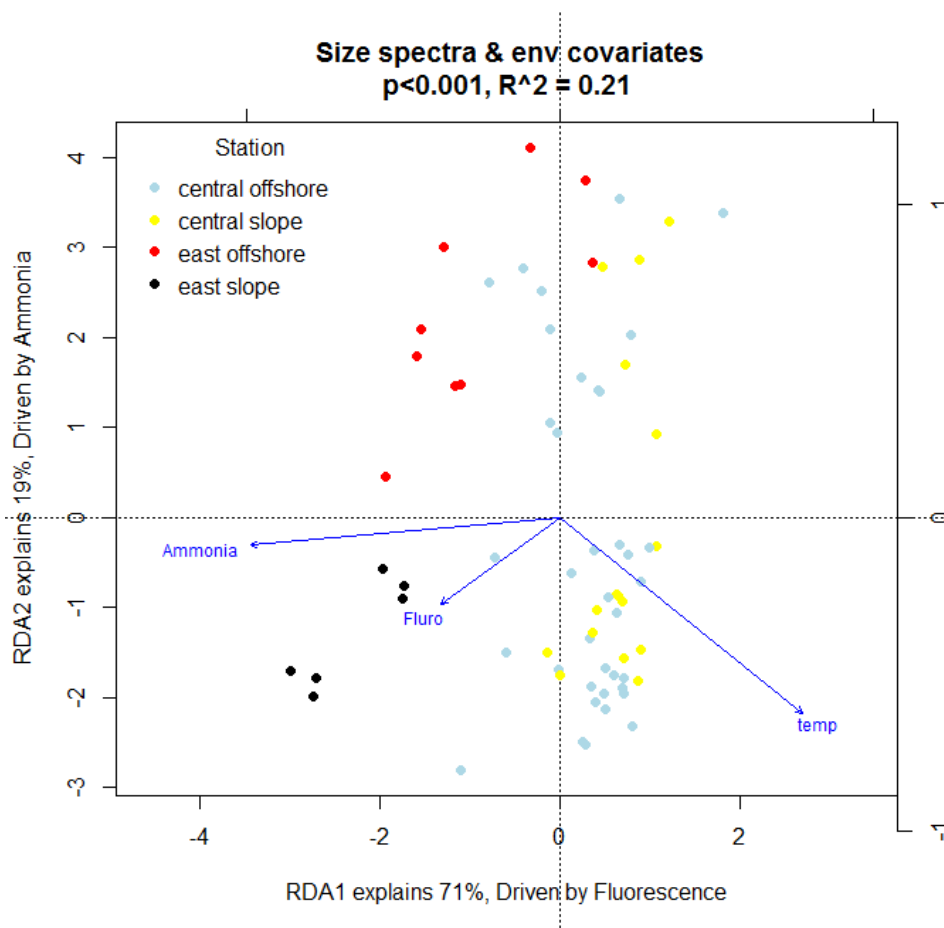


Figure 5.2-4 Redundancy Analysis on zooplankton size spectra and environmental variables. Arrows show direction of environmental variables, colour coding of points refers to sampling location.

#### *Environmental profiles and the vertical structure of meso-zooplankton communities*

Fluorescence profiles indicate the presence of strong subsurface chlorophyll layers (Figure 5.2-5). Layers occurred below the thermocline and nutricline but varied in magnitude and depth by region and habitat. E-Us stations displayed elevated fluorescence values over the greatest depth range with maximum values of  $34 \mu\text{g l}^{-1}$  at 51 m, E-Off and C-Off stations displayed similar peaks,  $33\text{--}34 \mu\text{g l}^{-1}$  at 70–73 m depth respectively. However at E-Off stations higher surface chlorophyll values were observed in the mixed layer. Chlorophyll values at C-Us were more consistent with depth than other stations and displayed maximum values  $26 \mu\text{g l}^{-1}$  at 91 m.

The vertical structure of particulate normalised biovolume (proxy for meso-zooplankton biomass) display interesting patterns by region and habitat (Figure 5.2-6). At offshore stations particulate biovolume indicate peak abundances occur at similar depth ranges to deep chlorophyll maximum layers at offshore stations (Figure 5.2-6 b, d). In contrast to offshore stations, E-Us stations display low particulate biovolume at the deep chlorophyll maximum (Figure 5.2-6 a). Particulate biovolume at C-Us sites is evenly distributed with depth and explained by relatively consistent fluorescence values from surface to 130 m (Figure 5.2-6 c).

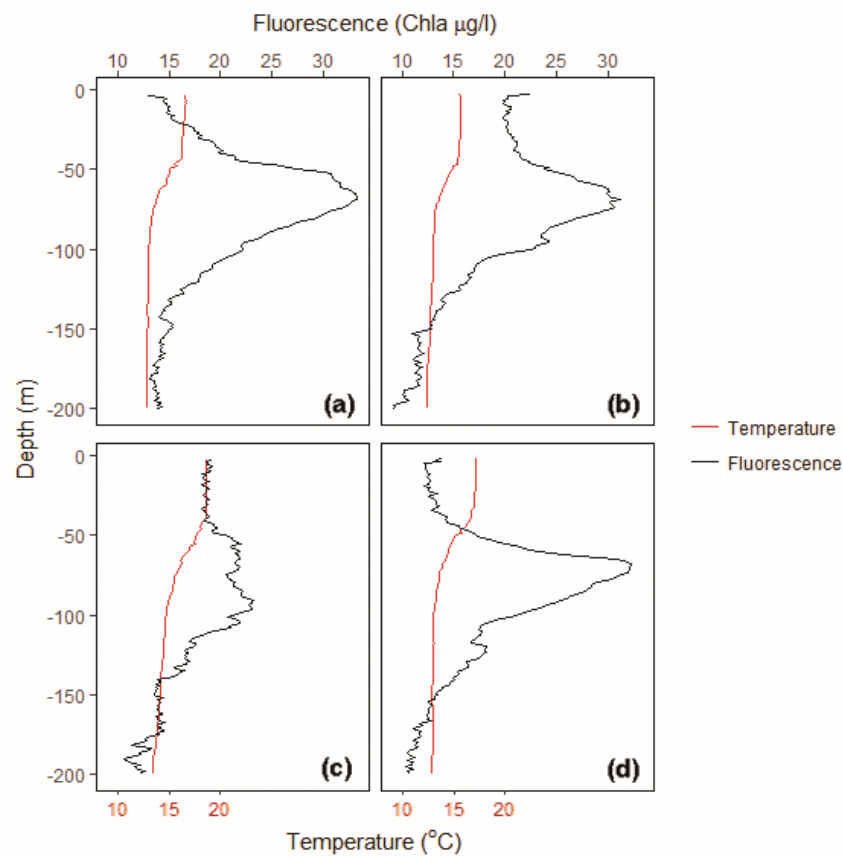


Figure 5.2-5. Temperature and Fluorescence profiles by region and habitat. ((a) E-Us (b) E-Off (c) C-Us (d) C-Off

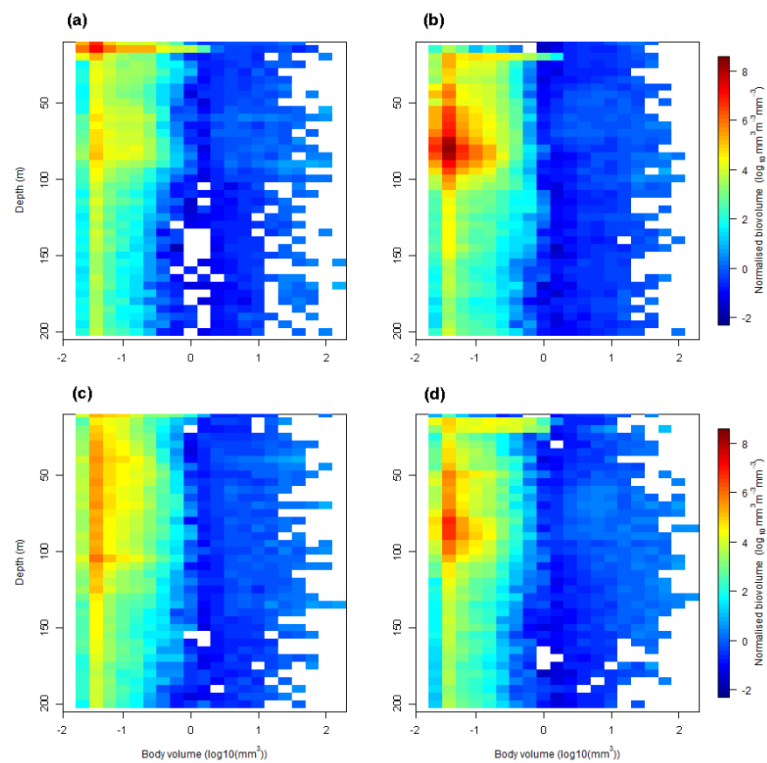


Figure 5.2-6 LOPC profiles of normalized biovolume. ((a) E-Us (b) E-Off (c) C-Us (d) C-Off

## Zooplankton

Meso-zooplankton samples from the EZ net suggest biovolume is greatest in the 0-100 m interval at E-Us and C-Off stations (Figure 5.2-7 a), and that biovolume is relatively consistent between 100-400 m. Broadly mean size of organisms is larger at offshore stations when compared slope stations and that mean size increases with depth (Figure 5.2-7 b). Copepod abundance was found to display a slight diurnal migration pattern in the central compared to the eastern GAB (Figure 5.2-8).

Table 5.2-1 provides a summary of surface net NBSS and size based metrics per transect for upper-slope and offshore waters. This was of interest, to gauge how representative T2 was of the central GAB. It highlights that the mean size and slope metrics of T1, T2 and T3 upper-slope and offshore communities were similar – when compared to E-Us. However, the total biovolume of communities at slope and offshore stations on T2 is higher than on T1 and T3.

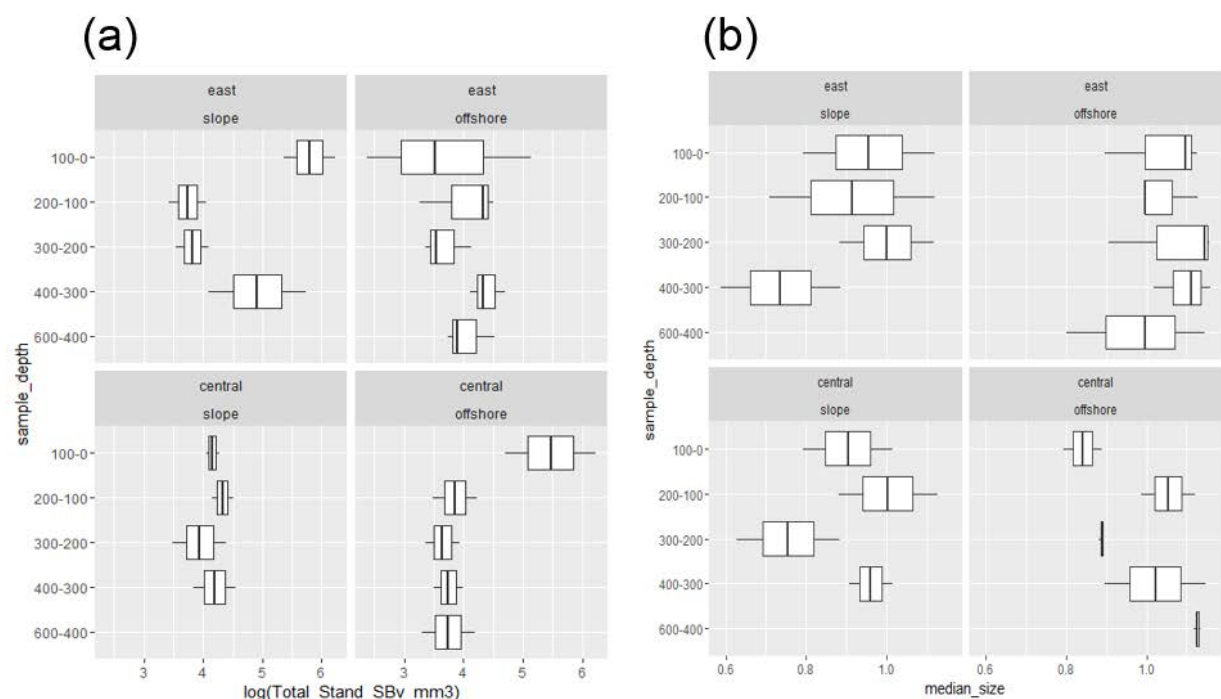


Figure 5.2-7. Depth stratified net samples from the EZ net (a) log total biovolume of meso-zooplankton communities by depth interval sampled (b) median size of meso-zooplankton communities by depth interval sampled



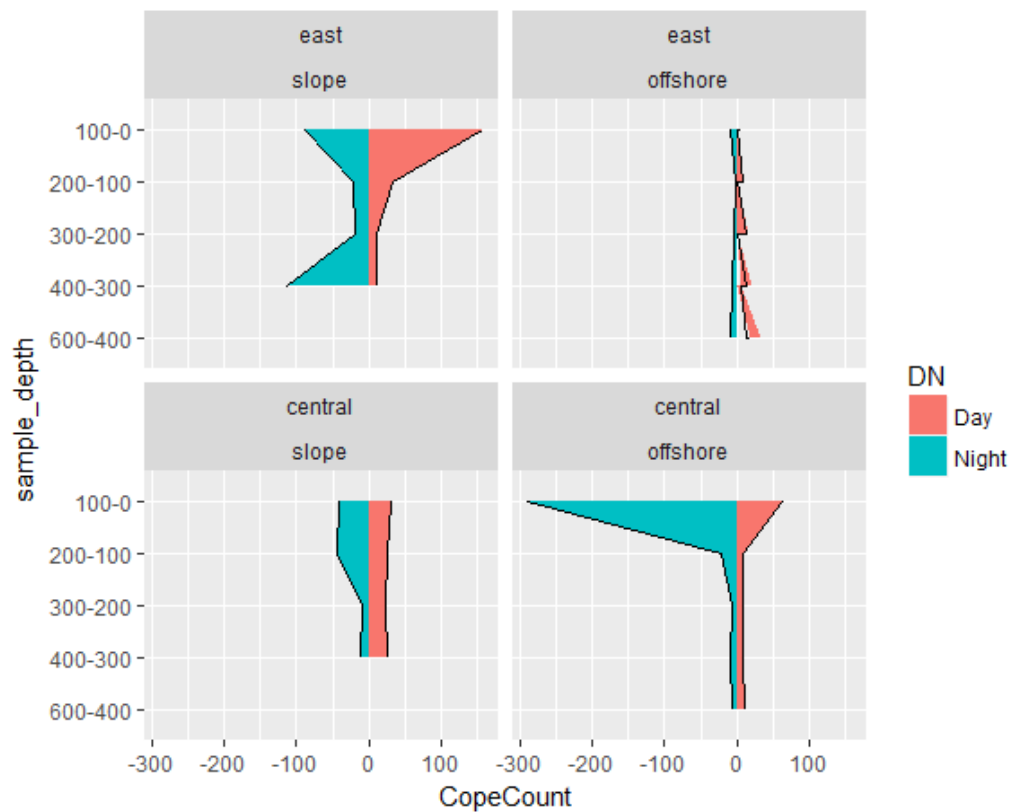


Figure 5.2-8. Copepod abundance (number of individuals  $m^{-3}$ ) by depth, Region, Habitat and Day/Night. Negative numbers on x axis refers to number of individuals at night.

*The consistency of surface meso-zooplankton communities the central GAB.*

Table 5.2-1 provides a summary of meso-zooplankton NBSS metrics on for each transect, to interpret how consistent T2 is with other transects in the central GAB (T1 and T3).

Table 5.2-1. Comparison of zooplankton samples from T1, T2, T3 and T6.

Transect	Region	Habitat	N	Slope mean	Slope std err	Biomass $m^3$	Biomass se	mean Size m	mean Size std err
T1	Central	offshore	9	-0.53	0.03	143.09	28.58	6.16	0.62
T1	Central	slope	3	-0.55	0.04	358.87	143.48	7.44	0.90
T2	Central	offshore	15	-0.52	0.05	333.54	129.11	5.71	0.47
T2	Central	slope	11	-0.41	0.03	157.30	48.39	6.60	0.48
T3	Central	offshore	13	-0.53	0.03	122.82	21.34	6.70	0.50
T3	Central	slope	2	-0.44	0.04	76.61	14.47	6.50	1.46
T6	East	offshore	9	-0.51	0.02	66.86	11.90	5.97	0.66
T6	East	slope	6	-0.81	0.03	359.60	73.16	3.69	0.46

## 5.2.4 Discussion

Differences in size structure and biovolume of meso-zooplankton communities in the upper-slope and offshore waters of the GAB are explained by regional differences in physical oceanography (chapter 3.2), nutrient supply and primary production (chapter 4.2). In offshore waters the mean size and biovolume of meso-zooplankton communities is similar. While at slope stations in the east meso-zooplankton communities are smaller and display higher biovolume than communities in the central GAB. In support of our hypothesis, we report that the size structure and biovolume of meso-zooplankton communities at E-US are representative of a more efficient ecosystem (steeper slopes)

than C-Us, C-Off and E-Off ecosystems (flatter slopes). A result that was contrary to expectation was that meso-zooplankton communities at E-Us displayed smaller mean size, which was explained by the relatively recent primary productivity (< 22 days prior) (Chapter 3.1).

A redundancy analysis supports this finding, where the environmental variable that explains the greatest proportion of variation in community size structure is fluorescence and sites group with similar size spectra and high fluorescence. Comparable studies in shelf and offshore waters of Norway observed similar trends in meso-zooplankton communities (Zhou et al., 2009). Waters with elevated primary productivity generated steeper slope metrics, which were explained by a greater abundance of smaller size classes identified as herbivorous zooplankton. Flatter slopes were observed in regions of low production (Zhou et al., 2009). In other regions, size spectra analyses of meso-zooplankton communities associated with differences in regional primary productivity are consistent with the findings of this study, where NBSS slopes steepen and biovolume increases in regions of higher primary production (Rissik et al., 1997; Herman and Harvey, 2006; Suthers et al., 2006; Zhou et al., 2009; Marcolin et al., 2013; Vandromme et al., 2014; Dai et al., 2016).

Results from depth-integrated environmental, net and LOPC observations indicate that subsurface production influences meso-zooplankton communities in C-Us and offshore waters of the GAB. At offshore stations, subsurface chlorophyll maximum layers were observed at ~70 m; peak meso-zooplankton abundance was also observed around this depth. While chlorophyll *a* is not a direct measure of phytoplankton biomass, Chapter 4.2 of this report noted that the deep chlorophyll maximum accounts for the greatest proportion of primary production in the photic zone of offshore waters of the GAB. These findings are consistent with other locations, e.g., in the South Indian Central Water mass, where up to 70% of net water column production was found to occur at the deep chlorophyll maximum (Hanson et al., 2007). The co-occurrence of chlorophyll *a*, phytoplankton biomass and meso-zooplankton biovolume suggests that subsurface primary production makes notable contributions to secondary production and ecosystem productivity in offshore waters of the GAB.

Vertical structure of meso-zooplankton profiles from LOPC at E-Us and C-Us stations are challenging to interpret. Fluorescence profiles at E-Us stations depict elevated chlorophyll concentrations, over the greatest depth range out of all stations, yet LOPC profiles indicate that there is a relatively low abundance of meso-zooplankton at deep chlorophyll maximums. There are several possible explanations of this trend: i) that recent upwelling disturbed meso-zooplankton communities are characteristic of stable waters, and insufficient time had elapsed for them to recolonise these waters, which would take several weeks to months (Colebrook, 1979; Thomas and Nielsen, 1994); ii) that grazing by higher trophic levels exert top-down control of meso-zooplankton communities at depth in the E-Us (Casini et al., 2008); or iii) that observations are subject to sampling bias due to the spatial patchiness of meso-zooplankton communities and limited replication. The first explanation is most likely, as discussed in Chapter 3.1, because the summer upwelling season had only been active less than a month prior to the voyage (~22 days), thus sampled water had been recently advected into the photic zone of the continental slope. The vertical structure of meso-zooplankton communities at C-Us stations are distributed relatively evenly between 50-100 m with a minor peak in abundance at 90 m, consistent with chlorophyll concentrations. The lack of a pronounced deep chlorophyll maximum is most likely explained by recent offshore hydrographic flow, which resulted in a deeper than usual mixed layer and thus deeper chlorophyll maximum (Chapter 3.2).

Depth stratified net sampling resolved that the biovolume of meso-zooplankton was highest in surface samples (0-100 m) of the E-Us and C-Off stations. Results that were consistent with observations from surface net samples and LOPC profiles. At C-Us stations, the biovolume of

communities were relatively low and evenly distributed vertically, results consistent with LOPC and chlorophyll concentrations. At E-Off stations biovolume was variable in 0-100 m samples, but lower than at C-Off stations, a result that conflicted with LOPC profiles. This may be an artefact of sampling, explained by the patchy distribution of zooplankton and that net sampling is subject to larger biases due to its larger surface area and large volume filtered. Finally, copepod abundance was plotted to look at the extent to which numerically-dominant genera undergo diel vertical migration, and there is evidence of weak diel vertical migration in the central GAB communities.

To summarise, we found that meso-zooplankton communities showed spatial differences in their size structure and biovolume that was explained by differences in regional chlorophyll concentrations. Consistent with our hypothesis, we observed greater biovolume of zooplankton in regions of elevated chlorophyll. In offshore waters, primary productivity was low and particulate biovolume peaked at similar depths to the deep chlorophyll maximum, indicating the importance of sub-surface productivity to pelagic ecosystem productivity in offshore waters.

In contrast to our hypothesis, we observed smaller mean size and greater biovolume of smaller size classes in regions of elevated productivity, which was explained by the relatively recent upwelling activity (~ 22 days prior).

## References

- ABRES, 2016. Australia : Fishery status reports released, MENA Report. Albawaba (London) Ltd., London.
- Blanchard, J.L., Heneghan, R.F., Everett, J.D., Trebilco, R., Richardson, A.J., 2017. From Bacteria to Whales: Using Functional Size Spectra to Model Marine Ecosystems. *Trends in Ecology and Evolution*, 32: 174-186.
- Cao, Y., Larsen, D.P., Thorne, R.S.-J., 2001. Rare species in multivariate analysis for bioassessment: some considerations. *Journal of the North American Benthological Society*, 20: 144-153.
- Casini, M., Lövgren, J., Hjelm, J., Cardinale, M., Molinero, J.-C., Kornilovs, G., 2008. Multi-level trophic cascades in a heavily exploited open marine ecosystem. *Proceedings of the Royal Society B: Biological Sciences*, 275: 1793.
- Cirano, M., Middleton, J.F., 2004. Aspects of the Mean Wintertime Circulation along Australia's Southern Shelves: Numerical Studies. *Journal of Physical Oceanography*, 34: 668-684.
- Colebrook, J.M., 1979. Continuous Plankton Records: Seasonal cycles of phytoplankton and copepods in the North Atlantic ocean and the North Sea. *Marine Biology*, 51: 23-32.
- Cullen, J.J., 1982. The Deep Chlorophyll Maximum: Comparing Vertical Profiles of Chlorophyll a. *Canadian Journal of Fisheries and Aquatic Sciences*, 39: 791-803.
- Cullen, J.J., 2015. Subsurface chlorophyll maximum layers: enduring enigma or mystery solved? *Annual Review of Marine Science*, 7: 207-239.
- Dai, L., Li, C., Yang, G., Sun, X., 2016. Zooplankton abundance, biovolume and size spectra at western boundary currents in the subtropical North Pacific during winter 2012. *Journal of Marine Systems*, 155: 73-83.
- Gorsky, G., Ohman, M.D., Picheral, M., Gasparini, S., Stemmann, L., Romagnan, J.-B., Cawood, A., Pesant, S., García-Comas, C., Prejger, F., 2010. Digital zooplankton image analysis using the ZooScan integrated system. *Journal of Plankton Research*, 32: 285-303.
- Grosjean, P., Picheral, M., Warembourg, C., Gorsky, G., 2004. Enumeration, measurement, and identification of net zooplankton samples using the ZOOSCAN digital imaging system. *Ices Journal of Marine Science*, 61: 518-525.
- Hanson, C.E., Pesant, S., Waite, A.M., Pattiaratchi, C.B., 2007. Assessing the magnitude and significance of deep chlorophyll maxima of the coastal eastern Indian Ocean. *Deep Sea Research Part II: Topical Studies in Oceanography*, 54: 884-901.
- Herman, A.W., Beanlands, B., Phillips, E.F., 2004. The next generation of Optical Plankton Counter: the Laser-OPC. *Journal of Plankton Research*, 26: 1135-1145.
- Herman, A.W., Harvey, M., 2006. Application of normalized biomass size spectra to laser optical plankton counter net intercomparisons of zooplankton distributions. *Journal of Geophysical Research: Oceans*, 111: C05S05.
- Jitts, H.R., 1969. Seasonal variations in the Indian Ocean along 110°E. IV. Primary production. *Marine and Freshwater Research*, 20: 65-76.
- Kämpf, J., 2010. On preconditioning of coastal upwelling in the eastern Great Australian Bight. *Journal of Geophysical Research: Oceans*, 115: C12071.
- Kämpf, J., Doubell, M., Griffin, D., Matthews, R.L., Ward, T.M., 2004. Evidence of a large seasonal coastal upwelling system along the southern shelf of Australia. *Geophysical Research Letters*, 31 L09310.
- Kemp, A.E.S., Villareal, T.A., 2013. High diatom production and export in stratified waters – A potential negative feedback to global warming. *Progress in Oceanography*, 119: 4-23.

- Legendre, P., Gallagher, E.D., 2001. Ecologically meaningful transformations for ordination of species data. *Oecologia*, 129: 271-280.
- Legendre, P., Oksanen, J., ter Braak, C.J.F., 2011. Testing the significance of canonical axes in redundancy analysis. *Methods in Ecology and Evolution*, 2: 269-277.
- Longhurst, A., 1995. Seasonal cycles of pelagic production and consumption. *Progress in Oceanography*, 36: 77-167.
- Marcolin, C.d.R., Schultes, S., Jackson, G.A., Lopes, R.M., 2013. Plankton and seston size spectra estimated by the LOPC and ZooScan in the Abrolhos Bank ecosystem (SE Atlantic). *Continental Shelf Research*, 70: 74-87.
- Middleton, J.F., Platov, G., 2003. The Mean Summertime Circulation along Australia's Southern Shelves: A Numerical Study. *Journal of Physical Oceanography*, 33: 2270-2287.
- Mignot, A., Claustre, H., Uitz, J., Poteau, A., D'Ortenzio, F., Xing, X., 2014. Understanding the seasonal dynamics of phytoplankton biomass and the deep chlorophyll maximum in oligotrophic environments: A Bio-Argo float investigation. *Global Biogeochemical Cycles*, 28: 856-876.
- Moore, C.M., Mills, M.M., Arrigo, K.R., Berman-Frank, I., Bopp, L., Boyd, P.W., Galbraith, E.D., Geider, R.J., Guieu, C., Jaccard, S.L., Jickells, T.D., La Roche, J., Lenton, T.M., Mahowald, N.M., Maranon, E., Marinov, I., Moore, J.K., Nakatsuka, T., Oschlies, A., Saito, M.A., Thingstad, T.F., Tsuda, A., Ulloa, O., 2013. Processes and patterns of oceanic nutrient limitation. *Nature Geoscience*, 6: 701-710.
- Motoda, S., Kawamura, T., Taniguchi, A., 1978. Differences in productivities between the Great Australian Bight and the Gulf of Carpentaria, Australia, in summer. *Marine Biology*, 46, 93-99.
- PIRSA Fisheries and Aquaculture, 2015. Status of South Australian fisheries report: fisheries snapshot for 2012–13. South Australian Fisheries Management Series paper 69, Primary Industries and Regions South Australia (PIRSA), Adelaide, South Australia, pp 137.
- R, 2013. R: A language and environment for statistical computing. R Foundation for Statistical Computing, Vienna, Austria.
- Rissik, D., Suthers, I.M., Taggart, C.T., 1997. Enhanced zooplankton abundance in the lee of an isolated reef in the south Coral Sea: the role of flow disturbance. *Journal of Plankton Research*, 19: 1347-1368.
- Rogers, P.J., 2013. Physical processes, biodiversity and ecology of the Great Australian Bight region : a literature review / Paul Rogers, Tim Ward, Paul van Ruth, Alan Williams ; contributing authors, Barry Bruce, Sean Connell, David Currie, Campbell Davies, Karen Evans, Bronwyn Gillanders, Simon Goldsworthy, David Griffin, Nick Hardman-Mountford, Alex Ivey, Rudy Kloser, John Middleton, Anthony Richardson, Andrew Ross, Jason Tanner and Jock Young. CSIRO, [Hobart, Tasmania].
- Sheldon, R.W., Prakash, A., Sutcliffe, W.H., 1972. THE SIZE DISTRIBUTION OF PARTICLES IN THE OCEAN1. *Limnology and Oceanography*, 17: 327-340.
- Signorini, S.R., Franz, B.A., McClain, C.R., 2015. Chlorophyll variability in the oligotrophic gyres: mechanisms, seasonality and trends. *Frontiers in Marine Science*, 2: 1-11.
- Suthers, I.M., Taggart, C.T., Rissik, D., Baird, M.E., 2006. Day and night ichthyoplankton assemblages and zooplankton biomass size spectrum in a deep ocean island wake. *Marine Ecology Progress Series*, 322: 225-238.
- Thomas, K., Nielsen, T.G., 1994. Regulation of zooplankton biomass and production in a temperate, coastal ecosystem. 1. Copepods. *Limnology and Oceanography*, 39: 493-507.
- Treusch, A.H., Vergin, K.L., Finlay, L.A., Donatz, M.G., Burton, R.M., Carlson, C.A., Giovannoni, S.J., 2009. Seasonality and vertical structure of microbial communities in an ocean gyre. *ISME Journal*, 3: 1148-1163.

- Uitz, J., Claustre, H., Gentili, B., Stramski, D., 2010. Phytoplankton class-specific primary production in the world's oceans: Seasonal and interannual variability from satellite observations. *Global Biogeochemical Cycles*, 24: GB3016.
- van Ruth, P.D., Ganf, G.G., Ward, T.M., 2010. Hot-spots of primary productivity: An Alternative interpretation to Conventional upwelling models. *Estuarine, Coastal and Shelf Science*, 90: 142-158.
- Van Ruth, P.D., Ward, T.M., 2009. Meso-Zooplankton Abundance, Distribution and Community Composition in the Eastern Great Australian Bight. *Transactions of the Royal Society of South Australia*, 133: 274-283.
- Vandromme, P., Nogueira, E., Huret, M., Lopez-Urrutia, Á., González-Nuevo González, G., Sourisseau, M., Petitgas, P., 2014. Springtime zooplankton size structure over the continental shelf of the Bay of Biscay. *Ocean Science*, 10: 821-835.
- Vandromme, P., Stemmann, L., García-Comas, C., Berline, L., Sun, X., Gorsky, G., 2012. Assessing biases in computing size spectra of automatically classified zooplankton from imaging systems: A case study with the ZooScan integrated system. *Methods in Oceanography*, 1: 3-21.
- Ward, T.M., McLeay, L.J., Dimmlich, W.F., Rogers, P.J., McClatchie, S.A.M., Matthews, R., Kämpf, J., Van Ruth, P.D., 2006. Pelagic ecology of a northern boundary current system: effects of upwelling on the production and distribution of sardine (*Sardinops sagax*), anchovy (*Engraulis australis*) and southern bluefin tuna (*Thunnus maccoyii*) in the Great Australian Bight. *Fisheries Oceanography*, 15: 191-207.
- Zhou, M., Tande, K.S., Zhu, Y., Basedow, S., 2009. Productivity, trophic levels and size spectra of zooplankton in northern Norwegian shelf regions. *Deep Sea Research Part II: Topical Studies in Oceanography*, 56: 1934-1944.

### 5.3 Gelatinous zooplankton

Lisa Gershwin, Rudy Kloser and Caroline Sutton

#### 5.3.1 Introduction

While plankton in general are poorly known compared to economically or socially important species, perhaps the most poorly studied of all groups is the gelatinous zooplankton (i.e., medusae, siphonophores, ctenophores, and pelagic tunicates (salps and their kin): “jellyfish” or “jellies”). Zooplankton and micronekton were highlighted in the review of the GAB (Rogers et al., 2013), and we focus on the gelatinous components that make up those size classes and demonstrate their significance in understanding ecosystem structure and function and their importance in monitoring ecosystem change.

The primary objectives of the GAB project (Section 2.2) include describing the community structure, testing the hypothesis of the microbial food web, and comparing the eastern and central GAB ecosystems. However, we have been limited by the lack of resolution on gelatinous groups in assessing these objectives. In the present study, gelatinous biota comprised 48% of the total micronekton catch, and in some areas, e.g. central GAB offshore, they were as high as 74% (Section 6.1.3, page 185). These large fractions of gelatinous biota are similar to those elsewhere. For example, off California, gelatinous biomass may be as high as 70% of the total (Bruce Robison, MBARI, pers. comm. 2014), while in the Arabian Sea, gelatinous fauna comprised up to 74% of the total catch (Gjøsaeter, 1984). In southern Australia, previous studies have also found that gelatinous biota dominate net catches. For example, Williams and Koslow (1997) found that gelatinous zooplankton off southern Tasmania comprised 60% of their net samples, while Young et al. (1996) found that the dry weight of this fraction off eastern Tasmania exceeded 50%. A metadata analysis of these and other studies found that the gelatinous zooplankton of southeastern Australia comprised 56-86% of the total biomass (CSIRO, unpublished data). We assert that not understanding up to 86% of the biomass is a critical gap limiting our understanding of the whole ecosystem.

#### *Background on GAB gelatinous zooplankton studies*

Only scant knowledge exists of gelatinous zooplankton in the GAB. Despite their importance in marine ecosystems, gelatinous taxa represent challenges for observation science in quantifying their ecology, biomass, diversity and changes over time due to their patchy nature and fragile form (Hamner et al., 1975; Haddock, 2004). As we are coming to appreciate their ecological role, robust trend analyses are impaired by poor historical temporal-spatial sampling (Hamilton, 2016).

Gelatinous collections from the GAB are few. The Baudin Expedition (1800-1803) found several species of medusae new to science (Péron and Lesueur, 1810). Several later expeditions have recorded a small number of gelatinous taxa in GAB waters. The Challenger Expedition stopped in Melbourne and sampled briefly on its way to Sydney (Haeckel, 1881, 1888). Margulis (1979) reported the distribution of 23 species of siphonophores in the eastern GAB. Later, Gaughan and Fletcher (1997) studied the carnivorous zooplankton in the western GAB, but were unable to identify most of the species they found, finally reporting only one medusa species and 10 species of siphonophores; no salps or ctenophores were reported.

More recently, Gershwin and Zeidler (2003) sampled the medusae, siphonophores, and ctenophores of the Nuyts Archipelago, reporting 17 species of hydromedusae (including 8 new to science), one species of siphonophore (which was later described as new to science), one species of scyphomedusa, and two species of ctenophores (one of which was new to science).



Other relevant collections include opportunistic new species and new records of medusae from around Adelaide (Kramp, 1965a; Gershwin and Zeidler, 2008a), and a nearby survey of midwater medusae of Bass Strait (Blackburn, 1955). Salps were reported by Thompson (1948), but have been virtually ignored since. Most species have not been studied past the original reports.

## General gelatinous zooplankton ecology

Until recently, ecologists studying plankton thought in terms of a linear trophic structure often conceptualised as a food chain (Sheldon et al., 1977). In particular, diatoms as primary producers are grazed by herbivores such as copepods and larvae; these herbivores, in turn, are consumed by small fish, which are eaten by larger fish, and so on, up the food chain to apex predators like sharks, whales, and humans. This is now typically conceptualised as a food web rather than a chain, with trophic linkages far more complex than originally imagined (Andersson et al., 2017).

Parsons and Lalli (2002) detailed an alternative to the classic food chain, whereby two trophic structures co-exist. In their view, the classic high energy or diatom-based food chain supports high energy visual predators, primarily vertebrates. The low energy or flagellate-based food chain, in contrast, comprises smaller phytoplankton, which are consumed by smaller grazers, supporting low-energy tactile predators, primarily jellyfish. These two trophic structures can operate side by side, with little obligate overlap (Scheffer et al., 2001). In recent years, research has focused on this latter structure, often referred to as the “microbial web” (see section 4 and references therein). An often overlooked component of the microbial web is the dual role that jellyfish play as both input and output effectors.

Firstly, jellyfish can operate distinct from, or overlapping with, both the classic food chain and the microbial web, conceptualised by Robison (2004) as a “jelly web” (

Figure 5.3-). The dual role of jellyfish as low trophic level members in high energy food webs and high trophic level members in low energy food webs offers them opportunistic flexibility to either persist or expand (Gershwin, 2013).

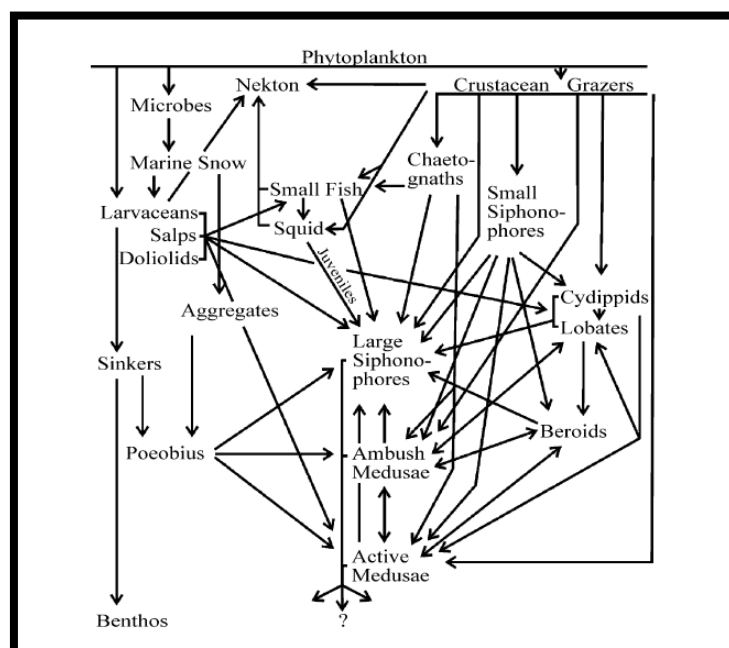


Figure 5.3-1 Diagram of the “Jelly Web”, a low-energy food web that is hypothesized to exist in tandem with the traditional high-energy food web. Illustration by Robison, B.H. (2004), *Deep pelagic biology. J. Exp. Mar. Biol. Ecol.* 300: 260.

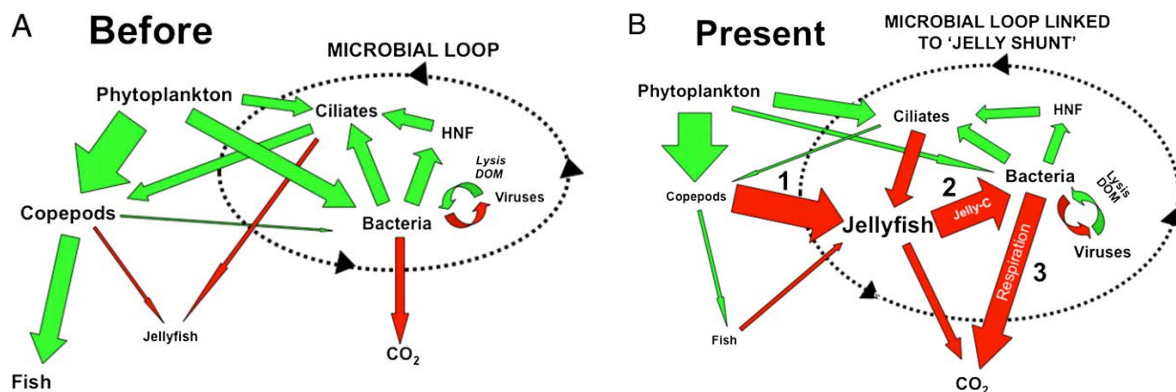


Figure 5.3-2 Diagram of the “Jelly Shunt”, wherein carbon is diverted from food production to carbon dioxide production via jellyfish blooms and microbes. A. The high energy food web. B. The low energy food web. Illustration modified from Condon et al. (2011), "Jellyfish blooms result in a major microbial respiratory sink of carbon in marine systems." *Proc. Nat. Acad. Sciences* **108**(25): 10225–10230.

Secondly, the chemistry of jellyfish mucus and excreta (dissolved organic matter, or DOM) can alter the microbial community. As elucidated by Condon et al. (2011), jellyfish waste (either as DOM or mucus) is particularly rich in a type of carbon that favours CO<sub>2</sub>-producing bacteria over edible bacteria (Figure 5.3-). Through jellyfish, carbon is shunted away from the food chain and contributes to a microbial community more favourable to a low energy regime.

Gelatinous zooplankton populations naturally fluctuate on numerous temporal and spatial scales. However, some blooms around the world persist beyond normal seasonal and geographical boundaries (Mills, 1995, 2001), entering a positive feedback loop whereby increased numbers of jellyfish exert heavy predation pressure on fish eggs and larvae, resulting in fewer predators and competitors (Purcell & Arai, 2001; Richardson et al., 2009). Semi-enclosed systems seem particularly vulnerable to these changes (Purcell et al., 2001); however, of notable interest to the GAB, the open Benguela Current system off Namibia has become dominated by two species of jellyfish, with no signs of reversal (Flynn et al., 2012; Roux et al., 2013).

Recent ecosystem modeling has suggested that these runaway blooms can be caused by any of multiple disturbances (CSIRO, unpublished data). Specifically, any perturbation that enhances jellyfish populations or negatively impacts predator and competitor populations has the capacity to trigger or exacerbate a feedback loop. These perturbations include jellyfish-enhancing processes like warming water or creation of new substrate through trawling or coastal construction, and predator/competitor-impacting processes like overfishing, eutrophication, pollution, warming water, ocean acidification, or species translocations. In combination, these processes can be particularly transformative to local ecosystems (Gershwin, 2013).

#### *Purpose of this study*

Gelatinous zooplankton offer a unique opportunity for early detection of ecosystem changes. With their rapid growth rates, short life cycles, and large body and population sizes, it is often difficult to overlook these species, making them ideal as monitoring subjects. However, gelatinous invertebrates are poorly known, particularly in the GAB.

The purpose of this study was to provide a baseline understanding of the gelatinous biodiversity of the GAB. Knowing the fauna (and flora) of a region is fundamental to understanding ecological relationships and assessing change.

### 5.3.2 Methods

To establish a baseline biodiversity understanding of the gelatinous invertebrates of the GAB, a list of all known jellyfish species in the region was compiled from available data (Table 5.3-3), including peer-reviewed studies, online databases, museum and voucher specimens, and new sampling.

Newly collected gelatinous specimens in the central and eastern GAB were sampled with nets (Figure 5.3- and see Chapter 6.1) and optically with the Profiling Lagrangian Acoustic Optical System (PLAOS) (Figure 5.3-4, Figure 5.3-5, and see Chapter 6.4).

Preliminary identifications were made in the field where possible, based on field guides developed for this purpose (Gershwin et al. 2013a-d). Identifications were subsequently confirmed under a dissecting microscope and identified to the lowest practical taxonomic level.

### 5.3.3 Results

We found 17 new records of jellyfish in our sampling, along with many other species previously documented. These 17 new records bring the total to 139 gelatinous zooplankton species now known from the GAB (and Bass Strait, assumed to be fed from the GAB), comprising 12 scyphomedusae, 2 cubomedusae, 53 hydromedusae, 39 siphonophores, 7 ctenophores, and 26 pelagic tunicates (see Table 5.3-3). These span 8 classes in three phyla.

Within these findings are at least two species that are new to science, at least three species newly reported in the Southern Hemisphere, at least three species newly reported in Australian waters, and at least nine species newly added to the GAB fauna (Table 5.3-1).

*Table 5.3-1 Alphabetical list of significant new records of gelatinous zooplankton species found by the R/V Investigator in the Dec 2015 GAB Survey.*

Atolla vanhoeffeni	Mesopelagic, cosmopolitan	*New GAB Record Herein
Beroe cf abyssicola	Mesopelagic; Oceanic	*New Record S. Hemisphere
Calyropsis n. sp.	Mesopelagic, East & Central GAB	*New Species Herein
Crossota pedunculata	Epibenthic; Central GAB	*New Record S. Hemisphere
Dendrogramma enigmatica	Benthic; Eastern & Central GAB; endemic	O'Hara et al., 2016; *New GAB Record on this Voyage
Enneagonum hyalinum	Mesopelagic; Central GAB	*New GAB Record Herein
?Halistemma n. sp.	Mesopelagic	*New Species Herein
Maresearsia praeclara	Mesopelagic; Central GAB	*New Australian Record Herein
Nanomia sp.	Mesopelagic	*New GAB Record Herein
Nectadamas diomedaeae	Mesopelagic; Central GAB	*New Australian Record Herein
Periphylla periphylla	Mesopelagic, cosmopolitan	*New GAB Record Herein
Physophora gilmeri	Mesopelagic; Central GAB	*New Record S. Hemisphere
Poralia rufescens	Mesopelagic, cosmopolitan	*New Australian Record Herein
Pyrosoma spinosum	Epipelagic, cosmopolitan	*New GAB Record Herein

Rosacea plicata	Mesopelagic	*New GAB Record Herein
Soestia zonaria	Bass Strait; East & Central GAB	*New GAB Record Herein
Thalia democratica	Bass Strait; Eastern GAB	*New GAB Record Herein

### 5.3.4 Discussion

Gelatinous zooplankton (“jellyfish”) of the GAB are among the least-studied of all groups. This gap in gelatinous knowledge is pervasive, from primary knowledge like taxonomy to secondary and tertiary knowledge of their biology, ecology, complex interactions, and value as ecological indicators. What little we do know about gelatinous species as a whole, suggests that they can disrupt ecosystems through heavy predation and competition. Although often overlooked, the dual roles of jellies as low trophic level members in high energy food webs and high trophic level members in low energy food webs make them important to include in ecosystem studies.

This is the first biodiversity review of gelatinous zooplankton of the GAB. Our studies add 17 new records to the GAB fauna, thus increasing the number of GAB jellyfish species considerably: there are now 139 known species in eight classes in three phyla. Within these findings are at least two species that are new to science, at least three species newly reported in the Southern Hemisphere, at least three species newly reported in Australian waters, and at least nine more species newly added to the GAB fauna. Here we discuss some unique aspects of jellyfish ecology that provide compelling bases for further study, as well as sampling challenges to consider.

There is a need to further enhance our understanding of the ecological role of gelatinous zooplankton. In particular, investigations into their function in the carbon cycle and ecosystem dynamics are only just beginning to be studied overseas, and remain largely unstudied in Australia. We envisage that the field guides developed in this study will help with identification so that jellyfish can more readily be incorporated into local studies (Gershwin et al. 2013a-d). We further anticipate that additional volumes produced by this study for other pelagic invertebrate groups will similarly facilitate their identification for finer-scale inclusion in future work (Gershwin et al. 2017a-d).

Three implications of jellyfish that were not possible to investigate within the limitations of this study are discussed below: their role as visible indicators of change, the role they play in ecosystem phase shifts, and the intriguing concept of pelagic endemism.

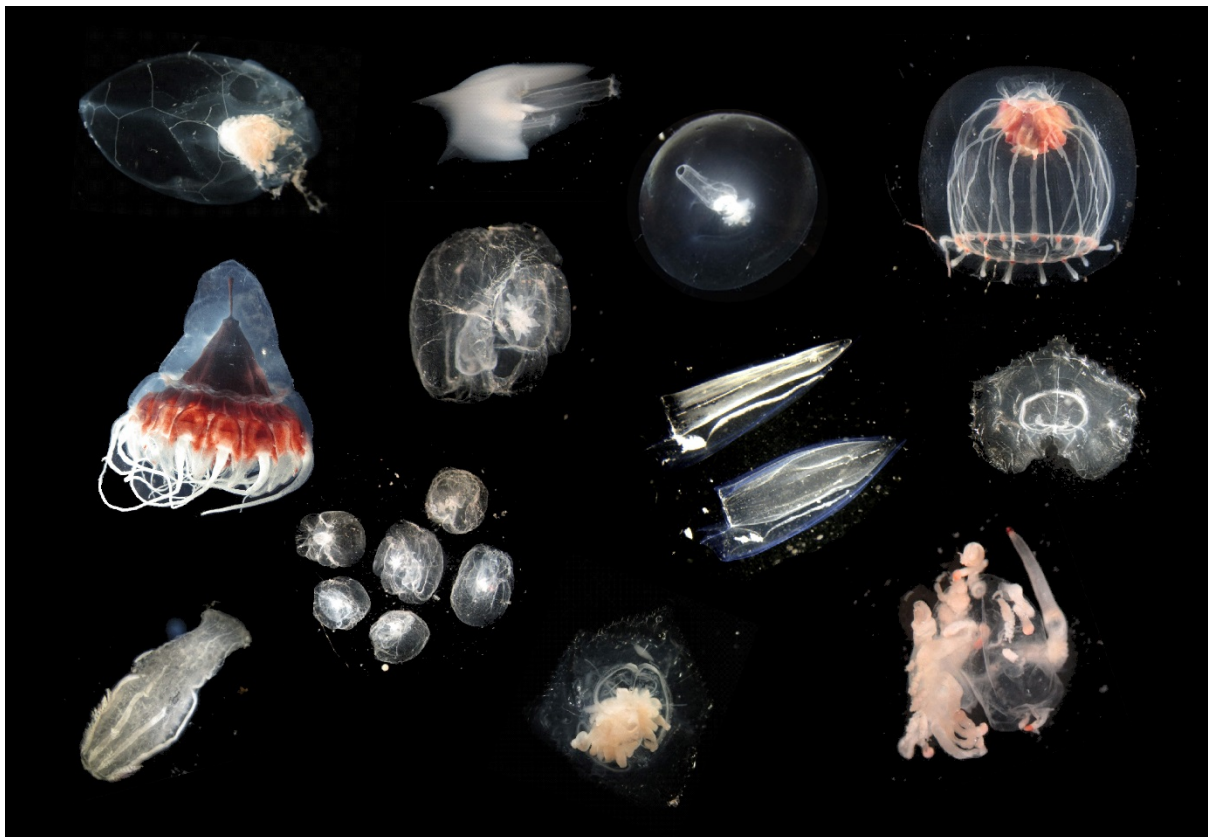
#### *Highly visible early indicators of ecosystem change*

Although often ignored in favour of more familiar species like fish and crustaceans (Purcell et al., 2001; Boero, 2013), jellyfish have proven to be a useful asset in ecosystem studies because of their unique highly-visible, quick-response nature (Boero, 2013). For example, large jellyfish species in Port Philip Bay appear to have undergone a shift in species dominance and population size, coinciding with long-term and probably irreversible changes to the benthic ecosystem and small pelagic fish populations (Fancett, 1986; Currie and Parry, 1999; Parry et al., 2009; Parry and Stokie, 2009; Hirst et al., 2010).

Many other examples exist around the world where large jellyfish species have undergone similar shifts, and often in an inverse relationship with small pelagics (Oguz et al., 2008; Quinones et al.,

2013; Roux et al., 2013; Brodeur et al., 2014; Greene et al., 2015; Schnedler-Meyer et al., 2016). In particular, carnivorous medusae and small pelagic fish are often each others' predators and competitors (Brodeur et al., 2011). In healthy waters fish may have the advantage because their vision makes them superior predators; however, in compromised visibility or where fish populations are reduced, medusae may reproduce and grow faster, giving them the competitive advantage.

While typically only large, visible jellyfish blooms are studied, smaller species may offer greater insight. Globally, about 90% of known medusa species are less than 2 cm in diameter. The only longitudinal study of small hydromedusae monitored this fauna in Chinese waters for 20 years (Sun et al., 2012). Over the study period, the biomass increased five-fold and there was a complete shift in species dominance. These changes were attributed to eutrophication, seawater warming, and salinity decrease, as well as aquaculture and coastal construction activities around the bay.





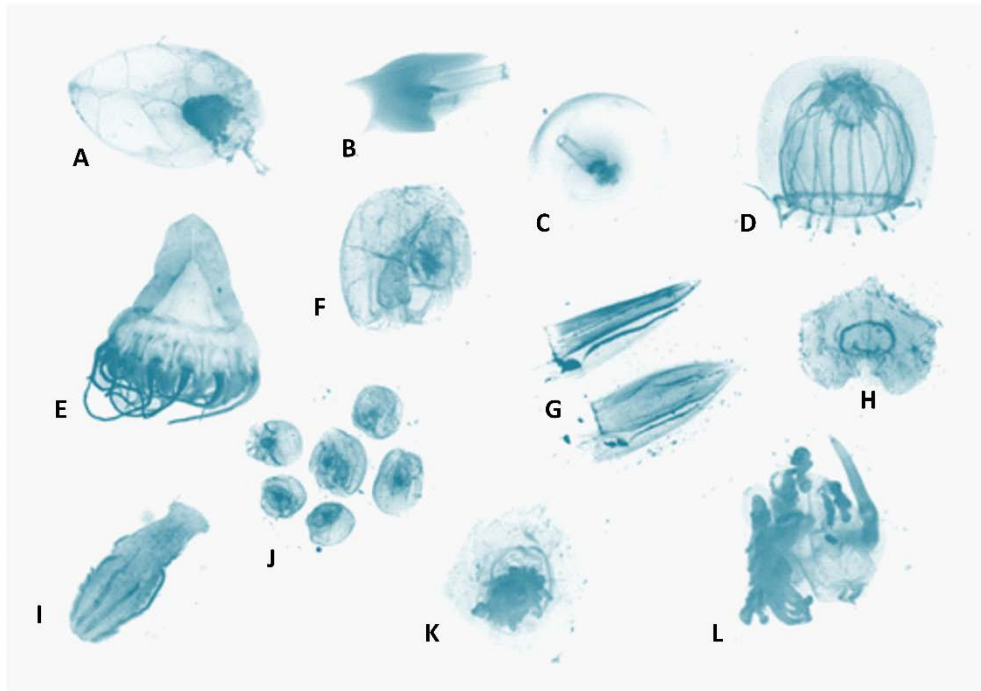


Figure 5.3-3 Jellyfish specimens collected from net samples in the GAB. A. *Nectadamas diomedea* (new record for Australia). B. *Ceratocymba*. C. *Maresearsia praeclara* (new record for Australia). D. *Calycopsis* (new species). E. *Periphylla*. F. *Amphicaryon*. G. *Chelophyes*. H. *Vogtia*. I. *Beroe cf abyssicola* (new record for Australia). J. *Amphicaryon*. K. *Vogtia*. L. *Physophora gilmeri* (new record for southern hemisphere).



Figure 5.3-4 Siphonophores in the GAB, taken by PLAOS. Left, *Nanomia* sp. (new GAB record). Top, *Praya* sp.. Centre, *Halistemma* sp. (new species). Right, *Nanomia* sp. (new GAB record).



Figure 5.3-5 Jellyfish in the GAB, taken by PLAOS. Clockwise from top left, *Praya* sp., *Hippopodius hippopus*, *Ocyropsis* sp. (new GAB record), *Hippopodius hippopus*. Centre, *Solmissus* sp.

#### Community dynamics and phase shifts

Jellyfish are often patchy temporally and spatially, confounding efforts to observe or understand their population changes. Moreover, these population fluctuations often appear to come and go with very little effect on other biota. Even when large populations of jellies persist, they may do so with little apparent effect on the system overall. Then abruptly, the ecosystem collapses, with jellyfish becoming the apex predator (Mills, 1995, 2001).

Phase shift dynamics are fairly well studied for some other groups, but are poorly studied in jellyfish (Figure 5.3-6). Speculatively, high and low energy trophic systems may exist in tandem as alternative stable states, until some trigger perpetuates a switch; this may include removal of competitors by overfishing of small pelagics, provision of new polyp settling space via coastal construction or extensive trawling, ecosystem disruption through invasion of exotic species, radical alteration through eutrophication, or a prolonged season of favourable climatic conditions. Regardless of the nature of the stimulus, it seems that when alternative stable states are present, the activation potential for a shift may be much lower than if a healthy state were dominant (Scheffer et al., 2001; Fauchald, 2010).



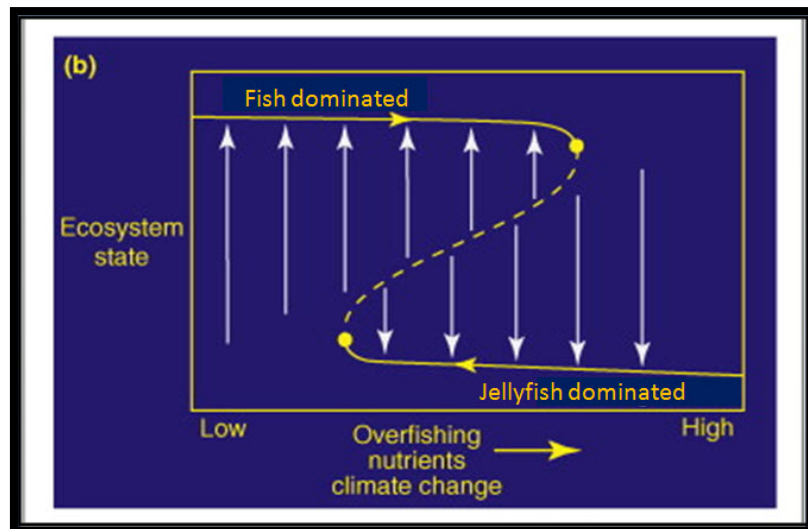


Figure 5.3-6 Diagrammatical representation of phase shifts or alternative stable states. Figure modified from Hughes et al. 2010. Rising to the challenge of sustaining coral reef resilience. *TREE* 25(11): 634.

One GAB species of particular concern is the lobate ctenophore *Bolinopsis*, closely related to *Mnemiopsis*, the comb jellyfish that collapsed the Black Sea ecosystem in the 1990s (Zaitsev and Mamaev, 1997). After being introduced from the US in ballast water, *Mnemiopsis* multiplied out of control. Within a few years, its population was estimated to comprise 95% of the Black Sea biomass (Travis, 1993). *Mnemiopsis* has since spread to the seas in Europe (Gershwin, 2013). In fact, *Bolinopsis* is a superior predator and competitor to *Mnemiopsis*, lives longer, and reproduces faster (Kasuya et al., 1994; Hiromi et al., 2005; Lučić et al., 2012; Båmstedt and Martinussen, 2015). The population density of *Bolinopsis* in Spencer Gulf has been repeatedly observed to be “off the scale”, “blanketing”, and “cheek-by-jowl” (Gershwin, unpublished notes). Both the effect on the Spencer Gulf ecosystem and the potential as a source for a greater Bight invasion remain unstudied. This GAB species is unidentified.

### CASE STUDY: Siphonophores

We highlight here an enigmatic but severely understudied group that is coming to light as a dominant predator in oceanic ecosystems. Long debated as evolutionary marvels – not quite a colony, not quite an individual – siphonophores are more recognised today for their taxonomic and trophic complexity (Figure 5.3-). Most notoriously embodied in the Portuguese Man-o-war or Blue Bottles, an array of form and function makes this group simultaneously challenging and compelling to study.

These colonial pelagic cnidarians were found in high abundance during the GAB Survey. Neuston (surface) nets collected large numbers of Blue Bottles (*Physalia utriculus*), while tethered cameras and videos recorded large abundance and diversity in epipelagic and mesopelagic species, including some new to science.

In these sorts of numbers, there may be cause for concern. Each siphonophore colony contains dozens to hundreds of mouths, which can consume small prey singly or large prey cooperatively. To fish for prey, the colony sets a curtain of tentacles, each armed with thousands of stinging cells. In some species, these tentacle arrays may span 50 metres. In bloom conditions, these organisms may disrupt food web dynamics or even collapse trophic structures (Rogers et al., 1978).

Currently, about 180 siphonophore species are recognised globally, divided into three main groups: those with swimming bells and a float (Order Physonectae), those with only a float (Order Cystonectae), and those with only swimming bells (Order Calycophorae). Some 90-100% of the cystonect diet is comprised of fish larvae (Purcell, 1985), while others tend to prey most heavily on copepods and other small plankton (Greve, 1994; Pagès et al., 2001). In addition to their trophic impact, siphonophore blooms have also caused heavy losses for net fisheries and aquaculture through clogging and stinging, respectively (Rogers, 1976; Båmstedt et al., 1998).

Siphonophores may also offer us a unique opportunity to detect early changes in oceanic ecosystems. Like many other gelatinous invertebrates, siphonophores “bloom” as a natural part of their life cycle, as well as in response to favourable conditions. Numerous studies have shown a correlation between ecological change and increased siphonophore abundance (Brotz et al., 2012; Licandro et al., 2012; Lo et al., 2012; Luo et al., 2014).

Despite these important concerns and opportunities presented by siphonophores, they are almost completely unstudied in Australia. We can better understand them through technological advancements like the PLAOS (see Section 6.5) and the multi-methodological approach used during the GAB Survey.

### Pelagic endemism

The GAB ecosystem has long been recognised as unique and still holds great potential for meaningful discovery. Trapped between the two warm currents of the Indian and Pacific Oceans, some 85-90% of marine flora and fauna in this temperate Southern Ocean habitat are estimated to be endemic to the region (SARDI, 2008).

Prior to 2000, the total number of gelatinous zooplankton species reported in the GAB was 79, including three endemic species; this study now brings the total to 139, with 21 apparently endemic (see Table 5.3-3). This should be interpreted only as a preliminary assessment.

With the current jellyfish endemic index at 15%, it seems almost certain to increase significantly with further study. Many of the large and conspicuous forms previously thought to be identical to overseas forms (e.g., *Aurelia aurita*, *Cyanea capillata*, *Physalia physalis*), have proven to be unique regional species. Furthermore, many of the small species have likewise proven to be new to science and endemic. It is likely that a progressively higher percentage of small species will be found with targeted collecting effort, and many of these will be endemic to the GAB.

### 5.3.5 Sampling challenges and future research focus

Although our sampling was only preliminary, it added substantially to our understanding of the biodiversity of offshore gelatinous communities of the GAB. We anticipate that further sampling of gelatinous zooplankton will find many more new species and new records, thus enhancing our baseline knowledge that underpins all other types of study.

Micronekton and mesozooplankton are difficult to sample due to their small size, residency depths, and patchiness on numerous temporal and spatial scales. Gelatinous species are even more difficult. Below, we examine some of the challenges in sampling bias and practicalities associated with these species.

#### *Sampling bias and practical challenges*

Preliminary comparisons between conventional net sampling, acoustics, and still/video imagery have demonstrated a high level of bias associated with different sampling methodologies (see Table 5.3-2 and Section 6.4).

Net sampling, for example, favours “tougher” species that remain intact through mechanical damage in the net; many types of jellyfish are destroyed upon contact with the net, or degrade beyond recognition during sorting if not quickly removed from the remainder of the sample (Purcell et al., 2001; CSIRO, unpublished notes). The delicate nature of gelatinous species means that most rarely look like the photos often found in field guides: medusae lose their tentacles, soft bodies are fragmented, and other useful characters are abraded away during collection. Moreover, many gelatinous specimens do not preserve with standard techniques like alcohol or formalin, requiring custom-made (and sometimes carcinogenic) mixtures, or are limited to photo-documentation (Adams et al. 1976; Matsumoto, 1988). However, net sampling remains the preferred method for identification for those that lend themselves to this collection technique.

Acoustics only reveal those forms with an acoustic signature and in high enough population density to be “seen”; however, species identification is typically not possible. Still and video imagery offer a much more thorough sampling, particularly of delicate species; however, because specimens are not retained, identification to species is often not possible unless a suitably ideal photo occurs serendipitously.

These methodologies further complicate sampling efforts by altering the behaviour of certain species, such as those responding to the pressure wave of an approaching net, or those reacting to the lights associated with photography. It is apparent from these comparisons that no one method is universal, but rather, a combination of methods offers the greatest sampling efficacy.

## Zooplankton

Table 5.3-2 Table 2. Comparison of efficacy of sampling methodologies for midwater zooplankton.

	Net sampling	Acoustic sampling	Photos	Videos
Biomass	moderate	high	low	moderate
Species richness	moderate	very low	low	moderate
Species ID	high	very low	high	moderate
Selectivity	high	high	high	moderate

### Challenges

To better understand the gelatinous community and its dual role in the carbon cycle and ecosystem function, this requires quantitative sampling. The types of data required include:

- (1) Systematic sampling to define the coastal and oceanic gelatinous biodiversity of the GAB, with particular emphasis on endemic species, new species, new locality records, and general distribution within the GAB;
- (2) Ecosystem reference points and early warning criteria for assessing impacts, including the identification of key gelatinous indicator taxa, based on local species and conditions in the GAB;
- (3) Baseline population estimates for key indicator taxa;
- (4) Regular monitoring of gelatinous communities to detect population shifts and species turnover rates in large and small species;
- (5) Targeted study of siphonophores to better understand the role of these predators in community dynamics and their value as early warning indicators of ecosystem health.
- (6) Specimens designated for morphological identification preserved in dilute formalin (2-4%) to allow for proper identification.

Table 5.3-3 Gelatinous zooplankton species currently reported from oceanic and coastal waters of the Great Australian Bight (GAB). Other abbreviations: AFD (Australian Faunal Directory); sp. (species); n. sp. (new species); gen. et sp. nov. (new genus and species).

SPECIES	LOCALITY	REFERENCE
SCYPHOMEDUSAE		
Coronatae		
Atolla vanhoeffeni	Mesopelagic, cosmopolitan	*New GAB Record Herein
Atolla wyvillei	Mesopelagic, cosmopolitan	Gershwin & Zeidler, 2003; Herein
Nausithoe sp.	Nuyts Archipelago	Gershwin & Zeidler, 2003
Periphylla periphylla	Mesopelagic, cosmopolitan	*New GAB Record Herein
Rhizostomeae		
Cassiopea ndrosia	Coastal, introduced	Southcott, 1982
Pseudorhiza haeckelii	Coastal, type locality	Haacke, 1884
Semaeostomae		
Poralia rufescens	Mesopelagic	*New Australian Record Herein
Aurelia coerulea	Coastal	Kramp, 1965a (ID error)

<i>Chrysaora southcotti</i>	Coastal, endemic	Gershwin & Zeidler, 2008a
<i>Cyanea muellerianthe</i>	Coastal, endemic	Haacke, 1887
<i>Cyanea rosella</i>	Coastal, endemic	Gowlett-Holmes, 2008
<i>Desmonema scoresbyanna</i>	Coastal, endemic	Gershwin & Zeidler, 2008a
CUBOMEDUSAE		
<i>Carybdea rastonii</i>	Coastal, type locality	Haacke, 1886
<i>Copula sivickisi</i>	Coastal, ?introduced	Gershwin 2005: 114
HYDROMEDUSAE		
Trachymedusae		
<i>Aglantha elongata</i>	Bass Strait	Blackburn, 1955
<i>Aglaura hemistoma</i>	Bass Strait; Western shelf waters	Blackburn, 1955; Gaughan & Fletcher, 1997
<i>Aglaura</i> sp.	Nuyts Archipelago	Gershwin & Zeidler, 2003
<i>Colobonema sericeum</i>	Bass Strait	Blackburn, 1955
<i>Crossota pedunculata</i>	Epibenthic; Central GAB	*New Australian Record Herein
<i>Halicreas minimum</i>	Bass Strait	Blackburn, 1955
<i>Halitrephes valdiviae</i>	Bass Strait	Blackburn, 1955
<i>Liriope tetraphylla</i>	Oceanic	Gershwin & Zeidler unpublished
<i>Pantochogon haeckeli</i>	Bass Strait	Blackburn, 1955
<i>Persa incolorata</i>	Bass Strait	Blackburn, 1955
<i>Rhopalonema velatum</i>	Bass Strait	Blackburn, 1955
<i>Sminthea eurygaster</i>	Bass Strait	Blackburn, 1955
Narcomedusae		
<i>Aegina citrea</i>	Bass Strait	Blackburn, 1955
<i>Cunina octonaria</i>	Bass Strait	Blackburn, 1955
<i>Cunina rubiginosa</i>	Bass Strait	Blackburn, 1955
<i>Solmaris rhodoloma</i>	Bass Strait	Blackburn, 1955
<i>Solmaris</i> sp.	Nuyts Archipelago, Port Lincoln	Gershwin & Zeidler, 2003
<i>Solmissus marshalli</i>	Bass Strait	Blackburn, 1955
<i>Solmundella bitentaculata</i>	Bass Strait	Blackburn, 1955
Anthomedusae		
<i>Amphinema cheshirei</i>	Nuyts Archipelago; endemic	Gershwin & Zeidler, 2003
<i>Australomedusa baylii</i>	Inland salt lakes; endemic	Russell, 1970
<i>Bougainvillia</i> sp.	Coastal: Port Lincoln, Ceduna	Gershwin & Zeidler unpublished
<i>Calycopsis</i> n. sp.	Mesopelagic, East & Central GAB	*New Species Herein
<i>Cladonema timmsii</i>	Inland salt lake; endemic	Gershwin & Zeidler, 2008b
<i>Cladonema</i> sp.	Coastal: Cowell, Ceduna	Gershwin & Zeidler unpublished
<i>Ectopleura</i> sp.	Nuyts Archipelago, coastal	Gershwin & Zeidler, 2003
<i>Euphysa</i> sp.	Coastal: Robe	Gershwin & Zeidler unpublished
<i>Euphysa</i> n. sp.	Coastal: Port Lincoln; endemic	Gershwin & Zeidler unpublished
<i>Halitiara thierryi</i>	Nuyts Archipelago, coastal; endemic	Gershwin & Zeidler, 2003
<i>Heterotiara ausgeoana</i>	Nuyts Archipelago; endemic	Gershwin & Zeidler, 2003
<i>Hydractinia</i> sp.	Nuyts Archipelago	Gershwin & Zeidler, 2003
<i>Turritopsis lata</i>	Coastal: Ceduna	Gershwin & Zeidler unpublished
<i>Turritopsis rubra</i>	Coastal	Southcott, 1982 (ID error)
<i>Velella velella</i>	Bight-wide, Pleuston	Gershwin et al., 2010b; Herein

## Zooplankton

<i>Zanclea baudini</i>	Nuyts Archipelago; endemic	Gershwin & Zeidler, 2003
<i>Zanclea carinata</i>	Nuyts Archipelago; endemic	Gershwin & Zeidler, 2003
<i>Zanclea ngeriana</i>	Nuyts Archipelago; endemic	Gershwin & Zeidler, 2003
<i>Zanclea sardii</i>	Nuyts Archipelago; endemic	Gershwin & Zeidler, 2003
Leptomedusae		
<i>Aequorea</i> 1 (pink)	Nuyts Archipelago	Gershwin & Zeidler, 2003
<i>Aequorea</i> 2 (blue)	Nuyts Archipelago	Gershwin & Zeidler, 2003
<i>Aequorea eurodina</i>	Bass Strait	Péron & Lesueur, 1810
<i>Aequorea kurangai</i>	Coastal	Gershwin et al., 2010b
<i>Eirene menoni</i>	Coastal	Kramp, 1965b
<i>Laodicea</i> sp.	Nuyts Archipelago	Gershwin & Zeidler, 2003
<i>Obelia</i> sp.	Coastal: Port Lincoln	Gershwin & Zeidler unpublished
<i>Phialopsis diegensis</i>	Coastal	Kramp, 1965b
<i>Staurodiscus</i> n. sp.	Coastal; endemic	Gershwin & Zeidler unpublished
<i>Staurophora falklandica</i>	Coastal; introduced	Gershwin & Zeidler, 2003
Limnomedusae		
<i>Craspedacusta sowerbyi</i>	Freshwater	Thomas, 1950, 1951
<i>Gonionemus hamatus</i>	St Vincent Gulf; endemic	Kramp, 1965b
<i>Hexaphilia scoresbyi</i>	Nuyts Archipelago; endemic	Gershwin & Zeidler, 2003
<i>Olindias singularis</i>	Coastal	Kramp, 1965b
Fam. Olindiidae gen. et sp. nov.	Coastal: Robe; endemic	Gershwin & Zeidler unpublished
SIPHONOPHORES		
Cystonectae		
<i>Physalia utriculus</i>	Pleuston GAB-wide	Gershwin et al., 2010b; Herein
<i>Rhizophysa</i> sp.	Mesopelagic, Epipelagic	Gaughan & Fletcher, 1997
Physonectae		
<i>Dendrogramma enigmatica</i>	Eastern & Central GAB, benthic; endemic	O'Hara et al., 2016; *New GAB Record on this Voyage
<i>Halistemma rubra</i>	Epipelagic, Western shelf waters	Margulis, 1976
? <i>Halistemma</i> n. sp.	Mesopelagic; endemic	*New Species Herein
<i>Physophora gilmeri</i>	Central GAB	*New Record S. Hemisphere
<i>Physophora hydrostatica</i>	Western shelf waters	Margulis, 1976
<i>Agalma elegans</i>	Western shelf waters	Gaughan & Fletcher, 1997
<i>Nanomia</i> sp.	Mesopelagic	*New GAB Record Herein
Calycophorae		
<i>Abylopsis eschscholtzii</i>	Epipelagic, Western & Eastern shelf waters	Margulis, 1976; Gaughan & Fletcher, 1997
<i>Abylopsis tetragona</i>	Epipelagic, Western shelf waters	Margulis, 1976; Gaughan & Fletcher, 1997
<i>Amphicaryon acaule</i>	Mesopelagic, all GAB waters	Margulis, 1976; Herein
<i>Bassia bassensis</i>	Western shelf waters	Gaughan & Fletcher, 1997
<i>Ceratocymba dentata</i>	Epipelagic, Western shelf waters	Margulis, 1976
<i>Ceratocymba sagittata</i>	Mesopelagic, Western & Eastern shelf waters	Margulis, 1976; Herein
<i>Chelophyes appendiculata</i>	Mesopelagic, Bight-wide	Margulis, 1976; Gaughan & Fletcher, 1997; Herein
<i>Diphyes dispar</i>	Epipelagic, Western shelf waters	Margulis, 1976
<i>Enneagonum hyalinum</i>	Central GAB	*New GAB Record Herein

<i>Eudoxoides spiralis</i>	Mesopelagic, W & E shelf waters	Margulis, 1976; Gaughan & Fletcher, 1997
<i>Hippopodius hippopus</i>	Mesopelagic, W & E shelf waters	Margulis, 1976; Herein
<i>Lensia conoidea</i>	Epipelagic, Western shelf waters	Margulis, 1976
<i>Lensia fowleri</i>	Mesopelagic, Western shelf waters	Margulis, 1976
<i>Lensia hardy</i>	Epipelagic, Western shelf waters	Margulis, 1976
<i>Lensia multicristata</i>	Mesopelagic, Western shelf waters	Margulis, 1976
<i>Lensia subtilis</i>	Mesopelagic, W & E shelf waters	Margulis, 1976; Gaughan & Fletcher, 1997
<i>Lensia subtiloides</i>	Western shelf waters	Gaughan & Fletcher, 1997
<i>Maresearsia praeclara</i>	Central GAB	*New Australian Record Herein
<i>Nectadamas diomedae</i>	Central GAB	*New Australian Record Herein
<i>Praya dubia</i>	Western & Eastern shelf waters	Quoy & Gaimard, 1833; Herein
<i>Praya reticulata</i>	Western & Eastern shelf waters	Margulis, 1976; Herein
<i>Rosacea plicata</i>	Mesopelagic	*New GAB Record Herein
<i>Sphaeronectes tasmanica</i>	Nuyts Archipelago, Tasmania	Gershwin & Zeidler, 2003; Gershwin et al., 2013b
<i>Sulculeolaria angusta</i> (as <i>Galetta</i> )	Epipelagic, Western shelf waters	Margulis, 1976
<i>Sulculeolaria biloba</i> (as <i>Galetta</i> )	Mesopelagic, W & E shelf waters	Margulis, 1976
<i>Sulculeolaria</i> sp.	Western shelf waters	Gaughan & Fletcher, 1997
<i>Vogtia glabra</i>	Mesopelagic, W & E shelf waters	Margulis, 1976
<i>Vogtia pentacantha</i>	Epipelagic, Western shelf waters	Margulis, 1976
<i>Vogtia serrata</i>	Mesopelagic, W & E shelf waters	Margulis, 1976
<i>Vogtia spinosa</i>	Mesopelagic, Western shelf waters	Margulis, 1976; Herein
CTENOPHORES		
<i>Cydippida</i>		
<i>Euplokamis evansae</i>	Tasmania, VIC	Gershwin et al., 2010a
<i>Pleurobrachia</i> sp.	Coastal, oceanic	Gershwin et al., 2010a
<i>Lobata</i>		
<i>Bolinopsis</i> sp.	Coastal, oceanic	Gershwin et al., 2010a
<i>Leucothea filmersankeyi</i>	Nuyts Archipelago, Tasmania	Gershwin et al., 2010a
<i>Nuda</i>		
<i>Beroe</i> cf <i>abyssicola</i>	Oceanic	*New Australian Record Herein
<i>Beroe cucumis</i>	Coastal, oceanic	Gershwin et al., 2010a
<i>Neis cordigera</i>	Coastal	Gershwin et al., 2010a
PELAGIC TUNICATES		
<i>Appendicularia</i>		
<i>Oikopleura longicauda</i>	SA, VIC	Thompson, 1948
<i>Oikopleura fusiformis</i>	VIC	Thompson, 1948
<i>Oikopleura dioica</i>	SA, VIC	Thompson, 1948
<i>Oikopleura cornutogastra</i>	VIC	Thompson, 1948
<i>Oikopleura rufescens</i>	SA, VIC	Thompson, 1948
<i>Megalocercus huxleyi</i>	VIC	Thompson, 1948
<i>Oikopleura cophocerca</i>	VIC	Thompson, 1948
<i>Fritillaria pellucida</i>	VIC	Thompson, 1948
<i>Fritillaria borealis</i> (f. <i>sargassi</i> )	VIC	Thompson, 1948
<i>Fritillaria megachile</i>	SA	Thompson, 1948



## Zooplankton

<i>Dolioletta gegenbauri</i>	Bass Strait	AFD
Thaliacea		
<i>Pyrosoma atlanticum</i>	All GAB shelf waters	AFD; Herein
<i>Pyrosoma spinosum</i>	All GAB waters	*New GAB Record Herein
<i>Cyclosalpa bakeri</i>	M.V. Warreen: off the coast SA; Bass Strait	Thompson, 1948; AFD
<i>Cyclosalpa pinnata</i>	M.V. Warreen: off the coast SA	Thompson, 1948
<i>Brooksia rostrata</i>	Bass Strait	AFD
<i>Ihleia megalhanica</i>	Bass Strait	AFD
<i>Pegaea confoederata</i>	All GAB shelf waters	Thompson, 1948; AFD
<i>Ritteriella amboinensis</i>	Bass Strait	AFD
<i>Salpa fusiformis</i>	GAB coast; Bass Strait	Thompson, 1948; AFD; Herein
<i>Salpa maxima</i>	Bass Strait	AFD; Herein
<i>Soestia zonaria</i>	Bass Strait; East & Central GAB	*New GAB Record Herein
<i>Thalia democratica</i>	Bass Strait; Eastern GAB	Thompson, 1948; CSIRO SS2013; *New GAB Record Herein
<i>Thetys vagina</i>	Southern Tas	AFD

## References

- Adams, H. R., A. P. Flerchinger and H. F. Steedman. 1976. Ctenophora fixation and preservation. Monographs in Oceanic Methodology, vol. 4, Zooplankton fixation and preservation. H. F. Steedman. Paris, UNESCO Press. 4: 270-271.
- Andersson, A., T. Tamminen, S. Lehtinen, K. Jürgens, M. Labrenz and M. Viitasalo. 2017. The pelagic food web. In: P. Snoeijs-Leijonmalm, et al., Biological Oceanography of the Baltic Sea. Springer, Dordrecht.
- Båmstedt, U., J. H. Fosså, M. B. Martinussen and A. Fosshagen. 1998. Mass occurrence of the physonect siphonophore *Apolemia uvaria* (Lesueur) in Norwegian waters. Sarsia 83: 79–85.
- Båmstedt, U. and M. B. Martinussen. 2015. Ecology and behavior of *Bolinopsis infundibulum* (Ctenophora: Lobata) in the Northeast Atlantic. Hydrobiologia 759(1): 3–14.
- Blackburn, M. 1955. Trachymedusae and Narcomedusae of south-east Australian waters. Australian Journal of Marine and Freshwater Research 6(3): 410–428.
- Boero, F. 2013. Review of jellyfish blooms in the Mediterranean and Black Sea. FAO, Rome: 63 pp.
- Brodeur, R. D., J. J. Ruzicka and J. H. Steele. 2011. Investigating Alternate Trophic Pathways through Gelatinous Zooplankton and Planktivorous Fishes in an Upwelling Ecosystem Using End-to-End Models. Interdisciplinary Studies on Environmental Chemistry-Marine Environmental Modeling & Analysis. K. Omori, X. Guo, N. Yoshie et al. TERRAPUB, Tokyo: 57-63.
- Brodeur, R. D., C. Barcelo, K. L. Robinson, E. A. Daly and J. J. Ruzicka. 2014. Spatial overlap between forage fishes and the large medusa *Chrysaora fuscescens* in the northern California Current region. Marine Ecology Progress Series 510: 167–181.
- Brotz, L., W. W. L. Cheung, K. Kleisner, E. Pakhomov and D. Pauly. 2012. Increasing jellyfish populations: trends in Large Marine Ecosystems. Hydrobiologia 690(1): 3–20.
- Condon, R. H., D. K. Steinberg, P. A. del Giorgio, T. C. Bouvier, D. A. Bronk, W. M. Graham and H. W. Ducklow. 2011. Jellyfish blooms result in a major microbial respiratory sink of carbon in marine systems. Proceedings of the National Academy of Sciences 108(25): 10225–10230.
- Currie, D. R. and G. D. Parry. 1999. Changes to benthic communities over 20 years in Port Phillip Bay, Victoria, Australia. Marine Pollution Bulletin 38(1): 36–43.

- Fancett, M. S. 1986. Species composition and abundance of scyphomedusae in Port Phillip Bay, Victoria [Australia]. *Australian Journal of Marine and Freshwater Research* 37(3): 379–384.
- Fauchald, P. 2010. Predator–prey reversal: A possible mechanism for ecosystem hysteresis in the North Sea? *Ecology* 91(8): 2191–2197.
- Flynn, B. A., A. J. Richardson, A. S. Brierley, D. C. Boyer, B. E. Axelsen, L. Scott, N. E. Moroff and e. al. 2012. Temporal and spatial patterns in the abundance of jellyfish in the northern Benguela upwelling ecosystem and their link to thwarted pelagic fish recovery. *African Journal of Marine Science* 34: 131–146.
- Gaughan, D. J. and W. J. Fletcher. 1997. Effects of the Leeuwin current on the distribution of carnivorous macrozooplankton in the shelf waters off southern Western Australia. *Estuarine Coastal and Shelf Science* 45(1): 89–97.
- Gershwin, L. 2005. Taxonomy and phylogeny of Australian Cubozoa. School of Marine Biology and Aquaculture. James Cook University, Townsville, Queensland: 221 pp., 49 plates.
- Gershwin, L. 2013. *Stung! On Jellyfish Blooms and the Future of the Ocean*. University of Chicago Press, Chicago.
- Gershwin, L., M. Lewis, K. Gowlett-Holmes and R. Kloser. 2013a. The Medusae. Pelagic Invertebrates of South-Eastern Australia: A field reference guide. CSIRO Marine and Atmospheric Research Hobart: 49 pp.
- Gershwin, L., M. Lewis, K. Gowlett-Holmes and R. Kloser. 2013b. The Siphonophores. Pelagic Invertebrates of South-Eastern Australia: A field reference guide. CSIRO Marine and Atmospheric Research Hobart.
- Gershwin, L., M. Lewis, K. Gowlett-Holmes and R. Kloser. 2013c. Ctenophores. Pelagic Invertebrates of South-Eastern Australia: A field reference guide. CSIRO Marine and Atmospheric Research Hobart.
- Gershwin, L., M. Lewis, K. Gowlett-Holmes and R. Kloser. 2013d. Pelagic Tunicates. Pelagic Invertebrates of South-Eastern Australia: A field reference guide. CSIRO Marine and Atmospheric Research Hobart.
- Gershwin, L., C. Sutton, K. Gowlett-Holmes and R. Kloser. Scheduled for 2017a. Worms. Pelagic Invertebrates of South-Eastern Australia: A field reference guide. CSIRO Marine and Atmospheric Research Hobart.
- Gershwin, L., C. Sutton, K. Gowlett-Holmes and R. Kloser. Scheduled for 2017b. Pelagic snails. Pelagic Invertebrates of South-Eastern Australia: A field reference guide. CSIRO Marine and Atmospheric Research Hobart.
- Gershwin, L., C. Sutton, K. Gowlett-Holmes and R. Kloser. Scheduled for 2017c. Euphausiids. Pelagic Invertebrates of South-Eastern Australia: A field reference guide. CSIRO Marine and Atmospheric Research Hobart.
- Gershwin, L., C. Sutton, K. Gowlett-Holmes and R. Kloser. Scheduled for 2017d. Pelagic Echinoderms. Pelagic Invertebrates of South-Eastern Australia: A field reference guide. CSIRO Marine and Atmospheric Research Hobart.
- Gershwin, L. and W. Zeidler. 2008a. Some new and previously unrecorded Scyphomedusae (Cnidaria: Scyphozoa) from southern Australian coastal waters. *Zootaxa* 1744: 1–18.
- Gershwin, L. and W. Zeidler. 2008b. *Cladonema timmsii*, a new species of hydromedusa (Cnidaria: Hydrozoa) from a salt lake in South Australia. *Zootaxa* 1826: 59–68.
- Gershwin, L., W. Zeidler and P. J. F. Davie. 2010a. Ctenophora of Australia. *Memoirs of the Queensland Museum* 54(3): 1–45.
- Gershwin, L., W. Zeidler and P. J. F. Davie. 2010b. Medusae of Moreton Bay. *Memoirs of the Queensland Museum* 54(3): 47–108.

- Gershwin, L. and W. Zeidler. 2003. Encounter 2002 expedition to the Isles of St Francis, South Australia: Medusae, siphonophores and ctenophores of the Nuyts Archipelago. Transactions of the Royal Society of South Australia 127(Part 2): 205–241.
- Gjøsaeter, J. 1984. Mesopelagic fish, a large potential resource in the Arabian Sea. Deep Sea Research Part A. Oceanographic Research Papers 31(6-8): 1019-1035.
- Gowlett-Holmes, K. 2008. A field guide to the marine invertebrates of South Australia. Notomares, Tasmania.
- Greene, C., L. Kuehne, C. Rice, K. Fresh and D. Penttila. 2015. Forty years of change in forage fish and jellyfish abundance across greater Puget Sound, Washington (USA): anthropogenic and climate associations. Marine Ecology Progress Series 525: 153–170.
- Greve, W. 1994. The 1989 German Bight invasion of *Muggiaea atlantica*. ICES Journal of Marine Science 51(4): 355–358.
- Haacke, W. 1884. *Pseudorhiza haeckelii*, sp.n. der Endspross des Discomedusenstammes. Biologisches Zentralblatt Bd. 4: 291–294.
- Haacke, W. 1886. Über die Ontogenie der Cubomedusen. Zoologischer Anzeiger 9: 554–555.
- Haacke, W. 1887. Die Scyphomedusen des St. Vincent Golfes. Jenaische Zeitschrift für Naturwissenschaft 20: 588–638, 3 plates.
- Haddock, S. H. D. 2004. A golden age of gelata: past and future research on planktonic ctenophores and cnidarians. Hydrobiologia 530/531: 549–556.
- Haeckel, E. 1881. Report on the deepsea medusae dredged by the H.M.S. Challenger during the years 1873–1876. Rept. Challenger Expd. (Zoology), Section V 4(Part 2): 1–154, pl. 1–32.
- Haeckel, E. 1888. Report on the scientific results of the voyage of H.M.S. Challenger during the years 1873–76 under the command of Capt. George S. Nares and Capt. Frank Tourle Thomson, R.N. / prepared under the superintendence of the late Sir C. Wyville Thomson ... and now of John Murray ... published by order of Her Majesty's Government [Siphonophorae]. Challenger Reports 35: 1–380, Tafel 1–50.
- Hamilton, G. 2016. The secret lives of jellyfish. Nature 531(7595): 432-434.
- Hamner, W. M., L. P. Madin, A. L. Alldredge, R. W. Gilmer and P. P. Hamner. 1975. Underwater observations of gelatinous zooplankton : Sampling problems, feeding biology, and behavior. Limnology and Oceanography 20(6): 907-917.
- Hiromi, J., T. Kasuya and H. Ishii. 2005. Impacts of massive occurrence of jellyfish on pelagic ecosystem. Bulletin of Plankton Society of Japan 52(2): 82–90. [In Japanese, with English abstract].
- Hirst, A. J., C. A. White, G. D. Parry, S. Heislors, G. F. Werner and D. R. Spooner. 2010. Baywide Anchovy Sub-program Milestone Report No. 3 (2010). Fisheries Victoria Technical Report Series No. 114 November 2010. Department of Primary Industries, Queenscliff, Victoria: 21 pp.
- Hughes, T. P., N. A. J. Graham, J. B. C. Jackson, P. J. Mumby and R. S. Steneck. 2010. Rising to the challenge of sustaining coral reef resilience. Trends in Ecology & Evolution 25(11): 633–642.
- Kasuya, T., T. Ishimaru and M. Murano. 1994. Feeding characteristics of the lobate ctenophore *Bolinopsis mikado* Moser. Bulletin of Plankton Society of Japan 41(1): 57–68.
- Kramp, P. L. 1965a. Some medusae (mainly Scyphomedusae) from Australian coastal waters. Transactions of the Royal Society of South Australia 89: 257–278, plates 1–3.
- Kramp, P. L. 1965b. The hydromedusae of the Pacific and Indian Oceans. Dana Report 63: 1–161.
- Licandro, P., S. Souissi, F. Ibanez and C. Carré. 2012. Long-term variability and environmental preferences of calycophoran siphonophores in the Bay of Villefranche (north-western Mediterranean). Progress in Oceanography 97–100: 152–163.

- Lo, W. T., P. R. Kang and H. Y. Hsieh. 2012. Siphonophores from a transect off southern Taiwan between the Kuroshio current and South China sea. *Zoological Studies* 51(8): 1354–1366.
- Lučić, D., B. Pestoric, A. Malej, L. Lopez-Lopez, D. Drakulovic, V. Onofri, M. Miloslavić, B. Gangai, I. Onofri and A. Benović. 2012. Mass occurrence of the ctenophore *Bolinopsis vitrea* (L. Agassiz, 1860) in the nearshore southern Adriatic Sea (Kotor Bay, Montenegro). *Environmental Monitoring and Assessment* 184(8): 4777–4785.
- Luo, J. Y., B. Grassian, D. Tang, J.-O. Irisson, A. T. Greer, C. M. Guigand, S. McClatchie and R. K. Cowen. 2014. Environmental drivers of the fine-scale distribution of a gelatinous zooplankton community across a mesoscale front. *Marine Ecology Progress Series* 510: 129–149.
- Margulis, R. Y. 1979. Siphonophores from the Great Australian Bight. *Kompleksnye Issledovaniya Prirody Okeana* 6: 219–230 [in Russian].
- Matsumoto, G. I. 1988. A new species of lobate ctenophore, *Leucothea pulchra* sp. nov., from the California Bight. *Journal of Plankton Research* 10(2): 301–311.
- Mills, C. E. 1995. Medusae, siphonophores, and ctenophores as planktivorous predators in changing global ecosystems. *ICES Journal of Marine Science* 52(3-4): 575–581.
- Mills, C. E. 2001. Jellyfish blooms: Are populations increasing globally in response to changing ocean conditions? *Hydrobiologia* 451: 55–68.
- Oguz, T., B. Fach and B. Salihoglu. 2008. Invasion dynamics of the alien ctenophore *Mnemiopsis leidyi* and its impact on anchovy collapse in the Black Sea. *Journal of Plankton Research* 30(12): 1385–1397.
- O'Hara, T. D., A. F. Hugall, H. MacIntosh, K. M. Naughton, A. Williams and A. Moussalli. 2016. *Dendrogramma* is a siphonophore. *Current Biology* 26(11): R457–8.
- Pagès, F., H. E. Gonzalez, M. Ramon, M. Sobarzo and J. M. Gili. 2001. Gelatinous zooplankton assemblages associated with water masses in the Humboldt Current System, and potential predatory impact by *Bassia bassensis* (Siphonophora: Calycophorae). *Marine Ecology Progress Series* 210: 13–24.
- Parry, G., A. Hirst, T. Stokie, C. Green, C. White, S. Heislars and G. Werner. 2009. Baywide Anchovy Study Sub-Program. Milestone Report No. 2 (2009). Technical Report No. 73. Department of Primary Industries Queenscliff, Victoria: 26 pp.
- Parry, G. and T. Stokie. 2009. Baywide Anchovy Study Sub-Program. Milestone Report No. 1 (2008). Technical Report No. 23. Fisheries Victoria. Department of Primary Industries Queenscliff, Victoria: 28 pp.
- Parsons, T. R. and C. M. Lalli. 2002. Jellyfish population explosions: Revisiting a Hypothesis of Possible Causes. *La Mer* 40: 111–121.
- Péron, F. and C. A. Lesueur. 1810. Tableau des caractères génériques et spécifiques de toutes les espèces de méduses connues jusqu'à ce jour. *Annales du Museum d'Histoire Naturelle, Paris* 14: 325–366.
- Purcell, J. E. 1985. Predation on fish eggs and larvae by pelagic cnidarians and ctenophores. *Bulletin of Marine Science* 37(2): 739–755.
- Purcell, J. E. and M. N. Arai. 2001. Interactions of pelagic cnidarians and ctenophores with fish: a review. *Hydrobiologia* 451: 27–44.
- Purcell, J. E., D. L. Breitburg, M. B. Decker, W. M. Graham, M. J. Youngbluth and K. A. Raskoff. 2001. Pelagic cnidarians and ctenophores in low dissolved oxygen environments: a review. *Coastal Hypoxia: consequences for living resources and ecosystems*. N. N. Rabalais and R. E. Turner. Washington DC, American Geophysical Union: Coastal and Estuarine Studies Series 58: 77–100.

- Quinones, J., A. Monroy, E. M. Acha and H. Mianzan. 2013. Jellyfish bycatch diminishes profit in an anchovy fishery off Peru. *Fisheries Research* 139: 47–50.
- Quoy, J. R. C. and J. P. Gaimard. 1833. Zoophytes. *Voyage de decouvertes de l'Astrolabe, execute par ordre du roi, pendant les annees 1826-1827-1828-1829, sous le commandement de M.J. Dumont D'Urville, Zoologie*. J. D. d'Urville. Paris, J. Tastu. Tome 4. Zoophytes: 1–390, plus Atlas.
- Richardson, A. J., A. Bakun, G. C. Hays and M. J. Gibbons. 2009. The jellyfish joyride: causes, consequences and management responses to a more gelatinous future. *Trends in Ecology and Evolution* 24(6): 312–322.
- Robison, B. H. 2004. Deep pelagic biology. *Journal of Experimental Marine Biology & Ecology* 300: 253–272.
- Rogers, C. A. 1976. Impact of autumn-winter swarming of a siphonophore ("Lipo") on fishing in coastal waters of New England. *Woods Hole Oceanographic Institute*, February 1976. <http://www.nefsc.noaa.gov/publications/series/whlrd/whlrd7603.pdf>.
- Rogers, C. A., D. C. Biggs and R. A. Cooper. 1978. Aggregations of the siphonophore *Nanomia cara* Agassiz 1865 in the Gulf of Maine: observations from a submersible. *Fishery Bulletin* (Washington, D.C.) 76(1): 281–284.
- Rogers, P.J., T. Ward, P. van Ruth, A. Williams; contributing authors, B. Bruce, S. Connell, D. Currie, C. Davies, K. Evans, B. Gillanders, S. Goldsworthy, D. Griffin, N. Hardman-Mountford, A. Ivey, R. Kloser, J. Middleton, A. Richardson, A. Ross, J. Tanner and J. Young. 2013. Physical processes, biodiversity and ecology of the Great Australian Bight region: a literature review. CSIRO, Hobart, Tasmania. 227 pp.
- Roux, J.-P., C. van der Lingen, M. J. Gibbons, N. E. Moroff, L. J. Shannon, A. D. M. Smith and P. M. Cury. 2013. Jellyfication of Marine Ecosystems as a Likely Consequence of Overfishing Small Pelagic Fishes: Lessons from the Benguela. *Bulletin of Marine Science* 89(1): 249–284.
- Russell, F. S. 1970. On a new species of medusa from an inland salt lake in South Australia. *Journal of Zoology* (London) 162: 449–452.
- SARDI. 2008. South Australia's Marine Temperate Environment. *South Australian Research & Development Institute* 7 February. [http://www.sardi.sa.gov.au/pages/aquatic/mee/ocean/temp\\_env.htm:sectID=246&tempID=1](http://www.sardi.sa.gov.au/pages/aquatic/mee/ocean/temp_env.htm:sectID=246&tempID=1).
- Scheffer, M., S. Carpenter, J. A. Foley, C. Folke and B. Walker. 2001. Catastrophic shifts in ecosystems. *Nature* 413: 591–596.
- Schnedler-Meyer, N. A., P. Mariani and T. Kiørboe. 2016. The global susceptibility of coastal forage fish to competition by large jellyfish. *Proceedings of the Royal Society B* 283: 20161931 (pp. 1–8).
- Sheldon, R. W., W. H. Sutcliffe Jr. and M. A. Paranjape. 1977. Structure of Pelagic Food Chain and Relationship Between Plankton and Fish Production. *Journal of the Fisheries Research Board of Canada* 34(12): 2344–2353.
- Southcott, R. V. 1982. Jellyfishes (Classes Scyphozoa and Hydrozoa). *Marine Invertebrates of Southern Australia, Part 1*. S. A. Shepherd and I. M. Thomas. D. J. Woolman, South Australia: 115–159.
- Sun, S., Y. Li and X. Sun. 2012. Changes in the small-jellyfish community in recent decades in Jiaozhou Bay, China. *Chinese Journal of Oceanology and Limnology* 30(4): 507–518.
- Thomas, I. M. 1950. The medusa *Craspedacusta* in Australia. *Nature* 166(4216): 312–313.
- Thomas, I. M. 1951. *Craspedacusta sowerbyi* in South Australia, with some notes on its habits. *Transactions of the Royal Society of South Australia* 74: 59–65.

- Thompson, H. 1948. Pelagic Tunicates of Australia. Commonwealth Council for Scientific and Industrial Research, Melbourne.
- Travis, J. 1993. Invader threatens Black, Azov Seas. *Science* 262: 1366–1367.
- Williams, A., and Koslow, J. 1997. Species composition, biomass and vertical distribution of micronekton over the mid-slope region off southern Tasmania, Australia. *Marine Biology*, 130: 259-276.
- Young, J. W., R. W. Bradford, T. D. Lamb and V. D. Lyne. 1996. Biomass of zooplankton and micronekton in the southern bluefin tuna fishing grounds off eastern Tasmania, Australia. *Marine Ecology Progress Series* 138: 1–14.
- Zaitsev, Y. and V. Mamaev. 1997. Biological diversity in the Black Sea: a study of change and decline. United Nations Publications, New York.

## 6. MICRONEKTON

Rudy Kloser, Adrian Flynn, Caroline Sutton, Andy Revill, Tim Ryan and Lisa Gershwin

Micronekton describes small (typically < 20 cm length) free-swimming teleosts, crustaceans, cephalopods and gelatinous organisms. These organisms are referred to as “mid-trophic” as they typically feed through a wide range of niches at the third trophic level (Choy et al., 2012). Therefore, micronekton populations mediate trophic transfer of primary productivity to higher order predators. In temperate and Southern Ocean pelagic systems, predators such as cephalopods (Phillips et al., 2001), toothed whales, tunas (Young et al., 1997; Young et al., 2010), seals (Robinson et al., 2002), penguins (Hindell, 1988a; Hindell, 1988b; Hindell, 1988c; Robinson and Hindell, 1996; Robinson et al., 2002) and demersal fishes (Williams and Koslow, 1997; Bulman et al., 2001; Goldsworthy et al., 2001; Williams et al., 2001) are among the predators that feed directly on micronekton or on predators of micronekton. As such, micronekton have been recognised as an important element in trophodynamic models (Bax et al., 2001; Griffiths et al., 2010; Lehodey et al., 2010; Lehodey et al., 2014).

Recent reviews of the key micronekton species in the GAB have highlighted the general lack of knowledge with little to no research in the central GAB region (e.g. McClatchie et al. (2006)). In particular, the interaction of the deep slope waters with the general pelagic food web is poorly understood (McClatchie and Young, 2006). For the important mesopelagic fish on shelf edge and slope waters, McClatchie and Young (2006) conclude that no synoptic independent surveys of mesopelagic organisms have been done, and that the significance of mesopelagic organisms to the food web are not known but are likely to have similar roles as in continental slope waters off Tasmania (Koslow et al., 1997; Williams and Koslow, 1997; Young et al., 1997; Williams et al., 2001). These mesopelagic organisms that make up the deep scattering layer from 200 to 1000 m depth occur throughout the world’s oceans with minimal to no information about their ecological role and spatial and temporal variability in the central GAB. As the central GAB is characterised by a dominant downwelling northern boundary current it is hypothesised that mesopelagic biomass will be less than that found in eastern Tasmanian waters.

One view of the micronekton from net catches for the central GAB (~132 °E) is recorded within Kloser et al. (1998), who found that in February 1998 micronekton biomass was low in shelf waters and highest on the shelf break reducing for offshore and inshore waters. They noted high abundance of salps in shelf break and inshore regions, which may be an important food component of southern bluefin tuna (Shingu, 1981). They recommend that future studies should be directed at identifying the seasonal and temporal distribution of micronekton in these waters as well as a better understanding of their importance to the tuna’s diet as well as that of other predators. The high abundance of micronekton has also been reported for the eastern GAB upwelling region (Ward and McLeary, 2006). This high abundance of micronekton is also expected to be associated with other key ecological features of the region such as canyons and persistent eddy fields (Pattiaratchi, 2007; Currie et al., 2012). Micronekton distribution and abundance can also be inferred by the distribution of apex predators such as New Zealand fur seals in shelf, shelf break and offshore waters (Page et al., 2006).

The importance of micronekton to the distribution and abundance of top predators has been reported for the eastern and western GAB inshore and shelf region (Page et al., 2005a; Page et al., 2005b; Ward et al., 2006; Goldsworthy et al., 2011). However, little is known about micronekton in mesopelagic waters and their diurnal connectivity with epipelagic production. A major impediment to our understanding of micronekton has been the ability to quantify the distribution and abundance



of the dominant species, their life histories and trophic interactions. Typically pelagic nets are used to sample micronekton but these have known catchability and selectivity issues (Koslow et al., 1997; Pakhomov and Yamamura, 2010). A better approach is the combined use of multiple methods using optics, acoustic and nets (Demer et al., 2009). An advantage of the acoustic method is that large areas can be sampled from a range of vessels with suitably equipped echosounders (Kloser et al., 2009)s. Large temporal and spatial data sets can be acquired to detect decadal trends (<http://imos.org.au/basoop.html>). Physical capture of organisms is also required to document species specific changes, life history parameters as well as trophic relationships. This chapter addresses objectives 1 and 3 of the project.

## References

- Bax, N., Burford, M., Clementson, L., and Davenport, S. 2001. Phytoplankton blooms and production sources on the south-east Australian continental shelf. *Marine and Freshwater Research*, 52: 451-462.
- Bulman, C., Althaus, F., He, X., Bax, N. J., and Williams, A. 2001. Diets and trophic guilds of demersal fishes of the south-eastern Australian shelf. *Marine and Freshwater Research*, 52: 537-548.
- Choy, C. A., Davison, P. C., Drazen, J. C., Flynn, A., Gier, E. J., Hoffman, J. C., McClain-Counts, J. P., et al. 2012. Global trophic position comparison of two dominant meopelagic fish families (Myctophidae, Stomiidae) using amino acid nitrogen isotopic analyses. *PLoS ONE*, 7: e50133.
- Currie, D. R., McClatchie, S., Middleton, J. F., and Nayar, S. 2012. Biophysical Factors Affecting the Distribution of Demersal Fish around the Head of a Submarine Canyon Off the Bonney Coast, South Australia. *PLoS ONE*, 7: e30138.
- Demer, D. A., Kloser, R. J., MacLennan, D. N., and Ona, E. 2009. An introduction to the proceedings and a synthesis of the 2008 ICES Symposium on the Ecosystem Approach with Fisheries Acoustics and Complementary Technologies (SEAFACS). *ICES Journal of Marine Science*, 66: 961-965.
- Goldsworthy, S., He, X., Williams, R., Lewis, M., Gaskett, A. C., Bulman, C., Young, J., et al. 2001. The Diet of Toothfish and Pelagic Fish around Macquarie Island. *In Ecologically Sustainable Development of the Fishery for Patagonian Toothfish (Dissostichus eleginoides) around Macquarie Island: Population Parameters, Population Assessment and Ecological Interactions*, pp. 219-240. Ed. by X. He, and D. Furlani. CSIRO Marine Research, Australian Antarctic Division, and Austral Fisheries Pty Ltd, Hobart.
- Goldsworthy, S. D., Page, B., Rogers, P. J., and Ward, T. M. 2011. Establishing ecosystem-based management for the South Australian Sardine Fishery : developing ecological performance indicators and reference points to assess the need for ecological allocations : final report to the Fisheries Research and Development Corporation / Simon D. Goldsworthy ... [et al.], SARDI Aquatic Sciences, West Beach, SA.
- Griffiths, S. P., Young, J. W., Lansdell, M. J., Campbell, R. A., Hampton, J., Hoyle, S. D., Langley, A., et al. 2010. Ecological effects of longline fishing and climate change on the pelagic ecosystem off eastern Australia. *Reviews in Fish Biology and Fisheries*, 20: 239-272.
- Hindell, M. A. 1988a. Diet of rockhopper penguin *Eudyptes chrysocome* at Macquarie Island. *Emu*, 88: 227-233.
- Hindell, M. A. 1988b. The diet of the King Penguin *Aptenodytes patagonicus* at Macquarie Island. *Ibis*, 130: 193-203.
- Hindell, M. A. 1988c. The diet of the royal penguin *Eudyptes schlegeli* at Macquarie Island. *Emu*, 88: 219-226.

- Kloser, R., Ryan, T., Sokov, P., Young, J., Stanley, C., and Davis, T. 1998. Assessment of acoustics as a research tool to determine the distribution, biomass and behaviour of southern bluefin tuna schools and their prey in the GReat Australian Bight. 1.
- Kloser, R. J., Ryan, T., Young, J., and Lewis, M. E. 2009. Acoustic observations of micronekton fish on the scale of an ocean basin: potential and challenges. *ICES J. Mar. Sci.*, 66: 998-1006.
- Koslow, J., Kloser, R., and Williams, A. 1997. Pelagic biomass and community structure over the mid-continental slope off southeastern Australia based upon acoustic and midwater trawl sampling. *Marine Ecology Progress Series*, 146: 21-35.
- Lehodey, P., Conchon, A., Senina, I., Domokos, R., Calmettes, B., Jouanno, J., Hernandez, O., et al. 2014. Optimization of a micronekton model with acoustic data. *ICES Journal of Marine Science*, doi: 10.1093/icesjms/fsu233.
- Lehodey, P., Murtugudde, R., and Senina, I. 2010. Bridging the gap from ocean models to population dynamics of large marine predators: A model of mid-trophic functional groups. *Progress in Oceanography*, 84: 69-84.
- McClatchie, S., Middleton, J., Pattiaratchi, C., Currie, D., and Kendrik, G. 2006. The South-west Marine Region: Ecosystems and Key Species Groups.
- McClatchie, S., and Young, J. 2006. South-west Marine Region: Ecosystems and key species groups - Part 2: Key species groups. Mesopelagic fish. 144-158 pp.
- Page, B., McKenzie, J., and Goldsworthy, S. 2005a. Inter-sexual differences in New Zealand fur seal diving behaviour. *Marine Ecology Progress Series*, 304: 249-264.
- Page, B., McKenzie, J., and Goldsworthy, S. D. 2005b. Dietary resource partitioning among sympatric New Zealand and Australian fur seals. *Marine Ecology Progress Series*, 293: 283-302.
- Page, B., McKenzie, J., Sumner, M., Coyne, M., and Goldsworthy, S. 2006. Spatial separation of foraging habitats among New Zealand fur seals.
- Pakhomov, E., and Yamamura, O. 2010. Report of the advisory panel on micronekton sampling inter-calibration experiment.
- Pakhomov, E.A., Perissinotto, R., and McQuaid, C.D. 1996. Prey composition and daily ration of myctophid fishes in the Southern Ocean.
- Pattiaratchi, C. 2007. Understanding areas of high productivity within the South-west Marine Region.
- Phillips, K. L., Jackson, G. D., and Nichols, P. D. 2001. Predation on myctophids by the squid *Moroteuthis ingens* around Macquarie and Heard Islands: stomach contents and fatty acid analysis. *Marine Ecology Progress Series*, 215: 179-189.
- Robinson, S. A., Goldsworthy, S. D., van den Hoff, J., and Hindell, M. A. 2002. The foraging ecology of two sympatric fur seal species, *Arctocephalus gazella* and *Arctocephalus tropicalis*, at Macquarie Island during the austral summer. *Marine & Freshwater Research*, 53: 1071-1082.
- Robinson, S. A., and Hindell, M. A. 1996. Foraging ecology of Gentoo Penguins *Pygoscelis papua* at Macquarie Island during the period of chick care. *Ibis*, 138: 722-731.
- Shingu, C. 1981. Ecology and stock of southern bluefin tuna / [Chiomi Shingu] ; translated by M.A. Hintze, CSIRO Division of Fisheries and Oceanography, Cronulla, N.S.W.
- Suntsov, A. V. and Brodeur, R. D., 2008. Trophic ecology of three dominant myctophid species in the northern California Current region. *Marine Ecology Progress Series*, 373: 81-96.
- Ward, T. M., and McLeary, L. J. 2006. Pelagic ecology of a northern boundary current system: effects of upwelling on the production and distribution of sardine (*Sardinops sagax*), anchovy (*Engraulis australis*) and southern bluefin tuna (*Thunnus maccoyii*) in the Great Australian Bight. *Fisheries Oceanography*, 15: 191-207.

- Ward, T. M., Sorokin, S. J., Currie, D. R., Rogers, P. J., and McLeay, L. J. 2006. Epifaunal assemblages of the eastern Great Australian Bight: Effectiveness of a benthic protection zone in representing regional biodiversity. *Continental Shelf Research*, 26: 25-40.
- Williams, A., and Koslow, J. 1997. Species composition, biomass and vertical distribution of micronekton over the mid-slope region off southern Tasmania, Australia. *Marine Biology*, 130: 259-276.
- Williams, A., Koslow, J., Terauds, A., and Haskard, K. 2001. Feeding ecology of five fishes from the mid-slope micronekton community off southern Tasmania, Australia. *Marine Biology*, 139: 1177-1192.
- Young, J. W., Lamb, T. D., Le, D., Bradford, R., and Whitelaw, A. W. 1997. Feeding ecology and interannual variations in diet of southern bluefin tuna, *Thunnus maccoyii*, in relation to coastal and oceanic waters off eastern Tasmania, Australia. *Environmental Biology of Fishes*, 50: 275-291.
- Young, J. W., Lansdell, M. J., Campbell, R. A., Cooper, S. P., Juanes, F., and Guest, M. A. 2010. Feeding ecology and niche segregation in oceanic top predators off eastern Australia. *Marine Biology*, 157: 2347-2368.

## 6.1 Micronekton abundance and diversity regional comparison.

Caroline Sutton, Adrian Flynn and Rudy Kloser

### 6.1.1 Introduction

The distribution of micronekton in the world's oceans is heterogeneous but not random. In oceanic environments they are often concentrated at frontal zones, eddies and other oceanographic features that are associated with enhanced production. Distributions are influenced by both passive entrainment and active swimming orientation to areas of high productivity or desirable habitat (Benoit-Bird and Au, 2006; McManus et al., 2008). There is often a time lag in the biological response to influential biological and physical events, and so, distributions do not always directly correlate with conditions at time of sampling (Young et al., 2015). While an understanding of oceanographic regimes at the basin- and meso-scale is useful for interpreting biological patterns, their taxonomic diversity and high mobility of some taxa means there will be sampling bias regardless of the method employed.

The vertical dimension of micronekton behaviour is typified by diel vertical migration (DVM). For many micronekton taxa this is a central aspect of mesopelagic ecology as it relates to feeding in shallow strata and transport of production to deep strata, a process known as the biological pump. At basin scales, micronekton community composition and mesopelagic biogeography more broadly, is structured by water masses (Backus, 1986). At sub-basin scales, and moving from offshore to inshore, interactions between vertically stratified micronekton populations and the continental slope can establish particular foraging regimes that may include benthopelagic predators; thus there may also be a cross shelf component to the DMV (Williams and Koslow, 1997; Flynn and Williams, 2012). With these fundamentals in mind, at a minimum a micronekton sampling program needs to incorporate both day /night sampling replication as well as horizontal sampling to capture inshore and offshore movements. In addition, there are seasonal and inter-annual factors that should also be considered.

Traditionally, net trawls are used to sample for micronekton and are generally good at sampling fishes and crustaceans but under-sample cephalopods (Battaglia et al., 2013). While gelatinous taxa are represented in trawl samples, their fragility and gaps in the taxonomic knowledge has meant that their contribution is not well understood (CSIRO unpublished data). Lanternfishes (family Myctophidae) are usually the most diverse teleost group in micronekton communities in the open ocean, and typically account for the majority of the biomass in midwater trawls. Therefore, this family of fishes is generally the most studied component of the micronekton and underpins many generalisations about mesopelagic ecology.

Net sampling in the GAB represents part of a multiple-lines-of-evidence approach to investigating micronekton communities, trophic level interactions and species distributions by linking with studies associated with acoustic and optical sensing, oceanography, phytoplankton and zooplankton, and isotopes. Results of this component should be viewed with reference to these partner studies.

The objectives of the micronekton net sampling component of this study are:

- To describe micronekton community structure, species richness and biomass
- To compare the eastern and central GAB micronekton communities in terms of species composition, size spectra, biomass, habitat and trophic processes.
- To provide samples of micronekton across multiple size ranges and trophic guilds for isotopic analyses.

- To sample micronekton species data to assist in the interpretation of acoustic and optical sensing data.
- To provide specimens for morphological identification and biodiversity studies

### 6.1.2 Methods

#### *MIDOC Trawl methodology*

A multiple closing cod-end device (MIDOC) was attached to the rear of an International Young Gadoid Pelagic Trawl (IYGPT) (Figure 6.1-1). The MIDOC comprises six separate cod-ends that are programmed to open and close on a timer. Depth strata to be sampled were planned to provide coverage of observed acoustic scattering layers and consistency between sampling locations. The net was trawled to the target depth strata at target opening-and-closing times by controlling winch speed, wire out length on the dual trawl warps and vessel speed. The net depth, distance behind vessel, headline height (used to calculate net mouth area) and altitude above seabed were monitored using a Simrad ITI system. Echograms from shipboard bioacoustic systems were monitored to observe the seabed, onset of DVM and scattering layers. The IYGPT was trawled via dual trawl wires attached to depressor wings (known as “trawl doors”) that acted to maintain spreading and downward force and to lower the mouth of the net. Additional Simrad ITI sensors in the depressor wings were used to monitor “door spread”. The dual trawl wires were controlled via dual trawl winches. Collectively, vessel speed, trawl wire payout and retrieval rates, and hydrodynamic behaviour of the trawl doors were optimised to achieve the target depths and maintain mouth opening. The MIDOC logged both depth and opening-closing events so that actual trawl profiles could be ascertained.

Mesh size of the IYGPT graduated from 200 mm stretched mesh width at the mouth to 10 mm stretched mesh width at the rear. In the MIDOC, cod-end socks were made from 10 mm knotless mesh and the final terminal removable cod-ends were 500 µm mesh size.

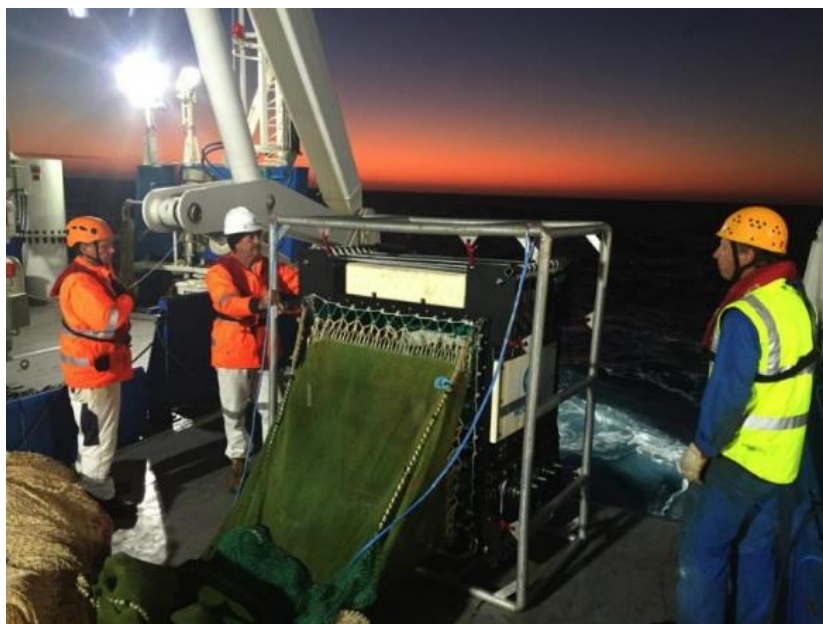
#### *Survey Design*

Regional comparisons for the MIDOC trawls were conducted along the two main transects used for the Central (T2) and East (T6) GAB regions. Inshore (Mid and Upper Slope) and Oceanic trawls were conducted within each region and replicated for Day and Night where possible. Time constraints prevented complete sample replication for both regions. The sample design and relevant statistics for trawls are given in Table 6.1-1.

Table 6.1-1 IYGPT- MIDOC trawl details. Depth = depths towed (m), VF = volume filtered (m<sup>3</sup>)

Region	Habitat	Site	Bottom Depth (m)	Time	Datum	Net 1	Net 2	Net 3	Net 4	Net 5	Net 6
East	Oceanic	T6-5000	5306	Day	Depth	0-18	18-166	166-290	290-405	450-230	230-0
					VF	1029767	339870	323831	232276	122652	129251
	<b>Mid Slope</b>	<b>T6-400</b>	<b>969</b>	<b>Day</b>	Depth	<b>0-645</b>	<b>645-363</b>	<b>363-336</b>	<b>336-270</b>	<b>270-153</b>	<b>153-0</b>
					VF	<b>1163263</b>	<b>361628</b>	<b>168583</b>	<b>172417</b>	<b>162278</b>	<b>139043</b>
		<b>T6-400</b>	<b>884</b>	<b>Night</b>	Depth	<b>0-608</b>	<b>608-408</b>	<b>408-302</b>	<b>302-223</b>	<b>223-143</b>	<b>143-0</b>
					VF	<b>831035</b>	<b>318432</b>	<b>168357</b>	<b>172225</b>	<b>165443</b>	<b>134049</b>
*	Targeted shelf break	Transit	270-560	Night	Depth	0-250	25-94	94-206	206-250	250-140	140-0
					VF	691256	207113	204414	197836	193668	204006
* Mid Zone	Upper Slope	T4-400	250-540	Night	Depth	0-386	386-288	288-202	202-124	124-26	62-0
					VF	893334	212798	222401	218533	221137	217797
<b>Central</b>	<b>Oceanic</b>	<b>T2-3000</b>	<b>3042</b>	<b>Day</b>	Depth	<b>0-611</b>	<b>611-411</b>	<b>411-330</b>	<b>330-211</b>	<b>211-100</b>	<b>100-0</b>
					VF	<b>1567201</b>	<b>430605</b>	<b>200435</b>	<b>203873</b>	<b>202512</b>	<b>300895</b>
		<b>T2-3000</b>	<b>2874</b>	<b>Night</b>	Depth	<b>0-625</b>	<b>625-405</b>	<b>405-293</b>	<b>293-209</b>	<b>209-101</b>	<b>101-0</b>
					VF	<b>151884</b>	<b>428573</b>	<b>206710</b>	<b>211441</b>	<b>218121</b>	<b>357926</b>
	<b>Upper slope</b>	<b>T2-400 m</b>	<b>383</b>	<b>Day</b>	Depth	<b>0-354</b>	<b>354-310</b>	<b>310-222</b>	<b>222-95</b>	<b>95-63</b>	<b>63-0</b>
					VF	<b>866176</b>	<b>189507</b>	<b>190712</b>	<b>191819</b>	<b>195280</b>	<b>179069</b>
		<b>T2-400</b>	<b>393</b>	<b>Night</b>	Depth	<b>0-375</b>	<b>375-305</b>	<b>305-213</b>	<b>213-115</b>	<b>115-70</b>	<b>70-0</b>
					VF	<b>946907</b>	<b>203990</b>	<b>208506</b>	<b>205642</b>	<b>197256</b>	<b>171438</b>
	<b>Mid Slope</b>	<b>T2-800</b>	<b>819</b>	<b>Day</b>	Depth	<b>0-650</b>	<b>650-427</b>	<b>427-326</b>	<b>326-238</b>	<b>238-150</b>	<b>150-0</b>
					VF	<b>1459079</b>	<b>439797</b>	<b>221663</b>	<b>211780</b>	<b>205353</b>	<b>212932</b>
		<b>T2-800</b>	<b>830</b>	<b>Night</b>	Depth	<b>0-590</b>	<b>590-396</b>	<b>396-315</b>	<b>315-210</b>	<b>210-120</b>	<b>120-0</b>
					VF	<b>1169310</b>	<b>418424</b>	<b>211056</b>	<b>213272</b>	<b>209502</b>	<b>183273</b>
*	Targeted shelf break	T1-200	206	Night	Depth	0-150	150-150	150-113	113-95	95-85	85-0
					VF	644650	200314	209054	204684	204684	176321

Footnote: Trawls in bold and shaded provided day-night and east-central data for comparison of standardised abundance and biomass. \* Exploratory trawl to investigate dense scattering layers on the shelf break/upper slope



a). MIDOC cod-end system sewn into the rear of the IYGPT. Six cod-ends are trailing astern.



b) Net system being retrieved.

*Figure 6.1-1 IYGPT midwater trawl with MIDOC cod-end system. The body of the IYGPT is laid on the deck and then wound up onto net drum. The six cod-ends of the MIDOC system are shown in both a and b trawling down the stern ramp.*

### *Sample processing*

Catches were sorted fresh in the ship-board laboratory at sea. The sorted catch was photographed and species were identified, enumerated, measured and weighed on a shipboard motion-compensated balance. Length measurements were standard length for fishes and total length for decapod crustaceans. Where very large numbers were sampled (e.g. multiple thousands of krill), the bulk biomass was weighed and a sub-sample of 20 - 50 individuals was measured and weighed separately. On-board specialists identified fishes, crustacea, gelatinous zooplankton and cephalopods specimens to the lowest possible level and a photographic log of species and observable taxonomic units was retained. Identification of gelatinous zooplankton sampled by nets is problematic as they tend to be fragile and easily damaged and fragmented. For this reason the bulk of the gelatinous biota were classified undifferentiated gelatinous biota. Where possible the gelatinous biota were identified to the lowest possible taxa, based on the identifiable biota from



each sample the undifferentiated fraction was grouped into gelatinous herbivores (i.e. salps and pyrosomes) or gelatinous carnivores (i.e. siphonophores, medusae and ctenophores).

Representatives of all taxa were retained for laboratory identification, genetic barcoding. Selected specimens were retained for isotope analysis (see Section 3.2). All biological material was returned to CSIRO or partner museums for further taxonomic study and archiving. The taxonomic information presented herein is derived from shipboard identifications and some post-field laboratory identifications. Future genetic work and more detailed morphological investigations may uncover some additional cryptic species diversity.

### *Data processing and analysis*

Biological data were entered into a centralised database that tracked sampling operations in study regions, net catch data and sub-samples taken for analysis. MIDOC net samples were classified according to the depth ranges traversed as follows:

- Epipelagic: 0 - 200 m
- Upper Mesopelagic: 200 - 400 m
- Lower Mesopelagic: 400 - 600 m

Taxa were classified into broad categories (termed “acoustic categories” herein) that are known to be (or postulated to be) acoustically distinguishable as follows:

- Crustaceans
- Cephalopods
- Fish - Swim bladder
- Fish - Non swim bladder
- Fish - Unknown swim bladder
- Gelatinous Herbivores (predominantly salps)
- Gelatinous Carnivores (predominantly medusae, pyrosomes and siphonophores)
- Other (e.g. worms and pteropods)

Individuals weighing more than 100 g were excluded to ensure large cephalopods and fish were not included as micronekton. Biomass was standardised to trawl volumes ( $\text{m}^3$ ) for each sample, calculated from net mouth area ( $\text{m}^2$ ) and distance trawled (m). Previous experience with this net indicates that effective mouth area is approximately  $188 \text{ m}^2$  (21m wing spread x 8.9 m headline height). Distance trawled was calculated from the ships' position at the start and finish of each net. Standardised biomass density is presented as  $1000 \text{ g} \cdot \text{m}^{-3}$  and was calculated by dividing the total biomass (g) in each net by the volume filtered ( $\text{m}^3$ ) and multiplying by 1000. Biomass per surface area ( $\text{m}^2$ ) is presented as  $\text{g} \cdot \text{m}^{-2}$  and was calculated for each net by multiplying the density ( $\text{g} \cdot \text{m}^{-3}$ ) by the vertical distance travelled by the net (m). During a single MIDOC deployment, multiple nets may have traversed a depth stratum. Total biomass densities ( $\text{g} \cdot \text{m}^{-3}$ ) for a depth stratum is the average for the number of nets contributing to that depth stratum. Biomass per surface area ( $\text{m}^2$ ) of each depth stratum is the sum of biomass contributing to that depth stratum.

Data analysis followed the approach of comparing and contrasting the Central and Eastern regions with respect to the whole-of-community results, stepping through to more detailed descriptions of particular indicator species. Total biomass was compared between regions habitats and by depth. Species diversity and evenness (Shannons and Pielou's) and Whittikers rank dominance was calculated on species abundance data for each region and habitat sampled. An nMDA cluster

analysis using Bray-Curtis dissimilarity on square root log transformed abundance data was performed on MIDOC species abundance data for central and east regions of the GAB.

### *Biogeographic analysis*

The micronekton fish community composition in the GAB was put into a bioregional context by comparing with data available for Western Tasmania (WT), Southern Tasmania (Southern Hills, SH), the Southern Tasman Sea Abyssal Basin (STAB), the North Tasman Sea (NT, north of the Tasman Front in the vicinity of Britannia Seamount) and Macquarie Island (MI). These data are described in a separate report (CSIRO unpublished data) and published papers (Williams and Koslow, 1997; Young et al., 2010; Young et al., 2011; Flynn and Williams, 2012; Flynn and Marshall, 2013). Micronekton catches in all regions were made using the same net type as that used in the GAB and all abundance data were standardised (n. 1000 m<sup>-3</sup>). First, species distributions were explored using a hierarchical distance measure known as UniFrac in the R package *phyloseq*. This method uses hierarchical taxonomic relatedness in the calculation of between-sample dissimilarity. A weighted version of UniFrac was used whereby the branch lengths of the phylogenetic tree are weighted by differences in abundances associated with each node (Lozupone et al., 2007; Lozupone et al., 2011). However, as will be described in the results below, the analysis was compromised by the dispersive nature of the taxonomic identifications across multiple surveys. For the purpose of this report, the regional fish community data were analysed using hierarchical clustering of the Myctophid abundance data alone. Abundance data were standardised to presence-absence of taxa and a 'Kulczynski' dissimilarity matrix constructed using the R package *vegan*. The results of the cluster analysis were compared with existing oceanographic regionalisations (Condie and Dunn, 2006; Longhurst, 2007) that represent *a-priori* biogeographic regions.

## 6.1.3 Results

### *Whole-of-community*

Total biomass captured for the 12 trawls at all sites was 69.5 kg. Total micronekton biomass was 62.5 kg: 35.9 kg from 7 trawls in the Central region, 21.1 kg from 4 trawls in the East region, and 5.5 kg from 1 trawl in the mid-zone. Average standardised biomass estimated from the MIDOCs used in the regional comparisons (i.e. excluding targeted trawls and depth integrated net 1s) was higher in the East (3.11 g 1000 m<sup>-3</sup>) compared to the Central (1.93 g 1000 m<sup>-3</sup>) region. Biomass density was highly variable among trawls in both regions, ranging from 0.62 g 1000 m<sup>-3</sup> (Day, Mid Slope, Central) to 5.14 g 1000 m<sup>-3</sup> (Night, Mid Slope, East). The highest densities were recorded from the shallow targeted trawls which primarily sampled the epipelagic depth stratum on or near the shelf break, namely station T1-200m in the Central region (6.9 g 1000 m<sup>-3</sup>) and the Transit station in the East region (4.47 g 1000 m<sup>-3</sup> or 8.57 g 1000 m<sup>-3</sup> excluding the upper mesopelagic net).

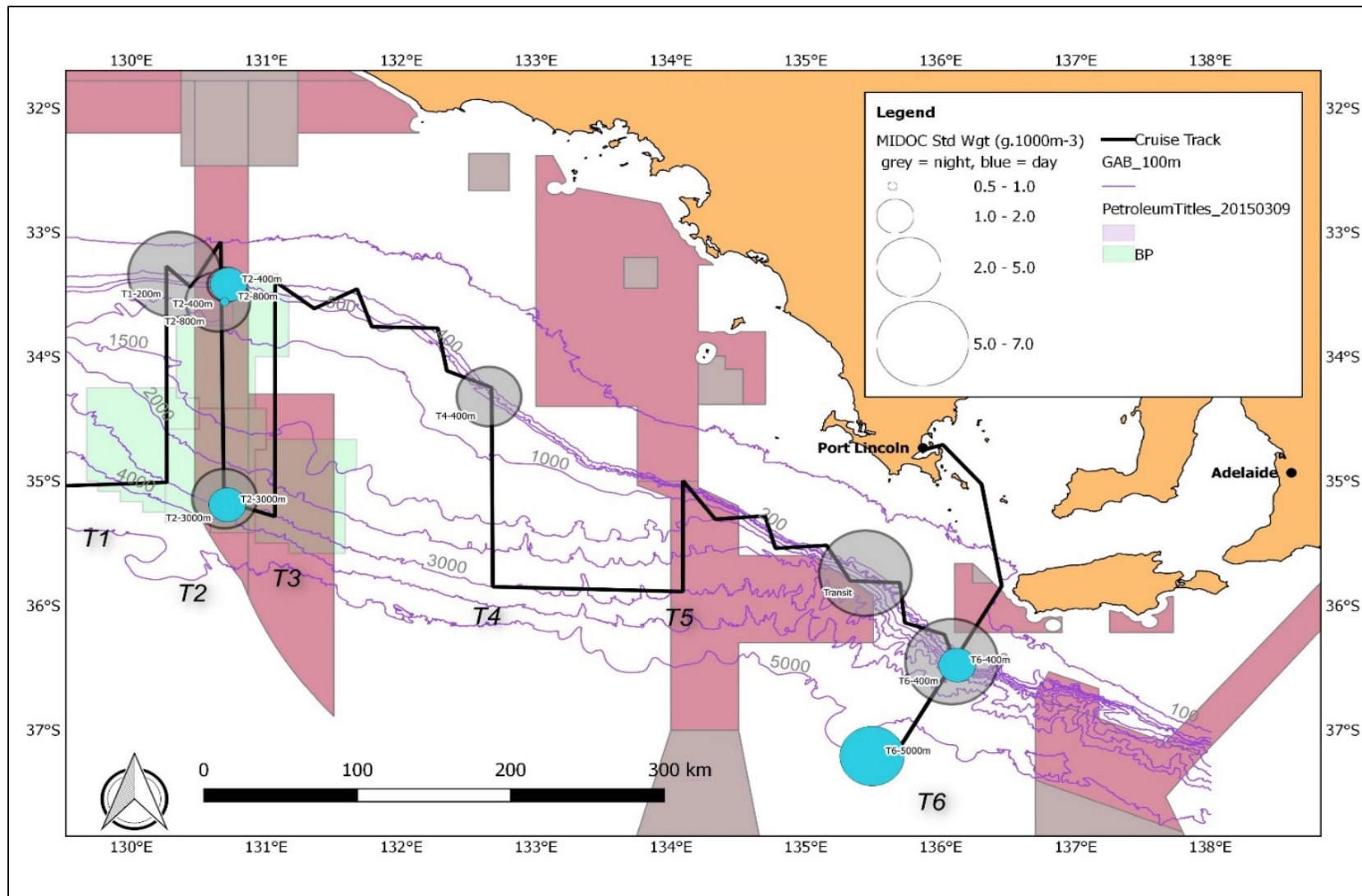


Figure 6.1-2 Shows the location and average standardised densities estimates from the 12 MIDOC trawls. Table 6.1-6 in Appendix gives the standardised density estimates for each location, trawl and depth stratum.

The total biomass for the survey was dominated by gelatinous taxa (48%), and followed by fish (collectively 27%) then crustaceans (19%). On a regional scale the Central region was dominated by gelatinous taxa (collectively 60%), and the total biomass in the East was split between fish (collectively 37%), crustaceans (33%) and gelatinous zooplankton (28% collectively) (Figure 6.1-3).

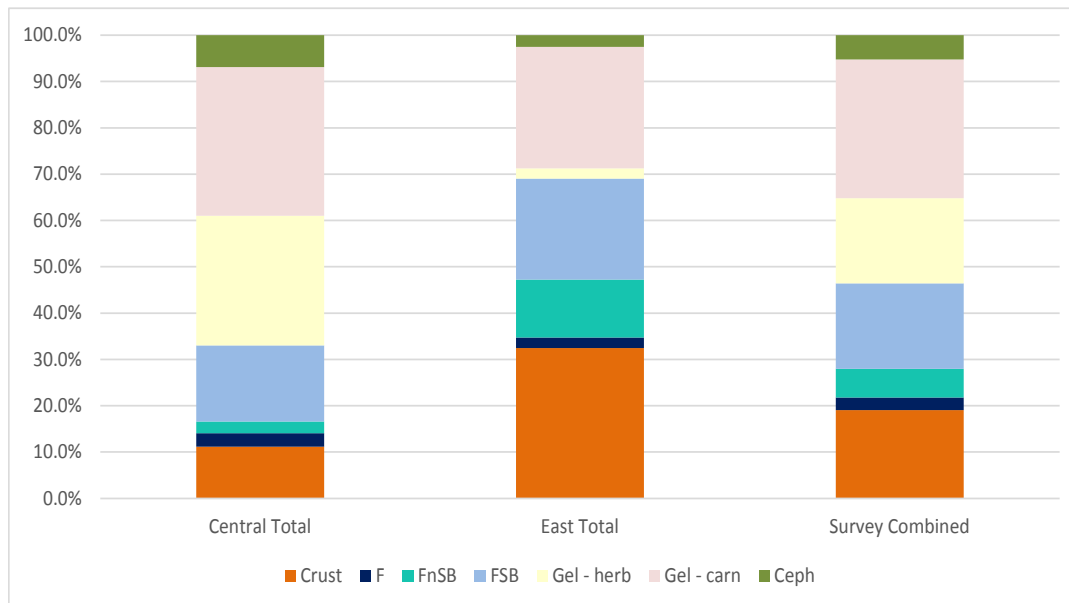


Figure 6.1-3 Proportion biomass contribution for each acoustic category for the Central and East Regions (T2 and T6 respectively) and for the Survey Combined. Note the depth integrated nets (net 1) and targeted MIDOC trawls are excluded from the results shown. Crust = crustaceans, F = fish – unknown swim bladder, FnSB = Fish with no swim bladder, FSB = Fish with swim bladder, Gel – herb = Gelatinous herbivores, Gel – carn = Gelatinous carnivores, Ceph = cephalopods

The Shelf Break / Upper Slope habitats of both the Central and East regions as sampled by the targeted MIDOC trawls were dominated by crustaceans. All other habitats in the Central region were dominated by gelatinous zooplankton, particularly for the Oceanic habitat where gelatinous zooplankton comprised 74% of the total biomass. The feeding guilds of gelatinous zooplankton in the Central region were composed of half carnivorous and half herbivorous taxa, most of herbivorous taxa were found in Oceanic habitat while the carnivorous taxa dominated the Slope. Fishes were dominant on the Slope for both regions, the second most dominant group for Central Slope, comprising between 32% and 35% of the biomass and the most dominant group in the East comprising 48% of biomass. The east region Oceanic habitat was dominated by gelatinous zooplankton which comprised 52% of the biomass and these were principally carnivorous taxa. Crustaceans comprised a relatively large portion of the biomass for both the Oceanic (40%) and the Mid Slope (30%) habitats of the East region.

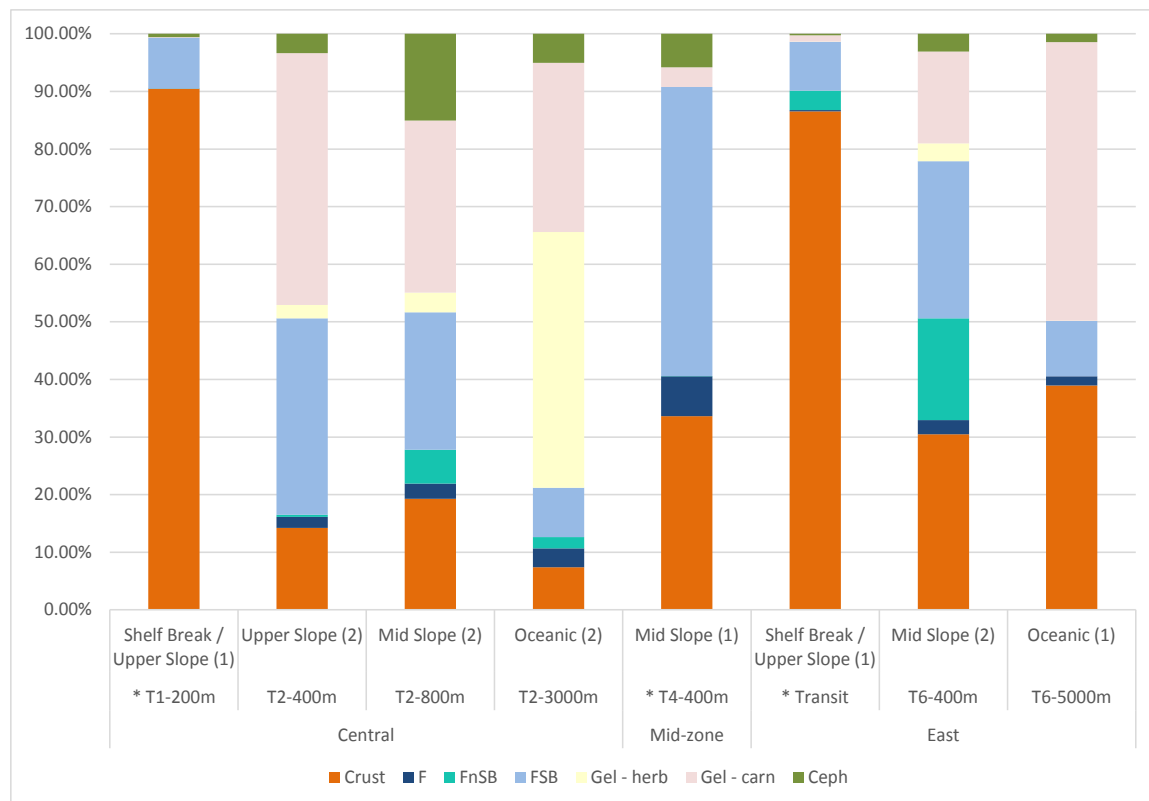


Figure 6.1-4 Proportion biomass contribution of each acoustic category for all the MIDOC trawls of the GAB Survey by Habitats (Shelf Break, Upper Slope, Mid Slope and Oceanic) sampled in each region (Central, Mid Zone and East). Depth integrated nets (net 1) are excluded. \* indicates targeted MIDOC trawls, number in brackets refers to the number of trawls conducted i.e. day and night trawls. Crust = crustaceans, F = fish – unknown swim bladder, FnSB = Fish with no swim bladder, FSB = Fish with swim bladder, Gel – herb = Gelatinous herbivores, Gel – carn = Gelatinous carnivores, Ceph = cephalopods.

A total of 319 taxa were identified at-sea from all trawls. Taxon richness by acoustic categories is listed in Table 6.1-2. Collectively, fishes dominated the catch richness at all sites and crustaceans were the second most taxon rich group. Cephalopod richness exceeded that of gelatinous zooplankton at all sites with the exception of the daytime sample in the Central area where a relatively high diversity of gelatinous taxa were recorded.

Table 6.1-2 Total micronekton taxon richness for the Central and East Regions by acoustic category. (Including data from T1, T2, T6 and Transit stations)

	Central (T1, T2)				Central (T2)			East (T6, Transit)			East (T6)			Survey
	Nos of trawls / habitat				Nos of trawls / time			Nos of trawls / habitat			Nos of trawls / time			Nos of trawls
	1	2	2	2	3	3	6	1	2	1	2	1	3	11
Taxa Group – Acoustic Category	Shelf break	Upper Shelf	Mid Shelf	Oceanic	Day	Night	Total	Shelf Break	Mid Shelf	Oceanic	Day	Night	Total	GAB
Cephalopod	5	18	18	16	15	33	36	11	20	18	26	12	30	53
Crustacean	4	24	34	36	41	37	60	9	31	16	32	18	39	73
Fish - with swimbladder	1	9	31	31	28	42	44	16	25	14	26	21	32	53
Fish - without swimbladder	2	3	10	9	8	12	15	4	6		1	6	6	19
Fish - with unknown swim bladder	9	14	18	33	18	42	49	17	26	21	31	18	40	78
Gelatinous - carnivore	3	8	14	11	16	12	20	6	7	8	10	3	12	28
Gelatinous - herbivore	1	4	7	4	7	4	7	4	4	2	5	1	5	12
Other - worm or pteropod			2			2	2		1			1	1	3
<b>All taxa</b>	<b>25</b>	<b>80</b>	<b>134</b>	<b>140</b>	<b>133</b>	<b>184</b>	<b>233</b>	<b>67</b>	<b>120</b>	<b>79</b>	<b>131</b>	<b>80</b>	<b>165</b>	<b>319</b>

There was no significant difference in diversity and evenness between central and east (Mann-Whitney,  $p > 0.05$ ) (Figure 6.1-5). Further, within areas, there was no significant difference between inshore and offshore stations. For the whole micronekton community, rank-dominance plots indicate that, in general, species distributions were typified by moderately strong dominance and a long tail of rare species (Figure 6.1-6).

Among the fishes only, there were also no significant differences in diversity and evenness between regions or stations within a region.

## Micronekton

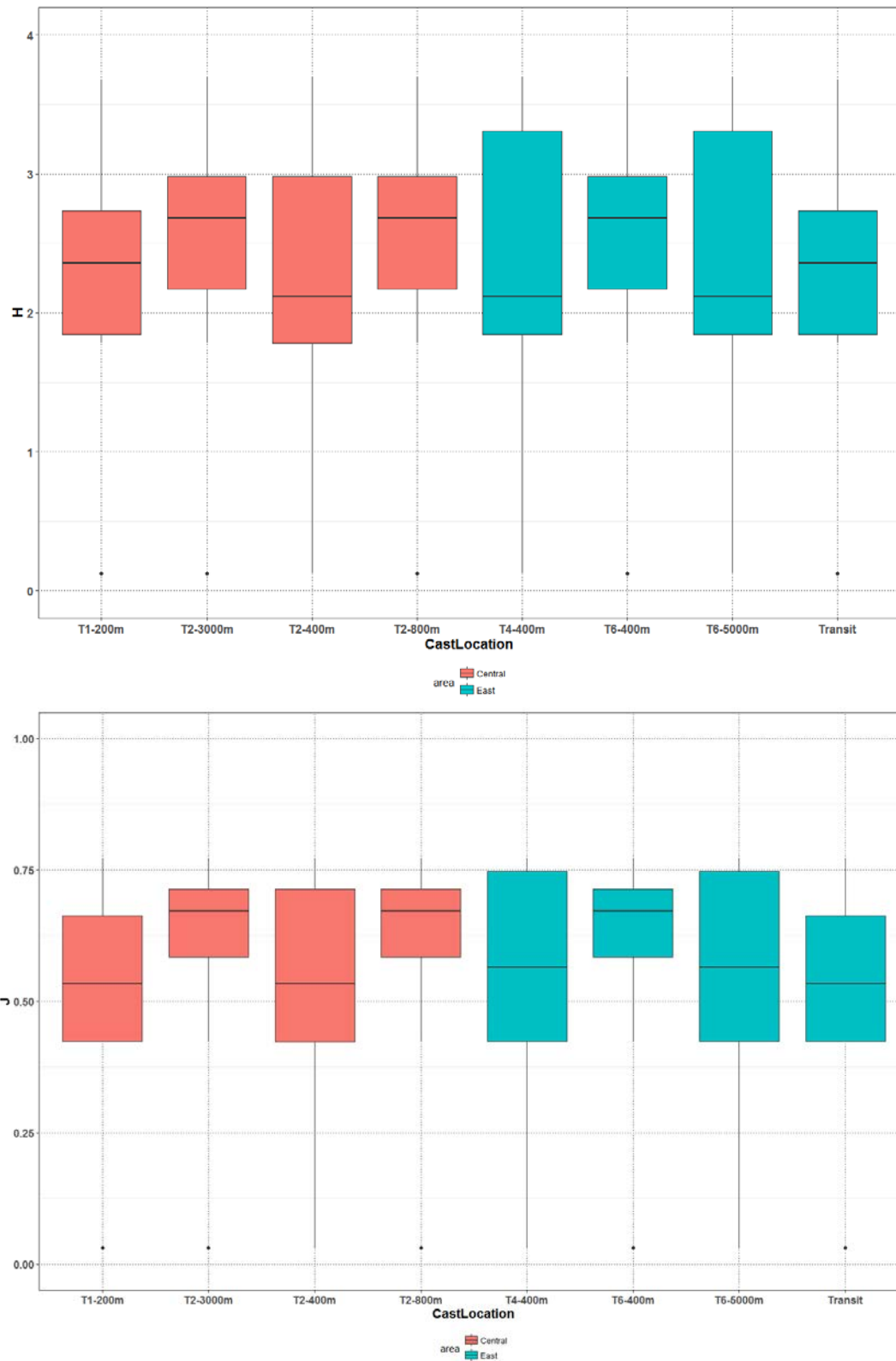


Figure 6.1-5 Shannon's diversity (top) and Pielou's evenness (bottom) for the whole micronekton community



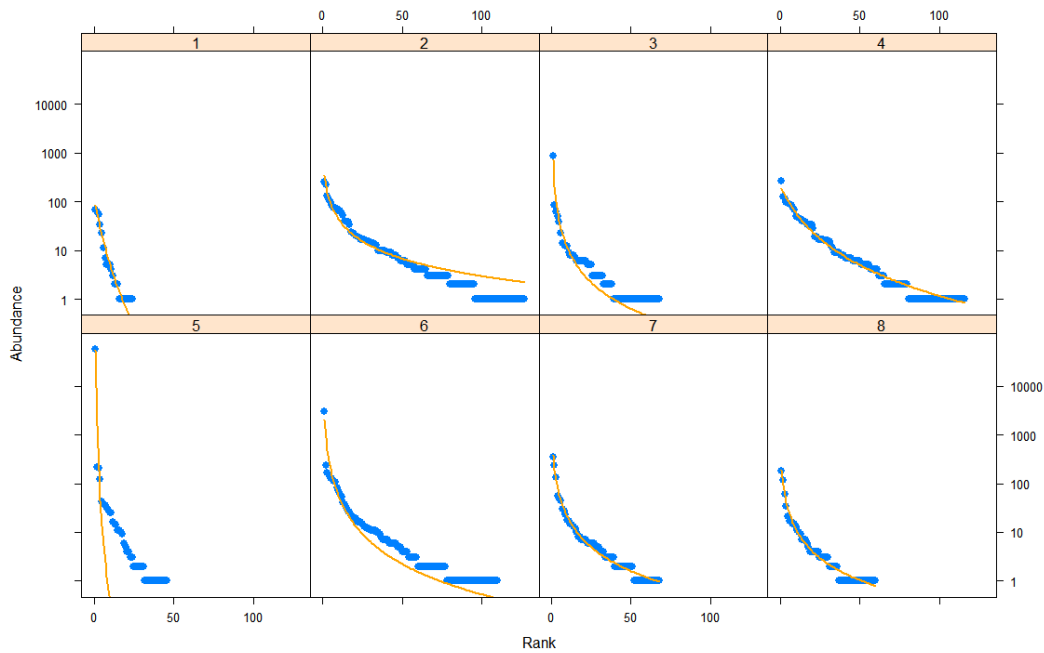


Figure 6.1-6 Whittaker plot of rank dominance (x-axis) by log abundance (y-axis). Graph panels labelled 1-8 in same order of stations listed from left to right in Figure 1.1. Line = Zipf-Mandelbrot model estimate that provides best model fit for distributions with strong dominance and long tail of rare species.

Cluster analysis indicated differences in the micronekton community composition between the East and Central regions (ANOSIM,  $R=0.29$ ,  $p=0.001$ ). Samples from the two regions formed separate but diffuse clusters (Figure 6.1-7). SIMPER analysis indicated that the key species abundances contributing to the differences between Central and East regions were the fish, *Maurolicus australis*, that was prevalent in the Central region and krill, *Nematoscelis megalops*, *Nyctiphanes australis* and *Euphausia similis*, that were recorded in relatively high abundance in the East.

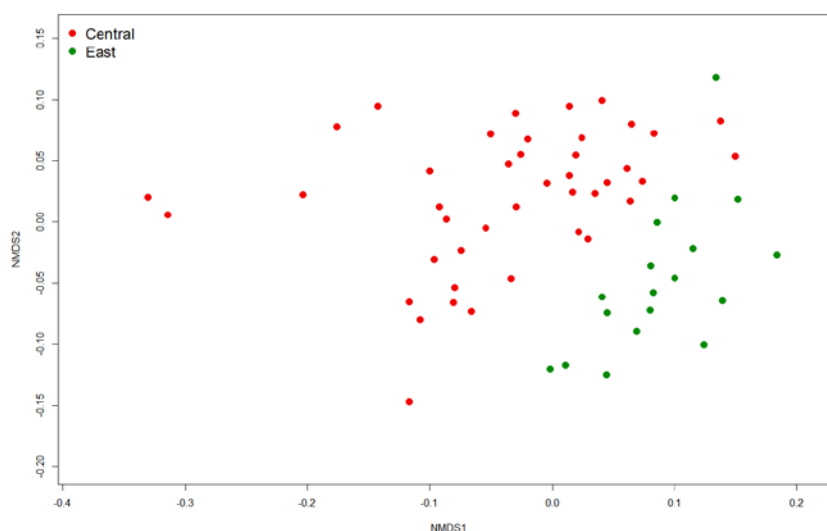


Figure 6.1-7 nMDS of MIDOC samples in Central and East regions, based on micronekton abundance (square-root transformed data, Bray-Curtis dissimilarity). Analysis omits stations T4-400 m and Transit.

Examination of the cumulative percentage biomass contribution of the top 10 most dominant species (Table 6.1-3 and Table 6.1-4) revealed further key distinctions between regions and habitats. In the Central region, gelatinous zooplankton were dominant in all three habitats. For the Slope habitat the gelatinous biomass was comprised of undifferentiated jelly medusae while the Oceanic

habitat it was the pelagic tunicate, *Pyrostremma spinosum*. The Upper Slope habitat in the Central region was characterised by relatively high dominance of *Maurolicus muelleri*, *Euphausia similis* and *Symbolophorus barnardi*. While the Mid-Slope habitat of the Central region was characterised by relatively low biomass with no obvious dominants. By contrast, in the East region gelatinous zooplankton were dominant only in the Oceanic habitat and the Upper Slope was characterised by dominance of *Xenodermichthys copei* and the krill species *Euphausia similis* and *Nyctiphanes australis*.

Among the krill communities, *Nyctiphanes australis* and *Euphausia similis* dominated the Slope habitats while *Nematoscelis megalops* dominated the Oceanic habitats (East only). Krill catches in the Central region were relatively low with the exception of a very large catch of *N. australis* (14.4 mm TL) on the Shelf Break/Upper Slope (T1-200 m). *E. similis* (21.4 mm TL) was the dominant krill species for the Central region Slope community, while in the East region the Slope community was dominated by both *E. similis* (21.5 mm TL) and *N. australis* (15 mm TL). This could indicate a size-dominance difference in the Slope krill community between Central and East regions. The oceanic habitat in the East region was dominated by *Nematoscelis megalops* (17.7 mm TL) and again krill were not dominant in the oceanic habitat of the Central region, although *N. megalops* and *Nematobrachion flexipes* (21.8 mm TL) were present. The cardinal fish *Verilus anomalus* was ranked in the top 10 for the Upper Slope of the Central Region only. Redbait, *Emmelichthys nitidus*, ranked in the top 10 most dominant species by biomass only in the East region and all specimens were juveniles (mean = 32.7 mm SL).

Among the total combined fish community alone, family Acropomatidae (represented by one species, *Verilus anomalus*) contributed most to the total standardised biomass at the Shelf-Break in the Central region (T1-200 m) and the Mid Zone (T4-400 m) (Figure 6.1-8). The dominance of *V. anomalus* in trawls in Shelf-Break and Upper Slope habitats confirms the known habitat preference and distribution of this species across southern Australia. Only three *V. anomalus* were captured in the East: one in the targeted Transit trawl in water depth between 250-560 m that missed the observed acoustic targets; and two at T6-400 m, which despite its name, was in water depth of 841 m.

The family Phosichthyidae (lightfishes) contributed significantly to total biomass in deeper offshore stations in the Central and East regions (see Figure 6.1-8). Sternoptychidae (hatchfishes and pearlsides) contributed significantly to total biomass in the Central region. In this family, there was again a distinction between offshore and slope/shelf break species, with *Maurolicus australis* the dominant species inshore while offshore, *Argyropelecus gigas*, *A. hemigymnus*, *Sternoptyx pseudodiaphana* and *Polyipnus* spp. were dominant. Further commentary on distribution patterns of key groups and species is provided below.

Table 6.1-3 Cumulative biomass contributions of the 10 most dominant micronekton species, listed in order of rank standardised biomass contribution by habitats for the Central region. Data shown are averages for the depth stratified nets only (excluding depth integrated net 1).

Habitat	Location (nos of nets)	taxon	Ave. Biomass: occurrence (g.1000 m <sup>-3</sup> )	Occurrence (nos of nets)	Ave. Biomass: weighted by all nets (g.1000 m <sup>-3</sup> )	Cumulative Biomass (g.1000 m <sup>-3</sup> )	Cumulative % Biomass
Upper Slope	T2-400m (10)	Gelatinous zooplankton - undifferentiated	0.92	7	0.64	0.64	43 %
		<i>Maurolicus australis</i>	0.28	10	0.28	0.93	61 %
		<i>Euphausia similis</i>	0.42	5	0.21	1.14	75 %
		<i>Symbolophorus barnardi</i>	0.51	3	0.15	1.29	85 %
		<i>Verilus anomalus</i>	0.19	2	0.04	1.32	88 %
		<i>Soestia zonaria</i>	0.08	3	0.03	1.35	89 %
		Sepiidae - undifferentiated	0.15	1	0.02	1.37	90 %
		<i>Iridoteuthis sp. 1</i>	0.02	8	0.01	1.38	91 %
		<i>Polyipnus tridentifer</i>	0.02	5	0.01	1.39	92 %
		<i>Lampanyctodes hectoris</i>	0.05	2	0.01	1.40	93 %
Mid Slope	T2-800m (10)	<i>Histioteuthis macrohista</i>	2.03	1	0.20	0.20	14 %
		Gelatinous zooplankton - undifferentiated	0.19	10	0.19	0.39	26 %
		<i>Lampanyctus spp.</i>	0.21	4	0.08	0.47	32 %
		<i>Euphausia spp.</i>	0.77	1	0.08	0.55	37 %
		<i>Praya sp.</i>	0.25	3	0.08	0.63	42 %
		<i>Phosichthys argenteus</i>	0.24	3	0.07	0.70	47 %
		<i>Gennadas sp. 2</i>	0.12	6	0.07	0.77	52 %
		<i>Pasiphaea sp. 1</i>	0.17	4	0.07	0.84	56 %
		<i>Symbolophorus barnardi</i>	0.15	4	0.06	0.90	60 %
		<i>Gennadas sp. 1</i>	0.11	4	0.05	0.94	63 %
Oceanic	T2-3000m (10)	<i>Pyrostremma spinosum</i>	5.45	2	1.09	1.09	38 %
		Gelatinous zooplankton - undifferentiated	0.43	7	0.58	1.67	58 %
		Order Siphonophora - undifferentiated	0.47	4	0.19	1.86	65 %
		<i>Phronima sp. 1</i>	0.11	9	0.10	1.96	69 %
		<i>Teuthowenia pellucida</i>	0.22	3	0.07	2.03	71 %
		Class Hydrozoa - undifferentiated	0.20	3	0.06	2.09	73 %
		<i>Thetys vagina</i>	0.28	2	0.06	2.14	75 %
		Salpidae - undifferentiated	0.09	5	0.05	2.19	77 %
		<i>Praya sp.</i>	0.44	1	0.04	2.23	78 %
		<i>Ceratoscopelus warmingii</i>	0.21	2	0.04	2.27	80 %

## Micronekton

**Table 6.1-4** Cumulative biomass contributions of the 10 most dominant micronekton species, listed in order of rank standardised biomass contribution by habitats for the East region. Depth stratified samples only (excluding depth integrated net 1).

Habitat	Location (nos of nets)	taxon	Ave. Biomass: occurrence (g.1000 m <sup>-3</sup> )	Occurrence (nos of nets)	Ave. Biomass: weighted by all nets (g.1000 m <sup>-3</sup> )	Cumulative Biomass (g.1000 m <sup>-3</sup> )	Cumulative % Biomass
Mid Slope	<b>T6-400m (10)</b>	<i>Xenodermichthys copei</i>	1.27	5	0.63	0.63	18 %
		<i>Nyctiphanes australis</i>	2.04	3	0.61	1.25	36 %
		<i>Euphausia similis</i>	1.93	3	0.58	1.82	52 %
		<i>Phosichthys argenteus</i>	0.49	7	0.34	2.16	62 %
		<i>Symbolophorus barnardi</i>	0.78	4	0.31	2.47	71 %
		Gelatinous zooplankton - undifferentiated	0.45	6	0.27	2.74	79 %
		Penaeoidea & Caridea - undifferentiated	0.19	4	0.08	2.82	81 %
		<i>Maurolicus australis</i>	0.13	5	0.07	2.89	83 %
		<i>Histioteuthis macrohista</i>	0.31	2	0.06	2.95	84 %
		<i>Emmelichthys nitidus</i>	0.13	4	0.05	3.00	86 %
Oceanic	<b>T6- 5000m (5)</b>	Gelatinous zooplankton - undifferentiated	1.74	3	1.05	1.05	38 %
		<i>Nematoscelis megalops</i>	0.63	5	0.63	1.68	61 %
		Order Siphonophora - undifferentiated	1.03	2	0.41	2.09	76 %
		<i>Praya sp.</i>	0.38	2	0.15	2.24	81 %
		<i>Maurolicus spp.</i>	0.11	5	0.11	2.35	85 %
		<i>Phosichthys argenteus</i>	0.16	3	0.10	2.45	89 %
		<i>Emmelichthys nitidus</i>	0.20	2	0.08	2.53	92 %
		Pronoidae - undifferentiated	0.12	2	0.05	2.57	93 %
		<i>Lycoteuthis sp.</i>	0.08	1	0.02	2.59	94 %
		"Superclass" Pisces - undifferentiated larvae	0.02	3	0.01	2.60	94 %

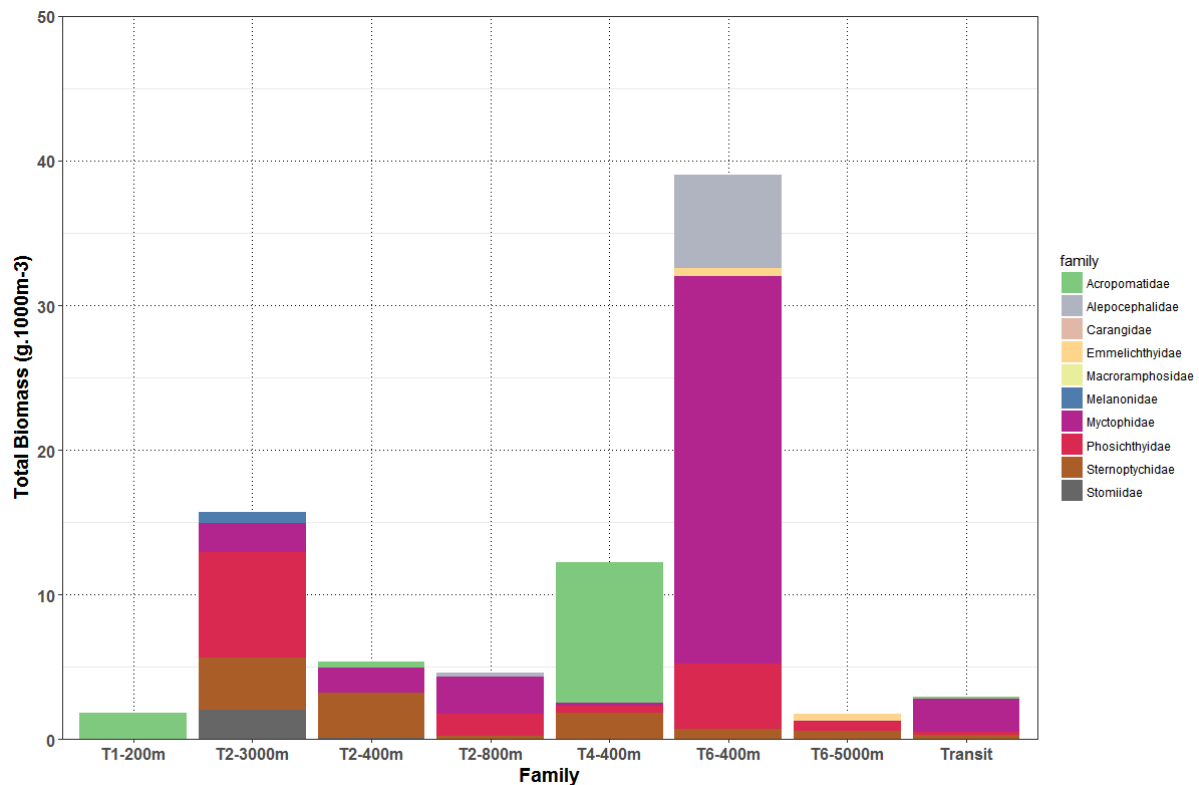


Figure 6.1-8 Contribution of fish families to the total overall fish catch from all trawls at each station, limited to the top 5 families represented at each station.

#### Vertical distributions: total micronekton community

For all habitats total micronekton biomass was highest in the epipelagic stratum (0-200 m) at night (Figure 6.1-9). For the Central Oceanic habitat (T2-3000 m) the high night-time epipelagic biomass resulted principally from relatively large catches of the pelagic tunicate, *Pyrostremma spinosum* and the lightfish, *Phosichthys argenteus*. For the Central Mid Slope (T2-800 m) there was no single dominant species that contributed to the relatively high night-time epipelagic biomass but rather this stratum was characterised by a high diversity of fishes, cephalopods and crustaceans, with the highest biomass contribution from a small number of squid, *Histioteuthis macrohista*.

The East Oceanic habitat (T6-5000 m) was only sampled during the day; gelatinous zooplankton and krill, *Nematoscelis megalops*, dominated the epipelagic biomass. At the East Mid Slope station (T6-400m), the high night time epipelagic biomass was contributed primarily by a large catch of krill, *E. similis* and *N. australis* with secondary contribution from the lanternfish, *Symbolophorus barnardi*. At this station, the slickhead, *Xenodermichthys copei*, dominated night time biomass in the upper mesopelagic stratum, while gelatinous zooplankton dominated the biomass in the lower mesopelagic stratum.

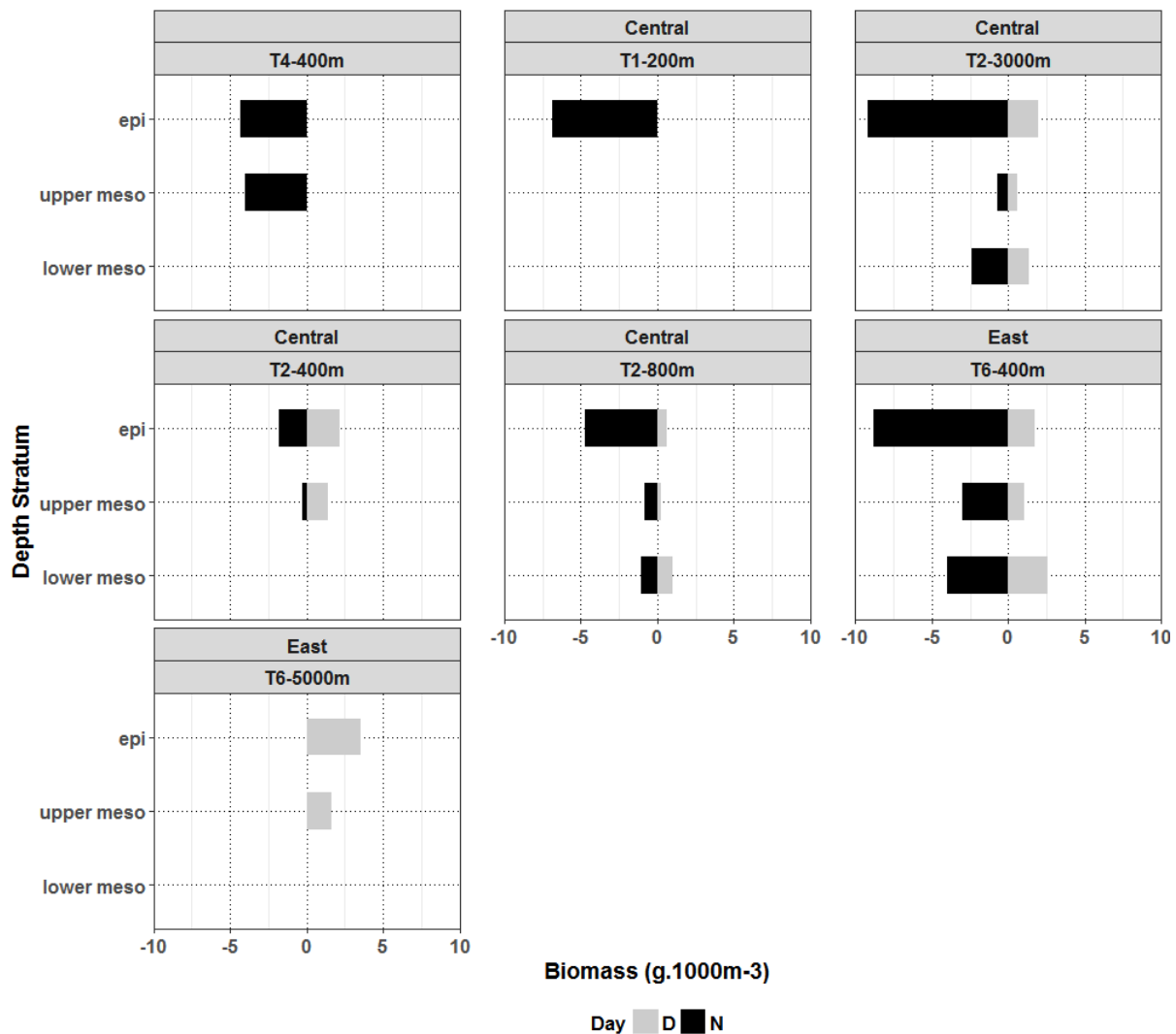


Figure 6.1-9 Distribution of total micronekton biomass in depth strata from Central region (top row) and East region (bottom row).

There is evidence of vertical migration for the crustaceans (comprised predominantly of krill, mentioned above) for both mid-slope stations and the oceanic station of the east. In contrast, for the central oceanic station, the crustaceans were dominant in the lower mesopelagic stratum with the highest contribution from, *Phronima sp. 1*, an amphipod that carves a shelter out of gelatinous organisms. Swimbladder fish (FSB), which are known vertical migrators, contributed proportionally more to biomass in the deeper strata during the day than to the shallower strata at night. The vertical pattern for the gelatinous taxa is less clear, although the herbivorous taxa like salps and pyrosomes were not present in the lower mesopelagic stratum. This is in contrast to the carnivorous taxa like medusae, ctenophores and siphonophres which comprised between 20% and 80% the total biomass in mesopelagic strata (Figure 6.1-10).

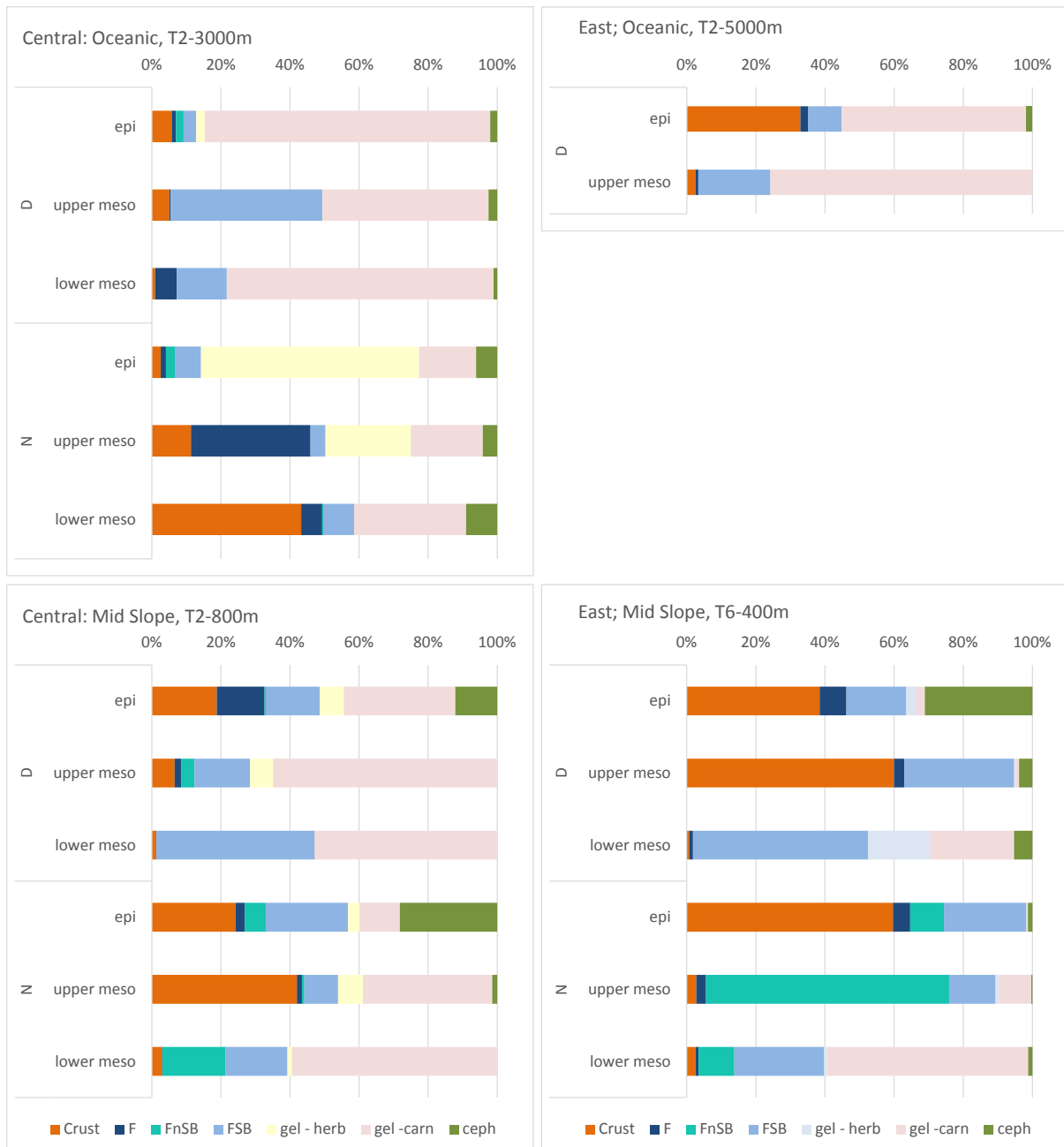


Figure 6.1-10 Day and Night vertical distribution for the Central and East region by the Oceanic and Mid Slope habitats.



*Distributions of key species*

Vertical distribution characteristics of species that contribute highly to total biomass, that are represented in catches from the Central and East regions, and that were selected for stable isotopes analysis (Section 6.2) are described here.

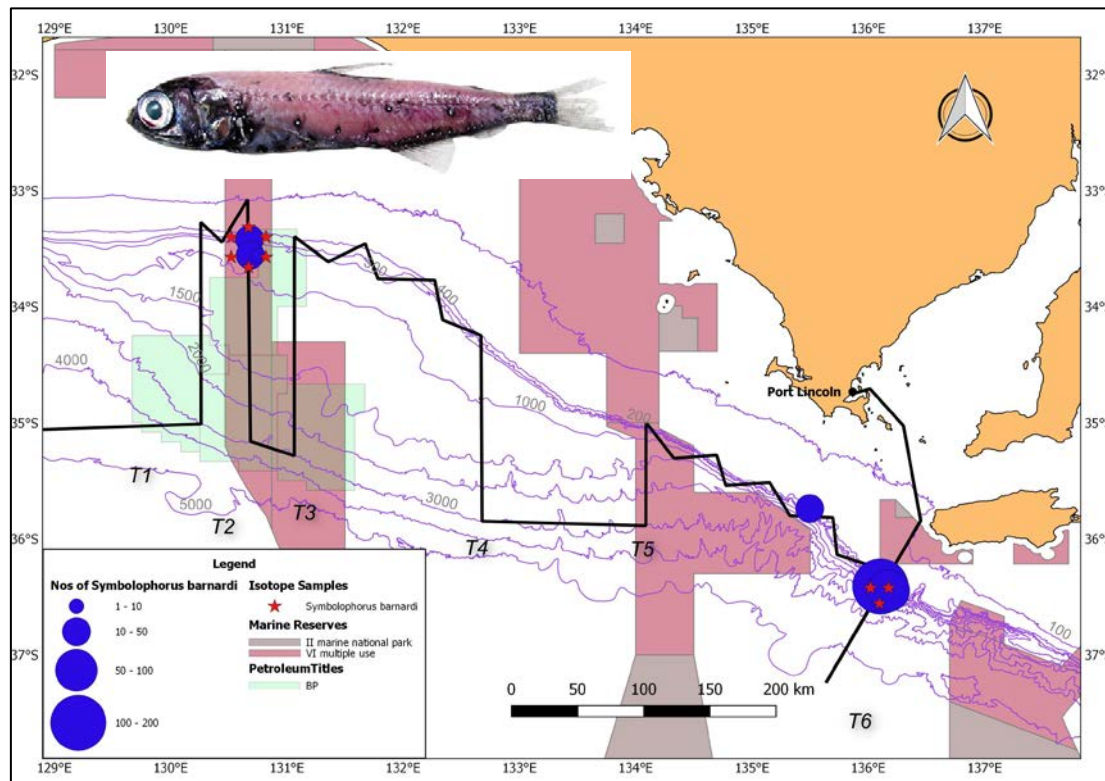
*Symbolophorus barnardi*

Figure 6.1-11 IN2015\_C02 MIDOC catch distribution for *Symbolophorus barnardi* (number of fish)

*Symbolophorus barnardi* is one of the larger bodied lanternfishes in the micronekton community of the GAB. In the Tasman Sea, the species is characterised as a “moderate to strong” migrator, occurring from 500-1000 m during the day and migrating to 0-100 m at night (Williams et al., 2001; Flynn and Pogonoski, 2012). Over the mid-slope off southern Tasmania, this species ranked third highest to total micronekton biomass contributions (Williams et al., 2001). In the GAB, the species was only recorded from Slope stations where the night time biomass of this species was highest in the epi-pelagic stratum (Figure 6.1-12). The species was not recorded from the Oceanic stations or the Day station in the Central region and in relatively low densities in the meso-pelagic stratum on the Slope in the East Region. Apparently the trawls did not sample the deep daytime residence depths of this species. This result suggests that there is significant vertical migration of this species and, importantly, offshore (deep daytime) to onshore (shallow night-time) diel movements.

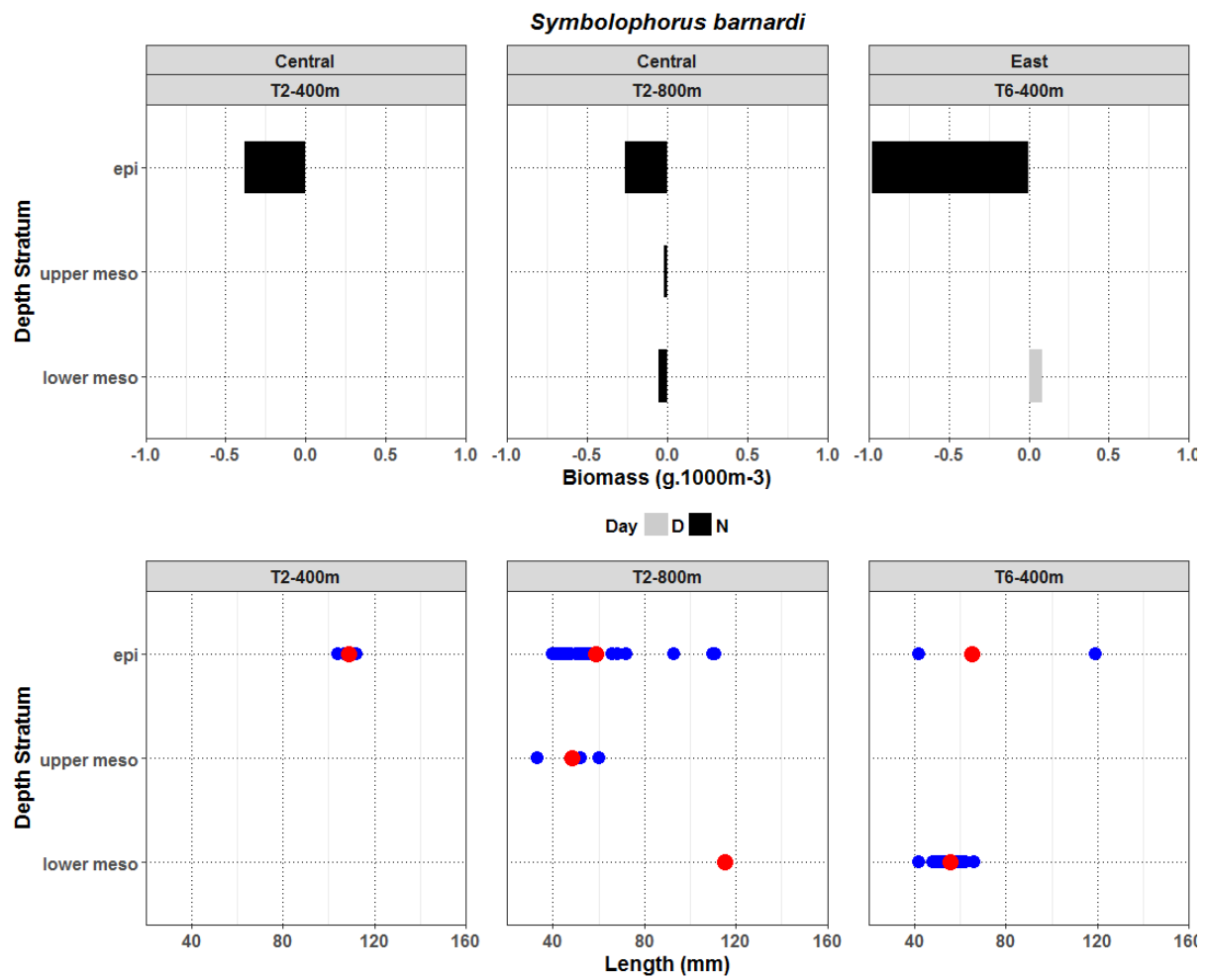


Figure 6.1-12 Distribution of *Symbolophorus barnardi* biomass in depth strata from Central and East regions (top row) and standard length range (blue dots) and mean (red dots) (bottom row).

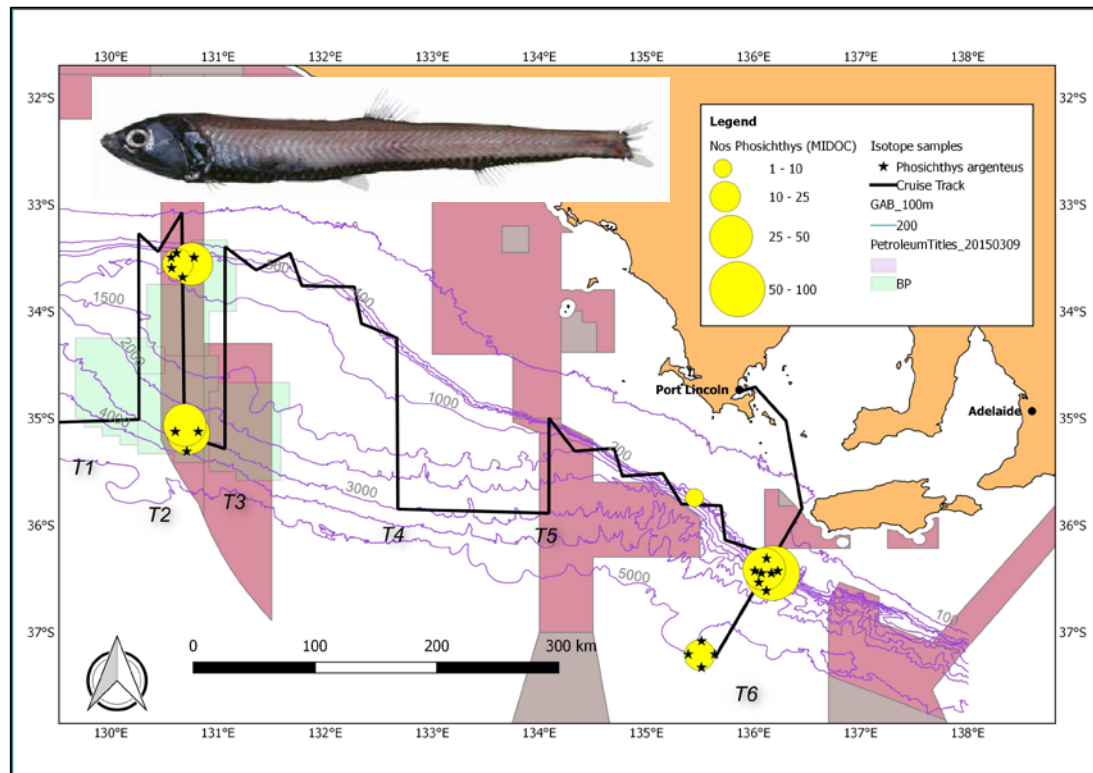
*Phosichthys argenteus*

Figure 6.1-13 IN2015\_C02 MIDOC catch distribution for *Phosichthys argenteus* (number of fish)

The silver lightfish, *Phosichthys argenteus* is another of the larger bodied member micronekton community of the GAB. The species is recorded from a depth range of 50 - 800 m in the Tasman Sea. It is the most dominant fish in terms of biomass in the micronekton community of the mid-slope off southern Tasmania (Williams et al., 2001) and the sixth most dominant fish off the West Coast of Tasmania (CSIRO unpublished data). Individuals in the 35-230 mm standard length (SL) size range were recorded from depth stratified nets in the GAB (Figure 6.1-14) and larger individuals to 360 mm SL range were recorded from the vertically integrated net (not included in Figure 6.1-14). Largest biomass of this species was recorded in the East region at the shelf-break where daytime and night time biomass was highest in the lower mesopelagic stratum. This is in agreement with Williams et al. (2001) who categorised this species as a lower mesopelagic non-migrator. In general, deeper strata recorded larger specimens.

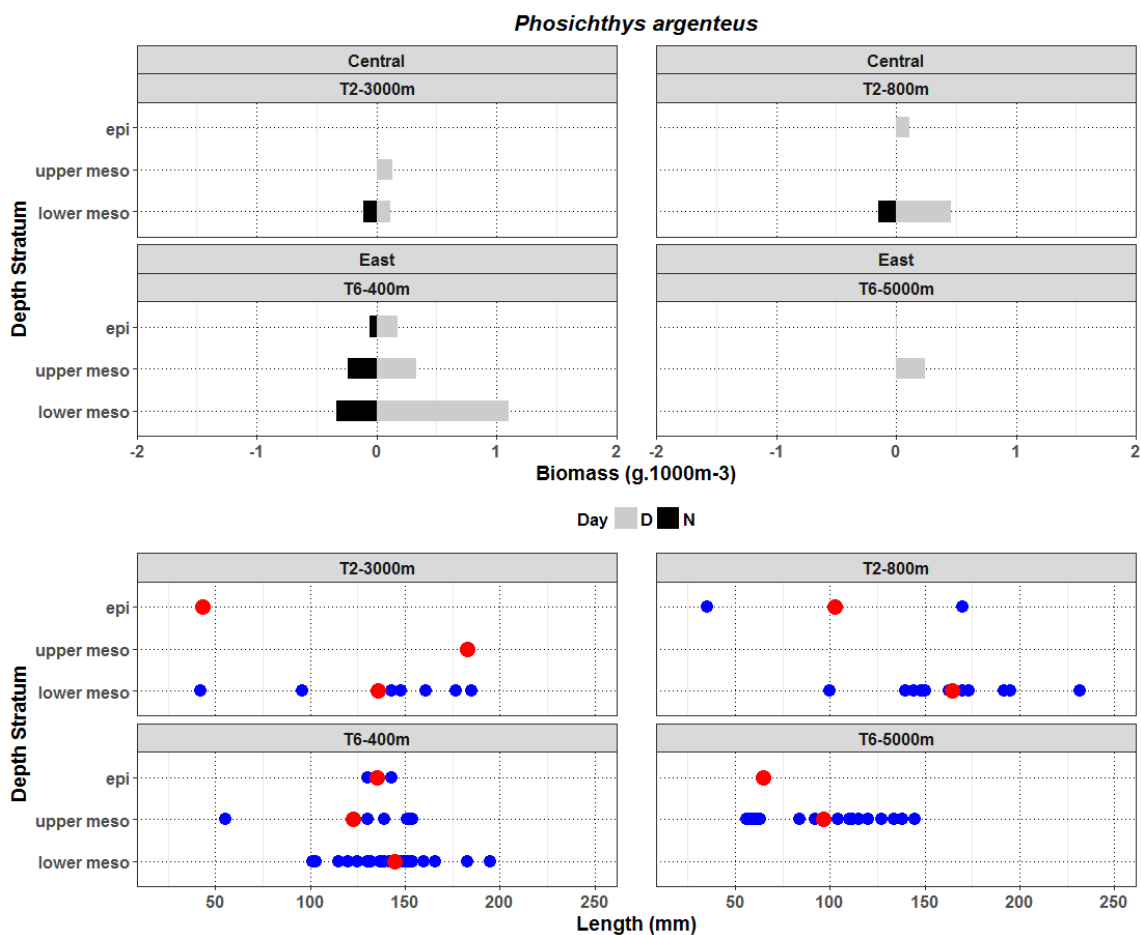


Figure 6.1-14 Distribution of *Phosichthys argenteus* biomass in depth strata from Central and East regions (top row) and standard length range (blue dots) and mean (red dots) (bottom row).

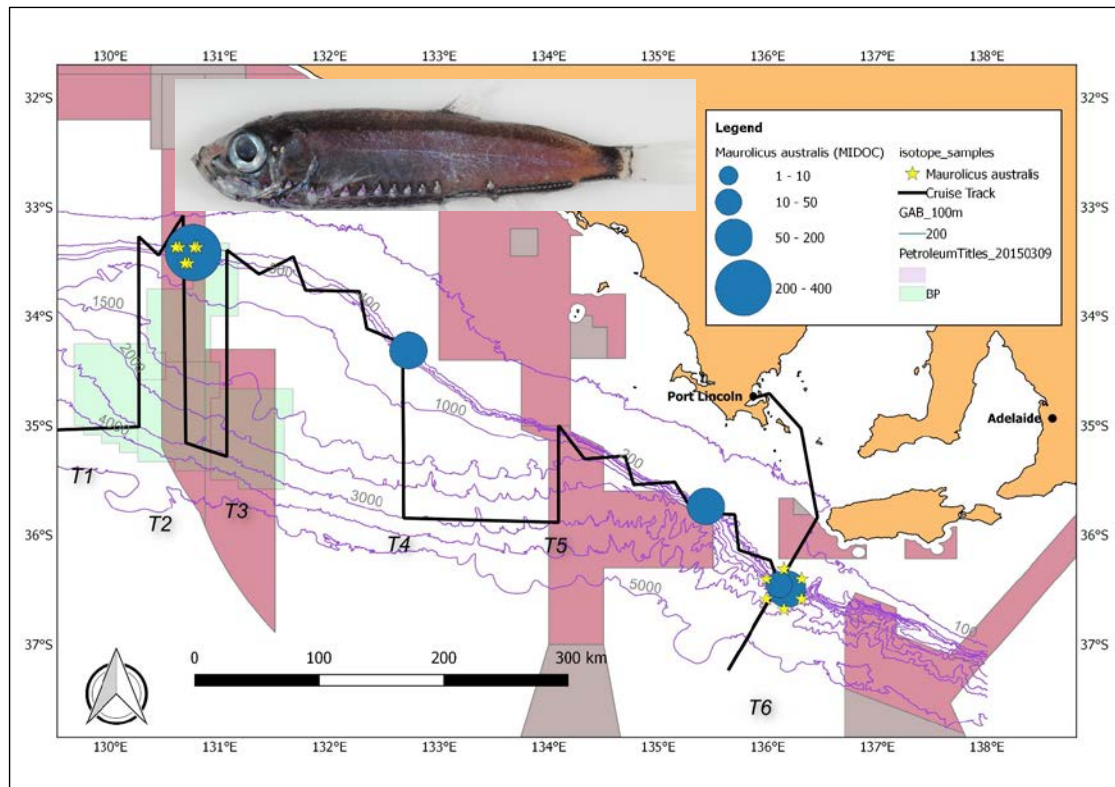
*Maurolicus australis*

Figure 6.1-15 IN2015\_C02 MIDOC catch distribution for *Maurolicus australis* (number of fish)

The pennant pearlside, *Maurolicus australis*, is a small-bodied species attaining about 5 cm length. During the 1970s - 80s, the species was the subject of investigations of NSW and Victoria to assess its fisheries potential. This species is generally prevalent in midwaters of southern and eastern Australia (Clarke, 1982) and has been reported to be one of the dominant mesopelagic fish off Western Tasmania (CSIRO unpublished data), where it was distributed throughout the water column to depths of 550 m. Most information about distributions of this species is inferred from studies on the related species *M. muelleri*. *Maurolicus muelleri* is generally considered to be most abundant at the shelf break and over the continental slope (Robertson et al., 1978; Clarke, 1982), where it can form dense schools (Kaartvedt et al., 1998). In the southern Benguela System, *M. muelleri* is considered an important food resource for commercially valuable mid-slope fish species (Armstrong and Prosch, 1991). Off southeastern Australia, *M. australis* (as *M. muelleri*) is reported to be important in the diets of jack mackerel (*Trachurus declivis*) and mirror dory (*Zenopsis nebulosus*) (Clarke, 1982). *Maurolicus muelleri* is generally considered to be a vertical migrator (Staby and Aksnes, 2011) but the extent of vertical migration is limited by the relatively shallow depths of its habitat. Off southeastern Australia, the *M. australis* (as *M. muelleri*) resides close to the seabed during the day at depths of 150-400 m (Clarke, 1982).

In the GAB, *Maurolicus australis* was recorded in relatively high abundance in trawls associated with the Upper to Mid Slope. Vertical migration from the upper mesopelagic (the limit of sampling at the stations where this species was recorded) to the epipelagic zone is evident (Figure 6.1-16). In the Central region (T2-400m), the smallest individuals were recorded in the epipelagic layer and in the East region small were relatively abundant in the epipelagic nets of the Oceanic station. Clarke (1982) observed that juveniles *M. australis* migrate to shallower strata than adults; it is possible then that small *Maurolicus* sp. we observed could in fact be juvenile *M. australis*.

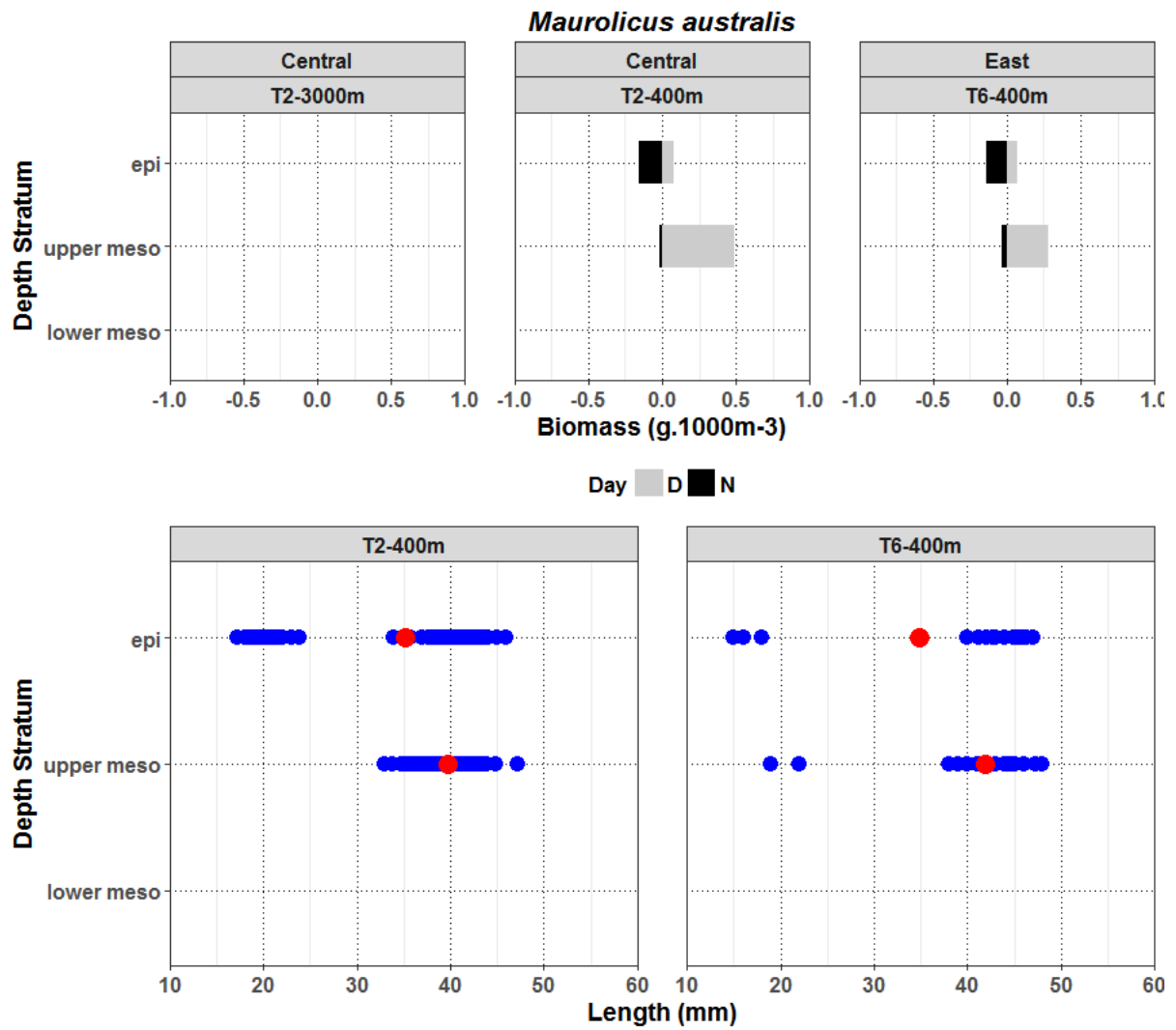


Figure 6.1-16 Distribution of *Maurolicus australis* biomass in depth strata from Central and East regions (top row) and standard length range (blue dots) and mean (red dots) (bottom row).



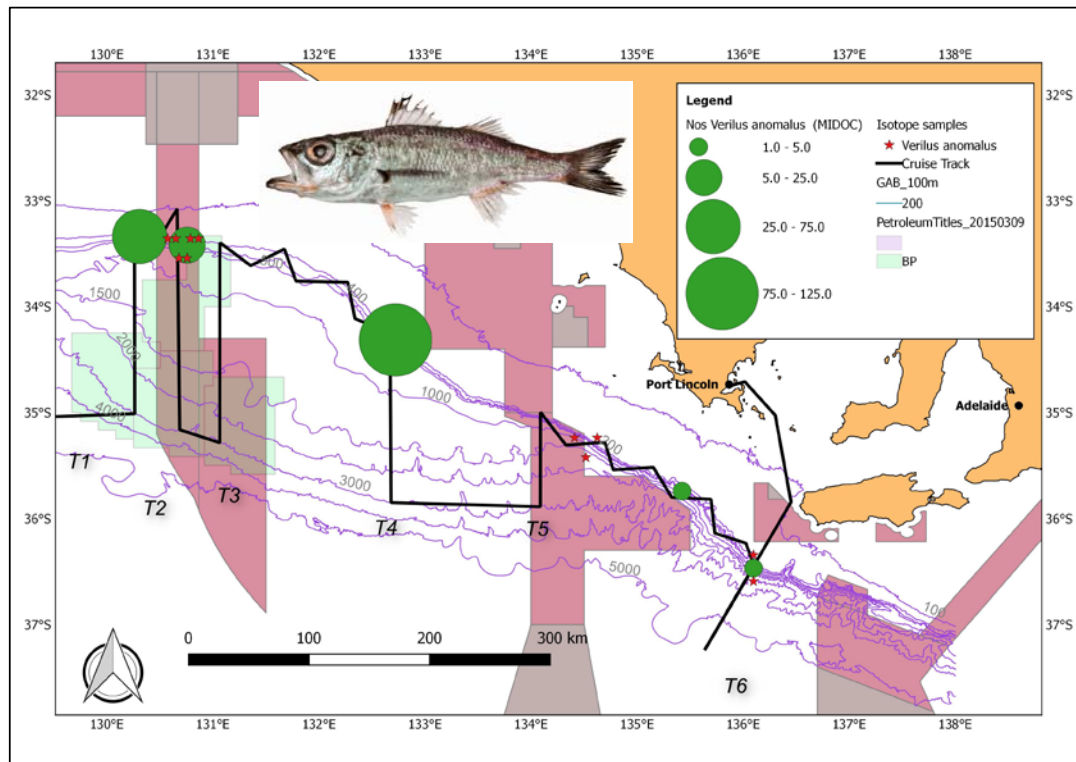
*Verilus anomalus*

Figure 6.1-17 IN2015\_C02 MIDOC catch distribution for *Verilus anomalus* (number of fish)

The threespine cardinalfish, *Verilus anomalus* (recently revised from *Apogonops anomalus*), forms aggregations on the continental shelf, shelf break and upper slope, where it is considered to represent a considerable food resource for predatory fish species (Gomon, 2008; Bulman and Blaber, 1986; Gray and Otway, 1994). It was one of the ten most dominant mesopelagic fish off West Coast Tasmania where the majority of *V. anomalus* (108 mm SL) were captured in mesopelagic stratum at night (550 m max depth) (CSIRO unpublished data). This species appears to be an important predator of the mesopelagic lanternfish fish such as the lanternfish *Lampanyctodes hectoris* in eastern Tasmania (Bulman et al., 2001) and *Diaphus danae*, *Lampanyctus australis* and *Lampanyctus procerus* in western Tasmania (CSIRO unpublished data). A similar dominance of *L. hectoris* in the diet of *Verilus anomalus* may be expected in the GAB as *L. hectoris* was recorded in moderately high abundance at the shelf break and upper slope. *V. anomalus* may also feed on *Maurolicus australis*, particularly during the day when the latter resides close to the bottom. This is supported by observations from western Tasmania (CSIRO unpublished data). Bulman et al. (2001) classified *V. anomalus* (*A. anomalus*) as a pelagic piscivore on the southeast Australian shelf, where stomach contents were dominated by “unknown fish”, “pelagic fish” and “pelagic crustacean”.

In the GAB, the species was recorded at the Shelf Break and Upper Slope stations. Catches in the GAB were predominantly made at night and nets usually integrated catches over the depths in question due to the generally shallow depths at these stations. Largest catches were recorded from the Upper Shelf at station T4-400m (Figure 6.1-18). Here, average length was greater in the portion of the population that were sampled from the upper mesopelagic zone (corresponding to near-seabed catches on the upper slope), potentially indicating that smaller fish were predominant among the vertically migrating component of the population.



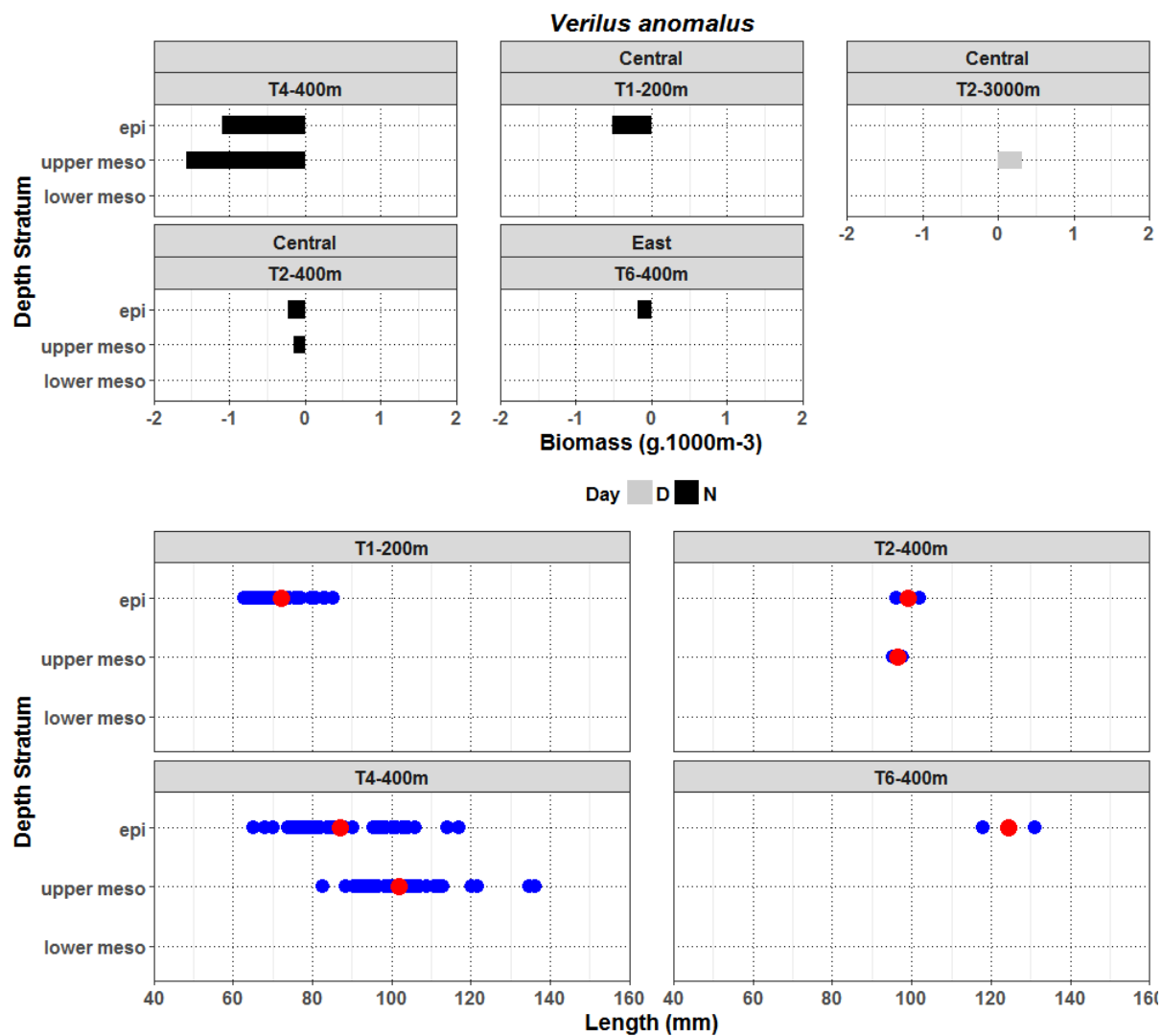


Figure 6.1-18 Distribution of *Verilus anomalus* biomass in depth strata from Central and East regions (top row) and length (standard length) range (blue dots) and mean (red dots) (bottom row).

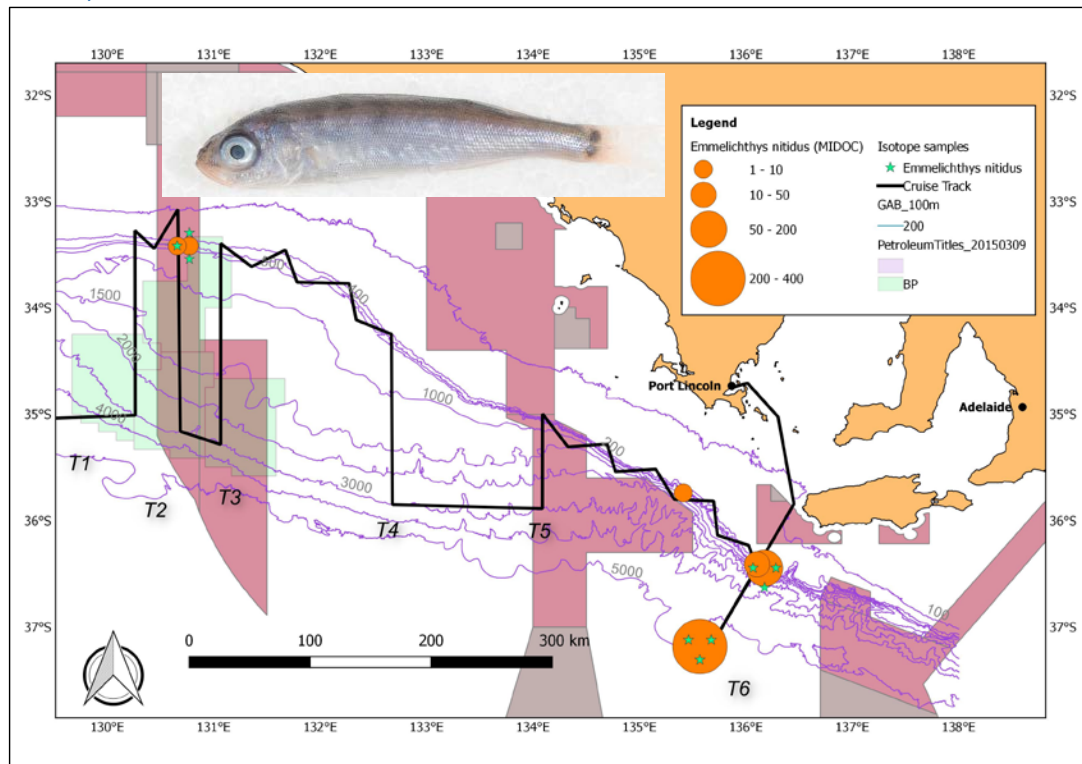
*Emmelichthys nitidus*

Figure 6.1-19 IN2015\_C02 MIDOC catch distribution for *Emmelichthys nitidus* (number of fish)

Redbait, *Emmelichthys nitidus*, is recognised as an abundant component of small pelagic fish assemblages and important in the diet of shelf populations of Southern Bluefin Tuna (SBT, *Thunnus maccoyii*) in southeastern Australia, along with jack mackerel (*Trachurus declivis*) and arrow squid (*Nototodarus gouldii*) (Young et al., 1997). Other predators in Tasmanian waters include seabirds (albatross and gannet) and Australian fur seals (Welsford and Lyle, 2003). The diet of redbait appears to be almost exclusively krill for size classes under 280 mm length while cephalopods and lanternfishes appear in the diets of individuals larger than 281 mm (Welsford and Lyle, 2003). This species dominates the catch from the small pelagic fishery off Tasmania (Welsford and Lyle, 2003). Small numbers of *E. nitidus* (180 mm) were present the epipelagic stratum of the depth stratified sampling off western Tasmania (CSIRO unpublished data). The species attains over 30 cm total length (Gomon, 2008) and all catches of this species in the present study involved juveniles less than 60 mm in standard length (Figure 6.1-20). All catches were from the epipelagic zone in the GAB.

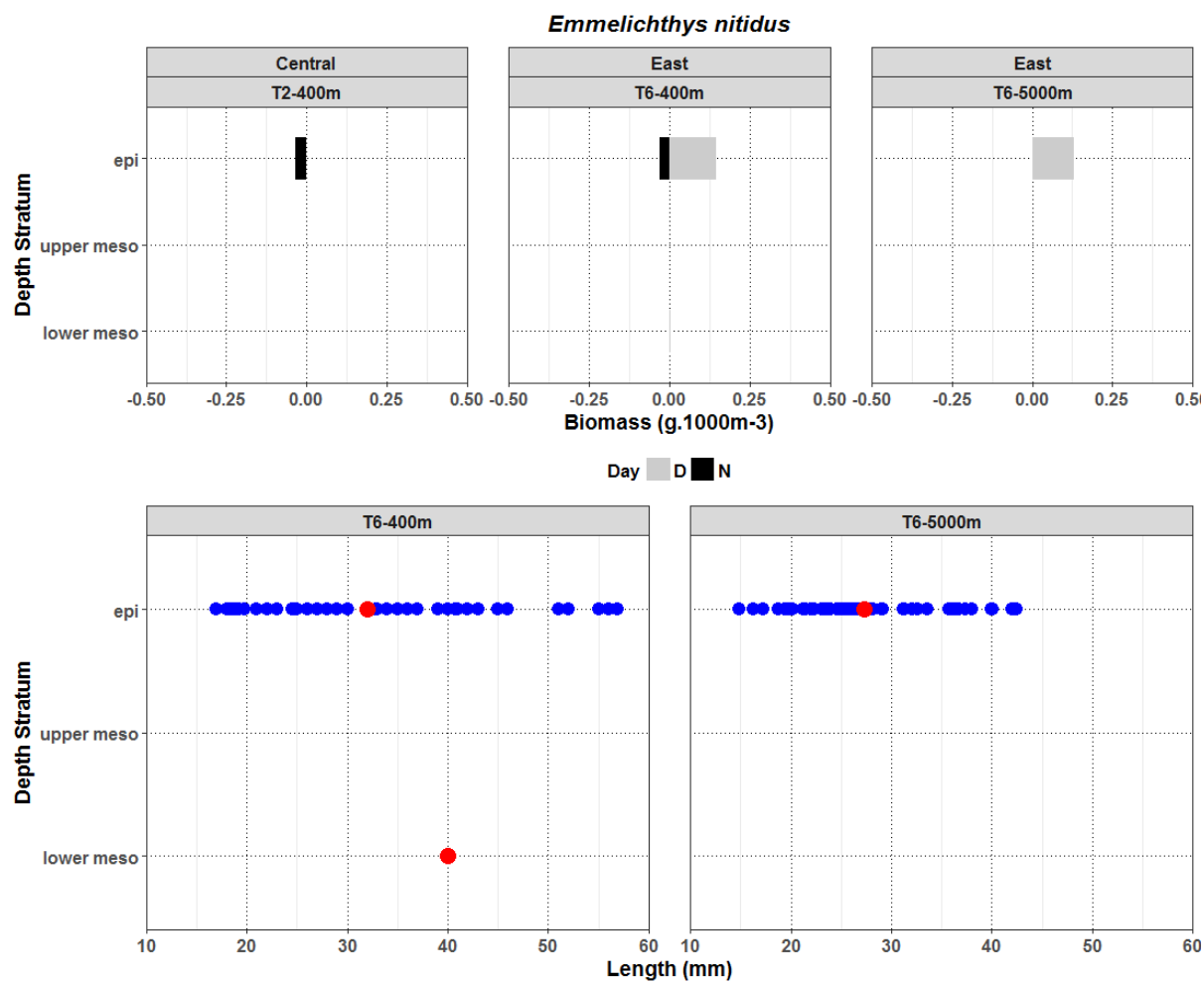


Figure 6.1-20 Distribution of *Emmelichthys nitidus* biomass in depth strata from Central and East regions (top row) and length (standard length) range (blue dots) and mean (red dots) (bottom row).

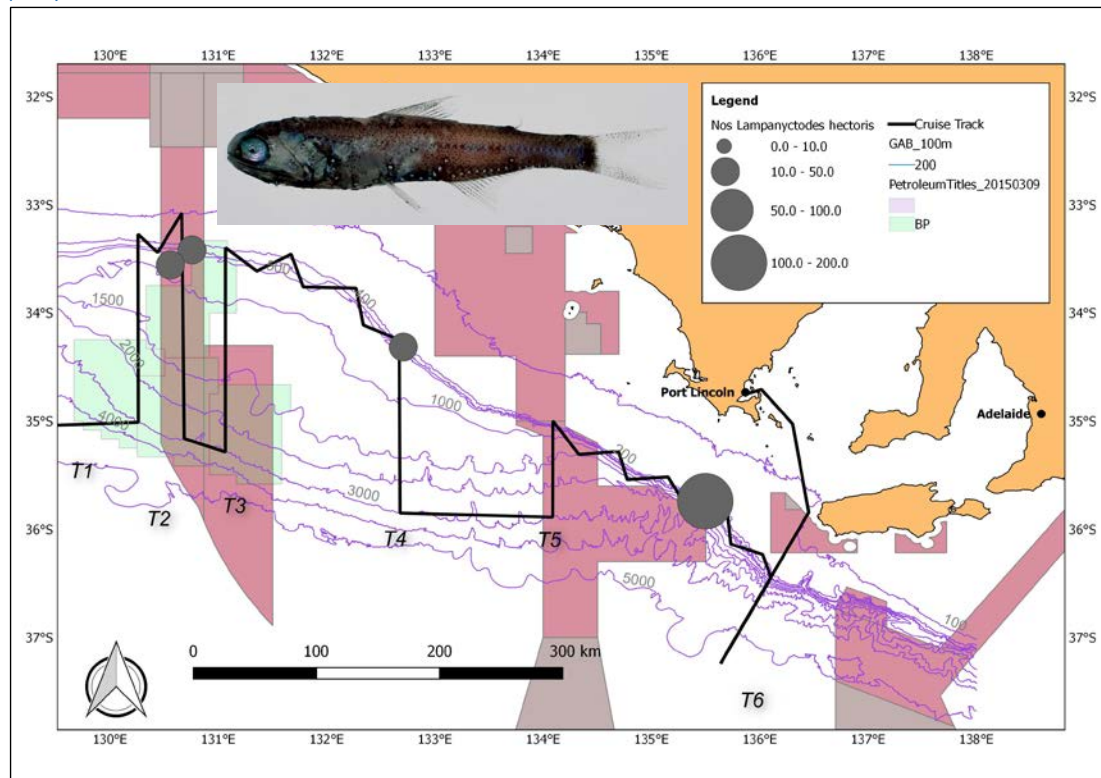
*Lampanyctodes hectoris*

Figure 6.1-21 IN2015\_C02 MIDOC catch distribution for *Lampanyctodes hectoris* (number of fish)

*Lampanyctodes hectoris* is a lanternfish species that is widespread in the southern hemisphere and common over the shelf break and upper-to mid-continental slope in Africa (Hulley, 1992), New Zealand (Robertson, 1977) and eastern Australia (May and Blaber, 1989). This species was not included in the top-10 species contributing to biomass in the present study. However, it is included here as it is a key species in the Tasman Sea and East Australian Current ecosystems. It is a dominant species of western Tasmania (CSIRO unpublished data) and off eastern Tasmania, the species can occur in very high abundance during autumn-winter (May and Blaber, 1989,) where it feeds primarily on seasonally abundant euphausiids (Young and Blaber, 1986). *Lampanyctodes hectoris* in turn is a major component in the diets of predatory fishes of the continental slope (Blaber and Bulman, 1987). In New Zealand, *L. hectoris* was the second most abundant lanternfish (second to *Symbolophorus* sp.) in the diet of New Zealand fur seals (*Arctocephalus forsteri*) (Carey, 1992). *Lampanyctodes hectoris* is generally considered as having habitat affinities with the Subtropical Convergence and southern Tasman Sea off eastern Australia.

In the present study, *L. hectoris* was recorded from the slope in the Central region and Shelf-Break / Upper Slope stations in the East, but in lower abundance than *Maurollicus muelleri* and *Symbolophorus barnardi* (Figure 6.1-22). *Lampanyctodes hectoris* was only recorded in night-time trawls in the Central region (17 captured in the night-time integrated net of T2\_800m not shown), despite the daytime trawls for this station sampling benthopelagic depth strata here. This indicates that the daytime habitat of this species was not effectively sampled and may suggest that there is a similar up-slope-down-slope (horizontal) element to the diel vertical migrations of this species similarly hypothesised for *Symbolophorus barnardi*.

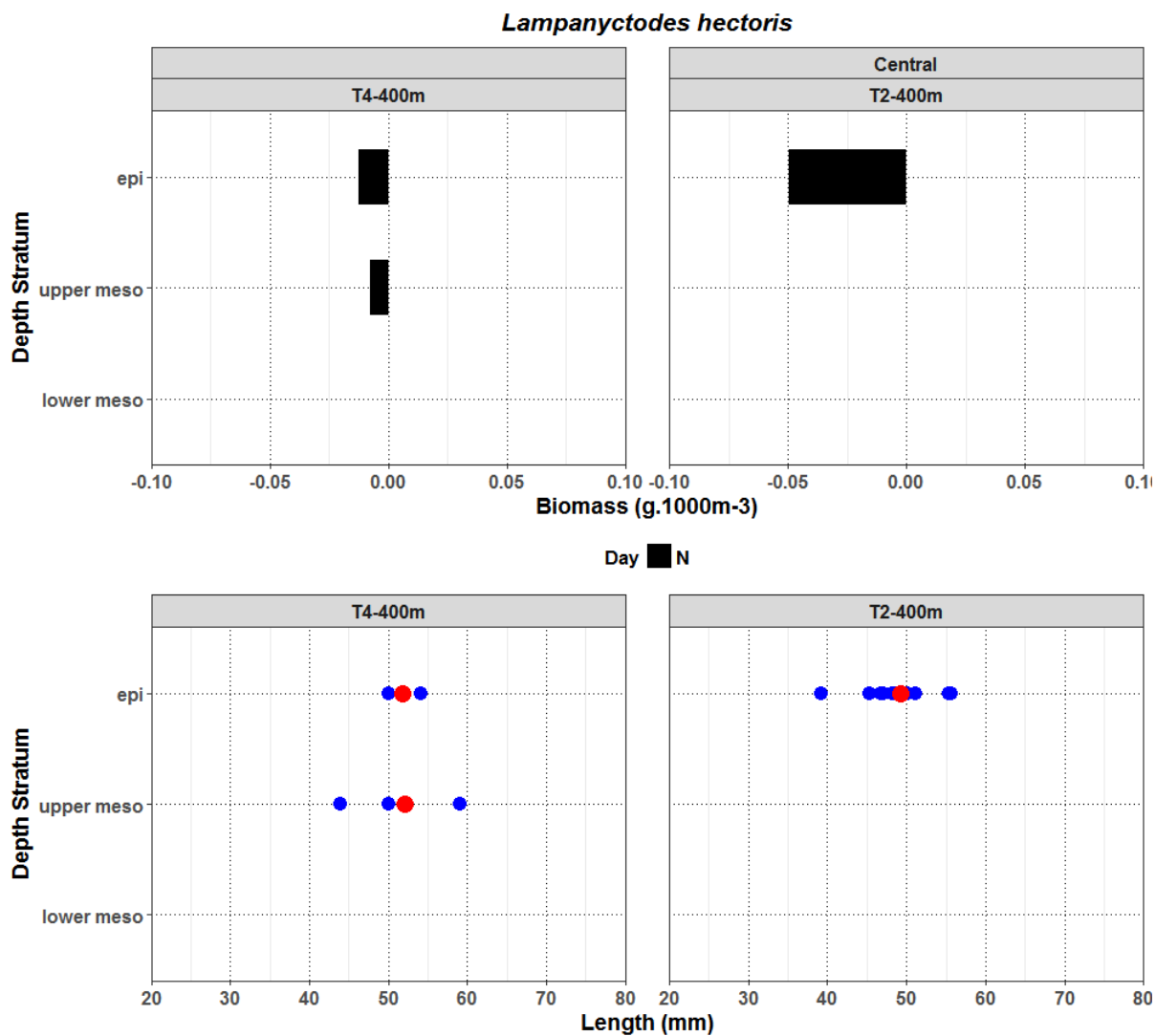


Figure 6.1-22 Distribution of *Lampanyctodes hectoris* biomass in depth strata from Central and East regions (top row) and length (standard length) range (blue dots) and mean (red dots) (bottom row).

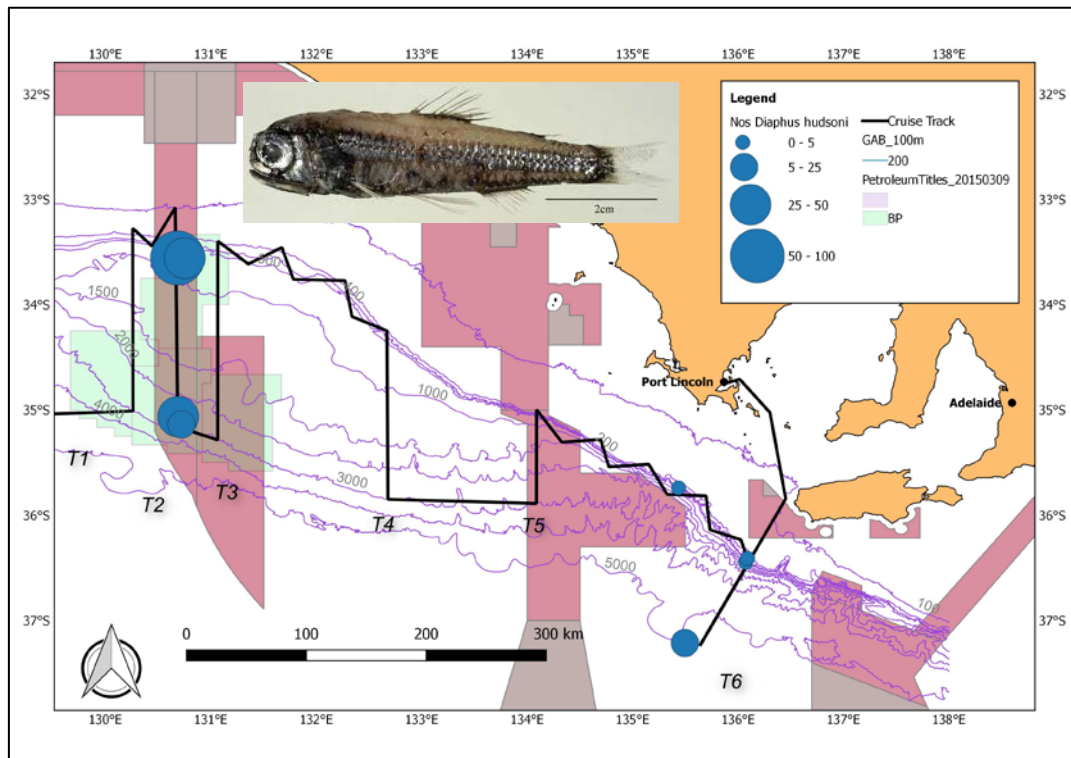
*Diaphus hudsoni*

Figure 6.1-23 N2015\_C02 MIDOC catch distribution for *Diaphus hudsoni* (number of fish)

*Diaphus hudsoni* was not among the top-10 species contributing to biomass for any of the GAB stations. However the distribution of this species is illustrative of habitat segregation among lanternfishes related to the interactions between water mass and the continental slope. *Diaphus hudsoni* is in a similar size range to *Lampanyctodes hectoris*, but occupies non-overlapping adjacent oceanic and mid- to lower-slope habitat. This is in agreement with distribution of *Diaphus hudsoni* in the southern Tasman Sea abyssal basin, where it was among the most abundant lanternfish species (Flynn and Kloser 2012) and for southern Tasmania where it was one of the top 10 most dominant fish species (CSIRO unpublished data). Where *Diaphus hudsoni* was recorded on the mid-slope (T6-400m, bottom depth ~900 m), the night time distributions were suppressed to the upper and lower mesopelagic zones (Figure 6.1-24). Such segregation in vertical distribution are hypothesised as primarily feeding niche segregation (Flynn and Kloser 2012). In the present study, larger individuals of *D. hudsoni* were recorded in deeper strata than small individuals.

The species is generally considered to have zoogeographic affinities to the Subtropical Convergence and southern Tasman Sea off eastern Australia (Flynn and Kloser, 2012).

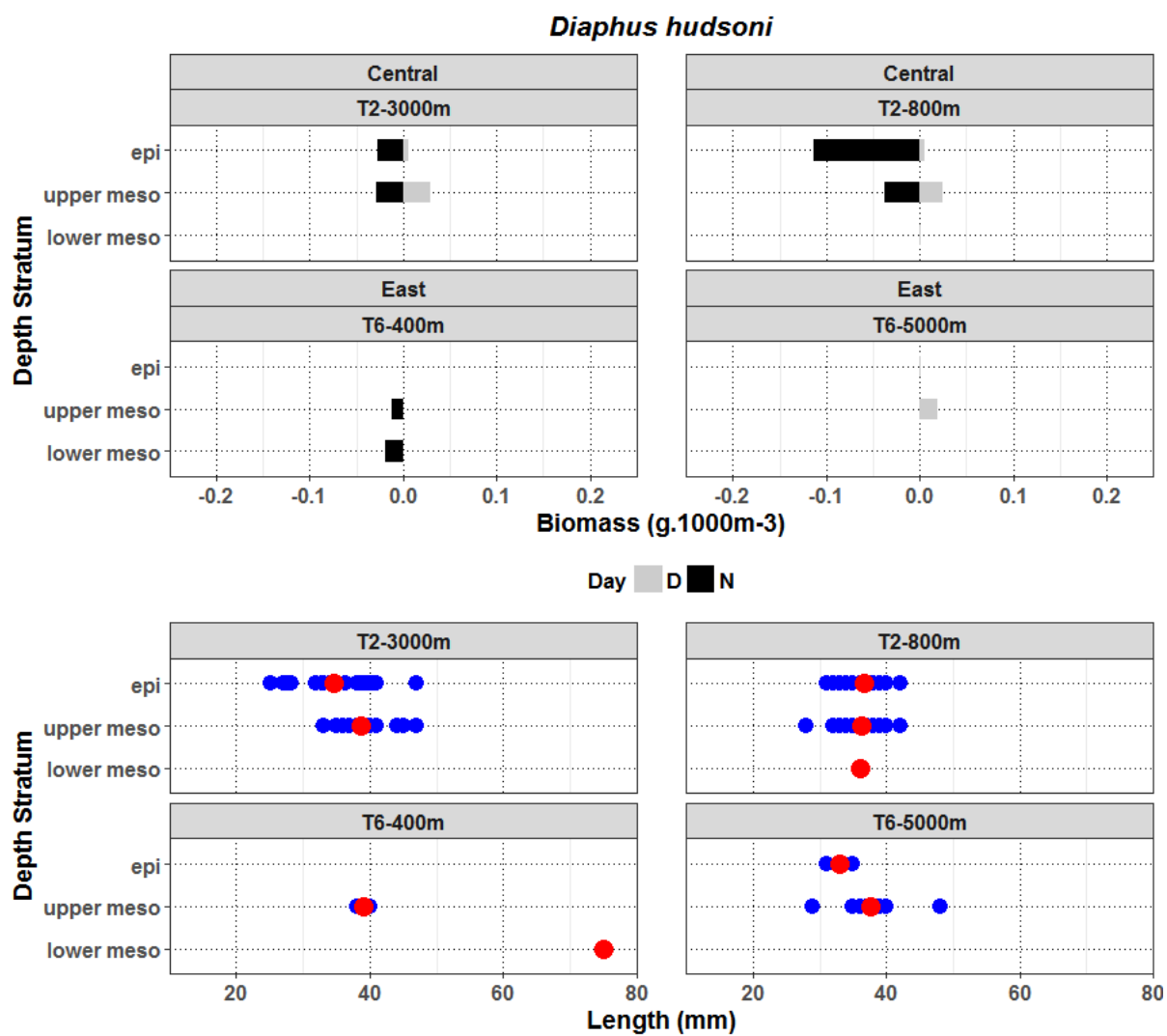


Figure 6.1-24 Distribution of *Diaphus hudsoni* biomass in depth strata from Central and East regions (top row) and length (standard length) range (blue dots) and mean (red dots) (bottom row).



## Dominant krill species

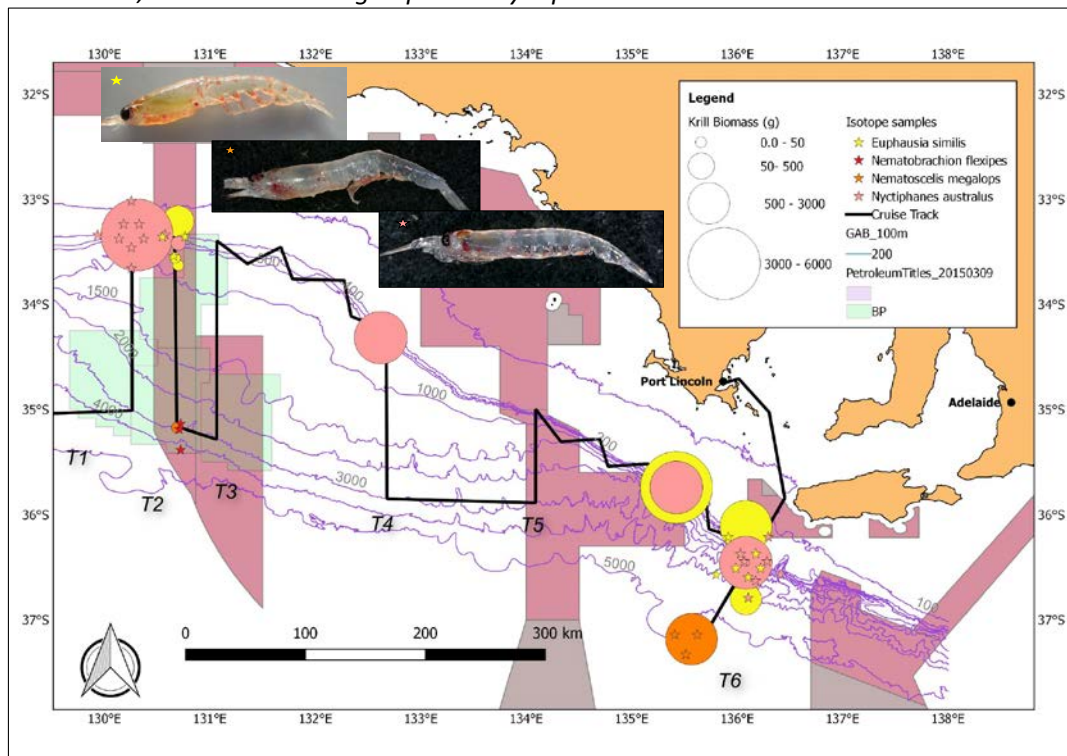
*Euphausia similis*, *Nematoscelis megalops* and *Nyctiphanes australis*

Figure 6.1-25 N2015\_C02 MIDOC catch distribution for the dominant krill species (total weight (g)).

*Nyctiphanes australis*

The krill, *Nyctiphanes australis* is a key prey species of blue whales *Balaenoptera musculus (brevicaudata)* in the Bonney Coast region of the GAB during the summer upwelling period (Gill et al., 2011). Off eastern Tasmania, *N. australis* forms a major component of coastal zooplankton assemblages where it is fed upon by seabirds and other neritic predators (O'Brien, 1988; Young et al., 1993). *N. australis* has been recorded in the diets of southern bluefin tuna (SBT, *Thunnus maccoyii*) and jack mackerel (*Trachurus declivis*), which is itself an important prey species of SBT (Young and Blaber, 1986). Off eastern Tasmania, *N. australis* is characteristic of northward-flowing cold water penetration of the Subtropical Convergence (STC) and thus population densities are driven by inter-related oceanographic and production regimes. Eastern Tasmanian populations were not reported to undertake regular diel vertical migrations (Young et al., 1993). There is some evidence to suggest that off eastern Tasmania, *N. australis* over-winters by residing close to the seabed where they are fed upon by benthic fish species (Young et al., 1993), although this is unconfirmed.

In the present study, *N. australis* was recorded from Shelf-Break and Upper Shelf stations with relatively large numbers in the Central region (Figure 6.1-26). This species was recorded only from the epipelagic zone with highest catches at night. Daytime catches were generally low and the results are inconclusive with regards to vertical migration behaviour, although the apparent epipelagic habitat for this species during the day (O'Brien, 1988; Gill, 2002) appears to be supported. Size structure was comparable between the Central and East regions and within the range reported off Eastern Tasmania (O'Brien, 1988) and correspond to Size Class IV of Young et al. (1993). *Nyctiphanes australis* populations are likely to provide a food resource for the shelf-break and slope resident lanternfish *Lampanyctodes hectoris*, the pearlside, *Maurollicus australis*, and the lanternfish

*Symbolophorus barnardi* that is an apparent diel migrator to the upper slope to shelf break. Myctophid species (Suntsov and Brodeur 2008), including *M. australis* and *L. hectoris* (Young and Blaber 1986) are known to feed on krill of this size range. The benthopelagic threespine cardinalfish, *Verilus anomalus*, is also likely to feed on *N. australis* swarms, particularly at night.

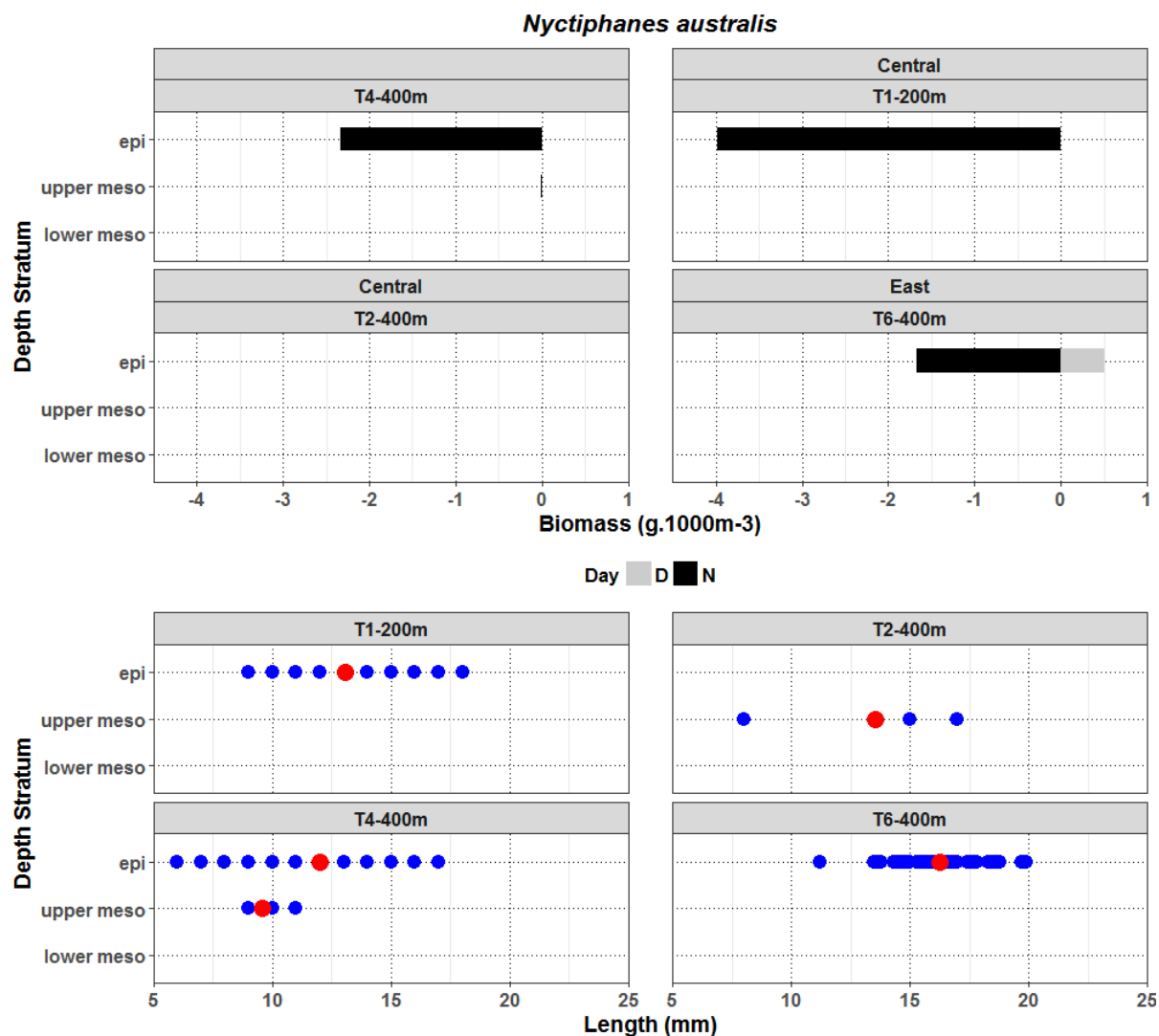


Figure 6.1-26 Distribution of *Nyctiphanes australis* biomass in depth strata from Central and East regions (top row) and length (standard length) range (blue dots) and mean (red dots) (bottom row).

*Euphausia similis*

Moving offshore from shelf waters, where *Nyctiphanes australis* was dominant, *Euphausia similis* and *Euphausia spinifera* became more abundant in the offshore zone off Eastern Tasmania characterised by cold 'Subantarctic Water' (Young et al., 1996). These two species were also among the most dominant identifiable crustaceans in the stomach contents of abundant lanternfishes on the southern Tasmania mid-slope (Williams et al., 2001) and in the Tasman Sea abyssal basin (Flynn and Kloser, 2012). Off eastern New Zealand, *E. similis* was characteristic of a region south of the Chatham Rise bathed in 'subantarctic water masses' (Robertson et al., 1978), while the congener *E. spinifera* was characteristic of subtropical front waters north of Chatham Rise.

In the present study, *E. similis* was most abundant at the Upper Slope station of the East region (T6-400m) (Figure 6.1-27). The occurrence of this species with habitat affinity with Subantarctic water may indicate the presence of upwelled water onto the mid- to upper-slope, an indication that will be discussed in the context of partner studies herein. Average length of *E. similis* was generally greater than that of *Nyctiphanes australis*. Data on diel vertical migrations are inconclusive but supportive of migratory behaviours in adult *Euphausia similis* reported off eastern Australia in the EAC (Harris et al., 2014).

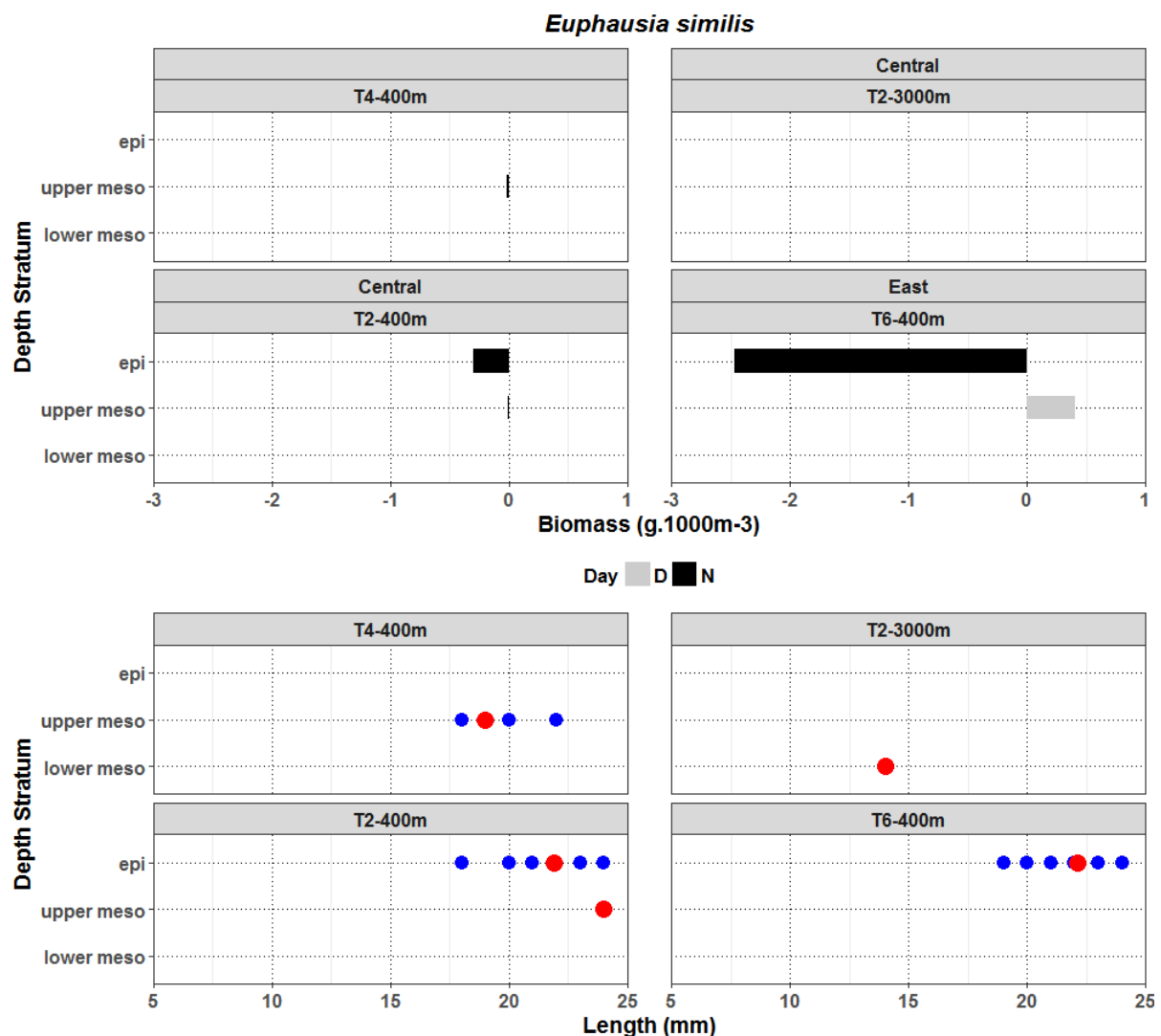


Figure 6.1-27 IN2015\_C02 MIDOC catch distribution of *Euphausia similis* biomass in depth strata from Central and East regions (top row) and length (standard length) range (blue dots) and mean (red dots) (bottom row).

*Nematoscelis megalops*

*Nematoscelis megalops* has been reported over the mid-slope off southern Tasmania, usually in lower abundance than *Euphausia similis* and *E. spinifera* (Williams et al., 2001). The species was not among those that were abundant in shelf assemblages off eastern Tasmania (Young 1996) but has been recorded as one of the common prey species for midwater fish (Young and Blaber, 1986) in the same area. This species was the second most abundant euphausiid in shelf assemblages for the northern Tasman (Griffiths, 1979). Off eastern New Zealand, *N. megalops* was the most abundant euphausiid recorded (Robertson et al., 1978). Off New Zealand, while the species was recorded across a relatively wide latitudinal range, abundance was higher in waters of the Subtropical Convergence. Similarly, in the Northwest Atlantic, the species appears to have habitat affinities with 'transitional' waters (Wiebe and Boyd, 1978). In the Southern Ocean, the species is considered to be more carnivorous than *Euphausia* spp. (Gurney et al., 2001). The species is generally considered to be a vertical migrator in the Benguela upwelling system, within narrower depth strata than were sampled in the present study (Barange, 1990).

In the present study, *N. megalops* was recorded from oceanic stations in the Central and East regions, and over the mid slope in the East region (station T6-400 m, water depth ~970 m) (Figure 6.1-28). Biomass was highest in the East region at the oceanic station. There was a substantial difference in mean length between populations sampled from the offshore and inshore stations in the Eastern regions, with inshore populations characterised by larger individuals. The size and habitat difference suggest that we may be dealing with two species. While the previous Australian observations have all been relatively low densities in shelf-break habitats, globally it is recognised as a common oceanic species. In addition the observed sizes are within the range reported for this species and the observed vertical distribution are also consistent to previous reports where smaller individuals are found predominantly in the epipelagic waters with the larger individuals in the deeper mesopelagic zone (Lindley, 1982).

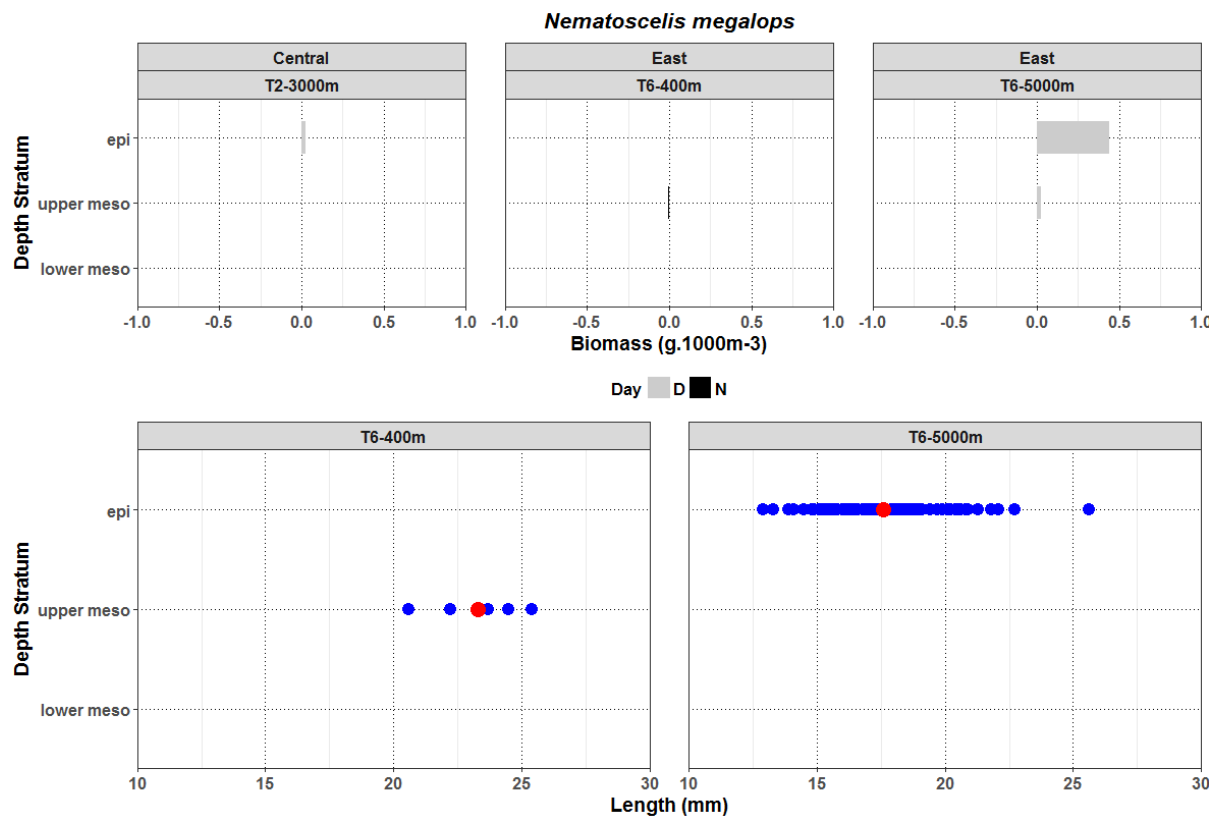


Figure 6.1-28 Distribution of *Nematoscelis megalops* biomass in depth strata from Central and East regions (top row) and length (standard length) range (blue dots) and mean (red dots) (bottom row).

### Small cephalopods – dumpling squid

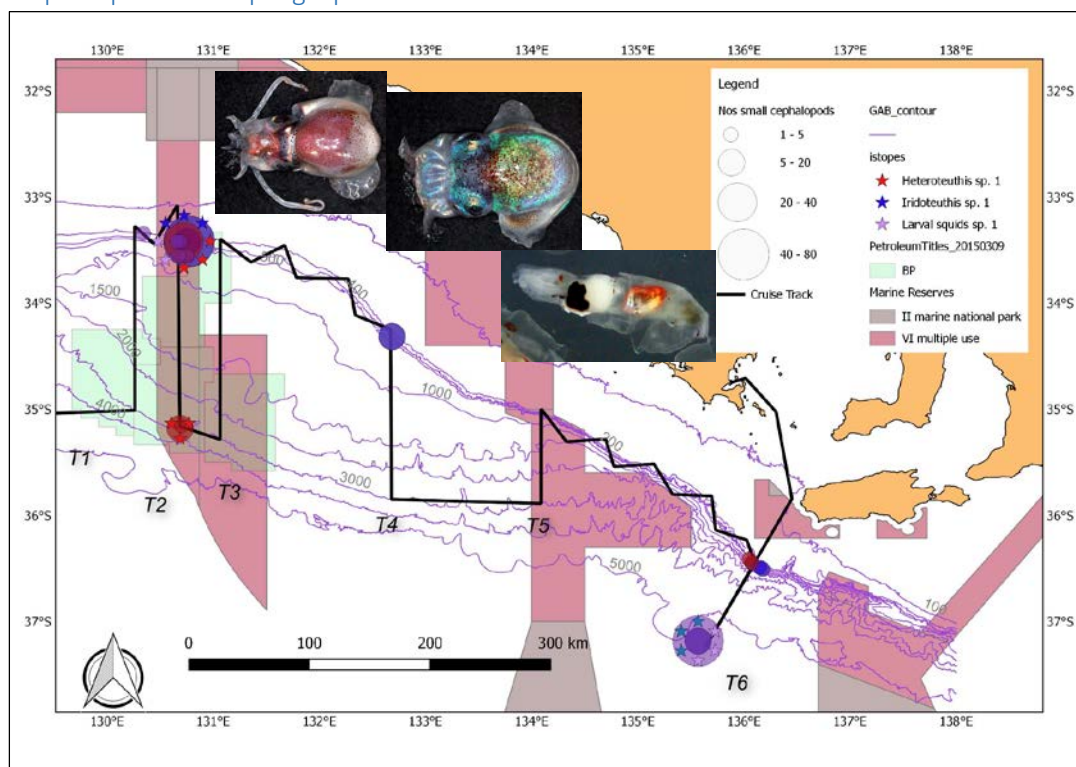


Figure 6.1-29 IN2015\_C02 MIDOC catch distribution of small cephalopods; Sepioids and larval squids (number of individuals).



The majority of the small cephalopods were pelagic species of the genera *Heteroteuthis* and *Iridoteuthis* within the Sepiolidae, a family of mostly benthic cephalopods. The species are likely to be *I. maoria*, which has been recorded from New Zealand the Southwest Pacific, and *H. hawaiiensis*, which has been recorded from the GAB (Jereb and Roper, 2005). The larvae squid sp. 1 are Pyroteuthids, a family of pelagic squids. There is little known about the ecology of the non-commercial cephalopods; however, the distribution of cephalopod larvae tend to be associated with distinct oceanographic features that lead to high productivity such as upwellings, and they are able to respond relatively quickly to changes in environmental conditions (Battaglia et al., 2013). Cephalopods are a significant prey source for apex predators (Young et al., 1997; Young et al., 2010), of which the small squid of the Sepiolidae can contribute a significant proportion of the diet of tuna (Battaglia et al., 2013). Of particular note is that both the Albacore and Southern Bluefin Tuna captured by handlines on this voyage had small cephalopods in their guts.

The cephalopods contributed only 2% of total combined biomass; net avoidance of this group is high and it is likely that they were under-sampled. Many may have slipped through the nets. As it is unknown if juvenile cephalopods school like fish and euphausiids which allow them to be herded into the cod-end of the net. Overall, catches were highest in the central region; in epipelagic depth stratum at stations on the slope. The exception was a relatively large catch of larval squid in the east at the epipelagic depth stratum of the oceanic station.

#### Gelatinous zooplankton

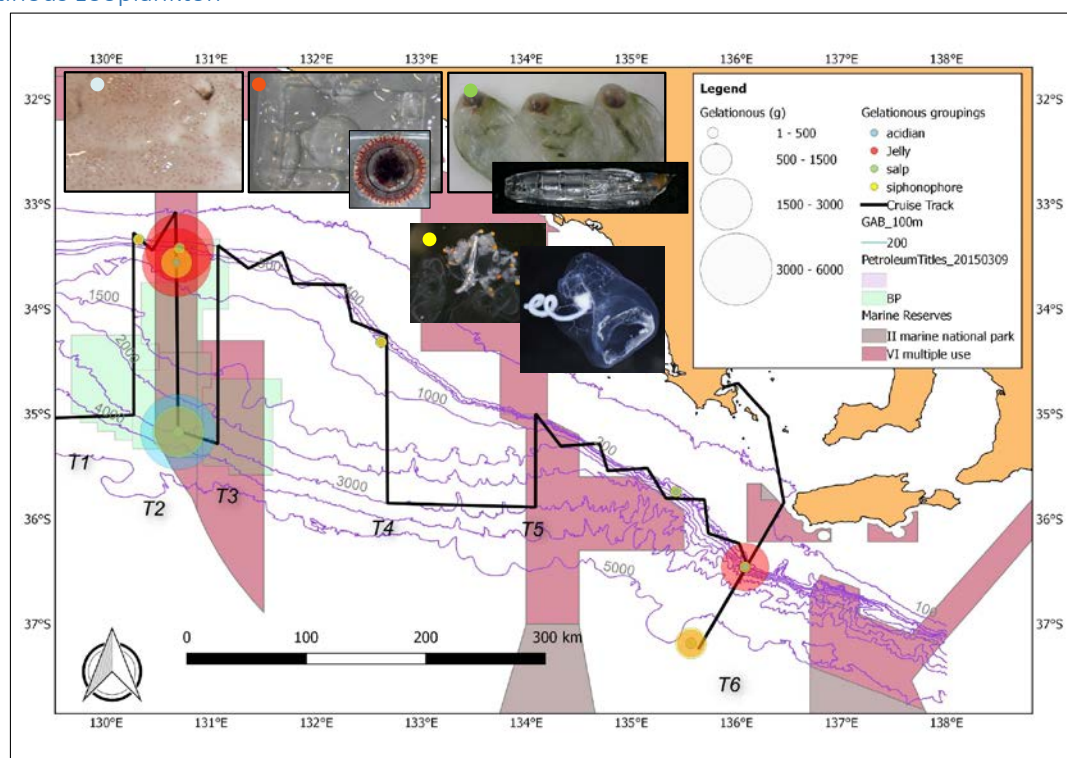


Figure 6.1-30 IN2015\_C02 MIDOC catch distribution for Gelatinous taxa (Total weight (g)). Gelatinous herbivores (pyrosomes and salps) and Gelatinous carnivores (medusae, ctenophores and siphonophores) are shown.

Oceanographic features influence the relative distribution of dominant feeding guilds of gelatinous zooplankton. Herbivorous or passive feeders like salps are reported to be associated with boundary areas where there are often high concentrations of detritus-related bacteria and protozoans. While the siphonophores have been associated with oligotrophic waters as they are able to capture faster

swimming zooplankton, unlike jellies which are slower moving and associated with high nutrient waters (Vinogradov and Shushkina, 2002).

Dominance of the gelatinous zooplankton in mesopelagic communities has been reported in waters associated with the Subtropical Convergence, Tasman Front and Subantarctic, and is relatively high compared with more northerly waters, e.g. Northern Tasman (CSIRO unpublished data; Young et al., 1996; Williams and Koslow, 1997). Within a regional scale Young et al. (1996) reported highest gelatinous biomass on the shelf off eastern Tasmania, suggesting that nutrient-rich subantarctic water is augmented by shelf-break upwelling leading to high productivity. Dominant species reported for waters associated with the subtropical convergence and the Tasman front are the salps *Thalia democratica* and *Thetys vagina* and the colonial ascidian *Pyrosoma atlanticum* (Young et al., 1996; Williams and Koslow, 1997; CSIRO unpublished data), both *T. vagina* and *P. atlanticum* were dominant in the central GAB but with much lower biomass (Figure 6.1-31). In the east, the dominant carnivorous guild was distributed predominantly in the mesopelagic stratum, which is consistent with the vertical distributions of jellyfish reported for subantarctic waters (CSIRO unpublished data). While much of the captured gelatinous biota were damaged, they were classed as jellyfish as some intact specimens were able to be identified as *Solmissus sp.*, an active predator and one of the most abundant cnidarian in warm and temperate waters worldwide (Robison, 2004). See Section 5.3 for more details.

#### Regional Biomass comparison

Excluding gelatinous biota, the average biomass ( $\text{g.m}^{-3}$ ) observed for the GAB, is lower but within the range recorded for other areas within the similar water masses such as the Tasman Sea and off western Tasmania (Figure 6.1-31, Table 6.1-5). The comparison is problematic due the limited replication of MIDOC trawls over time, habitats and regions (CSIRO unpublished data).



Figure 6.1-31 Micronekton density estimates ( $\text{g.1000 m}^{-3}$ ) for the southern Australian region. For comparative purposes data are for night time MIDOC samples in the epipelagic and mesopelagic depth strata and excluding gelatinous biota.



Table 6.1-5 Micronekton density estimates (g.1000 m<sup>-3</sup>) for the southern Australian region. For comparative purposes data are for night time MIDOC samples in the epipelagic and mesopelagic depth strata and excluding gelatinous biota.

Region	Depth Interval	Nos MIDOCs	n (nos of nets)	Micronekton density excluding Gelatinous biota (g 1000m <sup>-3</sup> )	Standard Deviation
GAB Central	epi		7	2.43	2.26
GAB Central	upper meso		6	0.38	0.23
GAB Central (0 -400 m)		3	13	1.48	1.92
GAB East	epi		2	8.41	8.42
GAB East	upper meso		2	2.82	0.44
GAB East (0 -400 m)		1	4	5.62	5.84
GAB (0 -400 m)		4	17	2.45	3.53
Northern Tasman	epi		16	3.93	1.71
	upper meso		16	1.52	0.67
Northern Tasman (0-500 m)		8	32	2.73	1.77
Western Tasmania	epi		16	2.26	3.75
	upper meso		16	2.11	2.24
Western Tasmania (0 -400 m)		8	32	2.18	3.04
Southern Tasman Abyssal Basin	epi		9	2.76	1.68
	upper meso		9	2.53	2.12
Southern Tasman Abyssal Basin (0 -400 m)		9	18	2.64	1.86
Southern Hills	epi		16	5.54	6.16
	upper meso		16	3.65	4.80
Southern Tasmania (0-400 m)		8	32	4.60	5.52
Macquarie Island	epi		5	3.15	1.81
	upper meso		5	2.96	2.20
Macquarie Island (0-400 m)		5	10	3.06	1.90

### Biogeography

There was concordance between species and regions that would potentially provide robust dissimilarity metrics, particularly for groups which had complete species-level identifications. For example, among the lanternfishes (Family Myctophidae), phylogenetic analysis indicated there was clustering of species assemblages among regions (Figure 6.1-32). Identifications of lanternfish species by various workers has been relatively consistent and confident. However, when up-scaled to whole-of-community comparisons, there were large numbers of incomplete species identifications in the regional dataset which forced incongruous similarities between taxa and

regions thus masking any biogeographic patterns. It was demonstrated through this work that biogeographic variability among the fish fauna was only tractable at the species level - that is, a genus may span multiple regions, but species within a genus inhabit specific regions.

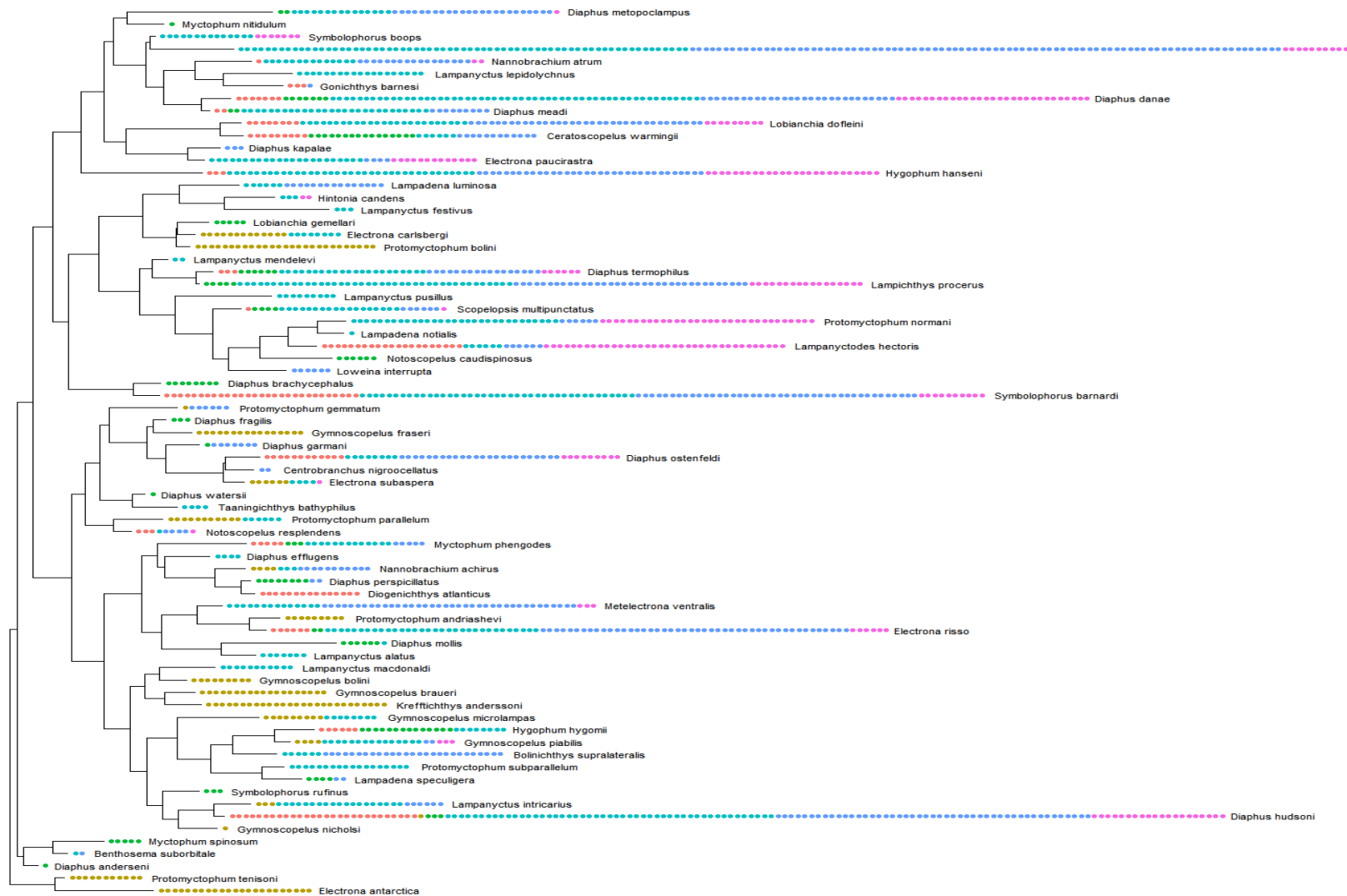


Figure 6.1-32 Lanternfish (family Myctophidae) species distribution by basin (water mass region, see text for abbreviations). The tree depicted is a 'random' phylogenetic tree for visualisation purposes only and does not depict actual phylogeny of lanternfishes. GAB = red, MI = yellow, NT = green, SH = aqua, STAB = blue, WT = pink.

For the whole-of-community, hierarchical clustering of the fish abundance data (standardised to presence-absence) showed that the GAB transects clustered together (in single-linkage clustering) and were nested within a group that included the Western Tasman, Southern Hills and Southern Tasman Abyssal Basin regions at the ~50% dissimilarity level (Figure 6.1-33). Macquarie Island and Northern Tasman groups clustered separately and were highly dissimilar. The dispersive nature of the cluster containing the GAB transects reflects the relatively low replication per habitat for those samples.

These results indicate that micronekton communities of the GAB have biogeographic affinities with the Subtropical Convergence (STC) and the southern Tasman Sea. Therefore, the fauna is expected to have similarities with the 'STC/South Tasman' zoogeographic region hypothesised by Flynn and Marshall (2013). However, the differentiation of the GAB fauna at the ~50% dissimilarity is indicative of a distinctive GAB micronekton bioregion. Further analyses will investigate this, but preliminary results concord with Condie and Dunn (2006) physicochemical regionalisation that erected a 'Southern Indian Central Water' region extending into the GAB that is distinct from an latitudinally constrained STC region located further south. Conversely, Longhurst (2007) erected a STC region that was latitudinally broader and extended north into the GAB.

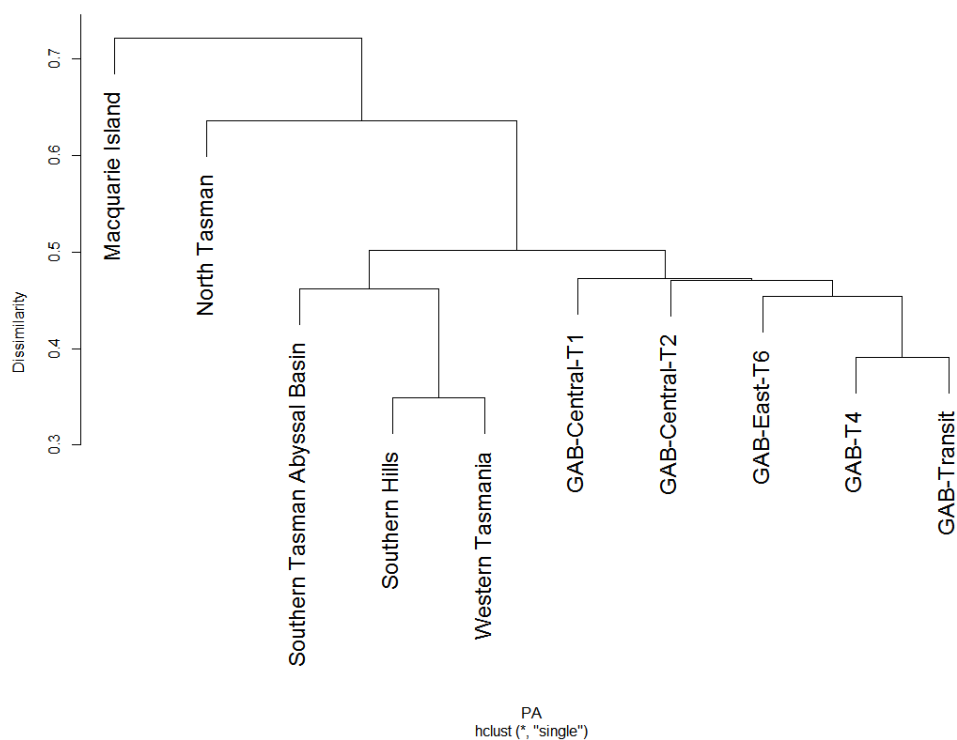


Figure 6.1-33 Dendrogram (single linkage clustering) of micronekton fish community dissimilarity among regions.

#### 6.1.4 Discussion

MIDOC net estimates for total biomass were higher for the Eastern GAB than the Central GAB, although this was not consistent for all taxa or habitats. On a regional scale, the biomass estimates are lower than, but within the range of, similar studies in waters associated with Sub Tropical Convergence such as the Tasman Sea and western Tasmania (CSIRO unpublished data). Species distributions and community composition, and in conjunction with the stable isotope results

presented in Section 6.2, indicate that species and processes indicative of upwelling can be identified. Also differences in day and night catches are observed which in part can be attributed to vertical migrations.

Based on the acoustic records there is clear evidence of diel vertical migration (DVM) in all regions that vary in intensity depending on species specific scattering (see Chapter 6.3 and 6.4). From the net retained catches there was clear evidence of DVM for known vertical migrators in both regions e.g. *Symbolophorus barnardi* and *Maurolicus australis*. The high backscatter in the epipelagic and lower mesopelagic (for lower frequencies which are a proxy for taxa with small gas bladders e.g. myctophids and siphonophores) can provide insights into distributions of organisms where net samples were lacking and requires further exploration. Transect 4 (Figure 6.3-3) is a good example where the backscatter signal in the mesopelagic increases as organisms migrate into deeper depths, although there is still a portion of non-migrating organisms and therefore, the relationship between night epipelagic and day mesopelagic backscatter is dependent on the community composition. For this transect, fish with swimbladders (FSB) comprised 50% of the total catch (Figure 6.1-4); of which *Verilus anomalus* was dominant and likely an important species contributing to the DVM signal. Day and night catches were combined when comparing areas for diversity and evenness to avoid vertical migration effects.

There was no significant difference in diversity or evenness between the regions or habitats. However, there was an observable difference in the micronekton community composition between the East and Central regions. In the Central region, gelatinous zooplankton were dominant in the inshore and oceanic habitats, while in the East region, the inshore habitat was dominated by fishes and the oceanic habitat was dominated by euphausiids (krill). In both the Central and East regions, the Shelf Break and Upper Slope habitat was dominated by large catches of the important coastal and key prey species, *Nyctiphanes australis*. The relatively large krill biomass on the slope and offshore in the east could be an indicator of upwelling. The dominant species observed in the GAB have all been associated with upwelling in other regions, namely *Nematoscelis megalops* in the Benguela (Barange 1990), *Euphausia similis* in New Zealand (Robertson et al. 1978), and *N. australis* off eastern Tasmania (Young et al. 1996).

The micronekton communities of the GAB have biogeographic affinities with the Subtropical Convergence (STC), a region defined on the basis of physicochemical (Condie and Dunn 2006; Longhurst 2007) and biological (Flynn and Marshall 2013) properties. There is some evidence to suggest that the GAB may represent a distinct biogeographic zone within the STC region. The STC is a latitudinally constrained water mass at the northern boundary of the Southern Ocean. As such, in a regional context, the micronekton community composition in the GAB is similar to those occurring from western Tasmania, south and southeastern Tasmania, the Southern Tasman Sea and south-southeastern New Zealand, but distinct to those in the higher latitudes of the Southern Ocean and the central and northern sectors of the Tasman Sea.

## References

- Armstrong, M. J., and Prosch, R. M. 1991. Abundance and distribution of the mesopelagic fish *Maurolicus muelleri* in the southern Benguela system. *South African Journal of Marine Science*, 10: 13-28.
- Backus, R. H. 1986. Biogeographic boundaries in the open ocean. *In* Pelagic biogeography, p. 291. Ed. by A. C. Pierrot-Bults, S. van der Spoel, B. J. Zahuranec, and R. K. Johnson. *Unesco Technical Papers in Marine Science*, The Netherlands.
- Barange, M. 1990. Vertical migration and habitat partitioning of six euphausiid species in the northern Benguela upwelling system. *Journal of Plankton Research*, 12: 1223-1237.

- Battaglia, P., Pedà, C., Sinopoli, M., Romeo, T., and Andaloro, F. 2013. Cephalopods in the diet of young-of-the-year bluefin tuna (*Thunnus thynnus* L. 1758, Pisces: Scombridae) from the southern Tyrrhenian Sea (central Mediterranean Sea). *Italian Journal of Zoology*, 80: 560-565.
- Benoit-Bird, K. J., and Au, W. W. 2006. Extreme diel horizontal migrations by a tropical nearshore resident micronekton community. *Marine Ecology Progress Series*, 319: 1-14.
- Blaber, S. J. M., and Bulman, C. 1987. Diets of fishes of the upper continental slope of eastern Tasmania: content, calorific values, dietary overlap and trophic relationships. *Marine Biology*, 95: 345-356.
- Bulman, C., Althaus, F., He, X., Bax, N. J., and Williams, A. 2001. Diets and trophic guilds of demersal fishes of the south-eastern Australian shelf. *Marine and Freshwater Research*, 52: 537-548.
- Bulman, C. M., and Blaber, S. J. M. 1986. Feeding ecology of *Macruronus novaezelandiae* (Hector) (Teleostei: Merluciidae) in south-eastern Australia. *Australian Journal of Marine and Freshwater Research*, 37: 621-639.
- Carey, P. W. 1992. Fish prey species of New Zealand fur seal (*Arctocephalus forsteri*, Lesson). *New Zealand Journal of Ecology*, 16: 14-46.
- Clarke, T. A. 1982. Distribution, growth and reproduction of the lightfish, *Maurolicus muelleri* (Sternoptychidae) off South-east Australia. ICES Document Report 145. 13 pp.
- Condie, S. A., and Dunn, J. R. 2006. Seasonal characteristics of the surface mixed layer in the Australasian region: implications for primary production regimes and biogeography. *Marine and Freshwater Research*, 57: 569-590.
- Flynn, A., and Pogonoski, J. J. 2012. Guide to mesopelagic fishes of the southern Tasman Sea / Adrian Flynn and John Pogonoski ; contributors Alastair Graham ... [et al.], CSIRO Marine & Atmospheric Research, Hobart, Tas.
- Flynn, A. J., and Kloser, R. J. 2012. Cross-basin heterogeneity in lanternfish (family Myctophidae) assemblages and isotopic niches ( $\delta^{13}\text{C}$  and  $\delta^{15}\text{N}$ ) in the southern Tasman Sea abyssal basin. *Deep-Sea Research I*, 69: 113-127.
- Flynn, A. J., and Marshall, N. J. 2013. Lanternfish (Myctophidae) zoogeography off Eastern Australia: a comparison with physicochemical biogeography. *PLoS ONE*, 8: e80950.
- Flynn, A. J., and Williams, A. 2012. Lanternfish (Pisces: Myctophidae) biomass distribution and oceanographic-topographic associations at Macquarie Island, Southern Ocean. *Marine & Freshwater Research*, 63: 251-263.
- Gill, P. C. 2002. A blue whale (*Balaenoptera musculus*) feeding ground in a southern Australian coastal upwelling zone. *Journal of Cetacean Research and Management*, 4: 179-184.
- Gill, P. C., Morrice, M. G., Page, B., Pirzl, R., Levings, A. H., and Coyne, M. 2011. Blue what habitat selection and within-season distribution in a regional upwelling system off southern Australia. *Marine Ecology Progress Series*, 421: 243-263.
- Gomon, M. F. 2008. Family Emmelichthyidae: Rovers, Bonnetmouths. *In* Fishes of Australia's Southern Coast, p. 585. Ed. by M. Gomon, D. Bray, and R. Kuitert. New Holland Publishers (Australia) Pty Ltd, Museum Victoria.
- Gray, C. A., and Otway, N. M. 1994. Spatial and temporal differences in assemblages of demersal fishes on the inner continental shelf off Sydney, South-eastern Australia. *Australian Journal of Marine and Freshwater Research*, 45: 665-676.
- Griffiths, F. 1979. Euphausiids in the Coral and Tasman Seas during May 1972. II. Horizontal Distribution in relation to Circulation Patterns. *Marine and Freshwater Research*, 30: 569-577.

- Gurney, L. J., Froneman, P. W., Pakhomov, E. A., and McQuaid, C. D. 2001. Trophic positions of three euphausiid species from the Prince Edward Islands (Southern Ocean): implications for the pelagic food web structure. *Marine Ecology-Progress Series*, 217: 167-174.
- Harris, B. P., Young, J. W., Revill, A. T., and Taylor, M. D. 2014. Understanding diel-vertical feeding migrations in zooplankton using bulk carbon and nitrogen stable isotopes. *Journal of Plankton Research*, 36: 1159-1163.
- Hulley, P. A. 1992. Upper-slope distributions of oceanic lanternfishes (family: Myctophidae). *Marine Biology*, 114: 365-383.
- Jereb, P., and Roper, C. 2005. An annotated and illustrated catalogue of cephalopod species known to date. Volume 1: Chambered nautilus and sepioids (Nautilidae, Sepiidae, Sepiolidae, Sepiadariidae, Idiosepiidae and Spirulidae). *FAO Species Catalogue for Fishery Purposes* 4(1). FAO, Rome. 262p., 9 colour plates. available online at <ftp://ftp.fao.org/docrep/fao/009/a0150e/A0150e00.pdf> [details]. Rome.
- Kaartvedt, S., Knutsen, R., and Holst, J. C. 1998. Schooling of the vertically migrating mesopelagic fish *Maurolicus muelleri* in light summer nights. *Marine Ecology Progress Series*, 170: 287-290.
- Lindley, J. A. 1982. Population dynamics and production of euphausiids. *Marine Biology*, 71: 1-6.
- Longhurst, A. R. 2007. *Ecological Geography of the Sea*, Academic Press, Burlington, USA. 525 pp.
- Lozupone, C., Lladser, M. E., Knights, D., Stombaugh, J., and Knight, R. 2011. UniFrac: an effective distance metric for microbial community comparison. *The ISME journal*, 5: 169-172.
- Lozupone, C. A., Hamady, M., Kelley, S. T., and Knight, R. 2007. Quantitative and Qualitative  $\beta$  Diversity Measures Lead to Different Insights into Factors That Structure Microbial Communities. *Applied and Environmental Microbiology*, 73: 1576-1585.
- May, J. L., and Blaber, S. J. M. 1989. Benthic and pelagic fish biomass of the upper continental slope off eastern Tasmania. *Marine Biology*, 101: 11-25.
- McManus, M. A., Benoit-Bird, K. J., and Woodson, C. B. 2008. Behavior exceeds physical forcing in the diel horizontal migration of the midwater sound-scattering layer in Hawaiian waters. *Marine Ecology Progress Series*, 365: 91-101.
- O'Brien, D. P. 1988. Surface schooling behaviour of the coastal krill *Nyctiphanes australis* (Crustacean: Euphausiacea) off Tasmania, Australia. *Marine Ecology Progress Series*, 42: 219-233.
- Robertson, D. A. 1977. Planktonic eggs of the lanternfish *Lampanyctodes hectoris* (family Myctophidae). *Deep Sea Research*, 24: 849-852.
- Robertson, D. A., Roberts, P. E., and Wilson, J. B. 1978. Mesopelagic faunal transition across the Subtropical Convergence east of New Zealand. *New Zealand Journal of Marine and Freshwater Research*, 12: 295-312.
- Robison, B. H. 2004. Deep pelagic biology. *Journal of Experimental Marine Biology and Ecology*, 300: 253-272.
- Staby, A., and Aksnes, D. L. 2011. Follow the light - diurnal and seasonal variations in vertical distribution of the mesopelagic fish *Maurolicus muelleri*. *Marine Ecology Progress Series*, 422: 265-273.
- Sutton, C., Kloser, R., and Ryan, T. in prep. Micronekton biomass, abundance and distribution: comparison of vertically integrated MIDOC net samples for southern Australian and subantarctic waters. CSIRO Marine and Atmospheric Research, Hobart.
- Vinogradov, M. E., and Shushkina, E. A. 2002. Vertical Distribution of Gelatinous Macroplankton in the North Pacific Observed by Manned Submersibles Mir-1 and Mir-2. *Journal of Oceanography*, 58: 295-303.



- Welsford, D. C., and Lyle, J. M. 2003. Redbait (*Emmelichthys nitidus*): A synopsis of fishery and biological data. Technical Report Series Number 20.
- Wiebe, P. H., and Boyd, S. H. 1978. Limits of *Nematoscelis megalops* in the Northwestern Atlantic in relation to Gulf Stream cold core rings. I. Horizontal and Vertical Distributions, . Journal of Marine Research, 36: 119-142.
- Williams, A., and Koslow, J. 1997. Species composition, biomass and vertical distribution of micronekton over the mid-slope region off southern Tasmania, Australia. Marine Biology, 130: 259-276.
- Williams, A., Koslow, J., Terauds, A., and Haskard, K. 2001. Feeding ecology of five fishes from the mid-slope micronekton community off southern Tasmania, Australia. Marine Biology, 139: 1177-1192.
- Young, J. W., and Blaber, S. J. M. 1986. Feeding ecology of three species of midwater fishes associated with the continental slope of eastern Tasmania, Australia. Marine Biology, 93: 147-156.
- Young, J. W., Bradford, R., Lamb, T. D., and Lyne, V. 1996. Biomass of zooplankton and micronekton in the southern bluefin tuna fishing grounds off eastern Tasmania, Australia. Marine Ecology Progress Series, 138: 1-14.
- Young, J. W., Hobday, A. J., Campbell, R. A., Kloser, R. J., Bonham, P. I., Clementson, L. A., and Lansdell, M. J. 2011. The biological oceanography of the East Australian Current and surrounding waters in relation to tuna and billfish catches off eastern Australia. Deep Sea Research Part II: Topical Studies in Oceanography, 58: 720-733.
- Young, J. W., Hunt, B. P. V., Cook, T. R., Llopiz, J. K., Hazen, E. L., Pethybridge, H. R., Ceccarelli, D., et al. 2015. The trophodynamics of marine top predators: Current knowledge, recent advances and challenges. Deep Sea Research Part II: Topical Studies in Oceanography, 113: 170-187.
- Young, J. W., Jordan, A. R., Bobbi, C., and Johannes, R. E. 1993. Seasonal and interannual variability in krill (*Nyctiphanes australis*) stocks and their relationship to the fishery for jack mackerel (*Trachurus declivis*) off eastern Tasmania, Australia. Marine Biology, 116: 9-18.
- Young, J. W., Lamb, T. D., Le, D., Bradford, R., and Whitelaw, A. W. 1997. Feeding ecology and interannual variations in diet of southern bluefin tuna, *Thunnus maccoyii*, in relation to coastal and oceanic waters off eastern Tasmania, Australia. Environmental Biology of Fishes, 50: 275-291.
- Young, J. W., Lansdell, M. J., Campbell, R. A., Cooper, S. P., Juanes, F., and Guest, M. A. 2010. Feeding ecology and niche segregation in oceanic top predators off eastern Australia. Marine Biology, 157: 2347-2368.

## 6.1.5 Appendix: Micronekton ancillary data

Table 6.1-6 Total Weight and Standardised biomass for MIDOC trawls

Values for depth stratified nets, integrated nets excluded					Sum	Average – Micronekton		
Region	Location	Time	Depth Stratum	nos of samples	Total Weight (g)	Micro (g)	Micro (g 1000 m <sup>-3</sup> )	Micro (g m <sup>-2</sup> )
<b>Values for each MIDOC and depth stratum</b>								
Central	T1-200m	N		5	6841.2	1232.44	6.90	0.54
	T2-3000m	D	epi	2	933.2	466.60	1.94	0.21
	T2-3000m	D	upper meso	2	577.6	114.80	0.57	0.05
	T2-3000m	D	lower meso	1	229.6	577.60	1.34	0.27
	T2-3000m	N	epi	2	7352.4	3180.20	9.18	0.93
	T2-3000m	N	upper meso	2	1160	155.00	0.74	0.07
	T2-3000m	N	lower meso	1	310	1008.00	2.35	0.52
	T2-400m	D	epi	3	1183.7	394.57	2.13	0.12
	T2-400m	D	upper meso	2	520.5	260.25	1.37	0.10
	T2-400m	N	epi	3	1488.1	332.37	1.81	0.12
	T2-400m	N	upper meso	2	116.6	58.30	0.28	0.02
	T2-800m	D	epi	2	252.2	126.10	0.60	0.08
	T2-800m	D	upper meso	2	455.6	51.80	0.24	0.02
	T2-800m	D	lower meso	1	103.6	455.60	1.04	0.23
	T2-800m	N	epi	2	1771.6	885.80	4.73	0.54
	T2-800m	N	upper meso	3	2400.51	266.84	0.90	0.12
East	T6-400m	D	epi	2	478.81	239.41	1.71	0.26
	T6-400m	D	upper meso	3	1288.8	429.60	1.55	0.28
	T6-400m	N	epi	2	2344.5	1172.25	8.45	1.13
	T6-400m	N	upper meso	2	1270.5	508.75	2.99	0.27
	T6-400m	N	lower meso	1	1017.5	1270.50	3.99	0.80
	T6-5000m	D	epi	3	2196.9	732.30	3.52	0.69
	T6-5000m	D	upper meso	2	636.5	318.25	1.61	0.24
	Transit	N	epi	4	6938.2	1734.55	8.57	1.15
Mid Zone	Transit	N	upper meso	1	73	73.00	0.37	0.02
	T4-400m	N	epi	3	3440.8	945.27	4.33	0.30
	T4-400m	N	upper meso	2	1776	888.00	4.02	0.35
<b>Values for each MIDOC trawl</b>								
Central	T1-200m	N	epi	1	1368.24	1232.44	6.90	0.54
	T2-3000m	D	epi - lower meso	3	386.33	386.33	1.28	0.53
	T2-3000m	N	epi - lower meso	3	1663.73	1447.73	4.09	1.52
	T2-400m	D	epi - upper meso	2	327.41	327.41	1.75	0.22
	T2-400m	N	epi - upper meso	2	277.17	195.33	1.04	0.15
	T2-800m	D	epi - lower meso	3	211.17	211.17	0.62	0.33
	T2-800m	N	epi - upper meso	2	842.99	576.32	2.81	0.67
East	T6-400m	D	epi - upper meso	2	334.50	334.50	1.63	0.54
	T6-400m	N	epi - lower meso	3	983.83	983.83	5.14	2.20

## Micronekton

	T6-5000m	D	epi - upper meso	2	525.28	525.28	2.57	0.93
	Transit	N	epi - upper meso	2	903.78	903.78	4.47	1.17
Mid Zone	T4-400m	N	epi - upper meso	2	1017.47	916.63	4.18	0.65
<b>Values for each Location of the Regional comparison (T2 and T6)</b>								
Central	T2-3000m		epi - lower meso	2	6150	917.03	2.69	1.02
	T2-400m		epi - lower meso	2	1209	261.37	1.40	0.18
	T2-800m		epi - lower meso	2	2319	393.74	1.72	0.50
East	T6-400m		epi - lower meso	2	2319	659.17	3.39	1.37
	T6-5000m		epi - upper meso	1	3621	525.28	2.57	0.93
<b>Values for each Region (T2 and T6)</b>								
Central			epi - lower meso	6	9679	524.05	1.93	0.57
East			epi - lower meso	3	4671	614.54	3.11	1.23
GAB			epi - lower meso	9	14350	554.21	2.33	0.79

## 6.2 Trophic linkages and food webs based on stable isotopes

Andy Revill, Rudy Kloser, Adrian Flynn and Caroline Sutton

### 6.2.1 Introduction

A key objective of the study was to, “compare the eastern and central GAB continental margin zooplankton and micronekton communities in terms of their species composition, size range, biomass, nutrient source/trophic pathways and habitat”. To investigate the trophic linkages and pathways between regions and species, stable isotope methods were proposed based on cost/expertise and effectiveness. This decision was based on a review of methods used in dietary studies and to characterise marine food webs (Young et al., 2015) which found visual identification of stomach contents is the most conventional method used but that, over the last decade, there has been a growth in the use of more specific biochemical tracers. These include bulk stable carbon and nitrogen isotopes, and, most promisingly, methods based on compound-specific stable isotopes.

Growth in the use of methods using biochemical tracers is because they better meet the challenge of detecting the influence of variability at the base of food webs in higher trophic levels. Long standing techniques for trophic studies such as stomach contents and bulk stable isotopes analysis (SIA) are vulnerable to a variety of errors. Stomach contents, while providing the only way of confirming prey items, will often reflect only the last meal and represent what was ingested rather than what was integrated. The issues of empty stomachs (up to 50-60%) and selective preservation of prey dictate that large sample sizes are required. Bulk stable isotope analysis (usually nitrogen in foodweb studies) reflects a more integrated diet but interpretation is complicated by variable trophic fractionation factors and the need to sample multiple trophic positions in order to assess the trophic position of the target organism.

More recently, compound specific nitrogen isotopes (CSIA) in individual amino acids have been used to investigate a wide variety of trophic interactions (McClelland and Montoya, 2002; Chikaraishi et al., 2007; Chikaraishi et al., 2009; Lorrain et al., 2009; Dale et al., 2011; ). This technique utilises the fact that certain “source” amino acids are incorporated with very little isotopic fractionation and are thus indicative of isotopic composition of the foodweb base, while other “trophic” amino acids undergo a relatively large degree of  $^{15}\text{N}$  enrichment with each trophic step and are indicative of the fractional trophic position of the consumer (Figure 6.2-1) (Popp et al., 2007). Thus, a sample from a single organism within an ecosystem can be used to estimate its trophic position and the likely isotopic composition of primary producers which can provide insights into nutrient source (McClelland et al., 2003). Further, unlike SIA, CSIA used in the present study targets amino acids that are associated with protein and therefore provide the best estimate of integration of prey into the growth of a predator. This acknowledges issues of variable nitrogen residency times in the tissue and how predator temporal food requirements may affect uptake of nitrogen of the prey into the tissue.

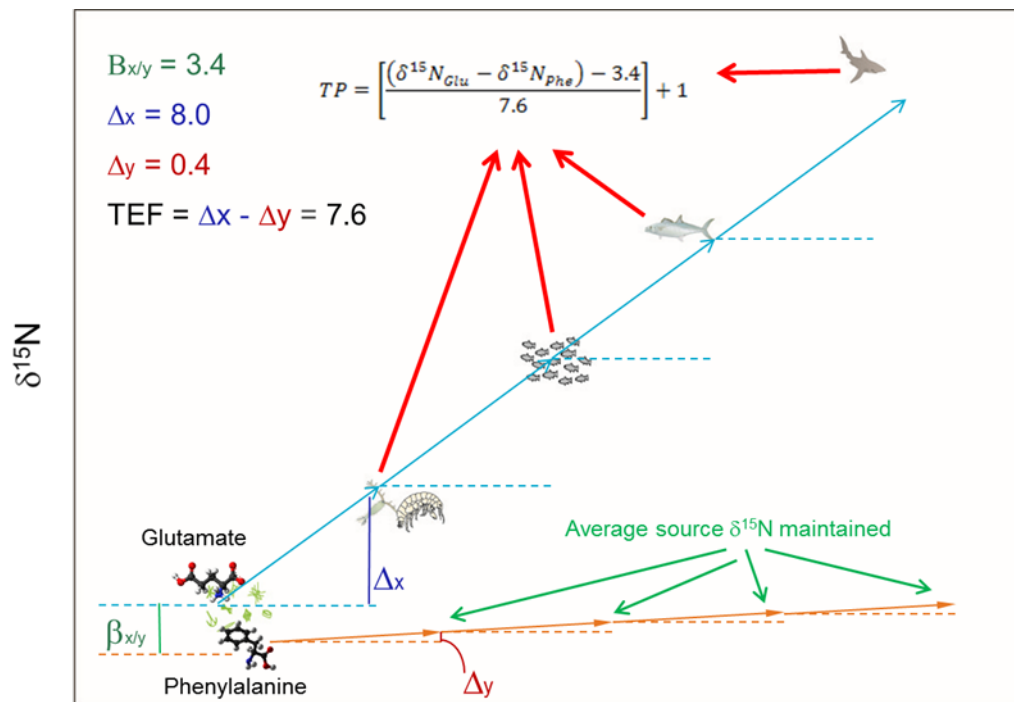


Figure 6.2-1 Explanation of fractionation (enrichment) of glutamate and phenylalanine through a food web and derivation of calculated trophic position (after Chikaraishi, Ogawa et al. 2009)

Given their ability to estimate trophic position, we have employed compound-specific methods in our study as a way to maximise information on food webs within the GAB to address Objective 3.

## 6.2.2 Methods

### Sample collection and Selection

Samples were obtained predominantly from MIDOC net trawls described in Section 6.1 but also from benthic beam trawls and handline fishing. Handline fishing was used to target the higher trophic level species such as tuna and large squid that were unlikely to be captured in the trawl nets. Species for analysis were chosen to address the key questions of the study that:

- Represented the main taxonomic groups of interest: crustaceans, squids and fishes;
- Were the most dominant in catches and sampled from both the Central and Eastern regions;
- Spanned a range of body sizes; and
- Were representative of the shelf-break, upper-slope, mid-slope and oceanic habitats.

Priority was given to dominant species that occurred in both the Central and East regions and in the offshore and upper slope habitats within the region as well as the ecologically significant species as identified in the literature for regional comparisons. Where possible, a minimum of three specimens was sampled for each region and habitat. Due to sampling limitations, full replication of species-specific depth ranges over day-night cycles within a region was not feasible.

After shipboard processing (counting, weighing and measuring), all specimens identified for isotope samples were wrapped in foil and frozen at sea for post voyage tissue dissection. Where time permitted, a minimum of 1 g muscle tissue sample was dissected from the specimen at sea and wrapped individually in foil or a glass vial with metal lined cap then stored at -20 °C. Post-voyage specimens identified for isotope samples were thawed and a minimum of 1 g muscle sample was dissected from the specimen and placed in glass scintillation vial and frozen. For very small

specimens such as the euphausiids, four individuals were pooled per sample and the whole body was used for analysis.

To enable examination of size class differences within species, some samples preserved in ethanol and formalin were included in the analysis. The preserved samples were processed in the same manner as the frozen samples as described above and it should be noted that preservation has no impact on amino acid compound specific isotopes, unlike traditional bulk isotope analyses.

### *Sample Processing and Analysis*

Samples for amino acid compound specific stable isotope analysis (CSIA) were prepared from a modified procedure to that of Brand et al. (1994) and Hofmann et al. (2003). Portions of white muscle tissue (60 – 80 mg, wet wt.) were placed in 16 mm ID screw top test tubes. One ml of 6 M HCl was added, the tubes flushed with N<sub>2</sub>, heated to 110 °C for 12 hr and samples then evaporated to dryness under a stream of N<sub>2</sub> at 60 °C. Samples were re-dissolved in 0.01 M HCl and amino acids purified using GracePure™ SPE Cation-X cartridges (#5141488). Cartridges were prepared for use by eluting 4 ml 0.01 M HCl. Samples were then applied to the top of the cartridge and a further 1 ml 0.01 M HCl rinsed through and discarded. Amino acids were then eluted from the cartridges with 4 ml 2 M NH<sub>4</sub>OH. Samples were evaporated until dry under a stream of N<sub>2</sub> at 60 °C.

Derivatives suitable for gas chromatography were obtained by firstly esterifying samples by adding 1 ml of acetyl chloride in isopropanol (1:4) and heating to 110 °C for 1 hr. Samples were again evaporated until dry under a stream of N<sub>2</sub> at 60 °C. Samples were trifluoroacetylated with the addition of 200 µl trifluoroacetic anhydride and 800 µl CH<sub>2</sub>Cl<sub>2</sub> and heated to 100 °C for 15 min. Samples were evaporated to dryness under a stream of N<sub>2</sub> at 60 °C and redissolved in 1 ml of hexane / dichloromethane (4:1) and 1 ml of aqueous phosphate buffer (pH 7.0, 5.36 g K<sub>2</sub>HPO<sub>4</sub> and 2.62 g KH<sub>2</sub>PO<sub>4</sub> in 500 ml of milli Q H<sub>2</sub>O). Samples were vortex mixed for 1 minute, centrifuged at 2000 rpm for 2 minutes and the top layer of hexane / dichloromethane containing the amino acids was extracted by pipette into a clean reaction tube. This procedure was performed twice more with two further 1 ml additions of hexane / dichloromethane mixture to ensure all the amino acid containing fraction had been extracted. Samples were evaporated to dryness under a stream of N<sub>2</sub> at 60 °C and were trifluoroacetylated again using the same procedure as above. Finally, samples were evaporated until dry under a stream of N<sub>2</sub> at 60 °C and redissolved in dichloromethane for analysis.

Amino acids were first analysed by gas chromatography (Thermo Scientific 1310, GC conditions as below) to determine relative proportions of each amino acid by measuring peak areas. The  $\delta^{15}\text{N}$  isotope composition of the amino acids were determined with a Trace GC gas chromatograph interfaced with a Delta V Plus isotope ratio mass spectrometer (IRMS) through a GC-C combustion furnace (980 °C), reduction furnace (650 °C) and liquid N<sub>2</sub> cold trap. The samples (0.5 µl) were injected splitless (split/splitless injector, 10:1 split ratio) onto a forte BPX5 capillary column (30 m × 0.32 mm × 1.0 µm film thickness) at an injector temperature of 180 °C with a constant helium flow rate of 1.5 ml min<sup>-1</sup>. The column was initially held at 50 °C for 2 min and then increased to 120 °C at a rate of 10 °C min<sup>-1</sup>. Once at 120 °C, the temperature was increased at a rate of 4 °C min<sup>-1</sup> to 195 °C and then at 5 °C min<sup>-1</sup> to 235 °C where it was held for 5 min. The temperature was then further increased to 300 °C at 15 °C min<sup>-1</sup> and held for 8 minutes. All samples were analysed at least in triplicate.

The  $\delta^{15}\text{N}$  values were normalised as follows: each sample analysis consisted of three separate IRMS analyses bracketed by a suite of amino acids with known  $\delta^{15}\text{N}$  values. The slope and intercept of known vs measured values were then used to correct the measured values for the sample set. In

addition, an internal reference compound, norleucine, also of known nitrogen isotopic composition, was co-injected with samples. The norleucine provided a check of combustion conditions and the consistency of normalisation using the bracketing standards.

Reproducibility associated with isotopic analysis of glutamic acid and phenylalanine averaged  $\pm 0.44$  ‰ (1 SD) and ranged from  $\pm 0.06$  ‰ to  $\pm 0.85$  ‰.

Trophic position was calculated according to the following equation:

$$TP = \frac{\delta^{15}N_{Glu} - \delta^{15}N_{Phe} - \beta}{TDF} + 1$$

Where  $\beta$  = the isotopic offset between phenylalanine and glutamate in primary producers (usually 3.4 ‰ in marine phytoplankton) and TDF is the Trophic Discrimination Factor initially assigned as 7.6 ‰ by Chikaraishi et al. (2009) with a suggested revision for teleosts to 5.0 ‰ by Nielsen et al. (2015). In this study we used TDF=7.6 for a consistent comparison as little is known about isotopic fractionation in many of the species studied but have applied TDF=5.0 for interpretation of fish results. All data were subsequently analysed using the R statistical package (ver. 3.3.2).



### 6.2.3 Results

A total of 134 individual samples across 19 species were analysed for compound-specific amino acid nitrogen isotopes (Table 6.2-1). A wide range of values were recorded for the three main parameters:

1. Ratio of Glutamate (trophic) to Phenylalanine (source) amino acids
2. Calculated trophic position, and
3.  $\delta^{15}\text{N}$  of the source amino acid phenylalanine

The ratio of glutamate (trophic) to phenylalanine (source) amino acid content was quite variable with the largest range observed in the squids, followed by the fish, with the crustaceans exhibiting the lowest range and most consistent values (Table 6.2-1). Within the squids, most variation in this parameter appears to be derived from *Heteroteuthis* sp. and within the fishes, the silver lightfish *Phosichthys argenteus* had the most variable results (Table 6.2-1, Figure 6.2-2).

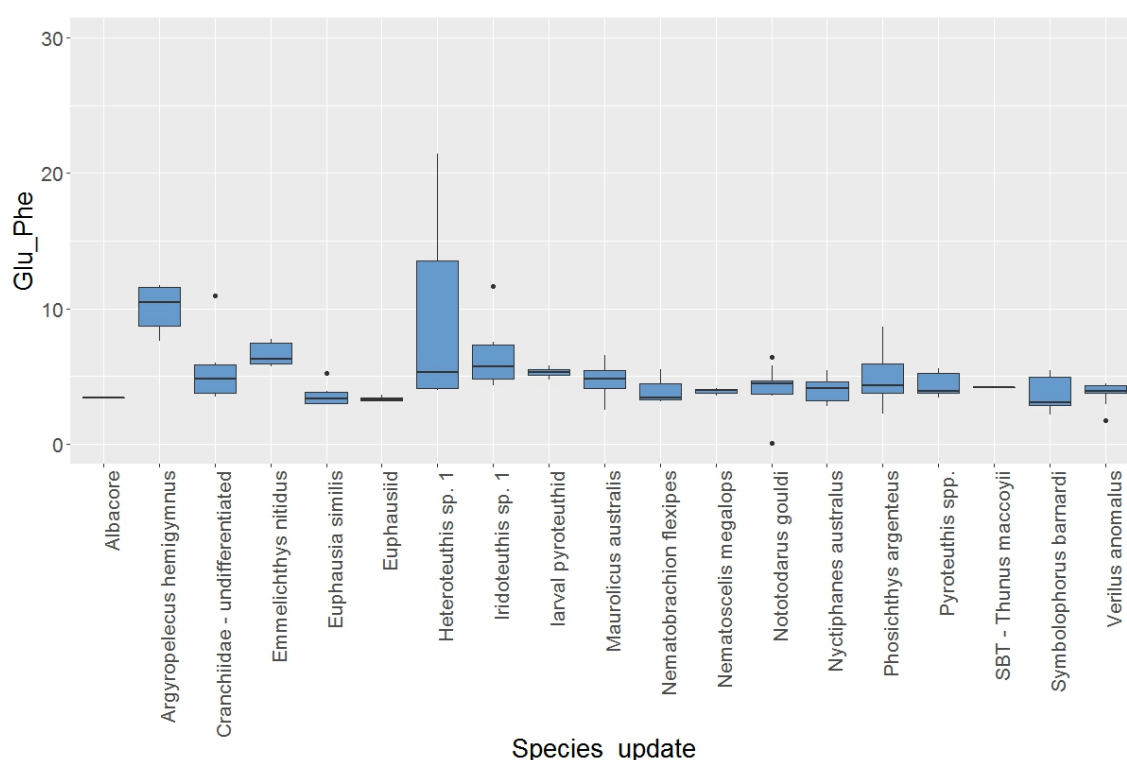


Figure 6.2-2 Measured Glutamate to phenylalanine ratios for all species.

## Micronekton

Table 6.2-1 Summary of amino acid results for each species analysed. Glu:Phe = peak area ratio of Glutamate:Phenylalanine, TP = calculated trophic position (for crustaceans and squid TDF=7.6; for fish TDF=5.0) and Phe =  $\delta^{15}\text{N}$  value of the "source" amino acid phenylalanine

	n	Glu:Phe			TP			Phe		
		min	max	mean	min	max	mean	min	max	mean
Fish	62	1.7	11.7		1.4	5.5		-1.3	13.2	
<i>Phosichthys argenteus</i>	13	2.2	8.6	4.9	2.9	4.6	3.7	2.7	9.5	6.1
<i>Maurolicus australis</i>	12	2.5	6.6	4.7	2.0	4.1	3.4	2.9	10.3	5.4
<i>Emmelichthys nitidus</i>	9	5.7	7.7	6.6	2.8	3.2	3.0	7.5	12.9	10.1
<i>Verilus anomalus</i>	11	1.7	4.5	3.8	1.4	5.5	3.4	-1.3	7.1	3.7
<i>Argyropelecus hemigymnus</i>	6	7.6	11.7	10.0	0.3	3.7	2.7	8.9	13.2	10.6
<i>Thunnus maccoyii</i> (820 mm S.L.)	1			4.2			3.5			10.1
<i>Thunnus alalunga</i> (720 mm S.L.)	1	3.4	3.4	3.4			3.4	2.4	2.4	2.4
<i>Symbolophorus barnardi</i>	9	2.1	5.4	3.6	3.2	4.9	3.9	2.6	11.1	4.8
Crustacean	30	2.8	5.5		1.6	3.7		-1.0	13.8	
<i>Nematoscelis megalops</i>	3	3.5	4.1	3.9	2.2	2.9	2.7	4.8	2.9	7.9
<i>Nyctiphanes australis</i>	15	2.8	5.4	3.9	1.6	3.7	2.5	-1.0	3.7	3.0
<i>Euphausiidae undifferentiated</i>	3	3.2	3.6	3.4	2.7	3.0	2.8	2.9	3.2	3.0
<i>Nematobrachion flexipes</i>	3	3.5	4.1	3.9	2.2	2.9	2.7	4.8	13.8	7.9
<i>Euphausia similis</i>	6	3.0	5.2	3.6	2.2	3.3	2.9	0.8	5.2	3.5
Squids	42	0.0	21.5		1.9	3.7		0.1	14.9	
<i>Heteroteuthis</i> sp. 1	6	4.0	21.5	9.3	2.8	3.4	3.1	0.1	7.2	5.0
<i>Iridoteuthis</i> sp. 1	6	4.3	11.7	6.6	2.3	3.3	2.9	1.5	14.9	7.0
Pyroteuthidae larvae	4	4.7	5.8	5.3	3.1	3.7	3.5	2.8	5.0	4.0
Cranchiidae - undifferentiated	6	3.5	11.0	5.6	2.0	3.5	2.7	3.4	11.0	6.0
<i>Pyroteuthis</i> spp.	5	3.4	5.6	4.4	2.6	3.5	3.0	3.0	10.5	7.5
<i>Iridoteuthis</i> sp. 1	6	4.3	11.7	6.6	2.3	3.3	2.9	1.5	14.9	7.0
<i>Nototodarus gouldi</i>	9	0.0	6.4	4.1	1.9	3.7	2.8	1.5	14.2	6.9

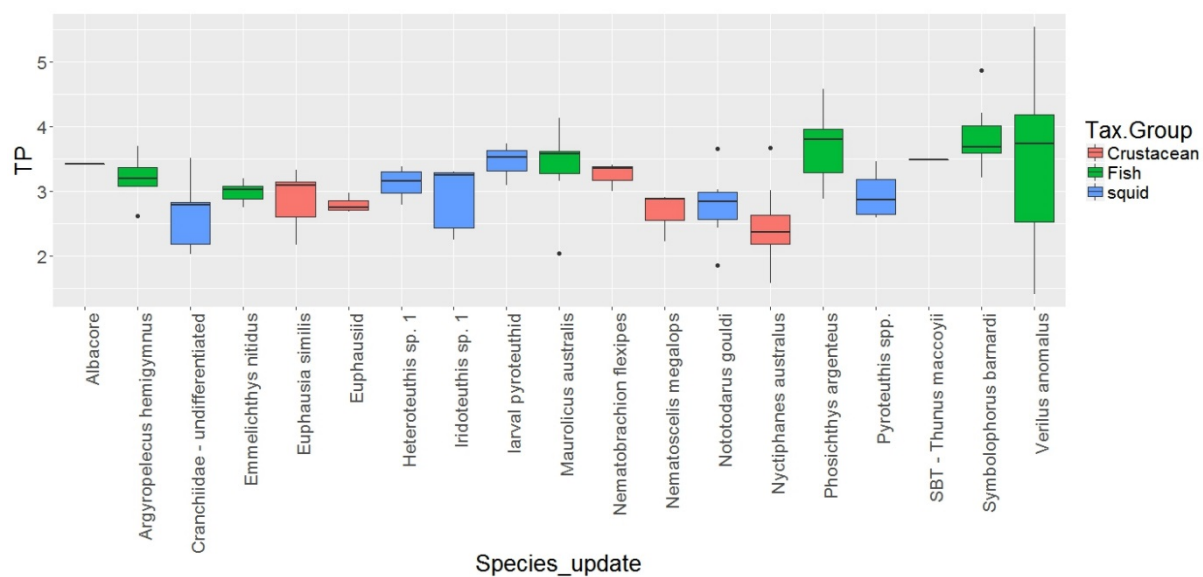


Figure 6.2-3 Trophic position calculated from compound specific amino acid data for all species analysed. Note: For crustaceans and squid TDF=7.6 and for fish TDF=5.0.

Variation in calculated trophic position appears to be similar across the three classes analysed with a range of approximately 1.5 to 5.5 (Table 6.2-1, Figure 6.2-3). Interestingly, even within the crustaceans there was a range of 2 trophic positions for some species (*N. australis*), potentially indicating the influence of factors such as local variation in food web structure or size related effects.

## Crustaceans

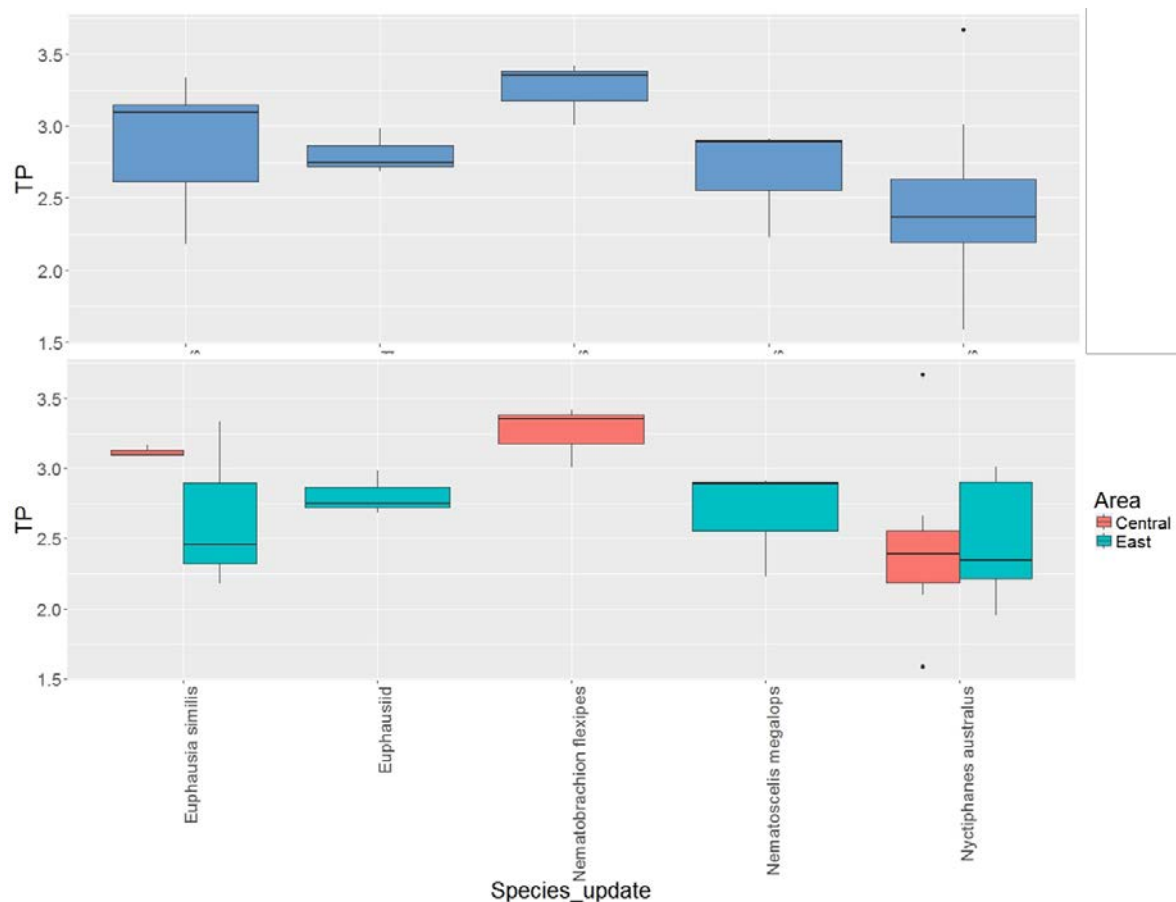


Figure 6.2-4 Average calculated trophic position (top) and categorised by catch region (bottom) for each species of crustacean analysed.

For crustaceans that were represented in the central and eastern GAB, mean calculated trophic position for two species was higher in the central GAB than the east (Figure 6.2-4). This appears to correlate with an increased occurrence of picoplankton in the central region (chapter 4.1) suggesting that an increase in the dominance of phytoplankton in the <2  $\mu\text{m}$  size range has resulted in an elevated trophic position, which is in agreement with the proposed hypothesis outlined in Figure 2.1-2.

In the central GAB, *Euphausia similis* and *Nematobrachion flexipes* had higher calculated TP than *Nyctiphanes australis* (Figure 6.2-4). The mean length of *E. similis* (21.6 mm) and *N. flexipes* (21.8 mm) in the GAB catches was higher than that of *N. australis* (13.7 mm) and this size differential may correspond to differential prey selection and may partly explain the TP differences. The habitat of *N. australis* in both the central and east regions of the GAB was exclusively the shelf-break to upper-slope, whereas *N. flexipes* was exclusively oceanic. *E. similis*, was recorded in oceanic and mid-slope habitats. However, the mean phenylalanine  $\delta^{15}\text{N}$  for these three species/habitats does not indicate a significant difference in source (base of foodweb) values indicating that habitat-derived differences are not driving the differences observed in the calculated TPs. This suggests that *E. similis* and *N. flexipes* feed at higher trophic positions than *N. australis*, at least in the Central GAB.

Phenylalanine  $\delta^{15}\text{N}$  for *N. australis* in the central region was highly variable and significantly more depleted than that in the East (Figure 6.2-5). As this species is confined to the shelf break and upper-

slope habitats in both regions, this result indicates that the shelf-break and upper-slope waters in the central and eastern regions are exposed to different sources of nutrients at the base of the foodweb, probably driven by differential water mass influences on these habitats.

*Nematoscelis megalops* from the eastern region of the GAB was sampled from oceanic habitat and recorded significantly enriched, and variable, phenylalanine  $\delta^{15}\text{N}$  values compared to the other crustacean species (Figure 6.2-5). This result concords with a working hypothesis of a more enriched phenylalanine  $\delta^{15}\text{N}$  value associated with the eastern region.

*E. similis* was sampled from mid-slope and oceanic habitats of the central and eastern regions and again phenylalanine  $\delta^{15}\text{N}$  was more enriched in the Eastern region (Figure 6.2-5), although means were not significantly different. This potentially indicates a mixing of water mass influences in these habitats.

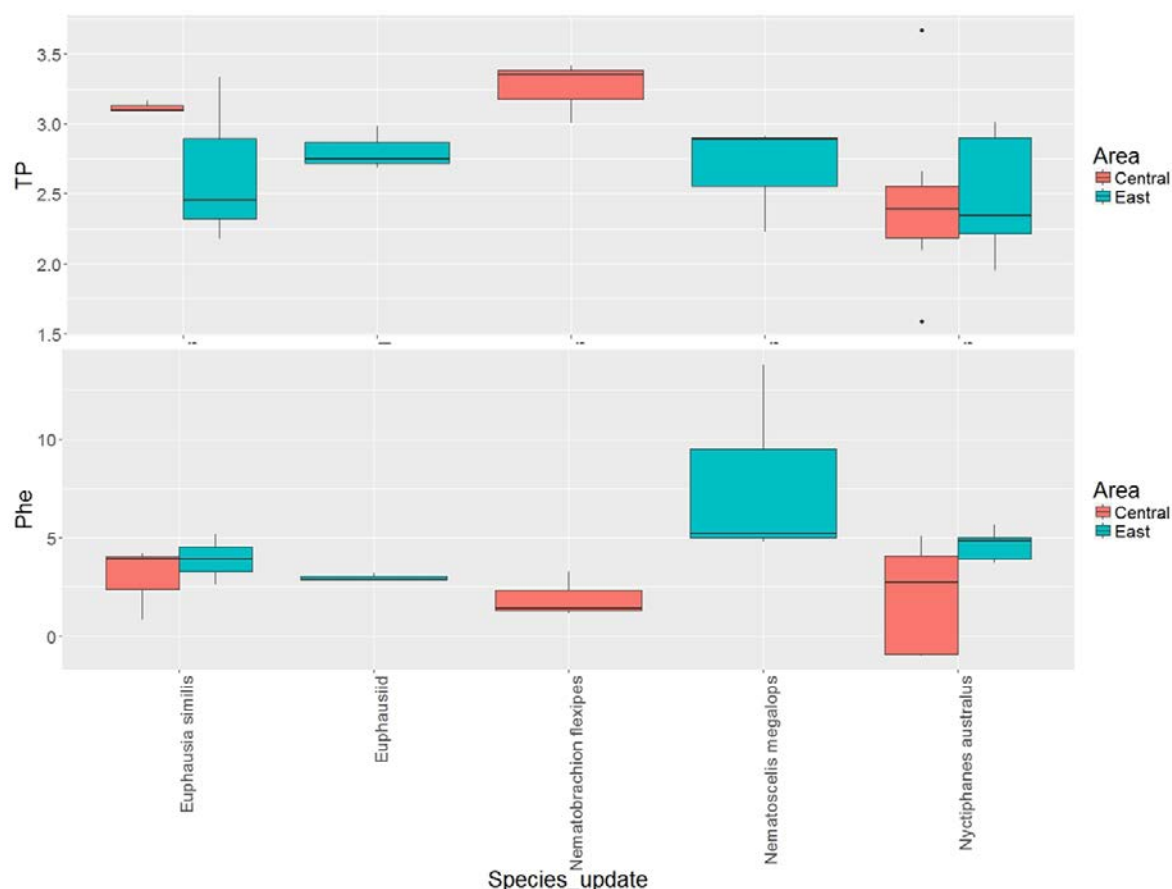


Figure 6.2-5 Comparison of crustacean calculated trophic position (top) and phenylalanine  $\delta^{15}\text{N}$  values (bottom) across the central and eastern GAB.

A comparison between calculated trophic positions and the  $\delta^{15}\text{N}$  values of the “source” amino acid phenylalanine, suggests that there is a difference in the source of nitrogen driving the two food webs, with values in the central GAB consistently more depleted, indicating more nitrogen derived from nitrogen fixation and less drawdown compared to the east (Figure 6.2-5). As described above, there was an increased abundance of picoplankton observed in the central region (Section 4.1) and this sub-set of phytoplankton is known to contain nitrogen fixing photosynthetic cyanobacteria and other diazotrophs, more generally associated with warmer, oligotrophic waters. It’s not clear if these organisms are actively fixing nitrogen but they do appear to be influencing the baseline  $\delta^{15}\text{N}$  of the food web in the central region and one species, *N. australis*, appears to have some individuals feeding directly on these organisms as shown by the occurrence of heavily depleted phenylalanine

$\delta^{15}\text{N}$  (Figure 6.2-5). It is also possible that there is an increase in heterotrophic bacteria leading to high levels of nitrogen re-mineralisation. Any influence from these is likely to be isotopically “invisible” (Gutierrez-Rodriguez et al., 2014) which would potentially conserve the depleted  $\delta^{15}\text{N}$  phenylalanine value but would not therefore lead to the observed elevated trophic position in two of the three crustacean species.

### Fish

Calculated trophic positions for fish using standard trophic discrimination factors of 7.6 ‰ and a recently recommended value of 5.0 ‰ (Nielsen et al., 2015) are presented in Table 6.2-2. The values derived by using a discrimination factor of 5.0 ‰ (Figure 6.2-3 and Figure 6.2-6) are considered most appropriate because they are in general agreement with those presented for lanternfishes and other micronekton in the region and known stomach contents (Choy et al., 2012; Flynn and Kloser, 2012).

*Verilus anomalus* (a benthopelagic species that occupies shelf and shelf-break habitat) and *Emmelichthys nitidus* (epipelagic juveniles sampled from the shelf-break and upper- to mid-slope habitat with replicates also taken from the oceanic habitat in the Eastern region) recorded significantly more enriched phenylalanine  $\delta^{15}\text{N}$  values in the eastern region than the central region (Figure 6.2-7). This is in agreement with the results for shelf-break and upper- to mid-slope crustacean species above and supports the hypothesis that the inshore habitats of the eastern and central regions are influenced by processes that introduce different nutrient sources.

The two species that are diel vertical migrators (*Symbolophorus barnardi* and *Maurolicus australis*) and a lower mesopelagic non-migrator (*Phosichthys argenteus*) were generally associated with mid-slope to oceanic habitat and recorded a pattern in phenylalanine  $\delta^{15}\text{N}$  values that contrasts with those for the shelf-break/upper-slope. For these species, mean phenylalanine  $\delta^{15}\text{N}$  was more depleted in the eastern region (Figure 6.2-7). For *P. argenteus*, the lower-mesopelagic non-migrator, this difference was significant. The interactions between these species and deep water masses is one factor that may be influencing source amino acid  $\delta^{15}\text{N}$  values (see below). It is unclear why this potential enrichment of phenylalanine  $\delta^{15}\text{N}$  in deep water masses differs between the central and eastern regions. *Argyropelecus hemigymnus* undergoes moderate diel vertical migrations from the upper mesopelagic to the epipelagic zone. Samples of this species were only analysed from the central region and recorded among the most enriched phenylalanine  $\delta^{15}\text{N}$  values.

Table 6.2-2 Comparison of average calculated trophic position for fish species using two different trophic enrichment factors (TEF). For TP TDF=7.6; for TP2 TDF=5.0.

Species	TP	TP2
<i>Phosichthys argenteus</i>	2.8	3.7
<i>Maurolicus australis</i>	2.6	3.4
<i>Emmelichthys nitidus</i>	2.3	3.0
<i>Verilus anomalus</i>	2.6	3.4
<i>Argyropelecus hemigymnus</i>	2.4	2.7
<i>Thunnus maccoyii</i>	2.6	3.5
<i>Thunnus alalunga</i>	2.6	3.4
<i>Symbolophorus barnardi</i>	2.9	3.9

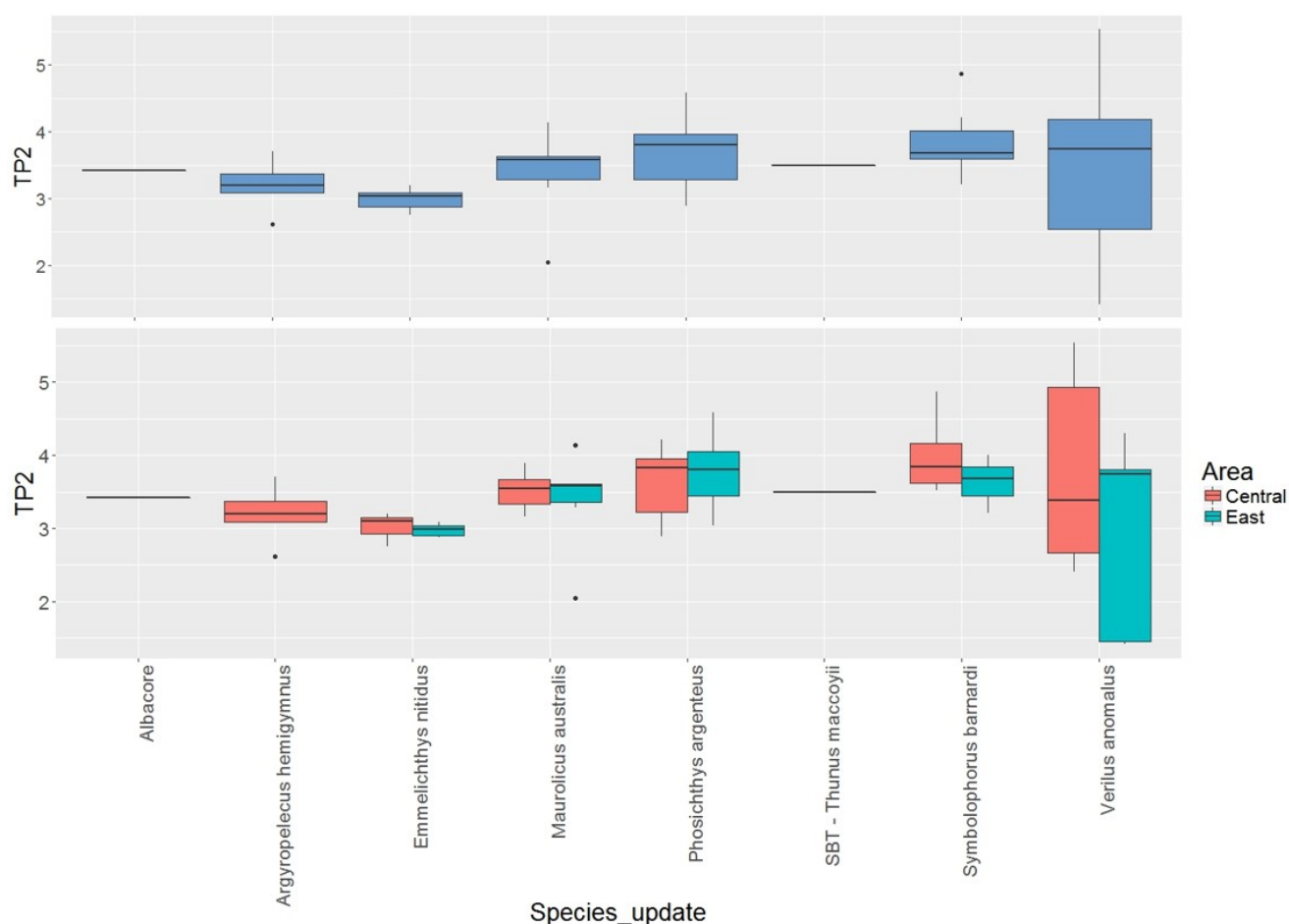


Figure 6.2-6 Calculated trophic position for fish species as mean of all individuals (top) and by species in central and east areas (bottom).



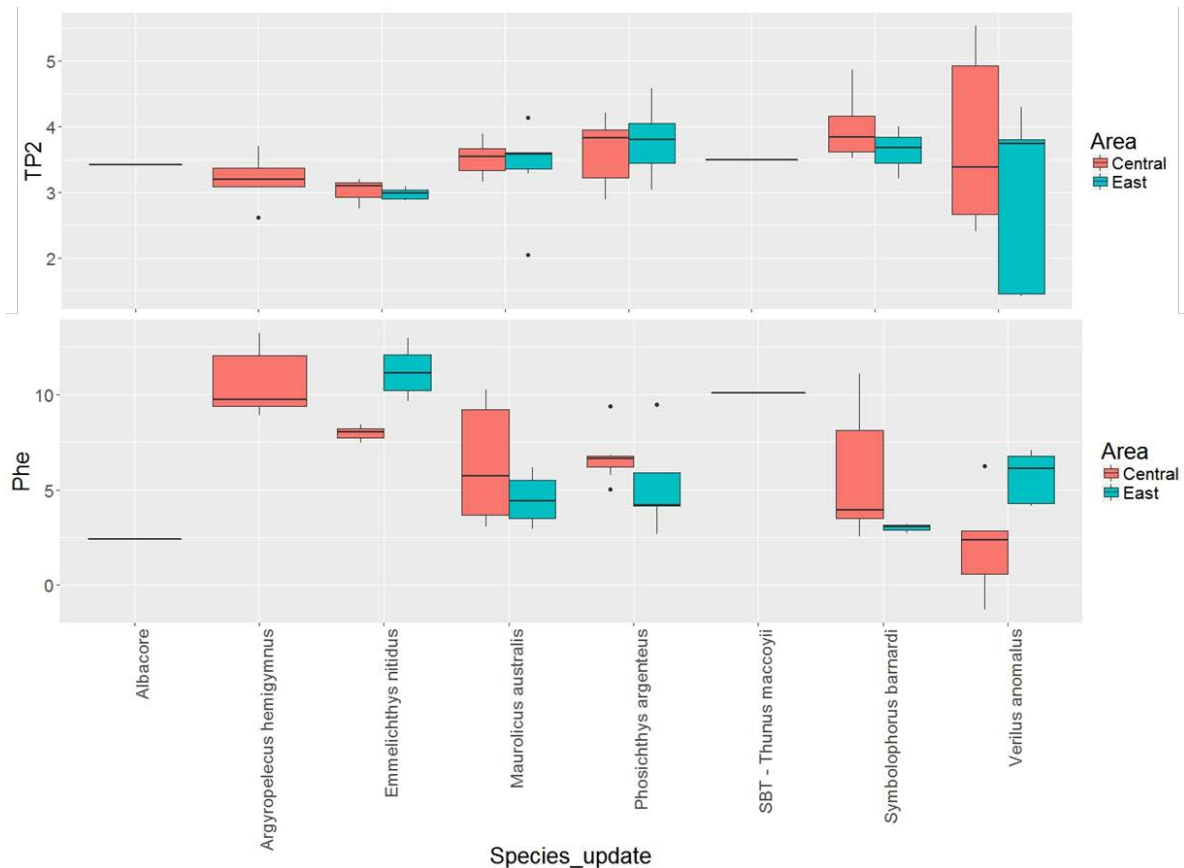


Figure 6.2-7 Comparison of fish calculated trophic position (top) and phenylalanine  $\delta^{15}\text{N}$  values (bottom) in the central and eastern GAB.

Phenylalanine  $\delta^{15}\text{N}$  values for *Thunnus maccoyii* and *Thunnus alalunga* were markedly different (Figure 6.2-7), suggesting contrasting feeding histories for these species in the GAB, although the lack of replication for these species must be considered. *Thunnus alalunga* is circumglobal but core habitat is considered tropical-subtropical<sup>1</sup> (Williams et al., 2015) while *Thunnus maccoyii* is principally a temperate species (Hartog et al., 2011). *Thunnus maccoyii* attains a larger maximum size than *T. alalunga*, but the individual of the former species analysed in the present study was a juvenile and approximately the same size as the *T. alalunga* specimen. The vertical foraging behaviours of these two species is similar although *T. maccoyii* appears to make deeper dives (Patterson et al., 2008). Trophic position for the two species, was calculated to be similar, at the mid-third level. Off Tasmania, Young et al. (1997) reported that *T. maccoyii* prey was habitat specific but contained high proportions of crustaceans and molluscs along with fishes and cephalopods and that prey diversity was highest in stomach samples from offshore stations. The authors also noted foraging of *Nyctiphanes australis* by *T. maccoyii* at inshore stations. Duffy et al. (2017) reported that the proportion of euphausiids and molluscs in *T. alalunga* diet exceeded that of squid and fish prey in some areas. Similarly, Williams et al. (2015) reported a high proportion of crustaceans in diets of *T. alalunga* from NZ. Therefore, the calculated TPs for the two tuna species, from these preliminary data, are in agreement with diet studies. A more depleted phenylalanine  $\delta^{15}\text{N}$  value for *T. alalunga* is consistent with tropical feeding as these environments generally have a higher proportion of nitrogen fixation. This suggests that this specimen had not been resident in the GAB or feeding in the area long enough to alter the tissue isotopic “source” value.

<sup>1</sup> <http://www.afma.gov.au/portfolio-item/albacore-tuna/>

## Squid

The squid species analysed generally occupied Trophic Positions (TP) of 2.5 to 3.5 (Figure 6.2-8). Three species were analysed in both the eastern and central regions and there were no marked differences or consistent patterns. The result for larval pyroteuthid squids is unexpected as larval squids are generally known to have a small feeding tube that necessitates the ingestion of very small prey.

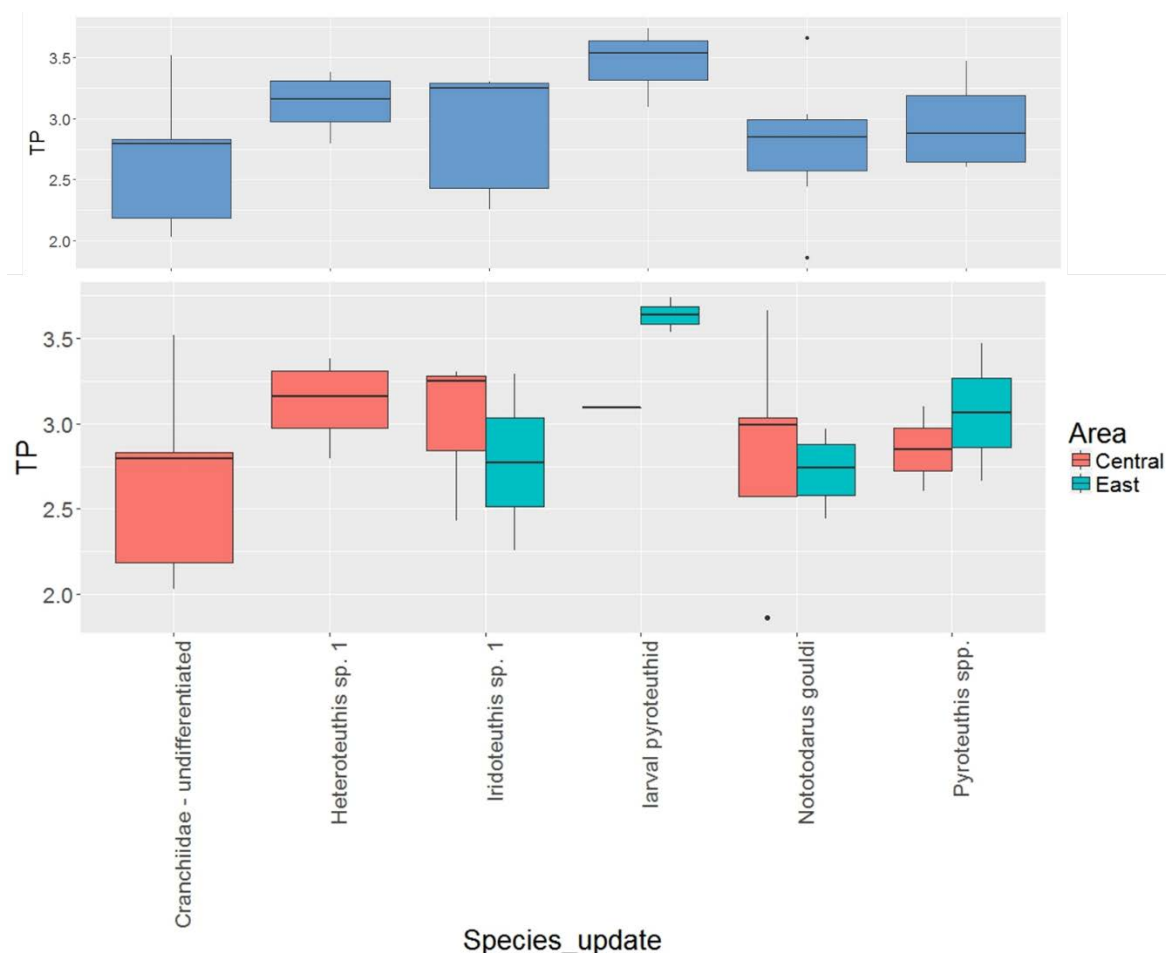


Figure 6.2-8 Calculated trophic position (TP) for squid species as mean of all individuals (top) and by species in central and east areas (bottom).

The  $\delta^{15}\text{N}$  values for phenylalanine for the *Nototodarus gouldi*, *Pyroteuthis* spp. and larval pyroteuthids is similar to that described for vertically migrating and deep-resident fishes, that is, more enriched values in central compared to eastern regions (Figure 6.2-9). This result is somewhat unexpected for *N. gouldi* because this species is typically considered an epipelagic species, although Norman and Reid (2000) note that the species occurs throughout the water column; over 95% of New Zealand's arrow squid (*Nototodarus sloanii*) catch is taken by deepwater trawls (~300 - 500 m depth) and are known to at least 825 m and taken as incidental catch in the Great Australian Bight Trawl Sector<sup>2</sup>. Until further sampling can be done, the working hypothesis is that differences in the interactions between vertical habitat use and water mass influence in the eastern and central regions account for differences in phenylalanine  $\delta^{15}\text{N}$  values in squids. Further, a working hypothesis is that squids occupy a lower, but overlapping range of trophic positions than micronekton fishes.

<sup>2</sup> <http://www.afma.gov.au/portfolio-item/goulds-squid/>

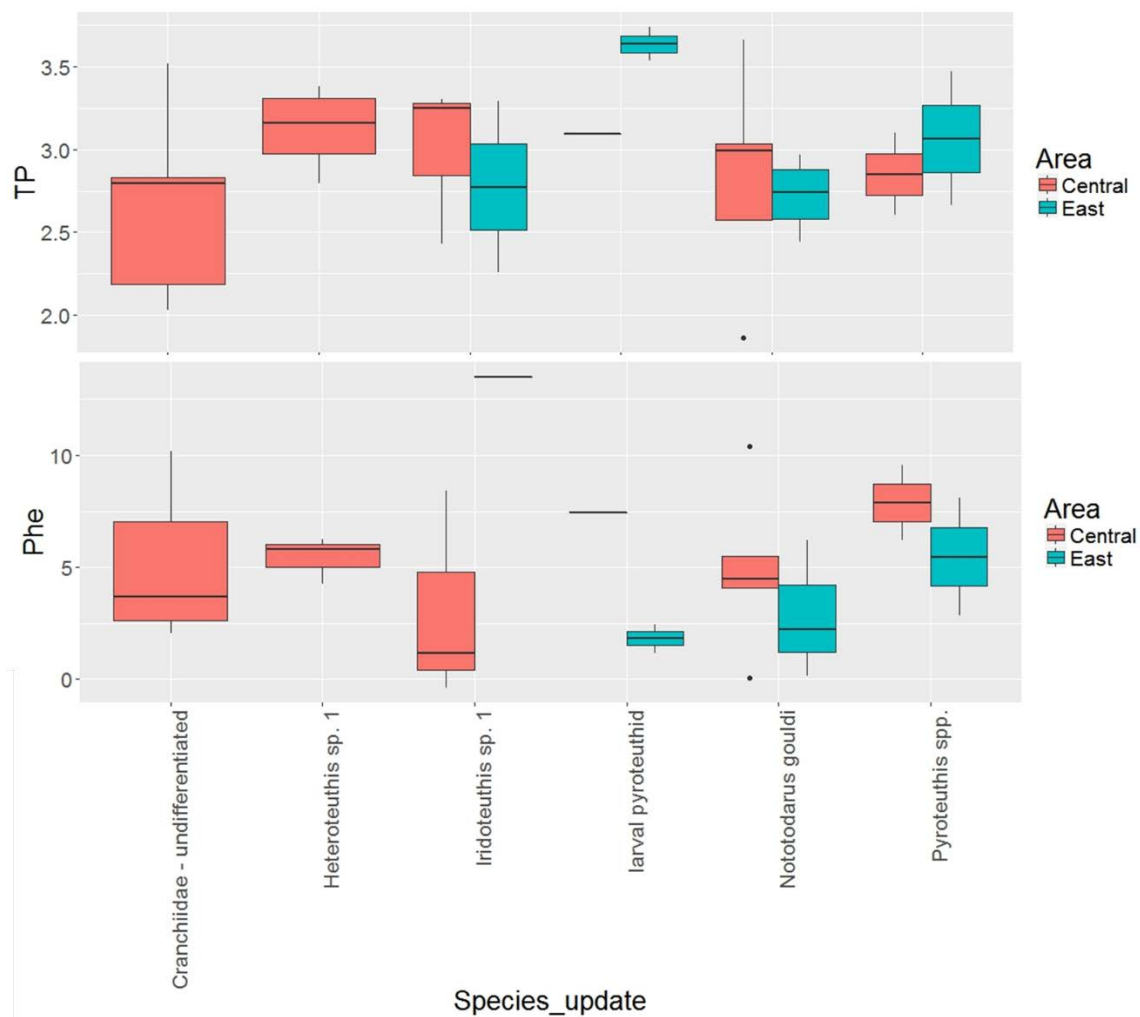


Figure 6.2-9 Comparison of squid calculated trophic position (top) and phenylalanine  $\delta^{15}\text{N}$  values (bottom) across the central and eastern GAB.

#### Water Mass Source Differentiation

Categorisation of the samples by the depth zone from which they were sampled indicated that there are significant differences in phenylalanine  $\delta^{15}\text{N}$  values among depth zone for the fish samples (Figure 6.2-10). Further, the phenylalanine  $\delta^{15}\text{N}$  value for the upper and lower mesopelagic zones differs significantly between the central and eastern regions. Together, these results indicate that vertically stratified water masses within a region have different source isotopic values and that between regions, the processes controlling the baseline isotopic properties of these water masses differs. This finding supports the hypothesis that contrasting broad scale oceanographic regimes exist in the two central and eastern regions. Therefore, the vertical niche selection and migration behaviours of pelagic species in the mid-slope and oceanic habitats in particular, superimposed on this vertically structured baseline isotopic regime, are likely to explain some of the variability observed among the fish species sampled. This highlights the importance of the vertical dimension in sample design and elucidation of food web interactions.

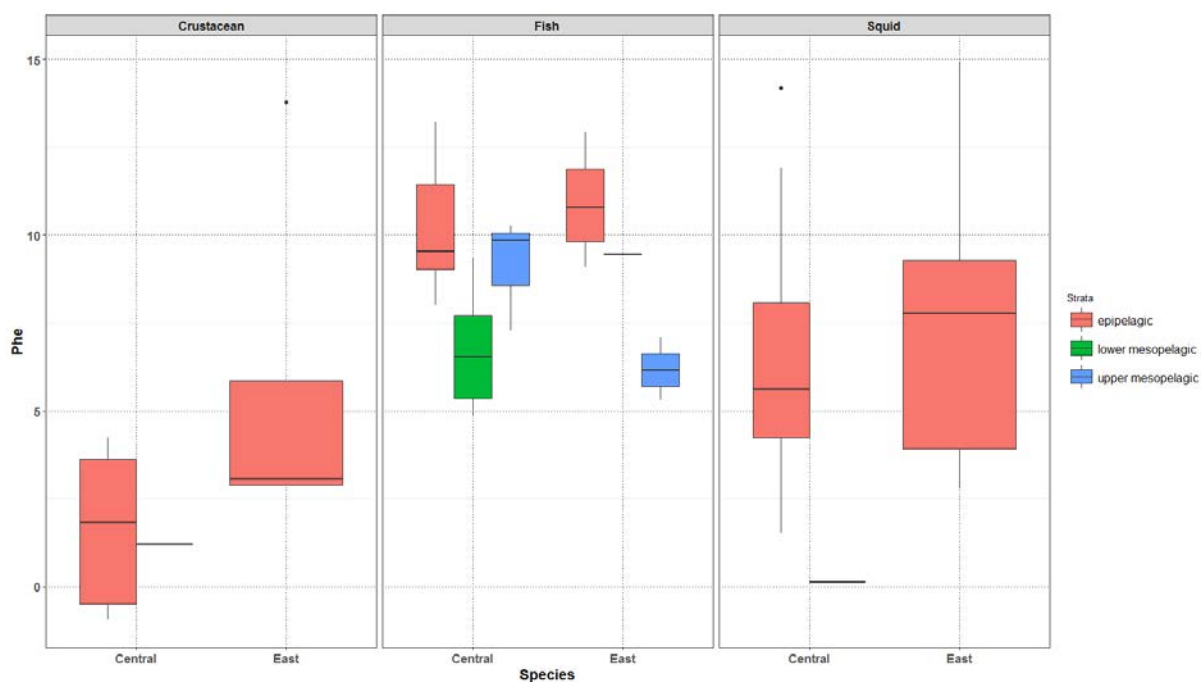


Figure 6.2-10 Phenylalanine  $\delta^{15}\text{N}$  (Phe) values in depth stratum for each faunal group.

## 6.2.4 Discussion

### Regional differences

Oceanographic processes in the GAB, most notably upwelling, are hypothesised to influence food webs of the continental shelf and upper pelagic communities, but to date there has been little direct evidence of this. Crustaceans are primary consumers and as such are often utilised to infer differences in primary production, which can be difficult to sample directly. In the present study, there is evidence that the  $\delta^{15}\text{N}$  of the “source” amino acid, phenylalanine, is relatively enriched by up to 2 ‰ in crustaceans sampled in the eastern region of the GAB compared to those from the central region, a pattern that is most evident for the shelf-break and upper slope habitats where populations of *Nyctiphanes australis* occur. This is consistent with a model of nitrate-based upwelling or influence of higher latitude water masses via the Flinders Current in the eastern region compared with microbially mediated N-recycling or oligotrophic conditions in central region. Indications of apparent enrichment of phenylalanine  $\delta^{15}\text{N}$  in the mid-slope and oceanic habitats of the eastern region, with respect to crustaceans, are complicated by reduced sample replication and vertical migration behaviour of the crustacean species in those habitats. The relative depletion of source  $\delta^{15}\text{N}$  in the central region may explain the apparently higher trophic position of crustaceans in that region as it may reflect the presence of a higher proportion of picoplankton (Section 4.1) and therefore an additional trophic step.

Similarly for fishes, the results are most conclusive for *Verilus anomalus* and *Emmelichthys nitidus*, which are shelf-break/upper slope species and that showed a marked enrichment of phenylalanine  $\delta^{15}\text{N}$  values in the eastern region compared to the central region. For vertically migrating and deep non-migrating species, there appears to be a contrasting pattern of relative enrichment in the central region. It is hypothesised that this is driven by interactions between the

behaviour of these species and deep water masses that have a different base isotopic composition or source between regions.

The results of this study, and in particular the results relating to shelf-break and upper slope species of crustaceans and fishes, are consistent with the hypotheses outlined in bold that:

1. *The “microbial food web” is the dominant planktonic food web over the deep GAB continental margin, particularly in the central GAB where year-round downwelling is thought to be the prevailing cross-margin flow, and that the more efficient “classic food web” only dominates in the eastern GAB during periods of nutrient-rich upwelling.*
2. *The zooplankton and micronekton communities of the central GAB continental margin have lower biomass, smaller species, different composition and **longer trophic pathways than those on the eastern GAB. This is due to the nutrient source being “microbial food web” dominated in the central GAB and “classical” food web dominated in the eastern GAB***

### *Trophic interactions*

Shelf-break/upper slope crustaceans (*Nyctiphanes australis*) appear to feed at a lower trophic level than mid-slope and oceanic species. This is generally consistent with the finding that Davenport and Bax (2002) calculated the TP of ‘pelagic zooplankton’ on the continental shelf off southeastern Australia as TP 2 and that Flynn and Kloser (2012) calculated for the *Euphausia similis/spinifera* complex as TP 3 in the southern Tasman Sea abyssal basin. It should also be acknowledged that *N. australis* is among the smallest crustacean species sampled in the present study, which dictates prey size handling and thus trophic position.

A key assumption of the calculation of trophic position of fishes is that the Trophic Discrimination Factor (TDF) is applicable uniformly in all taxa. Choy et al. (2012) recognised that calculated trophic position for *Chauliodus sloani* (a dragonfish in the family Stomiidae) based on CSIA was unexpectedly low and suggested that sporadic feeding and low locomotion may equate to low metabolic rate and slower protein turnover in dragonfishes. The same may be true for *Phosichthys argenteus* which had a mean calculated trophic position that was slightly higher than *Maurolicus australis* and in a similar range to *Symbolophorus barnardi*, despite the relatively large size of *P. argenteus* (144.7 mm SL) and the reported dominance of fishes in the diet of this species off southern Tasmania (Williams et al., 2001). It is interesting to note that the calculated TP for *P. argenteus* was in a similar range to that for *C. sloani* in the southern Tasman Sea abyssal basin (Choy et al., 2012). *Phosichthys argenteus* is a non-migrating lower mesopelagic predator with a body form and ecology similar to dragonfishes. It is possible that the TDF applied, which generated TP estimates that are concordant with stomach contents and previous studies for the other fish species analysed, is less applicable to *P. argenteus*.

*Symbolophorus barnardi* recorded the highest mean TP among the fishes, but the highest maximum values were recorded in *Verilus anomalus*. These two species represent contrasting life-histories: *S. barnardi* is a relatively short-lived (2-3 years), oceanic, vertically-migrating species that was among the larger-sized lanternfishes (mean 70.9 mm S.L.) sampled in the GAB, while *V. anomalus* is a larger-bodied (mean sampled in GAB 101.8 mm S.L., maximum size reported to 150 mm) shelf-break/upper slope/mid-slope benthopelagic species. Like most other lanternfishes, the main prey of *S. barnardi* is considered to be pelagic crustaceans, dominated by krill, but some species and larger individuals are known to feed on juvenile lanternfishes (Young and Blaber, 1986). The results of the present study support the observation that *V. anomalus* appears to be an important predator of the mesopelagic fishes such as the lanternfish *Lampanyctodes hectoris* in eastern Tasmania (Bulman et al., 2001) and *Diaphus danae*, *Lampanyctus australis* and *Lampanyctus procerus* in western Tasmania (CSIRO

Unpub. data). A similar dominance of *Lampanyctodes hectoris* in the diet of *V. anomalus* may be expected in the GAB as *L. hectoris* was recorded in moderately high abundance at the shelf break and upper slope. *Verilus anomalus* may also feed on *M. australis*, particularly during the day when the latter resides close to the bottom this is supported by observations from western Tasmanian.

Trophic position of the single specimens of juvenile *Thunnus maccoyii* and *T. alalunga* are consistent with known stomach contents. These species appear to feed at a middle position of the third trophic level and do not appear to be feeding on mesopelagic fishes that occupy the same or higher trophic position. However, pyroteuthid squid remains were observed in the stomach contents of the single *T. alalunga* specimen. Further sampling and consideration of temporal/ontogenetic changes in feeding behaviour of tunas is required for more conclusive results.

The squid species sampled had a mean trophic position ranging from 2.8 to 3.1 (omitting the anomalous value recorded for larval pyroteuthids of 3.5). Squids are generally fast growing and short lived. Little is known about the trophic isotopic fractionation of squid and it may well be that the TDF used in the present study (7.6 ‰) is not the most appropriate, although the results are generally consistent with the findings of Coll et al. (2013). Squids are known to have diverse feeding behaviours that are reflected in a large range of TPs, with most generally spanning the third to fourth trophic level (Coll et al., 2013; Navarro et al., 2013). Micronekton sampling recorded diverse and abundant cephalopod communities in the GAB and recent research has highlighted the role of squid in particular in pelagic systems (see Young et al. 2015 for overview). While the details of trophic interactions of the diverse range of squids in the GAB is unconfirmed, it is clear that squids in the Southern Ocean (Rodhouse, 2013) and other ocean basins (Young et al., 2015) are important predators and prey and play an important role in mediating mid-trophic interactions.

### Summary

It is clear from this work that the use of compound specific stable isotope analysis of individual amino acids has been able to elucidate differences between the food webs operating in the eastern and central upper slope GAB with the east apparently more reliant on upwelled nutrients and the central GAB under an increased influence by picoplankton and nitrogen fixation. In addition, this study has identified potential interactions between the isotopic regimes of vertically stratified water masses and the vertical niche selection and migration behaviour of pelagic species that need to be considered in trophic studies. While these findings appear to support the initial hypothesis, there is no information on the consistency and temporal extent of these differences and future work should be targeted to address these deficiencies through:

1. Increased focus on crustaceans – as the primary consumers, crustaceans most consistently reflect differences in productivity and nutrient sources, so more effort needs to be given to obtaining greater numbers and more consistency of species across habitats in the two regions.
2. Seasonal sampling – it is important to understand how the strength of these differences vary (or not) across time scales of oceanographic processes and particularly the role, if any, that the Leeuwin current might play in transporting picoplankton to the area.
3. Importance of microbial remineralisation – at present little is known about the role of heterotrophic microbial remineralisation of nitrogen within the water column. In an oligotrophic environment this may be sufficiently complete to conserve the isotopic value and therefore be “invisible”. Techniques are starting to appear that may help elucidate their



role but application would require a larger and more consistent data set between the regions.

4. Include other trophic groups - additional trophic groups could be targeted to more fully elucidate pelagic trophic webs include benthic fish species, additional tuna samples and mobile small pelagic fishes, and potentially species of conservation significance including Australian sea lions and seabirds (via fecal or blood samples).

## References

- Brand, W.A., Tegtmeier, A.R., Hilkert, A., 1994. Compound-specific isotope analysis - extending toward  $^{15}\text{N}/^{14}\text{N}$  and  $^{18}\text{O}/^{16}\text{O}$ . *Organic Geochemistry*, 21: 585-594.
- Bulman, C., Althaus, F., He, X., Bax, N.J., Williams, A., 2001. Diets and trophic guilds of demersal fishes of the south-eastern Australian shelf. *Marine and Freshwater Research*, 52: 537-548.
- Chikaraishi, Y., Kashiyama, Y., Ogawa, N.O., Kitazato, H., Ohkouchi, N., 2007. Metabolic Control of Nitrogen Isotope Composition of Amino Acids in Macroalgae and Gastropods: Implications for Aquatic Food Web Studies. *Marine Ecology-Progress Series*, 342: 85-90.
- Chikaraishi, Y., Ogawa, N.O., Kashiyama, Y., Takano, Y., Suga, H., Tomitani, A., Miyashita, H., Kitazato, H., Ohkouchi, N., 2009. Determination of aquatic food-web structure based on compound-specific nitrogen isotopic composition of amino acids. *Limnology and Oceanography-Methods*, 7:740-750.
- Choy, C.A., Davison, P.C., Drazen, J.C., Flynn, A., Gier, E.J., Hoffman, J.C., McClain-Counts, J.P., Miller, T.W., Popp, B.N., Ross, S.W., 2012. Global trophic position comparison of two dominant mesopelagic fish families (Myctophidae, Stomiidae) using amino acid nitrogen isotopic analyses. *PLoS ONE* 7, e50133.
- Coll, M., Navarro, J., Olson, R.J., Christensen, V., 2013. Assessing the trophic position and ecological role of squids in marine ecosystems by means of food-web models. *Deep Sea Research Part II: Topical Studies in Oceanography*, 95: 21-36.
- Dale, J.J., Wallsgrave, N.J., Popp, B.N., Holland, K.N., 2011. Nursery habitat use and foraging ecology of the brown stingray *Dasyatis lata* determined from stomach contents, bulk and amino acid stable isotopes. *Marine Ecology Progress Series*, 433: 221-236.
- Davenport, S.R., Bax, N.J., 2002. A trophic study of a marine ecosystem off southeastern Australia using stable isotopes of carbon and nitrogen. *Canadian Journal of Fisheries and Aquatic Sciences*, 59: 514-530.
- Duffy, L.M., Kuhnert, P.M., Pethybridge, H.R., Young, J.W., Olson, R.J., Logan, J.M., Goñi, N., Romanov, E., Allain, V., Staudinger, M.D., 2017. Global trophic ecology of yellowfin, bigeye, and albacore tunas: Understanding predation on micronekton communities at ocean-basin scales. *Deep Sea Research Part II: Topical Studies in Oceanography*.
- Flynn, A.J., Kloser, R.J., 2012. Cross-basin heterogeneity in lanternfish (family Myctophidae) assemblages and isotopic niches ( $\delta^{13}\text{C}$  and  $\delta^{15}\text{N}$ ) in the southern Tasman Sea abyssal basin. *Deep-Sea Research*, 69: 113-127.
- Gutierrez-Rodriguez, A., Decima, M., Popp, B.N., Landry, M.R., 2014. Isotopic invisibility of protozoan trophic steps in marine food webs. *Limnology and Oceanography*, 59: 1590-1598.
- Hartog, J.R., Hobday, A.J., Matear, R., Feng, M., 2011. Habitat overlap between southern bluefin tuna and yellowfin tuna in the east coast longline fishery—implications for present and future spatial management. *Deep Sea Research Part II: Topical Studies in Oceanography*, 58: 746-752.
- Hofmann, D., Gehre, M., Jung, K., 2003. Sample preparation techniques for the determination of natural N-15/N-14 variations in amino acids by gas chromatography-combustion-isotope



- ratio mass spectrometry (GC-C-IRMS). ISOTOPES IN ENVIRONMENTAL AND HEALTH STUDIES, 39; 233-244.
- Lorrain, A., Graham, B., Menard, F., Popp, B., Bouillon, S., van Breugel, P., Cherel, Y., 2009. Nitrogen and carbon isotope values of individual amino acids: a tool to study foraging ecology of penguins in the Southern Ocean. *Marine Ecology-Progress Series*, 391: 293-306.
- McClelland, J.W., Holl, C.M., Montoya, J.P., 2003. Relating low delta n-15 values of zooplankton to n-2-fixation in the tropical north atlantic: insights provided by stable isotope ratios of amino acids. *Deep-Sea Research Part I-Oceanographic Research Papers*, 50: 849-861.
- McClelland, J.W., Montoya, J.P., 2002. Trophic relationships and the nitrogen isotopic composition of amino acids in plankton. *Ecology*, 83: 2173-2180.
- Navarro, J., Coll, M., Somes, C.J., Olson, R.J., 2013. Trophic niche of squids: Insights from isotopic data in marine systems worldwide. *Deep Sea Research Part II: Topical Studies in Oceanography*, 95: 93-102.
- Nielsen, J.M., Popp, B.N., Winder, M., 2015. Meta-analysis of amino acid stable nitrogen isotope ratios for estimating trophic position in marine organisms. *Oecologia*, 178: 631-642.
- Norman, M., Reid, A., 2000. Guide to squid, cuttlefish and octopuses of Australasia. CSIRO publishing.
- Patterson, T.A., Evans, K., Carter, T.I., Gunn, J.S., 2008. Movement and behaviour of large southern bluefin tuna (*Thunnus maccoyii*) in the Australian region determined using pop-up satellite archival tags. *Fisheries Oceanography*, 17; 352-367.
- Popp, B.N., Graham, B.S., Olson, R.J., Hannidea, C.C.S., Lott, M.J., Lopez-Ibarra, G.A., Galvan-Magana, F., Fry, B., 2007. Insight into the trophic ecology of yellowfin tuna, *Thunnus albacares*, from compound-specific nitrogen isotope analysis of proteinaceous amino acids, in: Dawson, T., Siegwolf, R. (Eds.), *Stable isotopes in ecological change*. Elsevier/Academic press, p. 173-190.
- Rodhouse, P.G., 2013. Role of squid in the Southern Ocean pelagic ecosystem and the possible consequences of climate change. *Deep Sea Research Part II: Topical Studies in Oceanography*, 95: 129-138.
- Sutton, C., Kloser, R., Ryan, T., in prep. Micronekton biomass, abundance and distribution: comparison of vertically integrated MIDOC net samples for southern Australian and subantarctic waters. CSIRO Marine and Atmospheric Research, Hobart.
- Williams, A., Koslow, J., Terauds, A., Haskard, K., 2001. Feeding ecology of five fishes from the mid-slope micronekton community off southern Tasmania, Australia. *Marine Biology*, 139: 1177-1192.
- Williams, A.J., Allain, V., Nicol, S.J., Evans, K.J., Hoyle, S.D., Dupoux, C., Vourey, E., Dubosc, J., 2015. Vertical behavior and diet of albacore tuna (*Thunnus alalunga*) vary with latitude in the South Pacific Ocean. *Deep Sea Research Part II: Topical Studies in Oceanography*, 113: 154-169.
- Young, J.W., Blaber, S.J.M., 1986. Feeding ecology of three species of midwater fishers associated with the continental slope of eastern Tasmania, Australia. *Marine Biology*, 93: 147-156.
- Young, J.W., Hunt, B.P., Cook, T.R., Llopiz, J.K., Hazen, E.L., Pethybridge, H.R., Ceccarelli, D., Lorrain, A., Olson, R.J., Allain, V., 2015. The trophodynamics of marine top predators: Current knowledge, recent advances and challenges. *Deep Sea Research Part II: Topical Studies in Oceanography*, 113: 170-187.
- Young, J.W., Lamb, T.D., Le, D., Bradford, R., Whitelaw, A.W., 1997. Feeding ecology and interannual variations in diet of southern bluefin tuna, *Thunnus maccoyii*, in relation to coastal and oceanic waters off eastern Tasmania, Australia. *Environmental Biology of Fishes*, 50: 275-291.

### 6.3 Bioacoustic spatial and temporal summary

Tim Ryan and Rudy Kloser

#### 6.3.1 Introduction

A key objective of this project is to compare the eastern and central GAB continental margin zooplankton and micronekton communities in terms of their species composition, size range, biomass, nutrient source/trophic pathways and habitat. Vessel acoustic methods are well-suited to investigate biomass of micronekton organisms covering large spatial and (potentially) large temporal scales, providing measures of water column backscatter in the GAB. These measures can describe the distribution of micronekton at broad and fine scales (Kloser et al., 2009; Irigoien et al., 2014). A data mining exercise of CSIRO's data archives identified historic acoustic data in the central and eastern GAB. These opportunistic data sets complemented the centrepiece design-based acoustic data sets collected during the *Research Vessel (RV) Investigator* voyage (IN2015\_C02). The acoustic analysis considered four regions: Central offshore, Central upper slope (0-800 m), Eastern offshore (>5000 m) and Eastern upper slope (0-800 m). Due to the strong diurnal effects data were separated into day and night sets.

Following Kloser et al. (2009), we define micronekton as species of ~ 2 - 20 cm comprising a mix of small fish (many myctophid and bristlemouth species), squid, jellyfish (including siphonophores, ctenophores and salps) and crustaceans (krill and prawns). Individually these species will have different acoustic backscatter properties which are determined by their morphology (size, shape, density), behaviour (orientation), the depth at which they reside and the acoustic frequency. Complicating matters are those organisms that have a gas inclusion including the ubiquitous myctophid and bristlemouth species with small gas bladder and the pneumatophore of some siphonophore species. The density contrast caused by the gas/flesh interface will cause high backscatter that does not necessarily relate to the organism's size or weight. This is further complicated by a least an order of magnitude increase in backscatter at resonance, determined by the frequency, depth and size of the gas inclusion. Thus the use of multi-frequency acoustics adds complexity and also provides information to decode the dominant scatterers and potentially their gas bladder size through the water column (Kloser et al. 2016, and see Section 6.4).

This chapter summarises observations and measurements of acoustic backscatter, addressing Objective 3, to compare the relative biomass of micronekton in the central and eastern GAB.

#### 6.3.2 Methods

##### Bioacoustic data sets used

The bioacoustic characterisation of the central and eastern GAB pelagic ecosystem drew from both historic and recent data sets. These included data from *RV Investigator* (2015), *RV Southern Surveyor* (1998 and 2013) and the Integrated Marine Observing System (IMOS) Bio-Acoustic Ship of Opportunity (BASOOP) program. A review of all available acoustic data within the study region was made with a subset of these selected on the basis of relevance of location and suitability of data quality (Table 6.3-1). The *RV Investigator* and *RV Southern Surveyor*'s acoustic systems were calibrated using the standard sphere method (Foote et al., 1987; Demer et al., 2015). BP's Commercial Vessel (CV) *Ramform Sovereign* conducted full coverage seismic lines (750 m separation) of an area of approximately 100 km<sup>2</sup> over a five-month period in November 2014 and through to April 2015. This provided a rather unique data set of sustained observations in a central GAB region

centred approximately 50 km west of the central GAB study site. The opportunistic nature of the CV *Ramform Sovereign* acoustic data collection combined with the high logistical overheads of a large seismic vessel meant that calibration of its acoustic system has not been possible to date. The value of this dataset then is as a relative indicator of change, over a long period of time, where it is assumed that the acoustic system is stable, if not calibrated.

Table 6.3-1 Datasets used for characterisation of the pelagic ecosystems of the central and eastern GAB.

Vessel	Voyage	Date start	Date end	Frequencies (kHz)	Echosounder	Season	Region
RV <i>Investigator</i>	INV2015_C02	29/11/2015	21/12/2015	12, 18, 38, 70, 120, 200 and 333	Simrad EK60	Summer	Eastern, Central and Western
RV <i>Southern Surveyor</i>	SS01/1998	10/02/1998	06/03/1998	38 and 120	Simrad EK500	Summer	Central
RV <i>Southern Surveyor</i>	SS2013-C02	03/04/2013	22/04/2013	38 and 120	Simrad EK60	Autumn	Central
RV <i>Southern Surveyor</i>	SS2013-T02	17/06/2013	29/06/2013	38 and 120	Simrad EK60	Winter	Eastern, Central, Western
CV <i>Ramform Sovereign</i>	Nov-May GAB seismic surveys	17/11/2014	15/04/2015	12 and 38 *	Simrad EA600	Summer, Autumn	Central

\*CV *Ramform Sovereign* acoustic systems were uncalibrated. Nominal calibration values used.

### Acoustic data types

While different echosounders were used for the various voyages (Table 6.3-1), they record acoustic measurements of similar data types that can be processed to produce comparable data products. All systems record 'raw' digitised acoustic data from Simrad echosounders using the same or similar transducer models. These data are converted to logarithmic scale volume backscatter values ( $S_v$  dB re  $1\text{m}^{-1}$ ), through application of echosounder and calibration parameters to the sonar equation (MacLennan et al., 2002). These 'raw'  $S_v$  data may be resampled to a coarse resolution of horizontal distances of 10 or 100 m distance by 10 m cell heights to provide summary data where data volumes of original data are high, referred to as  $S_{v\ 10 \times 10}$  or  $S_{v\ 100 \times 10}$  from herein.  $S_v$  data were echo-integrated to convert the volume backscatter data to the linear term Nautical Area Scattering Coefficients (NASC,  $\text{m}^2/\text{n.mi}^2$ ), (MacLennan et al., 2002) for three pelagic layers: (1) epipelagic (20 m - 200 m), where surface portion is unavailable due to vessel draft + drop keel depth plus acoustic transmit pulse; (2) upper-mesopelagic (200 - 400 m), and (3) lower-mesopelagic (400 - 800 m). A total water column backscatter NASC was calculated by summing epipelagic, upper mesopelagic and lower mesopelagic NASC values.

### Multifrequency acoustics

The acoustic backscatter from an organism is dependent on its size, shape, tilt-angle, density, whether or not they have a gas inclusion and the frequency at which they are ensonified. The pelagic water column micronekton are very much a mix of species with highly varied morphology and behaviour resulting in complex backscattering possibilities. Multifrequency acoustics are well

established methods that exploit the frequency dependent differential in backscatter to infer species, or morphologically similar species groups (Kloser et al., 2002; Lavery et al., 2007). In simple terms, backscatter from small organisms (Rayleigh scattering, size  $\ll$  acoustic wavelength) increases with frequency, while for large organisms (Geometric scattering, size  $\gg$  acoustic wavelength), the scattering is similar across frequencies (Simmonds and MacLennan, 2005). A complicating factor is resonant scattering, where the backscatter can be greatly increased in magnitude compared to Rayleigh or geometric scatter, particularly for organisms with gas inclusions (e.g. many myctophid species, siphonophores with pneumatophores). This occurs when the size of the gas bubble is around the same size as the acoustic wavelength. Fully decoding the species-specific scattering regime in the GAB would require greater knowledge of the species composition and the acoustic backscatter (or target strength, TS) of the dominant species, and is beyond the scope of this report. Instead, as a simplified approach, the difference in signal between the two lowest frequencies, 18 kHz and 38 kHz, is used to give a broad overview of the dominant scattering communities in the water column. Section 6.4 describes how resonant scattering of organisms with small gas bladders are the most likely primary drivers of high backscatter in the 18 and 38 kHz echograms. See also (Davison et al., 2015).

#### Area of operation

The locations of the data sets spanning 1998 to 2015 are detailed in Table 6.3-1 and are shown in Figure 6.3-1.

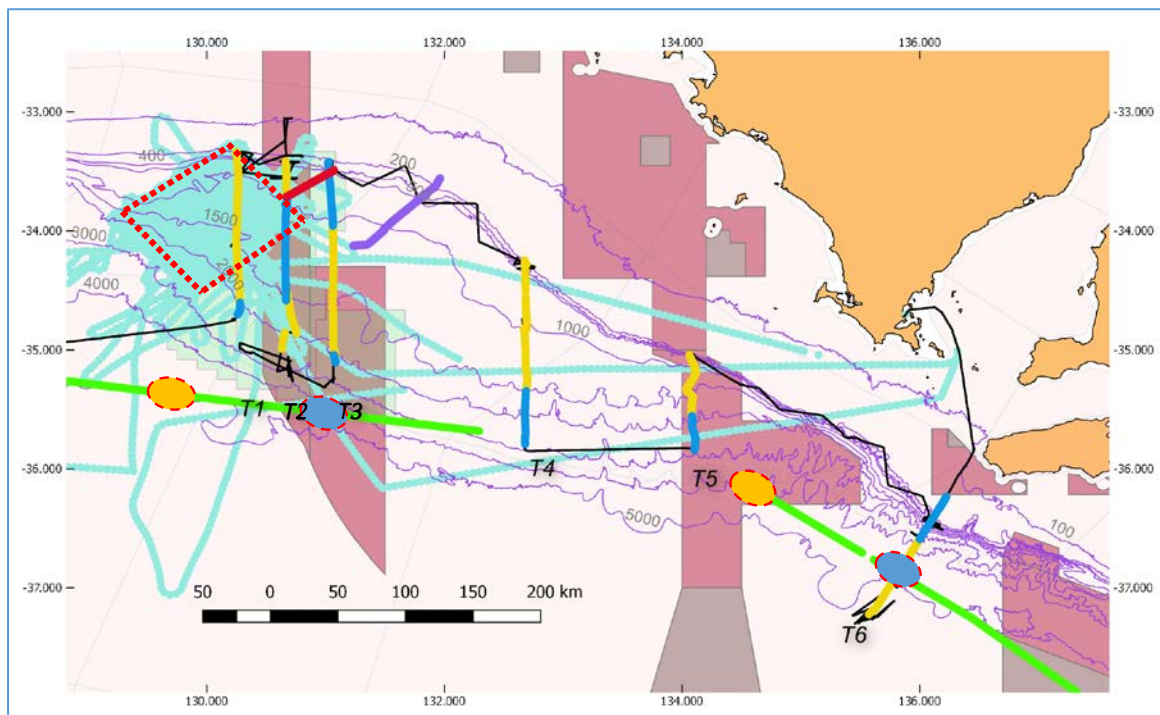


Figure 6.3-1 Map of underway acoustic sampling locations. Light blue: CV Ramform Sovereign – November 2014 to May 2015, Green: RV Southern Surveyor June 2013. The four red-dashed oblong shapes indicate where RV Southern Surveyor data was extracted from, with orange fill for day time and blue fill for night time. Black track – INV 2015\_CO2 voyage. Cross shelf transects T1 to T6, yellow track indicates day time, blue track indicates night. The red-dashed polygon indicates region from which CV Ramform Sovereign data were used. Solid red line in the central GAB indicates April 2013 RV Southern Surveyor data; solid purple line further east indicates February 1998 RV Southern Surveyor data.

## Analysis methods - RV Investigator INV2015\_CO2

### System calibration

The bioacoustic echosounders of *RV Investigator*'s were calibrated in October 2015, prior to the voyage (INV2015\_CO2), and again in August 2016. The differences in results between 2015 and 2016 are as follows: 18 kHz (1%), 38 kHz (10%), 70 kHz (5%), 120 kHz (20%) and 200 kHz (7%). Differences may be due to actual changes in the acoustic system and/or the error in the calibration measurement. With the exception of the 120 kHz (moderately anomalous), the system calibration stabilities are considered to be within acceptable limits. The pre-voyage 2015 results were applied to echosounders of *RV Investigator*'s for the voyage (INV2015\_CO2) (Table 6.3-2).

Table 6.3-2 INV2015\_CO2 bioacoustic echosounder settings.

Transducer	Frequency (kHz)	Power (W)	Pulse duration (ms)	Gain (dB)	Sa correction (dB)
ES18-11 (SN:2109)	18	2000	1.024	22.755	-0.70
ES38B (SN:31167)	38	2000	2.048	25.08	-0.40
ES38B (SN:31167)	38	2000	1.024	24.755	-0.71
ES70-7C (SN:255)	70	2000	2.048	27.32	-0.26
ES70-7C (SN:255)	70	2000	1.024	26.18	-0.4
ES120-7C (SN:876)	120	250	1.024	26.96	-0.38
ES200-7C (SN:530)	200	105	1.024	26.29	-0.25
ES333 (SN:132)	333	40	1.024	25.57	-0.36

### Bioacoustic sampling and analysis regimes

#### (1) Continuous underway data

Bioacoustic data were collected at all times throughout the voyage with settings optimised to maximise ping rate, sampling resolution and signal-to-noise when moving from shallower to deeper waters. The acoustic echograms provided information on the backscatter structure of the pelagic ecosystem helping to inform survey decisions, provide context to pelagic net sampling deployments and on selected occasions explicitly to guide the net systems to target specific layers. Subsets of the continuous data were selected for detailed analysis as described in the next two Sections.

#### (2) Cross-shelf transects

Six cross-shelf transects from shallow (on-shelf < 200 m) to deep (offshore up to +3000 m) or vice versa were conducted at east and central regions, and locations in between (Figure 6.3-1). These transects ranged in length from 50 to 100 nautical miles. The full sample resolution acoustic data was processed following CSIRO's IMOS BASOOP protocols (<http://imos.org.au/bioacoustic.html>) to produce quality-assured mean volume backscatter data at 100 m horizontal and 10 m vertical resolution,  $S_{v100 \times 10}$ . Visualisation of the  $S_{v100 \times 10}$  data is presented as single-panel echograms for each transect for the lower frequencies 18, 38 and 70 kHz, whose effective working range was at least 800 m, covering the water column depths of greatest interest. The effective range of the higher frequencies (120 kHz and above) limited use to the epipelagic zone. Synthetic echograms of 18 kHz

minus 38 kHz ( $S_{v\ 18-38}$  from herein) are presented to highlight the different scattering regimes across the shelf to offshore and with depth.

Qualitative descriptions of the cross-shelf transects, comparing eastern and central GAB regions are presented in the results.

The cross-shelf transects typically took between 5 to 10 hours to complete, but increased when other survey activities were conducted simultaneously. A consequence of variable times was that each transect had at least one transition from day to night or vice versa. This meant that a full set of comparison data for east-central, offshore-upper slope for both day and night was not available for extraction from the cross shelf transects. Instead, comparison data sets were derived from the 24 hour station-data as described in the next Section.

### (3) Station data

The biological sampling carried out by the EZ and MIDOC net systems were, by design, conducted at the offshore and upper slope of the central and eastern GAB for both day and night (Table 6.3-3). These activities provided well-defined periods where the vessel was going in a continuous direction for ~4 to 8 km and at low speed providing high-quality acoustic data.

*Table 6.3-3 Biological sampling stations from which bioacoustic data were extracted.*

Locality	Day/Night	Stations
<b>Central, Offshore</b>	Day	1
<b>Central, Offshore</b>	Night	2
Central, Upper slope	Day	4
Central, Upper slope	Night	2
<b>Eastern, Offshore</b>	Day	4
<b>Eastern, Offshore</b>	Night	1
Eastern, Upper slope	Day	2
Eastern, Upper slope	Night	2

Following basic quality checking, the full sample resolution acoustic data for 18, 38 and 70 kHz frequencies were echointegrated in NASC (Nautical Area Scattering Coefficient) values of 100 m horizontal distance and 10 m vertical height to a depth of 1000 m. These outputs were further resampled to give mean NASC values for each 100 m interval for epipelagic, upper mesopelagic and lower mesopelagic.

### *Analysis methods – CV Ramform Sovereign*

The *CV Ramform Sovereign* opportunistically collected 280 Gigabytes of continuous acoustic data at 12 kHz and 38 kHz over a 5 month period. Activities were focused on a survey region of 100 km<sup>2</sup>



centred at -33.9 S and 130.0 E, ~70 km west of the INV2015\_CO2 study site. The sampling design was intensive with 135 seismic survey transects separated by 750 m (Figure 6.3-2).

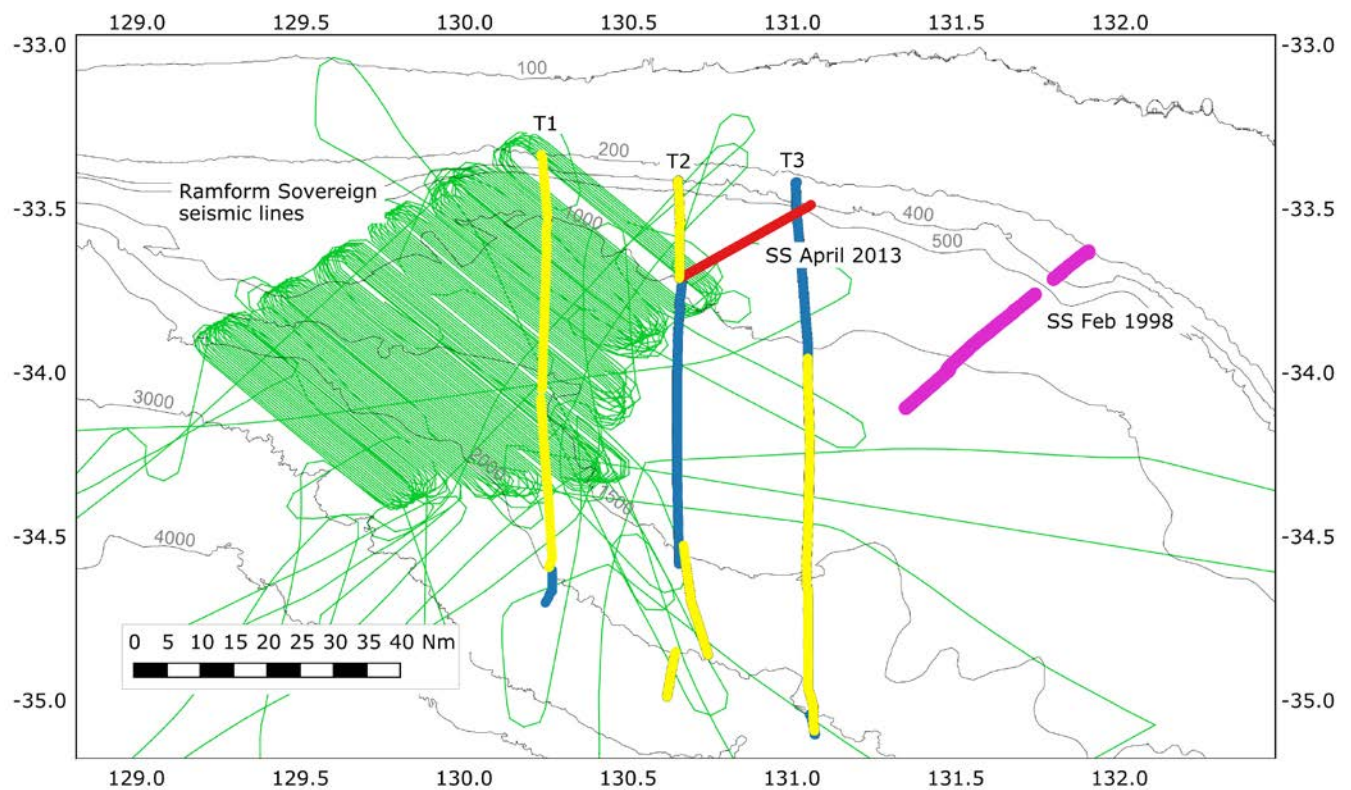


Figure 6.3-2 Area of operations for CV Ramform Sovereign seismic survey campaign are shown by the thin green lines. Yellow and blue north-south lines are transects T1 to T3 from the voyage (INV2015\_CO2) with colours representing day and night respectively. Red and purple lines are cross shelf transects from RV Southern Surveyor voyages in 2013 and 1998 respectively.

The Simrad EA600 hydrographic echosounder was uncalibrated, hence nominal manufacturer values were applied to the digitised raw acoustic data to produce  $S_v$  values at full sample resolution. These values may be in error by as much as a factor of 2 compared to calibrated systems. Thus, they are used as relative measures of backscatter. On occasions, changes were made to the echosounder power and pulse length, where some of the settings compromised the utility of the acoustic data, even as a relative measurement. The data recorded with such unsuitable echosounder settings were removed by the analysis procedures.

The large data volume and temporal span required analysis procedures to be rapid and, where possible, fully automated. A review of the data found that the 12 kHz had a great deal of interference from presumably the seismic air guns that would require intensive time consuming processing to possibly make it acceptable. Consequently, the focus of the analysis was on the 38 kHz frequency where data quality was not obviously affected by the seismic operations. Echograms were reviewed rapidly with seafloor manually excluded, and only the most obvious portions of bad data were manually removed. Finally, filters to remove attenuated signal and noise artefacts were applied through automated procedures to improve data quality (Ryan et al., 2015). This quality controlled



full-sample resolution raw data was resampled at a coarse resolution to produce mean volume backscatter values for 10 m horizontal distance by 10 m vertical height,  $S_{v\ 10 \times 10}$  data.

Two data products were derived from this lower resolution data. First, echointegration of the  $S_{v\ 10 \times 10}$  data was made to calculate the mean NASC values for each 100 m interval for epipelagic, upper mesopelagic and lower mesopelagic layers. These data were represented as a box-plot of NASC values for each layer for each month of the survey providing an indicator of temporal change over a five month period for the three depth-stratified layers (Figure 6.3-8).

A second data product identified schools within the top 500 m of the water column. To do this the original full-sample resolution raw data echograms were inspected to identify and characterise typical backscatter values associated with school regions. This established an empirically determined threshold where a mean  $S_v$  of -55 dB or above over a 10 m horizontal by 10 m vertical height was associated with school regions. This threshold was applied to the quality assured,  $S_{v\ 10 \times 10}$  data. Data points above the threshold were separated by day and night and mapped to show the spatial distribution (Figure 6.3-10). Boxplots of  $S_{v\ 10 \times 10}$  separated by day and night and sample depth of the  $S_v$  values are also presented.

#### *Analysis methods –RV Southern Surveyor*

##### *Winter 2013 Offshore*

*RV Southern Surveyor* provided acoustic data sets from February 1998, April 2013 and June 2013 (Table 6.3-1). The June 2013 data contained transect Sections in the east and central offshore regions. Analysis of these winter transects provided a seasonal contrast to the summer IN2015\_CO2 voyage. The June 2013 acoustic data had been quality controlled as part of the CSIRO bioacoustic ship of opportunity program (BASOOP). It has been posted as publically available data to the IMOS AODN web site (<https://portal.aodn.org.au/>), from where it was downloaded in netCDF format. Portions of the 38 kHz  $S_v$  acoustic data corresponding to east/day, east/night, central/day and central/night were extracted from the netCDF file (Figure 6.3-1). The  $S_v$  data for each region/time were echointegrated for epipelagic, upper mesopelagic and lower mesopelagic layers and presented as boxplots of NASC data (Figure 6.3-11).

##### *1998, 2013 and 2015 cross shelf transects in the Central GAB.*

Echograms at 38 kHz were recorded for three cross- shelf transects from ~ 400 m to 1000 m in similar localities in the central GAB, recorded in 1998, 2013 and 2015. A qualitative description of these echograms was made comparing dominant features for each of the three years.

### 6.3.3 Results

#### *IN2015\_CO2 cross-shelf transects*

Figure 6.3-3 visualises 18 kHz  $S_{v\ 100 \times 10}$  echograms for cross-shelf transects T1-T6, recalling that T1-T3 represent the central GAB, T6 Eastern GAB with T4 and T5 in-between (Figure 6.3-1). Figures for 38, 70 and 120 kHz  $S_{v\ 100 \times 10}$  cross-shelf echograms for T1 to T6 are included in the Appendix in Section 6.2.6. These echograms provide a broad-scale synopsis of the offshore and shelf backscatter from the assemblage of micronekton species. The 12-step colour legend spans 36 dB, where each step

from lowest (grey) to highest (brown) represents a doubling of backscatter. In general terms notable features include:

- (i) High backscatter in the epipelagic and lower mesopelagic regions with lesser backscatter in the upper mesopelagic region.
- (ii) Diurnal migration – e.g. observe Transect 4 at ~ latitude -35.35 degrees where dashed red line indicates transition from night (line at 800 m) to day (line at 200 m), where backscatter signal in the lower mesopelagic increases as organisms migrate into deeper waters during the day.
- (iii) At this sampling scale much of the backscatter has a high degree of structure forming contiguous regions and layers.
- (iv) The shelf length from 200 to 2000 m is ~170 km in the central GAB and ~12 km at the eastern GAB Transect 6, thus available habitat should be considered when comparing biomass of the central and eastern GAB upper slope.
- (v) These cross-shelf transects can provide a context for the biological multi-net sampling systems (EZ and MIDOC) which are towed through the epipelagic, upper mesopelagic and lower mesopelagic layers.

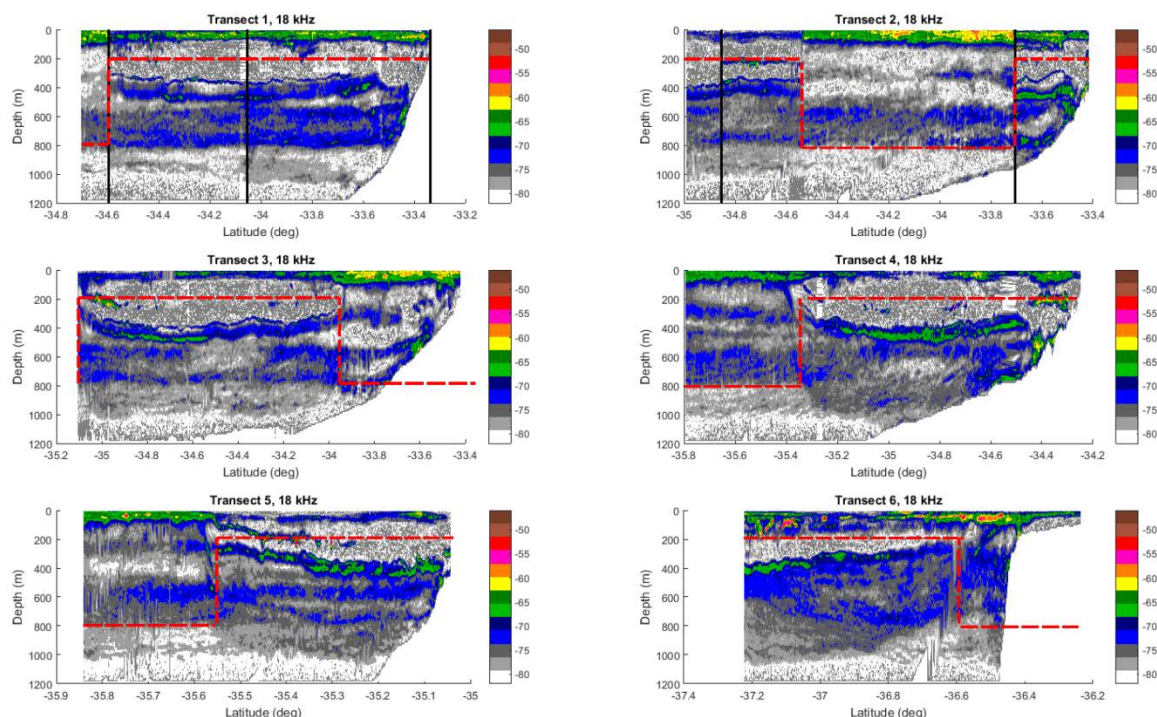


Figure 6.3-3 18 kHz Processed quality controlled echogram matrices of  $S_{v100 \times 10}$  values as a function of depth and latitude for cross-shelf transects T1-T6. Dashed red line at 200 m depth indicates daytime, at 800 m indicates night-time. Vertical black lines indicate occasions where there was a gap in data of greater than 4 hours.

Comparison of backscatter as a function of frequency provided insights into the dominant scattering regimes for eastern and central GAB regions. As diurnal effects have a strong effect on the

backscatter magnitude and distribution it was important to select cross-shelf transects that spanned similar time periods with respect to location. From inspection, Transect 3 (central GAB) and Transect 6 (eastern GAB) had a similar transition from day to night when moving towards the shelf.  $S_{v\ 100 \times 10}$  data for 18, 38, 70 and 18 kHz minus 38 kHz for Transect 3 and Transect 6 are presented in Figure 6.3-5 and Figure 6.3-6, respectively. Inspection of the echograms reveals high signal backscatter layers at one frequency that have greatly reduced signal at another. For example, both Transect 3 and Transect 6 have a high signal layer in the offshore region at ~ 400 m depth at 18 kHz but in the same region of the 38 and 70 kHz echograms is essentially absent. This is distinctly shown on the 18 minus 38 kHz echogram as the layer of red-brown pixels indicating that the 18 kHz is 8 – 10 dB (~ an order of magnitude) higher than 38 kHz. An opposite effect is observed in the 600 to 800 m region where 38 kHz backscatter is significantly higher than 18 kHz. This differential is more pronounced in the eastern region where 38 kHz backscatter is up to 10 dB higher (an order of magnitude) than 18 kHz in the 600 to 800 m depths. This difference is due to resonance scattering where the difference in scattering can be used to predict the gas bladder size at depth (see Section 6.4). This will be investigated further as part of ongoing developments.

A spatial view of the backscatter distribution between central and eastern GAB is provided in Figure 6.3-4, where total water column backscatter (epipelagic + upper mesopelagic + lower mesopelagic NASC) is visualised as a thematic map of along-track 38 kHz values where bubble-size is proportional to the total backscatter NASC. The night-time upper slope 38 kHz backscatter on eastern GAB T6 is noticeably higher than that of T3. Offshore daytime differences are not so pronounced between regions.

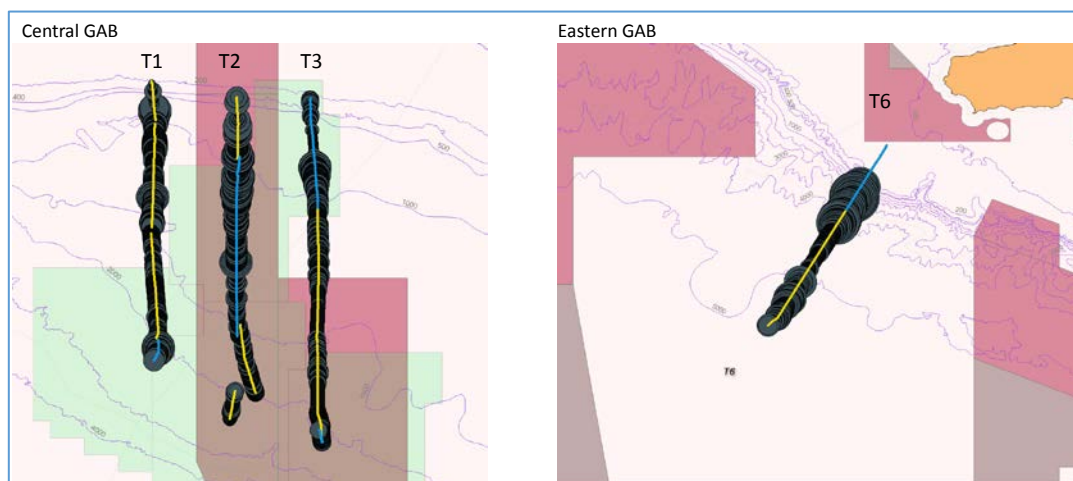


Figure 6.3-4 Along-track total water column NASC at 38 kHz where bubble size indicates magnitude of the backscatter value. The overlaid blue line indicates night time, the yellow line day time.



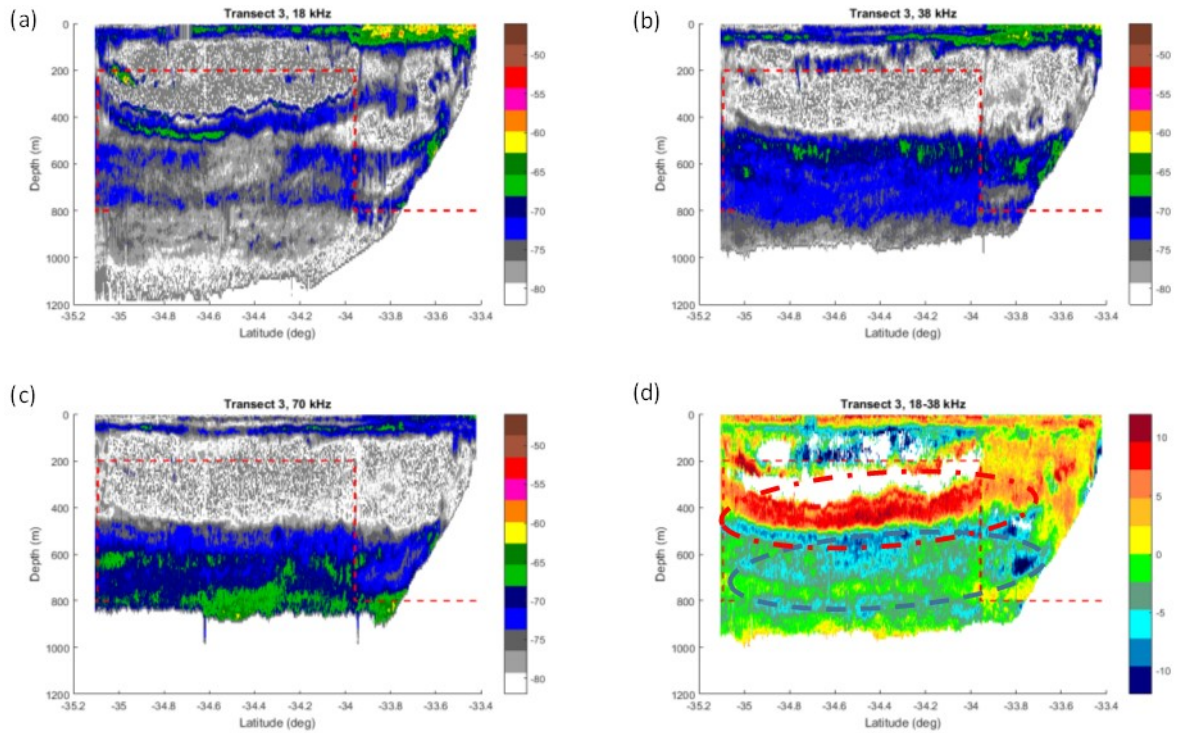


Figure 6.3-5 Transect 3.  $S_{v100 \times 10}$  echograms at 18, 38 and 70 kHz (a-c) plus decibel difference between 18 kHz  $S_{v100 \times 10}$  and 38 kHz  $S_{v100 \times 10}$  data, panel (d). Red dashed line indicates day (200 m) and night (800 m) periods. Blue dashed oblong and red dot-dash oblong (panel d) represent regions that are respectively higher and lower on 38 kHz compared to 18 kHz.

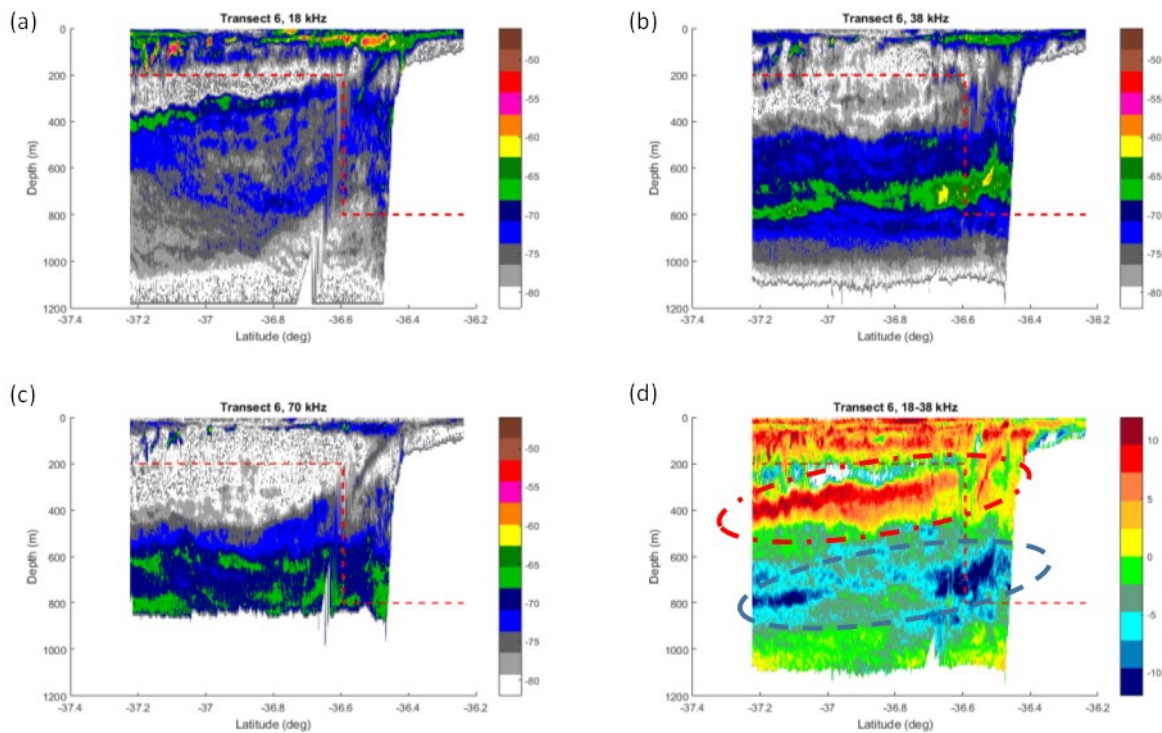


Figure 6.3-6 Transect 6.  $S_{v100 \times 10}$  echograms at 18, 38 and 70 kHz (a-c) plus decibel difference between 18 kHz  $S_{v100 \times 10}$  and 38 kHz  $S_{v100 \times 10}$  data, panel (d). Red dashed line indicates day (200 m) and night (800 m) periods. Blue dashed oblong and red dot-dash oblong (panel d) represent regions that are respectively higher and lower on 38 kHz compared to 18 kHz.

## IN2015\_CO2 station data

The per-100 m interval NASC values associated with biological net sampling stations were separated by locality (east/central), offshore/upper slope, day/night and epipelagic, upper mesopelagic and lower mesopelagic layers. Boxplots for each category are presented in the Appendix in Section 6.3.6 (Figure 6.3-14 to Figure 6.3-17). These plots show a degree of complexity where variability in acoustic backscatter produces a spread of values driven by day-night and upper slope-offshore variations and the often heterogeneous backscatter distribution both vertically and horizontally. Further complexity arises by measuring the same water column using multiple frequencies where resonant scattering of small gas-bearing organisms can confound the simple assumption that acoustic backscatter is proportionate to micronekton numeric density. To address the question of east vs central GAB biomass, the backscatter data were simplified, summing per-interval epipelagic, upper mesopelagic and lower mesopelagic NASC values to give a total water column backscatter from surface to 800 m and combining both day and night stations. These data are presented as box plots for upper slope and offshore regions for 18, 38 and 70 kHz frequencies (Figure 6.3-7).

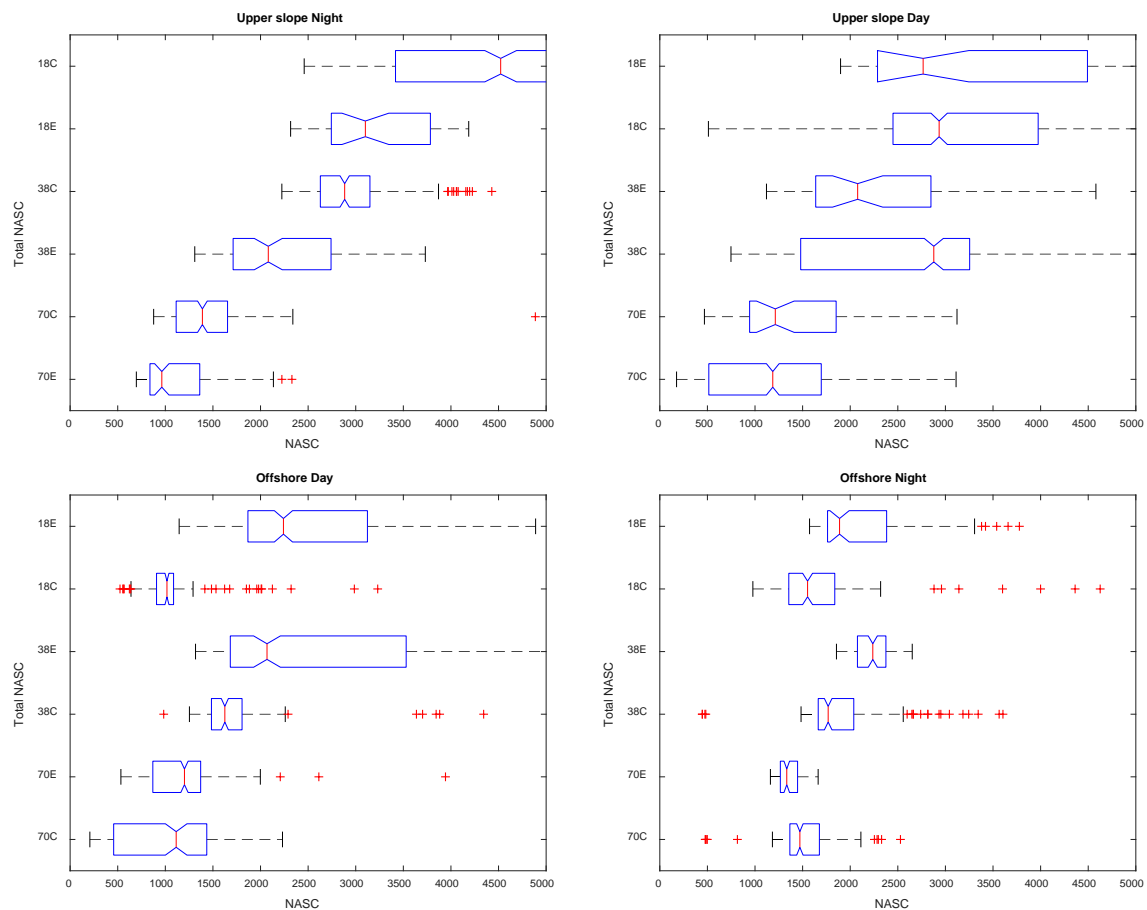


Figure 6.3-7 Box plots of NASC values per 100 m interval for 18, 38, 70 total backscatter, associated with eastern (E) and central (C) offshore biological net sampling stations in the GAB for upper slope (left panel) and offshore (right panel).

The backscatter data displayed in Figure 6.3-7 are summarised as mean and standard deviation of total water column NASC values for central and eastern regions in the GAB for 18, 38 and 70 kHz frequencies (Table 6.3-4). Included in this table is the ratio of Central GAB backscatter to Eastern GAB backscatter for 18, 38 and 70 kHz frequencies. At 18 and 38 kHz these ratios indicate that the

Eastern-Offshore GAB has 30% more backscatter than the Central-Offshore GAB. The ratio at 70 kHz is 10% lower backscatter for the Eastern-Offshore GAB. The opposite relationship is observed for the upper slope where 18 and 38 kHz Eastern-Upper Slope GAB backscatter is respectively lower by 10% and 30% than the Central-Upper Slope GAB. Minimal difference between Eastern-Upper Slope and Central was observed for 70 kHz backscatter.

*Table 6.3-4 Summary of mean per-interval NASC values for central and east GAB associated with offshore and upper slope net sampling stations. A ratio of central to east mean NASC is given for each frequency and upper slope and offshore regions.*

Offshore							
	Central			East			
Frequency	mean	std	number of samples	mean	std	number of samples	Central/East ratio
18	1838	2330	395	2818	1835	518	0.7
38	1806	442	401	2478	972	519	0.7
70	1278	478	394	1178	324	519	1.1
Upper slope							
	Central			East			
Frequency	mean	std	number of samples	mean	std	number of samples	Central/East ratio
18	4095	10990	1053	3857	2994	95	1.1
38	2991	9793	1053	2288	741	172	1.3
70	1201	607	1054	1228	503	172	1.0

A second ratio of mean backscatter values was made comparing upper slope to offshore backscatter for Central and Eastern GAB for 18, 38 and 70 kHz frequencies (Table 6.3-5). The data show that Central upper slope GAB had factor of 2.2 and 1.7 times more backscatter than the offshore region. For the Eastern GAB upper slope, backscatter is 1.4 times greater than offshore at 18 kHz but quite similar for 38 and 70 kHz (factor of 0.9 and 1.0, respectively).

*Table 6.3-5 Ratio of upper-slope to offshore backscatter NASC values for Central and East GAB for 18, 38 and 70 kHz frequencies.*

Frequency	Central	East
18	2.2	1.4
38	1.7	0.9
70	0.9	1.0

CV Ramform Sovereign

Long term observation of backscatter in the Central GAB

The distribution of monthly echointegrated 38 kHz acoustic backscatter (as uncalibrated NASC values) for epipelagic, upper mesopelagic and lower mesopelagic layers are presented in Figure 6.3-8. This long-term data series provides a number of insights into the acoustic backscatter of the central GAB over the summer and autumn periods. Over the course of the season, the average lower mesopelagic backscatter was highest, followed by epipelagic and then lower mesopelagic; season-long median values were 600, 278 and 57.1  $\text{m}^2/\text{nmi}^2$  for respectively epipelagic, upper mesopelagic and lower mesopelagic. With the exception of the November data, the epipelagic backscatter almost mirrored the trend of the lower mesopelagic. Epipelagic backscatter decreased from December to February (factor of 1.7 based on median values) and then increased by the same factor by April; median lower mesopelagic backscatter increased by a factor of 2.2 from December to February then decreased by a factor of 2.0 by April. Again with the exception of the November data, the trend of the lower mesopelagic backscatter matches that of the seafloor depth (Figure 6.3-8 d), where the lower mesopelagic backscatter increases as the survey vessel worked its way towards the shallower shelf region from December to February and then back deeper through to April. As noted already,



the epipelagic backscatter follows the opposite trend of the lower mesopelagic, and the opposite trend of the seafloor depth.

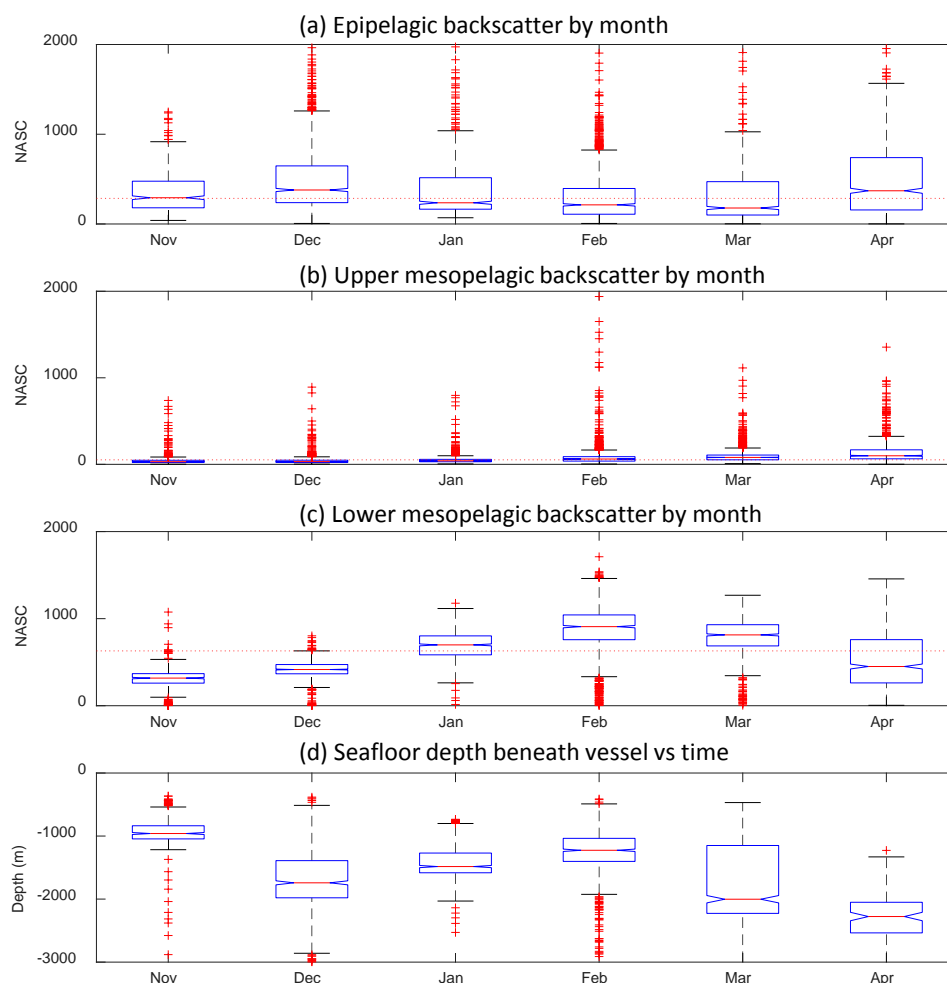


Figure 6.3-8 Boxplots showing monthly distribution of 38 kHz acoustic backscatter (NASC) values monthly for epipelagic (a), upper mesopelagic (b) and lower mesopelagic (c) layers from November 2014 to May 2015. Panel d shows the corresponding monthly distribution of seafloor depth along the transect lines.

#### Distribution of school regions

A second data product from the *CV Ramform Sovereign* voyage was to map the distribution of high-signal regions related to fish schools. Figure 6.3-9 shows an example of the high density schooling regions observed throughout the seismic survey campaign of the *CV Ramform Sovereign*. As described in the methods (Section 6.3.2), high-density school regions such as this were inspected to establish the empirical threshold of -55 dB, which was used to filter the processed  $S_V$   $10 \times 10$  data, where values above this threshold inferred schooling regions.

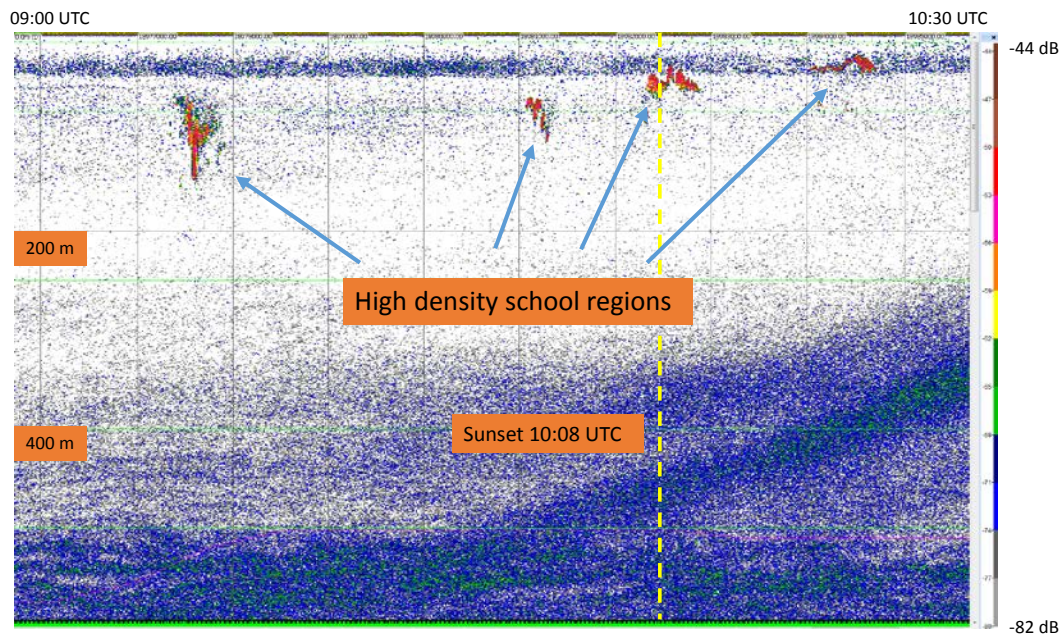


Figure 6.3-9 Example of high density school regions in the central GAB on February 19<sup>th</sup> 2015. Upward diurnal migration at sunset (10:08 UTC) of the lower mesopelagic layer can be observed while the high density school regions also move closer to the surface.

The distribution of acoustically-inferred school regions from CV *Ramform Sovereign* EA600 38 kHz acoustic data within the area of seismic operations from November 2014 to April 2015 is given in Figure 6.3-10a. There seems to be no obvious spatial or temporal pattern to the inferred fish schools where they appear to be randomly scattered throughout the survey region. Figure 6.3-10b shows the depth distribution of these schools over the same time period. A factor of 2.4 more above - threshold (-55 dB)  $S_{v\ 10 \times 10}$  samples were detected during the day compared to night (620 vs 259 respectively). This higher level of detectability may be due to fish behavior but appear to relate to the larger footprint of the acoustics where the chance of encountering schools that are deeper in the water column is increased by the larger acoustic footprint. At the median depth for day and night inferred fish schools, the acoustic footprint spans 47 and 18 m respectively at the 3dB points for the vessel's 7 degree transducer. Thus, the footprint at daytime school depths is higher by a factor of 2.6 which is in close agreement with the factor of 2.4 greater detections for daytime schools.

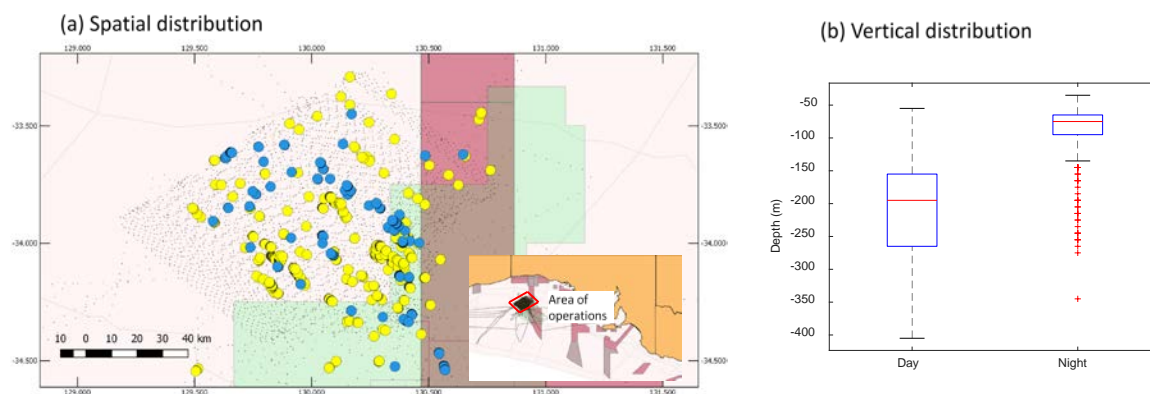


Figure 6.3-10 (a) Spatial distribution of acoustically-inferred school regions within the top 500 m of the water column within the CV Ramform Sovereign seismic survey area. Yellow circles indicate daytime, blue circles night-time. (b) Vertical distribution of acoustically-inferred schools separated by day and night.

#### *RV Southern Surveyor, winter offshore 2013*

Acoustic data from selected portions of June 2013 transect data from central and eastern GAB were echo-integrated to give to NASC values at 100 m intervals for epipelagic, upper mesopelagic and lower mesopelagic layers (Figure 6.3-11) with associated median values given in Table 6.3-6 *RV Investigator* data from December 2015 is presented to allow summer/winter comparisons.

Table 6.3-6 Median values for 38 kHz NASC values by east/central location for epipelagic, upper and lower mesopelagic layers, by day and night for winter 2013 and summer 2015 voyages in the offshore GAB. Total NASC (addition of NASC values for three layers) for east and central is given as is a percentage difference of this total between east and central offshore regions.

	Location	Day		Night	
		2013	2015	2013	2015
Epipelagic	E	29	513	249	392
	C	38	593	252	757
Upper mesopelagic	E	160	125	131	167
	C	112	69	181	91
Lower mesopelagic	E	2364	1350	1963	1605
	C	1987	959	1632	874
Total	E	2553	1988	2343	2164
	C	2137	1621	2064	1722
Total east compared to central %		16	18	12	20

Summer epipelagic backscatter is significantly higher than winter for both central and eastern regions. For daytime median summer epipelagic NASC is factor for 17 and 15 greater than for winter for east and central regions, respectively. For night-time, the difference is less pronounced where median summer epipelagic NASC is factor of 1.5 and 3 greater than winter for east and central regions respectively. For winter 2013, lower mesopelagic backscatter is greater than that of summer 2015 for both regions and also accounts for a greater proportion of the total backscatter. In both

summer and winter total 38 kHz backscatter (adding three pelagic layers) is between 12 and 20% higher in the east than the central GAB.

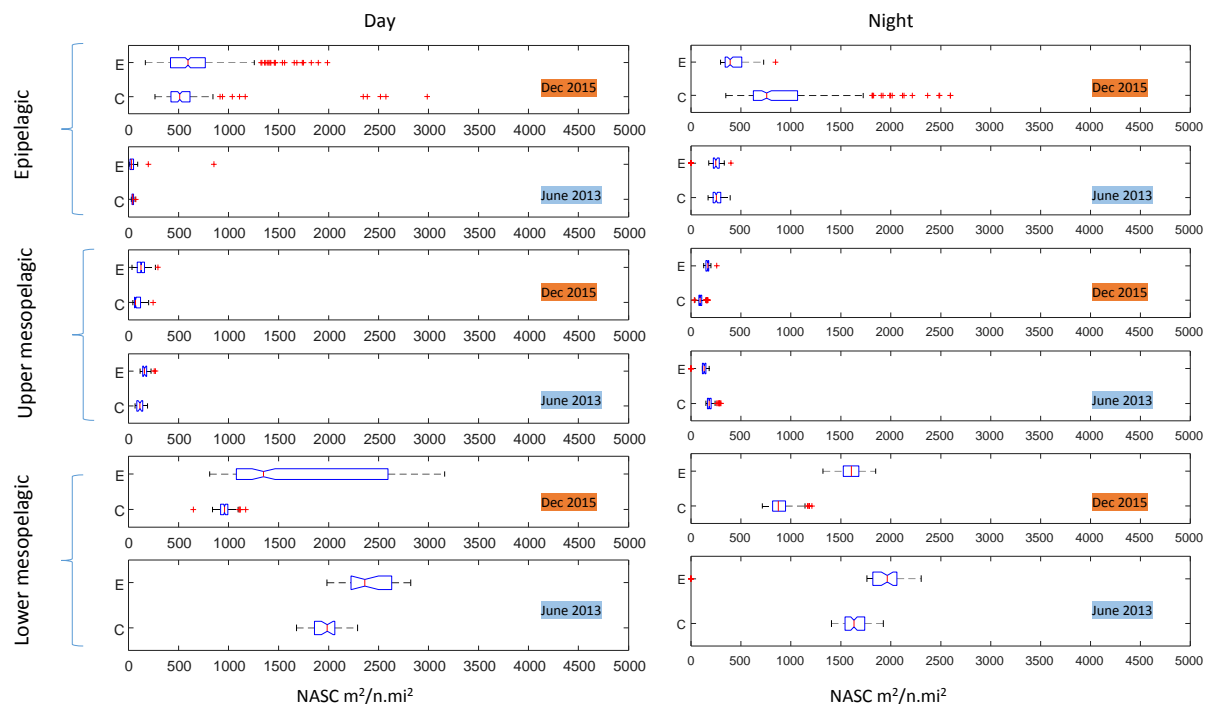


Figure 6.3-11 Box plots showing distribution of offshore 38 kHz calibrated backscatter (NASC values) for epipelagic, upper mesopelagic and lower mesopelagic layers for central (C) and east (E) GAB by day and night for RV Southern Surveyor (June 2013) and RV Investigator (Dec 2015).

#### 1998, 2013 and 2015 cross-shelf transects in the Central GAB.

As a point of comparison to the centrepiece IN2015\_CO2 voyage, 38 kHz echograms from RV *Southern Surveyor* 1998 and 2013 voyages are shown in Figure 6.3-12. The 1998 and 2013 echograms highlight a paradox in our understanding of the predominantly down-welling (inferred low production) central GAB where persistent large schools of micronekton were observed on the voyages. Based on biological sampling these were associated with Sternoptychidae hatchetfish (*Maurollicus australis* – previously identified as *Maurollicus muelleri*) and the Acropomatidae three-spined cardinal fish (*Verilus anomalus* previously identified as *Apogonops anomalus*). Such schools were noticeable by their absence in the IN2015\_CO2 echograms although the associated species were caught by the MIDOC net system. When considering what the 2015 acoustic data might infer regarding eastern and central biomass this review of two historic data sets suggests that inter -

annual seasonal effects may exist such that biomass differences between eastern and central GAB are variable.

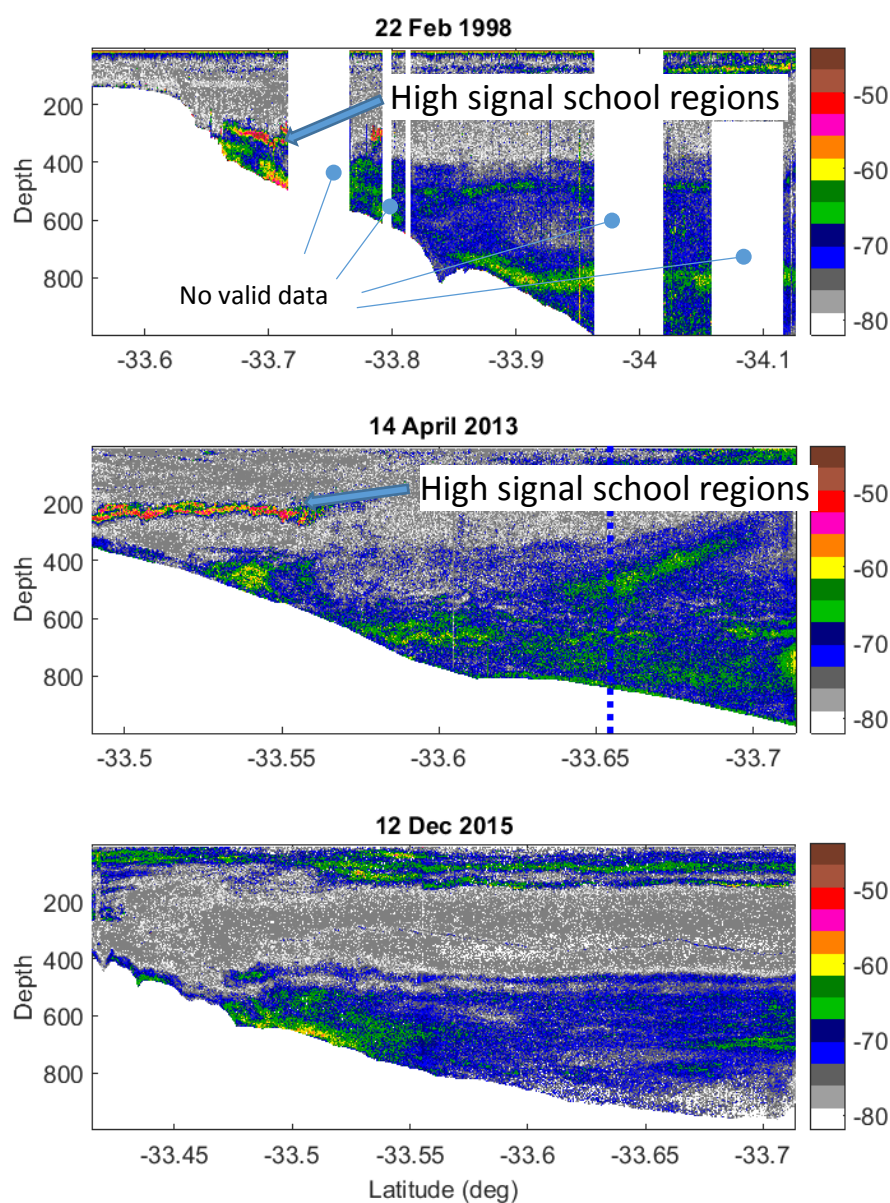


Figure 6.3-12 38 kHz echograms for three central GAB cross-shelf transects from 1998, 2013 and 2015. Vertical blue dotted line in middle echogram indicates time of sunset. Top and bottom echogram data were collected during daytime.

#### 6.3.4 Discussion

Comparison of eastern and central GAB pelagic ecosystems (Objective 3) through vessel-based bioacoustic methods was conducted using multiple lines of enquiry. The centrepiece December 2015 *RV Investigator* voyage provided high quality acoustic data at six frequencies, where the range of the lower three (18 kHz, 38 kHz and 70 kHz) recorded acoustic backscatter for three layers of relevance to the pelagic ecosystem: - epipelagic 0-200 m, upper mesopelagic 200-400 m and lower mesopelagic 400-800 m. Acoustic data included a series of six cross-shelf transects from upper-slope



to offshore depths in the east to central GAB, acoustic data associated with deeply deployed net systems conducted at specific locations (upper slope/offshelf, central/eastern and day/night) and continuous recording while underway enabling sustained observations through inspection of the acoustic echograms. Historic data was reviewed with data sets from summer 1998, autumn and winter 2013 found to be relevant to this study. Additionally opportunistic data from a seismic vessel provided continuous recording of 12 kHz and 38 kHz bioacoustic data in the central GAB over a five month period.

The IN2015\_CO2 cross-shelf transects showed similar structuring between east and central GAB. Diurnal migration effects were evident in both locations. Also at both locations decibel differences indicated high 18 kHz signal (+8 to +10 dB compared to 38 kHz for both east and central) at ~ 400 m and the opposite effect at ~ 600-800 m (-5 to -8 dB in the central, -8 to -10 dB in the east compared to 38 kHz). These differences in backscatter across frequencies are indicative of resonant scattering of gas-included organisms at the respective frequencies. It is notable that the pattern of decibel difference is similar at both locations, albeit with the effect stronger for the eastern region at depths of 600 to 800 m. 18 kHz echograms for central GAB showed regions of strong acoustic backscatter that from inspection do not appear to be dramatically different from those of the eastern GAB (e.g. Figure 6.3-5a, 18 kHz in the epipelagic layer, compared that of Figure 6.3-6a). Conversely along-track summation of 38 kHz backscatter (total NASC) indicated higher backscatter at the upper slope of the eastern GAB compared to the central GAB, while along-track offshore backscatter for both regions varied but did not indicate major differences (Figure 6.3-4).

The IN2015\_CO2 deeply deployed net-stations were designed to allow comparison between eastern and central regions, time of day and slope and offshore regions. Thus the acoustic data associated with these deployments provided a convenient data set that would allow the same comparisons. The station-based acoustic data when broken down by day/night and the epipelagic, upper mesopelagic and lower mesopelagic layers and at three frequencies, proved to be quite complicated (Figure 6.3-18); comparisons of eastern and central backscatter showed varying results where sometimes east backscatter was higher than central or vice versa depending on frequency, day/night, pelagic layer upper slope/offshore locality. Combining the station-acoustic data to give total backscatter for combined day and night helped provide a more straightforward view where whole-of-water column backscatter was an indicator of the regions biomass (Figure 6.3-7). A simple ratio of central-to-east backscatter for each frequency and for offshore and upper slope was used to quantify regional differences. This showed that at 18 kHz and 38 kHz offshore central backscatter was 30% less than eastern while conversely central upper-slope backscatter was higher than 10% and 30% respectively.

The winter 2013 *RV Southern Surveyor* offshore 38 kHz acoustic data gave a seasonal point of contrast with the IN2015\_CO2 voyage. In both winter and summer cases, median total offshore backscatter was higher in the eastern GAB by 12-20% (Table 6.3-6).

Differences in eastern and central GAB acoustic backscatter varied by no more than +/- 30% depending on frequency and upper slope/offshore locality. Differences may be due to changes in biomass (i.e. backscatter is proportional to biomass) or a change in the species mix (i.e. backscatter changes due to difference in reflectivity, not numeric density), noting that these changes may be more noticeable on one frequency than another. Statistical variability in the spatial distribution of the acoustic backscatter may also be responsible for observed differences. For example, Figure 6.3-13 shows two echograms from the central GAB obtained during daylight hours. The top panel shows a consistent pattern of vertical stratification through the water column with relatively homogeneous layers at the surface and closer to the seafloor at 800 m. The lower echogram shows a

highly dynamic heterogeneous structure. In this example, any metrics extracted would be highly dependent on which portion of the data set was used. To improve robustness of regional comparisons, sustained and repeated measurements are needed to account for such potential variability in the acoustic ‘echostructure’. Future monitoring should consider the issue of variability if designing vessel-based surveys, while moored acoustic systems may provide an effective method for obtaining sufficient data to account for variability in acoustic backscatter.

#### Variability in acoustic data and its implications

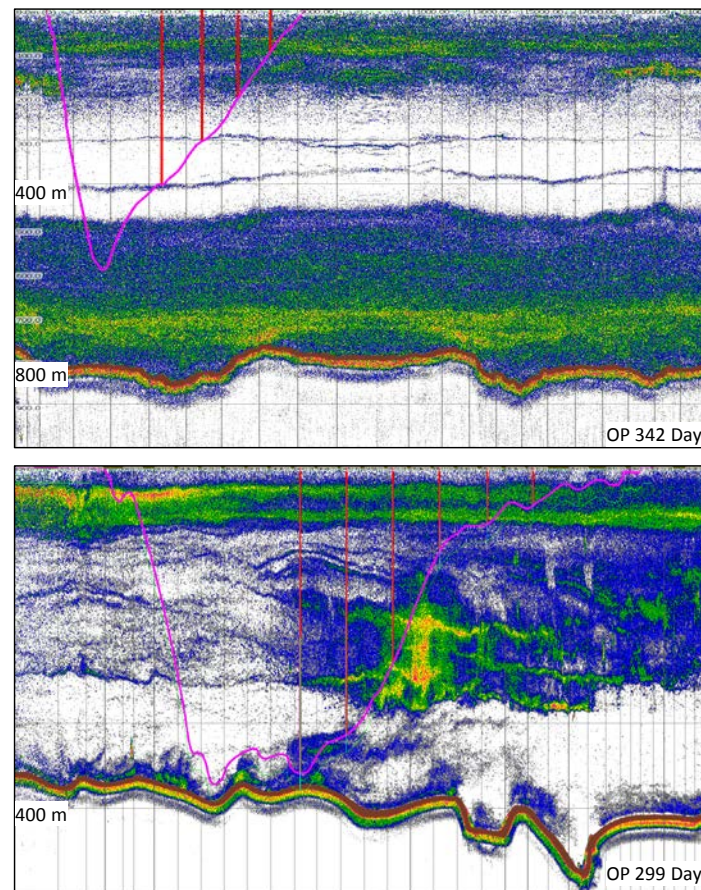


Figure 6.3-13 38 kHz echograms highlighting examples of relatively homogenous layers (top panel) and highly variable backscatter distribution in both vertical and horizontal directions.

The comparison of historic 38 kHz data (Feb 1998, April 2013 and Dec 2015) cross-shelf transects from the central GAB indicated regions of high intensity backscatter at ~ 250 – 300 m in 1998 and 2013 which were not observed in 2015. The lack of observed high signal regions in 2015 suggests multi-year observations are required to fully understand inter- and intra-annual variability. Complementing these observations was detection of many high-signal regions (inferring schools) distributed seemingly randomly over a 5 month period in the central GAB seismic survey region of the *CV Ramform Sovereign*. Although the trophic pathways may not be known, these high backscatter and presumably relatively high-biomass regions must be supported by a suitably high level of productivity.

The sustained recording obtained from *CV Ramform Sovereign* acoustics provided a unique opportunity to quantify season-long trends. Although clear trends were observed (e.g. lower mesopelagic increasing in summer then decreasing through to autumn with the opposite trend for



epipelagic), it is possible that depth (and thus movement into shallower and more productive waters) and not seasonality was the primary driver of these changes. Improved understanding would require control of the spatial sampling of vessel-based surveys or alternatively deployment of long term deep-water acoustic moorings to decouple spatial and temporal effects to monitor the marine environment over seasons and over multiple years.

### 6.3.5 Conclusions

A range of metrics based on bio-acoustic backscatter measurements indicated differences of no more than +/- 30% between central and eastern GAB depending on locality (upper slope/offshore) and what metrics were used. Statistical variability due to the underlying echostructure of the data selected for analysis may account for some of this variability. These metrics and visual inspection of the six cross-shelf acoustic transects did not indicate highly contrasting habitats that might be expected when comparing upwelling regions (expected higher biomass) with down-welling regions (expected lower biomass). The existence of schools in the central GAB upper slope and offshore regions indicates there should be a production source to sustain them.

### References

- Davison, P. C., Koslow, J. A., and Kloser, R. J. 2015. Acoustic biomass estimation of mesopelagic fish: backscattering from individuals, populations, and communities. *ICES Journal of Marine Science*, 72: 1413-1424.
- Demer, D., Berger, L., Bernasconi, M., Bethke, E., Boswell, K., Chu, D., and Domokos, R. 2015. Calibration of acoustic instruments. *ICES Cooperative Research Report*, 133.
- Foote, K. G., Knudsen, H. P., Vestnes, G., MacLennan, D. N., and Simmonds, E. J. 1987. Calibration of acoustic instruments for fish density estimation: a practical guide. *ICES Cooperative Research Report*, 144: 1-69.
- Irigoiien, X., Klevjer, T. A., Røstad, A., Martinez, U., Boyra, G., Acuña, J. L., Bode, A., et al. 2014. Large mesopelagic fishes biomass and trophic efficiency in the open ocean. *Nature Communications*, 5: 3271.
- Kloser, R. J., Ryan, T., Sakov, P., Williams, A., and Koslow, J. A. 2002. Species identification in deep water using multiple acoustic frequencies. *Canadian Journal of Fisheries and Aquatic Sciences*, 59: 1065-1077.
- Kloser, R. J., Ryan, T., Young, J., and Lewis, M. E. 2009. Acoustic observations of micronekton fish on the scale of an ocean basin: potential and challenges. *ICES J. Mar. Sci*, 66: 998-1006.
- Lavery, A. C., Wiebe, P. H., Stanton, T. K., Lawson, G. L., Benfield, M. C., and Copley, N. 2007. Determining dominant scatterers of sound in mixed zooplankton populations. *Journal of the Acoustical Society of America*, 122: 3304-3326.
- MacLennan, D. N., Fernandes, P. G., and Dalen, J. 2002. A consistent approach to definitions and symbols in fisheries acoustics. *Ices Journal of Marine Science*, 59: 365-369.
- Ryan, T. E., Downie, R. A., Kloser, R. J., and Keith, G. 2015. Reducing bias due to noise and attenuation in open-ocean echo integration data. *ICES Journal of Marine Science*, 72: 2482-2493.
- Simmonds, E. J., and MacLennan, D. N. 2005. *Fisheries Acoustics Theory and Practice*, Blackwell Science, Oxford. 437 pp.

### 6.3.6 Appendix – Additional acoustic figures

#### *IN2015\_CO2 cross shelf transects*

Echogram images for IN2015\_CO2 transects T1 to T6 at 38, 70 and 120 kHz are given in Figure 6.3-14 to Figure 6.3-16. Also presented is the subtraction of 38 kHz  $S_v$  data from 18 kHz for transects T1 to T6 (Figure 6.3-17).

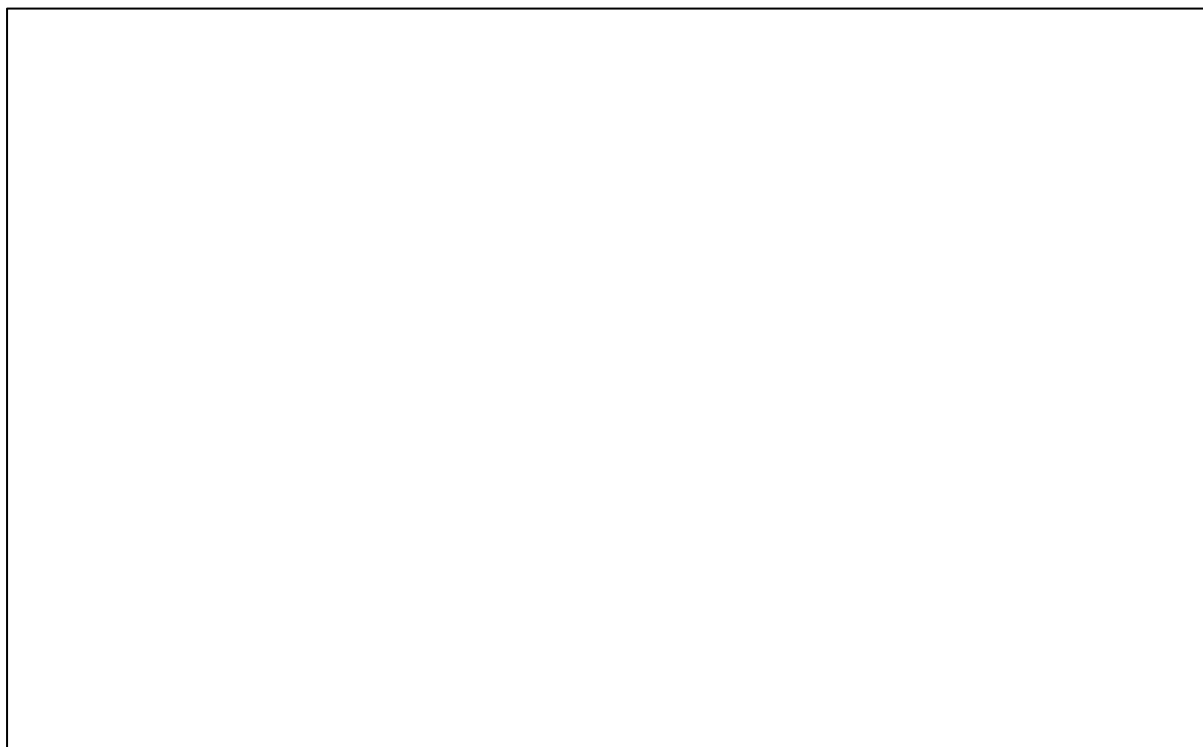


*Figure 6.3-14 38 kHz Processed quality controlled echogram matrices of  $S_v$  values as a function of depth and latitude for cross-shelf transects T1-T6. Dashed red line at 200 m depth indicates daytime, at 800 m indicates night-time. Vertical black lines indicate occasions where there was a gap in data of greater than 4 hours.*

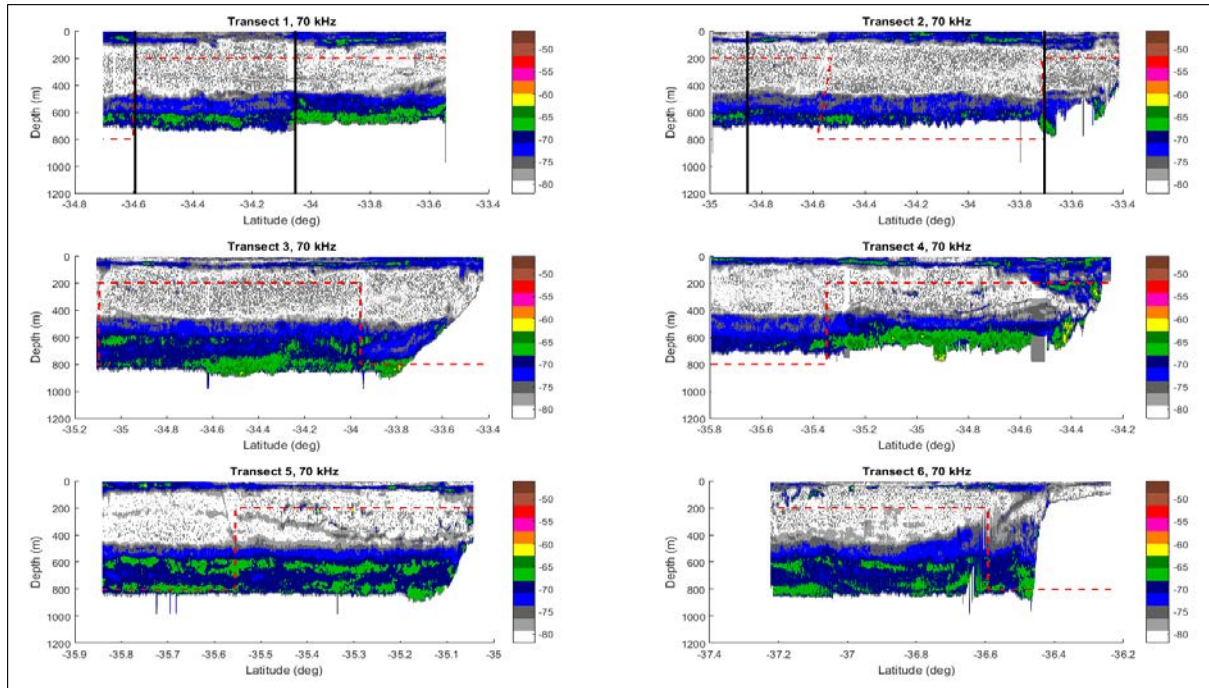


Figure 6.3-15 70 kHz Processed quality controlled echogram matrices of Sv values as a function of depth and latitude for cross-shelf transects T1-T6. Dashed red line at 200 m depth indicates daytime, at 800 m indicates night-time. Vertical black lines indicate occasions where there was a gap in data of greater than 4 hours.

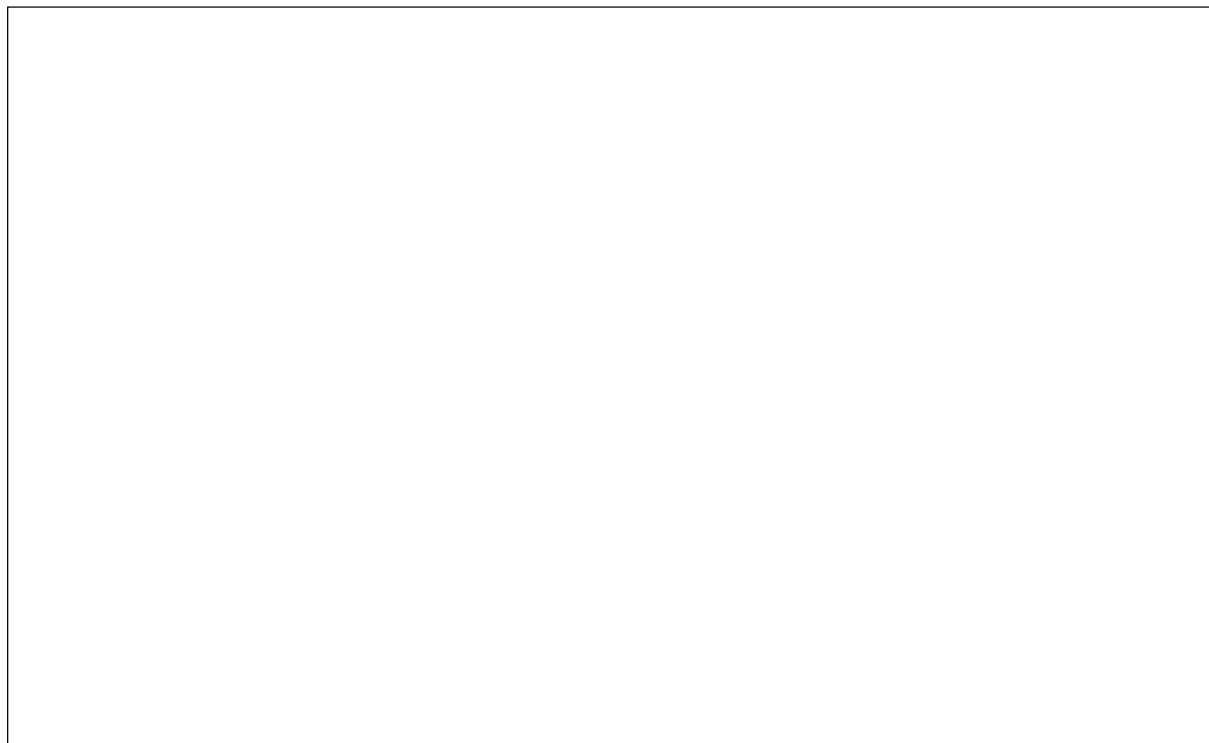


Figure 6.3-16 120 kHz Processed quality controlled echogram matrices of Sv values as a function of depth and latitude for cross-shelf transects T1-T6. Dashed red line at 200 m depth indicates daytime, at 800 m indicates night-time. Vertical black lines indicate occasions where there was a gap in data of greater than 4 hours.



*Figure 6.3-17 Decibel difference of 18kHz Sv data minus 38 kHz Sv data as a function of depth and latitude for cross-shelf transects T1-T6. Dashed red line at 400 m depth indicates daytime, at 1000 m indicates night-time. Vertical black lines indicate occasions where there was a gap in data of greater than 4 hours.*

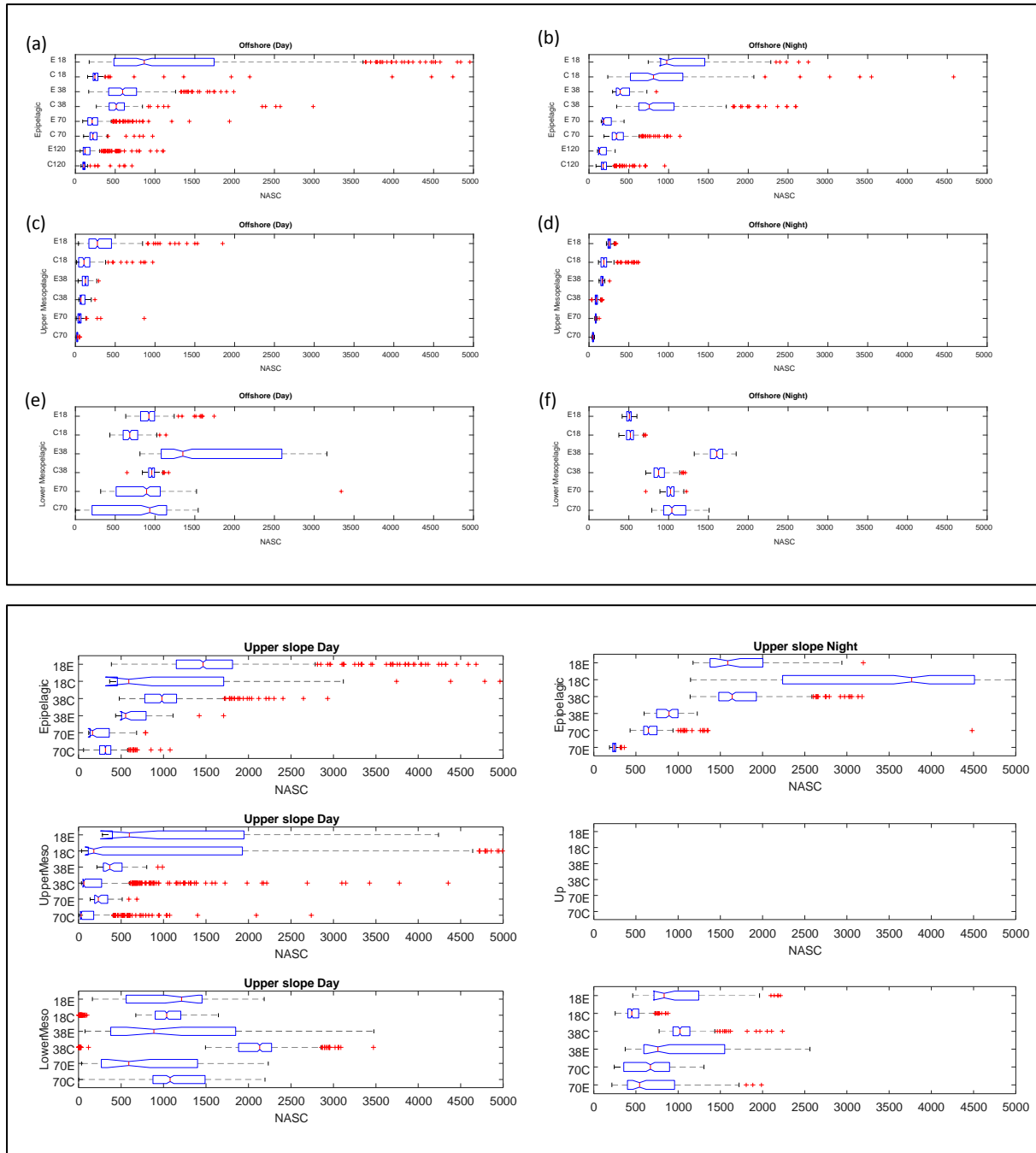


Figure 6.3-18 Box plots of NASC values per 100 m interval for 18, 38, 70 and 120 kHz for epipelagic, upper mesopelagic and lower mesopelagic layers associated with eastern (E) and central (C) offshore biological net sampling stations by day and night (top six panels, a to f) and upper slope stations by day and night (lower six panels, g-l).

## 6.4 Fine scale acoustic and optical sampling

Rudy Kloser, Lisa Gershwin, Arti Verma and Tim Ryan

### 6.4.1 Introduction

Knowledge of the structure and function of biota in the deep ocean is necessary to assist in managing human impacts, and especially to predict the behaviour of oceans in a changing climate using ecosystem models (Fulton et al., 2005; Lehodey et al., 2008; Lehodey et al., 2010; Maury, 2010;). Development of these ecosystem models will require an understanding of the biomass of the mid-trophic groups that link primary production to top predators. Here we define the mid-trophic group as those macrozooplankton and micronekton organisms of ~2 to 20 cm containing cephalopods, crustaceans and small fishes but also large gelatinous organisms (Lehodey et al., 2010). It is proposed that acoustic methods could help describe their biomass at regional and global scale, using a combination of existing or future developments (Handegard et al., 2010; Handegard et al., 2012; Lehodey and Maury, 2010; Lehodey et al., 2014).

A lot of attention is given to describe the biota in acoustic scattering layers and their diel vertical migrations. In particular, there has been a focus on organisms with gas-bladders that can make up the dominant component of the scattering (Barham, 1963; Davison et al., 2015). The dominant species that cause the scattering are identified using nets, and optics as gas-bladdered fishes or siphonophores with pneumatophores, or a combination of both (Benfield et al., 2003; Benoit-Bird and Au, 2001; Lavery et al., 2007; Davison et al., 2015; Kloser et al., 2016). With the advent of multi-frequency systems, acoustic methods have been used to classify broad categories of taxa of micronekton and nekton into dominant organisms that are gas-filled or fluid filled of different size classes (Kloser et al., 2002; D'Elia et al., 2016; Korneliussen et al., 2016).

Each sampling method of net, optics and acoustics has varying selectivity, making estimates of density of the various species and species groups problematic (Pakhomov and Yamamura, 2010; Kaartvedt et al., 2012). As an example, the current estimates of density and biomass of the gas-bladdered fish component using nets or acoustics vary by 1 to 2 orders of magnitude (Koslow et al., 1997; Kloser et al., 2009; Kaartvedt et al., 2012; Kloser et al., 2016). This difference could be due to the different selectivity of the gear types used. A particular problem for acoustics is resonance scattering where the scattering response is non-linear with fish size (Kloser et al., 2002; Davison et al., 2015). Therefore a combination of sampling methods is often used to enumerate the different micronekton taxa of gelatinous, crustacean, fish and squids.

As part of a study into the offshore pelagic habitat of the GAB, nets, optic and acoustic samplers were used from the *RV Investigator* in December 2015 to determine the taxonomy, size, biomass, trophic linkage and energetics of zooplankton and micronekton (see Sections 5 and 6). Each of these sampling methods has bias and uncertainty that needs to be quantified prior to attributing changes within and between regions. In particular, the gelatinous community covers a wide range of taxonomic and energetic groups that are difficult to sample with nets. To improve vessel-mounted acoustic and net-sampling methods of macrozooplankton and micronekton, a new profiling multi-frequency acoustic optical system was used based on a previous design (Marouchos et al., 2016). The system's 1000 m depth profiling method is lagrangian that enables the acoustic and optical data to track individuals and be linked at varying sampling ranges to explore species-specific optically-verified in situ acoustic signatures as well as organism movement. As an example, the physonect siphonophores are often damaged in nets but can be observed remotely and their acoustic signature



and depth distribution estimated. Based on this method, it is possible to compare acoustic echo-counting and echo-integration biomass estimates for a range of taxa (Kloser et al., 2016). The oblique optical imagery enables quantification of the larger zooplankton community.

In this Section, we compare the regions of the GAB as a test study for this new instrument to address biomass and size with a focus on gelatinous organisms and effects of fish behaviour.

#### 6.4.2 Methods

The Profiling Lagrangian Acoustic Optical System (PLAOS) was deployed 14 times during the *RV Investigator* voyage to depths between 400 m - 1000 m (Figure 6.4-1 a and Figure 6.4-2, Kloser et al. 2016). The PLAOS was lightly tethered to the ship and descended to depth at a set rate of  $0.4 \text{ m s}^{-1}$  recording 38 kHz, 120 kHz and 333 kHz split beam acoustics connected to Simrad EK60 echosounders, vertical video, vertical still photography (at 0.5 Hz) and oblique photos.

##### PLAOS description

The PLAOS described in Marouchos et al. (2016) recorded acoustic, optical, motion, conductivity, temperature and depth data internally. Relevant acoustic and optical specification and operating parameters of the system are given in Table 6.4-1 and Table 6.4-2.

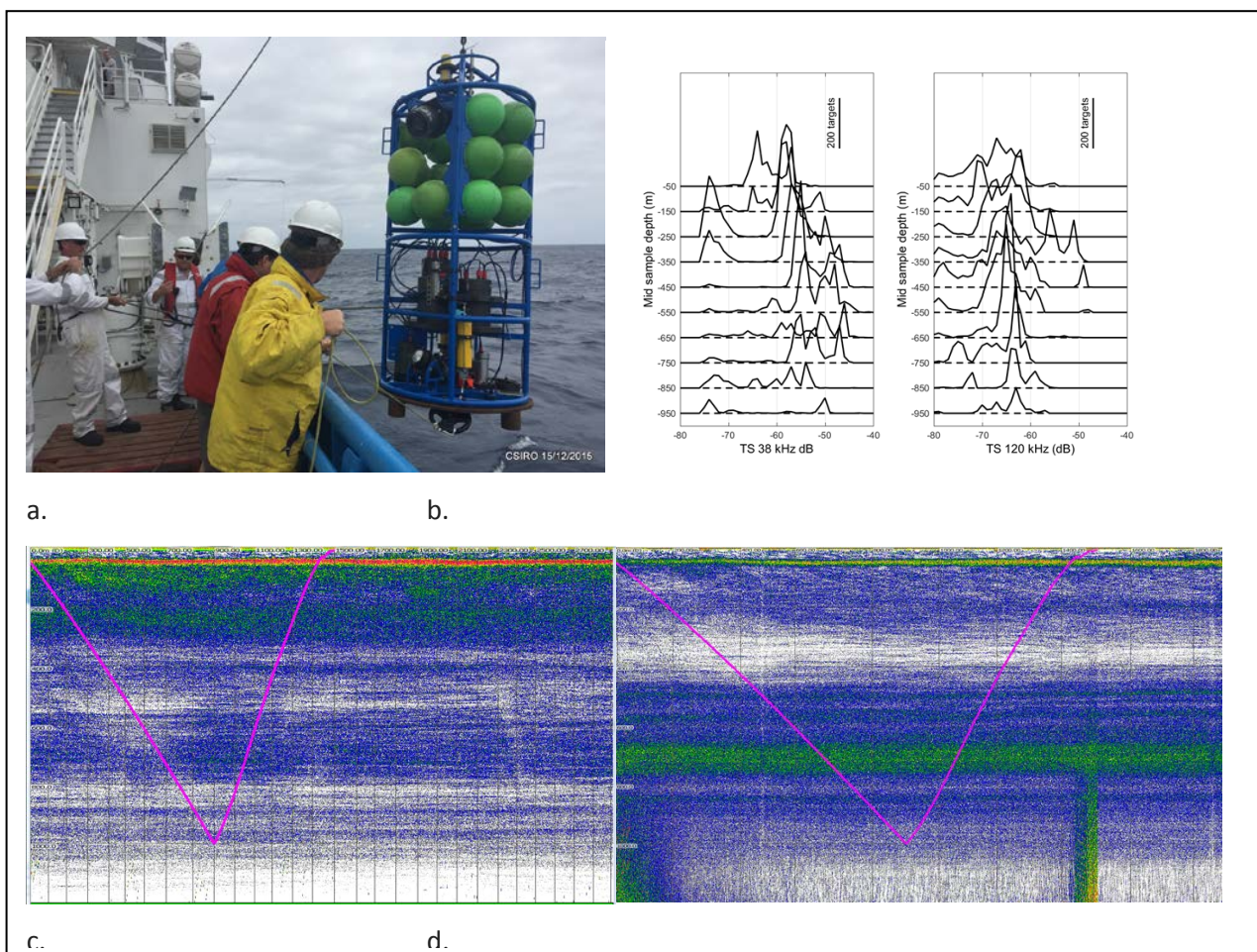


Figure 6.4-1 (a). An image of the PLAOS being deployed. (b) The number of single targets of strength in dB recorded per 100 m depth bin at 38 kHz and 120 kHz. (c) Vessel mounted 18 kHz. (d) 38 kHz echogram with the PLAOS profile overlaid.



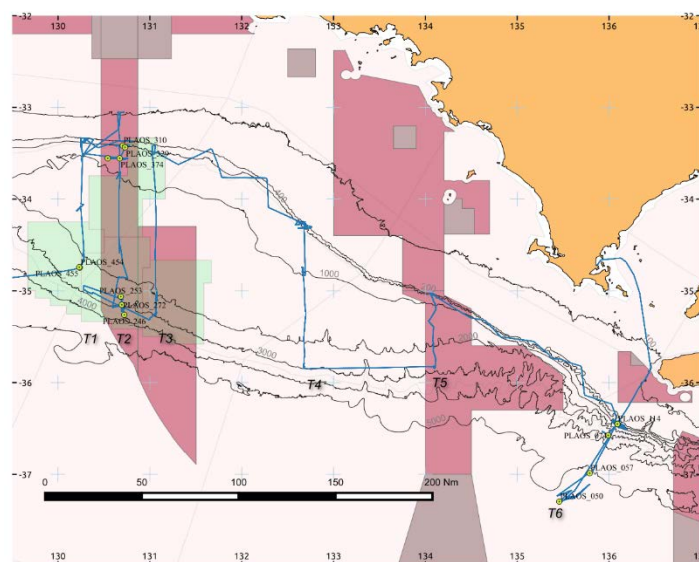


Figure 6.4-2 Profiling Lagrangian Acoustic Optical System (PLAOS) locations on voyage IN2015\_C02 with details in Kloser *et al.* (2016).

Table 6.4-1 Profiling Lagrangian Acoustic Optical System (PLAOS) acoustic system specifications and operating parameters used.

Variables	Units	MSI38	ES120	ES333
Frequency	<b>kHz</b>	<b>38</b>	<b>120</b>	<b>333</b>
Serial number			109	112
Beamwidth	Degrees	14	7	7
Transceiver	EK60	GPT 38 kHz 009072056078 1- 1 ES38-12	GPT 120 kHz 009072056154 2- 1 ES120-7CD	GPT 333 kHz 00907206047e 3- 1 ES333-7CD
Power	W	500	250	40
Pulse length	µs	512	256	512
Equivalent beam angle	dB re 1 Steradian	-15.5	-20.7	-20.7
Transducer Gain	dB	19.5	28	29
Sa corr	dB	0	0	0
Absorption coefficient	dB m <sup>-1</sup>	0.01	0.0374	0.078
Sound speed	ms <sup>-1</sup>	1494	1494	1494
Angle sensitivity		12.5	23	23
Sample interval	µs	1280	640	320
Calibration Sphere TC Diameter	mm	38.1	38.1	22

Table 6.4-2 Camera and video specifications and operating parameters and details of other sensors on the PLAOS.

Variables	Units	Oblique Camera	Vertical Camera	Vertical video
Optics	DSLR	Canon EOS-1D X	Canon EOS-1D X	
Focal length	mm	35	25	
Resolution	Pixels	5189 * 3456	5189 * 3456	
Resolution	dpi	72	72	
F-stop		f/6.3	f/16	
Exposure	s	1/250	1/250	
ISO speed		12800	3200	
Sensor size				
Light		Quantum stobe	Quantum stobe	2 Deepsea Power and Light
Platform motion:	Microstrain 3DM-GX1			
CTD	Seabird Electronics 37SI, SN 373150922-6286			

The geometry of the acoustic, video and still camera highlights the variable sampling volumes for the downward-looking sensors which overlap at ranges greater than 3 m (Figure 6.4-3). The volume-per-ping of water sampled by the downward-orientated acoustic sensors-per-ping between 5 m to 15 m and up to 4 degrees off the centre beam axis is  $16.5 \text{ m}^3$  (Figure 6.4-3). For the oblique camera, the volume of sampling is estimated to be  $1 \text{ m}^3$  based on the overlap of the camera and strobe (Figure 6.4-4).

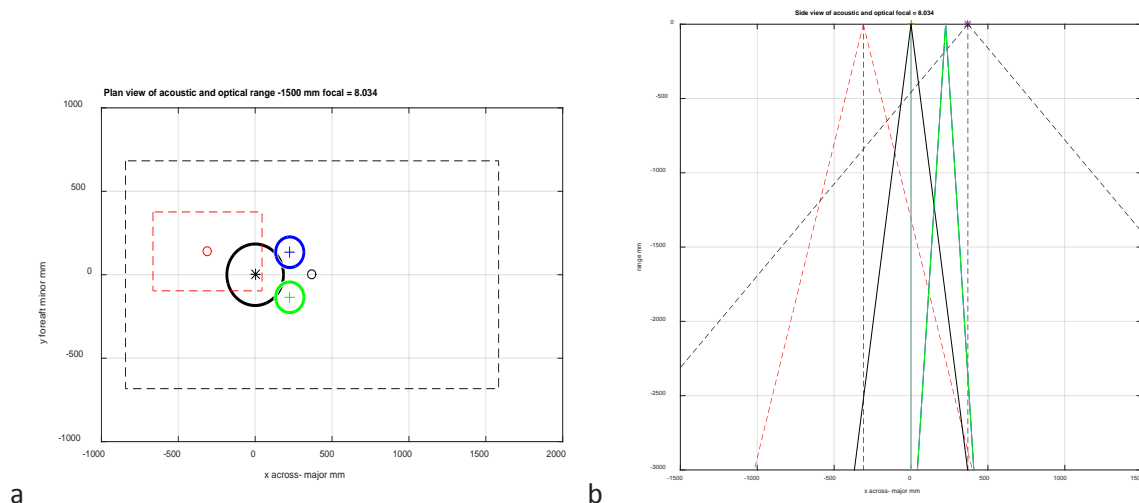


Figure 6.4-3 (a) plan view sampling area at a range of 1500 mm and (b) side view sampling area at a range of 3000 mm of the downward orientated acoustic sensors of beamwidth specified in Table 6.4-1 for the 38 kHz (black), 120 kHz (blue) and 333 kHz (green) frequencies and the video (black dashed) and still camera (red dashed) specified in

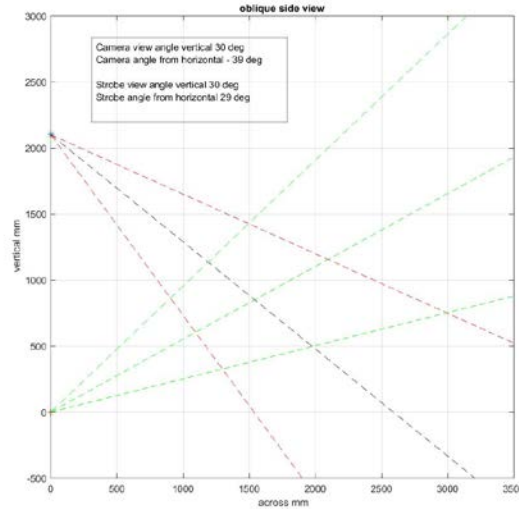


Figure 6.4-4 The side view sampling area at a range of 3500 mm of the oblique still camera (red-dashed) and the strobe light (green dashed) specified in

#### AOS Probe TS and Sv measurements

The analysis of the PLAOS data was as described in Kloser et al. (2016) with modifications as outlined below, where only the 38 kHz and 120 kHz data have been included for this analysis. Calibration at depth was done with a 38.1 mm tungsten carbide sphere suspended 4.5 m below the transducers with target strength of -42.3 dB and -39.5 dB at 38 kHz and 120 kHz, respectively. As the AOS probe was sinking and lightly tethered to the following vessel, the 38 kHz and 120 kHz transducers were operated at a ping-rate of 9 Hz and data recorded to 100 m. *In situ* target-strength data were derived using the Simrad split-beam method-2 algorithm in the Echoview acoustic-analysis software (Myriax, 2010), using settings as outlined in Kloser et al. (2016). Single targets from the 38 kHz and 120 kHz data were derived and recorded with depth, ping number and position. To minimize beam compensation errors, contamination by the calibration sphere and signal-threshold bias, only targets within 4° of the transducer axis and a range of 5–15 m were used. Target-strength frequency distributions were summarised into 100 m bins centred at 50 to 950 m depth. The density ( $d_{ij} \text{ m}^{-3}$ ) of the  $n$  target strength  $TS_{ij}$  (dB) targets in depth interval,  $i$ , with  $p_i$  pings is

$$d_{ij} = \frac{n}{p_i * V} \text{ m}^{-3},$$

where the insonified volume  $V = 16.5 \text{ m}^3$  for the 38 kHz and 120 kHz transducer for limits of off-axis angle of 4° and target range 5 to 15 m. The predicted volume-backscatter strength,  $Sv_i$ , of the  $k$  target strength classes for each depth interval,  $i$ , is:

$$Sv_i = 10 \log_{10} \left( \sum_{j=1}^k 10^{\frac{TS_{ij}}{10}} * d_{ij} \right) \text{ dB}.$$

#### Vessel mounted volume backscattering strength

The mean volume backscattering strength, MVBS, ( $Sv$ , dB re  $1 \text{ m}^{-1}$ ) just prior to the AOS probe experiment was obtained from 20 to 1000 m depths with a vessel-mounted Simrad EK80 echosounders operating at 18, 38, 70 and 120 kHz calibrated with appropriate standard spheres (MacLennan et al., 2002). Data were processed in EchoView (version 7.0 (Myriax, 2010)) where calibration offsets were applied, background and spike noise was removed and absorption and

sound speed applied as outlined in Section 6.3. MVBS was determined for each 20 m depth interval,  $i$ , using,  $n$ , volume backscattering strength,  $Sv_i$ , values in the depth interval:

$$Sv = 10 * \log_{10} \left( \frac{\sum_{j=1}^n 10^{\frac{Sv_j}{10}}}{n} \right) \text{ dB re m}^{-1}.$$

#### *Model predictions of resonance scattering target strength*

The following model was used to predict the resonance gas-bladder TS at each frequency and the logarithmic difference between frequencies,  $\Delta TS$ , at depth  $z$  metres for equivalent spherical radius,  $a_s$  from 0.1 mm to 6 mm at 0.1 mm intervals. The target strength  $TS_f$  at frequency  $f$  in dB form is  $TS_f = 10 * \log_{10}(\sigma_{bs})$  for the back-scattering cross-Section,  $\sigma_{bs}$ , derived from,

$$\sigma_{bs} = \frac{a_s^2}{\left[ \left( \frac{f_{RF}}{f} \right)^2 - 1 \right]^2 + \delta_{RF}^2} m^2,$$

at damping factor  $\delta_{RF} = 0.14$ . The resonance frequency,  $f_{RF}$ , was derived from,

$$f_{RF} \cong \frac{1}{2\pi a_s} \left( \frac{3\gamma P_A}{\rho_A} \right)^{0.5} \text{ Hz},$$

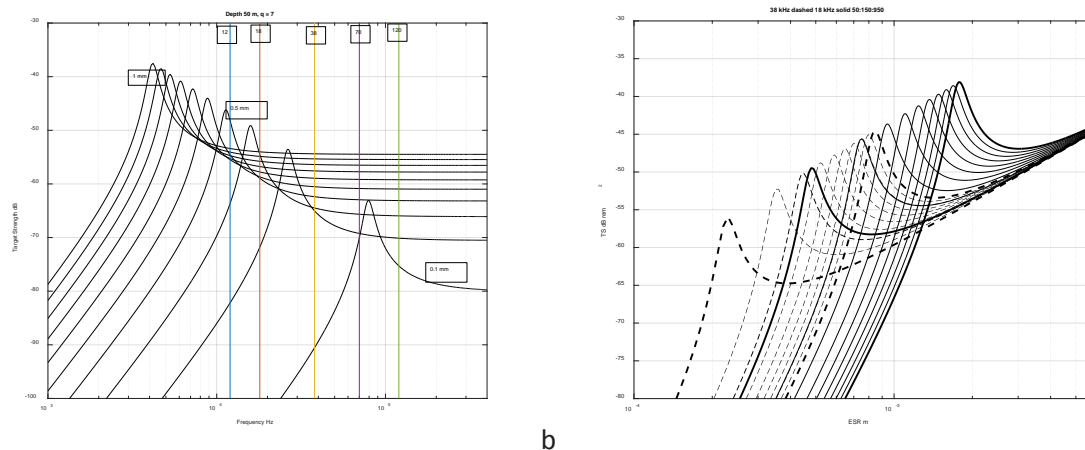
where it is assumed that the ratio of specific heat  $\gamma = 1.4$ , ambient pressure

$$P_A = 10^5 (1 + 0.1z) \text{ Pa at depth } z,$$

$$\rho_A = 1028 \text{ kg m}^{-3}$$

and  $a_s$  is the equivalent spherical radius (ESR) of the gas-bladder volume in metres as described by Clay and Medwin (1977) (p.221). Results of the model output at 50 m depth for a range of frequencies used in this study and the effect of depth on resonance scattering at 18 kHz and 38 kHz from 50 m to 950 m is shown in Figure 6.4-5.

The equivalent spherical radius of a target at depth  $z$  was assigned by matching the nearest consistent ESR across all model predicted frequency difference pairs to the *in situ* vessel mounted frequency difference,  $\Delta Sv$ , across several frequencies. The variance in the predicted ESR between the nearest model predictions was used to select the goodness of fit. The size and weight of fish assumed the gas bladder is 3 % of fish volume, density of flesh is 1030 kg m<sup>-3</sup> and shape described by a prolate spheroid of eccentricity of 6 (Kloser et al. 2016; Figure 6.4-5).



**a** **b**

Figure 6.4-5 Prediction of, (a) the resonance scattering target strength for frequency of various gas bubbles of ESR of 0.1 to 1 mm at 50 m depth highlighting the sampled frequencies on RV Investigator (12, 18, 38, 70, 120 kHz) and (b) the expected change in the target strength at 38 kHz (dashed) and 18 kHz (solid) for bubble sizes of 0.1 to 6 mm for depths from 50 to 950 m (bolded) in 100 m steps.

### Optical measurements

The oblique camera system Canon EOS-1D X digital SLR (DSLR) camera (Figure 6.4-4), were operated at 0.5 Hz image capture rate as the PLAOS descended, representing an image every 0.8 m of water depth. Optical images were reviewed and recorded in Transect Measure software by a taxonomic expert (co-author Lisa Gershwin) to identify dominant vertebrate and invertebrate taxa (Seager, 2008). At the top level the Fauna categories of Fish, Squid, Crustaceans, Worms, Gelatinous, Other and Uncertain were defined, and based on taxonomic knowledge these were further classified where in some cases it was possible to get to species. Each identification was given a score between low, medium and high confidence in identification. Density was estimated from the optical measures assuming the sample volume per image was 1 m<sup>3</sup> based on the camera and strobe geometry. The vertical depth distance between images was 0.8 m due to the 0.4 ms<sup>-1</sup> profiling rate (Figure 6.4-4).

### 6.4.3 Results

Of the 14 sampling sites, 8 were conducted at the 24 hr sampling stations that enabled a comparison of east (transect T6) and central (transect T2) GAB upper-slope and offshore regions (Table 6.4-3, Figure 6.4-2). At these stations, avoidance presumably by fishes could be observed in the vessel's acoustics as it descended, predominantly with the 18 kHz echosounder. This observation guided the interpretation of the data to ensure unbiased regional comparisons as outlined below.

Table 6.4-3 Location of the PLAOS profiles with the paired day and night stations of the offshore and slope stations in bold at the eastern GAB (transect T6) and central GAB (transect T2) (Figure 6.4-2).

Cast_ID	Transect	Location	Day (D) or Night (N)	Date (UTC)	Time (UTC)	Longitude DD	Latitude DD
50	T6	Offshore	D	2015-12-02	03:05:00	135.4570	-37.2970
57	T6	Offshore	N	2015-12-02	11:06:35	135.7877	-36.9881
95	T6	Upper Slope	N	2015-12-03	14:03:30	136.0893	-36.4515
114	T6	Upper Slope	D	2015-12-03	23:11:21	136.0904	-36.4517
253	T2	Offshore	D	2015-12-11	08:19:00	130.6824	-35.0628
272	T2	Offshore	N	2015-12-11	18:02:00	130.6930	-35.1530
310	T2	Upper Slope	D	2015-12-13	08:14:53	130.7033	-33.4167
329	T2	Upper Slope	N	2015-12-13	16:49:00	130.7281	-33.4359

#### Acoustic single target data analysis

A summary of the PLAOS deployments highlights large day-night differences in sampling where there are four times more targets at night for the 38 kHz sounder and 1.1 times more targets on the 120 kHz sounder. There was also an increase in the mean target strength (TS) at night on both the 38 kHz and 120 kHz of 1.5 dB. The observed behaviour appeared to be consistent at day and night within and between regions suggesting data can be used as a relative indicator. The two offshore eastern and central regions had similar densities of targets for both frequencies with slightly higher (0.1 to 1.0 dB) mean 38 kHz TS in the central GAB but lower (-1.0 to -1.2 dB) at 120 kHz frequency. There was a marked difference between the eastern and central GAB upper slope sites. The central region had higher densities (20 – 30 %) of targets day and night with higher target strengths (2-9 dB) compared to the eastern region for both the 38 kHz and 120 kHz frequencies (Table 6.4-4).

Table 6.4-4 Summary of the PLAOS acoustic data at 38 kHz and 120 kHz with number of targets between 5 and 15 m range from the transducer and out to 4 degrees off axis for the GAB regions of east and central, offshore and upper slope.

Station	N pings	# targets 38 kHz	# targets 120 kHz	mean TS 38 kHz	mean TS 120 kHz	Time	region	Depth
OP50	16458	1914	16072	-56.50	-64.3	Day	East	offshore
OP246	16877	1605	16356	-54.85	-65.5	Day	Central	offshore
OP57	16295	7271	15686	-53.80	-62.6	Night	East	offshore
OP272	18122	8859	16968	-53.77	-63.8	Night	Central	offshore
OP114	9368	666	4291	-54.92	-68.17	Day	East	Upper slope
OP329	6997	718	5339	-52.54	-64.18	Day	Central	Upper slope
OP95	8362	2359	4877	-56.87	-65.52	Night	East	Upper slope
OP310	6615	1977	5625	-48.33	-63.77	Night	Central	Upper slope

The high difference in the day and night number of targets and their mean target strength is explored by comparing the predicted PLAOS 38 kHz volume backscatter to the vessel 38 kHz volume backscatter (just prior to the PLAOS deployment) at offshore sites (Table 6.4-6). There is close agreement between the vessel 38 kHz profile and the predicted PLAOS 38 kHz volume backscatter (Sv) during the day, but at night the PLAOS 38 kHz backscatter greatly exceeds the vessel 38 kHz Sv.

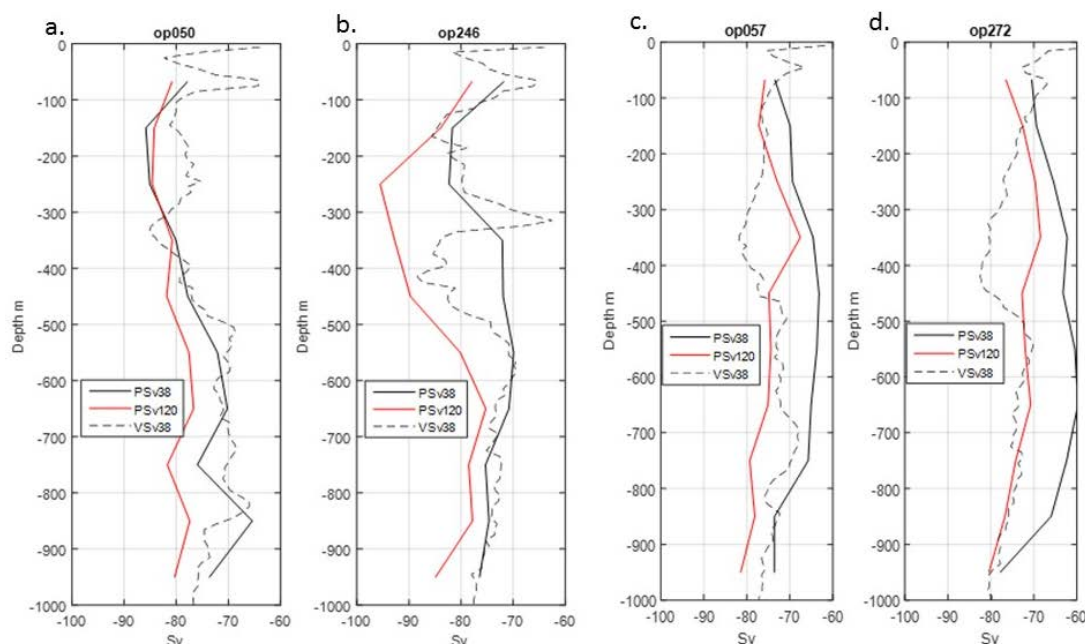


Figure 6.4-6 Comparison of the predicted volume backscatter (Sv dB re 1m-1) of the PLAOS at 38 kHz (black line) and 120 kHz (re- line) to the measured vessel volume backscatter (dashed black line) for day profiles at (a) Eastern and (b) Central and night-time (c) Eastern and (d) Central offshore sites.

The mean Sv for the vessel 38 kHz transducer is 23% lower during the night than at day which is expected to reflect changes in the organisms target strengths rather than changes in biomass. For the PLAOS there was a 600% increase in the night time predicted 38 kHz Sv compared to daytime for both the central and eastern regions. This observation was also consistent with the 120 kHz PLAOS predicted Sv (

Table 6.4-5). This increase between day and night Sv can be attributed to attraction of fish to the PLAOS during the night profile as observed on the systems video. This is also supported by the PLAOS predicted Sv being 740% (8.7 dB) higher than the measured vessel Sv (

Table 6.4-5). Inferred resonance-scattering effects are observed both day and night with the 38 kHz predicted volume backscatter being 7 dB higher than the 120 kHz frequency.

Table 6.4-5 Comparison of the estimated mean volume backscatter (Sv dB m-1 from 25-975 m) from the PLAOS and the measured backscatter from the vessel at 38 kHz between the day and night sampling of the eastern and central sites.

	Day east Sv dB	Day central Sv dB	Night east Sv dB	Night central Sv dB	Mean Sv Day – Night dB
PLAOS Sv120	-79.9	-80.2	-73.9	-72.2	-7.0
PLAOS Sv38	-72.5	-73.2	-66.6	-63.6	-7.8
Vessel Sv38	-72.2	-73.2	-73.3	-73.9	0.9
P38 – V38	-0.3	0	<b>6.7</b>	<b>10.3</b>	<b>-8.7</b>
P38 - P120	7.4	7	7.3	8.6	<b>-0.8</b>

#### Interpretation of vessel acoustic data and resonance scattering

Based on the resonance-scattering model, it is possible to interpret the size of gas bladders and their depth using both the vessel and PLAOS data. Resonance scattering by small gas bladders of



predicted ESR size of 0.45 mm at 165 m depth is clearly noticeable in the daytime vessel mounted echograms (Figure 6.4-7). The PLAOS data at this location predicts a mode of high density gas bladder size of 0.3 mm ESR at depths from 100 to 200 m (Figure 6.4-8). The 0.15 mm difference in estimates of gas bladder size between the vessel and PLAOS estimates is small and may be due to calibration, model frequency uncertainty or avoidance of the PLAOS by larger gas-bladdered organisms. We infer this layer to be dominated by small fishes with an estimated minimum standard length of between 3 to 5 mm of weight 4 to 18 mg. No evidence of a large number of small-sized organisms was evident in the PLAOS video or still imagery at these depths which could be due to the resolution of the imagery and focal distance used. This highlights the difficulty in validating and estimating acoustic biomass estimates of small gas-bladdered targets.

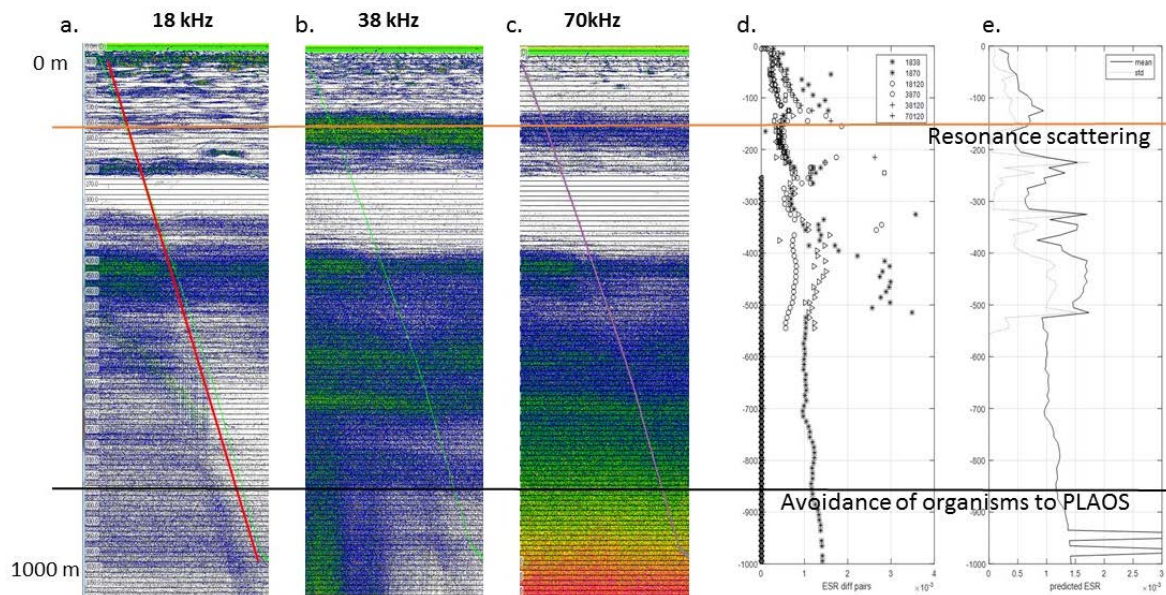


Figure 6.4-7 Example of resonance scattering (orange line) at 165 m observed on the stationary vessel mounted echograms at (a) 18 kHz (red line shows PLAOS decent to 1000 m), (b), 38 kHz, and (c) 70 kHz frequency. The predicted gas bubble size 0.45 mm (ESR) at 165 m based on (d) the Sv frequency difference pairs (symbols in legend) from 18 to 120 kHz and the mean (solid) and standard deviation (std) of the predicted ESR of all frequency estimates combined. Low standard deviation implies no ambiguities within and between frequencies. Avoidance to the lowered PLAOS by presumably mobile fish at depths from 600 m to 1000 m is highlighted (black line 850 m) where the response is more evident on the 18 kHz frequency.

Predicted gas bladder sizes at this location from the PLAOS range from 0.2 - 2 mm ESR with larger gas bladders predicted with depth (Figure 6.4-8). Based on the predicted ESR, the size of organisms range from 2 - 21 mm standard length and weight from 0.001 - 1.1 grams. Of note is the avoidance response to the PLAOS of presumably larger more mobile fishes as the PLAOS descends (Figure 6.4-7). This avoidance is most noticeable at depths from 600 - 1000 m on the 18 kHz vessel mounted frequency, that displace the assumed fishes when the PLAOS is within 100 m to a greater depth through the profile. These targets would not be detected in the 5 - 15 m processing window of PLAOS. Hence in this daytime deployment avoidance of targets would presumably bias PLAOS estimates to small, less mobile fishes.

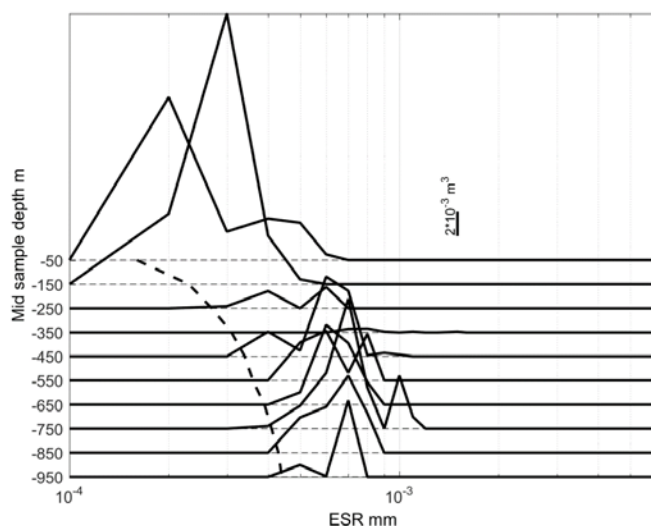


Figure 6.4-8 Estimate of gas bladder size and density of targets from the PLAOS 38 and 120 kHz data from 50 to 950 m depth highlighting larger gas bladder sizes with depth and the high number of small gas bladder sizes (0.3 mm ESR) between 100 and 200 m depth.

#### *Oblique camera analysis*

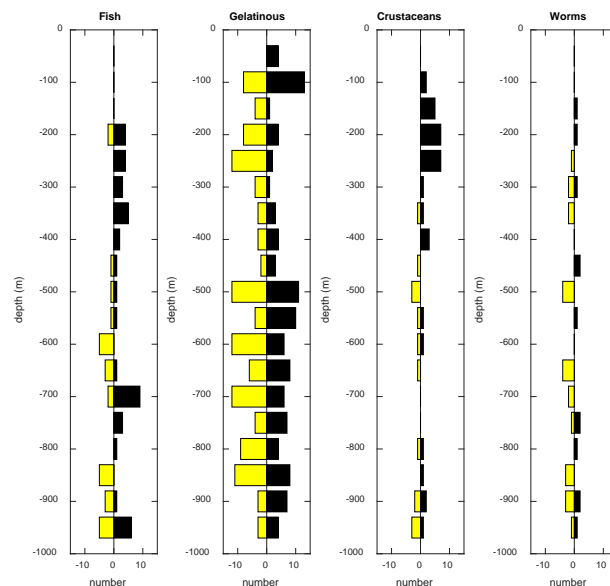
The oblique camera on the PLAOS was designed to image and census macrozooplankton and micronekton with a primary focus on the gelatinous community, which is an important part of the ecosystem and indicator for change, yet very difficult to sample (see Section 5.3). From the eight PLAOS profiles 10 022 oblique images were obtained at an image rate of 0.5 Hz, which is nominally every 0.8 m in depth (Table 6.4-6). From the images, 1542 large taxa were identified, comprised of gelatinous (46 %), crustaceans (22 %), fish (16 %), worms (6 %) and squid (2 %), with other taxa or uncertain identification accounting for 8% of image scores. During the night deployments, consistently higher numbers of fish (4-fold), crustaceans (8-fold) and squid (1.4-fold) were scored. This is presumably due to attraction to the PLAOS lights. The depth distribution of the scored imagery highlights the day-night differences for the fish and crustaceans in particular and distribution throughout the water column to 1000 m (Figure 6.4-6). The focus of this analysis is on the gelatinous community that showed no significant difference between total day and night biomass.

Table 6.4-6 Summary of the oblique camera imagery for macro-zooplankton and micronekton in broad fauna groups.

Cast_ID	Transect	Location	Day (D) or Night (N)	# images down	# images with biota scored	'Gelatinous'	'Fish'	'Worm'	'Crustaceans'	'Squid'	'Other'	'uncertain'
50	T6	Offshore	D	1254	236	128	28	25	18	2	1	34
57	T6	Offshore	N	1186	235	110	44	12	35	5	3	26
246	T2	Offshore	D	1300	141	68	14	28	12	11	2	6
272	T2	Offshore	N	1331	246	84	106	16	12	7	8	13
114	T6	Slope	D	671	89	78	3	2			3	3
95	T6	Slope	N	593	147	81	39	2	15	4		6
310	T2	Slope	D	493	113	93	6	1	5		1	7
329	T2	Slope	N	530	335	68	12	10	236	2		7
Totals				10022	1542	710	252	96	333	31	18	102

Based on the scored imagery there were higher densities (70 %) of gelatinous organisms in eastern offshore compared to the central offshore GAB at 50 - 950 m depths. Gelatinous organisms were also slightly less dense (20 %) in the eastern upper slope compared to the central upper slope region. Both eastern and central profiles show diel migration of gelatinous organisms most notably from the 150 - 450 m depth in the day to less than 100 m at night (Figure 6.4-9).

a.



b.

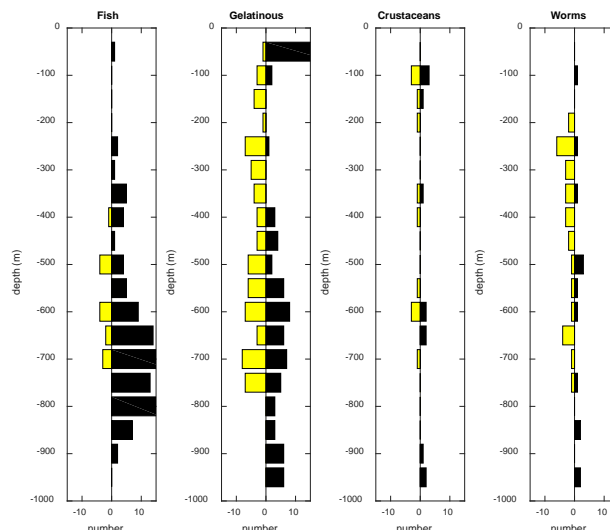


Figure 6.4-9 Depth distribution of the offshore major fauna categories scored (day yellow, night black) in the oblique camera for (a) Eastern and (b) central GAB regions (Table 6.4-6).

Gelatinous organisms were separated into classes of salps, medusae, siphonophores and ctenophores, with the siphonophores separated into physonect and non-physonect (see Section 5.3). Siphonophores are a top predator in the pelagic ecosystem and many species (physonects) have a pneumatophore filled with gas that can produce a large acoustic signal when in resonance (Figure 6.4-10). An example of this potential is a layer at 800 m that has high backscatter at 38 kHz and low backscatter at 18 kHz where a number of physonect siphonophores have been observed (Figure 6.4-11). Other physonects observed at shallower depths do not have high backscatter at 38 kHz and presumably these have gas floats of a size that are not in resonance at either 18 kHz or 38 kHz frequencies. The estimated density of physonect siphonophores for this profile is  $0.012 \text{ m}^{-3}$ . Of interest is the layer at 600 to 900 m that reduces in backscatter at a range of 100 m from the PLAOS (presumably fish avoidance) at 18 kHz but not 38 kHz as the PLAOS descends (Figure 6.4-11).

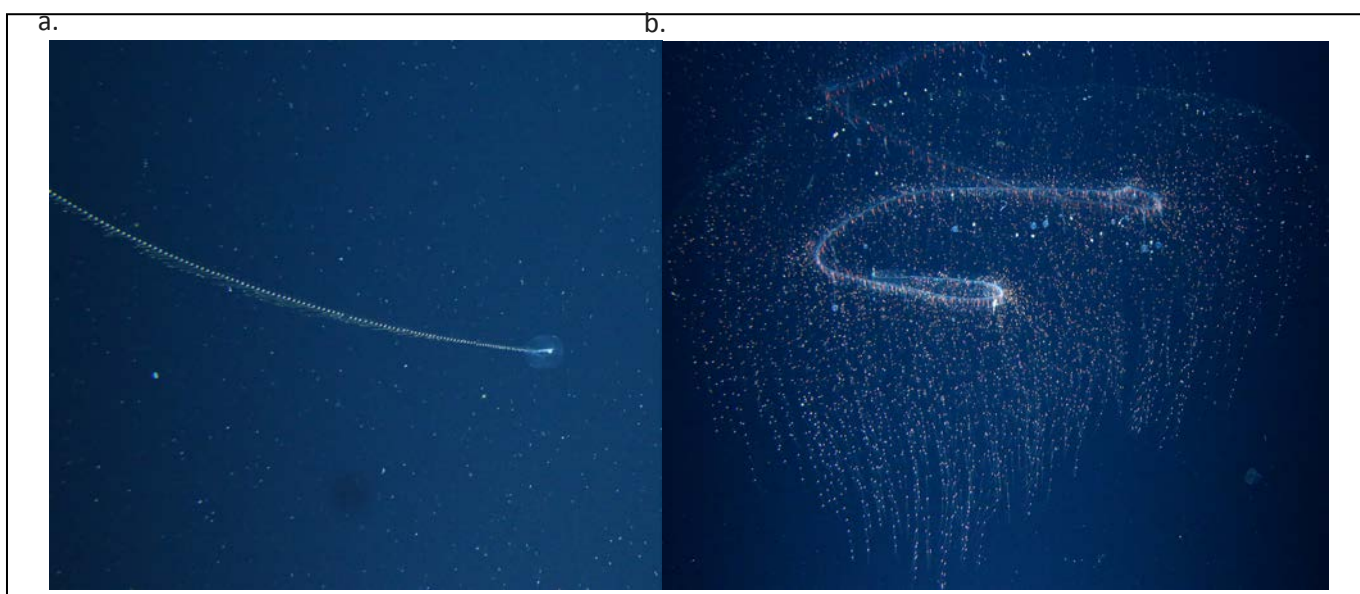


Figure 6.4-10 Imagery from the oblique cameras of siphonophores, (a) *Praya* species non – physonect and (b) a physonect species believed to be new to science, 0.8 m high and 2 m long in a feeding mode, highlighting their top predator status in the pelagic ecosystem.

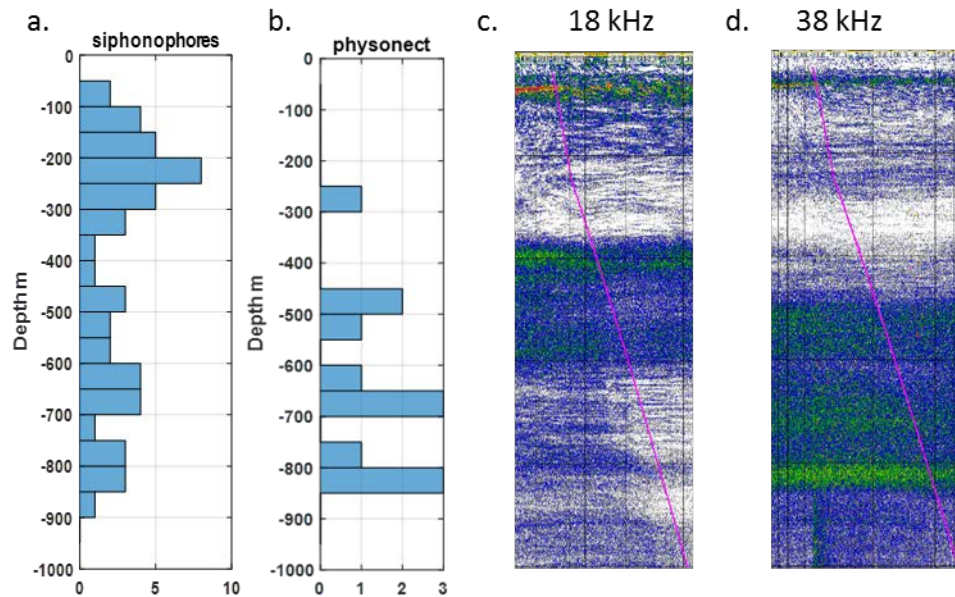


Figure 6.4-11 Example of the depth distribution of, (a), non-physonect siphonophores scored with the oblique camera (Table 6.4-6), and the, (b), identified gas-filled physonect siphonophores with the corresponding vessel mounted, (c), 18 kHz and, (d), 38 kHz acoustic echograms (minimum Sv -76 dB) highlighting the passage of the PLAOS (purple line) as it descends through the water column. Note the layer at 600 to 900 m that reduces in backscatter (presumably fish avoidance) at 18 kHz but not 38 kHz as the PLAOS descends and a layer at 800 m associated with high backscatter at 38 kHz that remains and associated with a number of physonect siphonophores and potentially resonance scattering due to the lack of 18 kHz backscatter.

It is possible that we are underrepresenting some gelatinous taxa due to avoidance. Video observations showed physonect siphonophores swimming downward and sideways away from the PLAOS as it descended with an estimated speed of 0.2 to 0.3 ms<sup>-1</sup>. It is possible that these siphonophores would not be captured by the oblique camera that sampled organisms at a range of 1 to 3 m to the side of PLAOS (Figure 6.4-4).

#### 6.4.4 Discussion

The PLAOS is a new tool to explore epipelagic and mesopelagic zooplankton and micronekton communities. The first use of the tool has elucidated some new insights into the distribution and behaviour of organisms. There was clear attraction by fish to the system at night and avoidance during the day. We presume that both the avoidance and attraction is due to a combination of factors with experiments subsequent to this voyage showing the continuous video lights were a dominant factor. Equal avoidance and attraction effects was observed within and between regions indicating the PLAOS could provide a relative estimate of the density of organisms and their acoustic size when occurring across multiple frequencies.

Comparison of east and central pelagic habitat implied that the offshore regions had similar densities and size (mean target strength similar across frequencies) that is in general agreement with MIDOC net sampling (Chapter 6.1). This differed for the upper slope habitat where the PLAOS density was higher with larger size (higher target strength on both frequencies) than the eastern region and in contrast to the MIDOC net sampling. In part, this may be due to the different selectivities of the two gear types. The PLAOS profiles highlight that the 38 kHz vessel mounted acoustic recordings are selective due to resonance scattering to small gas bladders in size range 0.2 to 1 mm ESR for predicted fish lengths of 2 to 21 mm. This size range would be under-represented in net samples compared to larger fishes. The higher PLAOS 120 kHz signal would not be due to



resonance gas bladders of that size and the signal would increase due to larger fishes or larger crustaceans. The vessel-mounted data in Chapter 6.3 across a range of frequencies (18 to 120 kHz) were in general agreement that the central upper slope region had higher biomass of biota. More investigation is required to verify which vessel acoustics and PLAOS or net estimate of density and size of which taxa is more representative of the ecosystem structure and function. It may be that avoidance by selected taxa is biasing the findings. In the central upper slope region avoidance of the net was observed by a dominant species, *Verilus anomalus* (Figure 6.1-15).

For the offshore regions at depths 400 - 1000 m, the 18 kHz vessel frequency is selective to species of larger gas bladders (2 - 3 mm ESR) and avoidance is observed as the PLAOS descends with fish reacting at 100 m range. Current PLAOS processing methods will not capture these larger gas bladder species. The PLAOS also shows that species with larger size gas bladders increase with depth. This avoidance reaction of larger species has implications for net sampling systems where the 5 - 6 m headline net opening would potentially miss a range of larger sized fishes. Avoidance by mesopelagic fishes has been well reported (e.g. Kaartvedt et al., 2012), and the PLAOS system with knowledge gained in this study will be used to modify the PLAOS to explore this bias. In particular, the implementation of broadband echo sounders that were trialled on the voyage and a subject of the PhD project detailed in the Appendix in Section 9.

A major advance in using the PLAOS has been the quantitative estimates of gelatinous macro- and mega- zooplankton. Scored imagery shows that gelatinous organisms are more numerous in the east than central offshore regions and counter to the MIDOC net findings. The upper-slope gelatinous densities were similar for both east and central regions and counter to the net observations (Chapter 6.1). In this case the PLAOS gelatinous density was from organisms in depths between 50 - 950 m and of large taxa which may be different for net sampling that retained a high number of small species. Behaviour of species was highlighted in the scored imagery which emphasized the attraction (presumably by continuous lighting) of fish and crustaceans. This work demonstrates the need to modify the lighting when using the system for obtaining reliable comparisons between day and night at a site. For the gelatinous organisms, there appeared to be no obvious day and night density bias and migration of large gelatinous organisms from depths of 400 m to the upper 100 m was observed. This will assist in quantifying mechanisms of transferring carbon from the epipelagic to deeper depths.

A top gelatinous predator of the system were physonect siphonophores which occurred throughout the water column. This trophic role and energetics of this species group are still largely unknown but are probably important in the transfer of carbon from epipelagic to mesopelagic waters and the remineralisation of nutrients as well as indicators of system change (Chapter 5.3). These organisms can also be a large contributor to scattering if the pneumatophore size is close to resonance at 18 or 38 kHz, and this study highlights a potential example of this for the vessel at 38 kHz at ~800 m depth. Of note for this study was the avoidance of the PLAOS by the fast-swimming siphonophores of different species. Estimates of swimming speeds between 0.2 - 0.3 ms<sup>-1</sup> for specimens observed, this could potentially bias our density estimates and needs further investigation.

The conflicting PLAOS and net estimates of biomass and size reinforce that multiple tools are required to ensure estimates are reliable both for relative and absolute estimates. Importantly, knowledge gained from this first use of PLAOS has informed modifications to provide a more robust instrument with the alteration of lighting and the addition of broad-band acoustics. We expect the further development and use of PLAOS will provide more robust estimates of distribution and abundance of a range of taxa including gelatinous organisms.

## References

- Barham, E. G. 1963. Siphonophores and deep-scattering layer. *Science*, 140: 826-8.
- Benfield, M. C., Lavery, A. C., Wiebe, P. H., Greene, C. H., Stanton, T. K., and Copley, N. J. 2003. Distributions of physonect siphonulae in the Gulf of Maine and their potential as important sources of acoustic scattering. *Canadian Journal of Fisheries and Aquatic Sciences*, 60: 759-772.
- Benoit-Bird, K. J., and Au, W. W. L. 2001. Target strength measurements of Hawaiian mesopelagic boundary community animals. *Journal of the Acoustical Society of America*, 110: 812-819.
- Clay, C. S., and Medwin, H. 1977. *Acoustical Oceanography*. John Wiley and Sons, New York, USA: 544 pp.
- D'Elia, M., Warren, J. D., Rodriguez-Pinto, I., Sutton, T. T., Cook, A., and Boswell, K. M. 2016. Diel variation in the vertical distribution of deep-water scattering layers in the Gulf of Mexico. *Deep Sea Research Part I: Oceanographic Research Papers*, 115: 91-102.
- Davison, P., Koslow, T. A., and Kloser, R. J. 2015. Acoustic biomass estimation of mesopelagic fishes: backscattering from individuals populations, and communities. *ICES J. Mar. Sci.*, 72(5): 1413-1424.
- Fulton, E., Smith, A., and Punt, A. 2005. Which ecological indicators can robustly detect effects of fishing. *ICES J. Mar. Sci.*, 62: 540-551.
- Handegard, N. O., Buisson, L. d., Brehmer, P., Chalmers, S. J., De Robertis, A., Huse, G., Kloser, R., et al. 2012. Towards an acoustic-based coupled observation and modelling system for monitoring and predicting ecosystem dynamics of the open ocean. *Fish and Fisheries: n/a-n/a*.
- Handegard, N. O., Demer, D. A., Kloser, R. J., Lehodey, P., Maury, O., and Simard, Y. 2010. Toward a Global Ocean Ecosystem Mid-Trophic Automatic Acoustic Sampler (MAAS). In *Proceedings of OceanObs'09: Sustained Ocean Observations and Information for Society* (2).
- Kaartvedt, S., Staby, A., and Aksnes, D. L. 2012. Efficient trawl avoidance by mesopelagic fishes causes large underestimation of their biomass. *Marine Ecology Progress Series*, 456: 1-6.
- Kloser, R., Ryan, T., Sakov, P., Williams, A., and Koslow, J. 2002. Species identification in deep water using multiple acoustic frequencies. *Canadian Journal of Fisheries and Aquatic Sciences*, 59: 1065-1077.
- Kloser, R. J., Ryan, T., Young, J., and Lewis, M. E. 2009. Acoustic observations of micronekton fish on the scale of an ocean basin: potential and challenges. *ICES J. Mar. Sci.*, 66: 998-1006.
- Kloser, R. J., Ryan, T. E., Keith, G., and Gershwin, L. 2016. Deep-scattering layer, gas-bladder density, and size estimates using a two-frequency acoustic and optical probe. *ICES Journal of Marine Science: Journal du Conseil*, 73: 2037-2048.
- Korneliussen, R. J., Heggelund, Y., Macaulay, G. J., Patel, D., Johnsen, E., and Eliassen, I. K. 2016. Acoustic identification of marine species using a feature library. *Methods in Oceanography*, 17: 187-205.
- Koslow, J. A., Kloser, R. J., and Williams, A. 1997. Pelagic biomass and community structure over the mid-continental slope off southeastern Australia based upon acoustic and midwater trawl sampling. *Marine Ecology-Progress Series*, 146: 21-35.
- Lavery, A. C., Wiebe, P. H., Stanton, T. K., Lawson, G. L., Benfield, M. C., and Copley, N. 2007. Determining dominant scatterers of sound in mixed zooplankton populations. *Journal of the Acoustical Society of America*, 122: 3304-3326.
- Lehodey, P., Conchon, A., Sennia, I., Domokos, R., Calmettes, B., Jouanno, J., Hernandez, O., et al. 2014. Optimization and evaluation of a micronekton model with acoustic data. *ICES Journal of Marine Science*, 72(5) 1399-1412.



- Lehodey, P., and Maury, O. 2010. Climate Impacts on Oceanic TOP Predators (CLIOTOP): Introduction to the Special Issue of the CLIOTOP International Symposium, La Paz, Mexico, 3-7 December 2007 Preface. *Progress in Oceanography*, 86: 1-7.
- Lehodey, P., Murtugudde, R., and Senina, I. 2010. Bridging the gap from ocean models to population dynamics of large marine predators: A model of mid-trophic functional groups. *Progress in Oceanography*, 84: 69-84.
- Lehodey, P., Senina, I., and Murtugudde, R. 2008. A spatial ecosystem and populations dynamics model (SEAPODYM) - Modeling of tuna and tuna-like populations. *Progress in Oceanography*, 78: 304-318.
- MacLennan, D. N., Fernandes, P. G., and Dalen, J. 2002. A consistent approach to definitions and symbols in fisheries acoustics. *ICES Journal of Marine Science: Journal du Conseil*, 59: 365.
- Marouchos, A., Sherlock, M., Kloser, R., Ryan, T., and Cordell, J. 2016. A profiling acoustic and optical system (pAOS) for pelagic studies; Prototype development and testing. *In OCEANS 2016-Shanghai*, pp. 1-6. IEEE.
- Maury, O. 2010. An overview of APECOSM, a spatialized mass balanced "Apex Predators ECOSystem Model" to study physiologically structured tuna population dynamics in their ecosystem. *Progress in Oceanography*, 84: 113-117.
- Myriax 2010. Echoview 4.90 Acoustic processing software. Myriax Pty Ltd. GPO Box 1387 Hobart, Tasmania, Australia, 7001.
- Pakhomov, E., and Yamamura, O. 2010. Report to the advisory panel on micronekton sampling inter-calibration experiment. PICES Scientific report No. 38 North Pacific Marine Science Organisation (PICES), Sidney, BC.
- Seager, J. W. 2008. SEAGIS CAL and Photomeasure stereo photogrametric calibration and analysis software. SEAGIS Pty Ltd, [www.seagis.com.au](http://www.seagis.com.au)

## 7. SYNTHESIS AND DISCUSSION

Rudy Kloser and Paul van Ruth

Significant advances in knowledge of pelagic ecosystem structure and function were made possible with the voyage on the 96 m MNF *RV Investigator* (Kloser et al. 2016). Sampling biota from microbes to tuna requires a large, diverse research team, using a wide range of technologies and methodologies, and is only possible on a large research vessel like *RV Investigator*. Inherent to this study were the multiple spatial and temporal scales that affect the composition, distribution and abundance of species. Given this complexity, and the complexities and precision of any one sampling method, a multiple-lines-of-evidence approach was adopted. The potential for bias in interpretation due to fast turnover (days – months) of microbes and plankton influenced by small scale local environmental changes, was augmented by characterising slow turn over (years) micronekton species. Similarly, studies of micronekton may be biased by gear selectivity and behaviour, and its temporal and spatial variability.

This synthesis of knowledge is based on historic data for temporal and spatial context, and new data collections made through this project, principally on a shared voyage in December 2015 on *RV Investigator*. A major limitation of the project was a reduction of the two planned *RV Investigator* voyages in each of summer and winter (20 days in each season) to a single 9 days of dedicated sampling in summer. The greatest impact of this change was on the ability to explore seasonal variation and, in the case of micronekton, replication in samples. Despite this it has been possible to combine historical data, information collected on the autumn *RV Southern Surveyor* voyage in 2013 and summer *RV Investigator* in 2015, and collections of bioacoustics and CPR data to address the key questions/hypotheses as outlined below in italics.

### *Community structure*

*“Describing the community structure, dynamics, biodiversity and endemism of microbes (i.e., viruses and bacteria), plankton (i.e., phytoplankton, zooplankton, ichthyoplankton) and micronekton (including squids, small pelagic and mesopelagic fish and gelatinous organisms).”*

Microbes (viruses and bacteria) and plankton (picophytoplankton, phytoplankton, and zooplankton) were sampled for the first time for shelf, slope and offshore waters of the eastern and central GAB in summer, highlighting differences in community composition and dynamics (Chapters 4 and 5) with major findings:

- No differences were detected in the abundance and composition of the microbial communities between the central and eastern GAB;
- Highest phytoplankton biomass always occurred below surface, with the biomass peak ~20-30 m deeper in the central GAB than in the east;
- Picoplankton (< 2 µm) (e.g. *Synechococcus* and *Prochlorococcus*) dominated phytoplankton biomass in the central GAB and nanoplankton (2 – 5 µm) (e.g. Prymesiophytes and Chlorophytes) dominated phytoplankton biomass in the east;
- Diatoms and dinoflagellates dominated the larger phytoplankton (> 5 µm) across the region, with Prasinophytes the next dominant taxa in the central GAB, and Chryptophytes the next dominant taxa in the eastern GAB; and

- The zooplankton community in the eastern GAB was dominated by copepods, with appendicularians, cladocerans, chaetognaths, echinoderms and the predatory dinoflagellate *Noctiluca* other dominant taxa. In the central GAB, copepods were also dominant, with appendicularians and thaliaceans the other dominant taxa;

Large zooplankton and micronekton were investigated for the first time in the central and eastern GAB with a combination of net, acoustic and optical sampling. This study highlights the dynamics of these organisms between regions, water depth and day-night gradients (Chapters 5 and 6). The main findings are:

- Based on net catches 319 taxa were identified where fish dominated the taxon richness showing that central and eastern GAB regions were similar in diversity and evenness;
- 18 new records of gelatinous organisms for the GAB that include 2 species new to science, 3 species newly reported to the Southern Hemisphere, 3 to Australia and 10 new species for the GAB, bringing the known species to 140; and
- A newly developed acoustic and optical probe (PLAOS) highlighted dynamics of micronekton to sampling gear quantified abundance and size and provided depth referenced images of the fragile gelatinous organisms.

#### *Planktonic food webs*

*“The “microbial food web” is the dominant planktonic food web over the deep GAB continental margin, particularly in the central GAB where year-round downwelling is thought to be the prevailing cross-margin flow, and that the more efficient “classic food web” only dominates in the eastern GAB during periods of nutrient-rich upwelling.”*

Physical, chemical, microbial, and planktonic data, together with information on rates from associated physiological processes, were synthesised to address the question/hypothesis above, and place those data in a regional context (Chapters 3 and 4). In summary, the GAB enrichment mechanisms driving primary productivity were found to differ between the eastern and central GAB at the time of the voyage (i.e. during the upwelling season). These can be summarised as being driven by physics (upwelling in summer) in the east, where enrichment is sporadic, but at times intense, and biological processes have a limited influence. In contrast, in the central GAB there is a stronger influence of biological processes (nitrification), with only intermittent input from turbulent fluxes at the shelf edge, resulting in a more constant but constrained enrichment.

The physical and chemical environment reflects the differences in food web dynamics that characterised the eastern and central GAB during the upwelling season, summarised below (Chapter 4).

- East:
  - DCM and nutricline ~40 – 60 m,  $Z_{eu}$  ~80-90 m.
  - Low nitrification rates.
  - Abundant high DMSP producing phytoplankton (Dinoflagellates, prymnesiophytes).
  - Nano phytoplankton dominate the autotrophic community.
  - High productivity driven by large volume of nutrient rich water above the euphotic depth, which contributes a significant proportion of total primary productivity in the euphotic zone.
  - More abundant mesozooplankton community with higher grazing rates.

- Higher rates of grazing on larger cells.  
→ Short food web underpinned by upwelled nitrogen.
- Central:
  - DCM ~80-90 m, nutricline ~100 m,  $Z_{eu}$  ~80-90 m.
  - High nitrification rates.
  - Abundant non/low DMSP producing phytoplankton (Smaller picophytoplankton, diatoms).
  - Picophytoplankton dominate the autotrophic community.
  - Productivity highest at the base of the euphotic zone, which makes a minimal contribution to total primary productivity in the euphotic zone.
  - Less abundant meso zooplankton community with low grazing rates.
  - Higher rates of grazing on small cells.  
→ Longer food web underpinned by regenerated nitrogen.

Despite these differences, long-term mean levels of remote sensed primary productivity were similar between the two regions. Primary productivity in the east is at times very high, but intermittent and variable, whereas in the central GAB primary productivity is more moderate and constant. Remote sensed data, which rely on surface measurements, likely underestimate total primary productivity in the eastern GAB by neglecting significant sub-surface primary productivity. However, our results indicate that the central GAB ecosystem is an important contributor to overall GAB productivity.

#### *Zooplankton and Micronekton*

*“That the zooplankton and micronekton communities of the central GAB continental margin have lower biomass, smaller species, different composition and longer trophic pathways than those on the eastern GAB. This is due to the nutrient source being “microbial food web” dominated in the central GAB and “classical” food web dominated in the eastern GAB.”*

Zooplankton and micronekton samples were used to address the above question and place those data in a regional context (Chapters 5 and 6). In summary, nutrient sources and trophic pathways (food web) were investigated for the first time in the offshore GAB using the compound-specific stable isotope analysis (CSIA) method (Chapter 6.2). The results highlight the complexity of predator-prey interactions of species within/between regions and depths with the main findings being:

- Clear evidence of a difference in source nitrogen between the eastern and central GAB upper slope crustacean species;
  - Eastern GAB source nitrogen indicative of upwelled or higher latitude water mass,
  - Central GAB source nitrogen indicative of atmospheric fixed nitrogen,
  - Longer trophic pathways in the central GAB for a high number of dominant species, and
  - These findings complement the plankton and primary production findings (Chapter 4);
- Mesopelagic fish have same or higher trophic position as sampled tuna, hence mesopelagic fish are not a significant prey of those tuna; and
- Meso zooplankton size and biovolume is consistent with plankton, production and isotope evidence that the eastern GAB upper slope is a distinct habitat consistent with upwelled nutrients (Chapter 5.2):
  - Precise size-based methods developed can be used to characterize mesozooplankton communities.

Whilst there were multiple lines of evidence to support dominant differences in nutrient enrichment and trophic pathways between the eastern and central region in summer, the assumed ecological response for zooplankton and micronekton of lower biomass, smaller species and different composition was difficult to assess. Zooplankton and micronekton biomass, size and species composition were similar between east and central regions but differed between species groups and sampling device, with highlights below:

- Meso zooplankton size smaller with higher biomass in the eastern upper slope region due to inferred recent nutrient enrichment (Chapter 5.2);
- Micronekton size ranges did not differ significantly between the eastern and central region;
- Macro zooplankton and micronekton biomass was higher in the eastern than central region but highly variable with limited sampling:
  - Shelf break and upper slope dominated by important krill prey species, and
  - Gelatinous community is an important component of the system, highest in the central region;
- Micronekton fish communities of the GAB have bio-geographic affinities with the Subtropical Convergence habitat zone:
  - No detectable east to central GAB differences in communities;
- Multi-frequency acoustic estimate of biomass was similar (within 30%) between regions;
- Profiling Lagrangian Acoustic Optical System (PLAOS) results infer slightly higher biomass with larger individuals in the central upper slope compared to the eastern GAB upper slope; and
- Large number of fish schools (hence biomass) in the central upper-slope and offshore GAB observed from acoustics highlights that the central GAB will have a production source to support them.

Spatial and temporal knowledge of zooplankton and micronekton distribution and abundance were investigated with Continuous Plankton Recorder (CPR) and bioacoustics methods. These methods are part of the Australian Integrated Marine Observing System (IMOS) and incorporating these methods enhanced this monitoring to place the GAB in an Australian and global context. These sampling methods also represented the most cost effective method of sampling at the time. Our sampling can also be placed in context with the overall oceanographic setting (see Chapter 3), the temporal changes (e.g. in the Leeuwin Current, GABRP, Theme 1) and the variation in inferred production (ocean colour time series, Chapter 4). Of note was the very weak Leeuwin Current prior to the December 2015 voyage but of normal strength during the voyage (GABRP, Theme 1). The influence of this on-transport of nutrients and biota from the western GAB could not be explored in this study as it may have contributed to the lower micronekton biomass in December 2015 compared to previous years. Based on the limited spatial and temporal context, this study provides a comprehensive state of the offshore environment that can be used to compare future environmental states.

### Summary

The prevailing hypothesis prior to this study was that the central GAB upper slope was an area of constant downwelling, implying low nutrients and hence low production and biomass that explained the sparse (low biomass) benthic fauna when compared to the upwelling eastern and western GAB

regions (Middleton et al., 2014, fig. 8). This study questions the validity of this hypothesis with the following observations:

- yearly production in the central GAB are similar to the eastern region based on remote sensed net primary productivity analysis, and
- high levels of micronekton biomass observed at the central region are similar to eastern region and other moderate production regions in Australia.

As a result of this study, we hypothesise that the central and eastern regions have similar production, sustained by the biology in the central and eastern GAB and for the eastern upper slope and shelf enrichment driven by the physics (during the summer upwelling season). In support of this we found that production and trophic transfer in the central region is more constant and appears to be dominated by regenerated nitrogen while the eastern region also receives pulses of upwelled nitrogen. This is reflected in the base nitrogen and reworked nitrogen trophic transfer to zooplankton and micronekton (Figure 8-1).

The findings in this work would benefit from longer temporal sampling to improve their significance. Clear differences in nutrient sources between the eastern and central upper slope at the time of sampling were highlighted from multiple lines of evidence. An understanding of the significance of these findings over a longer time frame is required to test our conclusions. We hypothesise, based on our findings, that the central GAB has lower but more consistent production supporting the micronekton schools observed by acoustics. Interestingly, our initial work on predator interactions using the CSIA method raises more questions than answers. The variability and complexity in these results highlights the difficulty in deriving simple functional relationships, but suggests that many mesopelagic fish are operating as top predators, with no overlap with the sampled tuna diet for this region. More detailed investigation of trophic interactions using stomach analysis and CSIA species specific trophic enrichment factor would assist in unravelling the complexities of the mesopelagic communities and their role in supplying food to other more charismatic “top predators”.

## 8. CONCLUSION

This study has advanced our knowledge of the structure and function of the ecosystem in the central and eastern offshore GAB. In general, the biomass of organisms in the offshore GAB is similar between regions, but nutrient and production sources differ for upper slope habitats in times of upwelling. Primary productivity in the east (upper slope) is at times very high, but intermittent and highly variable, whereas in the central GAB primary productivity is more moderate and constant. Hence the central GAB ecosystem is an important contributor to overall GAB productivity. This is reflected in the isotopic base and trophic enriched nitrogen transfer for zooplankton and micronekton. Interestingly, we found many micronekton fish had similar isotopic signatures to the few tuna sampled. These micronekton fish were calculated to be at a similar if not higher trophic level as tuna when using the same trophic enrichment factor for both groups. In general, there is more reworking of nitrogen in the central upper slope region with a different source nitrogen (Figure 8-1). We therefore conclude that the central offshore region is an important contributor to the production and biomass of pelagic organisms in the offshore GAB.



## Conclusion

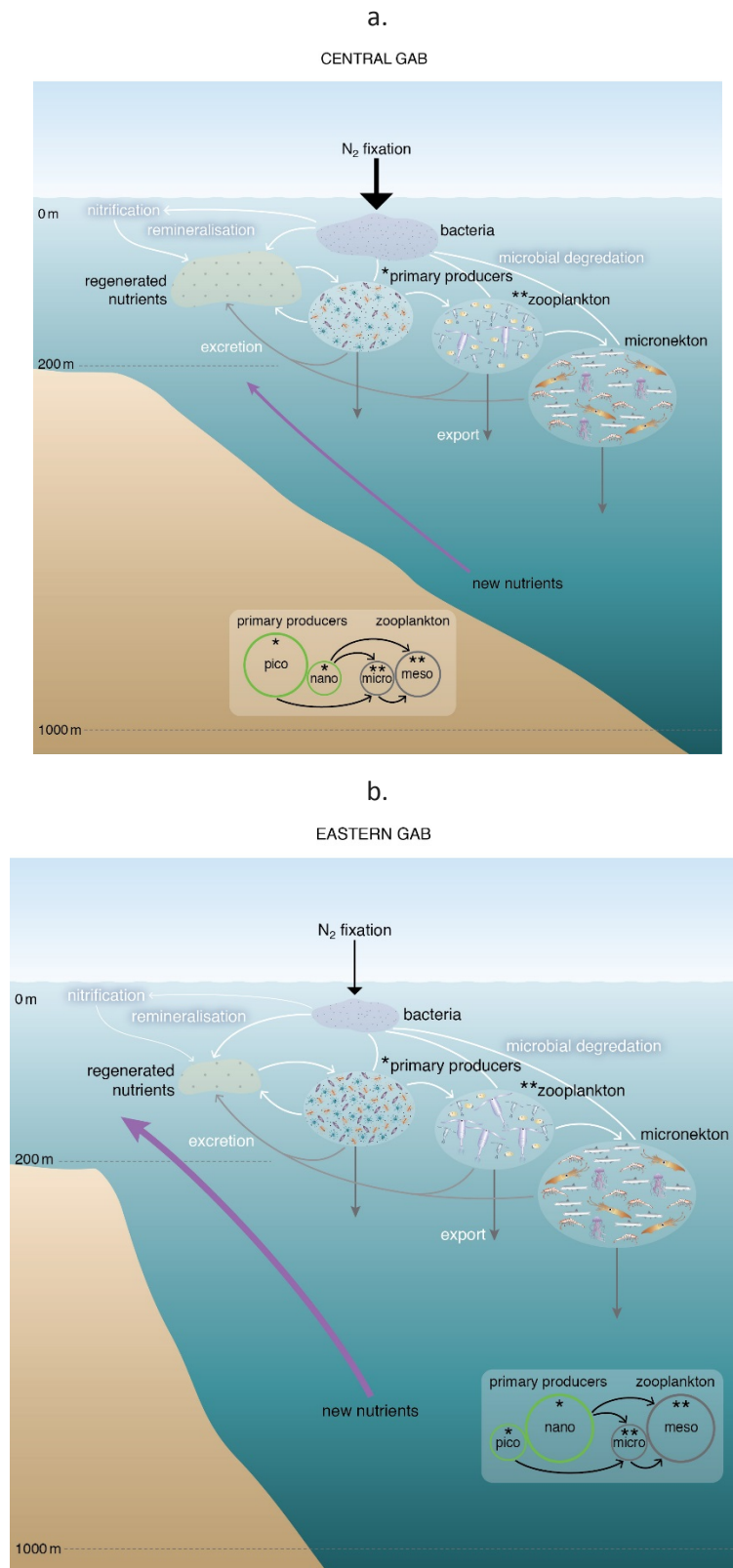


Figure 8-1 Diagram of functioning of the upper slope GAB highlighting dominant production drivers, (a). Central GAB where nutrient supply is constant but constrained and biological processes dominate nitrogen supply supporting production. (b), Eastern region where nutrient supply is characterized by addition of pulses of upwelled nutrients with a reduced pathway of biological processes. In general zooplankton and micronekton biomass is similar in the eastern and central region.

## 9. APPENDIX: STUDENT PROJECTS

### 9.1 Student name

Arti Verma

### 9.2 Degree type, project title and institution

**Degree:** Degree of Doctorate of Philosophy

**Title:** Development of wideband acoustic classification techniques for mesopelagic micronekton.

**Institution:** Centre for Marine Science and Technology

Department of Imaging and Applied Physics,

Curtin University

Perth

### 9.3 Status of student project

#### 9.3.1 Aim

Distributed beneath the territory of light in the ocean's dark and cold mesopelagic region exists a highly diverse community of micronekton, which are organisms ranging from 2-20 cm in size capable of swimming freely (Brodeur et al. 2005).

This project is a part of a wider research programme that focusses on the application of advanced acoustical and optical sensors to investigate the distribution and identification of micronekton, which form the mid-trophic level (MTL) organisms in the mesopelagic zone of the Great Australian Bight (GAB). The mesopelagic zone in the ocean is the region between the depth of 200 m and 1000 m underwater, which has limited exposure to sunlight. The prime objective of this research is to simulate and design an acoustic based mathematical model to solve the forward scattering problem, which is predicting the received echo level from the knowledge of scatterer physical and biological properties. Different models and approaches based on scatterer anatomical structure and scattering properties will be considered and applied subsequently. The statistical variability due to frequency dependency and spatial distribution of the received echo will be considered in addition to acoustic resonance and scattering. Simulations of the received echo levels from sound sources would be compared with the images obtained, enabling precise validation. The inverse problem, which is species identification from the received echo, will also be investigated.

The overall research objectives are:

- *In situ* evaluation of back scattering cross-Section and target strength of the prominent acoustic scatterers distributed within the mesopelagic region and determining the major scattering groups present within the GAB region.
- Investigate the frequency dependency and statistics of the backscattered echo amplitude and determine whether there is any relation between the length, shape, orientation of the animal, material properties of the animal and the echo characteristics.
- Compare and contrast the possibilities and results from sonars that transmit discrete narrowband signals and those that transmit signals with a continuous broadband frequency spectrum.

- Develop a simulation to quantify the received echo level through an integrated multi-disciplinary modelling approach for the dominant scatterer, taking into account all the biological and physical parameters including the size, aspect ratio, density, tilt angle, animal's behavior and morphology.
- Validate model output through application to different experimental data and quantification of the differences.
- Formulate the inverse problem, which is prediction of the biophysical characteristics of the target from the measured acoustic parameters and apply this to experimental data.

### 9.3.2 Progress on chapters

The preliminary goal was to calibrate the broadband echosounder for off axis angles and the depth variability, which has been accomplished in the first phase of the research. The research at present is in the second phase where resonant scattering models are being developed and applied to the *in situ* datasets. Moving further into second phase, we plan to integrate approximate scattering models and compare the experimental datasets with the modelling estimates. The final phase of the research is thesis writing which is expected to commence from January 2018.

#### *Progress and Accomplishments*

The first phase of the research aiming to collect acoustic, optics and net samples from the research region has been attained. The research is in the second phase where various acoustic scattering models are being developed and tested. At present, the research is almost following the scheduled timeline. We plan to continue analysis up to December 2017. The third phase of this research is writing the thesis.

The following objectives have been attained

Data acquisition: Broadband acoustic data and ancillary data required for the research has been collected in the last two years.

1. In August 2015, experiments were conducted in a laboratory set-up to calibrate the broadband echo sounder EK80 at Hobart harbor.
2. A field trip in the Great Australian Bight for the multidisciplinary data collection was conducted by *RV Investigator* from 30 November to 22 December 2015, providing integrated datasets for the research.
3. CT scan of major micronekton groups were conducted in January 2017 at Royal Hobart Hospital. The objective of the scan is to obtain the external and internal morphology of the biological specimens collected from the GAB region.

#### *Chapter wise Progress*

Chapter 1. Introduction (Literature review done)

Chapter 2. Broadband Theory (A Technical Paper to be submitted to IEEE)

Chapter 3 Acoustic Forward scattering Modelling (Working at Present)

Chapter 4 Application of acoustic scattering models to visually verified micronektons (Working at Present)

## 10. APPENDIX: PROJECT PUBLICATIONS

### 10.1 Papers

- Kloser, R.J., Willams, A., Van Ruth, P.D., Tanner, J.E., Downie, R., Doubell, M., Flynn, A., Keith, G., Ryan, T.E., and Hughes, D. (2016) *RV Investigator* voyage summary IN2015\_C02: Great Australian Bight deep-water pelagic and benthic ecosystem study, 30th Nov. to 22nd Dec. [http://www.mnf.csiro.au/~media/Files/Voyage-plans-and-summaries/Investigator/Voyage%20Plans%20summaries/2015/IN2015\\_C02%20Voyage%20Summary-20160220-FINAL-optimised.ashx](http://www.mnf.csiro.au/~media/Files/Voyage-plans-and-summaries/Investigator/Voyage%20Plans%20summaries/2015/IN2015_C02%20Voyage%20Summary-20160220-FINAL-optimised.ashx).
- Verma, A., Duncan, A. & Kloser, R. J. 2016. Developing active broadband acoustic methods to investigate the pelagic zone of the Great Australian Bight. *Proceedings of Acoustics*. [https://www.acoustics.asn.au/conference\\_proceedings/AASNZ2016/papers/p109.pdf](https://www.acoustics.asn.au/conference_proceedings/AASNZ2016/papers/p109.pdf)
- Verma, A., Duncan, A. & Kloser, R. J.. Signal Processing Techniques for Calibration of Broadband Fisheries Sonars for Off-axis Targets. (*to be submitted to IEEE*)
- Verma, A., Duncan, A. & Kloser, R. J.. Micronekton classification using broadband acoustic method. (*to be submitted to Acoustics Australia*)

### 10.2 Presentations

- L. Gershwin, R. Kloser, C. Sutton, A. Flynn, R. Downie, T Ryan (2017). Siphonophores: fearsome predators in oceanic food webs. AMSA conference.
- R.A. Downie, A.J. Richardson, R.J. Kloser (2017). Mesozooplankton abundance, biovolume and size structure within pelagic ecosystems of the Great Australian Bight. AMSA conference.
- Kloser, R.J., Gershwin, L., Verma, A., and Ryan, T.E. (2016) New insights into mesopelagic macrozooplankton using a profiling lagrangian acoustic optical system. In proceedings, ICES/PICES 6th Zooplankton Production Symposium "New Challenges in a Changing Ocean", Bergen Norway May 2016.
- Kloser, R.J., Ryan, T.E., Verma, A., Sherlock, M., Flynn, A., Sutton, C., Downie, R., and Gershwin, L. (2016) New insights into pelagic habitat with combined vessel acoustics, nets and a Profiling Lagrangian Acoustic, Optical System (PLAOS). ICES Fisheries Acoustic Science Technology Working group, Vigo Spain April 2016.
- Kloser, R.J., Van Ruth, P.D., Doubell, M., Richardson, A.E., and Revill, A. (2017) Exploring the slope/offshore Great Australian Bight (GAB) pelagic habitat paradox. Australian Marine Sciences Association, Darwin July 2017.
- Verma, A., Duncan, A., and Kloser, R. (2015) Development of wideband acoustic classification techniques for mesopelagic micronekton. Australian Marine Science Association (AMSA) Marine Science Student Workshop, Rottneest June 2015.
- Verma, A., Duncan, A., and Kloser, R. (2015) Can you count?? Annual Great Australian Bight Research Program Meeting, Adelaide August 2015.
- Verma, A., (2016) Broadband Sonar, Demystifying The Great Australian Bight. Curtin Marine and Coastal Research Network Conference, Perth January 2016.
- Verma, A., Duncan, A., and Kloser, R. (2016) Ping to ping variations in the frequency dependent target strength of single targets using a broadband echosounder (EK80). ICES Fisheries Acoustic Science Technology Working group, Vigo Spain April 2016.
- Verma, A., Duncan, A., and Kloser, R. (2016) Developing active broadband acoustic methods to investigate the pelagic zone of the Great Australian Bight. Annual Great Australian Bight Research Program Meeting, Adelaide August 2016.

- Verma, A., Duncan, A., and Kloser, R. (2016) Developing active broadband acoustic methods to investigate the pelagic zone of the Great Australian Bight. Second Australasian Acoustical Societies Conference, Brisbane November 2016.
- Verma, A., Duncan, A., and Kloser, R. (2017) Calibration of broadband sonars operating at depth. ICES Fisheries Acoustic Science Technology Working group, Nelson New Zealand April 2017.
- Tanner, J. (convenor), (2017) Great Australian Bight – seeking whole-of-system understanding. Symposim 15, Annual Conference Australian Marine Science Association, Darwin, NT, July 2017.

### 10.3 Patents

Not applicable.

### 10.4 Media Releases

Refer to program summary.

## 11. APPENDIX: INTELLECTUAL PROPERTY

### 11.1 Unique discoveries

New species have been described for the region as outlined in Section 5.3.

### 11.2 Action plan

TBD

